Ollscoil na Gaillimhe
University of Galway

Provided by the author(s) and University of Galway in accordance with publisher policies. Please cite the published version when available.

Title	Development of a Two-Dimensional Estuarine Hydrodynamic Model in Cylindrical Co-ordinates
Author(s)	Boblea, Luminita-Elena
Publication Date	2014-02-03
Item record	http://hdl.handle.net/10379/4427

Downloaded 2024-04-26T19:17:45Z

Some rights reserved. For more information, please see the item record link above.

Development of a Two-Dimensional Estuarine Hydrodynamic Model in Cylindrical Co-ordinates

Luminita – Elena Boblea

Thesis submitted to the National University of Ireland, Galway
for the Degree of Doctor of Philosophy

College of Engineering and Informatics
Department of Civil Engineering
National University of Ireland, Galway

February 2014

Supervisor: Professor Michael Hartnett
Head of Department: Dr. Piaras Ó hEachteirn

Declaration

I declare that this dissertation, in whole or in part, has not been submitted to any University as an exercise for a degree. I further declare that, except where reference is given, the work is entirely my own.

Signed:

_____

Luminita-Elena Boblea February 2014

Abstract

Development of a novel two-dimensional estuarine hydrodynamic model in cylindrical co-ordinates is presented herein. The full non-linear Navier-Stokes equations are written in cylindrical co-ordinates with the advantage of the co-ordinate system fitting the estuary's shape. Thus the bending of the coastline can be more accurately described. Also, this way a fine mesh is obtained in the coastal area, while a coarse mesh is defined away from the coast provided that the position of the pole is appropriately chosen. The new model aims at improving the resolution of study areas and getting results without increasing computational costs.

Validation of the cylindrical co-ordinates numerical model is done by comparison with robust industry-standard models, tidal basin measurements and analytical solution. Three test cases are proposed for comparison with other numerical models: horizontal bed with constant value of the scale factors in the radial direction, horizontal bed with one variation of the scale factors in the radial direction, horizontal bed with two variations of the scale factors in the radial direction. Variation of the scale factors in the radial direction is done with an exponential function. Comparisons with results of the two numerical models show very good agreement. Comparison with tidal basin data is done in three cases: cylindrical co-ordinates (the rectangular geometry is generated from cylindrical co-ordinates), uniform Cartesian co-ordinates, and non-uniform Cartesian co-ordinates. Results showed that agreement was achieved in all cases. Finally, agreement between analytical solution and results of the numerical model shows the potential of the cylindrical co-ordinates numerical model for estuarine hydrodynamic modelling.

In terms of computational savings, the model proved to be four times faster than the Cartesian co-ordinates numerical model ran at the finest resolution in the cylindrical co-ordinates numerical model. Compared to the general orthogonal curvilinear co-ordinates model, the new model is three times slower since this is a preliminary development of the cylindrical co-ordinates model and further improvement is required.

Acknowledgements

Professor Michael Hartnett is acknowledged for his guidance, encouragements and support throughout the duration of the research.

My thanks are directed to the College of Engineering and Informatics and IBM Fellowship Programme who funded the research.

I would also like to acknowledge the help of Niall Madden, Martin Meere and Naresh Chadha in the mathematical development of the cylindrical co-ordinates numerical model.

I am grateful to the members of the Marine Modelling and Informatics Group for their friendship and help.

Table of Contents

Declaration.....**i**

Abstract.....**ii**

Acknowledgements ..... **iii**

Table of Contents .....**iv**

List of Figures.....**ix**

List of Tables .....**xix**

List of Abbreviations .....**xxii**

Nomenclature .....**xxiv**

Chapter 1. Introduction……..**1**

1.1. Background Context.....**1**

1.2. The Role of Numerical Models **5**

1.4. Research Aims and Objectives **8**

1.4. Thesis layout and contents **9**

Chapter 2. Literature Review……..**12**

2.1. Introduction.....**12**

2.2. Estuarine Hydrodynamic Modelling Methodology **13**

2.3. Review of Grid Systems for Hydrodynamic Models **16**

2.3.1. Structured versus Unstructured Grid and Mesh Free Hydrodynamic Models.....18

2.3.2. Cartesian Co-ordinates Grid Models 26

2.3.3. Orthogonal Curvilinear Co-ordinates Grid Models 28

2.3.4. Non-orthogonal Curvilinear Co-ordinates Grid Models.....31
2.3.5. Spherical Co-ordinates Grid Models 32
2.3.6. Horizontal Spatial Resolution.....34
2.3.7. Number of Extra-Terms due to Curvature of the Structured Grid.....40
2.3.8. Conclusions.....42

2.4. Review of Analytical Solutions and Numerical Models in Cylindrical Co-ordinates 44
2.4.1. Analytical Solution of Shallow Water Equations in Cylindrical Co-ordinates for Estuarine Hydrodynamic Modelling 44
2.4.2. Cylindrical Co-ordinates for Pipe Flow Simulations.....46
2.4.3. Storm Surge Modelling in Cylindrical Co-ordinates.....48
2.4.4. Cylindrical Co-ordinates for Study of Tidal Wave Variations around Small Cylindrical Islands.....50
2.4.5. Conclusions.....53

2.5. Summary and conclusions.....53

Chapter 3. Mathematical Formulation of a Cylindrical Co-ordinates Numerical Model……...58

3.1. Introduction.....58

3.2. Governing Equations of Fluid Motion 59
3.2.1. The Continuity Equation.....59
3.2.2. The Navier-Stokes Equations 61

3.3. Formulation of the Governing Equations in Cylindrical Co-ordinates 67
3.3.1. Navier-Stokes Equations with the Hydrostatic Pressure Assumption ..71
3.3.2. Body Force Terms.....73
3.3.3. Reynolds Averaging Concept 74
3.3.4. Turbulence Modelling.....79

3.4. Depth Integration of the Hydrodynamic Equations in Cylindrical Co-ordinates.....80
3.4.1. Depth Integration of the Continuity Equation 82

3.4.2. Depth Integration of the $r-$ direction Momentum Equation.....84
3.4.3. Depth Integration of the $\theta-$ direction Momentum Equation 87
3.4.4. Evaluation of Bed and Wind Shear Stresses.....89
3.4.5. Approximations for Evaluation of the Turbulence Term 91

3.5. Mapping Transformations 93
3.5.1. Physical and Computational Grid Generation 93
3.5.2. Transformation Relationships for Equation Equivalence between Physical and Computational Domain.....96
3.5.3. Transformation of the Continuity and Navier-Stokes Equations.....97

3.6. Boundary Conditions.....100
3.6.1. Open Boundary Conditions.....101
3.6.2. Closed Boundary Conditions 102

3.7. Summary.....104

Chapter 4. Solution Technique……..105

4.1. Introduction.....105

4.2. Further Explanation of the Terms in the Navier-Stokes Equations ...105

4.3. Mathematical Modelling Methodology 107

4.4. Numerical Discretization of the Equations Governing Water Motion108
4.4.1. Properties of the Finite Difference Approximations.....108
4.4.2. Finite Difference Approximations on Cartesian Meshes.....109
4.4.3. Finite Difference Approximations on Computational Domains.....114
4.4.4. Alternating Directions Implicit Method – General Considerations....116
4.4.5. Courant Criterion for Alternating Directions Implicit Method.....120
4.4. 6. Proposed Finite Difference Scheme.....121
4.4.7. Boundary Conditions 126

4.5. Solution Technique 129
4.5.1. Thomas Algorithm - General considerations.....134
4.5.2. Thomas Algorithm for the Governing Equations 136

4.5.3. Representation of the Recursion Coefficients in the Numerical Model 138
4.5.4. Implementation of Solution Procedure in the Numerical Model 141

4.6. Summary 148

Chapter 5. Cylindrical Co-ordinates Numerical Model Results 149

5.1. Introduction 149

5.2. Preliminary Results of the Cylindrical Co-ordinates Numerical Model 150
5.2.1. Computational Mode 150
5.2.2. The Robert-Asselin-Williams Filter 151

5.3. Case Studies 154
5.3.1. Case 1 – Horizontal Bed with Constant Scale Factors in the Radial Direction 158
5.3.2. Case 2 – Horizontal Bed with Variable Step in the Radial Direction 175
5.3.3. Case 3 – Horizontal Bed with Two Variations of the Scale Factors in the Radial Direction 188

5.4. Physical Modelling 201
5.4.1. General Considerations 201
5.4.2. Tidal Model Set-Up 206
5.4.3. Numerical Model Results versus Tidal Basin Measurements – Rectangular Domain from Cylindrical Co-ordinates 209
5.4.4. Numerical Model Results versus Tidal Basin Measurements – Cylindrical Co-ordinates Numerical Model Transformed into Uniform Cartesian Co-ordinates Numerical Model 215
5.4.5. Numerical Model Results versus Tidal Basin Measurements – Cylindrical Co-ordinates Numerical Model Transformed into Non-Uniform Cartesian Co-ordinates Numerical Model 219

5.5. Application of the Analytical Solution of the Shallow Water Equations in Cylindrical Co-ordinates 223
5.5.1. General Considerations 223

5.5.2. Numerical Model Results versus Analytical Solution 225

5.6. Summary and Conclusions 226

Chapter 6. Summary and Final Conclusions ……...…230

6.1. Summary..... 230

6.2. Discussion and Conclusions 234

6.3. Future Work..... 236

REFERENCES AND BIBLIOGRAPHY 237

***APPENDIX 1* 255**

APPENDIX 2* *260

***APPENDIX 3* 265**

***APPENDIX 4* 271**

***APPENDIX 5* 273**

***APPENDIX 6* 279**

***APPENDIX 7* 307**

***APPENDIX 8* 316**

***APPENDIX 9* 322**

***APPENDIX 10* 332**

***APPENDIX 11* 336**

***APPENDIX 12* 347**

***APPENDIX 13* 353**

List of Figures

Figure		Page
1.1	Global distributions of population and land in the near coastal region [Nicholls and Small (2002)].	1
1.2	Interactions between atmosphere, land, ocean and ice in the context of climate change [after Ross (1995)].	2
1.3	Summary of mechanisms of shelf sediment transport [McCave (2002)].	3
1.4	Wave energy assessment around the world [Fusco (2012)].	4
1.5	Various uses of coastal numerical models.	6
2.1	Some features for design/selection of grid-based hydrodynamic models.	17
2.2	Some Arakawa grids for finite difference horizontal discretizations [after Dyke (2007)].	20
2.3	Uniform Cartesian mesh for numerical modelling of Cork Harbour, Ireland [Nash et al. (2005)]	27
2.4	Non-uniform two-dimensional Cartesian mesh for numerical modelling.	28
2.5	General curvilinear orthogonal grid of Bohai Sea (left) and transformed plane (right) [Bao et al. (2000)].	30
2.6	Non-orthogonal curvilinear grid of the Messina Strait, Italy [Andronosov et al. (2002)].	31
2.7	$O\vec{M}$ vector in a two-dimensional non-orthogonal curvilinear co-ordinate system [George (2007)]. Condition of non-orthogonality: $\varepsilon \neq \nu$.	32
2.8	Spherical grid with orthogonal mapping transformations for numerical modelling of Narragansett Bay [Sankaranarayanan and Ward (2006)].	33
2.9	Spherical co-ordinates grid with non-orthogonal mapping transformation of Greenwich Bay, USA [Sankaranarayanan and Spaulding (2003)].	34

2.10 Boundary-fitted grid and contravariant components of velocity in the horizontal physical domain and computational domain. 37

2.11 Quarter annular geometry for verification of numerical models. 45

2.12 Cylindrical island for the study of tidal wave variations in constant water depth (h): a) without sill [after Lee and Kim (1999)]; b) with uniform water depth (h_0) sill [Kowalik and Marchenko (2002)]. 51

2.13 Amplitude and phase of semidiurnal Sverdrup wave around cylindrical island without sill (a,b) and with sill (c,d) in the presence of bed friction [Marchenko and Kowalik (2002)]. 52

2.14 Simplified physical and computational plane for a hypothetical estuary [after Roy et al. (1999), Morinishi et al. (2004)]. 57

3.1 Infinitesimal control volume for mass flow rate evaluation with centre of mass at point C. Green arrow represents inflow in the considered volume at point A for the inflow area; red arrow illustrates outflow at point B in the $x-$direction 60

3.2 Control volume for derivation of the Navier-Stokes equations. 63

3.3 Total stress tensor in a tetrahedron [after Aris(1989)]. Stress tensor decomposed after the three planes of a Cartesian co-ordinate system, with unit vectors $\vec{e}_1, \vec{e}_2, \vec{e}_3$. 64

3.4 Cylindrical co-ordinate system. 69

3.5 Schematics of the ζ and h terms: H is the total depth ($H = \zeta + h$); ζ is water elevation below or above still water elevation. 72

3.6 Instantaneous velocity decomposition into mean and fluctuating parts: $\tilde{v}_r$ is the instantaneous velocity (green arrow); $\bar{v}_r$ is the averaged velocity (orange arrow), v_r' is the

	fluctuating quantity (yellow arrow). The mean value of $\tilde{v}_r$ is approximated by a logarithmic law, i.e. $(v_r)_{\log}$ represented with red arrow.	75
3.7	Three-dimensional vertical variation of velocity components approximated by a logarithmic law.	81
3.8	Depth integrated velocity in the $r-$direction.	81
3.9	Physical (a) and computational (b) plane. Colours representation: grey cells represent land boundaries, light blue cells are for open boundary, darker blue cells illustrate wet cells. r_0 is identical with the pole of the cylindrical co-ordinate system.	94
4.1	Flowchart of the mathematical modelling methodology.	107
4.2	Flowchart of the numerical model.	108
4.3	Description of three grid based discretization methods.	109
4.4	Finite difference approximations of first-order derivatives [Hirsch (1988)].	112
4.5	Some time and space finite differences schemes for one-dimensional problems [Falconer (1976)].	114
4.6	Staggered grid configuration in the transformed plane for spatial discretization. Blue triangles represent transformed velocities in the angular direction (V_{ξ^θ}), green triangles are used for transformed velocities in the radial direction (V_{ξ^r}), "+" is for i.e. water elevation (ζ), Chezy coefficient (C), eddy viscosity ($\overline{E}$). Boundary velocity points are represented as circumscribed triangles.	115
4.7	Ghost point method for evaluation of no slip and free slip land boundary conditions in the ξ^r – direction: a) on a straight line boundary; b) on a curved boundary [Hirsch (1988)].	128
4.8	Velocities and water elevation representation on computer grid showing finite difference grid points as well. Circumscribed triangles represent boundary velocities.	141

4.9	Code flowchart based on the ADI technique.	142
4.10	Final form of Fortran code flowchart.	143
4.11	Structure of the numerical model.	144
4.12	Computational domain for solution technique in the $\xi^r -$ direction. Grey cells represent land, light blue cells show water cells, dark blue cells illustrate open boundary. Red arrows show direction of calculations in each integration section [Nash (2010)].	145
4.13	Flowchart of subroutine HYDMODX showing implementation of the solution procedure in the $\xi^r -$(or $I -$) direction.	146
5.1	Grid points within considered domain defined between two radii positioned at angles $\theta_1 = 252°$ and $\theta_2 = 288°$ with respect to the positive horizontal eastward $x -$ axis of a Cartesian co-ordinate system and two concentric circles ($r_1 = 7500m$, $r_2 = 27500m$), $\Delta r = 500m$; $\Delta\theta = 1°$.	152
5.2	Outputs of the model before introducing the Asselin filter: a) water elevations at point (10, 27); b) total velocities at point (10, 27); c) predicted velocities inside domain.	153
5.3	Domain representation in DIVAST.	155
5.4	Grid orthogonality deviation in EFDC: a) for the horizontal bed with constant step in the radial direction test case; b) for the horizontal bed with one variation of the step in the radial direction test case; c) for the horizontal bed with two variations of the step in the radial direction test case.	156
5.5	Domain representation in the cylindrical co-ordinates numerical model for first test case.	160
5.6	Domain representation in EFDC for first test case.	161
5.7	Computed water levels from the cylindrical co-ordinates model.	162
5.8	Dimensionless water elevation amplitude variation with dimensionless distance for: a) $n = 1.0$; b) $n = 1.1610138$.	163

5.9 Total velocities and water elevation time series comparison between the three models at point A inside domain for the first test case. 165
5.10 Total velocities and water elevation time series comparison between the three models at point B inside domain for the first test case. 166
5.11 Total velocities and water elevation time series comparison between the three models at point C inside domain for the first test case. 166
5.12 Total velocities and water elevation time series comparison between the three models at point D inside domain for the first test case. 167
5.13 Total velocities and water elevation time series comparison between the three models at point E inside domain for the first test case. 167
5.14 Flow inside domain for the first test case at time 36.00 hours (DIVAST). 168
5.15 Flow inside domain for the first test case at time 36.00 hours (cylindrical co-ordinates model). 168
5.16 Flow inside domain for the first test case at time 36.00 hours (EFDC). 169
5.17 Water elevations variation at points A-E inside domain (DIVAST) for the first test case. 169
5.18 Water elevations variation at points A-E inside domain (cylindrical co-ordinates model) for the first test case. 170
5.19 Water elevations variation at points A-E inside domain (EFDC) for the first test case. 170
5.20 Total velocities variation at points A-E inside domain (DIVAST) for the first test case. 171
5.21 Total velocities variation at points A-E inside domain (cylindrical co-ordinates model) for the first test case. 171
5.22 Total velocities variation at points A-E inside domain (EFDC) for the first test case. 172

5.23	Domain representation for the second test case in the new numerical model.	177
5.24	Domain representation for the second test case in EFDC.	177
5.25	Total velocities and water elevation time series comparison between the two models at point A inside domain for the second test case.	179
5.26	Total velocities and water elevation time series comparison between the two models at point B inside domain for the second test case.	180
5.27	Total velocities and water elevation time series comparison between the two models at point C inside domain for the second test case.	180
5.28	Total velocities and water elevation time series comparison between the two models at point D inside domain for the second test case.	181
5.29	Total velocities and water elevation time series comparison between the two models at point E inside domain for the second test case.	181
5.30	Analysis of dimensionless water elevation amplitude versus dimensionless distance for the second test case. Water elevation transformation exponent term in the cylindrical co-ordinates model: a) $n = 1.0$; b) $n = 1.238358$.	182
5.31	Flow inside domain for horizontal bed test case at time 36.00 hours (cylindrical co-ordinates model) for the second test case.	183
5.32	Flow inside domain for the second test case at time 36.00 hours (EFDC).	183
5.33	Water elevations variation at points A-E inside domain (cylindrical co-ordinates model) for the second test case.	184
5.34	Water elevations variation at points A-E inside domain (EFDC) for the second test case.	184
5.35	Total velocities variation at points A-E inside domain (cylindrical co-ordinates model) for the second test case.	185

5.36 Total velocities variation at points A-E inside domain (EFDC) for the second test case. 185
5.37 Domain representation for the third test case in cylindrical co-ordinates numerical model. 189
5.38 Domain representation for the third test case in EFDC. 189
5.39 Total velocities and water elevation time series comparison between the two models at point A inside domain for the third test case. 192
5.40 Total velocities and water elevation time series comparison between the two models at point B inside domain for the third test case. 193
5.41 Total velocities and water elevation time series comparison between the two models at point C inside domain for the third test case. 193
5.42 Total velocities and water elevation time series comparison between the two models at point D inside domain for the third test case. 194
5.43 Total velocities and water elevation time series comparison between the two models at point E inside domain for the third test case. 194
5.44 Analysis of dimensionless water elevation amplitude versus dimensionless distance for the third test case: a) $n = 1.0$; b) $n = 1.216087$. 195
5.45 Flow inside domain for horizontal bed test case at time 36.00 hours (cylindrical co-ordinates model) for the third test case. 196
5.46 Flow inside domain for horizontal bed test case at time 36.00 hours (EFDC) for third the test case. 196
5.47 Water elevations variation at considered points inside domain (cylindrical co-ordinates model) for the third test case. 197
5.48 Water elevations variation at points A-E inside domain (EFDC) for the third test case. 197
5.49 Total velocities variation at points A-E inside domain

	(cylindrical co-ordinates model) for the third test case.	198
5.50	Total velocities variation at points A-E inside domain (EFDC) for the third test case.	198
5.51	Techniques for study of coastal flows.	202
5.52	Tidal Model set-up [Olbert (2006)]: a) schematic view; b) lab arrangement.	207
5.53	Schematic layout of tidal basin [Olbert (2006)]: a) plan view; b) cross-section.	207
5.54	Rectangular geometry generation using cylindrical co-ordinates for the scale factors given in Table 5.25.	211
5.55	Grid representation (11x11 points) of the tidal basin for numerical model simulation ($\delta x = 0.5m$) [Olbert (2006)].	212
5.56	Comparison of the measurements and numerical model results for the r – direction velocity component at point A5.	213
5.57	Comparison of the r – direction velocity results at point D5.	213
5.58	Comparison of the water elevation time series resulted from numerical model (blue line) and measurements (green line) at point A5 for two tidal cycles.	214
5.59	Velocity currents at various water elevation stages: a) high water; b) low water; c) mid water during ebb tide; d) mid water during flood tide.	215
5.60	Cartesian co-ordinates mesh for representation of tidal basin in numerical model ($\delta x = 0.1m$).	216
5.61	Measured data and numerical model predicted I – direction velocity component at point A5 for uniform Cartesian grid.	217
5.62	Measured data (green line) and numerical model predicted water elevation (blue line) at point A5 for uniform Cartesian grid.	217
5.63	Measured data and numerical model predicted I – direction velocity component at point D5 for uniform Cartesian grid.	218
5.64	Velocity currents at various water elevation stages: a) high water; b) low water; c) mid water during ebb tide; d) mid water during flood tide.	219

5.65	Measured data and numerical model predicted I – direction velocity component at point A5 for irregular Cartesian mesh.	221
5.66	Measured data and numerical model predicted I – direction velocity component at point D5 for irregular Cartesian mesh.	221
5.67	Measured data (green line) and numerical model predicted water elevation (blue line) at point A5 for irregular Cartesian mesh.	222
5.68	Velocity currents at various water elevation stages: a) high water; b) low water; c) mid water during ebb tide; d) mid water during flood tide.	222
5.69	Water elevation amplitude at points A-E from cylindrical co-ordinates model and analytical solution of Lynch and Gray (1978) for horizontal bed with constant step in the radial direction.	225
5.70	r – direction velocity at points A-E from cylindrical co-ordinates model and analytical solution of Lynch and Gray (1978) for horizontal bed with constant step in the radial direction.	226
A1.1	Representation of the Cartesian co-ordinate system.	255
A1.2	Spherical polar co-ordinate system.	256
A1.3	Cylindrical polar co-ordinate system.	257
A1.4	General orthogonal curvilinear co-ordinate system. The angle between any two axes is $90°$.	259
A3.1	Representation of the generalised curvilinear co-ordinate system.	265
A3.2	Covariant basis vectors for curvilinear co-ordinates [Warsi (2006)].	266
A6.1	Graphical transformation of vector components from cylindrical co-ordinates to Cartesian co-ordinates.	282
A11.1	Domain for the study of analytical solution in convergent geometry.	336
A11.2	Domain representation for water elevation transformation.	341
A12.1	Representation of variables in DIVAST.	350

A13.1 Staggered grid representation of variables in EFDC. 360

List of Tables

Table		Page
4.1	Mathematical and code formulation of the NSE terms in the $\xi^r -$ direction.	106
4.2	Description of some variables and the equivalence between mathematical and numerical model representation of variables.	140
5.1	Parameters common to the three test cases for the new numerical model and EFDC, and for the first test case for DIVAST.	157
5.2	Parameters common to the three test cases for EFDC.	157
5.3	Scale factors for domain representation in the cylindrical co-ordinates numerical model for the first test case.	159
5.4	Water elevation amplitudes at points A-E inside domain for the first test case with $n = 1.0$ and $n = 1.160138$.	162
5.5	Dimensionless water elevation amplitudes at points A-E inside domain for horizontal bed test case with $n = 1.0$.	164
5.6	Dimensionless water elevation amplitudes at points A-E inside domain for horizontal bed test case with $n = 1.160138$.	165
5.7	High and low water levels and maximum total velocity at ebb and flood tide for the first test case for $n = 1.0$.	173
5.8	Time period between high water and low water in the three models along centreline.	174
5.9	Time period between maximum velocity at ebb tide and maximum velocity at flood tide in the three models along centreline.	174
5.10	Variation of scale factors inside domain for horizontal bed with variable scale factors in the radial direction test case.	176
5.11	Water elevation amplitudes at the considered points inside domain for the second test case with $n = 1.0$ and.	

	$n = 1.331587$	178
5.12	Dimensionless water elevation amplitudes at the considered points inside domain for the second test case with $n = 1.0$ and $n = 1.331587$ in the cylindrical co-ordinates model.	186
5.13	High and low water levels and maximum total velocity at ebb and flood tide for the second test case for $n = 1.0$.	187
5.14	Time period between high water and low water in the three models along centreline.	188
5.15	Time period between maximum velocity at ebb tide and maximum velocity at flood tide in the three models along centreline.	188
5.16	Variation of scale factors inside domain for horizontal bed with two variations of the space step in the radial direction test case.	190
5.17	Water elevation amplitudes at the considered points inside domain for third test case for $n = 1.0$ and $n = 1.216087$.	191
5.18	Dimensionless water elevation amplitudes at the considered points inside domain for second test case for $n = 1.0$ and $n = 1.216087$.	195
5.19	High and low water levels and maximum total velocity at ebb and flood tide for the third test case for $n = 1.0$.	199
5.20	Time period between high water and low water in the three models along centreline for $n = 1.0$.	200
5.21	Time period between maximum velocity at ebb tide and maximum velocity at flood tide in the three models along centreline.	201
5.22	Conditions of similitude from Froude ratio Olbert (2006).	209
5.23	Variables used in the physical model and prototype.	210
5.24	Parameters for tidal basin simulations in the new numerical model.	210
5.25	Scale factors for generation of tidal basin rectangular geometry grid using cylindrical co-ordinates ($\delta r = 0.5m$).	211

5.26 Variation of space step in the I – direction for simulation in the tidal basin. 220
5.27 Analytical solutions of the shallow water equations written in cylindrical co-ordinates [Lynch and Gray (1978)]. 224

List of Abbreviations

IOC	Intergovernamental Oceanographic Commission
GOOS	Global Ocean Observing System
GTOS	Global Terrestrial Observing System
EuroGOOS	European Global Ocean Observing System
UNCLOS	United Nations Convention on the Law of the Sea
SOLAS	Safety of Life at Sea
LOICZ	Land-Ocean Interactions in Coastal Zone
SETIS	Strategic Energy Technologies Information System
NOAA	National Oceanic and Atmospheric Administration
OTEC	Ocean Thermal Energy Conservation
BOD	biochemical oxygen demand
SOD	sediment oxygen demand
DO	dissolved oxygen saturation
DIVAST	Depth Integrated Velocities and Solute Transport
SLOSH	Sea, Land and Overland Surges from Hurricanes
POM	Princeton Ocean Model
ROMS	Regional Ocean Model System
GETM	General Estuarine Transport Model
EFDC	Environmental Fluid Dynamics Code
ADCIRC	Advanced Circulation Model
FVCOM	Finite Volume Coastal Ocean Model
OPW	Office of Public Works
ADI	Alternating Directions Implicit method
FDM	Finite Differene Model
FVM	Finite Volume Method
FEM	Finite Element Method
ECOM-si	Estuarine Coastal Ocean Model with semi-implicit time discretization
GWCE	Generalized Wave Continuity Equation
SPH	Smoothed Particle Hydrodynamics

RANS	Reynolds-Averaged Navier-Stokes equations
PVM	Parallel Virtual Machine
MPI	Message Passing Interface
TRIGRID	Modelling system for building Triangular Grids
NSE	Navier-Stokes Equations
OBC	Open Boundary Conditions
RAW	Roberts-Asselin_Williams filter

Nomenclature

τ	weighting parameter in GWCE
τ_{ADI}	relaxation parameter in ADI
ρ	particle density in SPH
ρ_W	water density in SPH
b	bottom elevation in SPH
S_f	bed friction source term
(ξ,η)	horizontal computational domain
σ	dimensionless co-ordinate on the vertical generated using mapping transformations
(R,θ,ϕ)	spherical co-ordinate system
(u^c,v^c)	contravariant velocity components in the horizontal domain
(u^s,v^s)	velocity components in spherical co-ordinates in the horizontal plane
$\Phi_\xi,\Phi_\eta,\theta_\xi,6$	partial derivatives with respect to subscripts indicated
J_s	Jacobian of the horizontal non-orthogonal transformation from spherical co-ordinates onto computational domain
S	area
V	control volume
dS	infinitesimal area
dV	infinitesimal control volume
$\vec{v}$	velocity vector
x, y, z	axes of the Cartesian co-ordinate system
v_x, v_y, v_z	Components of the velocity vector in the directions of a Cartesian co-ordinate system
$\vec{f}_{INT}$	force per unit area exerted by the material outside the boundary surface
$\vec{f}_{EXT}$	external force per unit volume and unit density
$\vec{n}$	unit outward normal to the bounding surface

$\underset{\sim}{t}_n$	total stress tensor
$\underset{\sim}{T}$	second order stress tensor
T_{lk}	components of the second order tensor $\tilde{T}$
F	continuous function
$F_{,k}$	continuous first derivative of function F with respect to the kth direction
e_{kl}	symmetric deformation tensor
p	hydrostatic pressure for incompressible fluids or thermodynamic pressure for compressible fluids
μ	dynamic viscosity of the fluid
λ	second viscosity coefficient
Θ	invariant under an orthogonal transformation
δ_{kl}	von Karman constant
P_{kl}	viscous stress tensor
υ	kinematic viscosity
P_a	atmospheric pressure
r, θ, z	axes of the cylindrical co-ordinate system
ζ	water elevation
$-h$	water depth as measured from the mean water level
H	total water depth
$\tilde{V}$	instantaneous velocity
$\tilde{v}_r, \tilde{v}_\theta, \tilde{v}_z$	instantaneous velocity components on the three axes of the cylindrical co-ordinate system
t	time
$\tilde{f}_{EXT}$	instantaneous external force
$\tilde{f}_r, \tilde{f}_\theta, \tilde{f}_z$	instantaneous external force components on the three axes of the cylindrical co-ordinate system
ρ	water density
$\tilde{p}$	instantaneous pressure
g	gravitational acceleration

E	eddy viscosity/diffusivity
V_r, V_θ	depth-averaged velocities in the $r-$ and $\theta-$ directions (horizontal plane)
J	Jacobian of the orthogonal transformation from Cartesian to cylindrical co-ordinates
h_r, h_θ	scale factors of the orthogonal transformation from Cartesian to cylindrical co-ordinates
f_C	Coriolis force
ω	angular velocity of the Earth
ϕ	latitude
k	turbulent kinetic energy
$-\rho\overline{v_i' v_j'}$	Reynolds normal and shear stresses, $i, j = r, \theta, z$
λ_t	absolute eddy viscosity
E_t	turbulent eddy viscosity
$\overline{E}$	mean eddy viscosity
τ_{ib}	bed shear stress in the $i-$ direction, $i = r, \theta$
C_d	bed drag coefficient
C_f	friction coeficient
C	Chezy coefficient
n	Manning's coefficient
k_s	Nikuradse equivalent sand roughness size
Re	Reynolds number
τ_{iw}	wind stress in the $i-$ direction, $i = r, \theta$
γ	air-water resistance coefficient
ρ_a	air density
W	wind speed
W_r, W_θ	wind velocity components in the $r-$ and $\theta-$ direction, respectively
$\left(\xi^r, \xi^\theta\right)$	axes defining the horizontal computational domain
J_ξ	Jacobian of the orthogonal transformation from cylindrical co-ordinates onto computational domain

$V_{\xi^r}, V_{\xi^\theta}$	velocity components in the directions of the computational domain
ω'	relative vorticity
V_t	tangential component of the velocity vector at a curved wall
R_W	radius of curvature at the wall
c	wave speed
$\Delta^{1/2}$	average operator
Δ^-	backward difference operator
$\overline{\Delta}$	central difference operator
Δ^+	forward difference operator
δx	spatial step
δt	time step
α	diffusivity coefficient in the parabolic diffusion equation
$L_x,\ L_y$	one-dimensional splitting operators for the Alternating Directions Implicit Method
τ	relaxation parameter in the Alternating Directions Implicit Method
$(C_r)_{\max}$	maximum Courant number
$r_{i-1/2}, r_{i+1/2},$ $s_i, s_{i+1/2}, s_{i+1}$	recursion coefficients for implementation of Thomas algorithm in the cylindrical co-ordinates numerical model
$A_{i,j}^{n-1/2},$ $B_{i+1/2,j}^{n-1/2}$	Terms containing a combination of terms containing known values of ς and q_{ξ^r} at time previous time step
P_i, Q_i, R_i, S_i	Recursion terms in numerical model
$AI,\ BI$	Terms in the numerical model equivalent to $A_{i,j}^{n-1/2}$ and $B_{i+1/2,j}^{n-1/2}$
$V = (u, v, w')$	velocity vector with three components: two in the horizontal plane (u, v) and one (w') in the stretched dimensionless direction
p_s	physical pressure at the free surface
b	buoyancy

A_v	vertical turbulent viscosity
A_b	vertical turbulent diffusivity
q	turbulence intensity
l	turbulence length scale
Ri_q	Richardson number
Q_b, Q_l	additional source-sink terms (sub-grid scale horizontal diffusion)
τ_{ij}	horizontal stress tensor, $i, j = x, y$
$\alpha_1,\ \alpha_2$	parameters in the RAW filter
P	subscript indicating values calculated for prototype
PM	subscript indicating values calculated for physical model
F_i	inertial force
F_p	pressure force
F_g	gravity force
F_υ	viscous force
F_γ	surface tension force
F_e	elasticity force
L	geometric scale for undistorted models
L_X	linear horizontal scale for distorted models
L_Z	linear vertical scale for distorted models
L_T	time scale
L_V	velocity scale
ν	vertical viscous shear
n	exponent term for transformation of the computed water elevation from the computational domain onto physical domain
n	exponent term for representation of the bed in the analytical solution of Lynch and Gray (1978)

Chapter 1

Introduction

1.1. Background Context

Estuaries and coastal zones are undeniable significant socio-economic regions, as well as valuable ecosystems (mangroves, seagrass meadows, salt marshes, coral reefs, rocky shores, Arctic shores, sandy beaches) hosting a wide range of biotic and abiotic species. Their role in sustaining large concentrations of human dwellings, e.g. 60% of human population lives in adjacent coastal land areas [Lindeboom (2002)], food and oil production, tourist and recreational activities, sewage and waste, etc. cannot be overlooked. Nicholls and Small (2002) performed a study of the estimated coastal population and found out that only 23% of the 1990 worldwide population lived in the near-coastal zone [Figure 1.1]. The near-coastal area was defined as 100m from sea level (e.g. vertical distance) and 100km from shoreline. Also, the study evidenced that, although the population density in the specified area was 2.5 times greater than other zones on the globe, most people lived in small cities and rural areas rather than highly urbanized regions (more than 10,000 people/km^2).

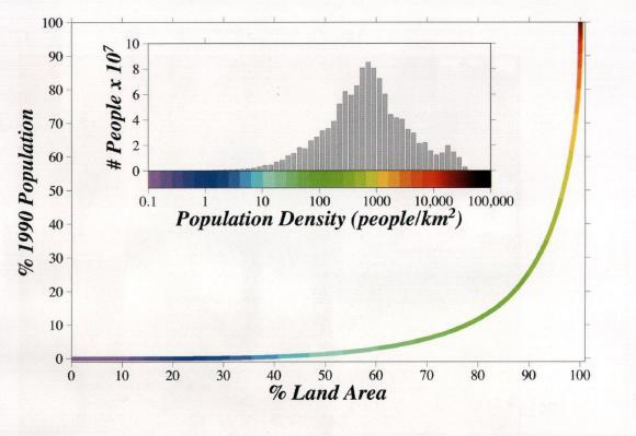

Figure 1.1. Global distributions of population and land in the near coastal region [Nicholls and Small (2002)]

From a geographical point of view, an estuary forms where a river discharges into the sea or ocean. In estuaries, water mixing can occur and salinity of estuarine waters can be less than 35‰ the value of ocean water salinity [Ross (1995)]. Rivers transport water rich in both nutrients and pollutants and these reach the deeper ocean by waves, currents and tides.

For the coastal zone various definitions have been proposed. Ross (1995) defined it as the part of the ocean affected by land and the part of land affected by ocean. According to Lindeboom (2002) the continental shelf represents the coastal region. Geographically speaking, the estuarine and coastal areas are positioned at the boundary of Earth's three major environments: land, ocean and atmosphere [Ross (1995)]. Figure 1.2 shows the interaction of the three environments when ice is also present in the context of climate changes. A schematic illustration of the complexity of interaction mechanisms between the three environments for shelf mechanism transport is presented in Figure 1.3.

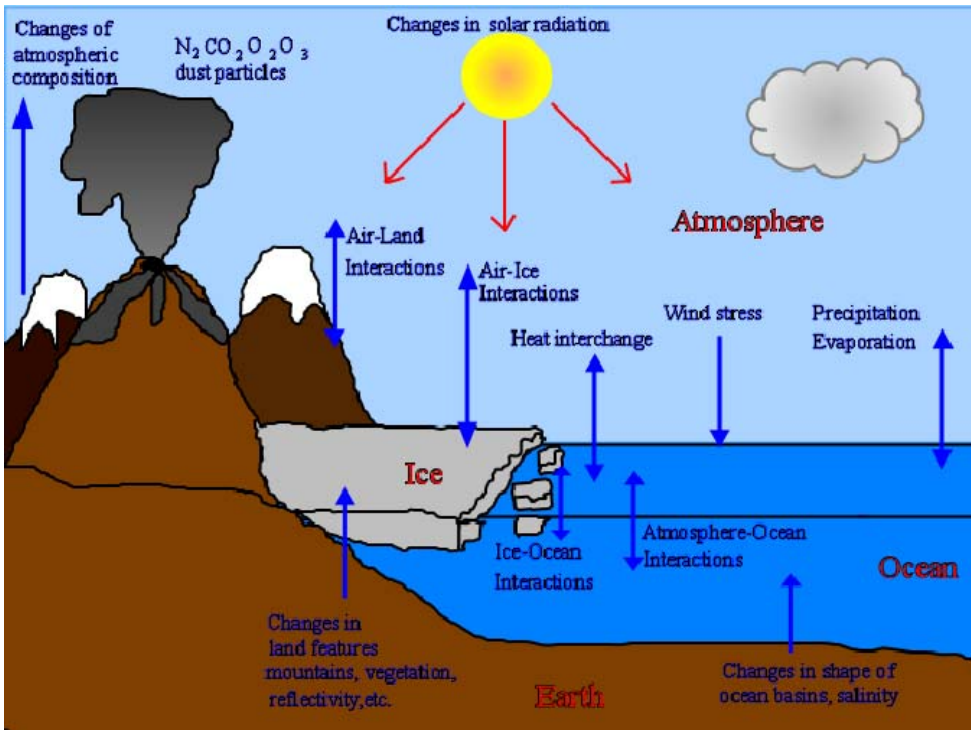

Figure 1.2. Interactions between atmosphere, land, ocean and ice in the context of climate change [after Ross (1995)]

Various pressures are applied to estuarine and coastal areas. Impacts of natural hazards, such as flooding due to tides, waves, or storm surges, as well as anthropogenic effects, such as modification of natural habitats, discharging pollutants in estuarine and coastal waters, and so on, have to be mitigated against. In Europe, Directives of the European Union, i.e. Water Framework Directive, Habitats Directive, etc., regulate the water quality legislative framework.

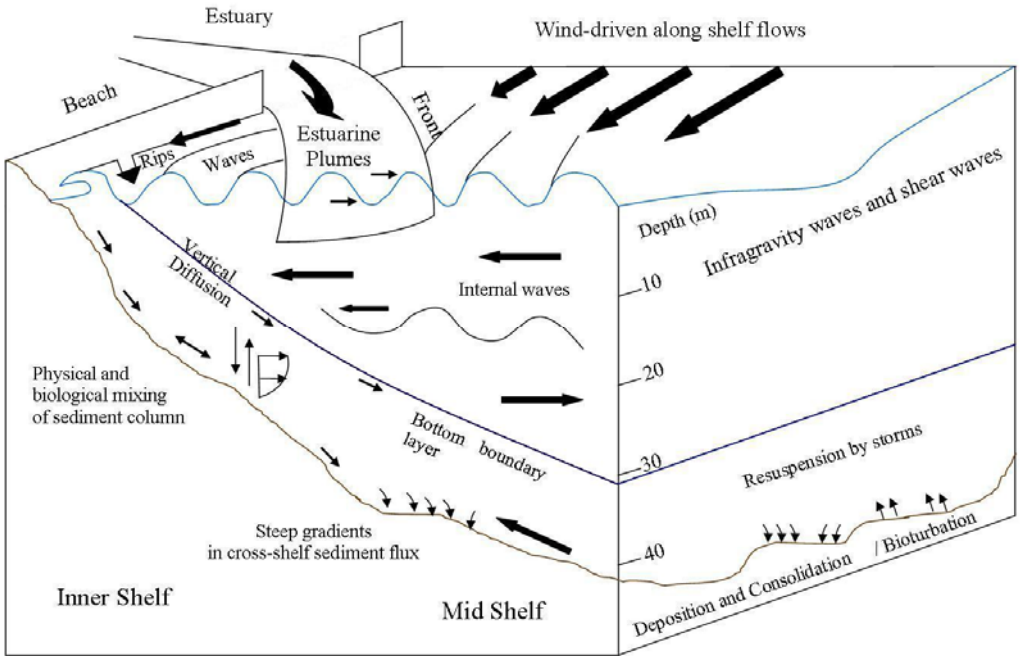

Figure 1.3. Summary of mechanisms of shelf sediment transport [McCave (2002)].

Worldwide, various international instruments have been developed in order to provide an integrated management system of these endangered environments: UNCLOS (United Nations Convention on the Law of the Sea), SOLAS (Safety of Life at Sea) Convention, Ramsar convention on Wetlands, etc. International research projects, such as LOICZ (Land-Ocean Interactions in Coastal Zone) investigate biological, chemical and physical changes in coastal area and identify human actions leading to coastal degradation. According to LOICZ, urbanization and environmental change were identified as the most significant pressures shaping human wellbeing and ecological integrity. GOOS (Global Ocean Observing System) is a permanent global system for observations,

modelling and analysis of marine and ocean variables, sponsored by the Intergovernamental Oceanographic Commission among others. The programme of the United Nations has two components: global GOOS and coastal GOOS, and the latter is linked to the coastal module of GTOS (Global Terrestrial Observing System) as part of the Coastal Theme [IGOS (2006)]. The two coastal modules recognize relationships and interactions between, and changes in, terrestrial and marine environments. EuroGOOS is the European Global Ocean Observing System, whose role is the development of Operational Oceanography in European Seas and adjacent oceans.

Figure 1.4. Wave energy assessment around the world [Fusco (2012)]

Over the last 10 years, marine renewable energies have come to the attention of policy makers, as a means of tackling climate changes and ensuring energy supply at competitive costs. Marine renewable energies include offshore wind, tidal and wave energy. Tidal and wave energy are considered as more reliable compared to other renewable energy resources such as sunlight or wind, since they do not depend on variability of weather. Economical advantages such as development of an industry creating devices for marine energy extraction cannot be overlooked. In the context of climate changes, marine renewable energies can help reducing the CO_2 emissions by 15-25 Mt/year if the full potential of wave energy is reached [SETIS (2011)]. Energy can also be created by salinity and temperature gradients [SETIS (2011)], but the area is still in its infancy. In the USA, NOAA (National Oceanic and Atmospheric Administration) has been

developing the OTEC (Ocean Thermal Energy Conservation) technology for tropical countries, where the difference between the surface layer and deep water is more than 20ºC all year-round. OTEC can be used for energy generation since the temperature gradients are used to power turbines.

Concerns related to the sustainable development of estuarine and coastal areas led to the subsequent development of hydrodynamic, sediment transport, water quality, storm surges, etc., numerical models. Moreover, besides existing information from Admiralty Charts, Admiralty Tidal Stream Atlases, or direct current meter readings, numerical models are useful tools for prediction of tidal stream flows, required in calculation of theoretical wave energy. An assessment of wave energy around the world is given in Figure 1.4.

1.2. The Role of Numerical Models

Numerical models were developed as the analytical solution of the system of equations describing the complex processes taking place in estuarine and coastal areas could not be found. In a simplistic illustration, an estuarine and coastal hydrodynamic numerical model is based on mathematical equations, more specifically the continuity and Navier-Stokes equations, domain and bathymetry representation, initial and boundary conditions, and forcings. According to Stewart (2008) numerical ocean models present the following advantages:

i) provide a detailed and realistic view of the ocean;
ii) include the influence of viscosity and non-linear dynamics;
iii) can be used for forecasting;
iv) interpolate between sparse observations of the ocean produced by ships, drifters, and satellites;

whereas, the shortcomings include:

i) usage of discretized equations that are necessarily different from continuous equations;

ii) turbulence calculation is difficult to achieve;

iii) simplifications such as hydrostatic and Boussinesq approximations, vertically integrated equations or bed topography representation at discrete points must be due to limited computer available resources;

iv) modelling of steep gradients and processes at different scales is problematic;

v) human and round-off errors in the calculation of the results.

So, without being perfect, numerical models give a better understanding of the processes taking place in the natural aquatic environments (rivers, lakes, coastal areas, oceans) using the existing knowledge and all the input data available. These models have various applications, some of them being summarized in Figure 1.5.

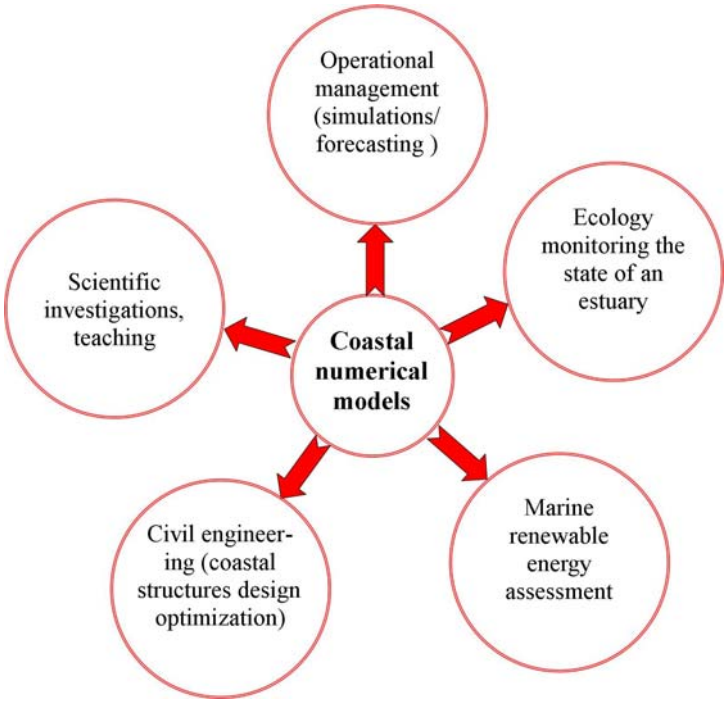

Figure 1.5. Various uses of coastal numerical models.

Computer models for estuarine and coastal areas can include:

- hydrodynamic models for current and water elevation predictions;

- sediment transport models for shelf mechanism transport or suspended particulate matter transport;
- water quality models that assess ecological and chemical status of water bodies according to the Water Framework Directive regulations;
- storm surge models for storm surge heights prediction, etc.

The Water Framework Directive prescribes the steps to be taken for achieving the good qualitative and quantitative status for ground and surface water bodies. Water quality models are needed for assessment of the ecological and chemical status of the water body. Water quality parameters typically include: salinity, biochemical oxygen demand (BOD), sediment oxygen demand (SOD), dissolved oxygen saturation (DO), ammoniacal and nitrate nitrogen, organic phosphorous, orthophosphate, phytoplankton, etc. Initial water conditions, nutrient fluxes, ambient environmental conditions and kinetic transformation rates and constants are necessary datasets for the development of the water quality model. Hartnett and Berry (2010) used DIVAST for heavy metals modelling in Mersey estuary.

Coastal flooding results from an increase of water levels above the astronomical tide. They are due to severe storm winds, waves and low atmospheric pressure. Hurricanes, extra-tropical storms and other severe storm conditions happen along coastal waters, estuaries and rivers and may result in serious economic damage and loss of life. Computer models for storm surge heights prediction and coastal flood risk assessment have been developed [i.e. SLOSH, Olbert and Hartnett (2010)].

Cost is a major parameter of any research and / or project management. In hydrodynamic modelling, costs are represented by computational burden and more specifically by the resolution of the grid used for spatial discretization, since grid resolution and time step are related by a mathematical relationship. A finer mesh offers better representation of the domain but subsequently increases computational time, whereas the costs are diminished using a coarser grid at the expense of poorer quality of the solution. In numerical modelling, domain discretization can be done on structured or unstructured grids. Structured grids

mainly use quadrilateral cells and are generally related to finite difference models; unstructured grids are developed with triangular or tetrahedral elements with mixed interconnectivity and are employed in finite element and finite volume methods. Estuarine and coastal models use structured grids with Cartesian (DIVAST – Depth Integrated Velocities and Solute Transport), orthogonal (POM – Princeton Ocean Model, ROMS – Regional Ocean Model System, GETM – General Estuarine and Transport Model, EFDC – Environmental Fluid Dynamics Code) and non-orthogonal curvilinear co-ordinates [Muin and Spaulding (1997), George (2007)] or unstructured grids [ADCIRC – Advanced Circulation Model, Namin et al. (2004), FVCOM – Finite Volume Coastal Ocean Model, TUFLOW, TELEMAC 2D]. Following the aforementioned financial considerations, multiscale models were developed as well. Comer (2011) developed a multiple nested model of Cork harbour. Resolutions varied from 90m at the forcing boundary (North-East Atlantic Ocean) to 2m at the city level after 3 levels nesting was performed (ratios 3:1, 5:1, 3:1). The model was used for coastal flooding simulation and comparisons with data available from OPW (Office of Public Works) for the flooding in 2007 showed good agreement. Research has shown that nested models provide increased resolution in the area of interest and subsequently computational costs are reduced compared to using a finer resolution over the entire domain. Still, they use the stair step representation for description of land boundaries and unrealistic solutions are produced in these regions. Also, fluxes have to be dynamically linked at the boundary between the coarse and fine grid [Nash (2010)] to ensure mass and momentum conservation.

1.4. Research Aims and Objectives

The objective of the research is to develop a new two-dimensional hydrodynamic model using an irregular grid that improves resolution in desired areas without increasing computational costs. The literature review showed that cylindrical co-ordinates offer more research possibilities compared to previously developed models based on structured grids, i.e., Cartesian, orthogonal

curvilinear and non-orthogonal curvilinear co-ordinate systems and unstructured grids. The advantage of using this approach is that the cylindrical co-ordinate system can be better fitted to an estuary's shape, so that fine resolution is obtained in coastal areas and coarse resolution away from the coast, provided the position of the pole is appropriately chosen. Moreover, the boundary error is reduced when compared to Cartesian co-ordinates, since the grid lines are curved in the radial direction. Computational time is reduced when using cylindrical co-ordinates compared to orthogonal and non-orthogonal curvilinear co-ordinates, since the number of extra terms to be discretized in the governing equations is smallest.

The aims of the research are subsequently presented:

i) to develop a novel cylindrical co-ordinates 2D hydrodynamic model;
ii) to verify results of the new model by comparing them with results from two models with extensive industrial applications;
iii) to validate the new model using experimental data obtained from measurements in a tidal basin;
iv) to show that cylindrical co-ordinates are a suitable choice as an orthogonal grid for domain discretization when the non-linear Navier-Stokes equations are used.

Model verification and validation are two important tasks that must be achieved in order to establish the credibility of the model. For a model to be verified one has to show that the code solves the relevant equations correctly. Model validation determines whether adequate fidelity is achieved in capturing the essential physical phenomena. Post and Votta (2005) emphasized the techniques to be used for model validation and verification and stated that the two processes were poorly implemented in numerical modelling. The recommendations in the aforementioned paper, as applied in present research, were to validate the model against existing analytical solutions, measurements, as well as results from well established numerical models. The recommendations were followed in this thesis.

1.4. Thesis layout and contents

The layout and contents of the thesis are as follows:

Chapter 2 offers an up-to-date literature review of the existing models in the area of estuarine and coastal models. The review begins with a general methodology for estuarine hydrodynamic modelling, followed by a review of structured, unstructured and mesh free methods used in hydrodynamic modelling. Since the structured grid models were found to be most computationally efficient, the review of structured grid models follows. Next, the models are analyzed from the point of view of two components affecting computational efficiency: spatial resolution and the number of extra terms introduced in the mathematical formulation of the hydrodynamic equations. It was found that Cartesian co-ordinates are advantageous from the point of view of number of extra terms, but do not accurately represent closed boundaries. Orthogonal co-ordinates provide better representation of irregular boundaries, but grid generation is difficult to achieve due to angle restriction, and are less computational efficient. Non-orthogonal curvilinear co-ordinates are easier to generate, but the co-ordinate metrics introduce a large number of terms to be discretized in the mathematical formulation of the model. An alternative that can introduce a minimum number of extra terms and vary the resolution inside the domain is represented by cylindrical co-ordinates. Subsequently it is shown that analytical solutions were found only for linearized forms of the Navier-Stokes equations in estuarine hydrodynamics, or for analyzing scattering of tidal waves around cylindrical islands. Numerical models in cylindrical co-ordinates were used for three-dimensional pipe flow simulations and in two-dimensional storm surge modelling; the latter using simplified formulations of the hydrodynamic equations. The Summary and Conclusions advocates for the use of cylindrical co-ordinates in estuarine hydrodynamic modelling.

Chapter 3 illustrates the theoretical considerations involved in development of the continuity and Navier-Stokes equations, which govern water flow inside a

given domain and conserve properties such as mass and momentum. Afterwards, the Author's own development of depth integrated equations written in cylindrical co-ordinates are presented and followed by the mapping transformations from the physical onto the computational domain. Mapping transformations represent a powerful tool in numerical discretization of the hydrodynamic equations because the methods already developed for Cartesian co-ordinates can be extended to other co-ordinate systems. The resulting equations are at the basis of numerical model development.

Chapter 4 shows the solution technique used to obtain results of the numerical model. Firstly, the finite discretization methods of the governing equations written in cylindrical co-ordinates suggested by various researchers are shown, and followed by the Author's proposed discretization scheme. Spatial discretization is performed on an Arakawa C grid, whereas time discretization scheme is a two-step finite difference Alternating Directions Implicit method (ADI). For the proposed discretization technique, the solution is obtained by means of Thomas algorithm. Details regarding implementation of the Thomas algorithm in the numerical model are given in this chapter. In the end of the Chapter the structure of the code is shown.

Chapter 5 validates the results of the numerical model. In order to assess the cylindrical co-ordinates numerical model results three test cases were used: a uniform horizontal bed with constant step in the radial direction; a uniform horizontal bed with one variation of the step in the radial direction, and a uniform horizontal bed with two variations of the step in the radial direction. The results for each test case are compared against results of two robust numerical models such as DIVAST and EFDC. The analytical solution of Lynch and Gray (1978) for simplified equations is used to verify numerical model results and agreement is observed. Tidal basin measurements are also used for validation and calibration of the cylindrical co-ordinates numerical model.

The thesis is enclosed by Chapter 6 presenting the summary and final conclusions.

Chapter 2

Literature Review

2.1. Introduction

The purpose of this chapter is to review existing numerical models in the area of coastal hydrodynamics and show that cylindrical co-ordinates present more research possibilities in this area. Processes like tides, waves, flooding due to storm surges taking place in estuaries and coastal areas can be described using hydrodynamic equations, also known as governing equations. Numerical modelling of estuaries and coastal regions is based on a set of partial differential governing equations which are solved by a computer, since an analytical solution to the given problem could not be established. Many researchers developed coastal hydrodynamic models generally using finite difference methods on structured grids, i.e. Cartesian, spherical, general orthogonal and non-orthogonal curvilinear grids. Also, unstructured grid models using finite element method or finite volume method, and mesh free models were developed. All the unstructured grid models are shown to be computationally expensive compared to traditional finite difference methods on structured grids, and the present review emphasizes the latter approach.

This chapter outlines the existing grid systems for hydrodynamic models with applications to estuarine and coastal areas. The analysis is performed from the point of view of computational costs, which are influenced by space and time resolution of the numerical models, and the number of extra terms in the governing equations due to curvature of the structured grid. The review focuses on two-dimensional models, used to represent well-mixed estuaries, and some three-dimensional models are presented as well, whenever needed for comparison or as a novel approach. Next, a summary of cylindrical co-ordinates usage in analytical and numerical modelling is given. At the end of the chapter, the summary and conclusions section advocates for the use of cylindrical co-ordinates in structured grid estuarine hydrodynamic modelling.

2.2. Estuarine Hydrodynamic Modelling Methodology

A numerical model can be developed based on the mathematical formulation of a given problem. In coastal hydrodynamics, the continuity and Navier-Stokes equations are used to represent mass and momentum conservation inside the domain. In these regions, water circulation is driven by: winds, tides, density gradients, large-scale circulation off the continental shelf, barometric pressure, and Coriolis force. Consequently, the equations used to model these areas have a non-linear character. Highly irregular land boundaries, sea boundaries and initial conditions inside the domain have to be accounted for, as well. The resulting problem is very complex and analytical solutions have not been found yet. Consequently, numerical models are often used.

Meteorological conditions and bathymetry represent input data on which the accuracy of the numerical model depends. Also, data at the boundaries, such as river inflows or tidal signals are required. The output of the model interferes with the quality of the input data. Therefore, the highest quality input data are required to generate best output. Hydrodynamic model outputs include: water surface elevation and current velocity.

The bathymetric module of the region of interest is the first input used in the hydrodynamic model. Bathymetric data can be obtained from field measurements or Admiralty Charts. Water depths may be obtained by digitisation of the Charts and interpolated onto the model grid at the required spatial resolution.

Freshwater inflows have a significant impact on estuary mixing, being responsible for the density difference inside the estuary. Freshwater flow rates can be used as inputs into models.

Wind speed, direction and duration affects the estuary depending on the latter's size and shape, resulting in wave action and surface currents. Martin and McCutcheon (1999) represented the wind induced stress as a function of wind

speed (u_w), the density of air (ρ_a) and the dimensionless drag or friction coefficient (C_D). The same stress can be defined using Munk formula as a function of the air/water resistance constant (γ), air density (ρ_a), wind velocity component in the direction of projection (W_x) and absolute wind speed at 10m above surface (i.e., $\sqrt{W_x^2 + W_y^2}$).

When modelling an estuary, open boundaries must be specified. There are clamped boundary conditions assuming that internal forces and processes do not affect boundary conditions and their effects are negligible. These simple boundary conditions over specify the boundary near the open boundaries or in small water bodies and cause artificial interactions between the internal flow and the boundary conditions. More elaborate boundary specifications such as radiation boundary condition, which passes transient events (tides, waves, coastal currents, storm surges, coastal jets, upwelling) through a transparent, non-reflective boundary, and slope boundary condition can be applied when the boundary critically affects internal conditions of the estuary. Phase errors are another type of open boundary problem. These errors appear whenever the water surface measurements or tide figure calculations are done at one point and are assumed to represent the conditions over the entire boundary. Interpolation between several points along the boundary reduces these errors. In order to avoid all these problems, a practical approach is damping the errors and reflections over distance by extending the simulated domain offshore. The experimentation with the location of boundaries and the existence of a small number of measurements results in increased computational burden. In FEM, boundary conditions can be specified writing down the equations for all nodes inside domain and replacing those for border nodes with appropriate functions describing the boundary conditions. Generally, solution of the system of equations is obtained by banded matrix inversion. When boundary conditions are included matrices loose their banded feature, but mathematical solutions exist for this problem, i.e. row operations [Dyke (2007)].

Water surface conditions are usually described using the rigid lid, i.e. external gravity waves are suppressed [Kantha and Clayson (2000)], or free-surface boundary condition by specifying the water surface and the vertical velocities. The former condition could be used in long term simulations of oceans since it allowed longer time steps. The latter condition could be used in storm surge modelling and tidal simulations in shallow waters. Bottom boundary conditions in estuaries can be expressed as: no-slip boundary condition ($u = v = w = 0$), hydraulically rough boundary condition (in this case the bed shear stress is defined using for example Colebrook-White or Manning equation) and canopy models (useful whenever the shallow waters of the estuaries are dominated by sea grass).

The Navier-Stokes equations for surface flows present the turbulence closure problem. Surface flows in estuarine and coastal zones are generally characterized by turbulence, a natural process due to high velocity gradients in the flow, which causes random, unsteady fluid motions. The disturbances in the fluid domain vary as a function of space and time, extending across scales of several orders of magnitude. Hence, numerical modelling of Navier-Stokes equations for turbulent flows requires the choice of an appropriate turbulence model. There are different types of turbulence models that can be used: algebraic models that do not require solution of any additional equations (also called zero-equation models), one-equation models solving one turbulent transport equation, models using the eddy viscosity concept (two-equation-models, multi-equation models), large eddy simulation approach represented by Smagorinsky model, and second-order closure schemes such as Mellor-Yamada scheme [Mellor and Yamada (1982)] or Reynolds-stress-models [Olbert (2006)]. Choice of the turbulence model is based on the ability of the model to describe the relevant physical problems, as well as the additional complexity introduced into the modelling equations. In coastal hydrodynamic models researchers use different turbulence models. Sheng (1989) used a simplified second-order closure turbulence model, Muin and Spaulding (1997) employed a one equation turbulent kinetic energy to calculate vertical eddy viscosity and diffusivity, Ye et al. (1998) used a $k-\varepsilon$ turbulence model to estimate turbulent viscosity, Falconer et al. (1998) closed the numerical model with a zero-equation model.

The $k-\varepsilon$ turbulence model was initially employed by Burchard and Bolding (2002); they subsequently made the interface to GOTM (General Ocean Transport Model) and used it as turbulence module. Chen et al. (2003) used a modified 2.5 level Mellor-Yamada scheme in FVCOM. Namin et al. (2004) developed the 2D finite volume model using the $k-\varepsilon$ turbulence scheme. Walters (2005) developed a three dimensional finite element primitive equations model using eddy viscosity turbulence parameterization. Also, the eddy viscosity turbulence closure was employed by White and Deleersnijder (2007) for the study of the tidal circulation around an island with a 3D finite element model.

2.3. Review of Grid Systems for Hydrodynamic Models

Numerical models for ocean and coastal ocean simulations are developed in the context of increasing concerns with respect to the health of the ocean. They were developed after the atmospheric computer modelling methods were established. Numerical models of estuarine and coastal areas are useful tools in predicting tidal stream velocity, variations of surface water levels, sediment transport, water quality, etc. Numerical models for estuaries and coastal areas require large computer resources, as these models are very complex. The regions are characterized as domains with highly irregular boundaries for numerical dicretization of the equations governing water flow. Moreover, in these regions, driving forces are winds, tides, density gradients and large-scale circulation off the continental shelf. On their proper representation inside the model depends the quality of the results. In hydrodynamic numerical modelling, there are a number of features to be considered for grid-based model design/selection and they are given in Figure 2.1.

Coastal hydrodynamic numerical models can be used for [Figure 1.5]:

1) simulations / forecasting, with applications to simulation of extreme events, i.e. for flood hazard due to storm surges in operational management;

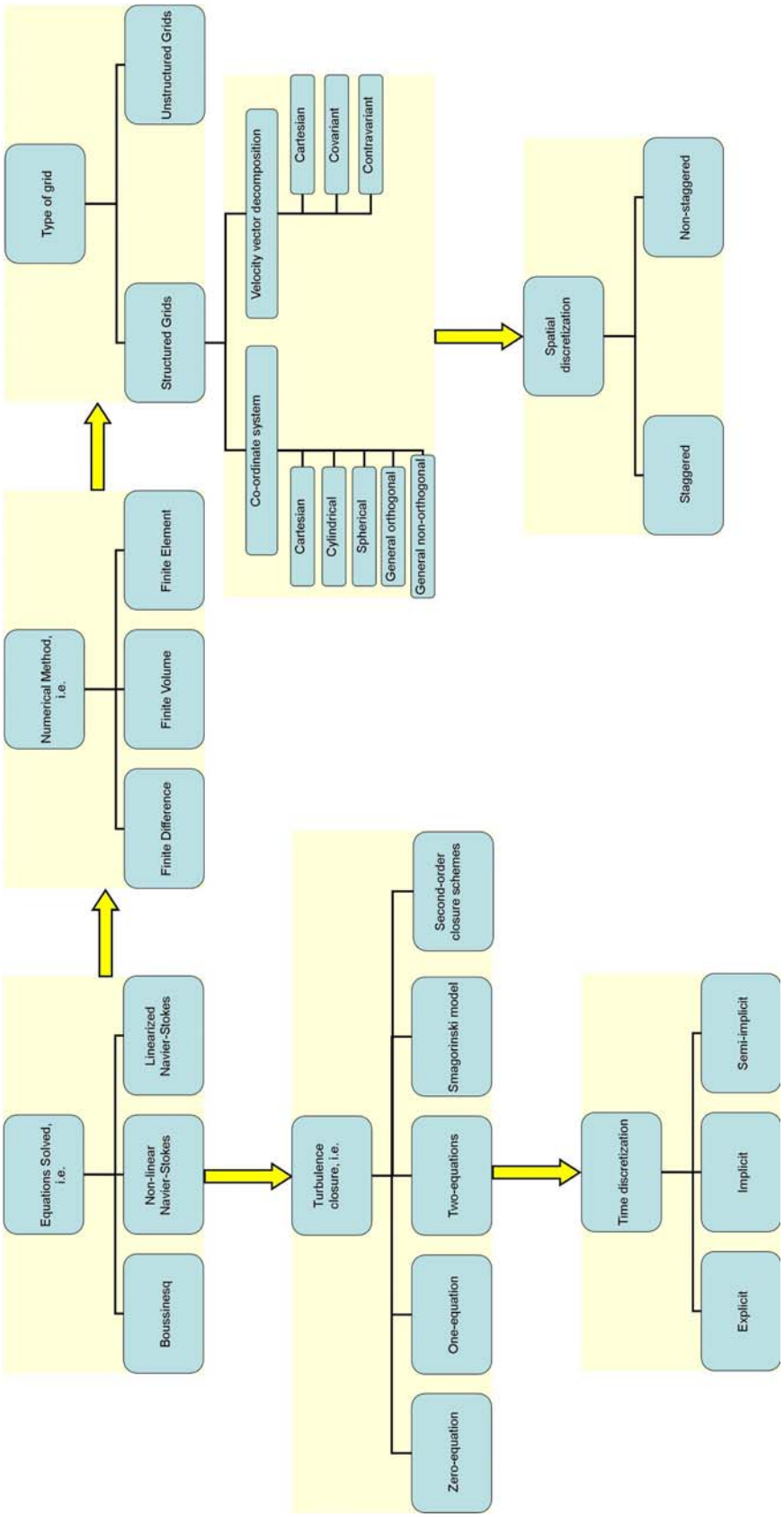

Figure 2.1. Some features for design/selection of grid-based hydrodynamic models.

2) monitoring the state of an estuary and to help establish best measures for conserving natural ecosystems (mangroves, wetlands, salt marshes, coral reefs) in ecology;
3) coastal structures design optimization, or to enhance construction operations in coastal and estuarine zones, marine renewable energy assessment for tidal and wave energy prediction in civil engineering;
4) scientific investigations in universities and research laboratories, as well as teaching.

Two-dimensional and three-dimensional numerical models can be used to simulate hydrodynamics, water quality, sediment transport, light attenuation, seagrass dynamics, and toxics in estuarine and coastal waters. 2D models assume velocity varies after a parabolic or logarithmic law in the vertical direction. The governing equations for 2D modelling are called shallow water equations. 3D models can perform computations on the horizontal grid and computed values can be next integrated over vertical layers in a method called mode splitting. All 2D and 3D models include simplifications of the problems being solved, for example hydrostatic and Boussinesq approximation, or depth averaging for 2D models, due to limited available computational resources. Hydrostatic approximation ignores the vertical accelerations in the Navier-Stokes equations. Boussinesq approximation uses an averaged value of density, where fluctuations in fluid density are small, but retains the buoyancy effects [Jones (2002)].

2.3.1. Structured versus Unstructured Grid and Mesh Free Hydrodynamic Models

Spatial discretization is the process of breaking down the domain into numerous components called elements. Grid based numerical models can be classified into two classes from the point of view of the space discretization method used: structured grid and unstructured grid approaches. Structured grids are mainly

related to finite difference methods, and can be represented using quadrilateral cells. Unstructured grids rely on finite element and finite volume techniques for which variably shaped elements with irregular connectivity separate the continuous domain of the problem.

Structured grids can use Cartesian, cylindrical, spherical, general orthogonal and non-orthogonal curvilinear co-ordinates to represent grid points. The choice of a suitable co-ordinate system is based on the type of geometries describing the boundaries and size of the domain. Cartesian co-ordinates handle simple rectangular geometries with application to small geographical areas, such as estuaries, bays, coastal areas; spherical co-ordinates can be best used to describe large regions, like oceans. Curvilinear co-ordinates, also known as boundary fitted co-ordinates, can be orthogonal or non-orthogonal. Orthogonal co-ordinates are more difficult to generate and distribution of the points is less flexible than for non-orthogonal ones because value of the angle between two directions is restricted to approximately 90º. Orthogonal co-ordinates achieve fewer computing operations, faster convergence and better stability and accuracy of the solution [Rodi (2004)]. Also, it was observed that accuracy of the shallow water equations on non-orthogonal grids is influenced by grid angle and grid resolution [Sankaranarayanan and Spaulding (2003)].

The finite difference method (FDM) is mainly used to solve the governing equations on structured grids; it is relatively straight forward and uses efficient algorithms. The considered region is divided into a grid of points, and approximations, based on Taylor's expansions, replace the partial derivative terms in the hydrodynamic differential equations at each point on grid. In FDM, spatial discretization of a domain can be done using either non-staggered or staggered grids. Non-staggered grids assume that all the unknowns are located at the same point on the grid, i.e. centre of the cell. This approach led to oscillations in solutions, which were identified to be generated by spatial discretization of the pressure gradient term. In 1970's Arakawa developed various staggered grids [Figure 2.2] which helped remove the oscillations generated by the pressure gradient term discretization; among these the Arakawa

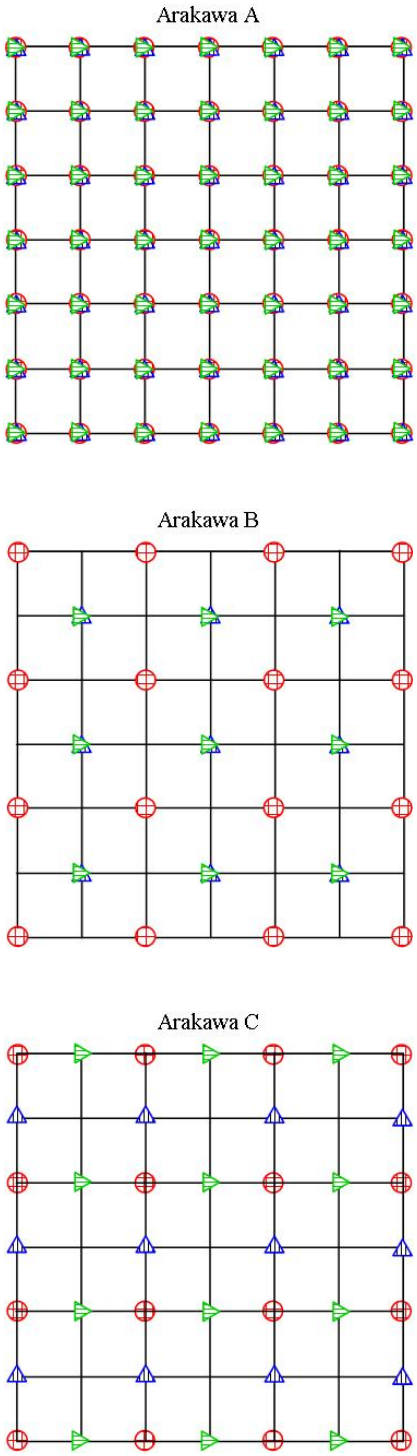

Figure 2.2. Some Arakawa grids for finite difference horizontal discretizations [after Dyke (2007)]

C grid is widely used in ocean and coastal modelling. The Arakawa C staggered grid defines components of velocity as follows: water elevation at the centre of the cell, the x-direction component to the left and right of water elevation, and the y-direction component to the north and south of water elevation. An equation is written at each grid point and the resulting system of equations can be solved by means of Thomas algorithm.

Estuaries and coastal areas present highly irregular land boundaries, which can accurately be described using non-orthogonal structured grids, at high computational prices. Consequently, unstructured grids were applied to estuarine domains in the quest to simultaneously solve the boundary representation problem and redue computational costs. The finite volume method (FVM) combines great flexibility of the unstructured grids with simplicity of finite difference methods. The method uses the integral formulation of the conservation laws. The Navier-Stokes equations written in their integral form are known as the conservative Navier-Stokes equations. Using this technique, the solution domain is separated into cells, named control volumes, and each conservation equation can be applied either at the centre or the vertices of the cell. The flux at the control surface is obtained by summing the control volume areas adjacent to the considered node.

In coastal modelling, the comparison made by Chen et al. (2003) showed that their triangular unstructured FVM model is more accurate than a FDM orthogonal co-ordinates model (ECOM-si) for three-dimensional modelling of the Bohai Sea and the Satilla River. For the first test case, the horizontal resolution in ECOM-si was uniform, 2km inside the domain, except for the area near open boundary where an unreasonable approximately 7km resolution was chosen. In FVCOM the horizontal resolution varied from 2.6km, in areas adjacent to closed boundaries and at the open boundary, to 15-20km in the interior of the domain. None of the models included flooding and drying processes for the presented results, which are essential in simulation of tidal elevation and currents. For the second test case, horizontal resolution varied from 100 m to 2.5km near open boundary in both models and reported results were better for FV model, while the FD model failed to resolve the upper

branches of the river. No details regarding allocation of computational resources for the two models were given and yet, the computational efficiency of the FD methods was generally recognized.

Initially developed to resolve structural analysis problems in the sixties, the finite element method (FEM) was extended to fluid dynamics in the seventies. FEM is based on a variational or weighted residual formulation and uses a large number of grid points. Numbering of the elements has to be carefully done, since it can be cumbersome. This method assumes writing the equations at each grid point, called node, and the resulting system of equations can be written in large sparse matrix form. The main obstacle in development of FEM models for coastal applications is that conservation of momentum is difficult to achieve.

Solutions of the primitive hydrodynamic equations using FE suffered from severe oscillations near the $2 \cdot \Delta x$ mode. Whereas for FDM, staggered grids solved these computational modes, introduction of the generalized wave continuity equation (GWCE) in FEM stabilized the model [Kantha and Clayson (2002), Walters (2005)]. GWCE is a second-order wave equation with role in smoothing out the spurious oscillations. GWCE contains a weighting parameter, τ, controlling the balance between the primitive continuity and wave equation portions of the GWCE, with recommended values in the literature of 0.0001-0.001. The approach was employed by Luettich et al. (1991), Westerink et al. (1994), Hagen et al. (2001), Walters (2005). A short time evolution of hydrodynamic models based on FEM was given by Walters (2005).

A first comparison of FEM with FDM, from the point of view of functional approximation, showed that FEM was restricted when dealing with equations containing highly non-linear terms, such as the advection term in the Navier-Stokes equations, due to the requirement of a single global functional approximation [Vinokur (1976)]. On the contrary, in FDM phenomena associated with the complexities of the Navier-Stokes equations were well resolved. Twenty years later, Lin and Chandler-Wilde (1996) emphasized that FEM is less computationally efficient than FDM and more sensitive to numerical errors. Chung (2002) specified that FDM cannot be compared to FEM

unless either the FD equations are written on unstructured grids, like in FVM, or FE equations are written on structured grids. Up to date, the Author has no knowledge of any comparison between FEM and FVM or FDM and FEM on structured grids in the area of coastal modelling. Jones and Davies (2005) compared FEM and FDM when modelling the west coast of Britain tides. A coarse grid 7 km FDM model, whose solutions showed agreement with observed values at various points in the considered domain, was compared with an approximately 7 km uniform finite element grid model, as well as various variable resolution FEM models. The element sizes for the various resolutions of the FEM model were established based on a water depth criterion. The comparison with observation points was done at nearest computed points for both FDM and FEM. Instead of using the advantage given by the finite element method in accurately representing the irregular boundaries, the finite difference coastal description was used for both models. For this representation, the uniform grid FEM model was less accurate and computationally less efficient than the FDM model. Best results of the FEM model were obtained using higher order elements, which resulted in a slight increase in accuracy at the price of computational effort. At this stage, the Author can conclude that FEM is more computationally expensive than FDM.

Based on the reasons presented in the previous paragraphs, many researchers developed coastal hydrodynamic models generally using structured grid models, for example: Cartesian [Blumberg and Mellor (1987), Falconer and Chen (1996), Burchard and Bolding (2002), Pietrzak et al. (2002), Chen (2003)], spherical [Sankaranarayanan and Ward (2006), Muin and Spaulding (1996,1997)], general orthogonal [Blumberg and Herring (1986), Lin and Chandler-Wilde (1996), Bao et al. (2000)], and non-orthogonal curvilinear [Spaulding (1984), Swanson et al. (1989), Sheng (1989), Barber and Scott (2000)] grids. Sheng's model (1989) can actually use any of the conformal, orthogonal or non-orthogonal curvilinear grids. Among the unstructured grid models with industrial applications in coastal modelling can be found ADCIRC (FEM), TELEMAC 2D (FEM and FVM), FVCOM (FVM).

Lately, the mesh free methods, among which smoothed particle hydrodynamics has many applications [Monaghan (2005)], came to the attention of hydrodynamic researchers [Bonet and Lock (1999), Shao and Lo (2003), Rodriguez-Paz and Bonet (2005), Dalrymple and Rogers (2006), Grenier et al. (2009), De Leffe et al. (2010), Ferrari (2010), Vacondio et al. (2012)].

When applied to estuarine and coastal areas, the so called mesh free models still use a Cartesian grid to specify bathymetry in the area of interest. The technique is to define the fluid continuum at discrete points, called particles, with properties such as density, volume, and mass. Each particle has neighbouring particles that represent the surrounding fluid. SPH estimates a property (i.e. density) by means of integral interpolation and uses a kernel function for this purpose. The kernel function can be chosen as a smoothed version of the Dirac delta function for accurate evaluation of the property at the considered point. A variable named smoothing length is associated with the kernel. Smoothing length is a measure of the spread of the kernel from its centre point and it can have either constant or variable values. The divergence and gradient of a scalar field can be established using the integral interpolation, as well. The property, property gradient or divergence of a vector field represented by integral interpolation can be discretized using a summation over the neighbouring particles [Monaghan (2005)]. The shallow water equations can be written in Lagrangian formulation, equations (2.1)-(2.2), formally equivalent to the Euler equations (3.6) and (3.22) when particle density (ρ) is defined as the product between water density (ρ_w) and water depth (H), i.e. $\rho = \rho_w H$. The Lagrangian formulation specifies the physical properties, including position, of each material particle as a function of time and this is sufficient for description of flow [Wesseling (2001)].

$$\frac{\partial H}{\partial t} = -\nabla \cdot (Hv) \tag{2.1}$$

$$\frac{d(Hv)}{dt} + \nabla \cdot (Hv) = -gH(H+b) + gHS_f \tag{2.2}$$

where:

H is water depth;

$\vec{v}$ is velocity vector with components (u,v) in a Cartesian co-ordinate system;

g is gravitational acceleration;

b is the bottom elevation;

S_f is the bed friction source term.

The expression of acceleration of a particle in the Lagrangian momentum equation can be derived considering the fluid continuum as a Hamiltonian system of particles and can include an acceleration term due to internal force obtained from the continuity equation. For specification of irregular bathymetries the bed gradient source term and the curvature tensor can be discretized with static bottom particles defined after a uniform Cartesian pattern.

A lack of resolution could be encountered in waters with small depth, when area of a particle is smaller than a threshold value, or for initially dry bottom due to the mathematical relationship for smoothing length, i.e. it is inversely proportional to water depth. Hence, a dynamic splitting procedure for particle refinement can be developed. The technique, based on a variable smoothing length, had to conserve both mass and momentum, and minimize the error in density and velocity field. Consequently, an increased number of particles is generated and no longer needed in regions where water depth was no longer very shallow. Hence, a coalescing procedure can be developed analogous to the splitting technique. Details regarding the particle coalescing can be found in Vacondio et al. (2011). Empirical criteria can be used for both splitting and coalescing in defining the minimum and maximum threshold values, respectively. The coalescing procedure was found to be computationally expensive and could be applied every 10 steps [Vacondio et al. (2011)]. The disadvantage of SPH is it requires generation of a large number of particles for good flow definition and results in increased computational burden compared to traditional mesh-based methods.

2.3.2. Cartesian Co-ordinates Grid Models

Initial estuarine and coastal water models were developed based on the continuity and Navier-Stokes equations written in a Cartesian co-ordinate system x, y, z defined with positive $x-$ direction towards east, $y-$ direction positive north and $z-$ direction positive upward [see Appendix 1]. They constitute a set of partial differential equations, governed by the laws of mass, and momentum conservation.

In a Cartesian co-ordinate system, the finite difference method can be employed for solving the partial differential equations which govern the hydrodynamic processes. The method requires the set up of a computational mesh to cover the modelling region. The cells composing the mesh are usually defined with the same width and length dimension in what is called a uniform grid [Figure 2.3]. Non-uniform meshes are characterized by variable dimensions of the cells [Figure 2.4]. Various space and time discretization schemes can be used for numerical modelling of the depth integrated Navier-Stokes equations. There are forward, backward and central differencing schemes, as well as hybrid schemes. In terms of space discretization, central differencing on the Arakawa C grid is widely used in estuarine hydrodynamic modelling.

Time discretization is performed using forward differentiation and some commonly used methods are leapfrog [EFDC, POM] and ADI [DIVAST] methods. The leapfrog time discretization scheme is explicit and based on central differencing. Alternating Directions Implicit (ADI) method uses a split time step with implicit representation of some variables (water elevation in continuity equation, velocity in one direction in hydrodynamic equation) during the first time step, while all other variables are represented explicitly. During the next time step, water elevation and velocity in the second direction are represented implicitly, while the remaining variables are explicitly described. A tridiagonal system of equations results and methods available for such problems are used.

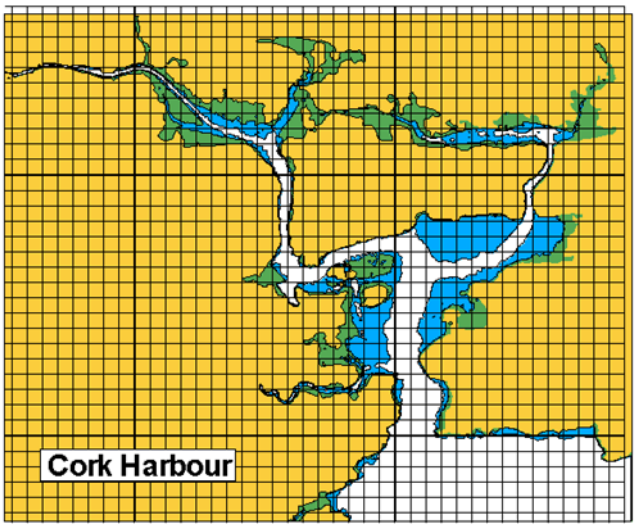

Figure 2.3.Uniform Cartesian mesh for numerical modelling of Cork Harbour, Ireland [Nash et al. (2005)]

Central spatial discretization on non-uniform meshes differs from that used for uniform meshes in that having different cell dimensions, differentiation of a variable does not contain only its value, but averaged values of the cell dimensions, as well [see Hirsch (1988)].

Also, three-dimensional hydrodynamic models for free-surface flows with non-hydrostatic pressure were developed by Kocyigit et al. (2002), Chen (2003). The pressure term can be decomposed in two components: hydrostatic and non-hydrostatic pressure. Chen's (2003) model solved the Reynolds Averaged Navier-Stokes (RANS) equations using a finite difference scheme containing two predictor-corrector steps. The non-hydrostatic pressure component was determined in the first step of a predictor-corrector scheme, followed by a second velocity field finding (the first velocity field was predicted using the hydrostatic pressure field at the previous time step) which lead to the computation of an intermediate free surface. A free surface correction method was employed in the second step in order to get the final free surface and the final solutions.

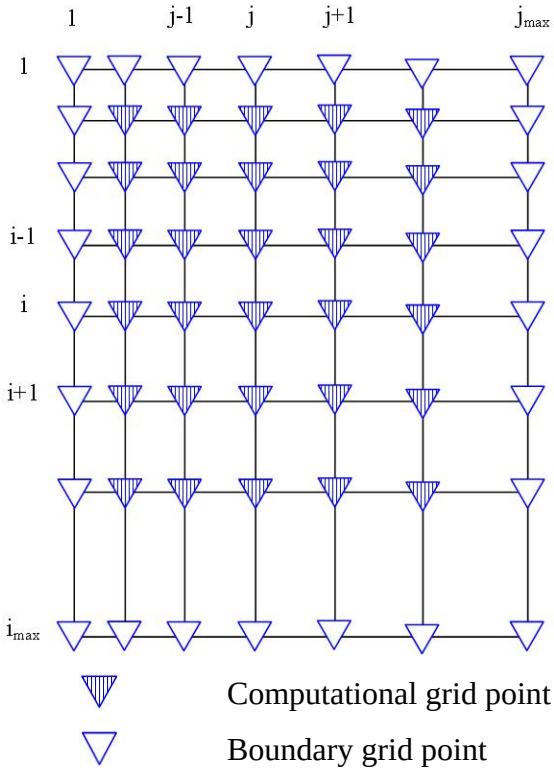

Figure 2.4. Non-uniform two-dimensional Cartesian mesh for numerical modelling.

Many estuarine and coastal models were developed in Cartesian co-ordinates [Blumberg and Mellor (1987), Falconer et al. (1998), Borchard and Bolding (2002), Pietrzak et al. (2002), MIKE21]. All models solving governing equations on a Cartesian grid presented the disadvantage of using a stair-step representation of land boundaries, generating unrealistic currents in these areas.

2.3.3. Orthogonal Curvilinear Co-ordinates Grid Models

In order to overcome the problems related to the inaccurate representation of the coastline and bathymetry using a uniform Cartesian grid when modelling estuaries and marine currents, different types of grids were developed, such as: conformal and orthogonal curvilinear grids. Some of the models developed using such grids are next reviewed. Conformal mapping is a special type of orthogonal transformation, which transforms the governing partial differential equations with the addition of a minimum number of extra terms, yet reducing the control over the grid line distribution. Details with respect to performing

conformal mapping transformations can be found in Lin and Chandler-Wilde (1996).

Two-dimensional orthogonal grid models were developed by Lin and Chandler-Wilde (1996) with applications to tidal simulations in Bristol Channel and Humber Estuary, as well as Shi et al. (1997) with applications to storm surge modelling in Huange Delta (China). In the later case the governing equations were written in a general orthogonal curvilinear co-ordinate system and orthogonal transformations were used to map the physical domain onto the computational domain. The resulting equations contained both Cartesian and contravariant velocity components.

Three-dimensional orthogonal grid models [Bao et al. (2000), POM, EFDC] can use two transformations: σ - stretched on the vertical and elliptic transformations to map the physical space onto a corresponding transformed space such that all boundaries are coincident with co-ordinate lines and the transformed grids are rectangular. The solution of the governing hydrodynamic equations in the transformed space can be obtained on a rectangular mesh of the transformed grid system [Figure 2.5]. The independent variables are transformed according to equations (2.3).

$$\xi = \xi(x, y, t) \tag{2.3a}$$

$$\eta = \eta(x, y, t) \tag{2.3b}$$

$$\sigma = \frac{h + z}{H} \tag{2.3c}$$

$$\tau = t \tag{2.3d}$$

where: $H = h(x, y) + \zeta(x, y, t)$.

The hydrodynamic equations can be written in both Cartesian and contravariant velocity components, while the expression of the continuity equation is given in terms of contravariant velocity components.

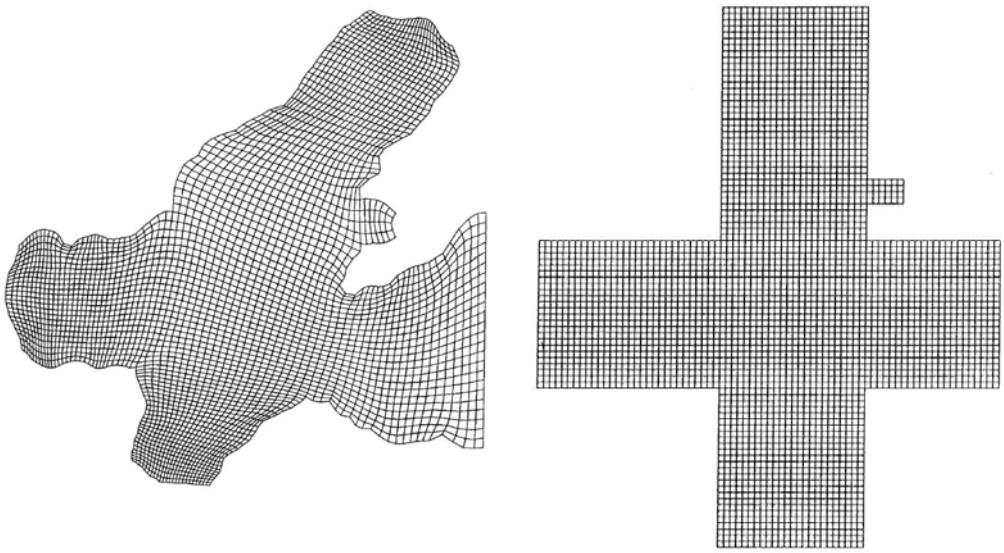

Figure 2.5. General curvilinear orthogonal grid of Bohai Sea (left) and transformed plane (right) [Bao et al. (2000)].

Generally, spatial discretization is done on an Arakawa C grid in both horizontal plane and vertical direction for three-dimensional modelling. The splitting mode technique can be used to reduce computational costs. For example, in POM :

i) the internal mode of time discretization scheme is three-dimensional and uses a long time step, based on the Courant-Friedrichs-Lewy condition along with the internal wave speed;

ii) the external mode is two-dimensional and uses a short time step satisfying the CFL condition and the external wave speed.

The three-dimensional velocity components can be expressed as superposition of vertically averaged velocity components and deviation of velocity components from the vertically averaged velocity. Forms of the deviation velocity equations of motion can be established as functions of the non-barotropic terms, which can be solved explicitly. The unknown velocity deviation results solving a tridiagonal set of equations with Thomas algorithm. The three-dimensional velocity structure is then obtained adding velocity deviations to the depth averaged values [Sankaranarayanan and Ward (2006)].

Other models developed using orthogonal curvilinear co-ordinate systems are: ROMS, EFDC, GETM. These models are extensively used for industrial applications.

2.3.4. Non-orthogonal Curvilinear Co-ordinates Grid Models

The difficulty of using orthogonal co-ordinates in regions with complicated geometry led to development of models written in non-orthogonal co-ordinates. The approach is to write the governing equations in non-orthogonal co-ordinates [Figure 2.6] and ulterior mapping transformations onto a computational domain can be performed. Mathematical formulation of the governing equations is complicated by the presence of co-ordinate metrics cross-derivatives and computer running times are longer compared to orthogonal curvilinear co-ordinates models.

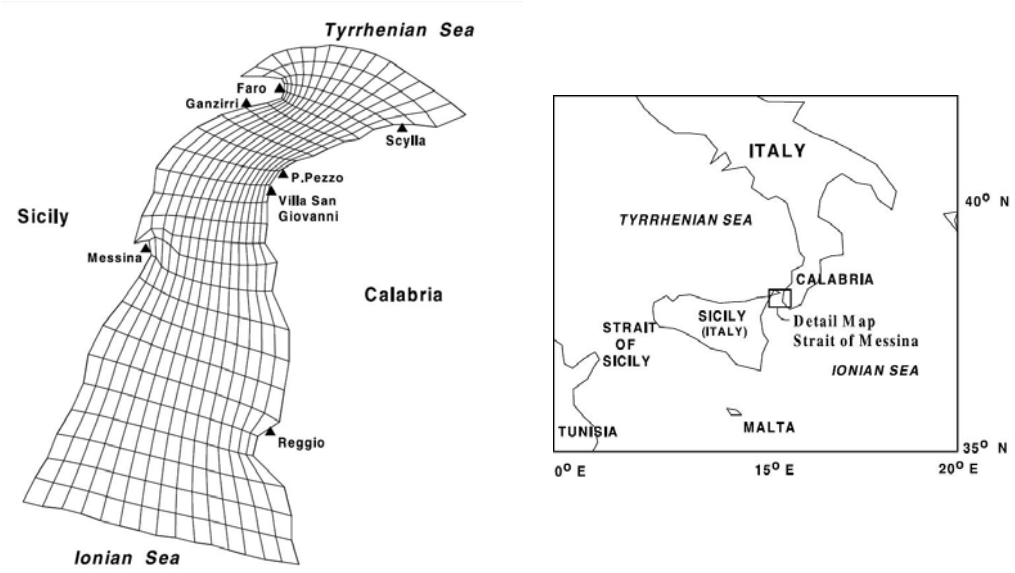

Figure 2.6. Non-orthogonal curvilinear grid of the Messina Strait, Italy [Andronosov et al. (2002)].

Two-dimensional modelling in non-orthogonal curvilinear co-ordinates was employed by Klevanny et al. (1994), Andronosov et al. (2002), and more recently by George (2007). The latter model had the Navier-Stokes equations written in two dimensions in terms of non-orthogonal co-ordinates, whereas the

continuity equation was written in terms of contravariant velocity components. The $\vec{OM}$ vector illustrated in Figure 2.7 could be written in the following forms: Cartesian co-ordinates (xOy), non-orthogonal co-ordinates ($x_N Oy_N$), and contravariant components.

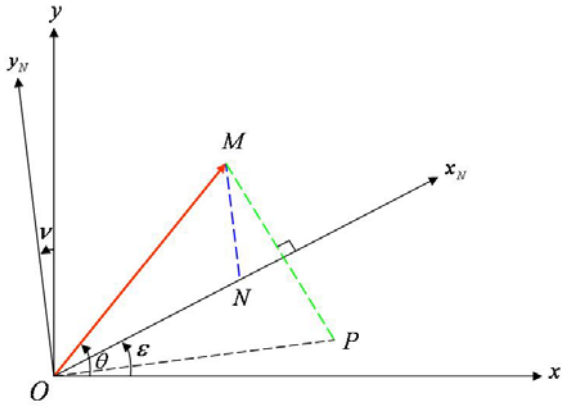

Figure 2.7. $\vec{OM}$ vector in a two-dimensional non-orthogonal curvilinear co-ordinate system [George (2007)]. Condition of non-orthogonality: $\varepsilon \neq \nu$.

Three-dimensional modelling on non-orthogonal grids follows the rules developed for orthogonal grids.

2.3.5. Spherical Co-ordinates Grid Models

Hydrodynamic models can be written in spherical co-ordinates and either orthogonal [Figure 2.8] or non-orthogonal [Figure 2.9] mapping transformations onto a computational plane are next used, in order to use methods already developed for Cartesian co-ordinates. First approach was used by Sankaranarayanan and Ward (2006) in a three-dimensional model, whereas the second technique was employed by Muin and Spaulding (1996) in two-dimensional modelling, as well as Muin and Spaulding (1997) in three-dimensional modelling. Spherical co-ordinate systems allow a design that follows the coastline, as well as the principal channels in drying zones with the disadvantage of complicating the mathematical procedure and resulting in even more increased computational time.

Two-dimensional modelling in spherical co-ordinates with non-orthogonal mapping transformations was described by Muin and Spaulding (1996). The relationships between velocities in spherical co-ordinates (u^s, v^s) and contravariant velocities $\left(u^c, v^c\right)$ are given by [Muin and Spaulding (1997)]:

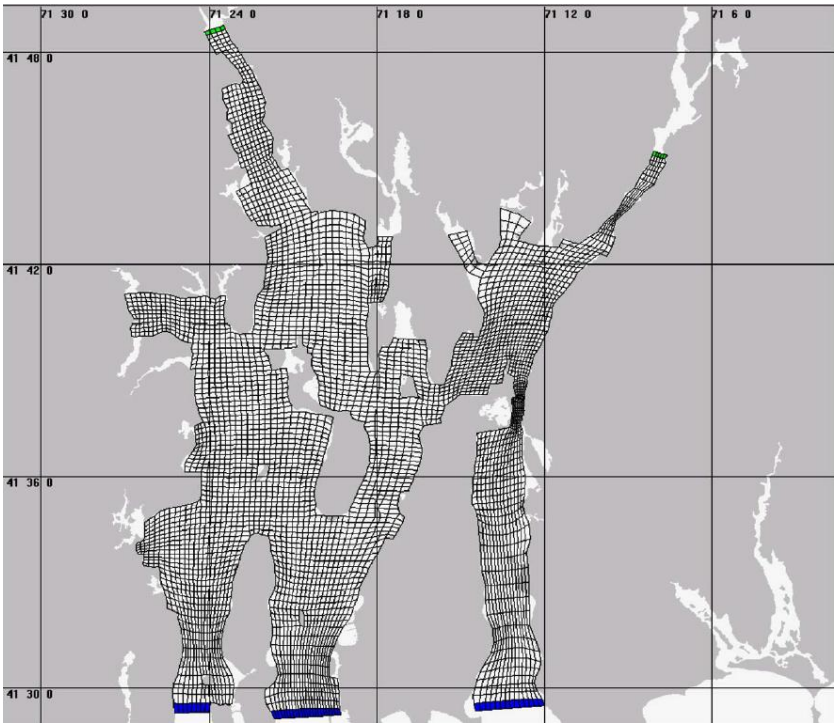

Figure 2.8. Spherical grid with orthogonal mapping transformations for numerical modelling of Narragansett Bay [Sankaranarayanan and Ward (2006)].

$$u^s = \Phi_\xi u^c \cos\theta + \Phi_\eta v^c \cos\theta \tag{2.4}$$

$$v^s = \theta_\xi u^c + \theta_\eta v^c \tag{2.4}$$

where the variables $\Phi_\xi, \Phi_\eta, \theta_\xi, \theta_\eta$ refer to derivatives with respect to subscripts indicated; they are called spatial derivatives. The Jacobian of the transformation has the expression: $J_s = \Phi_\xi \theta_\eta - \Phi_\eta \theta_\xi$.

In three-dimensional modelling using spherical co-ordinates transformation of the governing equations to a σ – co-ordinate system can resolve the bathymetric

variations with a constant number of grids [Muin and Spaulding (1997)]. The equations of momentum, continuity and concentration conservation in a curvilinear co-ordinate system can be written in terms of contravariant velocity components. Solution of the 3D problem is obtained using the mode splitting technique.

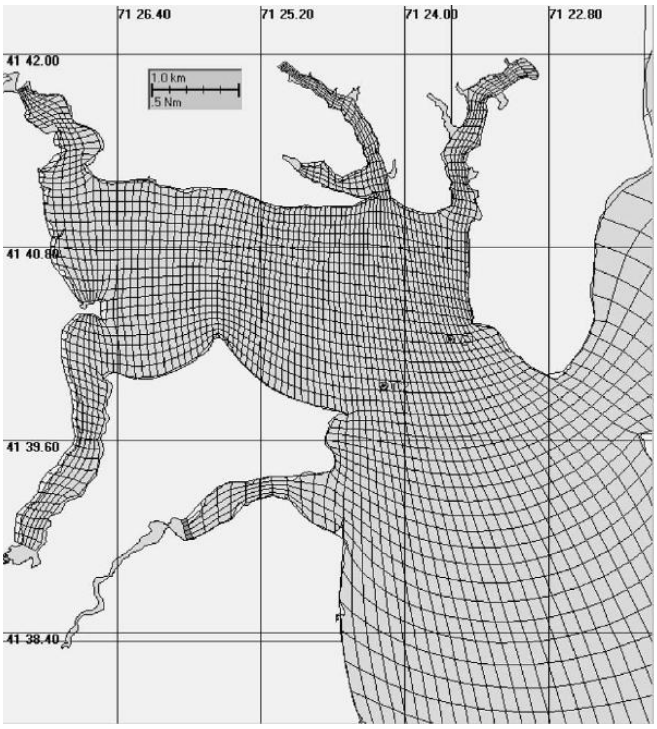

Figure 2.9. Spherical co-ordinates grid with non-orthogonal mapping transformation of Greenwich Bay, USA [Sankaranarayanan and Spaulding (2003)]

Next, an analysis of the hydrodynamic numerical models is made considering the elements affecting computational efficiency: horizontal spatial resolution of the numerical models and the number of extra terms due to the curvature of the grid added to the mathematical formulation of the governing equations written in Cartesian co-ordinates.

2.3.6. Horizontal Spatial Resolution

Spatial resolution of the domain dictates the number of grid points and represents a prohibitive factor that is linked with available computational

resources. Also, spatial resolution is dictated by the processes taking place in the area of interest. In many cases the spatial resolution of a model is not fine enough to accurately describe the processes taking place at scales that are smaller than the space step considered in the model [Zhang et al. (2007)]. The higher the resolution, the larger the number of grid points used in the simulation and the better the results are. Courant criterion dictates a direct relationship between time step and space step, resulting in longer running times for finer resolution and increased computational costs.

In orthogonal / non-orthogonal co-ordinates, grids can be generated by means of algebraic methods (such as domain vertex, or transfinite interpolation in multidirectional interpolation) or as solutions of partial differential equations. Curvilinear grids can be generated using solutions of elliptic, hyperbolic or parabolic partial differential equations. The limitations of the algebraic methods include higher sensitivity to distribution of the points at the boundary and presence of larger truncation errors due to lack of grid smoothness. Many researchers developed orthogonal grids based on solution of Laplace equations [Lin and Chandler-Wilde (1996)], or non-orthognal grids using solution of Poisson equations [Borthwick and Barber (1992), Klevanny et al. (1994), Muin and Spaulding (1996), (1997), Andronosov et al. (1997), Barber and Scott (2000)]. The approach to obtain the solution of the elliptic partial differential equations (the Poisson equations with Dirichlet boundary conditions) for curvilinear grids generation was presented in Thompson et al. (1977). The Laplace equations were transformed into a quasi-elliptical system of nonlinear Poisson equations (2.5)-(2.6) for the physical co-ordinate functions $x(\xi,\eta)$ and $y(\xi,\eta)$ in the transformed plane [Figure 2.10].

$$\left[\left(\frac{\partial x}{\partial \eta}\right)^2+\left(\frac{\partial y}{\partial \eta}\right)^2\right]\frac{\partial^2 x}{\partial \xi^2}+\left[\left(\frac{\partial x}{\partial \xi}\right)^2+\left(\frac{\partial y}{\partial \xi}\right)^2\right]\frac{\partial^2 x}{\partial \eta^2} - 2\left(\frac{\partial x}{\partial \xi}\frac{\partial x}{\partial \eta}+\frac{\partial y}{\partial \xi}\frac{\partial y}{\partial \eta}\right)\frac{\partial^2 x}{\partial \xi \partial \eta}=-J^2\left(P\frac{\partial x}{\partial \xi}+Q\frac{\partial x}{\partial \eta}\right) \tag{2.5}$$

$$\left[\left(\frac{\partial x}{\partial \eta}\right)^2+\left(\frac{\partial y}{\partial \eta}\right)^2\right]\frac{\partial^2 y}{\partial \xi^2}+\left[\left(\frac{\partial x}{\partial \xi}\right)^2+\left(\frac{\partial y}{\partial \xi}\right)^2\right]\frac{\partial^2 y}{\partial \eta^2} - 2\left(\frac{\partial x}{\partial \xi}\frac{\partial x}{\partial \eta}+\frac{\partial y}{\partial \xi}\frac{\partial y}{\partial \eta}\right)\frac{\partial^2 y}{\partial \xi \partial \eta}=-J^2\left(P\frac{\partial y}{\partial \xi}+Q\frac{\partial y}{\partial \eta}\right) \tag{2.6}$$

where $J=\frac{\partial x}{\partial \xi}\frac{\partial y}{\partial \eta}-\frac{\partial x}{\partial \eta}\frac{\partial y}{\partial \xi}$ is the Jacobian of the transformation, whose value dictates the possibility of performing a one-to-one mapping, i.e. J must be non-zero and with finite value for the mapping to be performed, and P and Q are functions that control the grid lines clustering degree and the angle at the boundaries. A form of the control functions can be established using amplification or decay factors [Chung (2002)]. The Poisson equations satisfy the maximum principle for reasonable values of P and Q. This principle implies that the maximum and minimum values of ξ and η occur on the boundary. Extreme choices for P and Q may cause a local grid overlap. Barber and Scott (2000) successfully considered the control functions as dependent on an equally distributed weight function, which depended on the depth of the estuary bed. However, the form of P and Q functions can be difficult to determine [Chung (2002)].

Some general design guidelines for curvilinear grids include the following:

- optimal grid arrangement is based on flow field which results in minimization of truncation errors for non-orthogonal curvilinear grids [Lee and Tsuei (1992)];
- ratio of the grid sizes in the two orthogonal directions should be approximately 3 - 5 for orthogonal grids [Kantha and Clayson (2002)];
- grid orthogonality should be preserved in the near-boundary area [Rodi (2004)].

All derivatives in the Poisson equations could be expressed using second-order central finite differences equations. Numerical solution of the equations could be obtained using point successive over-relaxation iteration [Muin and Spaulding

(1996), (1997)]. A disadvantage of the elliptic grid generator method consists of large computational time requirements.

Grid design in Cartesian co-ordinates is straightforward since the number of grid points dictates the resolution inside the domain. A solution that improves resolution in certain areas of a given domain is offered by Cartesian nested models.

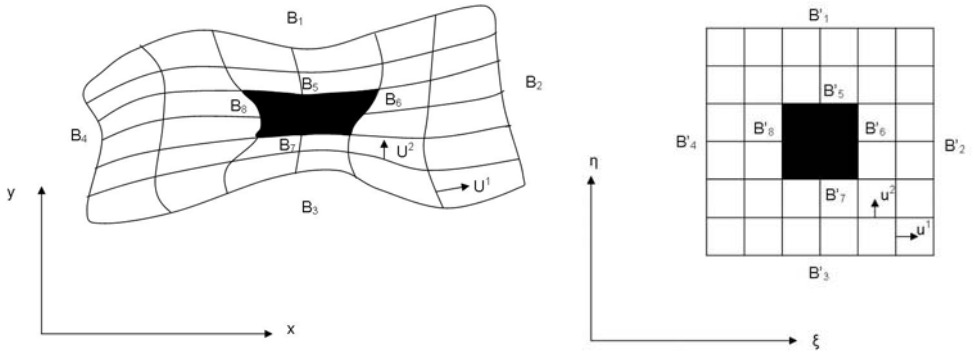

Figure 2.10. Boundary-fitted grid and contravariant components of velocity in the horizontal physical domain and computational domain

By using this approach a fine mesh is nested within a coarse mesh which saves computer time and memory space. The terminology used in nesting is “parent grid” for coarse mesh, and “child grid” for fine mesh. The advantage of the method comes from the fact that only the area of interest has higher resolution compared to having the same fine resolution over the entire domain. An important element in nesting is the nesting ratio. It represents the ratio between cell sizes in parent grid and child grid. Generally, nesting ratios have odd values, i.e. 3:1, 5:1, because the centre of one parent grid cell coincides with one centre of the child grid, reducing the number of interpolations, but even values can be used as well [Borthwick et al. (2001), Huang et al. (2010)]. There are two ways of implementing grid nesting: one-way nesting and two-way nesting. One-way nesting is characterized by the independence existing between the fine and coarse model. The boundary conditions for the child can be obtained by interpolating fluxes on the parent grid cells. The approach was developed due to requirements of simplicity and to reduce computational time. Two-way nesting presents exchange of information between the fine and coarse mesh resulting in

a better representation of the small-scale disturbances that are generated within the fine grid [Zhang et al. (2007)]. The condition for this approach to give good results is to dynamically couple the coarse and fine grid. More details with respect to development of nested models can be found in Blayo and Debreu (2006), Nash (2010). Telescoping can be used to further refine resolution in an area defining a child grid as a parent for another grid. One-way multiple nested models were developed by Kores and Lascaratos (2003), Staneva et al. (2009), while a two-way nested model using the telescoping approach was developed by Barth et al. (2005).

Adaptive meshes can be used when research problem requires a localized fine mesh that changes position in time and space. In an adaptive nested mesh model, the fine grid moves along with the process that requires increased resolution instead of defining a large number of points all over the domain. They have large applications in atmospheric modelling and during the last two decades were introduced in ocean numerical modelling. In two-dimensional hydrodynamic modelling, the finite volume discretization of the governing equations on a quadtree grid was applied to predict wind induced circulation in Lake Balaton, Hungary [Borthwick et al. (2001)]. Huang et al. 2010 also developed a two-dimensional model for the study of fluvial bed morphodynamics using a decoupled finite volume solution of the non-linear shallow water equations and a finite difference solver for the bed deformation equation on a dynamically adaptive quadtree grid.

Computational resource can be increased using a collection of individual computers interconnected by a variety of networks, such as Ethernet. These concurrent machines are called parallel computers. PVM (Parallel Virtual Machine) software system enables manual parallelization, as well as writing new parallel / distributed programs. Message Passing Interface (MPI) is another language independent communications protocol used to program parallel computers. Both PVM and MPI message-passing systems use domain decomposition techniques. The approach is to divide the computational domain into subdomains and assign each subdomain to different processors. Internal communications among partition boundaries, as well as communications for

boundary points with specification of periodic boundary points, are required. Ghost cells have to be specified on the side and corner boundaries with or without neighbouring subdomains for execution or consistency reasons, respectively. Boukas et al. (1999) parallelized POM with PVM programming model. MPI approach was used for parallelization of ROMS [Wang et al. (2005)].

Although structured grids were chosen for the present research based on their computational efficiency, a short presentation of the unstructured grid generation methods for coastal models is presented. General notions related to unstructured grid generation can be found in Mavriplis (1997), Chung (2002). As previously stated, the advantage of the unstructured over structured grid approaches stems from the flexibility of the grid in representation of irregular boundaries. Initially, the FEM models with applicability to water bodies suffered from artificial modes in sea level and/or velocity. The computational modes were grid scale waves that did not propagate and were superimposed on the desired solution. In the early days they were suppressed by artificial dissipation. Subsequently, the GWCE (section 2.2.2) was developed and results were similar to those obtained using staggered grids in FDM. Westerink et al. (1994) observed the resolution of the coastal boundary strongly influences the computed response particularly in near coastal regions and on continental shelf. Resolution requirements could be related to depth, gradients in topography, as well as the resolution of the coastal boundary. Furthermore, Jones and Davies (2005) underlined that the accuracy of a finite element method is critically dependent upon nearshore water depth. The finite element grids used in 2D coastal models could be uniform [Luettich et al. (1991)] or graded [Westerink et al. (1994), Jones and Davies (2005), Walters (2005]]. The grid for FEM could be generated using specialized software, i.e. TRIGRID [Henry and Walters (1993)], for generation of a mesh containing basic linear triangles in ADCIRC-2DDI. Legrand et al. (2000) developed a Delaunay triangulation generator on the sphere for a global ocean circulation model accounting for the closed boundaries, i.e. coastlines. A fully automatic generation procedure for graded unstructured meshes was described by Hagen et al. (2001) with application to shallow waters. The automatic generation procedure consisted of an error

estimation procedure which defined the local limits on element sizes, and a hierarchical technique for interpretation of the requirements.

2.3.7. Number of Extra-Terms due to Curvature of the Structured Grid

Up to this point, numerical models for estuarine hydrodynamics modelling were analysed from the point of view of spatial resolution. Another restrictive factor with respect to computational burden is the number of extra terms introduced in the hydrodynamic equations for other than Cartesian type of co-ordinates such as spherical, orthogonal or non-orthogonal curvilinear co-ordinates. In fully non-linear models written in two-dimensional Cartesian co-ordinates, there are seven terms included in the hydrodynamic equations on each direction, as can be seen in the $x-$direction momentum in DIVAST [equation (5.2)]:

1) local acceleration term: $\frac{\partial UH}{\partial t}$;

2) advective acceleration term: $\frac{\partial^2 UH}{\partial x}+\frac{\partial UVH}{\partial y}$;

3) Coriolis acceleration term: $-fVH$;

4) pressure term: $gH\frac{\partial \zeta}{\partial x}+\frac{H}{\rho}\frac{\partial P}{\partial x}\approx gH\frac{\partial \zeta}{\partial x}$;

5) wind stress term: $-\frac{1}{\rho}\tau_{xw}$;

6) bed stress term: $\frac{1}{\rho}\tau_{xb}$;

7) turbulence term: $-2\frac{\partial}{\partial x}\left[\left(\overline{E}\right)H\frac{\partial U}{\partial x}\right]+\frac{\partial}{\partial y}\left[\left(\overline{E}\right)H\left(\frac{\partial U}{\partial y}+\frac{\partial V}{\partial x}\right)\right]$

$\approx EH\left[\frac{\partial^2(UH)}{\partial x^2}+\frac{\partial^2(VH)}{\partial y^2}\right]$.

The quality of the results of the numerical model depends on the quality of the inputs and the accurate representation of these terms, among which the

advective acceleration term poses real challenges. This term gives the non-linear character of the Navier-Stokes equations.

The number of extra terms in the governing equations varies in all other than Cartesian co-ordinate systems from a minimum number of five extra terms in spherical co-ordinates and can reach up to 80 extra terms in non-orthogonal curvilinear co-ordinates. It is obvious that the greater number of terms to be discretized require larger computational resources. Orthogonal curvilinear co-ordinates introduce a smaller number of extra terms compared with non-orthogonal curvilinear co-ordinates. As an example the three-dimensional form of the governing equations written in spherical co-ordinates given in Aris (1989) can be analyzed. Three-dimensional governing equations written in spherical co-ordinates (θ, ϕ, R, with θ representing polar angle or co-latitude, ϕ the longitude, and R the radius of Earth) show an increase in the number of extra terms in the mathematical formulation of the equations. For example, in the $\theta-$ direction there are two extra terms $\left(V_r V_\theta / R, -V_\phi^2 \cot\theta / R\right)$, also known as source terms, in the advective acceleration term and three extra terms $\left(-V_\theta / R^2 \sin^2\theta, 2\partial V_R / R^2 \partial\theta, -2\cos\theta \partial V_\phi / R^2 \sin^2\theta \partial\phi\right)$ in the turbulence term, where $\left(V_\phi, V_\theta, V_R\right)$ are velocity vector components on the three axes of the considered co-ordinate system. These terms reflect that advective acceleration and turbulence are affected by the bending of two grid lines, i.e. in the latitudinal (θ) and longitudinal (ϕ) directions, as well as curvature of Earth. Two-dimensional formulation of the equations written in spherical co-ordinates showed that advection term contained only one extra term, $V_\phi V_\phi H \tan\theta / R$, in the $\theta-$direction [Muin and Spaulding (1996)], whereas the turbulence term was not included.

Hydrodynamic equations written in other than Cartesian co-ordinates can usually be solved using one-to-one mapping transformations from the physical domain onto the computational domain at the price of lengthy mathematical formulations due to the presence of co-ordinate metrics. Such mapping transformations allow all computation to be done on a fixed grid with uniform

square mesh in the transformed plane [Figure 2.10]. Both orthogonal and non-orthogonal transformations of the depth integrated equations written in spherical co-ordinates can increase the number of terms to be discretized due to the presence of Jacobian of the transformation and co-ordinate metrics. For example, the Navier-Stokes equations presented 6 extra terms due to an orthogonal transformation, as in Sankaranarayanan and Ward (2006), whereas a non-orthogonal transformation could result in circa 23 extra terms, as in Muin and Spaulding (1997), due to the presence of co-ordinate metrics cross-derivatives in the formulation of the Navier-Stokes equations in one horizontal direction.

Transformations can employ either independent variables [Borthwick and Barber (1992)] or both dependent and independent variables [Sheng (1989), Muin and Spaulding (1996, 1997), George (2007)] in order to satisfy lateral boundary conditions. Co-ordinate geometry components represent the independent variables and components of velocity are the dependent variables. Another important aspect to be considered when using mapping transformations for equations written in cylindrical, spherical, orthogonal or non-orthogonal curvilinear co-ordinates is the way velocity vectors can be represented in a process called velocity decomposition. There can be used: Cartesian, covariant and contravariant representations. Contravariant representations are recommended because velocity vectors are aligned with grid lines [Rodi (2004)], i.e. as done by Muin and Spaulding (1996), (1997). This approach is useful when boundaries do not coincide with Cartesian directions. When grid lines are curved, the axes chosen to resolve the velocity vector change direction from one field point to another and additional curvature terms arise in the momentum equations. The extra terms require a smooth grid in order to accurately solve the numerical equations and this is a severe restriction in practical problems.

2.3.8. Conclusions

An analysis of the structured grid models, due to their advantage in terms computational time when compared to both unstructured grids and mesh free models, is presented up to this point of the literature review.

From the point of view of horizontal spatial resolution, it can be seen that consensus cannot be achieved in the area of structured grid modelling:

i) Cartesian co-ordinate systems can easily be used to vary spatial resolution increasing the number of grid points, but they lack accurate representation of boundary irregularities;
ii) orthogonal curvilinear co-ordinates improve boundary representation, but grid generation is constricted by the orthogonality requirement;
iii) non-orthogonal curvilinear co-ordinates are easier to generate, since restriction on the grid angle exists only at the boundaries, yet the generation method (solution of elliptic partial differential equations) is time consuming.

From the point of view of the number of terms present in the mathematical formulation of the equations governing water flow, Cartesian co-ordinates present the advantage of a minimum number of terms to be discretized. Subsequent development of the equations in general orthogonal curvilinear co-ordinates have the advantage of better fitting the curvature of the irregular boundaries at the price of added complexity to mathematics, by introduction of extra terms in the governing equations, which result in additional computational costs. Still, grid generation is not easy due to constriction of the angle to be approximately $90°$. Furthermore, general non-orthogonal curvilinear co-ordinate models can be developed. These grids are easier to generate, but they introduce an even larger number of extra terms in the equations, due to the presence of co-ordinate metrics, resulting in higher computational costs.

At that stage of the research, the Author observed that no cylindrical co-ordinates non-linear numerical model was developed for estuarine and coastal hydrodynamic applications. The cylindrical co-ordinate system presents the advantages of being easy to generate, preserving orthogonality of the grid at all times and providing variable resolution in desired regions when position of the pole is appropriately chosen. Moreover, the curvature of the boundaries is better represented in the angular direction.

2.4. Review of Analytical Solutions and Numerical Models in Cylindrical Co-ordinates

Up to this point of the literature review, it has been established that cylindrical co-ordinates can be considered for estuarine hydrodynamic modelling. Applications of cylindrical co-ordinates to various problems related to hydrodynamics are next reviewed. Analytical solutions of the two-dimensional linearized hydrodynamic equations written in cylindrical co-ordinates were derived by Lynch and Gray (1978), followed by three-dimensional versions of Lynch and Officer (1985). Some applications of cylindrical co-ordinates in numerical modelling are: pipe flow simulations in three-dimensions, and storm surge simulations in two-dimensions. Moreover, scattered waves around small islands can be represented in a cylindrical co-ordinate system for the study of shelf circulation and some analytical solutions were derived. A short summary of these analytical solutions and numerical models is next presented.

2.4.1. Analytical Solution of Shallow Water Equations in Cylindrical Co-ordinates for Estuarine Hydrodynamic Modelling

Analytical solutions, in terms of Bessel functions, of the shallow water linearized governing equations written in cylindrical polar co-ordinates, equations (2.7)–(2.8), with application to estuarine hydrodynamics were obtained by Lynch and Gray (1978). They considered four shapes of the sea bed: horizontal, linearly sloping and two parabolic shaped beds. The forcing applied at the outer boundary of the domain was expressed as water elevation in terms of cosine function. Such solutions can be considered useful for verification of the results of a numerical model, as done in a three-dimensional orthogonal curvilinear co-ordinates model by Blumberg and Herring (1986), in a two-dimensional non-orthogonal co-ordinates model of Muin and Spaulding (1996), and in a three-dimensional spherical orthogonal co-ordinates model by

Sankaranarayanan and Ward (2006). An analysis of the verification method of estuarine numerical models using the annular geometry showed that:

1) simulations were performed mainly for annular sections with the angle defined between $\theta_1 = 0°$, and respectively $\theta_2 = 90°$ [Figure 2.11];

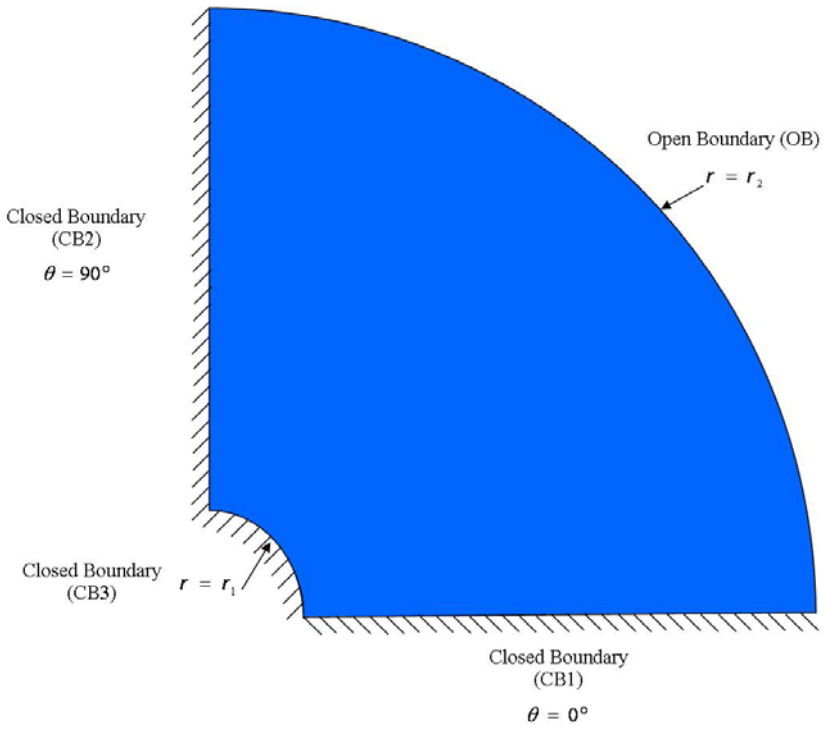

Figure 2.11. Quarter annular geometry for verification of numerical models.

2) large steps in the radial direction were used, of the order of kilometres, with subsequent choice of the time step of the order of minutes; these values are unrealistic for simulations in estuarine and coastal areas;

3) forcing at the outer boundary of the domain can be specified in terms of M_2 tides, represented using the sine function for two-dimensional models.

An interesting application would be to simulate different situations, i.e. with radial resolution varying between 50-500m, a different choice of θ_1 and θ_2 to represent shallower angles, and time steps of the order of seconds.

2.4.2. Cylindrical Co-ordinates for Pipe Flow Simulations

The equations governing water flow written in cylindrical co-ordinates present the singularity co-ordinate problem since the source terms in the Navier-Stokes equations, equations (2.7)-(2.10), in radial and angular directions are expressed using division by r; these terms cannot obviously be defined at $r = 0$. Solutions of the three-dimensional flow equations in cylindrical co-ordinates were obtained by Akselvoll and Moin (1996), Verzicco and Orlandi (1996), Priymak and Miyazaki (1998), Constantinescu and Lele (2001), Fukagata and Kasagi (2002), Morinishi et al. (2004), Barbosa and Daube (2005), Nikitin (2006).

$r-$ direction momentum:

$$\frac{\partial v_r}{\partial t} + v_r \frac{\partial v_r}{\partial r} + \frac{v_\theta}{r}\frac{\partial v_r}{\partial \theta} + v_z \frac{\partial v_r}{\partial z} - \frac{v_\theta^2}{r} = -\frac{1}{\rho}\frac{\partial p}{\partial r} + \\ + E_r\left(\nabla^2 v_r - \frac{v_r}{r^2} - \frac{2}{r^2}\frac{\partial v_\theta}{\partial \theta}\right) \tag{2.7}$$

$\theta-$ direction:

$$\frac{\partial v_\theta}{\partial t} + v_r \frac{\partial v_\theta}{\partial \theta} + \frac{v_\theta}{r}\frac{\partial v_\theta}{\partial \theta} + v_z \frac{\partial v_\theta}{\partial z} + \frac{v_r v_\theta}{r} = -\frac{1}{\rho r}\frac{\partial p}{\partial \theta} + \\ + E_\theta\left(\nabla^2 v_\theta + \frac{2}{r^2}\frac{\partial v_r}{\partial \theta} - \frac{v_\theta}{r^2}\right) \tag{2.8}$$

$z-$ direction:

$$\frac{\partial v_z}{\partial t} + v_r \frac{\partial v_z}{\partial r} + \frac{v_\theta}{r}\frac{\partial v_z}{\partial \theta} + v_z \frac{\partial v_z}{\partial z} = -\frac{1}{\rho}\frac{\partial p}{\partial z} + E_z \nabla^2 v_z \tag{2.9}$$

continuity equation

$$\frac{1}{r}\frac{\partial}{\partial r}(r v_r) + \frac{1}{r}\frac{\partial v_\theta}{\partial \theta} + \frac{\partial v_z}{\partial z} = 0 \tag{2.10}$$

where:

$v = (v_r, v_\theta, v_z)$ is the velocity vector with components on the $r-$, $\theta-$ and $z-$ axes, respectively;

r is the radius;

ρ is water density;

p is the pressure;

$E = (E_r, E_\theta, E_z)$ is the eddy viscosity;

$\nabla^2 = \frac{\partial^2}{\partial r^2} + \frac{1}{r}\frac{\partial}{\partial r} + \frac{1}{r^2}\frac{\partial^2}{\partial \theta^2} + \frac{\partial^2}{\partial z^2}$ is the vector Laplacian in cylindrical co-ordinates.

Akselvoll and Moin (1996) solved the temporal integration of the Navier-Stokes equations formulated in cylindrical co-ordinates. In order to overcome the time limitation restrictions if explicit time integration schemes were employed, they divided the computational domain into two sub-regions. Subsequently, derivatives in one direction were treated implicitly in each region. The resulting nonlinear equation could be easily linearized. Verzicco and Orlandi (1996) developed a finite difference scheme for incompressible flows using the fractional step and approximate factorization technique. Moreover, they treated the singularity of the Navier-Stokes equations at the axis $r = 0$ introducing the radial flux $q_r = rv_r$ on a staggered grid. Priymak and Miyazaki (1998) established an accurate spectral method for studying the transitional and turbulent flows in a circular pipe. The algorithm assumed transformation of the dependent variables in the unsteady incompressible flow equations in such a manner that the singularity problem was avoided at $r = 0$. Mohseni and Colonius (2000) established a method for treating the co-ordinate singularity in polar co-ordinates for compressible flows. The technique smoothly differentiated the data through the pole and no point was directly positioned at the pole. Constantinescu and Lele (2001) used series expansions for solving the flow equations in cylindrical co-ordinates on a non-staggered grid. Although the scheme was developed for compressible flows, the authors underlined the suitability of the scheme for incompressible flows. Their approach to singularity treatment was to map the computational domain in such a manner that no numerical boundary conditions specification was needed at $r = 0$. Fukagata and

Kasagi (2002) studied the energy conservation for second-order accurate finite difference methods in cylindrical co-ordinates. In their case a new FD scheme on a staggered grid was proposed and the source terms in momentum equations were called centrifugal force in $r-$direction and Coriolis force in $\theta-$direction, respectively. They also used the concepts of advecting velocity (i.e., rv_r, v_θ, v_z) and advected velocity (i.e., v_r) for discretization of advection terms. A normalization factor with value one for uniform grids and close to unity for non-uniform grids was proposed as well. Morinishi et al. (2004) transformed the geometry components from cylindrical co-ordinates onto a uniform rectangular mesh; therefore, the techniques developed for Cartesian co-ordinates could be employed for solving the flow equations. They developed both second- and fourth-order accurate finite difference methods. Barbosa and Daube (2005) employed mimetic discrete operators for discretization of the flow governing equations written in cylindrical co-ordinates. For regular cells they noticed that the discrete operators were similar to the continuous operators, and gave a form of the diffusion operator that could be discretized on a staggered grid.

Of all the methods presented in this section, the approach of Morinishi et al. (2004) for variable stepping in radial direction is appealing, since it can use techniques already developed for Cartesian co-ordinates numerical models.

2.4.3. Storm Surge Modelling in Cylindrical Co-ordinates

Applications of the cylindrical co-ordinates to estuarine hydrodynamic numerical modelling include storm surge models [Roy et al. (1999), Rahman et al. (2012)]. The governing equations used for mathematical formulation of the models were linearized and did not include the effects of turbulence, equations (2.11)-(2.13). The models only showed the evolution of water surface in time. The difference between the two models consisted of the grid representation, i.e. Roy et al (1999) used a grid with constant time stepping in the radial direction, whereas Rahman et al. (2012) used a nested cylindrical polar co-ordinates grid. While both models were developed for the same geometry, namely the coast of Bangladesh, the former model had 46x45 grid points (coarse grid), and the latter

model had 120x133 mesh points. In the coarse model space step in radial direction was 18.5km, whereas the step in angular direction varied from approximately 0 (close to pole) to 29 km (at the outer boundary). The nesting ratios used by Rahman et al. (2012) were 6:1 in the radial direction ($\Delta r \cong 2.6\,\text{km}$) until the eighteenth circular line in the coarse grid, and 3:1 in the angular direction ($\Delta\theta \cong 0.66°$).

$$\frac{\partial \zeta}{\partial t} + \frac{1}{r}\frac{\partial (rV_r H)}{\partial r} + \frac{1}{r}\frac{\partial (V_\theta H)}{\partial \theta} = 0 \tag{2.11}$$

$$\frac{\partial V_r}{\partial t} - fV_\theta = -g\frac{\partial \zeta}{\partial r} + \frac{\tau_r}{\rho H} - \frac{c_f V_r \left(V_r^2 + V_\theta^2\right)^{1/2}}{H} \tag{2.12}$$

$$\frac{\partial V_\theta}{\partial t} + fV_r = -\frac{g}{r}\frac{\partial \zeta}{\partial \theta} + \frac{\tau_\theta}{\rho H} - \frac{c_f V_\theta \left(V_r^2 + V_\theta^2\right)^{1/2}}{H} \tag{2.13}$$

where:

$(V_r, V_\theta) = \frac{1}{H}\int_{-h}^{\zeta} (\tilde{v}_r, \tilde{v}_\theta) dz$;

$\tilde{v}_r, \tilde{v}_\theta$ are the radial and tangential components of the Reynolds averaged velocity, respectively;

f is the Coriolis parameter;

c_f is the friction coefficient of the sea bed;

ρ is the density of sea water;

$(\tau_r, \tau_\theta) = C_D \rho_a V_a^2 (-\sin\delta, \cos\delta)$ are the radial and tangential components of the surface stress, respectively;

C_D is the drag coefficient;

ρ_a is the air density;

$$V_a = \begin{cases} V_0 \left(\frac{r_a}{R}\right)^{3/2}, r_a \le R \\ V_0 \left(\frac{r_a}{R}\right)^{1/2}, r_a > R \end{cases}$$

V_0 is the maximum sustained wind at the radial distance R;

r_a is the radial distance at which the wind field is desired.

In numerical modelling, storm surges can be represented using superposition of tides and surge at the open boundary of the domain. Nested model results were reported to be better compared to those obtained from the coarse grid model.

2.4.4. Cylindrical Co-ordinates for Study of Tidal Wave Variations around Small Cylindrical Islands

Cylindrical co-ordinates can also be used for a better representation of the island geometry in the study of shelf circulation around islands. Tides can be represented using either Helmholtz or Laplace equations. Helmholtz equation can be written with a source term as in equation (2.14) for a uniformly rotating plane ocean of uniform depth [Proudman (1914) cited by Larsen (1977)], or without a source term as in equation (2.15) [see Lee and Kim (1999)]. Proudman's research showed that amplitude and phase can change locally when tidal frequency waves are simulated around small cylindrical and elliptical islands. In theory, amplitude and phase variations can be due to the incident wave type. Tidal waves can be represented as superposition of free and forced tide. The free (or incident) tide can be expressed as Sverdrup, Poincare or Kelvin wave [Lee and Kim (1999)]. The forced tide can include two components: the equilibrium tide and the diffracted (or scattered) tide due to the presence of an island in the area [Larsen (1977)], or only the scattered tide [Lee and Kim (1993), Marchenko and Kowalik (2002)]. A rule of thumb is to represent the scattered waves in the cylindrical polar co-ordinate system and the incident waves in the Cartesian co-ordinate system. Laplace equation in equation (2.16) was used for simulation of Sverdrup waves (Larsen, 1977), Kelvin waves [Lee and Kim (1993)], or Sverdrup Poincare and Kelvin waves [Lee and Kim (1999)] around a small cylindrical island in a uniform depth ocean [Figure 2.12 a)]. This approach can be used based upon the assumption that the Rossby radius of deformation is very large compared with the scale of local disturbance generated by the presence of the island [Lee and Kim (1993)].

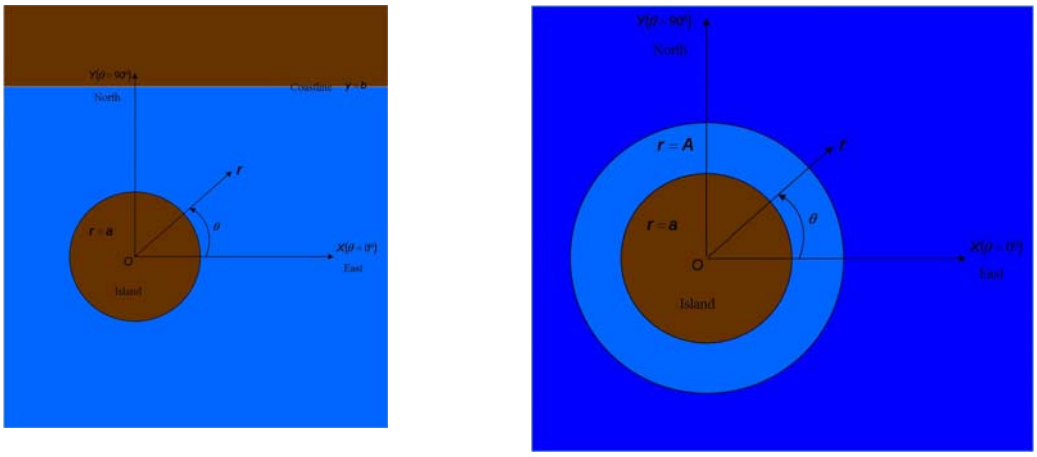

a) b)

Figure 2.12. Cylindrical island for the study of tidal wave variations in constant water depth (h): a) without sill [after Lee and Kim (1999)]; b) with uniform water depth (h_0) sill [Kowalik and Marchenko (2002)]

$$\nabla^2 Z + k^2 Z = \nabla^2 Z_E \tag{2.14}$$

$$\nabla^2 Z + k^2 Z = 0 \tag{2.15}$$

$$\nabla^2 Z = 0 \tag{2.16}$$

Initial studies in this area did not include the bottom friction term until the study of Lee and Kim (1993) for Kelvin waves, based on the work of Mojfeld (1980). Inclusion of bottom friction in representation of tides resulted in that it slanted the co-amplitude lines of the incident Kelvin wave backward relative to the direction of wave propagation [Lee and Kim (1993)]. Lee and Kim (1999) developed an analytical scattering solution that included bottom friction coefficient for Sverdrup, Poincare and Kelvin waves and worked for all frequency ranges, i.e. (sub-inertial, inertial and super-inertial frequencies). The frequency range could be established based on the values of the wave frequency (ω) and Coriolis parameter (f), as follows: $\omega < f$ represents sub-inertial frequency; $\omega = f$ defines inertial frequency; $\omega > f$ describes super-inertial frequency. For Lee and Kim (1999) the study of Sverdrup and Kelvin waves

with sub-inertial and super-inertial frequency could be used to interpret amplitude and phase variations around Cheju Island.

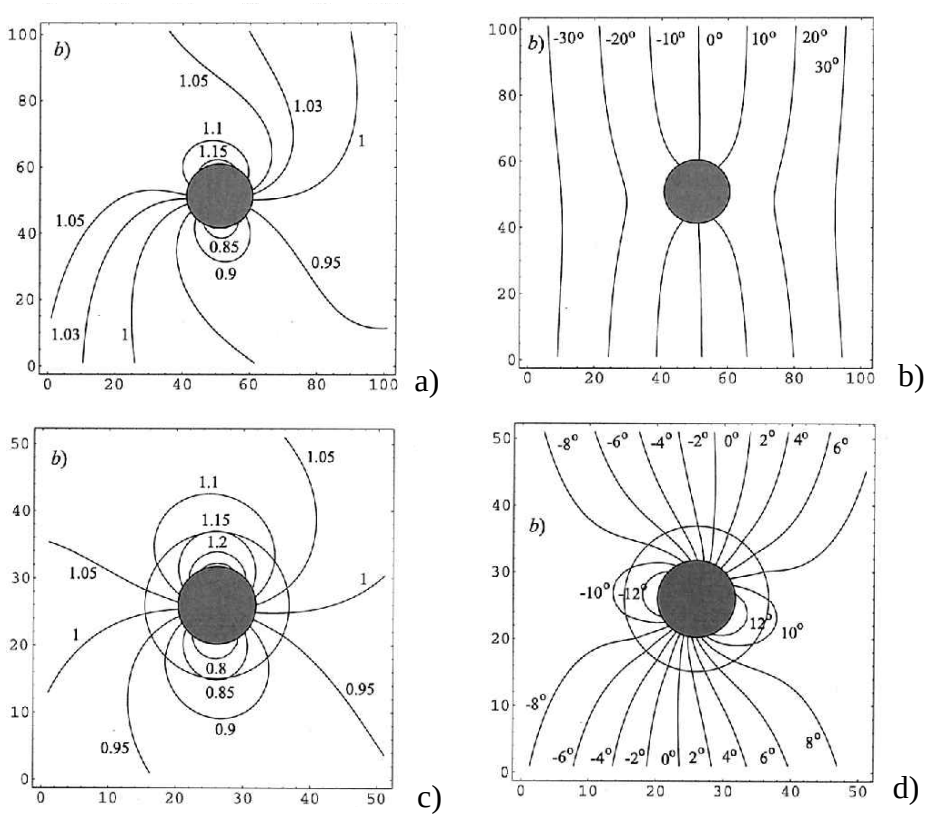

Figure 2.13. Amplitude and phase of semidiurnal Sverdrup wave around cylindrical island without sill (a,b) and with sill (c,d) in the presence of bed friction [Marchenko and Kowalik (2002)].

Kowalik and Marchenko (2002) further developed the theory and included a depth discontinuity around the circular island [Figure 2.12 b)] for the study of free Sverdrup and Kelvin wave variation. Compared with previous studies without sill, the presence of a uniform water depth sill around a cylindrical island introduced [Figure 2.13]:

i) high frequency gravity waves and low frequency topographic waves;
ii) additional modes of eigenoscillations, important for resonance with incident waves;
iii) additional bottom friction, with role in the wave modification.

2.4.5. Conclusions

The literature review of the analytical solutions and numerical models in cylindrical co-ordinates presented herein showed that:

i) analytical solutions were obtained only for simplified cases of the equations governing water flow, and for Helmholtz and Laplace equations;

ii) numerical models for storm surge modelling in cylindrical co-ordinates used simplified forms of the momentum equations, which did not include the advection, as well as the turbulence term.

iii) three-dimensional numerical modelling of pipe flow was done in cylindrical co-ordinates, with the assumption of rotational flow, the domain was represented by a full cylinder and no prescription of open boundaries at the outer radius existed;

iv) numerical methods already developed for Cartesian co-ordinates can be used for the cylindrical co-ordinates numerical model provided that proper mapping transformations are preformed.

2.5. Summary and conclusions

Water motion is described by the Navier-Stokes equations which together with the continuity equation represent the equations governing hydrodynamic modelling. The analytical solution of the governing equations cannot be obtained due to the complexity of the studied system. Hence, numerical methods are used for solving the complicated problems related to the hydrodynamic modelling of rivers, estuaries and oceans and they are applied to specific problems. There are two classes of numerical models commonly used: structured grid approaches (primarily finite difference algorithms) and unstructured grid approaches (including finite element and finite volume methods). The model grid results in a numerical method through the discretization of the domain. Discretization is the process of separating the

continuous domain of the problem into numerous components, called elements. Both structured and unstructured grids can be employed in discretization process. Structured grids are relatively straightforward and use efficient algorithms. Their main drawback is that they do not model bed topography very well. Cartesian grids can be used on domains with non-rectangular boundaries using the “cut-cell” method [Ketefian and Jacobson (2011)]. Unstructured grid models use variable triangular and tetrahedral elements, but also elements of mixed type with irregular connectivity. Factors such as problem size, problem complexity and the representation of reality converge to grid design in unstructured grid modelling [French and Clifford (2000)].

From a mathematical point of view, the degree of complexity of the modelled equations recommends usage of finite difference methods [Vinokur (1976)]. In the present literature review it has been established that allocation of computational resources is less advantageous when using unstructured grid models. Subsequently, structured grid models can be recommended for development of a new hydrodynamic model. The choice of a suitable co-ordinate system considers the type of geometries describing the boundaries for structured grids. Cartesian co-ordinates handle simple rectangular geometries with application to small geographical areas, whereas spherical co-ordinates are best used to describe large regions [Sankaranarayanan and Ward (2006)]. Curvilinear co-ordinates are a natural choice for complex geometries. Curvilinear, boundary-fitted co-ordinates can be either orthogonal or non-orthogonal. Orthogonal co-ordinates result in fewer computing operations, faster convergence and better stability and accuracy of the solution. Non-orthogonal co-ordinates are easier to generate since they are not constrained by the value of the angle, and provide greater flexibility in the distribution of the grid points but show a reduced convergence rate, accuracy and stability [Rodi et al. (2004)]. Most of the estuarine and coastal area structured grid models have been developed using Cartesian [i.e. DIVAST, Blumberg and Mellor (1987), Chen (2003)], spherical [Sankaranarayanan and Ward (2006)], orthogonal curvilinear [Blumberg and Herring (1986), EFDC, POM, ROMS, GETM], and non-orthogonal curvilinear grids [i.e. Sheng (1989), Muin and Spaulding (1996), (1997), George (2007)]. The Author observed that no structured grid cylindrical

co-ordinates coastal hydrodynamic models were developed up to the moment of writing the literature review.

Cylindrical co-ordinate systems can be used in estuarine hydrodynamic models since they offer a fine resolution close to the closed boundary of the domain and a coarse resolution away from the coast if the position of the pole is appropriately chosen. Simplified cylindrical co-ordinates momentum equations have been used in storm surge models, i.e. Roy et al. (1999). The governing equations missed the advective acceleration and turbulence terms. In three-dimensional form, cylindrical co-ordinates have been mainly used for pipe flow models. For estuarine applications, in 1978, Lynch and Gray obtained the analytical solutions of the two-dimensional linearized shallow water equations with various shapes of the bed assumed, i.e. horizontal, linear, parabolic, etc. These solutions were subsequently used for two-dimensional non-orthogonal curvilinear co-ordinates, and further development by Lynch and Officer (1985) led to three-dimensional non-orthogonal and FEM (ADCIRC) model verification. A better representation of the island geometry could be obtained in cylindrical co-ordinates in the study of shelf circulation around islands. Therefore, cylindrical co-ordinates present more research possibilities in the area of estuarine hydrodynamic modelling described by the non-linear Navier-Stokes equations.

In structured grid modelling, increasing the number of grid points to increase resolution in certain areas of interest, as in Cartesian nested models, is undoubtedly a huge improvement compared to using high resolution all over the domain. A more economical way of achieving a variable resolution is to use a grid that automatically varies resolution, without changing the number of points and keeps orthogonality at all times. Such a grid can be defined using cylindrical co-ordinates since many natural estuaries are more or less “V”-shaped. A rather intuitive representation of these domains could use annular geometries, like the ones obtained using cylindrical co-ordinates; domain could be defined between two concentric circles and two radii positioned at angles theta1 and theta2 from positive horizontal direction, respectively [Figure 2.14]. From the point of view of computational burden, cylindrical co-ordinates present the advantage of being

easiest orthogonal curvilinear co-ordinates that can be generated. Another advantage of using these co-ordinates is given by the variable resolution. Position of the pole can be chosen in a judicious manner and subsequently dictates the resolution inside a given domain, i.e. a higher resolution can be obtained in the coastal area and a coarser resolution away from the coast. Furthermore, the curvature of the coast in the angular direction can be more accurately described compared to rectilinear models. Also, orthogonality of the grid is preserved at all times. In order to prevent the singularity problem, the simulation domain does not include the pole.

In conclusion, development of a new two-dimensional estuarine hydrodynamic model in cylindrical co-ordinates is proposed herein. Governing equations are written in cylindrical co-ordinates and depth integrated, since two-dimensional models can be used for numerical simulations of well-mixed estuaries and coastal areas. Cylindrical co-ordinate grids can be easily generated and mapping transformations onto a computational domain can be performed using algebraic relationships. In Figure 2.14, the real plane is represented between angles θ_5 and θ_7, with all points on the land outside the physical plane represented on grey coloured background, water cells represented on blue background, and land points inside the domain on brown background. Subsequent mapping transformations onto the computational plane show that only points positioned on white background, equivalent to blue and brown background on the left hand side of Figure 2.14, are considered for domain modelling, whereas land cells outside the real domain are still represented on grey background. Both dependent and independent variables are transformed. The governing equations are discretized on an Arakawa C grid, and an Alternating Directions Implicit time discretization scheme is used. The tridiagonal system of equations is solved by means of Thomas algorithm and the water elevation and velocity components are correlated with the Cartesian co-ordinates again.

The new model represents an improvement of the existing cylindrical co-ordinate models, in that the model uses the Navier-Stokes equations written in cylindrical co-ordinates in their fully non-linear form to simulate

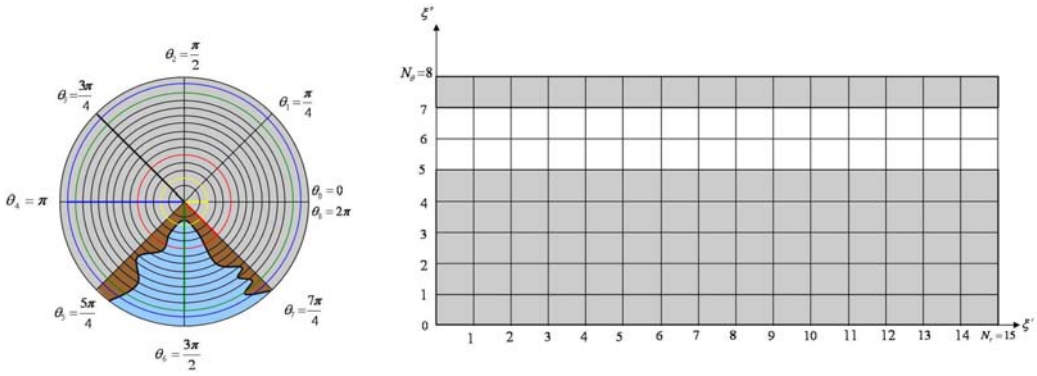

Figure 2.14. Simplified physical and computational plane for a hypothetical estuary [after Roy et al. (1999), Morinishi et al. (2004)].

hydrodynamics in the estuarine region, unlike the storm surge models or analytical solutions which use a simplified form of the equations and do not include advection and turbulence effects. Also, compared to the fully non-linear models used in pipe flow simulations, the domain of simulation differs in that an annular section can be used for simulation instead of the full circle, irrotational flow can be assumed and open boundary conditions can be applied on the curved boundary.

Chapter 3

Mathematical Formulation of a Cylindrical Co-ordinates Numerical Model

3.1. Introduction

In Chapter 2 it was established that cylindrical co-ordinates present more research opportunities compared with all other Eulerian co-ordinate systems in the area of coastal modelling. In this chapter the mathematical development of the equations governing water flow (Navier-Stokes equations) and ensuring conservation of properties such as mass and momentum are presented. The equations are written in terms of instantaneous velocities and time averaging in order to obtain the Reynolds stresses for turbulence modelling. Derivation of the hydrodynamic equations uses various approximations such as the hydrostatic or Boussinesq approximation described in Chapter 2. The equations are obtained in their 3D form and subsequently vertically integrated in order to achieve the 2D expression. The Author developed the formulation of the 2D continuity and Navier-Stokes equations. In the depth integrated equations, vertical variation of the velocities is considered small and postulated by a logarithmic profile. The resulting equations have applicability to well-mixed estuaries and describe the velocity distribution and water elevation variation on a horizontal plane. Following the presented approach, the effects of turbulence within the governing equations is reduced to bed shear and wind stresses, and viscosity terms.

The chapter is organized as follows: derivation of the continuity equation in a Cartesian co-ordinate system, followed by derivation of the Navier-Stokes equations, continued by the transformation of the equations written in cylindrical co-ordinates into Reynolds averaged form, depth integration of the resulting equations, mapping transformations of the depth integrated equations from a real plane onto a computational plane and ending with presentation of some open and closed boundary conditions.

3.2. Governing Equations of Fluid Motion

3.2.1. The Continuity Equation

A classical approach for derivation of the continuity equation is to use the principle of mass conservation written for an infinitesimal control volume [Wesseling (2001)]. It states that the rate of change of mass inside the considered volume equals the net inflow minus the outflow. For the present derivation an infinitesimal volume, with dimensions $\delta x, \delta y, \delta z$ and velocity components (u, v, w) in the directions of a Cartesian co-ordinate system (x, y, z), defined as in Figure 3.1, is considered. Point A is the centre of mass for the inflow face $\delta y \delta z$, whereas point B has the same significance for the outflow face in the $x-$ direction. Point C is the centre of mass of the infinitesimal volume. The mass flow rate in the $x-$direction can be written in terms of velocity component (u), density of the fluid (ρ) and area (S) at some point as $\rho u S$.

Mass flow rate across face $\delta y \delta z$ at point A in Figure 3.1 is $\rho u \delta y \delta z$. Mass flow rate variation from point A to point C, also known as the net inflow, can be written as the sum of mass flow rate at point A and its variation $(\partial \rho u / \partial x)$ in the $x-$direction over infinitesimal distance $(-\delta x/2)$, expressed as:

$$\left[\rho u - \frac{\partial(\rho u)}{\partial x}\frac{\delta x}{2}\right]\delta y \delta z \tag{3.1}$$

A similar explanation between points C and B helps establish the mass flow rate variation between the two points, named net outflow, as:

$$\left[\rho u + \frac{\partial(\rho u)}{\partial x}\frac{\delta x}{2}\right]\delta y \delta z \tag{3.2}$$

The difference between the net inflow and net outflow gives the mass gain across the area as: $-\frac{\partial(\rho u)}{\partial x}\delta x\delta y\delta z$.

Similar expressions can be obtained for mass production in the $y-$ and $z-$ directions (i.e face $\delta x\delta z$ and $\delta x\delta y$, respectively). Subsequently the variation of mass with respect to time in the infinitesimal volume can be written as the sum of mass flow rates across the three directions:

$$\frac{\partial \rho}{\partial t}\delta x\delta y\delta z = -\left[\frac{\partial(\rho u)}{\partial x}+\frac{\partial(\rho v)}{\partial y}+\frac{\partial(\rho w)}{\partial z}\right]\delta x\delta y\delta z \tag{3.3}$$

or

$$\frac{\partial \rho}{\partial t} = -\left[\frac{\partial(\rho u)}{\partial x}+\frac{\partial(\rho v)}{\partial y}+\frac{\partial(\rho w)}{\partial z}\right] \tag{3.4}$$

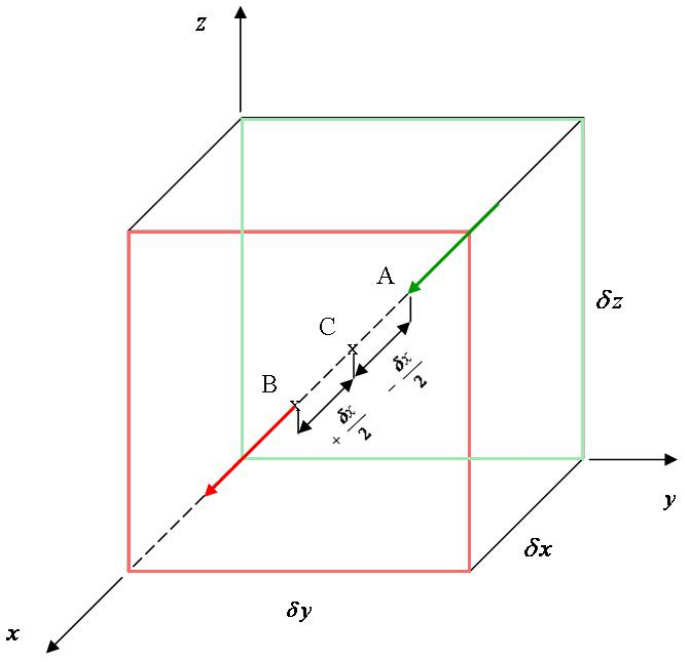

Figure 3.1: Infinitesimal control volume for mass flow rate evaluation with centre of mass at point C. Green arrow represents inflow in the considered volume at point A for the inflow area; red arrow illustrates outflow at point B in the $x-$direction.

In tensors form equation (3.4) can be written as:

$$\frac{\partial \rho}{\partial t} + \nabla \cdot (\rho \vec{v}) = 0 \tag{3.5}$$

where:

$\nabla \cdot (\rho \vec{v}) = \frac{\partial(\rho u)}{\partial x} + \frac{\partial(\rho v)}{\partial y} + \frac{\partial(\rho w)}{\partial z}$ is divergence of linear momentum $\rho \vec{v}$.

Equation (3.5) represents the continuity equation for a compressible fluid. It states that the sum of mass variation with respect to time and divergence of linear momentum inside a domain is null.

The condition for a flow to be incompressible is given by constant density. The mass conservation law for incompressible fluids has the following expression:

$$\nabla \cdot \vec{v} = 0 \tag{3.6}$$

Equation (3.6) characterizes a fluid with an isochoric motion (volume does not change during motion) or a solenoidal velocity field.

Details regarding vector calculus in orthogonal co-ordinate systems can be found in Appendix 2, whereas for non-orthogonal co-ordinates mathematical identities are presented in Appendix 3. The mass conservation equation can be written in Cartesian, spherical, general orthogonal or non-orthogonal curvilinear co-ordinate systems as can be seen in Appendix 4.

3.2.2. The Navier-Stokes Equations

The Navier-Stokes equations (NSE) are a set of partial differential equations that describe the motion of fluids. They could be derived from Newton's second law for fluid motion [Mellor (1996)], but also from Cauchy's equation of motion for

fluids with addition of the mechanical constitutive equation [Aris (1989)]. The NSE use a representation of the fluid stress tensor as the sum of a diffusing viscous stress tensor, proportional to the divergence of velocity, and a pressure term [Hirsch (1988), Aris (1989)]. The number of unknowns in the NSE is four (the 3 components of velocity on the axes of a co-ordinate system, i.e. Cartesian, and pressure). Therefore, solving the NSE requires an additional equation and that is the continuity equation derived in Section 3.2.1.

The present derivation of the NSE follows the work of Aris (1989). The principle of the conservation of linear momentum represents the rate of change of linear momentum ($\rho\vec{v}$) as the sum of external and internal forces acting on a control volume V :

$$\frac{d}{dt}\iiint_V \rho\vec{v}\,dV = \iiint_V \rho\vec{f}_{EXT}\,dV + \iint_S \vec{f}_{INT}\,dS \tag{3.7}$$

where:

$\rho\vec{f}_{EXT}$ is the external force per unit volume, for example $\vec{f}_{EXT}$ is the gravitational acceleration in the z – direction per unit mass;

$\vec{f}_{INT}$ is the force per unit area, represented at a point of the boundary surface S with unit outward normal $\vec{n}$, exerted by the material outside the surface S.

The control volume V, the bounding surface S and the forces acting on the control volume are illustrated in Figure 3.2.

The total stress tensor $\underset{\sim}{t}_n$ in Figure 3.2 is the internal force per unit area and can be represented as:

$$\vec{f}_{INT} = \vec{n} \cdot \underset{\sim}{T} \tag{3.8}$$

or in terms of kth component:

$$\left(f_{INT}\right)_k = T_{lk} n_l \tag{3.9}$$

where n_l is the normal outward to the bounding surface S_l, and T_{lk} are the components of a second order tensor $\underset{\sim}{T}$, i.e. T_{lk} is the kth component of $\underset{\sim}{t}_l$, $k = 1,2,3$, $l = 1,2,3$ in Figure 3.3.

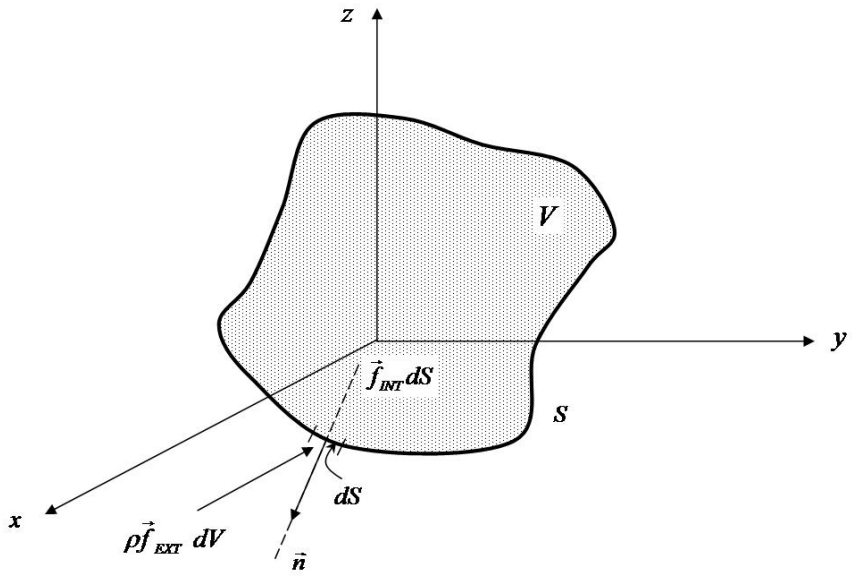

Figure 3.2: Control volume for derivation of the Navier-Stokes equations.

For any continuous function F with continuous derivatives ($F_{,k}$) in the considered volume V, the divergence theorem relates a volume integral to an integral over the bounding surface and is known as Green's theorem:

$$\iiint_V F_{,k}\, dV = \iint_S F n_k\, dS \tag{3.10}$$

Equation (3.10) can be applied on any composite volume V with a piecewise smooth boundary S. Using equation (3.7) and Green's theorem (3.10) results:

$$\iiint_V \frac{d\rho v_k}{dt} dV = \iiint_V \left[\rho\left(f_{EXT}\right)_k + T_{lk,l}\right] dV \tag{3.11}$$

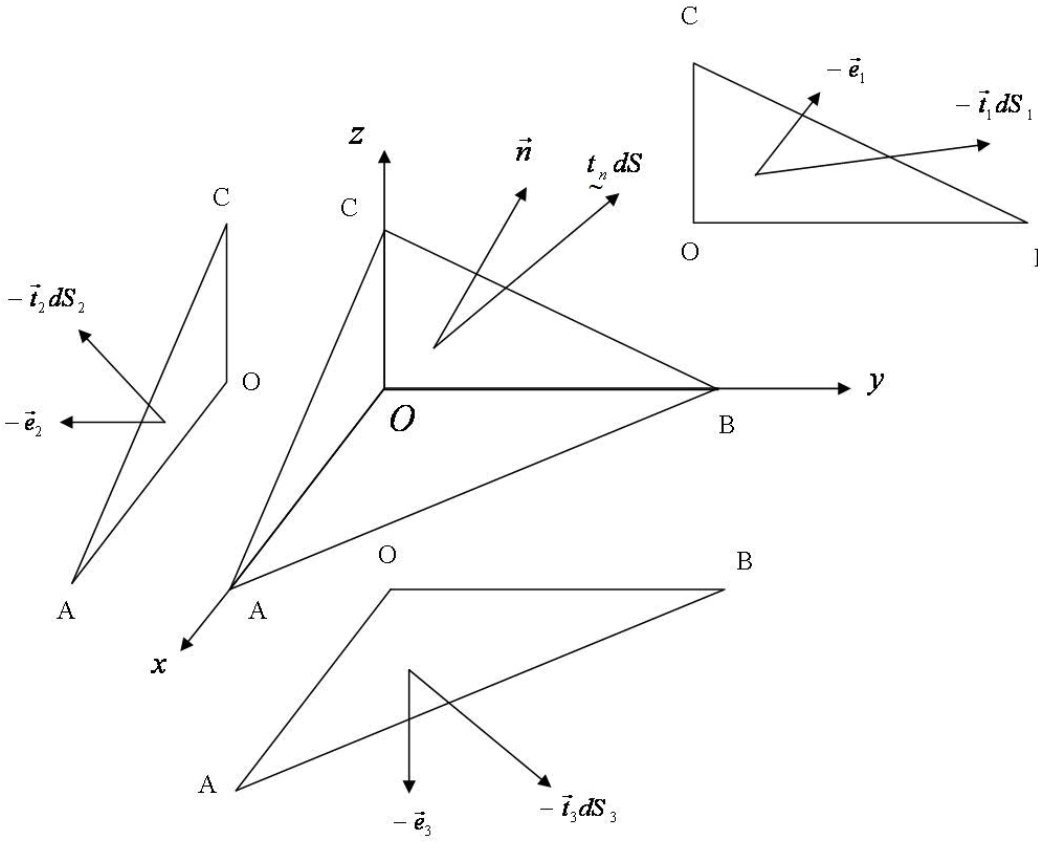

Figure 3.3: Total stress tensor in a tetrahedron [after Aris(1989)]. Stress tensor decomposed after the three planes of a Cartesian co-ordinate system, with unit vectors $\vec{e}_1, \vec{e}_2, \vec{e}_3$.

Cauchy's equation of motion for fluids is obtained in terms of kth component, since equation (3.11) can be written for an arbitrary volume V, as:

$$\frac{d\rho v_k}{dt} = \rho\left(f_{EXT}\right)_k + T_{lk,l} \tag{3.12}$$

or, in terms of instantaneous velocity $\vec{v}$:

$$\frac{d\rho\vec{v}}{dt} = \rho\vec{f} + \nabla \cdot \underset{\sim}{T} \tag{3.13}$$

The stress tensor in equation (3.13) is symmetric and it can be written in terms of the components of the second order tensor $\underset{\sim}{T}$ as: $T_{kl} = T_{lk}$. This symmetry can

be explained by the fact that two opposite internal forces with respect to any arbitrary point inside volume V cancel each other based on the principle of conservation of momentum, since the only internal forces considered in equation (3.7) are those acting on the points of the boundary surface.

Effects of viscosity can be included in Cauchy's equations of motion by writing the stress tensor components (T_{kl}) as continuous functions of the symmetric form of the deformation tensor components (e_{kl}). The mechanical constitutive equation for a Newtonian fluid gives the relationship between the stress tensor and the rate of strain tensor in a general co-ordinate system as [Hirsch (1988)]:

$$T_{kl} = \left(-p + \lambda\Theta\right)\delta_{kl} + 2\mu e_{kl} \tag{3.14}$$

where:

p is the hydrostatic pressure for incompressible fluids, or pressure of thermodynamics for compressible fluids;

$e_{kl} = \frac{1}{2}\left(\frac{\partial v_k}{\partial x_l} + \frac{\partial v_l}{\partial x_k}\right)$ is the symmetric form of the deformation tensor;

μ is the dynamic viscosity of the fluid;

λ is the second viscosity coefficient;

$$\delta_{kl} = \begin{cases} 1 & if \quad k = l \\ 0 & if \quad k \neq l \end{cases}$$

Θ is an invariant under an orthogonal transformation: $\Theta = \nabla \cdot \vec{v}$.

Equation (3.14) can be explained by the fact that any fluid at rest is subjected to the hydrostatic stress:

$$T_{kl} = -p\delta_{kl} \tag{3.15}$$

but a general formulation is given by:

$$T_{kl} = -p\delta_{kl} + P_{kl} \tag{3.16}$$

where P_{kl} is the viscous stress tensor, which vanishes when fluid is not in motion. For a Newtonian fluid, the form of the viscous stress tensor is given as [Chung (2002)]:

$$P_{kl} = \lambda(\nabla \cdot \vec{v})\delta_{kl} + 2\mu e_{kl} \tag{3.17}$$

The deformation tensor can be derived with respect to l to give [Aris (1998)]:

$$\begin{aligned} e_{kl,l} &= \frac{1}{2}\frac{\partial}{\partial x_l}\left(\frac{\partial v_k}{\partial x_l} + \frac{\partial v_l}{\partial x_k}\right) \\ e_{kl,l} &= \frac{1}{2}\frac{\partial^2 v_k}{\partial x_l \partial x_l} + \frac{1}{2}\frac{\partial}{\partial x_k}\frac{\partial v_k}{\partial x_l} \\ e_{kl,l} &= \frac{1}{2}\nabla^2 v_k + \frac{1}{2}\frac{\partial}{\partial x_k}(\nabla \cdot \vec{v}) \end{aligned} \tag{3.18}$$

The last term in equation (3.12) becomes:

$$T_{lk,l} = -\frac{\partial p}{\partial x_k} + (\lambda + \mu)\frac{\partial}{\partial x_k}(\nabla \cdot \vec{v}) + \mu\nabla^2 v_k \tag{3.19}$$

Introducing (3.19) into (3.12) gives:

$$\frac{d\rho v_k}{dt} = \rho(f_{EXT})_k - \frac{\partial p}{\partial x_k} + (\lambda + \mu)\frac{\partial}{\partial x_k}(\nabla \cdot \vec{v}) + \mu\nabla^2 v_k \tag{3.20}$$

The general form of the Navier-Stokes equations for compressible fluids is:

$$\frac{d\rho\vec{v}}{dt} = \rho\vec{f}_{EXT} - \nabla p + (\lambda + \mu)\nabla(\nabla \cdot \vec{v}) + \mu\nabla^2\vec{v} \tag{3.21}$$

For incompressible fluids the rate of change of the volume density of the outward flux of a vector field from an infinitesimal volume around a given point is zero: $\partial\rho/\partial t = 0$, which means that continuity equation has the expression given in equation (3.6), and $\nabla(\nabla \cdot \vec{v}) = 0$. Therefore, equation (3.21) becomes:

$$\frac{d\vec{v}}{dt} = \vec{f}_{EXT} - \frac{1}{\rho}\nabla p + \nu\nabla^2\vec{v} \tag{3.22}$$

The coefficient of the Laplacian is called kinematic viscosity ($\upsilon = \mu/\rho$). In equation (3.22) the second coefficient of viscosity is incorporated in μ. The NSE for incompressible fluids (3.22) can be written in various Eulerian co-ordinate systems in the same manner as the continuity equation. The forms of the equations are given in Appendix 5.

3.3. Formulation of the Governing Equations in Cylindrical Co-ordinates

In Chapter 2 of the present thesis it was established that cylindrical co-ordinates [Figure 3.4] present more research opportunities compared with all other Eulerian co-ordinate systems in the area of coastal modelling. Hence, the hydrodynamic equations written in cylindrical co-ordinates are presented herein. Derivation of the Navier-Stokes equations into cylindrical co-ordinates is presented in Appendix 6 and results are the same as the relationships given by Warsi (2006). The momentum equations of incompressible fluid can be written in terms of instantaneous velocities in cylindrical co-ordinates as follows:

$r-$ direction momentum:

$$\frac{\partial\tilde{v}_r}{\partial t} + \tilde{v}_r\frac{\partial\tilde{v}_r}{\partial r} + \frac{\tilde{v}_\theta}{r}\frac{\partial\tilde{v}_r}{\partial\theta} + \tilde{v}_z\frac{\partial\tilde{v}_r}{\partial z} - \frac{\tilde{v}_\theta^2}{r} = \tilde{f}_r - \frac{1}{\rho}\frac{\partial\tilde{p}}{\partial r} \tag{3.23}$$

$$+ E_r\left(\nabla^2\tilde{v}_r - \frac{\tilde{v}_r}{r^2} - \frac{2}{r^2}\frac{\partial\tilde{v}_\theta}{\partial\theta}\right)$$

$\theta-$ direction momentum:

$$\frac{\partial \tilde{v}_\theta}{\partial t}+\tilde{v}_r\frac{\partial \tilde{v}_\theta}{\partial r}+\frac{\tilde{v}_\theta}{r}\frac{\partial \tilde{v}_\theta}{\partial \theta}+\tilde{v}_z\frac{\partial \tilde{v}_\theta}{\partial z}+\frac{\tilde{v}_r\tilde{v}_\theta}{r}=\tilde{f}_\theta-\frac{1}{\rho}\frac{\partial \tilde{p}}{r\partial \theta} \tag{3.24}$$

$$+E_\theta\left(\nabla^2\tilde{v}_\theta+\frac{2}{r^2}\frac{\partial \tilde{v}_r}{\partial \theta}-\frac{\tilde{v}_\theta}{r^2}\right)$$

$z-$ direction momentum:

$$\frac{\partial \tilde{v}_z}{\partial t}+\tilde{v}_r\frac{\partial \tilde{v}_z}{\partial r}+\frac{\tilde{v}_\theta}{r}\frac{\partial \tilde{v}_z}{\partial \theta}+\tilde{v}_z\frac{\partial \tilde{v}_z}{\partial z}=\tilde{f}_z-\frac{1}{\rho}\frac{\partial \tilde{p}}{\partial z}+E_z\nabla^2\tilde{v}_z \tag{3.25}$$

while the equation of continuity can be expressed as:

$$\frac{1}{r}\frac{\partial}{\partial r}\left(r\tilde{v}_r\right)+\frac{1}{r}\frac{\partial \tilde{v}_\theta}{\partial \theta}+\frac{\partial \tilde{v}_z}{\partial z}=0 \tag{3.26}$$

The Laplacian in equations (3.23)-(3.25) is:

$$\nabla^2=\frac{\partial^2}{\partial r^2}+\frac{1}{r}\frac{\partial}{\partial r}+\frac{1}{r^2}\frac{\partial^2}{\partial \theta^2}+\frac{\partial^2}{\partial z^2} \tag{3.27}$$

where:

$\vec{v}$ is the instantaneous velocity vector with components on the three axes of the cylindrical co-ordinate system $\tilde{v}_r,\tilde{v}_\theta,\tilde{v}_z$;

t is the time;

$\tilde{f}_{EXT}$ is the instantaneous external force with components on the three axes of the cylindrical co-ordinate system $\tilde{f}_r,\tilde{f}_\theta,\tilde{f}_z$;

ρ is the water density;

$\tilde{p}$ is the instantaneous pressure;

g is the gravitational acceleration;

E is the eddy viscosity/diffusivity with components on the three axes of the cylindrical co-ordinate system E_r,E_θ,E_z.

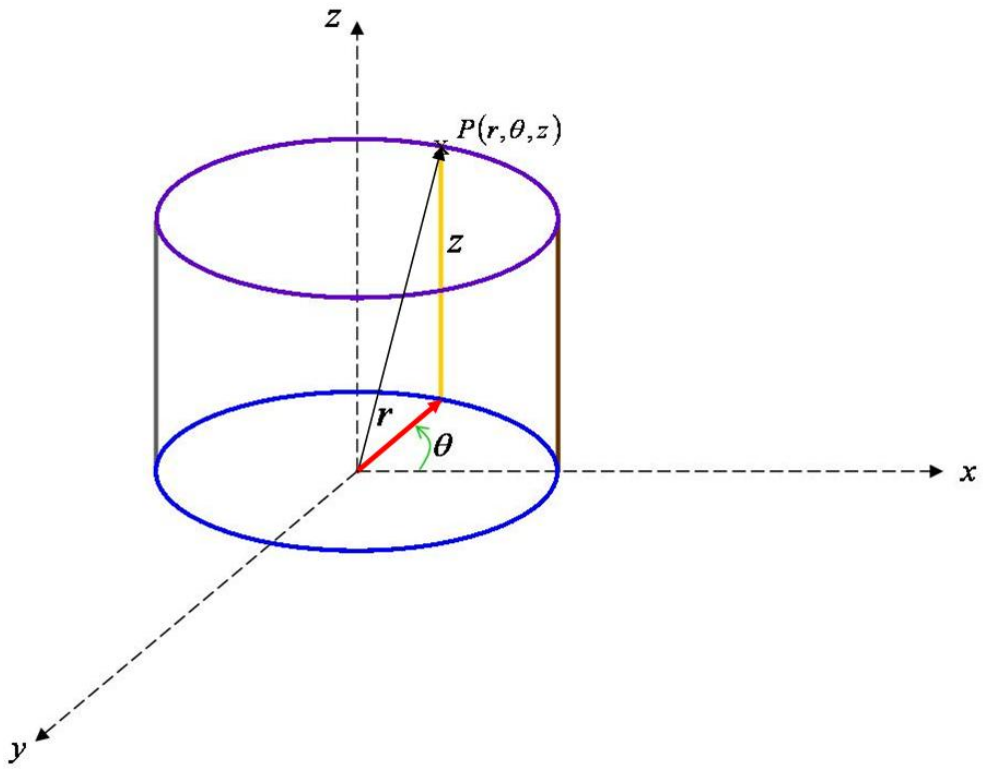

Figure 3.4: Cylindrical co-ordinate system.

With the hydrostatic pressure assumption, equation (3.25) can be written as:

$z-$ direction momentum:

$$\frac{1}{\rho}\frac{\partial \tilde{p}}{\partial z} = -g \tag{3.28}$$

According to Olbert (2006) for tide-induced flows, the hydrostatic pressure assumption (3.28) is found to be valid since tidal heights are very small compared to tidal wavelengths.

Momentum equation in the $r-$direction (3.23) can be re-arranged in flux form, when continuity equation (3.26) is multiplied by $\tilde{v}_r$:

$$\begin{aligned}
&\frac{\tilde{v}_r}{r}\frac{\partial}{\partial r}\left(r\tilde{v}_r\right)+\frac{\tilde{v}_r}{r}\frac{\partial \tilde{v}_\theta}{\partial \theta}+\tilde{v}_r\frac{\partial \tilde{v}_z}{\partial z} \\
&=\frac{1}{r}\frac{\partial\left(r\tilde{v}_r^2\right)}{\partial r}-\tilde{v}_r\frac{\partial \tilde{v}_r}{\partial r}+\frac{1}{r}\frac{\partial\left(\tilde{v}_r\tilde{v}_\theta\right)}{\partial \theta}-\frac{\tilde{v}_\theta}{r}\frac{\partial \tilde{v}_r}{\partial \theta}+\frac{\partial\left(\tilde{v}_r\tilde{v}_z\right)}{\partial z}-\tilde{v}_z\frac{\partial \tilde{v}_r}{\partial z} \\
&=0
\end{aligned} \tag{3.29}$$

and the resulting formulation is added to equation (3.23), into two equivalent forms:

$r-$ direction momentum:

$$\frac{\partial \tilde{v}_r}{\partial t}+\frac{1}{r}\frac{\partial\left(r\tilde{v}_r^2\right)}{\partial r}+\frac{1}{r}\frac{\partial\left(\tilde{v}_r\tilde{v}_\theta\right)}{\partial \theta}+\frac{\partial\left(\tilde{v}_r\tilde{v}_z\right)}{\partial z}-\frac{\tilde{v}_\theta^2}{r}=\tilde{f}_r-\frac{1}{\rho}\frac{\partial \tilde{p}}{\partial r} \\ +E_r\left(\nabla^2\tilde{v}_r-\frac{\tilde{v}_r}{r^2}-\frac{2}{r^2}\frac{\partial \tilde{v}_\theta}{\partial \theta}\right) \tag{3.30}$$

or

$r-$ direction momentum:

$$\frac{\partial \tilde{v}_r}{\partial t}+\frac{\partial \tilde{v}_r^2}{\partial r}+\frac{1}{r}\frac{\partial\left(\tilde{v}_r\tilde{v}_\theta\right)}{\partial \theta}+\frac{\partial\left(\tilde{v}_r\tilde{v}_z\right)}{\partial z}+\frac{\tilde{v}_r^2}{r}-\frac{\tilde{v}_\theta^2}{r} \\ =\tilde{f}_r-\frac{1}{\rho}\frac{\partial \tilde{p}}{\partial r}+E_r\left(\nabla^2\tilde{v}_r-\frac{\tilde{v}_r}{r^2}-\frac{2}{r^2}\frac{\partial \tilde{v}_\theta}{\partial \theta}\right) \tag{3.31}$$

A similar flux form of the momentum equation in the $\theta-$ direction can be found when continuity equation (3.26) is multiplied by $\tilde{v}_\theta$:

$$\frac{\tilde{v}_\theta}{r}\frac{\partial}{\partial r}\left(r\tilde{v}_r\right)+\frac{\tilde{v}_\theta}{r}\frac{\partial \tilde{v}_\theta}{\partial \theta}+\tilde{v}_\theta\frac{\partial \tilde{v}_z}{\partial z} \\ =\frac{1}{r}\frac{\partial\left(r\tilde{v}_r\tilde{v}_\theta\right)}{\partial r}-\tilde{v}_r\frac{\partial \tilde{v}_\theta}{\partial r}+\frac{1}{r}\frac{\partial\left(\tilde{v}_\theta^2\right)}{\partial \theta}-\frac{\tilde{v}_\theta}{r}\frac{\partial \tilde{v}_\theta}{\partial \theta}+\frac{\partial\left(\tilde{v}_\theta\tilde{v}_z\right)}{\partial z}-\tilde{v}_z\frac{\partial \tilde{v}_\theta}{\partial z} \\ =0 \tag{3.32}$$

and the resulting expression is added to equation (3.24):

$\theta-$ direction momentum:

$$\frac{\partial \tilde{v}_\theta}{\partial t}+\frac{1}{r}\frac{\partial\left(r\tilde{v}_r\tilde{v}_\theta\right)}{\partial r}+\frac{1}{r}\frac{\partial\left(\tilde{v}_\theta^2\right)}{\partial \theta}+\frac{\partial\left(\tilde{v}_\theta\tilde{v}_z\right)}{\partial z}+\frac{\tilde{v}_r\tilde{v}_\theta}{r}=\tilde{f}_\theta-\frac{1}{\rho}\frac{\partial \tilde{p}}{r\partial \theta} \\ +E_\theta\left(\nabla^2\tilde{v}_\theta+\frac{2}{r^2}\frac{\partial \tilde{v}_r}{\partial \theta}-\frac{\tilde{v}_\theta}{r^2}\right) \tag{3.33}$$

or

$\theta-$ direction momentum:

$$\frac{\partial \tilde{v}_\theta}{\partial t}+\frac{\partial\left(\tilde{v}_r \tilde{v}_\theta\right)}{\partial r}+\frac{1}{r} \frac{\partial\left(\tilde{v}_\theta^2\right)}{\partial \theta}+\frac{\partial\left(\tilde{v}_\theta \tilde{v}_z\right)}{\partial z}+\frac{2 \tilde{v}_r \tilde{v}_\theta}{r}=\tilde{f}_\theta-\frac{1}{\rho r} \frac{\partial \tilde{p}}{\partial \theta} + E_\theta\left(\nabla^2 \tilde{v}_\theta+\frac{2}{r^2} \frac{\partial \tilde{v}_r}{\partial \theta}-\frac{\tilde{v}_\theta}{r^2}\right) \tag{3.34}$$

For a non-hydrostatic model, the $z-$ direction momentum (3.25) equation could be written in the flux form as:

$z-$ direction momentum:

$$\frac{\partial \tilde{v}_z}{\partial t}+\frac{1}{r} \frac{\partial\left(r \tilde{v}_r \tilde{v}_z\right)}{\partial r}+\frac{1}{r} \frac{\partial\left(\tilde{v}_\theta \tilde{v}_z\right)}{\partial \theta}+\frac{\partial\left(\tilde{v}_z^2\right)}{\partial z}=\tilde{f}_z-\frac{1}{\rho} \frac{\partial \tilde{p}}{\partial z}+E_z \nabla^2 \tilde{v}_z \tag{3.35}$$

3.3.1. Navier-Stokes Equations with the Hydrostatic Pressure Assumption

Derivation of the pressure term from the equation for instantaneous hydrostatic pressure (3.28) is next considered. Neglecting all the vertical accelerations and shear stresses, the hydrostatic pressure distribution results in:

$$\int_p^{P_a} dp=-\int_Z^\zeta \rho g dz \Rightarrow P_a-p=-\rho g(\zeta-Z) \Rightarrow p=P_a+\rho g(\zeta-Z) \tag{3.36}$$

where g is the acceleration due to gravity; P_a is the atmospheric pressure.

The following boundary conditions [Figure 3.5] can be used:

i) at the bed ($Z=-h$): $p_{-h}=P_a+\rho g(\zeta+h)$;

ii) at the free surface ($Z = \zeta$): $p_\zeta = P_a$.

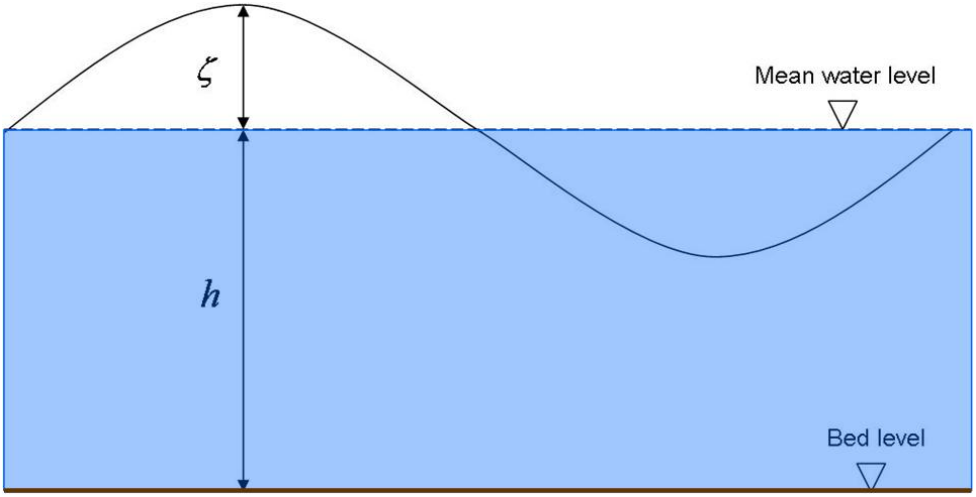

Figure 3.5: Schematics of the ζ and h terms: H is the total depth ($H = \zeta + h$); ζ is water elevation below or above still water elevation.

So that derivatives of the pressure in the $r-$ direction could be written at the free surface as:

$$\frac{\partial p}{\partial r} = \rho g \frac{\partial \zeta}{\partial r} + \frac{\partial P_a}{\partial r} \tag{3.37}$$

In the scale of motion being considered the atmospheric pressure gradient constitutes an insignificant part of the hydrodynamic pressure and can be neglected [Falconer (1976)]:

$$\frac{\partial p}{\partial r} \approx \rho g \frac{\partial \zeta}{\partial r} \tag{3.38}$$

Similar reasoning can be applied to the $\theta-$direction to give:

$$\frac{1}{r}\frac{\partial p}{\partial \theta} \approx \rho g \frac{1}{r}\frac{\partial \zeta}{\partial \theta} \tag{3.39}$$

Subsequently, equations (3.31) and (3.34) can be written as:

$r-$ direction momentum:

$$\frac{\partial \tilde{v}_r}{\partial t}+\frac{\partial \tilde{v}_r^2}{\partial r}+\frac{1}{r}\frac{\partial(\tilde{v}_r\tilde{v}_\theta)}{\partial \theta}+\frac{\partial(\tilde{v}_r\tilde{v}_z)}{\partial z}+\frac{\tilde{v}_r^2}{r}-\frac{\tilde{v}_\theta^2}{r} = \tilde{f}_r-g\frac{\partial \tilde{\zeta}}{\partial r}+E_r\left(\nabla^2\tilde{v}_r-\frac{\tilde{v}_r}{r^2}-\frac{2}{r^2}\frac{\partial \tilde{v}_\theta}{\partial \theta}\right) \tag{3.40}$$

and, respectively:

$\theta-$ direction momentum:

$$\frac{\partial \tilde{v}_\theta}{\partial t}+\frac{\partial(\tilde{v}_r\tilde{v}_\theta)}{\partial r}+\frac{1}{r}\frac{\partial(\tilde{v}_\theta^2)}{\partial \theta}+\frac{\partial(\tilde{v}_\theta\tilde{v}_z)}{\partial z}+\frac{2\tilde{v}_r\tilde{v}_\theta}{r} = \tilde{f}_\theta-\frac{1}{r}g\frac{\partial \tilde{\zeta}}{\partial \theta} + E_\theta\left(\nabla^2\tilde{v}_\theta+\frac{2}{r^2}\frac{\partial \tilde{v}_r}{\partial \theta}-\frac{\tilde{v}_\theta}{r^2}\right) \tag{3.41}$$

3.3.2. Body Force Terms

The body force $\tilde{f}$ terms considered in equations (3.31), (3.34) and (3.25), and subsequently derived equations, are the Coriolis acceleration:

$$\tilde{f}_r = f_C\tilde{v}_\theta \text{ in the } r-\text{direction} \tag{3.42}$$

$$\tilde{f}_\theta = -f_C\tilde{v}_r \text{ in the } \theta-\text{direction} \tag{3.43}$$

and acceleration due to gravity:

$$\tilde{f}_z = -g \text{ in the } z-\text{direction} \tag{3.44}$$

The Coriolis acceleration is due to the relative motion of Earth's rotation. Within a fixed frame of reference, the effect of Coriolis acceleration is to deflect the velocity vector to the right in the Northern Hemisphere. The expression of the Coriolis force (f_C) is given by:

$$f_C = 2\omega\sin\phi \tag{3.45}$$

where:

ω is the angular velocity of the Earth ($\omega = 7.27 \times 10^{-5} rad/s$);

ϕ is the latitude (degrees).

3.3.3. Reynolds Averaging Concept

Equations (3.31), (3.34), (3.28) and (3.26) are written in terms of instantaneous functions ($\tilde{v}_r, \tilde{v}_\theta, \tilde{v}_z, \tilde{p}$). Reynolds average concept can be used decompose an instantaneous function into a mean and a fluctuating part [Figure 3.6], as in equation (3.46), and these are next interpolated in time, see equation (3.47). The Reynolds averaged Navier-Stokes (RANS) equations can be used to describe turbulent flows.

$$\tilde{F} = F + F' \tag{3.46}$$

$$\int_{t_1}^{t_2} \tilde{F} dt = (t_2 - t_1) F \tag{3.47}$$

where:

$\tilde{F}$ is the instantaneous value of some function;

F is the resolvable mean quantity;

F' is the unresolvable fluctuating quantity;

$t_2 - t_1$ is a long time interval when compared with the scale of turbulent motion, but small compared with the scale of the mean flow variation.

Following this approach, the subsequent expressions are found:

$$\overline{F + F'} = \frac{1}{t_2 - t_1} \int_{t_1}^{t_2} (F + F') dt = F \tag{3.48}$$

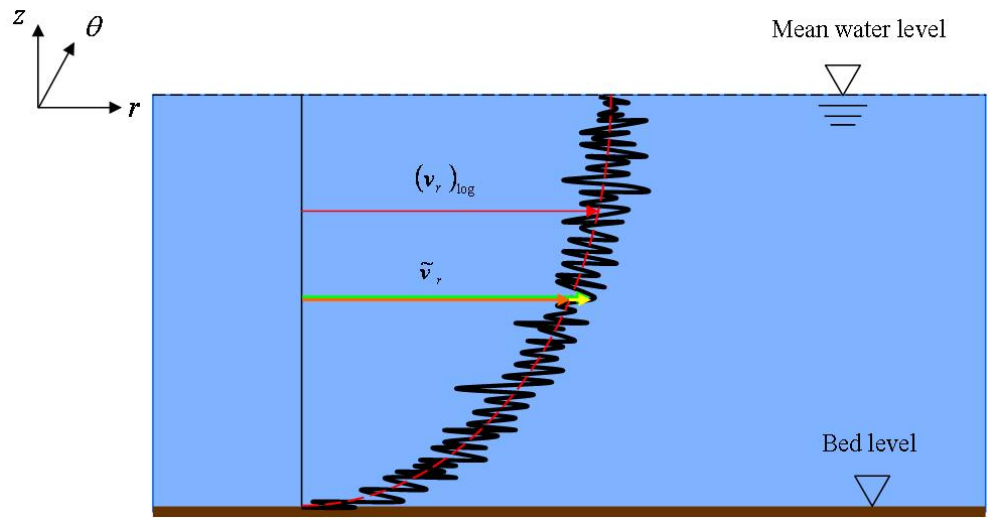

Figure 3.6: Instantaneous velocity decomposition into mean and fluctuating parts: $\tilde{v}_r$ is the instantaneous velocity (green arrow); $\bar{v}_r$ is the averaged velocity (orange arrow), $v_r^{'}$ is the fluctuating quantity (yellow arrow). The mean value of $\tilde{v}_r$ is approximated by a logarithmic law, i.e. $(v_r)_{\log}$ represented with red arrow.

$$\overline{F'} = \frac{1}{t_2 - t_1}\int_{t_1}^{t_2} F'\,dt = 0 \tag{3.49}$$

$$\overline{FF'} = \frac{1}{t_2 - t_1}\int_{t_1}^{t_2} FF'\,dt = 0 \tag{3.50}$$

This method transforms equation (3.31) into:

$r-$direction momentum

$$\begin{aligned}&\frac{\partial}{\partial t}(\bar{v}_r + v'_r) + \frac{\partial}{\partial r}(\bar{v}_r + v'_r)(\bar{v}_r + v'_r) + \frac{1}{r}\frac{\partial}{\partial \theta}(\bar{v}_r + v'_r)(\bar{v}_\theta + v'_\theta)\\ &+ \frac{\partial}{\partial z}(\bar{v}_r + v'_r)(\bar{v}_z + v'_z) + \frac{(\bar{v}_r + v'_r)(\bar{v}_r + v'_r) - (\bar{v}_\theta + v'_\theta)(\bar{v}_\theta + v'_\theta)}{r}\end{aligned} \tag{3.51}$$

$$= \bar{f}_r + f'_r - \frac{1}{\rho}\frac{\partial}{\partial r}(\bar{p} + p')$$

$$\begin{aligned}&+ E\left[\frac{\partial^2}{\partial r^2}(\bar{v}_r + v'_r) + \frac{1}{r^2}\frac{\partial^2}{\partial \theta^2}(\bar{v}_r + v'_r) + \frac{\partial^2}{\partial z^2}(\bar{v}_r + v'_r)\right.\\ &\left. + \frac{1}{r}\frac{\partial}{\partial r}(\bar{v}_r + v'_r) - \frac{2}{r^2}\frac{\partial}{\partial \theta}(\bar{v}_\theta + v'_\theta) - \frac{(\bar{v}_r + v'_r)}{r^2}\right]\end{aligned} \tag{3.51}$$

continued

The following calculus is required for further development of equation (3.51):

$$\overline{\left(\bar{v}_r\bar{v}_r+\bar{v}_r v'_r+\bar{v}_r v'_r+v'_r\,v'_r\right)}=\frac{1}{t_2-t_1}\int_{t_1}^{t_2}\left(\bar{v}_r\bar{v}_r+2v'_r\,\bar{v}_r+v'_r\,v'_r\right)dt$$

$$\overline{\left(\bar{v}_r\bar{v}_r+\bar{v}_r v'_r+\bar{v}_r v'_r+v'_r\,v'_r\right)}=\bar{v}_r\bar{v}_r+\overline{v'_r\,v'_r}$$

because:

$$\bar{v}_r\bar{v}_r=const.$$

$$\frac{1}{t_2-t_1}\int_{t_1}^{t_2}2v'_r\,\bar{v}_r dt=\frac{2\bar{v}_r}{t_2-t_1}\int_{t_1}^{t_2}v'_r\,dt=0$$

$$\frac{1}{t_2-t_1}\int_{t_1}^{t_2}v'_r\,v'_r dt=\overline{v'_r\,v'_r}$$

and gives:

$r-$ direction momentum

$$\begin{aligned}
&\frac{\partial}{\partial t}\overline{\left(\bar{v}_r+v'_r\right)}+\frac{\partial}{\partial r}\overline{\left(\bar{v}_r^2+2v'_r\,\bar{v}_r+v'_r\,v'_r\right)}+\\
&\frac{1}{r}\frac{\partial}{\partial\theta}\overline{\left(\bar{v}_r\bar{v}_\theta+\bar{v}_\theta v'_r+\bar{v}_r v'_\theta+v'_r\,v'_\theta\right)}\\
&+\frac{\partial}{\partial z}\overline{\left(\bar{v}_r\bar{v}_z+\bar{v}_z v'_r+\bar{v}_r v'_z+v'_r\,v'_z\right)}\\
&+\frac{\overline{\left(\bar{v}_r^2+2v'_r\,\bar{v}_r+v'^2_r\right)}-\overline{\left(\bar{v}_\theta^2+2v'_\theta\,\bar{v}_\theta+v'_\theta\,v'_\theta\right)}}{r}\\
&=\overline{\bar{f}_r+f'_r}-\frac{1}{\rho}\frac{\partial}{\partial r}\overline{\left(\bar{p}+p'\right)}\\
&+E\left[\frac{\partial^2}{\partial r^2}\overline{\left(\bar{v}_r+v'_r\right)}+\frac{1}{r^2}\frac{\partial^2}{\partial\theta^2}\overline{\left(\bar{v}_r+v'_r\right)}+\frac{\partial^2}{\partial z^2}\overline{\left(\bar{v}_r+v'_r\right)}\right.\\
&\left.+\frac{1}{r}\frac{\partial}{\partial r}\overline{\left(\bar{v}_r+v'_r\right)}-\frac{2}{r^2}\frac{\partial}{\partial\theta}\overline{\left(\bar{v}_\theta+v'_\theta\right)}-\frac{\overline{\left(\bar{v}_r+v'_r\right)}}{r^2}\right]
\end{aligned}\qquad(3.52)$$

Hence, equation (3.52) can be written as:

$r-$ direction momentum (3.53)

$$\frac{\partial \bar{v}_r}{\partial t}+\frac{\partial \bar{v}_r^2}{\partial r}+\frac{1}{r}\frac{\partial \bar{v}_r \bar{v}_\theta}{\partial \theta}+\frac{\partial \bar{v}_r \bar{v}_z}{\partial z}+\frac{\bar{v}_r^2-\bar{v}_\theta^2}{r}=\bar{f}_r-\frac{1}{\rho}\frac{\partial \bar{p}}{\partial r}$$
$$+E\left[\frac{\partial^2 \bar{v}_r}{\partial r^2}+\frac{1}{r^2}\frac{\partial^2 \bar{v}_r}{\partial \theta^2}+\frac{\partial^2 \bar{v}_r}{\partial z^2}+\frac{1}{r}\frac{\partial \bar{v}_r}{\partial r}-\frac{2}{r^2}\frac{\partial \bar{v}_\theta}{\partial \theta}-\frac{\bar{v}_r}{r^2}\right]$$
$$-\left(\frac{\partial \overline{v'_r v'_r}}{\partial r}+\frac{1}{r}\frac{\partial \overline{v'_r v'_\theta}}{\partial \theta}+\frac{\partial \overline{v'_r v'_z}}{\partial z}\right)-\frac{\left(\overline{v'_r v'_r}-\overline{v'_\theta v'_\theta}\right)}{r}$$

Time averaged expression of the momentum equation in the $\theta-$direction (3.34) is analogously derived to that in the $r-$ direction and results in:

$\theta-$ direction momentum

$$\frac{\partial \bar{v}_\theta}{\partial t}+\frac{\partial\left(\bar{v}_r \bar{v}_\theta\right)}{\partial r}+\frac{1}{r}\frac{\partial\left(\bar{v}_\theta^2\right)}{\partial \theta}+\frac{\partial\left(\bar{v}_\theta \bar{v}_z\right)}{\partial z}+\frac{2\bar{v}_r \bar{v}_\theta}{r}=\bar{f}_\theta-\frac{1}{\rho}\frac{\partial \bar{p}}{r\partial \theta}$$
$$+E_\theta\left(\frac{\partial^2 \bar{v}_\theta}{\partial r^2}+\frac{1}{r}\frac{\partial \bar{v}_\theta}{\partial r}+\frac{1}{r^2}\frac{\partial^2 \bar{v}_\theta}{\partial \theta^2}+\frac{\partial^2 \bar{v}_\theta}{\partial z^2}+\frac{2}{r^2}\frac{\partial \bar{v}_r}{\partial \theta}-\frac{\bar{v}_\theta}{r^2}\right) \qquad (3.54)$$
$$-\left(\frac{\partial \overline{v'_r v'_\theta}}{\partial r}+\frac{1}{r}\frac{\partial \overline{v'_\theta v'_\theta}}{\partial \theta}+\frac{\partial \overline{v'_\theta v'_z}}{\partial z}\right)-\frac{2\overline{v'_r v'_\theta}}{r}$$

A similar approach applied to the hydrostatic pressure equation (3.28) results in:

$z-$ direction momentum:

$$\frac{1}{\rho}\frac{\partial \bar{p}}{\partial z}=-g \qquad (3.55)$$

A quick look at the 3D momentum equations (3.53)-(3.55) written in cylindrical co-ordinates (r,θ,z) reveals two extra terms due to the curvature of the grid in the angular direction. In the $r-$direction the two extra terms are: $-\bar{v}_\theta^2/r$ in the advection term, and $\left(-2\partial \bar{v}_\theta/r^2\partial\theta\right)$ in the turbulence term. First term shows that magnitude of the advective acceleration term is influenced by the bending grid line normal to the flow which is proportional to the squared velocity in the angular direction, as dictated by the first derivative of the scale factor with respect to direction of flow. This term is called a source term. Second term

results from evaluation of the cross-derivatives in the turbulence term. The term $\left(-2\partial\overline{v}_\theta / r^2 \partial\theta\right)$ shows that turbulence in the radial direction is affected by a term proportional to the rate of change of angular velocity in the direction normal to the flow.

The Reynolds averaging concept can be applied to the continuity equation (3.26) written in terms of instantaneous velocities as:

$$\frac{\partial}{\partial r}\left(\overline{v}_r + v'_r\right) + \frac{1}{r}\left(\overline{v}_r + v'_r\right) + \frac{1}{r}\frac{\partial}{\partial\theta}\left(\overline{v}_\theta + v'_\theta\right) + \frac{\partial}{\partial z}\left(\overline{v}_z + v'_z\right) = 0 \tag{3.56a}$$

$$\frac{\partial}{\partial r}\overline{\left(\overline{v}_r + v'_r\right)} + \frac{1}{r}\overline{\left(\overline{v}_r + v'_r\right)} + \frac{1}{r}\frac{\partial}{\partial\theta}\overline{\left(\overline{v}_\theta + v'_\theta\right)} + \frac{\partial}{\partial z}\overline{\left(\overline{v}_z + v'_z\right)} = 0 \tag{3.56b}$$

where:

$$\overline{\left(\overline{v}_r + v'_r\right)} = \frac{1}{t_2 - t_1}\int_{t_1}^{t_2}\left(\overline{v}_r + v'_r\right)dt = \overline{v}_r$$

$$\overline{\left(\overline{v}_\theta + v'_\theta\right)} = \frac{1}{t_2 - t_1}\int_{t_1}^{t_2}\left(\overline{v}_\theta + v'_\theta\right)dt = \overline{v}_\theta$$

$$\overline{\left(\overline{v}_z + v'_z\right)} = \frac{1}{t_2 - t_1}\int_{t_1}^{t_2}\left(\overline{v}_z + v'_z\right)dt = \overline{v}_z$$

and gives:

$$\frac{\partial\overline{v}_r}{\partial r} + \frac{1}{r}\overline{v}_r + \frac{1}{r}\frac{\partial\overline{v}_\theta}{\partial\theta} + \frac{\partial\overline{v}_z}{\partial z} = 0 \tag{3.57}$$

or

$$\frac{1}{r}\frac{\partial\left(r\overline{v}_r\right)}{\partial r} + \frac{1}{r}\frac{\partial\overline{v}_\theta}{\partial\theta} + \frac{\partial\overline{v}_z}{\partial z} = 0 \tag{3.58}$$

In equations (3.53), (3.54), (3.55) and (3.58), the time averaged values of velocity, $\overline{v}_i$, $i = r, \theta, z$ and pressure, $\overline{p}$, replace the instantaneous quantities $\tilde{v}_i$, $\tilde{p}$ in equations (3.31), (3.34), (3.28) and (3.26). The additional term $(-\overline{v_i' v_j'})$,

$i = r, \theta, z$, $j = r, \theta, z$ on the right hand side of the averaged momentum equations (3.53) and (3.54) is called Reynolds stress and describes the transport of x_i - momentum in the x_j - direction (or vice versa). The assumption for the previous considerations is that density is uniform, so that the generality is not lost if $\rho = 1$. In the laminar flow, their value is zero. Both the transport of momentum and mass by turbulent motion terms are due to the nonlinearity of the Navier-Stokes equations (3.31) and (3.34).

3.3.4. Turbulence Modelling

Equations (3.48), (3.49), (3.50) and (3.53) represent an example of the closure problem of turbulence because they do not constitute a closed set. The derivation of the Reynolds stresses doesn't solve the turbulence closure problem due to the introduction of new unknowns in the higher order correlations. The modelling turbulence theory defines the turbulent fluxes using known or determinable variables and solves the previously presented problem.

There are two categories of turbulence transport models:
- the first class uses eddy viscosity concept;
- the second group solves directly the transport equations for the shear stresses ($-\overline{v_i' v_j'}$) and describes a second-order closure scheme.

In the present derivation of the hydrodynamic equations the first class of models is chosen, based on the advantages offered by the method in terms of computational time and stability of calculations. Eddy viscosity is the concept developed through an analogy between molecular and turbulent motions. The approach was proposed by Boussinesq [Boussinesq (1877)]. It is derived from the expression giving the proportionality between the turbulent viscosity and the gradient of the mean velocity:

$$-\overline{v_i' v_j'} = E_t \frac{1}{2}\left(v_{j,i} + v_{i,j}\right) - \frac{2}{3} k \delta_{ij} \tag{3.59}$$

where:

E_t is the turbulent or eddy viscosity;

δ_{ij} is the Kronecker delta;

k is the kinetic energy of turbulence defined as:

$k = \frac{1}{2}\overline{v_i' v_j'} = \frac{1}{2}\left(\overline{v_r'^2} + \overline{v_\theta'^2} + \overline{v_z'^2}\right)$.

The normal stresses in the equation (3.59), ignoring the kinetic energy of turbulence, are given by:

$$-\overline{v_i' v_i'} = -2E_t v^i_{,i} \tag{3.60}$$

the sum of which is zero because of the continuity equation.

A turbulent viscosity expression, originating from dimensional analysis, is given by:

$$E_t \propto \tilde{V} L \tag{3.61}$$

Generally, both L (the characteristic turbulent length) and $\tilde{V}$ (the velocity of the transport) that represent the size of eddies transporting momentum need to be determined. In zero-equation models $\tilde{V}$ is the mean flow velocity or its gradients and L is the empirical characteristic flow dimension.

3.4. Depth Integration of the Hydrodynamic Equations in Cylindrical Co-ordinates

Depth integration of the three-dimensional equations governing water motion is performed for flows that show little variation on the vertical direction, i.e. vertical variation of velocities can be postulated by a logarithmic law [Figure 3.7]. Hence, a simplification of the system of equations to be solved is

performed. Vertical integration is performed between free surface (ζ) and bed ($-h$), represented in Figure 3.3. For convenience, the over bars indicating time averaging of the governing equations are dropped.

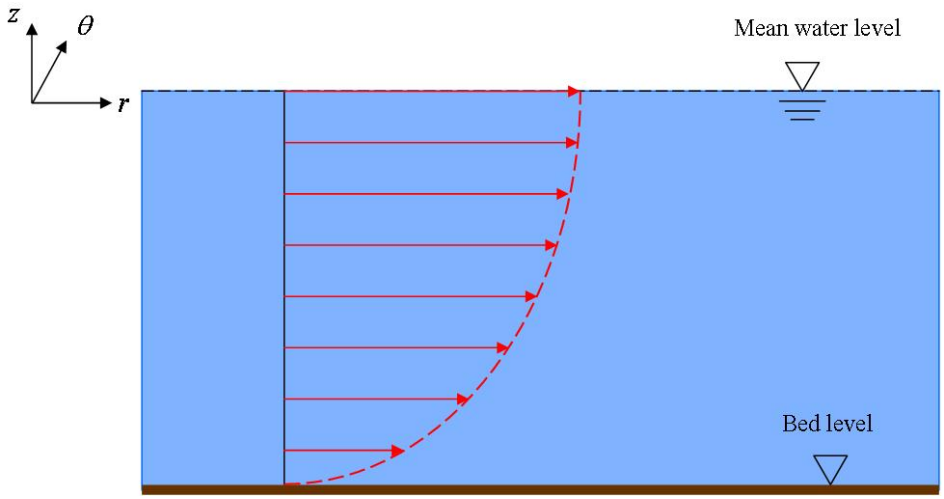

Figure 3.7: Three-dimensional vertical variation of velocity components approximated by a logarithmic law.

Velocity components in the three-dimensional cylindrical co-ordinate system (v_r, v_θ, v_z) reduce to two-dimensional depth averaged velocity components in the (r, θ) plane [Figure 3.8]:

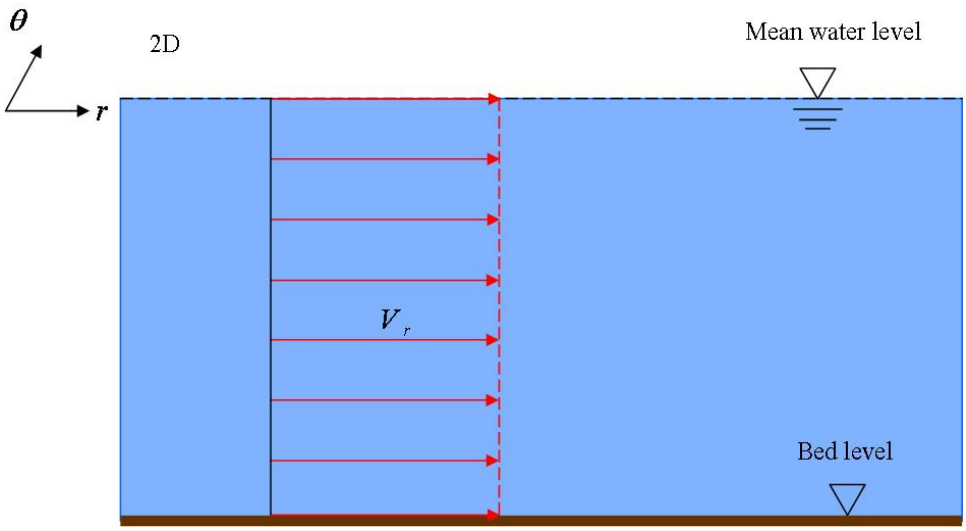

Figure 3.8: Depth integrated velocity in the $r-$direction.

$V_r = \frac{1}{H}\int_{-h}^{\zeta} v_r dz$ is the depth averaged velocity in $r-$direction

$V_\theta = \frac{1}{H}\int_{-h}^{\zeta} v_\theta dz$ is the depth averaged velocity in $\theta-$direction

where:

$H = \zeta + h$ is the total depth

ζ is the water surface elevation

$-h$ is the water depth as measured from the mean water level.

3.4.1. Depth Integration of the Continuity Equation

Depth integration of the continuity equation (3.58) gives:

$$\int_{-h}^{\zeta}\left[\frac{1}{r}\frac{\partial(rv_r)}{\partial r}+\frac{1}{r}\frac{\partial v_\theta}{\partial \theta}+\frac{\partial v_z}{\partial z}\right]dz = 0 \tag{3.62}$$

$$\int_{-h}^{\zeta}\left[\frac{1}{r}\frac{\partial(rv_r)}{\partial r}+\frac{1}{r}\frac{\partial v_\theta}{\partial \theta}\right]dz + v_{z\zeta} - (v_z)_{-h} = 0 \tag{3.63}$$

where: $\int_{-h}^{\zeta}\frac{\partial v_z}{\partial z}dz = (v_z)_\zeta - (v_z)_{-h}$.

Applying Leibnitz's rule:

$$\int_a^b \frac{\partial f(x,y)}{\partial y} = \frac{\partial}{\partial y}\int_a^b f(x,y)dx - f(b,y)\frac{\partial b}{\partial y} + f(a,y)\frac{\partial a}{\partial y} \tag{3.64}$$

where:

$$\int_{-h}^{\zeta}\frac{1}{r}\frac{\partial(rv_r)}{\partial r}dz = \frac{1}{r}\left[\frac{\partial}{\partial r}\int_{-h}^{\zeta}(rv_r)dz - (rv_r)_\zeta\frac{\partial \zeta}{\partial r} + (rv_r)_{-h}\frac{\partial(-h)}{\partial r}\right] \tag{3.65a}$$

$$\int_{-h}^{\zeta}\frac{1}{r}\frac{\partial v_\theta}{\partial\theta}dz=\frac{1}{r}\left[\frac{\partial}{\partial\theta}\int_{-h}^{\zeta}v_\theta dz-(v_\theta)_\zeta\frac{\partial\zeta}{\partial\theta}+(v_\theta)_{-h}\frac{\partial(-h)}{\partial\theta}\right] \tag{3.65b}$$

gives:

$$\begin{aligned}&\frac{1}{r}\frac{\partial}{\partial r}\int_{-h}^{\zeta}(rv_r)dz+\frac{1}{r}\frac{\partial}{\partial\theta}\int_{-h}^{\zeta}v_\theta dz-\frac{1}{r}(rv_r)_\zeta\left.\frac{\partial\zeta}{\partial r}\right|_\zeta+\frac{1}{r}(rv_r)_{-h}\left.\frac{\partial(-h)}{\partial r}\right|_{-h}\\&-(v_\theta)_\zeta\frac{1}{r}\left.\frac{\partial\zeta}{\partial\theta}\right|_\zeta+(v_\theta)_{-h}\frac{1}{r}\left.\frac{\partial(-h)}{\partial\theta}\right|_{-h}+(v_z)_\zeta-(v_z)_{-h}=0\end{aligned} \tag{3.66}$$

Since radius r is not a function of the water depth $(H=\zeta+h)$, equation (3.66) becomes:

$$\begin{aligned}&\frac{1}{r}\frac{\partial}{\partial r}\left(r\int_{-h}^{\zeta}v_r dz\right)+\frac{1}{r}\frac{\partial}{\partial\theta}\int_{-h}^{\zeta}v_\theta dz-(v_r)_\zeta\left.\frac{\partial\zeta}{\partial r}\right|_\zeta+(v_r)_{-h}\left.\frac{\partial(-h)}{\partial r}\right|_{-h}\\&-\frac{1}{r}(v_\theta)_\zeta\left.\frac{\partial\zeta}{\partial\theta}\right|_\zeta+\frac{1}{r}(v_\theta)_{-h}\left.\frac{\partial(-h)}{\partial\theta}\right|_{-h}+(v_z)_\zeta-(v_z)_{-h}=0\end{aligned} \tag{3.67}$$

At bed a no-slip boundary condition, which states that velocities at the impermeable bed are zero, can be employed:

$$(v_r)_{-h}=(v_\theta)_{-h}=(v_z)_{-h}=0 \tag{3.68}$$

reducing equation (3.67) to:

$$\begin{aligned}&\frac{1}{r}\frac{\partial}{\partial r}\left(r\int_{-h}^{\zeta}v_r dz\right)+\frac{1}{r}\frac{\partial}{\partial\theta}\int_{-h}^{\zeta}v_\theta dz-(v_r)_\zeta\left.\frac{\partial\zeta}{\partial r}\right|_\zeta-\frac{1}{r}(v_\theta)_\zeta\left.\frac{\partial\zeta}{\partial\theta}\right|_\zeta\\&+(v_z)_\zeta=0\end{aligned} \tag{3.69}$$

At the surface a kinematic condition is used to express the vertical velocity component as the total differential of the free surface with respect to time and assume that no fluid particle crosses the surface [Lamb (1932)]:

$$\frac{D\zeta}{Dt} = \left[\frac{\partial\zeta}{\partial t} + \frac{\partial\zeta}{\partial r}\frac{\partial r}{\partial t} + \frac{1}{r}\frac{\partial\zeta}{\partial\theta}\frac{\partial\theta}{\partial t}\right]_{\zeta}$$
$$= \left[\frac{\partial\zeta}{\partial t} + v_r\frac{\partial\zeta}{\partial r} + \frac{1}{r}v_\theta\frac{\partial\zeta}{\partial\theta}\right]_{\zeta} \quad (3.70)$$
$$= (v_z)_{\zeta}$$

$$(v_z)_{\zeta} - (v_r)_{\zeta}\left.\frac{\partial\zeta}{\partial r}\right|_{\zeta} - \frac{1}{r}(v_\theta)_{\zeta}\left.\frac{\partial\zeta}{\partial\theta}\right|_{\zeta} = \frac{\partial\zeta}{\partial t} \quad (3.71)$$

Equation (3.71) can be further introduced in equation (3.69):

$$\frac{1}{r}\frac{\partial}{\partial r}\left(r\int_{-h}^{\zeta} v_r dz\right) + \frac{1}{r}\frac{\partial}{\partial\theta}\int_{-h}^{\zeta} v_\theta dz + \frac{\partial\zeta}{\partial t} = 0 \quad (3.72)$$

to give the depth integrated continuity equation in cylindrical polar coordinates:

$$\frac{\partial\zeta}{\partial t} + \frac{1}{r}\frac{\partial(rV_rH)}{\partial r} + \frac{1}{r}\frac{\partial(V_\theta H)}{\partial\theta} = 0 \quad (3.73)$$

3.4.2. Depth Integration of the $r-$ direction Momentum Equation

Integration of the Reynolds averaged $r-$direction momentum equation (3.53) over the water depth between $-h$ (bed) and ζ (surface) can be written:

$r-$direction momentum

$$\int_{-h}^{\zeta}\frac{\partial v_r}{\partial t}dz + \int_{-h}^{\zeta}\frac{\partial v_r^2}{\partial r}dz + \int_{-h}^{\zeta}\frac{1}{r}\frac{\partial v_r v_\theta}{\partial\theta}dz + \int_{-h}^{\zeta}\frac{\partial v_r v_z}{\partial z}dz$$
$$+ \int_{-h}^{\zeta}\frac{v_r^2}{r}dz - \int_{-h}^{\zeta}\frac{\overline{v'_r v'_r}}{r}dz - \int_{-h}^{\zeta}\frac{v_\theta^2}{r}dz + \int_{-h}^{\zeta}\frac{\overline{v'_\theta v'_\theta}}{r}dz = \quad (3.74)$$

$$\int_{-h}^{\zeta} f_C v_\theta dz - \int_{-h}^{\zeta} \frac{1}{\rho}\frac{\partial p}{\partial r} dz + \int_{-h}^{\zeta} \frac{\partial}{\partial r}\left(E\frac{\partial v_r}{\partial r} - \overline{v'_r\, v'_r} \right) dz$$
$$+ \int_{-h}^{\zeta} \frac{1}{r}\frac{\partial}{\partial \theta}\left(\frac{1}{r} E\frac{\partial v_r}{\partial \theta} - \overline{v'_r\, v'_\theta} \right) dz + \int_{-h}^{\zeta} \frac{\partial}{\partial z}\left(E\frac{\partial v_r}{\partial z} - \overline{v'_r\, v'_z} \right) dz$$
$$+ \int_{-h}^{\zeta} \frac{1}{r} E\frac{\partial v_r}{\partial r} dz - \int_{-h}^{\zeta} \frac{2}{r^2} E\frac{\partial v_\theta}{\partial \theta} dz - \int_{-h}^{\zeta} E\frac{v_r}{r^2} dz$$

In equation (3.74) the over bars indicating time averaging of the instantaneous variables were dropped for convenience.

In cylindrical co-ordinates the Reynolds normal and shear stresses can be written, after evaluating them similar to equation (3.59), as:

$$-\rho\overline{v_r' v_r'} = 2\lambda_t\left(\frac{\partial v_r}{\partial r}\right) - \frac{2}{3}k \tag{3.75a}$$

$$-\rho\overline{v_\theta' v_\theta'} = 2\lambda_t\left(\frac{1}{r}\frac{\partial v_\theta}{\partial \theta} + \frac{v_r}{r}\right) - \frac{2}{3}k \tag{3.75b}$$

$$-\rho\overline{v_z' v_z'} = 2\lambda_t\left(\frac{\partial v_z}{\partial z}\right) - \frac{2}{3}k \tag{3.75c}$$

$$-\rho\overline{v_r' v_\theta'} = \lambda_t\left(\frac{\partial v_\theta}{\partial r} - \frac{v_\theta}{r} + \frac{1}{r}\frac{\partial v_r}{\partial \theta}\right) \tag{3.75d}$$

$$-\rho\overline{v_r' v_z'} = \lambda_t\left(\frac{\partial v_z}{\partial r} + \frac{\partial v_r}{\partial z}\right) \tag{3.75e}$$

$$-\rho\overline{v_\theta' v_z'} = \lambda_t\left(\frac{\partial v_\theta}{\partial z} + \frac{1}{r}\frac{\partial v_z}{\partial \theta}\right) \tag{3.75f}$$

where:

λ_t is the absolute eddy viscosity $\lambda_t = \rho E_t$;

k is the turbulent kinetic energy;

E_t is the eddy viscosity (similar to the kinematic viscosity E, which determines the extent to which fluid flow exhibits turbulence). In general, for turbulent flows: $E_t >> E$ [Goodwin (1988)], and $\lambda_t >> \rho E$.

The two dimensional depth-integrated form of the $r-$direction momentum equation becomes equation (A7.24):

$$
\begin{aligned}
&r-\text{direction momentum}\\
&\frac{\partial V_r H}{\partial t}+\beta\left[\frac{\partial\left(V_r^2 H\right)}{\partial r}+\frac{1}{r}\frac{\partial\left(V_r V_\theta H\right)}{\partial\theta}+\frac{V_r^2 H-V_\theta^2 H}{r}\right]=\\
&f_C V_\theta H-gH\frac{\partial\zeta}{\partial r}+\frac{1}{\rho}\tau_{rw}-\frac{1}{\rho}\tau_{rb}\\
&+\frac{\partial}{\partial r}\left[\left(E+2\overline{E}_t\right)H\frac{\partial V_r}{\partial r}\right]+\frac{1}{r}\frac{\partial}{\partial\theta}\left[\frac{1}{r}\left(E+\overline{E}_t\right)H\frac{\partial V_r}{\partial\theta}+\overline{E}_t H\frac{\partial V_\theta}{\partial r}\right]\\
&-\frac{1}{r^2}\left(3\overline{E}_t+2E\right)H\frac{\partial V_\theta}{\partial\theta}+\frac{1}{r}\left(E+2\overline{E}_t\right)H\frac{\partial V_r}{\partial r}-\frac{1}{r^2}\left(E+2\overline{E}_t\right)HV_r
\end{aligned}
\tag{3.76}
$$

The stresses resulted from depth averaging are difficult to quantify and can be neglected [Molls and Chaundray (1995)]. Hence, the depth averaged turbulent kinetic energy variation with respect to any horizontal direction is neglected: $2\partial\left(\overline{k}H\right)/3\partial r\approx 0$ in equation (3.76).

For the kinematic viscosity (E) and eddy viscosity ($\overline{E}_t$) terms, Falconer (1976) proposed a generalised version of Prandtl's mixing length. The approach is applicable to cases where neither the mean nor the turbulent motions are confined to two dimensions. An assumption is employed in this case, which states that one particular component of the mean rate deformation tensor is much greater than the others. Subsequently, the Reynolds stresses are approximated by equations (3.70). A form of the mean eddy viscosity ($\overline{E}$) is given in equation (3.77), which can replace the sum of kinematic viscosity E and turbulent viscosity $\overline{E}_t$:

$$
\overline{E}=\frac{k\sqrt{g}\sqrt{\left(V_r^2+V_\theta^2\right)}}{6C}H^2 \tag{3.77}
$$

Hence, equation (3.76) becomes:

$r-$direction momentum

$$\frac{\partial V_r H}{\partial t}+\beta\left[\frac{\partial\left(V_r^2 H\right)}{\partial r}+\frac{1}{r}\frac{\partial\left(V_r V_\theta H\right)}{\partial\theta}+\frac{V_r^2 H-V_\theta^2 H}{r}\right]=$$
$$f_C V_\theta H-gH\frac{\partial\zeta}{\partial r}+\frac{1}{\rho}\tau_{rw}-\frac{1}{\rho}\tau_{rb}$$
$$+2\frac{\partial}{\partial r}\left(\overline{E}H\frac{\partial V_r}{\partial r}\right)+\frac{1}{r}\frac{\partial}{\partial\theta}\left(\frac{1}{r}\overline{E}H\frac{\partial V_r}{\partial\theta}\right)+\frac{1}{r}\frac{\partial}{\partial\theta}\left(\overline{E}H\frac{\partial V_\theta}{\partial r}\right) \tag{3.78}$$
$$-\frac{3}{r^2}\overline{E}H\frac{\partial V_\theta}{\partial\theta}+\frac{2}{r}\overline{E}H\frac{\partial V_r}{\partial r}-\frac{2}{r^2}\overline{E}HV_r$$

3.4.3. Depth Integration of the $\theta-$ direction Momentum Equation

Depth integration of Reynolds averaged equation (3.54) is written as:

$\theta-$direction momentum

$$\int_{-h}^{\zeta}\frac{\partial v_\theta}{\partial t}dz+\int_{-h}^{\zeta}\frac{\partial v_r v_\theta}{\partial r}dz+\int_{-h}^{\zeta}\frac{1}{r}\frac{\partial v_\theta^2}{\partial\theta}dz+\int_{-h}^{\zeta}\frac{\partial v_z v_\theta}{\partial z}dz$$
$$+\int_{-h}^{\zeta}2\left(\frac{v_r v_\theta}{r}-\frac{\overline{v'_r\,v'_\theta}}{r}\right)dz$$
$$=-\int_{-h}^{\zeta}f_C v_r dz-\int_{-h}^{\zeta}\frac{1}{\rho r}\frac{\partial p}{\partial\theta}dz+\int_{-h}^{\zeta}\frac{\partial}{\partial r}\left(E\frac{\partial v_\theta}{\partial r}-\overline{v'_r\,v'_\theta}\right)dz \tag{3.79}$$
$$+\int_{-h}^{\zeta}\frac{1}{r}\frac{\partial}{\partial\theta}\left(\frac{1}{r}E\frac{\partial v_\theta}{\partial\theta}-\overline{v'_\theta\,v'_\theta}\right)dz+\int_{-h}^{\zeta}\frac{\partial}{\partial z}\left(E\frac{\partial v_\theta}{\partial z}-\overline{v'_\theta\,v'_z}\right)dz$$
$$+\int_{-h}^{\zeta}\frac{1}{r}E\frac{\partial v_\theta}{\partial r}dz+\int_{-h}^{\zeta}\frac{2}{r^2}E\frac{\partial v_r}{\partial\theta}dz-\int_{-h}^{\zeta}E\frac{v_\theta}{r^2}dz$$

Following the approach presented in section 3.5.2, the depth integrated form of the momentum equation in the $\theta-$ direction becomes:

θ – direction momentum

$$\begin{aligned}
&\frac{\partial V_\theta H}{\partial t}+\beta\left[\frac{\partial\left(V_r V_\theta H\right)}{\partial r}+\frac{1}{r}\frac{\partial\left(V_\theta V_\theta H\right)}{\partial\theta}+2\frac{V_r V_\theta H}{r}\right]\\
&=-f_C V_r H-gH\frac{1}{r}\frac{\partial\zeta}{\partial\theta}+\frac{1}{\rho}\left(\tau_{\theta w}-\tau_{\theta b}\right)\\
&+\frac{\partial}{\partial r}\left[\left(EH+\overline{E}_t H\right)\frac{\partial V_\theta}{\partial r}\right]+\frac{1}{r^2}\frac{\partial}{\partial\theta}\left[\left(EH+2\overline{E}_t H\right)\frac{\partial V_\theta}{\partial\theta}\right]\\
&+\frac{1}{r}\left[\left(2\overline{E}_t H+EH\right)\frac{\partial V_\theta}{\partial r}\right]-\frac{\partial}{\partial r}\left[\overline{E}_t H\frac{V_\theta}{r}\right]-\frac{1}{r^2}\left(EH+2\overline{E}_t H\right)V_\theta\\
&+\left(\overline{E}_t H+EH\right)\frac{2}{r^2}\frac{\partial V_r}{\partial\theta}+\frac{2}{r^2}\frac{\partial}{\partial\theta}\left[\overline{E}_t H V_r\right]+\frac{\partial}{\partial r}\left[\overline{E}_t H\frac{1}{r}\frac{\partial V_r}{\partial\theta}\right]
\end{aligned}\tag{3.80}$$

Assuming that for turbulent flows eddy viscosity is much larger than kinetic viscosity and using equation (3.77), equation (3.80) becomes:

θ – direction momentum

$$\begin{aligned}
&\frac{\partial V_\theta H}{\partial t}+\beta\left[\frac{\partial\left(V_r V_\theta H\right)}{\partial r}+\frac{1}{r}\frac{\partial\left(V_\theta V_\theta H\right)}{\partial\theta}+2\frac{V_r V_\theta H}{r}\right]\\
&=-f_C V_r H-gH\frac{1}{r}\frac{\partial\zeta}{\partial\theta}+\frac{1}{\rho}\left(\tau_{\theta w}-\tau_{\theta b}\right)\\
&+\frac{\partial}{\partial r}\left(\overline{E}H\frac{\partial V_\theta}{\partial r}\right)+\frac{2}{r^2}\frac{\partial}{\partial\theta}\left(\overline{E}H\frac{\partial V_\theta}{\partial\theta}\right)\\
&+\frac{2}{r}\left(\overline{E}H\frac{\partial V_\theta}{\partial r}\right)-\frac{1}{r}\frac{\partial}{\partial r}\left(\overline{E}HV_\theta\right)+\frac{1}{r^2}\overline{E}HV_\theta-\frac{2}{r^2}\overline{E}HV_\theta\\
&+\overline{E}H\frac{2}{r^2}\frac{\partial V_r}{\partial\theta}+\frac{2}{r^2}\frac{\partial}{\partial\theta}\left(\overline{E}HV_r\right)+\frac{1}{r}\frac{\partial}{\partial r}\left(\overline{E}H\frac{\partial V_r}{\partial\theta}\right)\\
&-\frac{1}{r^2}\frac{\partial}{\partial\theta}\left(\overline{E}H\frac{\partial V_r}{\partial\theta}\right)
\end{aligned}\tag{3.81}$$

Equations (3.73), (3.78) and (3.81) describe the velocity distribution and water elevation variation in the horizontal plane. The effect of turbulence within the depth integrated Navier-Stokes and continuity equations was reduced to bed shear stresses ($\tau_{rb,}\tau_{\theta b}$), wind stresses ($\tau_{rw,}\tau_{\theta w}$), and a mean viscosity term ($\overline{E}$). Next, some formulas for evaluation of bed and wind stresses are presented, whereas for the viscosity term a constant value is assumed.

3.4.4. Evaluation of Bed and Wind Shear Stresses

A quadratic friction law can be employed for approximation of the bed shear stress components. For example, in the $r-$ direction the bed shear stress component (τ_{rb}) is:

$$\tau_{rb} = C_d \rho V_r V \tag{3.82}$$

where:

C_d is the bed drag coefficient;

V_r is the depth-averaged velocity in the $r-$ direction;

$V = \sqrt{V_r^2 + V_\theta^2}$ is the depth-averaged total velocity.

The bed drag coefficient can be expressed as a function of the friction coefficient (C_f):

$$C_d = \frac{C_f}{2} \tag{3.83}$$

where:

$$C_f = \frac{2g}{C^2} \tag{3.84}$$

C is the Chezy roughness coefficient. It can be established using either Colebrook-White formula:

$$C = \sqrt{\frac{2g}{C_f}} = -32 \log_{10}\left(\frac{k_s}{12H} + \frac{5C}{\mathrm{Re}\sqrt{32g}} \right) \tag{3.85}$$

or Manning's equation:

$$C = \frac{H^{1/6}}{n} \tag{3.86}$$

The terms involved in Colebrook-White formula have the following meaning:

k_s is Nikuradse equivalent sand roughness size;

$\mathrm{Re} = \frac{VH}{E}$ is Reynolds number for wide channels (V is the depth-averaged total velocity; H is the flow depth; E is the kinematic viscosity). Turbulent flows occur at Reynolds numbers greater than 500.

Manning's roughness coefficient (n) varies between 0.015 and 0.04. When the bed roughness is known in terms of Manning's coefficient, the roughness k_s, expressed in meters, can be given by:

$$k_s = 0.3048\left(\frac{n}{0.031}\right)^6 \tag{3.87}$$

The wind shear stress in the $r-$ direction τ_{rw} can be similarly obtained from a quadratic friction law. Its expression is:

$$\tau_{rw} = \gamma \rho_a W_r W \tag{3.88}$$

where:

$\gamma = 0.0026$ is the air-water resistance coefficient;

$\rho_a = 1.25 kg/m^3$ is the air density;

W_r is the wind velocity component in the $r-$direction at 10m above surface;

$W = \sqrt{W_r^2 + W_\theta^2}$ is wind speed at 10m above surface.

3.4.5. Approximations for Evaluation of the Turbulence Term

The terms multiplied by the mean eddy viscosity in equations (3.78) and (3.81) respectively can be reduced to the laplacian component of velocity vector in the respective direction. Following Falconer and Chen (1996) within a Cartesian co-ordinate system these terms can be written in the $x-$ direction:

$$\begin{aligned} &2\frac{\partial}{\partial x}\left(\overline{E}H\frac{\partial U}{\partial x}\right)+\frac{\partial}{\partial y}\left[\overline{E}H\left(\frac{\partial U}{\partial y}+\frac{\partial V}{\partial x}\right)\right]= \\ &2\overline{E}H\frac{\partial^2 U}{\partial x^2}+\overline{E}H\frac{\partial}{\partial y}\left(\frac{\partial U}{\partial y}+\frac{\partial V}{\partial x}\right) \\ &+2\frac{\partial \overline{E}H}{\partial x}\frac{\partial U}{\partial x}+\frac{\partial \overline{E}H}{\partial y}\left(\frac{\partial U}{\partial y}+\frac{\partial V}{\partial x}\right)\cong \overline{E}H\left(\frac{\partial^2 U}{\partial x^2}+\frac{\partial^2 U}{\partial y^2}\right) \end{aligned} \tag{3.89}$$

and in the $y-$ direction, respectively:

$$2\frac{\partial}{\partial y}\left(\overline{E}H\frac{\partial V}{\partial y}\right)+\frac{\partial}{\partial x}\left[\overline{E}H\left(\frac{\partial U}{\partial y}+\frac{\partial V}{\partial x}\right)\right]\cong \overline{E}H\left(\frac{\partial^2 V}{\partial x^2}+\frac{\partial^2 V}{\partial y^2}\right) \tag{3.90}$$

Using equation (3.89), the terms multiplied by $\overline{E}H$ in the $r-$ direction momentum equation (3.78) can be written:

$$\begin{aligned} &r-\text{direction} \\ &2\frac{\partial}{\partial r}\left[\frac{1}{r}\overline{E}H\frac{\partial(rV_r)}{\partial r}\right]+\frac{1}{r}\frac{\partial}{\partial \theta}\left[\frac{1}{r}\overline{E}H\frac{\partial V_r}{\partial \theta}+\overline{E}H\frac{\partial V_\theta}{\partial r}\right] \\ &+\frac{1}{r}\frac{\partial}{\partial \theta}\left(\overline{E}_t H\frac{\partial V_\theta}{\partial r}\right)-\frac{3}{r^2}\overline{E}H\frac{\partial V_\theta}{\partial \theta} \\ &\approx \overline{E}H\left\{\frac{\partial}{\partial r}\left[\frac{1}{r}\frac{\partial(rV_r)}{\partial r}\right]+\frac{1}{r^2}\frac{\partial^2 V_r}{\partial \theta^2}-\frac{2}{r^2}\frac{\partial V_\theta}{\partial \theta}\right\} \end{aligned} \tag{3.91}$$

A similar approach can be applied in the $\theta-$ direction momentum equation (3.81), resulting in:

$\theta-$direction

$$\begin{aligned}
&\frac{\partial}{\partial r}\left(\overline{E}H\frac{\partial V_\theta}{\partial r}\right)+\frac{2}{r^2}\frac{\partial}{\partial\theta}\left(\overline{E}H\frac{\partial V_\theta}{\partial\theta}\right)\\
&+\frac{2}{r}\left(\overline{E}H\frac{\partial V_\theta}{\partial r}\right)-\frac{1}{r}\frac{\partial}{\partial r}\left(\overline{E}HV_\theta\right)+\frac{1}{r^2}\overline{E}HV_\theta-\frac{2}{r^2}\overline{E}HV_\theta\\
&+\overline{E}H\frac{2}{r^2}\frac{\partial V_r}{\partial\theta}+\frac{2}{r^2}\frac{\partial}{\partial\theta}\left(\overline{E}HV_r\right)+\frac{1}{r}\frac{\partial}{\partial r}\left(\overline{E}H\frac{\partial V_r}{\partial\theta}\right)\\
&-\frac{1}{r^2}\frac{\partial}{\partial r}\left(\overline{E}H\frac{\partial V_r}{\partial\theta}\right)\\
&\cong\overline{E}H\left\{\frac{\partial}{\partial r}\left[\frac{1}{r}\frac{\partial\left(rV_\theta\right)}{\partial r}\right]+\frac{1}{r^2}\frac{\partial^2V_\theta}{\partial\theta^2}+\frac{2}{r^2}\frac{\partial V_r}{\partial\theta}\right\}
\end{aligned}\tag{3.92}$$

The depth averaged forms of the Navier-Stokes equations in the horizontal directions are obtained as:

$r-$direction momentum

$$\begin{aligned}
&\frac{\partial V_rH}{\partial t}+\beta\left(\frac{\partial V_rV_rH}{\partial r}+\frac{1}{r}\frac{\partial V_rV_\theta H}{\partial\theta}+\frac{V_r^2H-V_\theta^2H}{r}\right)\\
&=f_CV_\theta H-gH\frac{\partial\zeta}{\partial r}+\frac{\rho_a}{\rho}\gamma W_rW-g\frac{V_rV}{C^2}+\\
&+\overline{E}H\left(\frac{\partial^2V_r}{\partial r^2}+\frac{1}{r^2}\frac{\partial^2V_r}{\partial\theta^2}+\frac{1}{r}\frac{\partial V_r}{\partial r}-\frac{2}{r^2}\frac{\partial V_\theta}{\partial\theta}-\frac{V_r}{r^2}\right)
\end{aligned}\tag{3.93}$$

and, respectively:

$\theta-$direction momentum

$$\begin{aligned}
&\frac{\partial V_\theta H}{\partial t}+\beta\left(\frac{\partial V_rV_\theta H}{\partial r}+\frac{1}{r}\frac{\partial V_\theta V_\theta H}{\partial\theta}+2\frac{V_rV_\theta H}{r}\right)=\\
&-f_CV_rH-\frac{1}{r}gH\frac{\partial\zeta}{\partial\theta}+\frac{\rho_a}{\rho}\gamma W_\theta W-g\frac{V_\theta V}{C^2}+\\
&+\overline{E}H\left(\frac{\partial^2V_\theta}{\partial r^2}+\frac{1}{r^2}\frac{\partial^2V_\theta}{\partial\theta^2}+\frac{1}{r}\frac{\partial V_\theta}{\partial r}+\frac{2}{r^2}\frac{\partial V_r}{\partial\theta}-\frac{V_\theta}{r^2}\right)
\end{aligned}\tag{3.94}$$

(3.94) *continued*

Equations (3.73), (3.93) and (3.94) are the mathematical equations governing hydrodynamics and mass conservation written in cylindrical co-ordinates for development of the numerical model in the present research.

3.5. Mapping Transformations

3.5.1. Physical and Computational Grid Generation

Solution of the depth integrated coupled system of equations can be obtained by means of methods already developed for a Cartesian co-ordinate system if proper mapping transformations from the physical onto computational domain [Figure 3.9] are performed. A proper transformation is defined when the Jacobian of the transformation is finite and nonzero [Aris (1989)].

Cylindrical (physical) domain [Figure 3.9a)] is generated based on the relationships:

$$\begin{aligned} x &= r\cos\theta \\ y &= r\sin\theta \end{aligned} \tag{3.95}$$

In the radial direction, for given values of r_0 and r_n the given domain can be discretized for a value Δr set by the user. Analogously, the resolution in the angular direction can be set with given values of θ_0, θ_n and $\Delta\theta$. The maximum number of points in each direction is:

$$\begin{aligned} M &= \frac{r_n - r_0}{\Delta r} + 1 \qquad \text{in the } r-\text{direction} \\ N &= \frac{\theta_n - \theta_0}{\Delta\theta} + 1 \qquad \text{in the } \theta-\text{direction} \end{aligned} \tag{3.96}$$

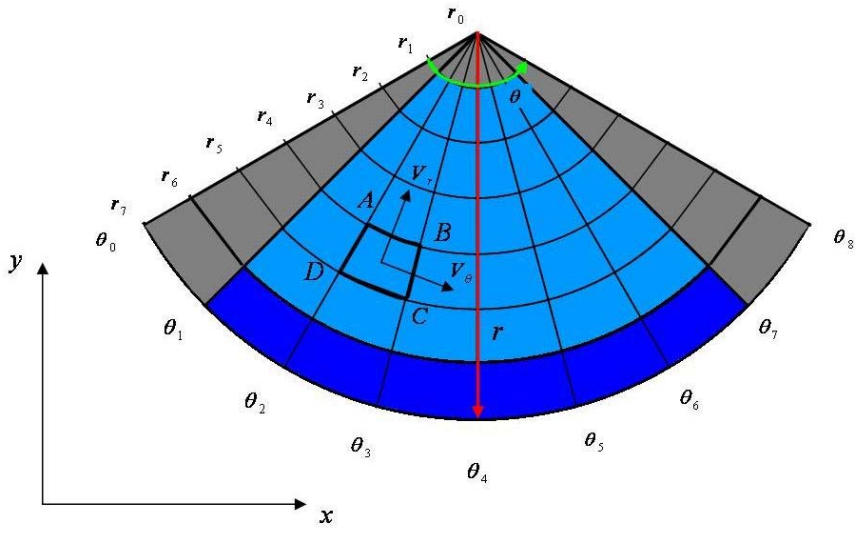

a)

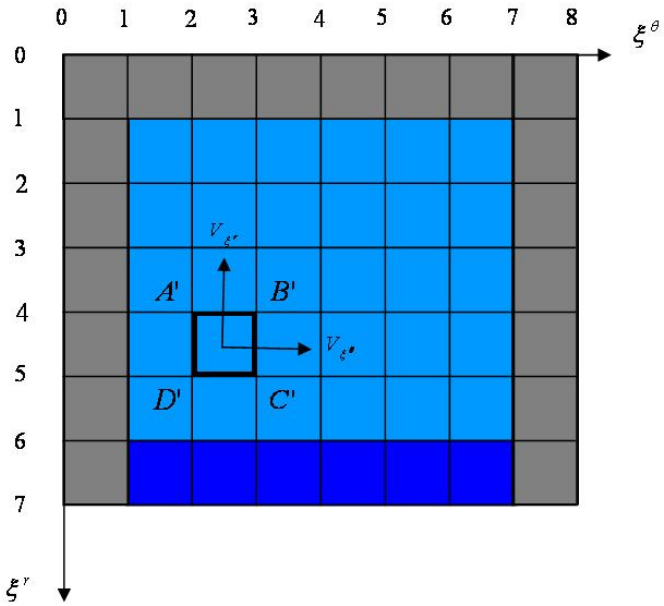

b)

Figure 3.9: Physical (a) and computational (b) plane. Colours representation: grey cells represent land boundaries, light blue cells are for open boundary, darker blue cells illustrate wet cells. r_0 is identical with the pole of the cylindrical co-ordinate system.

First, the radial points are obtained:

$$r_i = r_0 + i(r_i - r_0) \qquad \text{for } i = 1,...,M \tag{3.97}$$

and similarly the points in the angular direction are:

$$\theta_i = \theta_0 + i(\theta_i - \theta_0) \qquad \text{for } j = 1,..., N \tag{3.98}$$

Grid points are next generated in the two directions as:

$$\begin{aligned} x(i, j) &= r_i \cos(\theta_j) \qquad \text{for } i = 1,..., M \,, \quad j = 1,..., N \\ y(i, j) &= r_i \sin(\theta_j) \end{aligned} \tag{3.99}$$

The transformation from (r, θ) physical plane onto (ξ^r, ξ^θ) computational domain can be defined:

$$\begin{aligned} r &= r(\xi^r, \xi^\theta), \ \theta = \theta(\xi^r, \xi^\theta) \\ \xi^r &= \xi^r(r, \theta), \ \xi^\theta = \xi^\theta(r, \theta) \end{aligned} \tag{3.100}$$

A new co-ordinate system can be defined according to the following algebraic relationships [Morinishi et al. (2004)]:

$$\xi^r = \frac{r - r_1}{r_2 - r_1}, \ \Delta r = r_2 - r_1 \tag{3.101}$$

$$r = r_1 + (r_2 - r_1)\xi^r \tag{3.102}$$

$$\xi^\theta = \frac{\theta - \theta_1}{\theta_2 - \theta_1}, \ \Delta\theta = \theta_2 - \theta_1 \tag{3.103}$$

$$\theta = \theta_1 + (\theta_2 - \theta_1)\xi^\theta \tag{3.104}$$

Using equations (3.101) and (3.103), the new co-ordinates ξ^r and ξ^θ are nothing else but the number of the radius and angle, respectively, inside the domain.

Partial derivatives of the old co-ordinates (r, θ) with respect to the new co-ordinates (ξ^r, ξ^θ) can be written as in equation (3.105a), whereas partial derivatives of the new co-ordinates with respect to the cylindrical co-ordinates are given in equation (3.105b).

$$\frac{\partial r}{\partial \xi^r} = \Delta r\,,\ \frac{\partial r}{\partial \xi^\theta} = 0\,,\ \frac{\partial \theta}{\partial \xi^r} = 0\,,\ \frac{\partial \theta}{\partial \xi^\theta} = \Delta\theta \tag{3.105a}$$

$$\frac{\partial \xi^r}{\partial r} = \frac{1}{\Delta r}\,,\ \frac{\partial \xi^r}{\partial \theta} = 0\,,\ \frac{\partial \xi^\theta}{\partial r} = 0\,,\ \frac{\partial \xi^\theta}{\partial \theta} = \frac{1}{\Delta\theta} \tag{3.105b}$$

The scale factors and Jacobian of the transformation are computed using:

$$h_{\xi^r} = \frac{\partial r}{\partial \xi^r} \Leftrightarrow h_{\xi^r} = \Delta r \tag{3.106a}$$

$$h_{\xi^\theta} = r\frac{\partial \theta}{\partial \xi^\theta} \Leftrightarrow h_{\xi^\theta} = r\Delta\theta \tag{3.106b}$$

$$J_\xi = r_{\xi^r} \times r \times \theta_{\xi^\theta} - r_{\xi^\theta} \times r \times \theta_{\xi^r} \tag{3.106c}$$

$$J_\xi = h_{\xi^r} h_{\xi^\theta} \Rightarrow J_\xi = r\frac{\partial r}{\partial \xi^r}\frac{\partial \theta}{\partial \xi^\theta} \tag{3.106d}$$

3.5.2. Transformation Relationships for Equation Equivalence between Physical and Computational Domain

In order to perform the equations transformation, a number of transformation relationships have to be defined for: vector components on the computational plane $\left(V_{\xi^r}, V_{\xi^\theta}\right)$, scalars $\left(f\right)$ and scale factors $\left(h_{\xi^r}, h_{\xi^\theta}\right)$ cross derivatives. These relationships are next defined.

Vector components transform between physical ($r-\theta$) and computational ($\xi^r - \xi^\theta$) planes as [Aris (1989)]:

$$V_{\xi^r} = V_r\frac{h_{\xi^r}}{h_r}\frac{\partial \xi^r}{\partial r} + V_\theta\frac{h_{\xi^r}}{h_\theta}\frac{\partial \xi^r}{\partial \theta} \tag{3.107a}$$

$$V_{\xi^\theta} = V_r\frac{h_{\xi^\theta}}{h_r}\frac{\partial \xi^\theta}{\partial r} + V_\theta\frac{h_{\xi^\theta}}{h_\theta}\frac{\partial \xi^\theta}{\partial \theta} \tag{3.107b}$$

and scalars transform according to [Aris (1989)]:

$$\frac{\partial f}{\partial \xi^r} = \frac{\partial r}{\partial \xi^r}\frac{\partial f}{\partial r} + \frac{\partial \theta}{\partial \xi^r}\frac{1}{r}\frac{\partial f}{\partial \theta} \tag{3.108a}$$

$$\frac{\partial f}{\partial \xi^\theta} = \frac{\partial r}{\partial \xi^\theta}\frac{\partial f}{\partial r} + \frac{\partial \theta}{\partial \xi^\theta}\frac{1}{r}\frac{\partial f}{\partial \theta} \tag{3.108b}$$

Using equations (3.105a), equations (3.108a) and (3.108b) can be written:

$$\frac{1}{h_{\xi^r}}\frac{\partial f}{\partial \xi^r} = \frac{\partial f}{\partial r} \tag{3.109a}$$

$$\frac{1}{h_{\xi^\theta}}\frac{\partial f}{\partial \xi^\theta} = \frac{1}{r}\frac{\partial f}{\partial \theta} \tag{3.109b}$$

The scale factors cross derivation relationships are written as:

$$\frac{1}{J_\xi}\frac{\partial h_{\xi^\theta}}{\partial \xi^r} = \frac{1}{r\Delta r\Delta\theta}\frac{\partial(r\Delta\theta)}{\partial \xi^r} = \frac{1}{r\Delta r\Delta\theta}\Delta\theta\frac{\partial r}{\partial \xi^r} = \frac{1}{r} \tag{3.110a}$$

$$\frac{1}{J_\xi}\frac{\partial h_{\xi^r}}{\partial \xi^\theta} = \frac{1}{r\Delta r\Delta\theta}\frac{\partial(\Delta r)}{\partial \xi^\theta} = 0 \tag{3.110b}$$

3.5.3. Transformation of the Continuity and Navier-Stokes Equations

The partial differential form of the depth integrated continuity equation can be written as:

$$\frac{\partial \zeta}{\partial t} + \frac{1}{J}\frac{\partial(h_\theta V_r H)}{\partial r} + \frac{1}{J}\frac{\partial(h_r V_\theta H)}{\partial \theta} = 0 \tag{3.111}$$

or

$$\frac{\partial \zeta}{\partial t}+\frac{1}{J}\frac{\partial}{\partial r}\left(\frac{J}{h_r}q_r\right)+\frac{1}{J}\frac{\partial}{\partial \theta}\left(\frac{J}{h_\theta}q_\theta\right)=0 \tag{3.112}$$

where: $J=h_r h_\theta$ is the Jacobian of the transformation from cylindrical to Cartesian co-ordinates, the corresponding scale factors being: $h_r=1;\ h_\theta=r$; $q_r=V_r H, q_\theta=V_\theta H$ are the physical components of the discharges per unit width in the $r-$ and $\theta-$direction, respectively ($m^3/s/m$).

The partial differential momentum equations in the radial and angular directions, are given by equations (3.93) and (3.94), respectively. Mapping the NSE onto $\left(\xi^r,\xi^\theta\right)$ plane assumes transformation of the equations into ξ^r,ξ^θ coordinates.

Subsequently, in the new co-ordinate system the continuity equation can be written as:

$$\frac{\partial \zeta}{\partial t}+\frac{1}{J_\xi}\frac{\partial\left(h_{\xi^\theta}q_{\xi^r}\right)}{\partial \xi^r}+\frac{1}{J_\xi}\frac{\partial\left(h_{\xi^r}q_{\xi^\theta}\right)}{\partial \xi^\theta}=0 \tag{3.113}$$

Equations (3.93) and (3.94) become, after performing mapping transformations as shown in Appendix 9:

ξ^r-direction momentum equation

$$\frac{\partial q_{\xi^r}}{\partial t}+\beta\left(\frac{1}{h_{\xi^r}}\frac{\partial V_{\xi^r}q_{\xi^r}}{\partial \xi^r}+\frac{1}{h_{\xi^\theta}}\frac{\partial V_{\xi^\theta}q_{\xi^r}}{\partial \xi^\theta}+\frac{V_{\xi^r}q_{\xi^r}-V_{\xi^\theta}q_{\xi^\theta}}{h_\theta}\right) \tag{3.114}$$

$$=f_C V_{\xi^\theta}H-gH\frac{1}{h_{\xi^r}}\frac{\partial \zeta}{\partial \xi^r}+\frac{\rho_a}{\rho}\gamma W_{\xi^r}W-g\frac{V_{\xi^r}V}{C^2}$$

$$+\overline{E}H\left\{\frac{1}{h_{\xi^r}}\frac{\partial}{\partial \xi^r}\left[\frac{1}{J_\xi}\frac{\partial}{\partial \xi^r}\left(h_{\xi^\theta}V_{\xi^r}\right)\right]+\frac{1}{h_{\xi^\theta}}\frac{\partial}{\partial \xi^\theta}\left[\frac{1}{J_\xi}\frac{\partial\left(h_{\xi^r}V_{\xi^r}\right)}{\partial \xi^\theta}\right]\right.$$

$$\left.+\frac{1}{h_{\xi^r}}\frac{\partial}{\partial \xi^r}\left[\frac{1}{J_\xi}\frac{\partial}{\partial \xi^\theta}\left(h_{\xi^r}V_{\xi^\theta}\right)\right]-\frac{1}{h_{\xi^\theta}}\frac{\partial}{\partial \xi^\theta}\left[\frac{1}{J_\xi}\frac{\partial\left(h_{\xi^\theta}V_{\xi^\theta}\right)}{\partial \xi^r}\right]\right\} \tag{3.114}$$

continued

and, respectively:

ξ^{θ} – direction momentum equation

$$\frac{\partial q_{\xi^{\theta}}}{\partial t}+\beta\left(\frac{1}{h_{\xi^{r}}}\frac{\partial V_{\xi^{r}}q_{\xi^{\theta}}}{\partial\xi^{r}}+\frac{1}{h_{\xi^{\theta}}}\frac{\partial V_{\xi^{\theta}}q_{\xi^{\theta}}}{\partial\xi^{\theta}}+2\frac{V_{\xi^{r}}q_{\xi^{\theta}}}{h_{\theta}}\right)=$$
$$-f_{C}V_{\xi^{r}}H-\frac{1}{h_{\xi^{\theta}}}gH\frac{\partial\zeta}{\partial\xi^{\theta}}+\frac{\rho_{a}}{\rho}\gamma W_{\xi^{\theta}}W-g\frac{V_{\xi^{\theta}}V}{C^{2}}+ \qquad (3.115)$$
$$+\overline{E}H\left\{\frac{1}{h_{\xi^{r}}}\frac{\partial}{\partial\xi^{r}}\left[\frac{1}{J_{\xi}}\frac{\partial\left(h_{\xi^{\theta}}V_{\xi^{\theta}}\right)}{\partial\xi^{r}}\right]+\frac{1}{h_{\xi^{\theta}}}\frac{\partial}{\partial\xi^{\theta}}\left[\frac{1}{J_{\xi}}\frac{\partial}{\partial\xi^{\theta}}\left(h_{\xi^{r}}V_{\xi^{\theta}}\right)\right]\right.$$
$$\left.-\frac{1}{h_{\xi^{r}}}\frac{\partial}{\partial\xi^{r}}\left[\frac{1}{J_{\xi}}\frac{\partial\left(h_{\xi^{r}}V_{\xi^{r}}\right)}{\partial\xi^{\theta}}\right]+\frac{1}{h_{\xi^{\theta}}}\frac{\partial}{\partial\xi^{\theta}}\left[\frac{1}{J_{\xi}}\frac{\partial}{\partial\xi^{r}}\left(h_{\xi^{\theta}}V_{\xi^{r}}\right)\right]\right\}$$

Equations (3.114) and (3.115) are equivalent to writing:

ξ^{r} – direction momentum equation

$$\underbrace{\frac{\partial q_{\xi^{r}}}{\partial t}}_{(1)}+\beta\left\{\underbrace{\frac{1}{J_{\xi}}\left[\frac{\partial}{\partial\xi^{r}}\left(h_{\xi^{\theta}}V_{\xi^{r}}V_{\xi^{r}}H\right)+\frac{\partial}{\partial\xi^{\theta}}\left(h_{\xi^{r}}V_{\xi^{r}}V_{\xi^{\theta}}H\right)\right]}_{(2a)}\right. \qquad (3.116)$$
$$\left.+\underbrace{\frac{V_{\xi^{\theta}}}{J_{\xi}}\left(V_{\xi^{r}}H\frac{\partial h_{\xi^{r}}}{\partial\xi^{\theta}}-V_{\xi^{\theta}}H\frac{\partial h_{\xi^{\theta}}}{\partial\xi^{r}}\right)}_{(2b)}\right\}=$$
$$\underbrace{f_{C}V_{\xi^{\theta}}H}_{(3)}-\underbrace{gH\frac{1}{h_{\xi^{r}}}\frac{\partial\zeta}{\partial\xi^{r}}}_{(4)}+\underbrace{\frac{\rho_{a}}{\rho}\gamma W_{\xi^{r}}W}_{(5)}-\underbrace{g\frac{V_{\xi^{r}}V}{C^{2}}}_{(6)} \qquad (3.116)$$
$$+\overline{E}H\left\{\underbrace{\frac{1}{h_{\xi^{r}}}\frac{\partial}{\partial\xi^{r}}\left[\frac{1}{J_{\xi}}\frac{\partial}{\partial\xi^{r}}\left(h_{\xi^{\theta}}V_{\xi^{r}}\right)\right]+\frac{1}{h_{\xi^{\theta}}}\frac{\partial}{\partial\xi^{\theta}}\left[\frac{1}{J_{\xi}}\frac{\partial\left(h_{\xi^{r}}V_{\xi^{r}}\right)}{\partial\xi^{\theta}}\right]}_{(7a)}\right. \qquad \textit{continued}$$

$$+\underbrace{\frac{1}{h_{\xi^r}}\frac{\partial}{\partial\xi^r}\left[\frac{1}{J_\xi}\frac{\partial}{\partial\xi^\theta}\left(h_{\xi^r}V_{\xi^\theta}\right)\right]-\frac{1}{h_{\xi^\theta}}\frac{\partial}{\partial\xi^\theta}\left[\frac{1}{J_\xi}\frac{\partial\left(h_{\xi^\theta}V_{\xi^\theta}\right)}{\partial\xi^r}\right]}_{(7b)}\Bigg\}$$

and, respectively:

ξ^θ – direction momentum equation

$$\begin{aligned}
&\frac{\partial q_{\xi^\theta}}{\partial t}+\beta\left\{\frac{1}{J_\xi}\left[\frac{\partial}{\partial\xi^r}\left(h_{\xi^\theta}V_{\xi^\theta}V_{\xi^r}H\right)+\frac{\partial}{\partial\xi^\theta}\left(h_{\xi^r}V_{\xi^\theta}V_{\xi^\theta}H\right)\right]\right.\\
&\left.+\frac{V_{\xi^r}}{J_\xi}\left(V_{\xi^\theta}H\frac{\partial h_{\xi^\theta}}{\partial\xi^r}-V_{\xi^r}H\frac{\partial h_{\xi^r}}{\partial\xi^\theta}\right)\right\} \qquad (3.117)\\
&=-f_C V_{\xi^r}H-\frac{1}{h_{\xi^\theta}}gH\frac{\partial\zeta}{\partial\xi^\theta}+\frac{\rho_a}{\rho}\gamma W_{\xi^\theta}W-g\frac{V_{\xi^\theta}V}{C^2}\\
&+\overline{E}H\left\{\frac{1}{h_{\xi^r}}\frac{\partial}{\partial\xi^r}\left[\frac{1}{J_\xi}\frac{\partial\left(h_{\xi^\theta}V_{\xi^\theta}\right)}{\partial\xi^r}\right]+\frac{1}{h_{\xi^\theta}}\frac{\partial}{\partial\xi^\theta}\left[\frac{1}{J_\xi}\frac{\partial}{\partial\xi^\theta}\left(h_{\xi^r}V_{\xi^\theta}\right)\right]\right.\\
&\left.-\frac{1}{h_{\xi^r}}\frac{\partial}{\partial\xi^r}\left[\frac{1}{J_\xi}\frac{\partial\left(h_{\xi^r}V_{\xi^r}\right)}{\partial\xi^\theta}\right]+\frac{1}{h_{\xi^\theta}}\frac{\partial}{\partial\xi^\theta}\left[\frac{1}{J_\xi}\frac{\partial}{\partial\xi^r}\left(h_{\xi^\theta}V_{\xi^r}\right)\right]\right\}
\end{aligned}$$

Equations (3.113), (3.116) and (3.117) can be discretized on a structured computational grid using finite difference method.

3.6. Boundary Conditions

Boundary conditions play a significant role in obtaining the solution of the Navier-Stokes equations. Herzfeld (2009) defined boundary position as “the location in the grid where values for dependent variables are provided by a method different from solving the governing equations”.

3.6.1. Open Boundary Conditions

Open boundary conditions prescription is required in any coastal model for the closure of the governing equations. Open boundaries can be prescribed using radiation (active) conditions that allow the motions generated within the domain to leave without deteriorating the inside solution, or reflective (passive) conditions. Generally, the radiation OBC can be expressed by means of the Sommerfeld [equation (3.117)] or Flather [equation (3.118)] conditions. Blayo and Debreu (2005) emphasized in a study for hyperbolic equations that the Sommerfeld condition is justified for wave equations with constant wave speed ($c = \sqrt{gH}$). Equation (3.113) for normal velocity component to the boundary represents a well posed problem for inviscid shallow water equations [Blayo and Debreu (2005)]. It is obtained by mixing the Sommerfeld condition (with surface gravity wave speed) for surface elevation with a one-dimensional continuity equation [Flather (1988)].

$$\frac{\partial \phi}{\partial t} \pm c \frac{\partial \phi}{\partial n} = 0 \tag{3.118}$$

$$\frac{\partial}{\partial n}\left(v_n - \sqrt{\frac{g}{H}}\zeta \right) = 0 \tag{3.119}$$

where ϕ is one of the two components of velocity in a two-dimensional model, c is the phase speed, $n-$ defines the normal direction to the boundary, v_n is the normal component of velocity to the boundary, ζ is water elevation.

The importance of the OBC in accurately solving the governing equations in the considered domain cannot be underestimated and the literature dedicated to the subject proves this point [Flather (1988), Blumberg and Kantha (1985), Hedley and Yau (1988), Stevens (1990), Shulman and Lewis (1994), Nycander and Döös (2003), Marsalaiex et al. (2006)]. Reviews of the solutions to the Sommerfeld condition, with constant or varying phase speed, and / or Flather condition can be found in Chapman (1985), Palma and Matano (2000), Marchessielo et al. (2001), Blayo and Debreu (2005).

Carter and Merrifield (2007) identified three types of barotropic boundary conditions used for tidal simulations: clamped water elevation, clamped velocity and Flather condition. Clamped boundary conditions were found to be reflective to any flow not described by the boundary condition and resulted in very poor performance. In clamped (Dirichlet) boundary conditions either water elevation or normal component of velocity could be prescribed by an external value. Water elevation had to be clamped one cell in from the boundary, whereas velocity could be set in the boundary cell. Errors in the prescribed boundary values generated incorrect values of the solution. According to the study, the Flather condition was the least responsive to such errors.

The cylindrical co-ordinates numerical model developed in this thesis uses barotropic boundary conditions defined as clamped water elevation.

3.6.2. Closed Boundary Conditions

Closed (land) boundary conditions are usually expressed in terms of free slip or no slip boundary conditions. In the free slip boundary conditions there are two assumptions used: no normal velocity, i.e. normal component of velocity to the wall is zero [equation (3.120)], and tangential velocity expressed as the zero relative vorticity on the boundary [equation (3.121)]. The no-slip velocity ensures that no flow exists across the solid model boundaries using the mass conservation principle.

$$\vec{V} \cdot \vec{n} = 0 \tag{3.120}$$

where: $\vec{V}$ is the velocity vector, and $\vec{n}$ is the direction normal to the flow.

The relative vorticity on the boundary can be expressed as:

$$\omega' = \frac{\partial v}{\partial x} - \frac{\partial u}{\partial y} = 0 \tag{3.121}$$

where: ω' is the relative vorticity; and $\vec{V} = (u, v)$ velocity vector in a two-dimensional Cartesian co-ordinate system (x, y).

On a curved coastline the tangential velocity is expressed as vanishing vorticity writing [Hirsch (1990)]:

$$\frac{\partial V_t}{\partial n} = -\frac{V_t}{R_w} \tag{3.122}$$

where: V_t represents the local tangential velocity component; n is the direction normal to the wall; R_w is the radius of curvature at the wall.

The cylindrical co-ordinate system is orthogonal and equation (3.122) can be written in the physical domain as:

for north-south boundary, i.e. in the $r-$ direction:

$$\frac{1}{r}\frac{\partial V_r}{\partial \theta} = 0 \tag{3.123}$$

for west-east boundary, i.e. in the $\theta-$ direction:

$$\frac{\partial V_\theta}{\partial r} = -\frac{V_\theta}{R_w} \tag{3.124}$$

Equations (3.123) and (3.124) can be mapped onto a computational domain resulting in:

for north-south boundary, i.e. in the ξ^r- direction:

$$\frac{1}{h_{\xi^\theta}}\frac{\partial V_{\xi^r}}{\partial \xi^\theta} = 0 \tag{3.125}$$

for west-east boundary, i.e. in the $\xi^\theta-$ direction: (3.126)

$$\frac{1}{h_{\xi^r}}\frac{\partial V_{\xi^\theta}}{\partial \xi^r}+\frac{V_{\xi^\theta}}{R_w}=0$$

3.7. Summary

The NSE equations represent a useful tool in describing water motion. They are partial differential equations and have a nonlinear character, which makes them difficult to solve. The number of unknowns (p, v_r, v_θ, v_z) in the NSE is greater than the number of equations and the continuity equation is added to the system of equations. Also, they require a number of closures, such as turbulence closure and boundary conditions.

NSE can be written in various co-ordinate systems, making them useful in different situations. The present chapter shows the approach to obtain the equations governing mass and momentum conservation and write them in cylindrical co-ordinates. The shallow water equations result from assuming a logarithmic variation law of the vertical velocity and applying the specific properties of the estuary or coastal area to the continuity and momentum equations. The technicalities of depth integration of the continuity and Navier-Stokes equations written in cylindrical co-ordinates are shown. Solution of the depth integrated equations can be obtained with methods already developed for a Cartesian co-ordinate system if proper mapping transformations from physical onto computational plane are performed. A proper transformation is defined if the Jacobian of the transformation is finite and nonzero. In the present case algebraic mapping transformations are employed. The resulting equations are used in the ulterior development of the numerical hydrodynamic model. Also, some open and closed boundary conditions are presented.

Chapter 4

Solution Technique

4.1. Introduction

The depth integrated continuity and Navier-Stokes equations in cylindrical co-ordinates developed in Chapter 3 constitute a coupled system of equations. The analytical solution of the equations cannot be obtained due to the complexity of the problem. Therefore, numerical methods are employed. The equations can be solved in either cylindrical co-ordinates form or after performing mapping transformations onto a computational plane. The advantage of using mapping transformations stems from the fact that solution techniques developed for Cartesian co-ordinates can be used by other co-ordinate systems, such as cylindrical, spherical, general orthogonal, or non-orthogonal curvilinear co-ordinates.

The present chapter describes the terms in the NSE equations, modelling methodology for estuarine hydrodynamics, presents properties of the finite difference numerical models, finite difference formulations of the partial differential equations and the solution algorithm chosen to solve the coupled system of equations written in the transformed co-ordinate system $\left(\xi^r, \xi^\theta\right)$.

4.2. Further Explanation of the Terms in the Navier-Stokes Equations

The Navier-Stokes equations written in cylindrical co-ordinates were derived, depth integrated and mapped onto the computational plane in the preceding chapter. Their final form is given by equations (3.115) and (3.116), respectively. It can be observed that momentum equation (3.115) contains two extra terms, $\left(2b\right)$ and $\left(7b\right)$, compared to the Cartesian form of the equations [Olbert (2006)]. These additional terms are due to the curvature of the grid in the angular

direction and are called source terms. In the ξ^r – direction, the equivalent mathematical formulation and code notation of these terms is given in Table 4.1.

Term no. in eq. (3.115)	Description	Mathematical formulation in the ξ^r- direction	Representation within code
(1)	local acceleration	$\partial q_{\xi^r}/\partial t$	$[QXU(I,J)-QXL(I,J)]/DT$
(2a)	advective accelerations	$\frac{1}{J_\xi}\left[\frac{\partial}{\partial \xi^r}\left(h_{\xi^\theta} V_{\xi^\theta} V_{\xi^r} H\right)+\frac{\partial}{\partial \xi^\theta}\left(h_{\xi^r} V_{\xi^r} V_{\xi^\theta} H\right)\right]$	$DUUHIDX+DUVHIDY$
(2b)	source term in advective acceleration term	$\frac{V_{\xi^\theta}}{J_\xi}\left(V_{\xi^r} H \frac{\partial h_{\xi^r}}{\partial \xi^\theta}-V_{\xi^\theta} H \frac{\partial h_{\xi^\theta}}{\partial \xi^r}\right)$	$EXTRA1$
(3)	Coriolis force	$f_C V_{\xi^\theta} H$	$D3CORI * QYMAV$
(4)	pressure gradient	$gH\frac{1}{h_{\xi^r}}\frac{\partial \zeta}{\partial \xi^r}$	$PRESS$
(5)	wind shear force	$\rho_a W_{\xi^r} W/\rho$	$WSTRESS$
(6)	bed shear resistance	$g V_{\xi^r} V/C^2$	$D4BDFR * QXL(I,J)$
(7a)	turbulence induced shear force	$\frac{1}{h_{\xi^r}}\frac{\partial}{\partial \xi^r}\left[\frac{1}{J_\xi}\frac{\partial}{\partial \xi^r}\left(h_{\xi^\theta} V_{\xi^r}\right)\right]+\frac{1}{h_{\xi^\theta}}\frac{\partial}{\partial \xi^\theta}\left[\frac{1}{J_\xi}\frac{\partial\left(h_{\xi^r} V_{\xi^r}\right)}{\partial \xi^\theta}\right]$	$DIFUS$
(7b)	source term in turbulence induced shear force term	$\frac{1}{h_{\xi^r}}\frac{\partial}{\partial \xi^r}\left[\frac{1}{J_\xi}\frac{\partial}{\partial \xi^\theta}\left(h_{\xi^r} V_{\xi^\theta}\right)\right]-\frac{1}{h_{\xi^\theta}}\frac{\partial}{\partial \xi^\theta}\left[\frac{1}{J_\xi}\frac{\partial\left(h_{\xi^\theta} V_{\xi^\theta}\right)}{\partial \xi^r}\right]$	$EXTRA2$

Table 4.1: Mathematical and numerical code formulation of the NSE terms in the ξ^r- direction

4.3. Mathematical Modelling Methodology

The mathematical modelling methodology for two-dimensional estuarine hydrodynamics in cylindrical co-ordinates is shown in the flowchart in Figure 4.1. The first six components of the flowchart were presented in Chapter 3.

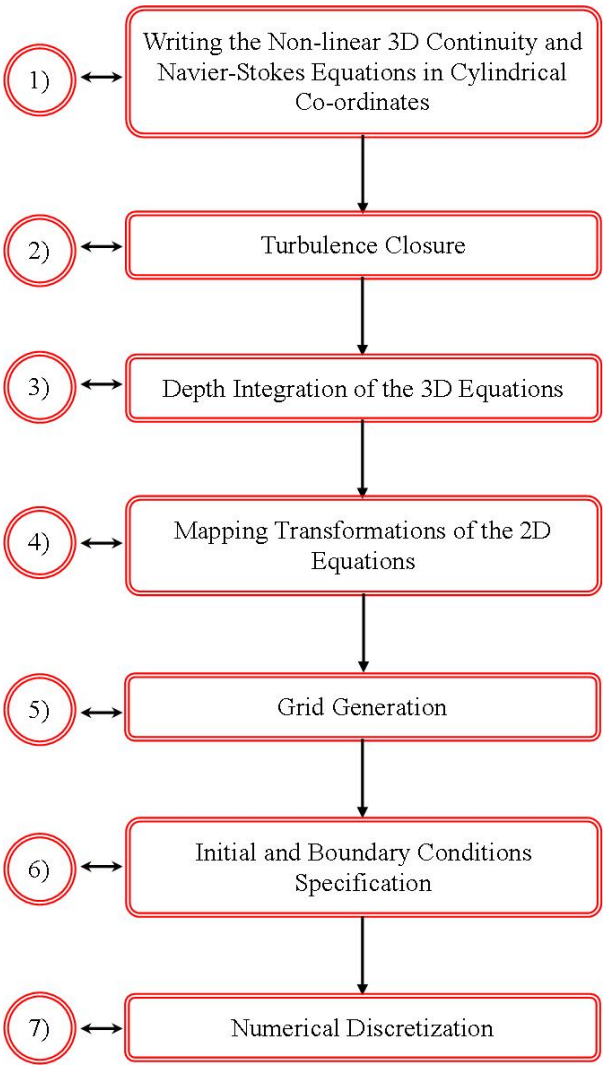

Figure 4.1: Flowchart of the mathematical modelling methodology

After numerical discretization of the governing equations is performed, the flowchart of the code can be represented as in Figure 4.2. The input data is read from the master input file and all other input files required by the model. Then, open boundary conditions are applied and the hydrodynamic solution proceeds. The solution of the model is next written to output files as time series or snapshots.

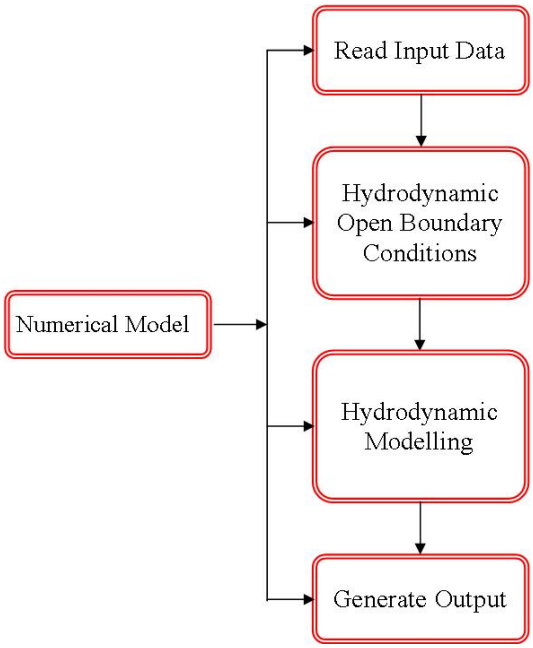

Figure 4.2: Flowchart of the numerical model.

4.4. Numerical Discretization of the Equations Governing Water Motion

4.4.1. Properties of the Finite Difference Approximations

In the present research, the finite difference method was chosen for solving the hydrodynamic equations based on the advantages in terms of computational time they present compared to both unstructured grid techniques (FEM, FVM), and mesh free methods. A description [Eymard et al. (2000)] of three mesh based methods is presented in Figure 4.3.

An analysis of consistency, stability, convergence and accuracy of the finite difference scheme representation ensures that the correct computational predictions are obtained. Consistency condition refers to the structure of numerical formulation, in that both the finite difference equation and the partial differential equation have to describe the same physical process. Both stability and convergence are conditions applied to solution of the numerical scheme [Hirsch (1988)]. Stability means that differences between computed and exact solutions of the finite difference equation are insignificant, while convergence

condition relates the computed solution of the finite difference equation to the exact solution of the partial differential equation. The truncation error for a finite difference scheme has its magnitude defined by the accuracy criterion.

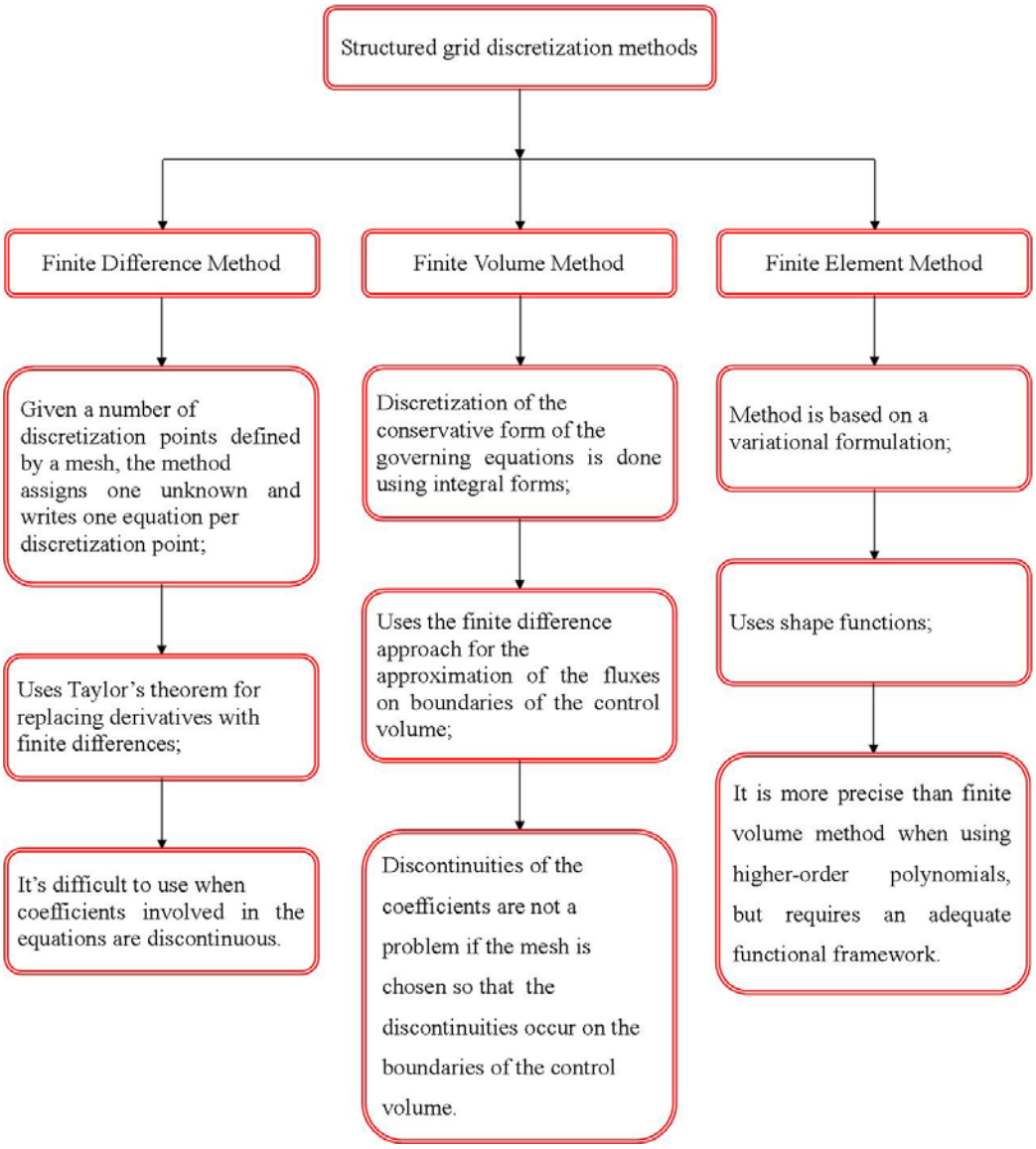

Figure 4.3: Description of three grid based discretization methods.

4.4.2. Finite Difference Approximations on Cartesian Meshes

Any continuous function $f(x)$ defined on an interval $[a,b]$ can be discretized on a uniform grid assuming the values of the function at two points on the grid. Let δx be a small finite value which represents the spatial step, i.e. the distance

between two consecutive points on the grid [Figure 4.4]. The following approximations can be used:

Backward difference: $\Delta^{-} f = f(x) - f(x - \delta x)$ (4.1)

Central difference: $\overline{\Delta} f = f(x + \delta x) - f(x - \delta x)$ (4.2)

Forward difference: $\Delta^{+} f = f(x + \delta x) - f(x)$ (4.3)

The backward and forward differences are called one-sided differences. An averaging (or interpolation) operator can be defined as:

Averaging : $\Delta^{1/2} f = \frac{1}{2}[f(x + \delta x) + f(x)]$ (4.4)

If the points in the interval are noted as: $x_i \equiv x$, $x_{i+1} \equiv x + \delta x$, $x_{i-1} \equiv x - \delta x$, then the above difference formulations can be rewritten as:

Backward difference: $\Delta^{-} f = f(x_i) - f(x_{i-1})$ (4.5)

Central difference: $\overline{\Delta} f = f(x_{i+1}) - f(x_{i-1})$ (4.6)

Forward difference: $\Delta^{+} f = f(x_{i+1}) - f(x_i)$ (4.7)

Averaging : $\Delta^{1/2} f = \frac{1}{2}[f(x_{i+1}) + f(x_i)]$ (4.8)

As seen in Figure 4.3, Taylor's series are used for development of discretized differential terms. Based on this approach, the term $f(x + \delta x) \equiv f(x_{i+1})$ can be developed as:

$$f(x+\delta x) = f(x) + \delta x \frac{\partial f(x)}{\partial x} + \frac{\delta x^2}{2} \frac{\partial^2 f(x)}{\partial x^2} + \ldots \tag{4.9}$$

Retaining the first two terms of the approximation, the derivative $\frac{\partial f(x)}{\partial x}$ of the first order in δx (the order of difference approximation is defined later in the text) becomes:

Forward difference: $$\frac{f(x+\delta x) - f(x)}{\delta x} = \frac{\partial f(x)}{\partial x} + 0(\delta x) \tag{4.10}$$

When the term $f(x-\delta x) \equiv f(x_{i-1})$ is represented using Taylor's expansions:

$$f(x-\delta x) = f(x) - \delta x \frac{\partial f(x)}{\partial x} + \frac{\delta x^2}{2} \frac{\partial^2 f(x)}{\partial x^2} + \ldots \tag{4.11}$$

the expression of the first derivative is written as:

Backward difference: $$\frac{f(x) - f(x-\delta x)}{\delta x} = \frac{\partial f(x)}{\partial x} + 0(\delta x) \tag{4.12}$$

When Taylor's expansion for $f(x-\delta x)$ is subtracted from the expression of $f(x+\delta x)$ in terms of Taylor's series, the expression of the central difference for the first derivative is obtained:

Central difference: $$\frac{f(x+\delta x) - f(x-\delta x)}{2\delta x} = \frac{\partial f(x)}{\partial x} + 0(\delta x^2) \tag{4.13}$$

This is a second-order approximation given by the term $0(\delta x^2)$.

In general forward differencing is used for prediction, whereas central differencing is considered the most accurate, containing information on both sides of the value in current position [Olbert (2006)].

In finite difference methods truncation error plays a significant role. It shows the error by which the approximation differs from the real value. Truncation error tends to zero as δx goes to zero. The order of approximation shows the variation law of the truncation error with respect to δx, i.e. first-order approximation means that the truncation error varies as the first power in δx, etc. [Hirsch (1988)].

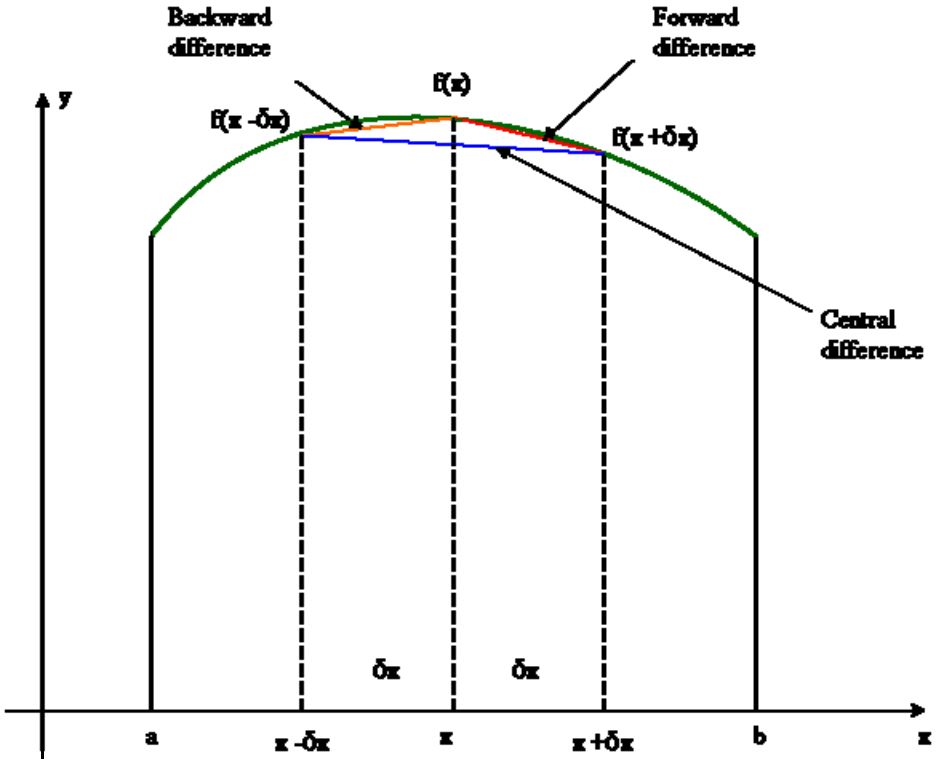

Figure 4.4: Finite difference approximations of first-order derivatives [Hirsch (1988)].

Second derivative can be obtained by repeated application of first-order formulas:

$$\frac{\partial^2 f(x)}{\partial x^2} \approx \frac{1}{\delta x}\left[\frac{\partial f}{\partial x}(x+\delta x) - \frac{\partial f}{\partial x}(x)\right] = \frac{f(x+\delta x) - 2f(x) + f(x-\delta x)}{\delta x^2} \tag{4.14}$$

In the above equation, with second-order accuracy, first derivatives at points $x+\delta x$ and x are approximated using backward differences.

General methods for finite difference formulas up to the fourth order derivative are presented by Hirsch (1988) with emphasis on first and second derivatives which are generally required to be discretized for solving the shallow water equations. The work also includes finite difference approximations on non-uniform Cartesian grids [equations (4.15)-(4.18)], where it is recommended that mesh size does not vary abruptly, since truncation error is proportional to the difference of two consecutive mesh lengths. An abrupt variation in cell size is defined as $\delta x_{i+1} \approx 2\delta x_i$. Extension of the formulas to two dimensions is straightforward and details are not given here. Figure 4.5 shows finite difference techniques combining time and spatial discretizations.

Second-order finite difference approximations on non-uniform Cartesian grids:

Backward difference: $$\frac{f(x)-f(x-\delta x)}{\delta x_i}=\frac{\partial f(x)}{\partial x}+0(\delta x) \tag{4.15}$$

Central difference:

$$\frac{1}{\delta x_i+\delta x_{i+1}}\left\{\frac{\delta x_i}{\delta x_{i+1}}\left[f(x+\delta x)-f(x)\right]+\frac{\delta x_{i+1}}{\delta x_i}\left[f(x)-f(x-\delta x)\right]\right\} \tag{4.16}$$
$$=\frac{\partial f(x)}{\partial x}+0(\delta x^2)$$

Forward difference: $$\frac{f(x+\delta x)-f(x)}{\delta x_{i+1}}=\frac{\partial f(x)}{\partial x}+0(\delta x^2) \tag{4.17}$$

Second derivative with central difference:

$$\frac{2}{\delta x_{i+1}+\delta x_i}\left[\frac{f(x+\delta x)-f(x)}{\delta x_{i+1}}-\frac{f(x)-f(x-\delta x)}{\delta x_i}\right]=\frac{\partial^2 f(x)}{\partial x^2}+0(\delta x^2) \tag{4.18}$$

where:

$\delta x_i = x_i - x_{i-1}$.

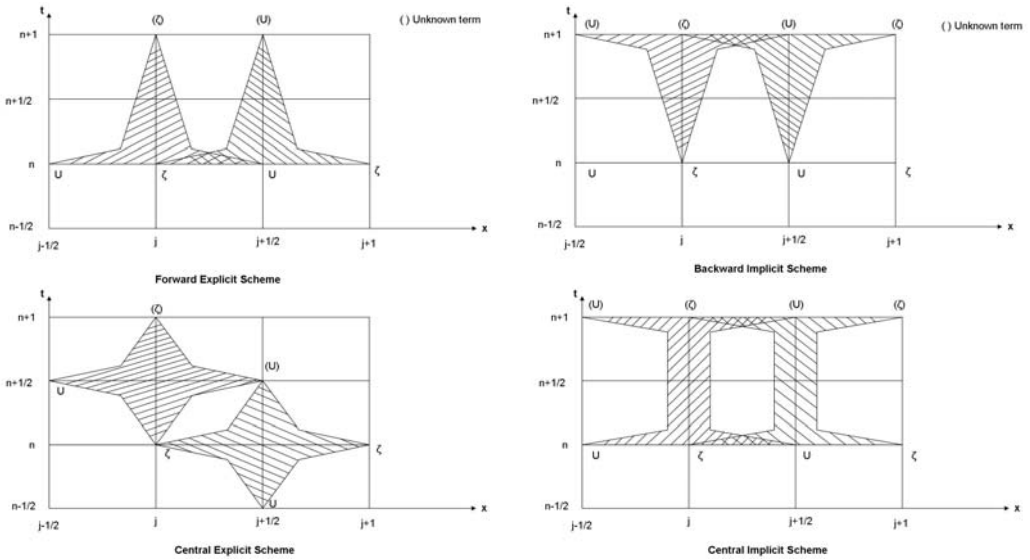

Figure 4.5: Some time and space finite differences schemes for one-dimensional problems [Falconer (1976)].

4.4.3. Finite Difference Approximations on Computational Domains

Finite difference approximations can be written on curvilinear grids. For example, for any curvilinear co-ordinates $\left(\xi^1, \xi^2\right)^c$ a mapping transformation can be performed: $\xi^1 = \xi^1(x, y)$, $\xi^2 = \xi^2(x, y)$ and the physical space (x, y) is mapped onto a computational plane $\left(\xi^1, \xi^2\right)$. In the computational plane a Cartesian mesh is set up and numerical discretization of the equations can be performed. When mapping transformations are effectuated, the presence of co-ordinate metrics derivatives complicates the form of the finite difference approximations.

For the present problem, where the computational domain is represented by the $\left(\xi^r, \xi^\theta\right)$ on an Arakawa C grid [Figure 4.6], a second-order accurate discretization of the first derivative in the advective acceleration term can be written as [Morinishi et al. (2004)]:

$$\frac{1}{\Delta^{1/2}_{\xi^i} J_\xi}\frac{1}{\delta\xi^j}\left[\Delta^{1/2}_{\xi^i}\left(\frac{J_\xi}{h_{\xi^j}}q_{\xi^j}\right)\Delta^{+}\left(\Delta^{1/2}_{\xi^j}V_{\xi^i}\right)\right]$$
$$-\frac{1}{\Delta^{1/2}_{\xi^i} J_\xi}\frac{1}{\delta\xi^j}\left[\Delta^{1/2}_{\xi^i}\left(\frac{J_\xi}{h_{\xi^j}}q_{\xi^j}\right)\Delta^{-}\left(\Delta^{1/2}_{\xi^j}V_{\xi^i}\right)\right] \qquad (4.19)$$

where:

$i = r$, $j = r, \theta$ in the ξ^r – direction;

$i = \theta$, $j = r, \theta$ in the ξ^θ – direction;

$\Delta^{1/2}_{\xi^i}$ is the average operator in the ξ^i direction, defined by equation (4.8).

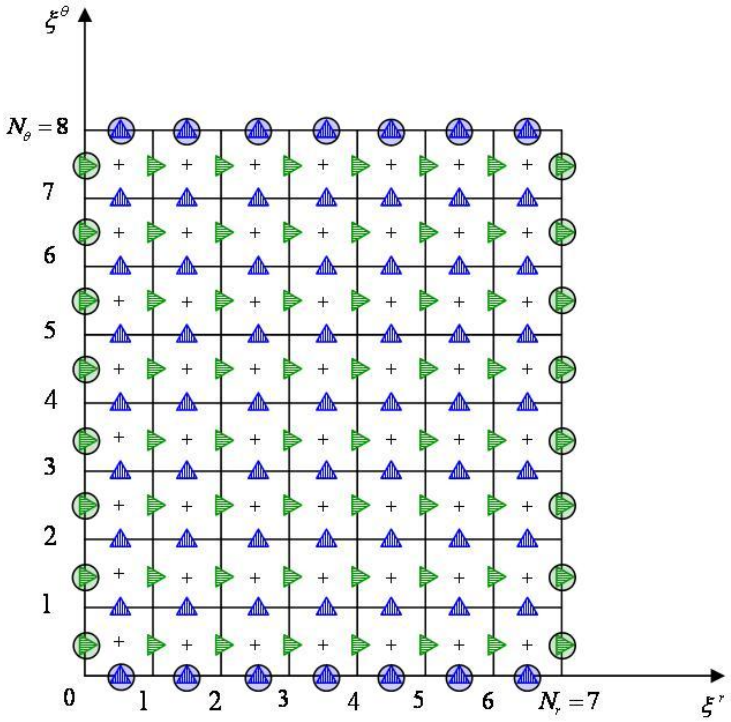

Figure 4.6: Staggered grid configuration in the transformed plane for spatial discretization. Blue triangles represent transformed velocities in the angular direction (V_{ξ^θ}), green triangles are used for transformed velocities in the radial direction (V_{ξ^r}), "+" is for i.e. water elevation (ζ), Chezy coefficient (C), eddy viscosity ($\overline{E}$). Boundary velocity points are represented as circumscribed triangles.

The source term, equivalent to writing $-V_\theta^2 / r$ in equation (3.115), can be evaluated for the non-zero term as:

$$\Delta_{\xi^r}^{1/2}\left(\frac{V_{\xi^\theta}}{J_\xi}\right)\frac{1}{\delta\xi^r}\left(\Delta_{\xi^r}^{1/2}h_{\xi^\theta}\right) \tag{4.20}$$

A second derivative, such as $\frac{1}{h_{\xi^r}}\frac{\partial}{\partial\xi^r}\left[\frac{1}{J_\xi}\frac{\partial\left(h_{\xi^\theta}V_{\xi^r}\right)}{\partial\xi^r}\right]$ in the turbulence term of equation (3.115), can be discretized as:

$$\begin{aligned}&\frac{1}{\Delta_{\xi^r}^{1/2}h_{\xi^r}}\frac{1}{\delta\xi^r}\left\{\frac{1}{\Delta_{\xi^r}^{1/2}J_\xi}\frac{1}{\delta\xi^r}\Delta^+\left[\Delta_{\xi^r}^{1/2}\left(\frac{J_\xi}{h_{\xi^r}}V_{\xi^r}\right)\right]\right.\\&\left.-\frac{1}{\Delta_{\xi^r}^{1/2}J_\xi}\frac{1}{\delta\xi^r}\Delta^-\left[\Delta_{\xi^r}^{1/2}\left(\frac{J_\xi}{h_{\xi^r}}V_{\xi^r}\right)\right]\right\}\end{aligned} \tag{4.21}$$

4.4.4. Alternating Directions Implicit Method – General Considerations

In two-dimensional hydrodynamic modelling the second-order accurate Alternating Direction Implicit (ADI) scheme is commonly employed, since it allows linearization of the Navier-Stokes equations. The method was introduced for study of heat problems by Peaceman and Rachford (1955), generalized by Douglas and Gunn (1964) and subjected to many research papers. Modifications of the ADI method to solve parabolic equations with mixed derivatives were described by Beam and Warming (1980), Craig and Sneyd (1988), in t'Hout and Welfert (2007). Last study showed that ADI method for parabolic equations with mixed derivatives terms is unconditionally stable. McKee et al. (1996) used ADI for parabolic equations with mixed derivative and convective terms in a heat study in curvilinear co-ordinates. Application of a second-order in time linear ADI method with applications to shallow water equations based on a Crank-Nicholson time discretization technique was described by Fairweather

and Navon (1980). When applied to coastal numerical models on Cartesian or orthogonal curvilinear grids, ADI results in a diagonal dominant system of equations, which can be solved using methods already available, such as Thomas algorithm, after addition of finite difference approximations to boundary condition equations. By using ADI methods in estuarine non-orthogonal curvilinear co-ordinates models, a tridiagonal solution matrix results and keeps its form as long as the non-orthogonal components of the barotropic term are solved explicitly. For dominating non-orthogonal components of the barotropic term the computational time step is restricted by the Courant number given by CFL condition. A semi-implicit method eliminates the problem since both orthogonal and non-orthogonal barotropic components can be solved implicitly [Muin and Spaulding (1996)]. Borthwick and Barber (1992) emphasized that for two-dimensional equations written in non-orthogonal curvilinear co-ordinates the second order accuracy in time could not be achieved using a single ADI cycle and recommended an iterative technique which obtained improved estimates for the otherwise lagged variables. ADI technique was employed by Klevanny et al. (1994), Andronosov et al (1997), Muin and Spaulding (1997), as well. Some variations of the method with applications to solute transport problems on Cartesian meshes are cited by Falconer et al. (1988): ADI-TOADSOD (Alternating Direction Implicit – Third Order Advection and Second Order Diffusion), ADI-QUICK (Alternating Direction Implicit – Quadratic Upwind Interpolation for Convective Kinematics) and ADI-QUICKEST (Alternating Direction Implicit – Quadratic Upwind Interpolation for Convective Kinematics, Estimated Streaming Term).

ADI is a time centred implicit finite difference method. The principle of the method is to split the time step into two halves (in two-dimensional problems):

i) at first half time-step some variables are solved explicitly in the x-direction and all others are solved explicitly;
ii) at second half time-step the corresponding variables are implicitly solved in the y-direction and the rest is solved explicitly.

The basic idea behind two-dimensional ADI on uniform Cartesian grids can be illustrated for the parabolic diffusion equation:

$$\frac{\partial u}{\partial t} = \alpha\left(\frac{\partial^2 u}{\partial x^2} + \frac{\partial^2 u}{\partial y^2}\right) \tag{4.22}$$

where α is the diffusivity coefficient.

Equation (4.22) can be written in terms of ADI operators as:

$$\frac{\partial u}{\partial t} = L_x u + L_y u \tag{4.23}$$

where:

$$L_x u = \frac{\alpha}{\delta_x^2}\left(u_{i+1,j}^n - 2u_{i,j}^n + u_{i-1,j}^n\right)$$
$$L_x u = \frac{\alpha}{\delta_y^2}\left(u_{i,j+1}^n - 2u_{i,j}^n + u_{i,j-1}^n\right)$$
$$L = L_x + L_y$$

Equation (4.23) can be discretized with a backward Euler time discretization method and becomes:

$$\frac{u^{n+1} - u^n}{\delta t} = \left(L_x + L_y\right)u^{n+1} \tag{4.24}$$

Moving unknown terms to the left gives:

$$\left[1 - \delta t\left(L_x + L_y\right)\right]u^{n+1} = u^n \tag{4.25}$$

A factorization of the right-hand-side operator can be written as a product of one-dimensional splitting operators:

$$\left(1-\tau_{ADI}\delta t L_x\right)\left(1-\tau_{ADI}\delta t L_y\right)u^{n+1}=u^n \tag{4.26}$$

The relaxation parameter (τ_{ADI}) in equation (4.26) can have various values: $\tau_{ADI}=1$ for the Douglas-Rachford scheme in equation (4.27), and $\tau_{ADI}=1/2$ for the Peaceman-Rachford method.

$$\left(1-\tau_{ADI}\delta t L_x\right)\left(1-\tau_{ADI}\delta t L_y\right)\delta_t u^n=\tau_{ADI}\delta t L u^n \tag{4.27}$$

The factorized scheme (4.26) can be solved in two steps:

$$\left(1-\tau_{ADI}\delta t L_x\right)u^{\overline{n+1}}=\left[1+\tau_{ADI}\delta t L_y\right]u^n \tag{4.28}$$

$$\left(1-\tau_{ADI}\delta t L_y\right)u^{n+1}=u^{\overline{n+1}}-\tau_{ADI}\delta t L_y u^n \tag{4.29}$$

The unconditionally stable, second-order accurate in time Peaceman-Rachford method is [Hirsch (1988)]:

$$\left(1-\frac{\delta t}{2}L_x\right)u^{\overline{n+1}}=\left[1+\frac{\delta t}{2}L_y\right]u^n \tag{4.30}$$

$$\left(1-\frac{\delta t}{2}L_y\right)u^{n+1}=\left(1+\frac{\delta t}{2}L_x\right)u^{\overline{n+1}} \tag{4.31}$$

The equations require appropriate boundary conditions for the variables represented at intermediate time steps. Dirichlet conditions for equations (4.28) and (4.29) can be written:

$$\delta_t u^{\overline{n+1}}\Big|_B=\left(1-\frac{\delta t}{2}L_y\right)\left(u^{n+1}-u^n\right)\Big|_B \tag{4.32}$$

where $\delta_t u^{\overline{n+1}}=u^{\overline{n+1}}-u^n$.

4.4.5. Courant Criterion for Alternating Directions Implicit Method

Finite difference discretization method is conditionally stable. This means that space step and time step are related by a criterion which establishes the maximum time step allowable for computations.

ADI can be unconditionally used on two-dimensional uniform Cartesian meshes. The accuracy of the solution requires a restriction for the time step dictated by the maximum Courant number [Falconer et al. (1998)]:

$$\left(C_r\right)_{\max} = \frac{\delta t}{2}\sqrt{gH\left(\frac{1}{\delta x^2}+\frac{1}{\delta y^2}\right)} \le \sqrt{2} \tag{4.33}$$

where:

δt is the time step employed;

δx is the grid spacing in the x-direction;

δy is the grid spacing in the y-direction.

Equation (4.33) can be used for curvilinear co-ordinates mapped onto a computational plane, with leapfrog time discretization method (in external mode of POM), for $\delta x = h_{\xi^r}\delta\xi^r$, and $\delta y = h_{\xi^\theta}\delta\xi^\theta$, respectively.

For two-dimensional curvilinear conformal co-ordinates mapped onto a computational domain, and using ADI, Lin and Chandler-Wilde (1996) defined the Courant number as:

$$\left(C_r\right)_{\max} = \frac{\delta t\sqrt{gH}}{\sqrt{\min\left(h_{\xi^r}\delta\xi^r h_{\xi^\theta}\delta\xi^\theta\right)}} \le \sqrt{2} \tag{4.34}$$

4.4. 6. Proposed Finite Difference Scheme

The transformed depth integrated continuity and Navier-Stokes equations have the form given by equations (3.112), (3.115) and (3.116). Spatial discretization of the equations governing shallow water motion follows the scheme outlined by Lin and Chandler-Wilde (1996). For time integration, the second-order accurate two-step finite difference Alternating Directions Implicit technique is employed. This scheme assumes that a two-time levels scheme is used:

i) at the first half time step ($n \to n+1/2$) the continuity and ξ^r – direction momentum equation are discretized;
ii) at the second half time step ($n+1/2 \to n+1$) the continuity and ξ^θ – direction momentum equation are discretized.

i) During the first time step $(n \to n+1/2)$ the finite difference approximations of the continuity and ξ^r – direction momentum equation are:

continuity equation:

$$\frac{\zeta_{i,j}^{n+1/2} - \zeta_{i,j}^{n}}{\delta t/2} + \frac{1}{J_\xi\big|_{i,j}} \frac{1}{\delta \xi^r} \left(h_{\xi^\theta}\big|_{i+1/2,j} q_{\xi^r}\Big|_{i+1/2,j}^{n+1/2} - h_{\xi^\theta}\big|_{i-1/2,j} q_{\xi^r}\Big|_{i-1/2,j}^{n+1/2} \right) + \frac{1}{J_\xi\big|_{i,j}} \frac{1}{\delta \xi^\theta} \left(h_{\xi^r}\big|_{i,j+1/2} q_{\xi^\theta}\Big|_{i,j+1/2}^{n} - h_{\xi^r}\big|_{i,j-1/2} q_{\xi^\theta}\Big|_{i,j-1/2}^{n} \right) = 0 \tag{4.35}$$

and, respectively:

ξ^r – direction momentum equation:

$$\frac{q_{\xi^r}\Big|_{i+1/2,j}^{n+1/2} - q_{\xi^r}\Big|_{i+1/2,j}^{n-1/2}}{\delta t} \tag{4.36}$$

$$+\beta\frac{1}{J_{\xi}\Big|_{i+1/2,j}}\left\{\frac{1}{\delta\xi^{r}}\left[\left(h_{\xi^{\theta}}V_{\xi^{r}}^{'}q_{\xi^{r}}^{'}\Big|_{i+1,j}^{n}\right)-\left(h_{\xi^{\theta}}V_{\xi^{r}}^{'}q_{\xi^{r}}^{'}\Big|_{i,j}^{n}\right)\right]\right.$$

$$+\frac{1}{\delta\xi^{\theta}}\left[\left(h_{\xi^{r}}q_{\xi^{\theta}}\right)_{i+1/2,j+1/2}^{n}V_{r}^{'}\Big|_{i+1/2,j+a^{*}}^{n}\right.$$

$$\left.\left.-\left(h_{\xi^{r}}q_{\xi^{\theta}}\right)_{i+1/2,j-1/2}^{n}V_{r}^{'}\Big|_{i+1/2,j-1+b^{*}}^{n}\right]\right.$$

$$+V_{\xi^{\theta}}\Big|_{i+1/2,j}^{n}\left[q_{\xi^{r}}^{'}\Big|_{i+1/2,j}^{n}\frac{1}{\delta\xi^{\theta}}\left(h_{\xi^{r}}\Big|_{i+1/2,j+1/2}^{n}-h_{\xi^{r}}\Big|_{i+1/2,j-1/2}^{n}\right)\right.$$

$$\left.\left.-q_{\xi^{\theta}}\Big|_{i+1/2,j}^{n}\frac{1}{\delta\xi^{r}}\left(h_{\xi^{\theta}}\Big|_{i+1,j}-h_{\xi^{\theta}}\Big|_{i,j}\right)\right]\right\}=$$

$$f\,q_{\xi^{\theta}}\Big|_{i+1/2,j}^{n}$$

$$-\frac{g}{2}\frac{1}{\delta\xi^{r}}\left(\frac{H}{h_{\xi^{r}}}\right)\Bigg|_{i+1/2,j}^{n}\left(\zeta\Big|_{i+1,j}^{n+1/2}-\zeta\Big|_{i,j}^{n+1/2}+\zeta\Big|_{i+1,j}^{n-1/2}-\zeta\Big|_{i,j}^{n-1/2}\right) \qquad (4.36)$$

continued

$$+\frac{\rho_{a}}{\rho}\gamma W_{\xi^{r}}W$$

$$-g\left(\frac{\left(V_{r}^{2}+V_{\theta}^{2}\right)^{1/2}}{HC^{2}}\right)\Bigg|_{i+1/2,j}^{n}\left(\frac{q_{\xi^{r}}\Big|_{i+1/2,j}^{n+1/2}+q_{\xi^{r}}\Big|_{i+1/2,j}^{n-1/2}}{2}\right)$$

$$-\left(\overline{E}H\right)_{i+1/2,j}^{n}\left\{\frac{1}{h_{\xi^{r}}\Big|_{i+1/2,j}}\frac{1}{\left(\delta\xi^{r}\right)^{2}}\left[\frac{1}{J_{\xi}\Big|_{i+1,j}}\left(h_{\xi^{\theta}}V_{\xi^{r}}^{'}\right)_{i+3/2,j}^{n}\right.\right.$$

$$\left.-\frac{1}{J_{\xi}\Big|_{i+1,j}}\left(h_{\xi^{\theta}}V_{\xi^{r}}^{'}\right)_{i+1/2,j}^{n}\right]$$

$$-\frac{1}{h_{\xi^{r}}\Big|_{i+1/2,j}}\frac{1}{\left(\delta\xi^{r}\right)^{2}}\frac{1}{J_{\xi}\Big|_{i,j}}\left[\left(h_{\xi^{\theta}}V_{\xi^{r}}^{'}\right)_{i+1/2,j}^{n}-\left(h_{\xi^{\theta}}V_{\xi^{r}}^{'}\right)_{i-1/2,j}^{n}\right]$$

$$+\frac{1}{h_{\xi^{\theta}}\Big|_{i+1/2,j}}\frac{1}{\left(\delta\xi^{\theta}\right)^{2}}\left[\frac{1}{J_{\xi}\Big|_{i+1/2,j+1/2}}\left(h_{\xi^{r}}V_{\xi^{r}}^{'}\right)_{i+1/2,j+1}^{n}\right.$$

$$\left.\left.-\frac{1}{J_{\xi}\Big|_{i+1/2,j+1/2}}\left(h_{\xi^{r}}V_{\xi^{r}}^{'}\right)_{i+1/2,j}^{n}\right]\right.$$

$$
\begin{aligned}
&- \frac{1}{h_{\xi^\theta}\Big|_{i+1/2,j}} \frac{1}{\left(\delta\xi^\theta\right)^2} \left[\frac{1}{J_\xi\Big|_{i+1/2,j-1/2}} \left(h_{\xi^r} V'_{\xi^r}\right)^n_{i+1/2,j} \right. \\
&\left. - \frac{1}{J_\xi\Big|_{i+1/2,j-1/2}} \left(h_{\xi^r} V'_{\xi^r}\right)^n_{i+1/2,j-1} \right] \\
&+ \frac{1}{h_{\xi^r}\Big|_{i+1/2,j}} \frac{1}{\delta\xi^r \delta\xi^\theta} \left[\frac{1}{J_\xi\Big|_{i+1,j}} \left(h_{\xi^r} V_{\xi^\theta}\right)^n_{i+1,j+1/2} \right. \\
&- \frac{1}{J_\xi\Big|_{i+1,j}} \left(h_{\xi^r} V_\theta\right)^n_{i+1,j-1/2} \\
&\left. - \frac{1}{J_\xi\Big|_{i,j}} \left(h_{\xi^r} V_{\xi^\theta}\right)^n_{i,j+1/2} + \frac{1}{J_\xi\Big|_{i,j}} \left(h_{\xi^r} V_{\xi^\theta}\right)^n_{i,j-1/2} \right] \\
&- \frac{1}{\left(h_{\xi^\theta}\right)_{i+1/2,j}} \left[\frac{1}{J_\xi\Big|_{i+1/2,j+1/2}} \left(h_{\xi^\theta} V_\theta\right)^n_{i+1,j+1/2} \right. \\
&- \frac{1}{J_\xi\Big|_{i+1/2,j+1/2}} \left(h_{\xi^\theta} V_{\xi^\theta}\right)^n_{i,j+1/2} \\
&\left. \left. - \frac{1}{J_\xi\Big|_{i+1/2,j-1/2}} \left(h_{\xi^\theta} V_{\xi^\theta}\right)^n_{i+1,j-1/2} + \frac{1}{J_\xi\Big|_{i+1/2,j-1/2}} \left(h_{\xi^\theta} V_{\xi^\theta}\right)^n_{i,j-1/2} \right] \right\}
\end{aligned}
\tag{4.36}
$$

continued

where:

$$
a^* = \begin{cases} 1 \text{ if } & V^*_{\xi^\theta} < 0 \\ 0 \text{ if } & V^*_{\xi^\theta} > 0 \end{cases}
$$

$$
V^*_{\xi^\theta}\Big|_{i+1/2,j} = \frac{1}{4}\left[V_{\xi^\theta}\Big|^n_{i,j+1/2} + V_{\xi^\theta}\Big|^n_{i,j-1/2} + V_{\xi^\theta}\Big|^n_{i+1,j+1/2} + V_{\xi^\theta}\Big|^n_{i+1,j-1/2} \right]
$$

and, similarly:

$$
b^* = \begin{cases} 1 \text{ if } & V^*_{\xi^r} < 0 \\ 0 \text{ if } & V^*_{\xi^r} > 0 \end{cases}
$$

$$V^{*}_{\xi^r}\Big|_{i,j+1/2} = \frac{1}{4}\left[V_{\xi^r}\Big|^{n}_{i+1/2,j} + V_{\xi^r}\Big|^{n}_{i-1/2,j} + V_{\xi^r}\Big|^{n}_{i+1/2,j+1} + V_{\xi^r}\Big|^{n}_{i-1/2,j+1} \right]$$

The primed terms in the discretized momentum equation (4.36) are defined as values corrected by time iterations:

$$V^{'}_{\xi^r}\Big|^{n} = \begin{cases} V^{n-1/2}_{\xi^r} & for\ \ the\ \ first\ \ iteration \\ \frac{1}{2}\left(V^{n-1/2}_{\xi^r} + V^{n+1/2}_{\xi^r} \right) & for\ \ the\ \ \text{sec}ond\ \ iteration \end{cases}$$

ii) During the second time step $(n+1/2 \to n+1)$ the finite difference approximations of the continuity and $\xi^{\theta}-$direction momentum equation can be written as:

continuity equation:

$$\frac{\zeta^{n+1}_{i,j} - \zeta^{n+1/2}_{i,j}}{\delta t/2} + \frac{1}{J_{\xi}\Big|_{i,j}} \frac{1}{\delta\xi^r} \left(h_{\xi^{\theta}}\Big|_{i+1/2,j} q_{\xi^r}\Big|^{n+1/2}_{i+1/2,j} - h_{\xi^{\theta}}\Big|_{i-1/2,j} q_{\xi^r}\Big|^{n+1/2}_{i-1/2,j} \right)$$
$$+ \frac{1}{J_{\xi}\Big|_{i,j}} \frac{1}{\delta\xi^{\theta}} \left(h_{\xi^r}\Big|_{i,j+1/2} q_{\xi^{\theta}}\Big|^{n+1}_{i,j+1/2} - h_{\xi^r}\Big|_{i,j-1/2} q_{\xi^{\theta}}\Big|^{n+1}_{i,j-1/2} \right) = 0 \qquad (4.37)$$

and, respectively:

$\xi^{\theta}-$direction momentum equation:

$$\frac{q_{\xi^{\theta}}\Big|^{n+1}_{i,j+1/2} - q_{\xi^{\theta}}\Big|^{n}_{i,j+1/2}}{\delta t} =$$
$$\frac{\beta}{J_{\xi}\Big|_{i,j+1/2}} \left\{ \frac{1}{\delta\xi^r} \left[\left(h_{\xi^{\theta}} q_{\xi^r} \right)^{n+1/2}_{i+1/2,j+1/2} V^{'}_{\xi^{\theta}}\Big|^{n+1/2}_{i+a^*,j+1/2} \right.\right.$$
$$\left.\left. - \left(h_{\xi^{\theta}} q_{\xi^r} \right)^{n+1/2}_{i+1/2,j-1/2} V^{'}_{\xi^{\theta}}\Big|^{n+1/2}_{i-1+b^*,j+1/2} \right] \right.$$
$$\left. + \frac{1}{\delta\xi^{\theta}} \left[\left(h_{\xi^r} V^{'}_{\xi^{\theta}} q^{'}_{\xi^{\theta}} \right)^{n+1/2}_{i,j+1} - \left(h_{\xi^r} V^{'}_{\xi^{\theta}} q^{'}_{\xi^{\theta}} \right)^{n+1/2}_{i,j+1} \right] \right. \qquad (4.38)$$

$$+V_r\Big|_{i,j+1/2}^{n+1/2}\left[q'_{\xi^\theta}\Big|_{i,j+1/2}^{n+1/2}\frac{1}{\delta\xi^r}\left(h_{\xi^\theta}\Big|_{i+1,j}^{n+1/2}-h_{\xi^\theta}\Big|_{i,j}^{n+1/2}\right)\right.$$

$$\left.-q_{\xi^r}\Big|_{i,j+1/2}^{n+1/2}\frac{1}{\delta\xi^\theta}\left(h_{\xi^r}\Big|_{i+1/2,j+1/2}^{n+1/2}-h_{\xi^r}\Big|_{i+1/2,j-1/2}^{n+1/2}\right)\right]\Bigg\}-f\,q_{\xi^r}\Big|_{i,j+1/2}^{n+1/2}$$

$$-\frac{g}{2}\frac{1}{\delta\xi^\theta}\left(\frac{H}{h_{\xi^\theta}}\right)\Bigg|_{i,j+1/2}^{n+1/2}\left(\zeta\Big|_{i,j+1}^{n}-\zeta\Big|_{i,j}^{n}+\zeta\Big|_{i,j+1}^{n+1}-\zeta\Big|_{i,j}^{n+1}\right)$$

$$+\frac{\rho_a}{\rho}\gamma W_\theta W-g\left(\frac{V}{HC^2}\right)\Bigg|_{i,j+1/2}^{n+1/2}\left(\frac{q_{\xi^\theta}\Big|_{i,j+1/2}^{n+1}+q_{\xi^\theta}\Big|_{i,j+1/2}^{n}}{2}\right)$$

$$-\left(\overline{E}H\right)_{i,j+1/2}^{n+1/2}\left\{\frac{1}{h_{\xi^r}\Big|_{i,j+1/2}}\frac{1}{\left(\delta\xi^r\right)^2}\frac{1}{J_\xi\Big|_{i+1/2,j+1/2}}\left[\left(h_{\xi^\theta}V'_{\xi^\theta}\right)\Big|_{i+1,j+1/2}^{n+1/2}\right.\right.$$

$$\left.-\left(h_{\xi^\theta}V'_{\xi^\theta}\right)_{i,j+1/2}^{n+1/2}\right]$$

$$-\frac{1}{h_{\xi^r}\Big|_{i,j+1/2}}\frac{1}{\left(\delta\xi^r\right)^2}\frac{1}{J_\xi\Big|_{i-1/2,j+1/2}}\left[\left(h_{\xi^\theta}V'_{\xi^\theta}\right)\Big|_{i,j+1/2}^{n+1/2}\right. \qquad (4.38)$$

continued

$$\left.-\left(h_{\xi^\theta}V'_{\xi^\theta}\right)_{i-1,j+1/2}^{n+1/2}\right]$$

$$+\frac{1}{h_{\xi^\theta}\Big|_{i,j+1/2}}\frac{1}{\left(\delta\xi^\theta\right)^2}\left[\frac{1}{J_\xi\Big|_{i,j+1}}\left(h_{\xi^r}V'_{\xi^\theta}\right)_{i,j+3/2}^{n+1/2}\right.$$

$$\left.-\frac{1}{J_\xi\Big|_{i,j+1}}\left(h_{\xi^r}V'_{\xi^\theta}\right)_{i,j+1/2}^{n+1/2}\right]$$

$$-\frac{1}{h_{\xi^\theta}\Big|_{i,j+1/2}}\frac{1}{\left(\Delta\xi^\theta\right)^2}\left[\frac{1}{J_\xi\Big|_{i,j}}\left(h_{\xi^r}V'_{\xi^\theta}\right)_{i,j+1/2}^{n+1/2}\right.$$

$$\left.-\frac{1}{J_\xi\Big|_{i,j}}\left(h_{\xi^r}V'_{\xi^\theta}\right)_{i,j-1/2}^{n+1/2}\right]$$

$$+\frac{1}{h_{\xi^r}\Big|_{i,j+1/2}}\frac{1}{\delta\xi^r\delta\xi^\theta}\left[\frac{1}{J_\xi\Big|_{i+1/2,j+1/2}}\left(h_{\xi^r}V_{\xi^r}\right)_{i+1/2,j+1}^{n+1/2}\right.$$

$$
-\frac{1}{J_\xi\Big|_{i+1/2,\,j+1/2}}\left(h_{\xi^r}V_{\xi^r}\right)\Big|_{i+1/2,\,j}^{n+1/2}
$$

$$
-\frac{1}{J_\xi\Big|_{i-1/2,\,j+1/2}}\left(h_{\xi^r}V_{\xi^r}\right)\Big|_{i-1/2,\,j+1}^{n+1/2}+\frac{1}{J_\xi\Big|_{i-1/2,\,j+1/2}}\left(h_{\xi^r}V_{\xi^r}\right)\Big|_{i-1/2,\,j}^{n+1/2}\Bigg]
$$

$$
-\frac{1}{h_{\xi^\theta}\Big|_{i,\,j+1/2}}\frac{1}{\delta\xi^r\delta\xi^\theta}\Bigg[\frac{1}{J_\xi\Big|_{i,\,j+1}}\left(h_{\xi^\theta}V_{\xi^r}\right)\Big|_{i+1/2,\,j+1}^{n+1/2} \qquad (4.38)
$$

continued

$$
-\frac{1}{J_\xi\Big|_{i,\,j+1}}\left(h_{\xi^\theta}V_{\xi^r}\right)\Big|_{i-1/2,\,j+1}^{n+1/2}
$$

$$
-\frac{1}{J_\xi\Big|_{i,\,j}}\left(h_{\xi^\theta}V_{\xi^r}\right)\Big|_{i+1/2,\,j}^{n+1/2}+\frac{1}{J_\xi\Big|_{i,\,j}}\left(h_{\xi^\theta}V_{\xi^r}\right)\Big|_{i-1/2,\,j}^{n+1/2}\Bigg]\Bigg\}
$$

4.4.7. Boundary Conditions

Open boundary condition can be specified in terms of water elevations or prescribed velocities at the open boundary, i.e. upper boundary in the ξ^r- (or $I-$) direction. A quasi-geostrophic relationship relates water elevations to velocities in the $I-$ direction and can be written:

$$
gH\frac{1}{h_{\xi^\theta}}\frac{\partial\zeta}{\partial\xi^\theta}=-f_C q_{\xi^r} \qquad (4.39)
$$

Approximation of the space derivative in the $\xi^\theta-$ (or $J-$) direction is:

$$
\frac{1}{h_{\xi^\theta}}\frac{\partial\zeta}{\partial\xi^\theta}\approx\frac{1}{h_{\xi^\theta}\Big|_{i,\,j+1/2}}\frac{\zeta\big|_{i,\,j+1}^{n+1}-\zeta\big|_{i,\,j}^{n+1}}{\delta\xi^\theta} \qquad (4.40)
$$

Coriolis acceleration can be represented at $J-$ direction point as:

$$- f_C V_{\xi^r} \approx - f_C \left(\Delta^{1/2}_{\xi^\theta} V_{\xi^r} \right) = - f_C \frac{1}{2} \left(V_{\xi^r} \Big|^{n}_{i-1, j+1} + V_{\xi^r} \Big|^{n}_{i-1, j} \right) \tag{4.41}$$

Substituting equations (4.40) and (4.41) in (4.39) gives the water elevation propagation relationship in the $\xi^\theta -$ direction along the open boundary:

$$\zeta \Big|^{n+1}_{i,j} = \zeta \Big|^{n+1}_{i,j+1} + \delta \xi^\theta h_{\xi^\theta} \Big|_{i, j+1/2} f_C \left(\Delta^{1/2}_{\xi^\theta} V_{\xi^r} \right) \Big/ g \tag{4.42}$$

A method commonly used in numerical modelling of the oceans for specification of closed boundary conditions is the “ghost point” method [Moore (2004)], which assumes definition of a mask (fictious land points) around the domain of wet grid cells where tangential velocity components can be specified. For a straight line western land boundary represented as in Figure 4.7a), the no-slip condition expresses the contravariant velocity on the land boundary as equal to zero ($V^{\xi^r} \Big|_{i+1/2, j-1/2} = 0$) in the $\xi^r -$ direction as:

$$\frac{V_{\xi^r}}{h_{\xi^r}} \Bigg|_{i+1/2, j-1} = - \frac{V_{\xi^r}}{h_{\xi^r}} \Bigg|_{i+1/2, j} \tag{4.43}$$

whereas the free slip condition with a no normal flow assumption is:

$$\frac{V_{\xi^r}}{h_{\xi^r}} \Bigg|_{i+1/2, j-1} = \frac{V_{\xi^r}}{h_{\xi^r}} \Bigg|_{i+1/2, j} \tag{4.44}$$

Numerical discretization of the boundary condition (3.125) can be written:

in the $\xi^\theta -$ direction:

$$\frac{1}{h_{\xi^\theta}} V_{\xi^r} \Bigg|_{i+1/2, j-1} = \frac{1}{h_{\xi^\theta}} V_{\xi^r} \Bigg|_{i+1/2, j} \tag{4.45}$$

a)

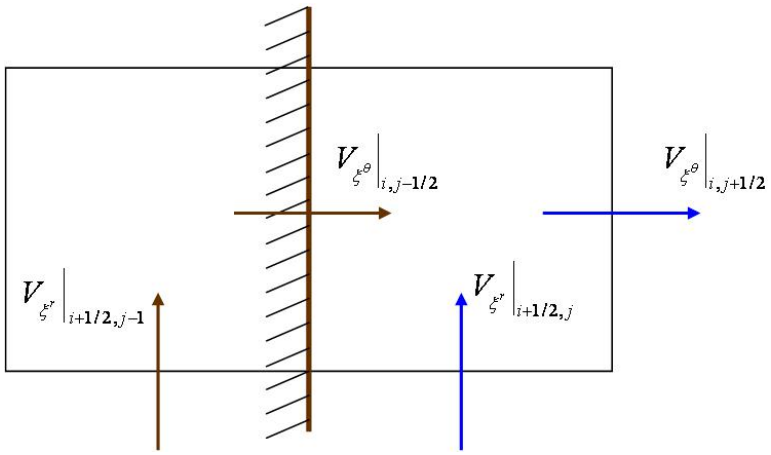

b)

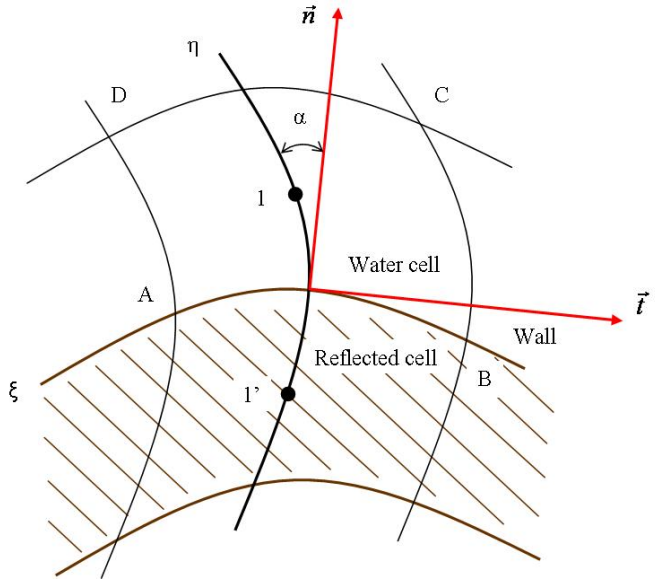

Figure 4.7: Ghost point method for evaluation of no slip and free slip land boundary conditions in the $\xi^r -$ direction: a) on a straight line boundary; b) on a curved boundary [Hirsch (1988)].

For equation (3.126) numerical discretization can be written:

in the $\xi^r -$ direction:

$$\frac{V_{\xi^\theta}\big|_{i,j+1/2} - V_{\xi^\theta}\big|_{i-1,j+1/2}}{h_{\xi^r}\big|_{i-1/2,j+1/2}\,\delta\xi^r} + \frac{V_{\xi^\theta}\big|_{i,j+1/2} + V_{\xi^\theta}\big|_{i-1,j+1/2}}{2R_w} = 0 \tag{4.46}$$

resulting in:

in the ξ^r – direction:

$$V_{\xi^\theta}\Big|_{i-1,\,j+1/2} = \frac{\left(1+h_{\xi^r}\Big|_{i-1/2,\,j+1/2}\delta\xi^r/2R_w\right)}{\left(1-h_{\xi^r}\Big|_{i-1/2,\,j+1/2}\delta\xi^r/2R_w\right)}V_{\xi^\theta}\Big|_{i,\,j+1/2} \tag{4.47}$$

Equation (4.47) is written for a positive radius, i.e. positive values of the normal to the curved boundary occur towards the inside of the flow domain. For a negative radius, or flow towards the boundary, the expression of vanishing vorticity is:

in the ξ^r – direction:

$$V_{\xi^\theta}\Big|_{i-1,\,j+1/2} = \frac{\left(1-h_{\xi^r}\Big|_{i-1/2,\,j+1/2}\delta\xi^r/2R_w\right)}{\left(1+h_{\xi^r}\Big|_{i-1/2,\,j+1/2}\delta\xi^r/2R_w\right)}V_{\xi^\theta}\Big|_{i,\,j+1/2} \tag{4.48}$$

4.5. Solution Technique

The solution technique employed in the numerical model is presented in this section. The example shown here is developed for the first time-step, i.e. $n \to n+1/2$.

The continuity equation can be written in differential form as in equation (3.112), with the finite difference representation given in equation (4.24). Rearranging equation (4.35) by moving all unknowns to LHS gives:

continuity equation

$$\begin{aligned}&\zeta_{i,j}^{n+½} + \frac{\delta t}{2\delta\xi^r}\frac{h_{\xi^\theta}\Big|_{i+1/2,\,j}}{J_\xi\Big|_{j,k}}q_{\xi^r}\Big|_{i+½,\,j}^{n+½} - \frac{\delta t}{2\delta\xi^r}\frac{h_{\xi^\theta}\Big|_{i-1/2,\,j}}{J_\xi\Big|_{i,\,j}}q_{\xi^r}\Big|_{i-½,\,j}^{n+½} \\ &= \zeta_{i,j}^{n} - \frac{\delta t}{2J_\xi\Big|_{i,\,j}}\frac{1}{\delta\xi^\theta}\left[\left(h_{\xi^r}q_{\xi^\theta}\right)\Big|_{i,\,j+½}^{n} - \left(h_{\xi^r}q_{\xi^\theta}\right)\Big|_{i,\,j-½}^{n}\right]\end{aligned} \tag{4.49}$$

Replacing known terms in (4.49) gives:

continuity equation

$$-r_{i-1/2}q_{\xi^r}\Big|_{i-\frac{1}{2},k}^{n+\frac{1}{2}}+\zeta_{i,j}^{n+\frac{1}{2}}+r_{i+1/2}q_{\xi^r}\Big|_{i+\frac{1}{2},j}^{n+\frac{1}{2}}=A_{i,j}^{n} \tag{4.50}$$

where:

$$r_{i-1/2}=\frac{\delta t}{2J_{\xi}\Big|_{i,j}}\frac{h_{\xi^\theta}\Big|_{i-1/2,k}}{\delta\xi^r} \tag{4.51}$$

$$r_{i+1/2}=\frac{\delta t}{2J_{\xi}\Big|_{i,j}}\frac{h_{\xi^\theta}\Big|_{i+1/2,j}}{\delta\xi^r} \tag{4.52}$$

$$A_{i,j}^{n}=\zeta_{i,j}^{n}-\frac{\delta t}{2J_{\xi}\Big|_{i,j}}\frac{1}{\delta\xi^\theta}\left[\left(h_{\xi^r}q_{\xi^\theta}\right)_{i,j+\frac{1}{2}}^{n}-\left(h_{\xi^r}q_{\xi^\theta}\right)_{i,j-\frac{1}{2}}^{n}\right] \tag{4.53}$$

At the same time step, the partial differential momentum equation in the ξ^r – direction is given by equation (3.115); equation (4.36) represents its finite difference equivalent. Hence, equation (4.36) can be written as:

ξ^r – direction momentum

$$\begin{aligned}
&q_{\xi^r}\Big|_{i+\frac{1}{2},j}^{n+\frac{1}{2}}=q_{\xi^r}\Big|_{i+\frac{1}{2},j}^{n-1/2}\\
&-\frac{\beta\delta t}{J_{\xi}\Big|_{i+1/2,j}}\left\{\frac{1}{\delta\xi^r}\left[\left(h_{\xi^\theta}V_{\xi^r}^{'}q_{\xi^r}^{'}\right)_{i+1,j}^{n}-\left(h_{\xi^\theta}V_{\xi^r}^{'}q_{\xi^r}^{'}\right)_{i,j}^{n}\right]\right.\\
&\left.+\frac{1}{\delta\xi^\theta}\left[\left(h_{\xi^r}q_{\xi^\theta}\right)_{i+1/2,j+1/2}^{n}V_{\xi^r}^{'}\Big|_{i+1/2,j+p}^{n}\right.\right.\\
&\left.\left.-\left(h_{\xi^r}q_{\xi^\theta}\right)_{j+1/2,k-1/2}^{n}V_{\xi^r}^{'}\Big|_{i+1/2,j-1+q}^{n}\right]\right.
\end{aligned} \tag{4.54}$$

$$+V_{\xi^\theta}\Big|^n_{i+1/2,j}\left[q'_{\xi^r}\Big|_{i+1/2,j}\frac{1}{\delta\xi^\theta}\left(h_{\xi^r}\Big|_{i+1/2,j+1/2}-h_{\xi^r}\Big|_{i+1/2,j-1/2}\right)\right.$$

$$\left.-q_{\xi^\theta}\Big|_{i+1/2,j}\frac{1}{\delta\xi^r}\left(h_{\xi^\theta}\Big|_{i+1,j}-h_{\xi^\theta}\Big|_{i,j}\right)\right]\Bigg\}+\delta tfq_{\xi^\theta}\Big|^n_{i+\frac{1}{2},j}$$

$$-\frac{g\Delta t}{2\Delta\xi^r}\frac{H}{h_{\xi^r}}\Bigg|^n_{i+\frac{1}{2},j}\left[\zeta^{n+\frac{1}{2}}_{i+1,j}-\zeta^{n+\frac{1}{2}}_{i,j}+\zeta^{n-\frac{1}{2}}_{i+1,j}-\zeta^{n-\frac{1}{2}}_{i,j}\right]$$

$$+\frac{\rho_a\Delta tC^*W_{\xi^r}(W_{\xi^r}{}^2+W_{\xi^\theta}{}^2)^{\frac{1}{2}}}{\rho}$$

$$-\frac{g\delta t(q_{\xi^r}{}'^2+q_{\xi^\theta}{}^2)^{\frac{1}{2}}}{2(HC)^2}\Bigg|^n_{i+1/2,j}\left(q_{\xi^r}\Big|^{n+\frac{1}{2}}_{i+\frac{1}{2},j}+q_{\xi^r}\Big|^{n-\frac{1}{2}}_{i+1/2,j}\right)$$

$$+\delta t\left(\overline{E}H\right)^n_{i+1/2,j}\left\{\frac{1}{h_{\xi^r}\Big|_{i+1/2,j}}\frac{1}{\left(\delta\xi^r\right)^2}\frac{1}{J_\xi\Big|_{i+1,j}}\left[\left(h_{\xi^\theta}V'_{\xi^r}\right)^n_{i+1/2,j}\right.\right. \tag{4.54}$$

continued

$$\left.-\left(h_{\xi^\theta}V'_{\xi^r}\right)^n_{i-1/2,j}\right]$$

$$-\frac{1}{h_{\xi^r}\Big|_{i+1/2,j}}\frac{1}{\left(\delta\xi^r\right)^2}\frac{1}{J_\xi\Big|_{i,j}}\left(\left(h_{\xi^\theta}V'_{\xi^r}\right)^n_{i+1/2,j}-\left(h_{\xi^\theta}V'_{\xi^r}\right)^n_{i-1/2,j}\right)\Bigg]$$

$$+\frac{1}{h_{\xi^\theta}\Big|_{i+1/2,j}}\frac{1}{\left(\delta\xi^\theta\right)^2}\left[\frac{1}{J_\xi\Big|_{i+1/2,j+1/2}}\left(\left(h_{\xi^r}V'_{\xi^r}\right)^n_{i+1/2,j+1}-\left(h_{\xi^r}V'_{\xi^r}\right)^n_{i+1/2,j}\right)\right.$$

$$\left.-\frac{1}{J_\xi\Big|_{i+1/2,j-1/2}}\left(\left(h_{\xi^r}V'_{\xi^r}\right)^n_{i+1/2,j}-\left(h_{\xi^r}V'_{\xi^r}\right)^n_{i+1/2,j-1}\right)\right]$$

$$+\frac{1}{h_{\xi^r}\Big|_{i+1/2,j}}\frac{1}{\delta\xi^r\delta\xi^\theta}\left[\frac{1}{J_\xi\Big|_{i+1,j}}\left(\left(h_{\xi^r}V_{\xi^\theta}\right)^n_{i+1,j+1/2}-\left(h_{\xi^r}V_{\xi^\theta}\right)^n_{i+1,j-1/2}\right)\right.$$

$$\left.-\frac{1}{J_\xi\Big|_{i,j}}\left(\left(h_{\xi^r}V_{\xi^\theta}\right)^n_{i,j+1/2}-\left(h_{\xi^r}V_{\xi^\theta}\right)^n_{i,j-1/2}\right)\right]$$

$$-\frac{1}{h_{\xi^\theta}\Big|_{i+1/2,j}}\frac{1}{\delta\xi^r\delta\xi^\theta}\left[\frac{1}{J_\xi\Big|_{i+1/2,j+1/2}}\left(\left(h_{\xi^\theta}V_{\xi^\theta}\right)^n_{i+1,j+1/2}-\left(h_{\xi^\theta}V_{\xi^\theta}\right)^n_{i,j+1/2}\right)\right.$$

$$-\frac{1}{J_{\xi}\Big|_{i+1/2,\,j-1/2}}\left(\left(h_{\xi^{\theta}}V_{\xi^{\theta}}\right)_{i+1,\,j-1/2}^{n}-\left(h_{\xi^{\theta}}V_{\xi^{\theta}}\right)_{i,\,j-1/2}^{n}\right)\Bigg]\Bigg\} \tag{4.54}$$

continued

Moving all the unknown terms in equation (4.54) to the left and replacing known terms gives the form of the momentum equation in the ξ^{r} – direction in terms of recursion coefficients:

$$-s_i\zeta_{i,j}^{n+1/2}+s_{i+1/2}q_{\xi}\Big|_{i+1/2,\,j}^{n+1/2}+s_{i+1}\zeta_{i+1,j}^{n+1/2}=B_{i+1/2,\,j}^{n-1/2} \tag{4.55}$$

where:

$$s_{i+1}=s_i=\frac{g\delta t}{2\delta\xi}\left(\frac{H}{h_1}\right)_{i+1/2,\,j}^{n} \tag{4.56}$$

$$s_{i+1/2}=1+\frac{g\delta t(q_{\xi^{r}}{}'^{2}+q_{\xi^{\theta}}{}^{2})^{1/2}}{2(HC)^{2}}\Bigg|_{i+1/2,\,j}^{n} \tag{4.57}$$

$$\begin{aligned}
&B_{i+1/2,\,j}^{n}\\
&=q_{\xi^{r}}\Big|_{i+1/2,\,j}^{n-1/2}-\frac{\beta\delta t}{J_{\xi}\Big|_{i+1/2,\,j}}\left\{\frac{1}{\Delta\xi^{r}}\left[\left(h_{\xi^{\theta}}V_{\xi^{r}}^{'}q_{\xi^{r}}^{'}\right)_{i+1,\,j}^{n}-\left(h_{\xi^{\theta}}V_{\xi^{r}}^{'}q_{\xi^{r}}^{'}\right)_{i,\,j}^{n}\right]\right.\\
&+\frac{1}{\delta\xi^{\theta}}\left[\left(h_{\xi^{r}}q_{\xi^{\theta}}\right)\Big|_{i+1/2,\,j+1/2}^{n}V_{\xi^{r}}^{'}\Big|_{i+1/2,\,j+p}^{n}\right.\\
&\left.\left.-\left(h_{\xi^{r}}q_{\xi^{\theta}}\right)\Big|_{j+1/2,k-1/2}^{n}V_{\xi^{r}}^{'}\Big|_{i+1/2,\,j-1+q}^{n}\right]\right.\\
&+V_{\xi^{\theta}}\Big|_{i+1/2,\,j}^{n}\left[q_{\xi^{r}}^{'}\Big|_{i+1/2,\,j}\frac{1}{\delta\xi^{\theta}}\left(h_{\xi^{r}}\Big|_{i+1/2,\,j+1/2}-h_{\xi^{r}}\Big|_{i+1/2,\,j-1/2}\right)\right.\\
&\left.\left.-q_{\xi^{\theta}}\Big|_{i+1/2,\,j}\frac{1}{\delta\xi^{r}}\left(h_{\xi^{\theta}}\Big|_{i+1,\,j}-h_{\xi^{\theta}}\Big|_{i,\,j}\right)\right]\right\}+\delta tfq_{\xi^{\theta}}\Big|_{i+1/2,\,j}^{n}\\
&-\frac{g\delta t}{2\delta\xi^{r}}\frac{H}{h_{\xi^{r}}}\Bigg|_{i+1/2,\,j}^{n}\left(\zeta_{i+1,\,j}^{n-1/2}-\zeta_{i,\,j}^{n-1/2}\right)
\end{aligned} \tag{4.58}$$

$$
+\frac{\rho_a \delta t C^* W_{\xi^r}\left(W_{\xi^r}{}^2+W_{\xi^\theta}{}^2\right)^{1/2}}{\rho}
$$

$$
-\frac{g\delta t\left(q_{\xi^r}{}'^2+q_{\xi^\theta}{}^2\right)^{1/2}}{2(HC)^2}\Bigg|_{i+1/2,j}^{n} q_{\xi^r}\Big|_{i+1/2,j}^{n-1/2}
$$

$$
+\delta t\left(\overline{E}H\right)_{i+1/2,j}^{n}\left\{\frac{1}{h_{\xi^r}\Big|_{i+1/2,j}}\frac{1}{\left(\delta\xi^r\right)^2}\times\right.
$$

$$
\left[\frac{1}{J_\xi\Big|_{i+1,j}}\left(\left(h_{\xi^\theta}V'_{\xi^r}\right)_{i+3/2,j}^{n}-\left(h_{\xi^\theta}V'_{\xi^r}\right)_{i+1/2,j}^{n}\right)\right.
$$

$$
\left.\left.-\frac{1}{J_\xi\Big|_{i,j}}\left(\left(h_{\xi^\theta}V'_{\xi^r}\right)_{i+1/2,j}^{n}-\left(h_{\xi^\theta}V'_{\xi^r}\right)_{i-1/2,j}^{n}\right)\right]\right.
$$

$$
+\frac{1}{h_{\xi^\theta}\Big|_{i+1/2,j}}\frac{1}{\left(\delta\xi^\theta\right)^2}\times
$$

$$
\left[\frac{1}{J_\xi\Big|_{i+1/2,j+1/2}}\left(\left(h_{\xi^r}V'_{\xi^r}\right)_{i+1/2,j+1}^{n}-\left(h_{\xi^r}V'_{\xi^r}\right)_{i+1/2,j}^{n}\right)\right.
$$

$$
\left.-\frac{1}{J_\xi\Big|_{i+1/2,j-1/2}}\left(\left(h_{\xi^r}V'_{\xi^r}\right)_{i+1/2,j}^{n}-\left(h_{\xi^r}V'_{\xi^r}\right)_{i+1/2,j-1}^{n}\right)\right]
$$

$$
+\frac{1}{h_{\xi^r}\Big|_{i+1/2,j}}\frac{1}{\delta\xi^r\delta\xi^\theta}\left[\frac{1}{J_\xi\Big|_{i+1,j}}\left(\left(h_{\xi^r}V_{\xi^\theta}\right)_{i+1,j+1/2}^{n}-\left(h_{\xi^r}V_{\xi^\theta}\right)_{i+1,j-1/2}^{n}\right)\right.
$$

$$
\left.-\frac{1}{J_\xi\Big|_{i,j}}\left(\left(h_{\xi^r}V_{\xi^\theta}\right)_{i,j+1/2}^{n}-\left(h_{\xi^r}V_{\xi^\theta}\right)_{i,j-1/2}^{n}\right)\right]
$$

$$
-\frac{1}{h_{\xi^\theta}\Big|_{i+1/2,j}}\frac{1}{\delta\xi^r\delta\xi^\theta}\times
$$

$$
\left[\frac{1}{J_\xi\Big|_{i+1/2,j+1/2}}\left(\left(h_{\xi^\theta}V_{\xi^\theta}\right)_{i+1,j+1/2}^{n}-\left(h_{\xi^\theta}V_{\xi^\theta}\right)_{i,j+1/2}^{n}\right)\right.
$$

$$
\left.\left.-\frac{1}{J_\xi\Big|_{i+1/2,j-1/2}}\left(\left(h_{\xi^\theta}V_{\xi^\theta}\right)_{i+1,j-1/2}^{n}-\left(h_{\xi^\theta}V_{\xi^\theta}\right)_{i,j-1/2}^{n}\right)\right]\right\}
$$

(4.58)

continued

In equations (4.53) and (4.58), $r_{i-1/2}, r_{i+1/2}, s_i, s_{i+1/2}, s_{i+1}$ are recursion coefficients. The terms $A_{i,j}^{n-1/2}$, $B_{i+1/2,j}^{n-1/2}$ consist of a combination of terms containing known values of ς and q_{ς^r} at time previous time step.

4.5.1. Thomas Algorithm - General considerations

A system of equations to be solved is tridiagonal if equation number *i* in the system only involves the *y* unknowns with numbers $i-1, i, i+1$. Following Morton and Myers (2005), the tridiagonal system for *n* unknowns can be written as:

$$-\alpha_i y_{i-1} + \beta_i y_i - \chi_i y_{i+1} = \lambda_i \quad \text{for } i = 1,...,n \tag{4.59}$$

with $\alpha_1 = 0$ and $\chi_n = 0$. In matrix form, equation (4.59) can be written:

$$\begin{pmatrix} \beta_1 & \chi_1 & & & 0 \\ \alpha_2 & \beta_2 & \chi_2 & & \\ & & & & \\ & & \alpha_{n-1} & \beta_{n-1} & \chi_{n-1} \\ 0 & & & \alpha_n & \beta_n \end{pmatrix} \cdot \begin{pmatrix} y_1 \\ y_2 \\ \\ y_{n-1} \\ y_n \end{pmatrix} = \begin{pmatrix} \lambda_1 \\ \lambda_2 \\ \\ \lambda_{n-1} \\ \lambda_n \end{pmatrix} \tag{4.60}$$

The condition for the matrix in equation (4.60) to be solved using Thomas algorithm is that the matrix is diagonally dominant:

$$|\alpha_i| + |\chi_i| < |\beta_i| \quad \text{for } i = 1,...,n-1 \tag{4.61}$$

Thomas algorithm reduces the system of equations to upper triangular form, by eliminating the term containing unknown y_{i-1} in each of the equations. This is done by treating each equation in turn. Suppose that the first *k* equations have been reduced to:

$$y_i - \chi_i^{'} y_{i+1} = \lambda_i^{'} \quad \text{for } i = 1,...,k \tag{4.62}$$

At $i = k$ the equation has the form:

$$y_k - \chi_k^{'} y_{k+1} = \lambda_k^{'} \tag{4.63}$$

At $i = k+1$ the equation is still in its original form:

$$-\alpha_{k+1} y_k + \beta_{k+1} y_{k+1} - \chi_{k+1} y_{k+2} = \lambda_{k+1} \tag{4.64}$$

Eliminating y_k between equations (4.63) and (4.64) gives:

$$\begin{aligned} &-\alpha_{k+1}\left(\chi_k^{'} y_{k+1} + \delta_k^{'}\right) + \beta_{k+1} y_{k+1} - \chi_{k+1} y_{k+2} = \lambda_{k+1} \\ &\left(-\alpha_{k+1}\chi_k^{'} + \beta_{k+1}\right) y_{k+1} - \chi_{k+1} y_{k+2} = \lambda_{k+1} + \alpha_{k+1}\lambda_k^{'} \\ &y_{k+1} - \frac{\chi_{k+1}}{-\alpha_{k+1}\chi_k^{'} + \beta_{k+1}} y_{k+2} = \frac{\lambda_{k+1} + \alpha_{k+1}\lambda_k^{'}}{-\alpha_{k+1}\chi_k^{'} + \beta_{k+1}} \end{aligned} \tag{4.65}$$

Identifying the recursion coefficients in equation (4.65) one gets:

$$\chi_{i+1}^{'} = \frac{\chi_{i+1}}{-\alpha_{i+1}\chi_i^{'} + \beta_{i+1}} \tag{4.66a}$$

$$\delta_{i+1}^{'} = \frac{\lambda_{i+1} + \alpha_{i+1}\lambda_i^{'}}{-\alpha_{i+1}\chi_i^{'} + \beta_{i+1}} \tag{4.66b}$$

The recursion coefficients have the expressions:

$$\chi_i^{'} = \begin{cases} \dfrac{\chi_1}{\beta_1} \text{ for i} = 1 \\ \dfrac{\chi_i}{\beta_i - \chi_{i-1}^{'}\alpha_i} \text{ for i} = 2,...,\text{n} - 1 \end{cases} \tag{4.67}$$

$$\lambda_i^{'} = \begin{cases} \dfrac{\lambda_1}{\beta_1} \text{ for i} = 1 \\ \dfrac{\lambda_i + \lambda_{i-1}^{'}\alpha_i}{\beta_i - \chi_{i-1}^{'}\alpha_i} \text{ for i} = 2,...,\text{n -1} \end{cases} \tag{4.68}$$

The unknowns y_i are obtained from equation (4.63): beginning from the known value of y_n one gets the values y_{n-1}, y_{n-2} and so on, finishing with y_1.

4.5.2. Thomas Algorithm for the Governing Equations

Solutions of the system of recursion equations (4.53) and (4. 58) can be found by means of Thomas algorithm and its implementation is presented next. Unknown values of q_{ξ^r} and ζ can be evaluated by a process of elimination of the unknowns. Starting at $i = 1$, and given that $\zeta_{1,j}^{n+1/2}$ is a known boundary condition, the unknown $q_{\xi^r}\Big|_{1+1/2,j}^{n+1/2}$ in (4.58) can be written in the form:

$$q_{\xi^r}\Big|_{1+1/2,j}^{n+1/2} = -R_1\zeta_{2,j}^{n+1/2} + S_1 \tag{4.69}$$

At $i = 2$, (4.69) can then be substituted into (4.53) to eliminate the flux $q_{\xi^r}\Big|_{1+1/2,j}^{n+1/2}$ obtaining an equation for $\zeta_{2,j}^{n+1/2}$ of the form:

$$\zeta_{2,j}^{n+1/2} = -P_2 q_{\xi^r}\Big|_{2+1/2,j}^{n+1/2} + Q_2 \tag{4.70}$$

At $i = 3$, (4.70) can then be substituted back into (4.34) to eliminate $\zeta_{2,j}^{n+1/2}$ and so on and so forth for $i = 1,2,...I_{\max}$. The elimination of unknowns in this manner is known as Gaussian elimination. In their general recursive forms the continuity and momentum equations may be written respectively as:

$$\zeta_{i,j}^{n+1/2} = -P_i q_{\xi^r}\Big|_{i+1/2,j}^{n+1/2} + Q_i \tag{4.71}$$

$$q_{\xi^r}\Big|_{i+\frac{1}{2},j}^{n+\frac{1}{2}} = -R_i \zeta_{i+1,j}^{n+\frac{1}{2}} + S_i \tag{4.72}$$

where P_i, Q_i, R_i, S_i are recursion terms computed at $i = 2,3,\ldots,I_{\max}$ as follows:

$$P_i = \frac{r_{i+1/2}}{1 + r_{i-1/2} R_{i-1}} \tag{4.73}$$

$$Q_i = \frac{A_{i,j}^n + r_{i-1/2} S_{i-1}}{1 + r_{i-1/2} R_{i-1}} \tag{4.74}$$

$$R_i = \frac{s_{i+1}}{s_{i+1/2} + s_i P_i} \tag{4.75}$$

$$S_i = \frac{B_{i+1/2,j}^n + s_i Q_i}{s_{i+1/2} + s_i P_i} \tag{4.76}$$

Recursion terms P_i, Q_i are not required at $i = 1$. For the case $i = 1$, the remaining recursion terms are computed as:

$$R_1 = \frac{s_{1+1}}{s_{1+1/2}} \tag{4.77}$$

$$S_1 = \frac{B_{1+1/2,j}^n + s_1 \zeta_{1,j}^{n+\frac{1}{2}}}{s_{1+1/2}} \tag{4.78}$$

Upon reaching $I_{\max} - 1$ one will have an equation in the form of (4.72) with $q_{\xi^r}\Big|_{I_{\max}-\frac{1}{2},j}^{n+\frac{1}{2}}$ is expressed in terms of $\zeta_{I_{\max},j}^{n+\frac{1}{2}}$. Water elevation is provided by the upper boundary condition and allows $q_{\xi^r}\Big|_{I_{\max}-\frac{1}{2},j}^{n+\frac{1}{2}}$ to be calculated. Backward

substitution is then used to determine $\zeta_{i,j}^{n+1/2}$ from (4.71) and $q_{\xi^r}\Big|_{i+1/2,j}^{n+1/2}$ from (4.72) at each value of i.

4.5.3. Representation of the Recursion Coefficients in the Numerical Model

The general forms of the recursion equations are represented in the new model as in equations (4.79)-(4.80) and notation of the variables in the Fortran code is given in Table 4.2. In equations (4.79)-(4.92), the formulation of the equation in the numerical model is first shown and it is followed by the equivalent mathematical expression.

$$\begin{aligned} &EU(I,J) = -P(I) * QXU(I,J) + Q(I) \rightarrow \\ &\zeta_{i,j}^{n+1/2} = -P_i q_{\xi^r}\Big|_{i+1/2,j}^{n+1/2} + Q_i \end{aligned} \tag{4.79}$$

$$\begin{aligned} &QXU(IM1,J) = -R(IM1) * EU(I,J) + S(IM1) \\ &\rightarrow \quad q_{\xi^r}\Big|_{i+1/2,j}^{n+1/2} = -R_i \zeta_{i+1,j}^{n+1/2} + S_i \end{aligned} \tag{4.80}$$

The recursion terms P_i, Q_i, R_i, S_i representation in the cylindrical co-ordinates numerical model is given in equations (4.81)-(4.84).

$$P(I) = \frac{RIP1}{1 + RIM1 * R(IM1)} \rightarrow P_i = \frac{r_{i+1/2}}{1 + r_{i-1/2} R_{i-1}} \tag{4.81}$$

$$Q(I) = \frac{AI + RIM1 * S(IM1)}{1 + RIM1 * R(IM1)} \rightarrow Q_i = \frac{A_{i,j}^n + r_{i-1/2} S_{i-1}}{1 + r_{i-1/2} R_{i-1}} \tag{4.82}$$

$$\begin{aligned} &R(I) = \frac{D1XDPC}{(1 + D4BDFR) + D1XDPC * P(I)} \quad \rightarrow \\ &R_i = \frac{s_{i+1}}{s_{i+1/2} + s_i P_i} \text{ for } i = 2,3,...,I_{\max} \end{aligned} \tag{4.83}$$

$$S_i = \frac{B^n_{i+1/2,j} + s_i Q_i}{s_{i+1/2} + s_i P_i} \rightarrow$$

$$S(I) = \frac{BI + D1XDPC * Q(I)}{(1 + D4BDFR) + D1XDPC * P(I)} \text{ for } i = 2,3,..., I_{\max} \tag{4.84}$$

From equations (4.81)-(4.84) it can be seen that the new model representations of the recursive coefficients $s_i, s_{i+1}, s_{i+1/2}, r_{i-1/2}, r_{i+1/2}, A^n_{i,j}, B^n_{i+1/2,j}$ are as follows:

$$D1XDPC \rightarrow s_{i+1} = s_i \tag{4.85}$$

$$TEMP1 = 1 + D4BDFR \rightarrow s_{i+1/2} \tag{4.86}$$

$$RIM1 = C1X * HGYAVB / HG2IJ \rightarrow r_{i-1/2} \tag{4.87}$$

$$RIP1 = C1X * HGYAVC / HG2IJ \rightarrow r_{i+1/2} \tag{4.88}$$

$$AI \rightarrow A^n_{i,j} \tag{4.89}$$

$$BI \rightarrow B^n_{i+1/2,j} \tag{4.90}$$

For the special case $i = 1$, R_i and S_i are represented as follows:

$$R(IBM1) = \frac{D1XDPC}{TEMP1} \rightarrow R_1 = \frac{s_{i+1}}{s_{i+1/2}} \tag{4.91}$$

$$S(IBM1) = \frac{BIBM1 + D1XDPC * EU(1,J)}{(1 + D4BDFR)} \rightarrow S_1 = \frac{B^n_{1+1/2,j} + s_1 \zeta^{n+1/2}_{1,j}}{s_{1+1/2}} \tag{4.92}$$

Variable Description	Mathematical Model	Numerical Model
Time step	δt	DT
Scale factor in the ξ^r – direction	$h_{\xi^r}\Big\|_{i+1/2,j}$	$HGEOMX(I,J)$
Scale factor in the ξ^θ – direction	$h_{\xi^\theta}\Big\|_{i,j+1/2}$	$HGEOMY(I,J)$
Total water depth in the ξ^r – direction	$H_{i+1/2,j}$	$DEPX(I,J)$
Total water depth in the ξ^θ – direction	$H_{i,j+1/2}$	$DEPY(I,J)$
Flux in the ξ^r – direction	$q_{\xi^r}\Big\|^{n+1/2}_{i+1/2,j}$	$QXU(I,J)$
	$q_{\xi^r}\Big\|^{n}_{i+1/2,j}$	$QXM(I,J)$
	$q_{\xi^r}\Big\|^{n-1/2}_{i+1/2,j}$	$QXL(I,J)$
Flux in the ξ^θ – direction	$q_{\xi^\theta}\Big\|^{n+1}_{i+1/2,j}$	$QYU(I,J)$
	$q_{\xi^\theta}\Big\|^{n+1/2}_{i+1/2,j}$	$QYM(I,J)$
	$q_{\xi^\theta}\Big\|^{n-1}_{i+1/2,j}$	$QYL(I,J)$
Water elevation in the ξ^r – direction	$\zeta\Big\|^{n+1/2}_{i,j}$	$EU(I,J)$
	$\zeta\Big\|^{n}_{i,j}$	$EM(I,J)$
	$\zeta\Big\|^{n-1/2}_{i,j}$	$EL(I,J)$
Water elevation in the ξ^θ – direction	$\zeta\Big\|^{n+1}_{i,j}$	$EU(I,J)$
	$\zeta\Big\|^{n+1/2}_{i,j}$	$EM(I,J)$
	$\zeta\Big\|^{n}_{i,j}$	$EL(I,J)$

Table 4.2: Description of some variables and the equivalence between mathematical and numerical model representation of variables.

Figure 4.8 shows the equivalence between finite difference grid and computer notations. Scale factors are defined at the same locations as velocities, namely: scale factors in the ξ^r – direction are located at the same point on the computer grid as the U velocity, and scale factors in the ξ^θ – direction are located at the same point on the computer grid as the V velocity, respectively. Main variables used in the mathematical and numerical model are given in Table 4.2.

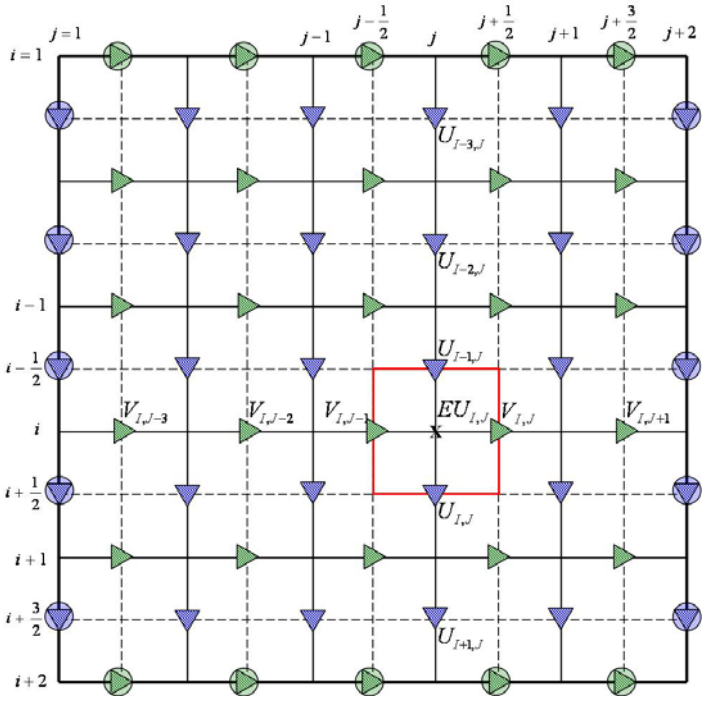

Figure 4.8: Velocities and water elevation representation on computer grid showing finite difference grid points as well. Circumscribed triangles represent boundary velocities.

4.5.4. Implementation of Solution Procedure in the Numerical Model

The flowchart in Figure 4.2 is changed to the one in Figure 4.9, in order to accommodate the ADI method, which applies hydrodynamic open boundary conditions and solution procedure in each direction at every half time step.

As will be later seen in Chapter 5, numerical solution exhibits a time splitting character at even-odd times, which can be corrected by introduction of a weak time filter, namely the Asselin filter. Based on the split character of the discretization method chosen for research, the time filter has to be applied at each half time step, after the hydrodynamic solution was obtained in one

direction. Therefore, the flowchart of the numerical model in its final form is given in Figure 4.10.

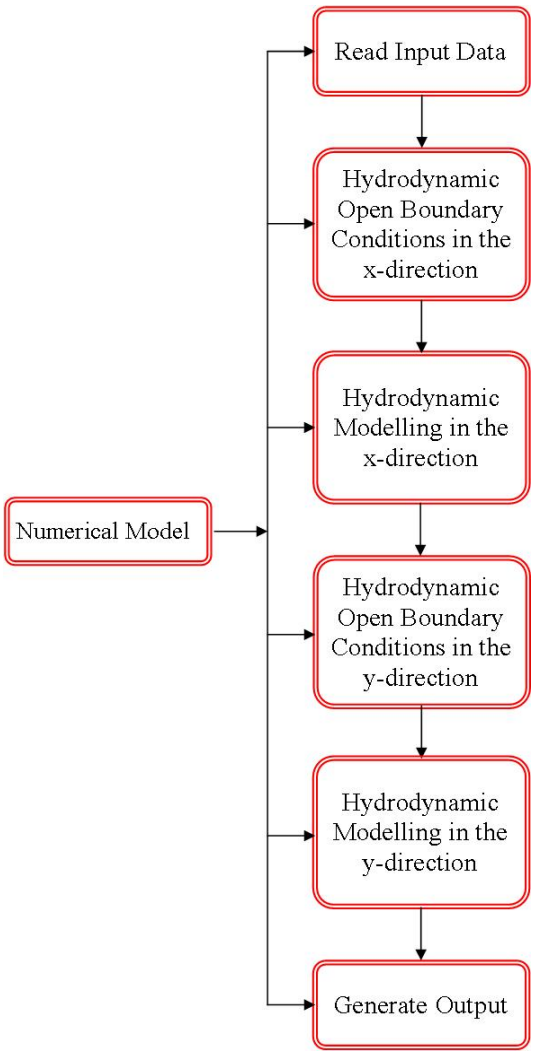

Figure 4.9: Code flowchart based on the ADI technique.

The code is structured into a Main Program which directly or indirectly calls 24 subroutines [Figure 4.11]. Also, in the Main Program the Author's transformation of the computed water elevation time series according to the wave energy conservation condition [Annex 11] is performed.

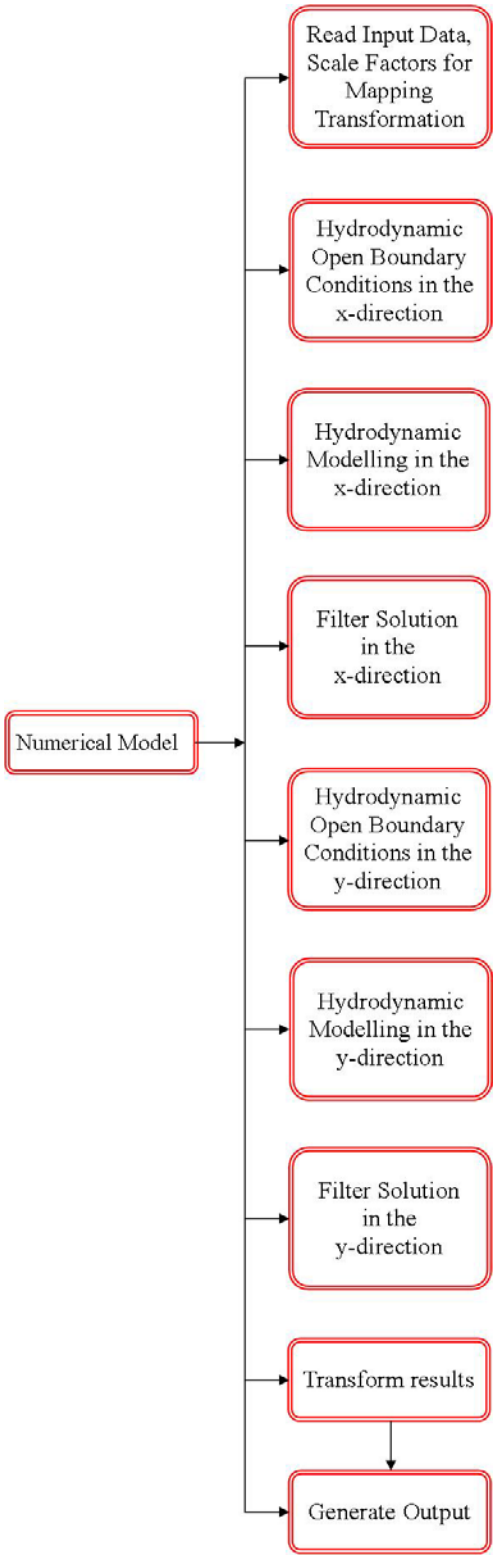

Figure 4.10: Final form of Fortran code flowchart.

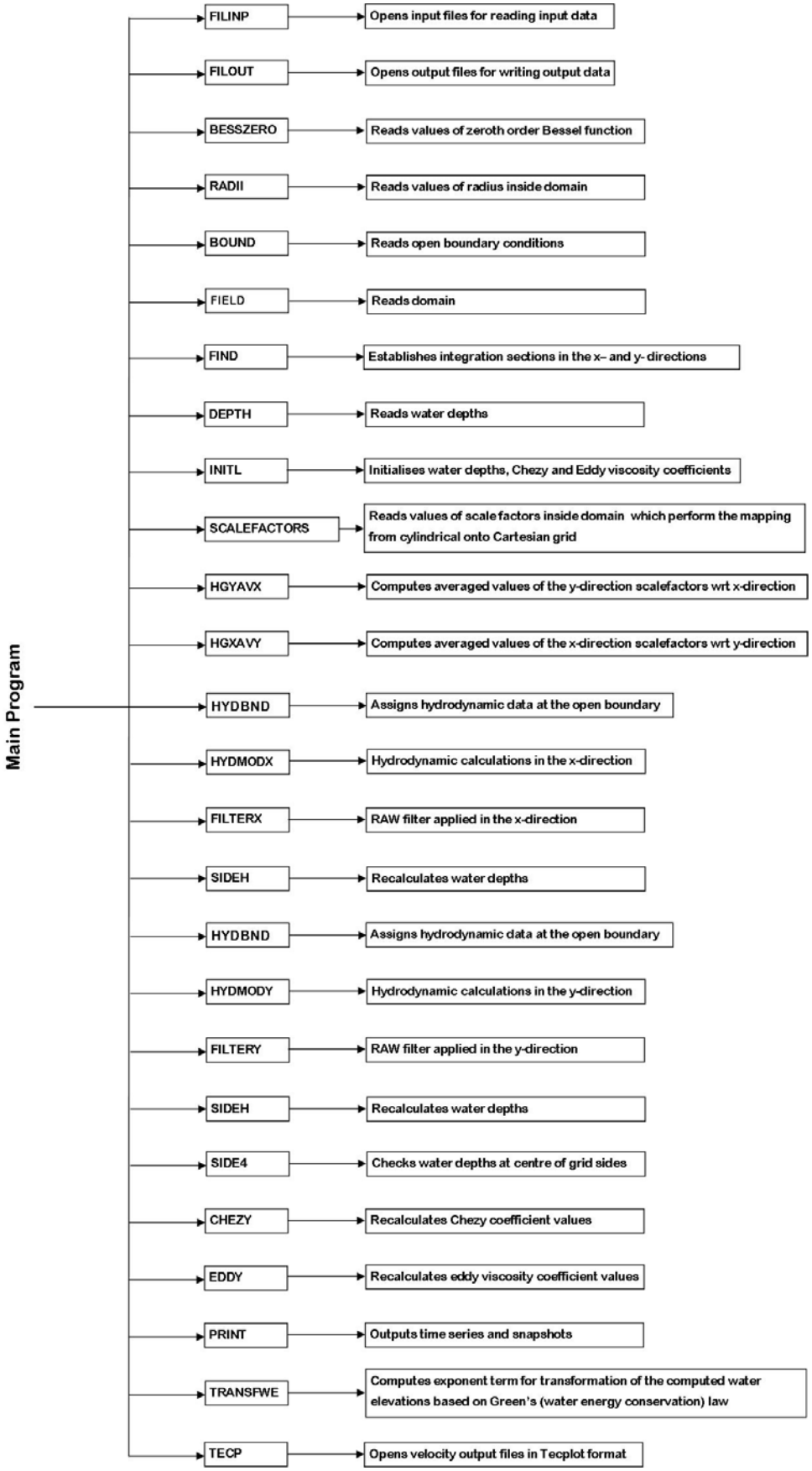

Figure 4.11: Structure of the numerical model.

In order to obtain the solution of the governing equations in the ξ^r – direction, the wet grid cells can be defined for $I = IB, IT$ as in Figure 4.12a). At the lower end of the wetted domain $I = IBM1$ represents the lower boundary, and similarly, at the upper end there is an upper boundary ($I = ITP1$). Both $I = IBM1$ and $I = ITP1$ can be used to represent either open or closed boundary conditions.

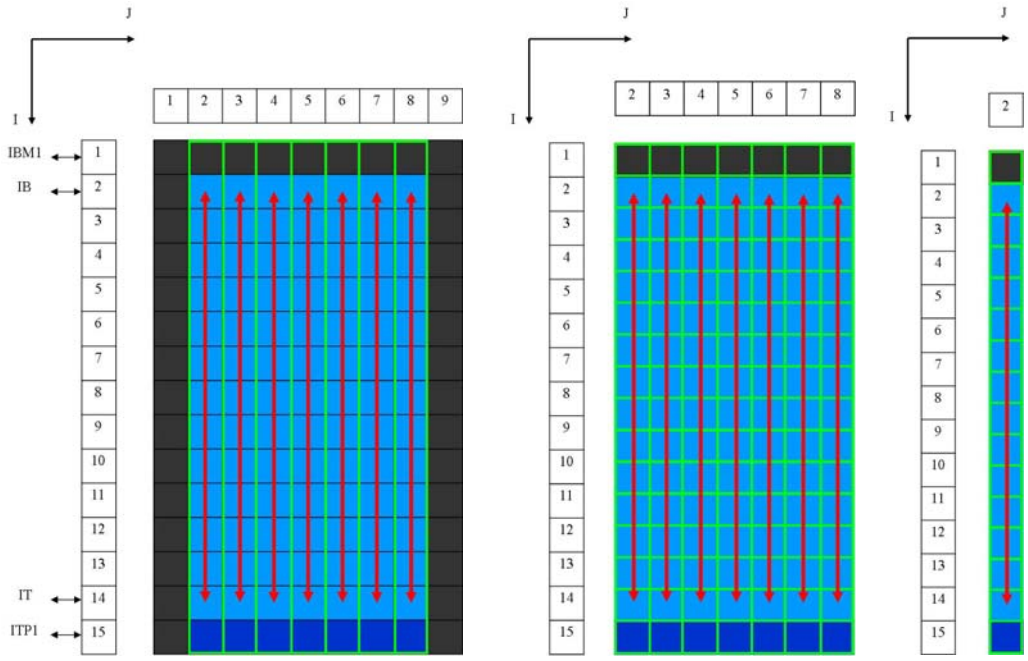

a) Model grid

b) Integration sections for given model grid

c) One integration section

Figure 4.12: Computational domain for solution technique in the ξ^r – direction. Grey cells represent land, light blue cells show water cells, dark blue cells illustrate open boundary. Red arrows show direction of calculations in each integration section [Nash (2010)].

For the calculus to be performed in the ξ^r –(or I –) direction, the wet grid cells are represented in the ξ^θ – (or J –) direction along columns, known as integration sections, or IS , represented in Figure 4.12b).

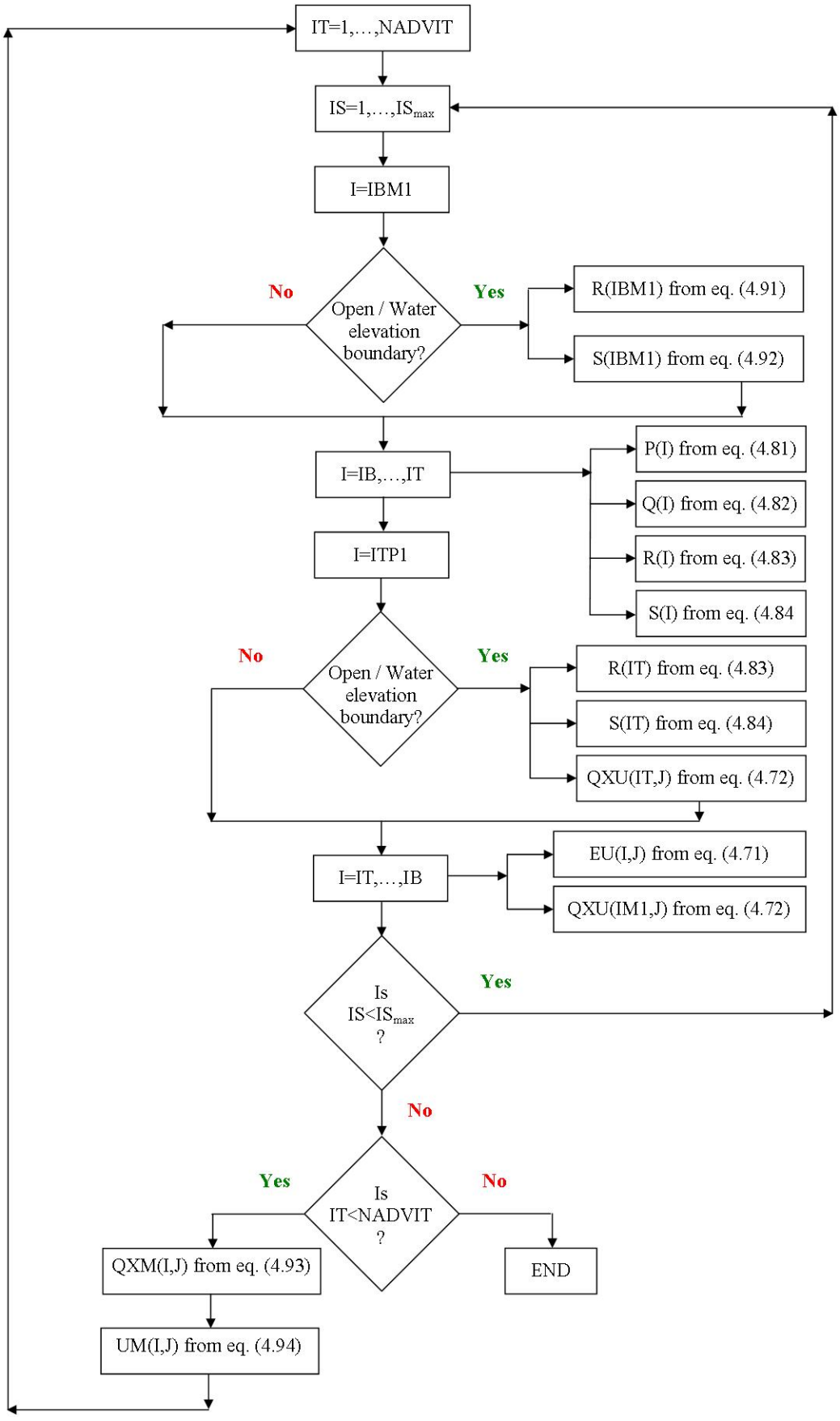

Figure 4.13: Flowchart of subroutine HYDMODX showing implementation of the solution procedure in the $\xi^r -$(or $I -$) direction.

During the first half time step solution for velocity components and water elevation is obtained in the ξ^r – direction. Calculus starts at first integration section (in the $J-$ or $\xi^\theta-$ direction) corresponding to value 2 in Figure 4.12c) and is performed for all wet cells. At $I = IBM1$ the values of recursion coefficients $R(IBM1)$ and $S(IBM1)$ are calculated using equations (4.91) and (4.92), for $I = IBM1$ representing open and water elevation boundary. Calculus progresses within the open boundary reach from IB to IT. During this first sweep all recursion coefficients are calculated. At $I = ITP1$ two recursion coefficients are recalculated, $R(IT)$ and $S(IT)$, and equation (4.72) is used to obtain $QXU(IT, J)$. Second sweep considers all I values between IT and IB, and for all wet or potentially wet cells computes $EU(I, J)$ using (4.71), and $QXU(IM1, J)$ using (4.72) and calculus can advance to the next integration section. The maximum number of iterations for advection terms was set to two. While the current number of the advection iteration is smaller than the maximum number of advection iterations set in the input file, $QXM(I, J)$ and $UM(I, J)$ are calculated based on equations (4.93) and (4.94). The procedure is iterated between integration sections corresponding to 2,3,4,...,8 in the ξ^θ – direction in Figure 4.12a) and 4.12b). The flowchart of solution procedure for all integration sections, included in subroutine HYDMODX, is given in Figure 4.13.

$$QXM(I, J) = \frac{1}{2}\left[QXU(I, J) + QXL(I, J)\right] \tag{4.93}$$

$$UM(I, J) = QXM(I, J) / DEPX(I, J) \tag{4.94}$$

4.6. Summary

Finite difference formulations of the equations governing water motion and conservation of mass were presented in this chapter. Spatial discretization of the equations was performed using finite differences on a staggered grid, the Arakawa C grid, and a two-step finite difference Alternating Direction Implicit technique was utilized for time discretization. Also, a general solution approach for the resulting tridiagonal system of equations was described, namely the Thomas algorithm. Application of the aforementioned procedure to the numerical model was shown. Representations of the recursion terms in the code were included as well. The initial flowchart of the code was modified to accommodate the ADI method and the weak Asselin time filter. The final structure of the code was presented herein.

Chapter 5

Cylindrical Co-ordinates Numerical Model Results

5.1. Introduction

The mathematical model developed in Chapter 3 and implemented in the numerical model as seen in Chapter 4 is used in various test cases. Results of the numerical model are compared against results of numerical models with extensive applications in industry. Two models are used for verification of the results: DIVAST and EFDC and short descriptions of their hydrodynamics modules are given in Appendix 12 and Appendix 13, respectively. There are three test cases used in the thesis for comparison with the two numerical models: horizontal bed with constant scale factors in the radial direction; horizontal bed with one variation of the scale factors in the radial direction; horizontal bed with two variations of the scale factors in the radial direction. Also, verification of the results is done against experimental data obtained in the tidal basin laboratory by Olbert (2006) and analytical solution of Lynch and Gray (1978). For the validation of the results versus measurements, again three test cases are considered: generation of the rectangular geometry from cylindrical co-ordinates, transformation of the numerical model from cylindrical to uniform Cartesian co-ordinates by setting up the scale factors to unity, and transformation of the numerical model from cylindrical to irregular Cartesian co-ordinates in the direction of flow.

The present chapter describes implementation of a weak filter that conserves the three-time-level mean in the numerical model due to solution splitting at odd-even times in preliminary results of the numerical model, evaluation of the numerical model results against two other robust numerical models for the three test cases mentioned in the previous paragraph, as well as validation of the results from tidal basin measurements and analytical solution.

5.2. Preliminary Results of the Cylindrical Co-ordinates Numerical Model

5.2.1. Computational Mode

In order to define the computational mode a simplified problem is presented. For example, equation (5.1) for the unknown quantity φ can be discretized using a three-time level leapfrog scheme [equation (5.2)].

$$\frac{\partial \varphi}{\partial t} + c\frac{\partial \varphi}{\partial x} = 0 \tag{5.1}$$

$$\varphi_l^{n+1} - \varphi_l^{n-1} = -C_r\left(\varphi_{l+1}^n - \varphi_{l-1}^n\right) \tag{5.2}$$

where: $c = \sqrt{gH}$ is the wave speed; $C_r = \frac{\delta t}{\delta x}\sqrt{gH}$ is the Courant number.

Representation of the variable φ_l^n as $\varphi^0 \lambda_l^n e^{ikl\delta x}$, with k the wavenumber, $i = \sqrt{-1}$ and n an exponent, leads to the following form of the discretized equation:

$$\begin{aligned}&\varphi^0 \lambda_l^{n+1} e^{ikl\delta x} - \varphi^0 \lambda_l^{n-1} e^{ikl\delta x} = \\ &-C_r\left(\varphi^0 \lambda_{l+1}^n e^{ik(l+1)\delta x} - \varphi^0 \lambda_{l-1}^n e^{ik(l-1)\delta x}\right)\end{aligned} \tag{5.2}$$

Dividing equation (5.2) by $\varphi^0 e^{ikl\delta x}$ and considering $\lambda_l^n = \lambda_{l+1}^n = \lambda_{l-1}^n = \lambda^n$ one gets:

$$\lambda^{n+1} - \lambda^{n-1} = -C_r \lambda^n \left(e^{ik\delta x} - e^{-ik\delta x}\right) \tag{5.3}$$

The term $\left(e^{ik\delta x} - e^{-ik\delta x}\right)$ can be written as $2i\sin(k\delta x)$ and the resulting equation has the form:

$$\lambda^{n+1} - \lambda^{n-1} = -C_r \lambda^n 2i \sin(k\delta x) \tag{5.4}$$

Equation (5.4) can be divided by λ^{n-1} giving:

$$\lambda^2 + 2i\lambda C_r \sin(k\delta x) - 1 = 0 \tag{5.5}$$

The two solutions of the above equation are:

$$\lambda_1 = iC_r \sin(k\delta x) + \sqrt{1 - [C_r \sin(k\delta x)]^2} \tag{5.6}$$

$$\lambda_2 = iC_r \sin(k\delta x) - \sqrt{1 - [C_r \sin(k\delta x)]^2} \tag{5.7}$$

Equation (5.6) represents the physical mode, since for $\delta x \to 0$ and $\delta t \to 0$ $\lambda_1 \to 1$. Equation (5.7) defines the computational mode, since for infinitesimal values of the time and space steps $\lambda_2 \to -1$.

Time discretization of the non-linear flow equations can generate a time splitting based on the presence of an undamped computational mode added to the physical mode.

5.2.2. The Robert-Asselin-Williams Filter

For a domain defined as in Figure 5.1, the time discretization scheme used within the cylindrical co-ordinates numerical model generated an odd-even decoupling of the solution [Figure 5.2] similar to the computational mode described in Section 5.2.1. In ocean numerical modelling the problem can be overcome introducing a correction step, as in EFDC, or a weak filter developed by Asselin (1972):

$$F_s^n = F_c^n - \frac{\alpha}{2}\left(F_c^{n+1} - 2F_c^n + F_s^{n-1}\right) \tag{5.8}$$

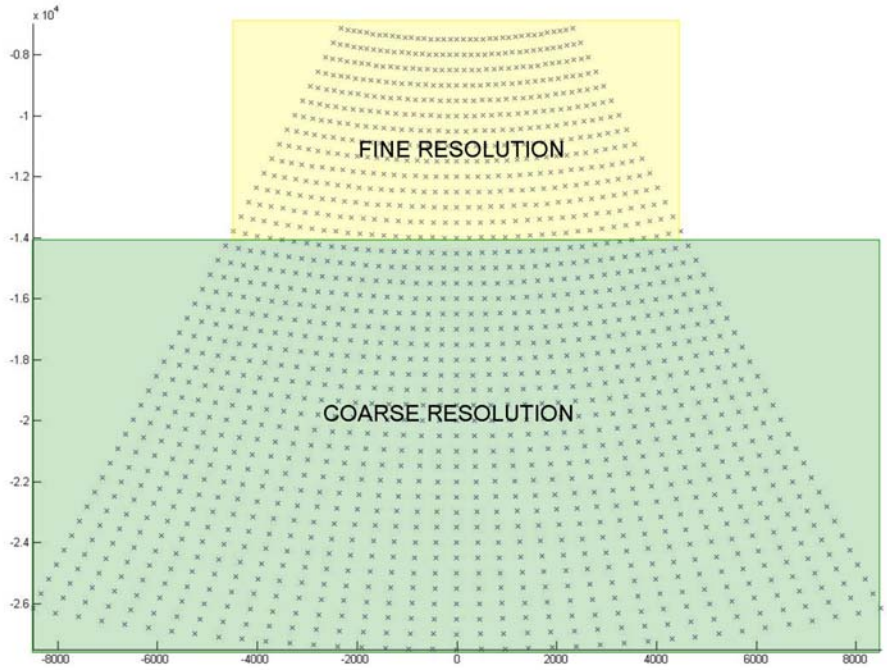

Figure 5.1: Grid points within considered domain defined between two radii positioned at angles $\theta_1 = 252°$ and $\theta_2 = 288°$ with respect to the positive horizontal eastward $x-$ axis of a Cartesian co-ordinate system and two concentric circles ($r_1 = 7500m$, $r_2 = 27500m$), $\Delta r = 500m$; $\Delta\theta = 1°$.

where subscipts s and c are used for smoothed and computed values, respectively; the filter parameter is $\alpha = 0.01 - 0.2$ [Asselin (1972), Williams (2009), Williams (2010), Amezcua et al. (2011)]. Kantha and Clayson (2000) recommended for the same parameter values of $\alpha = 0.1 - 0.3$ in ocean numerical modelling. With a value close to that used in POM ($\alpha = 0.05$), the numerical model showed good results for $\alpha = 0.08$ or $\alpha = 0.05$.

Williams (2009) further developed the Asselin filter, thus conserving the three time level (F^{n-1}, F^n, F^{n+1}) mean by introduction of a second filter parameter α_2 and applying the filter at next time step as well:

$$F_{s2}^n = F_s^n + \frac{\alpha_1\alpha_2}{2}\left(F_c^{n+1} - 2F_s^n + F_{s2}^{n-1}\right) \tag{5.9}$$

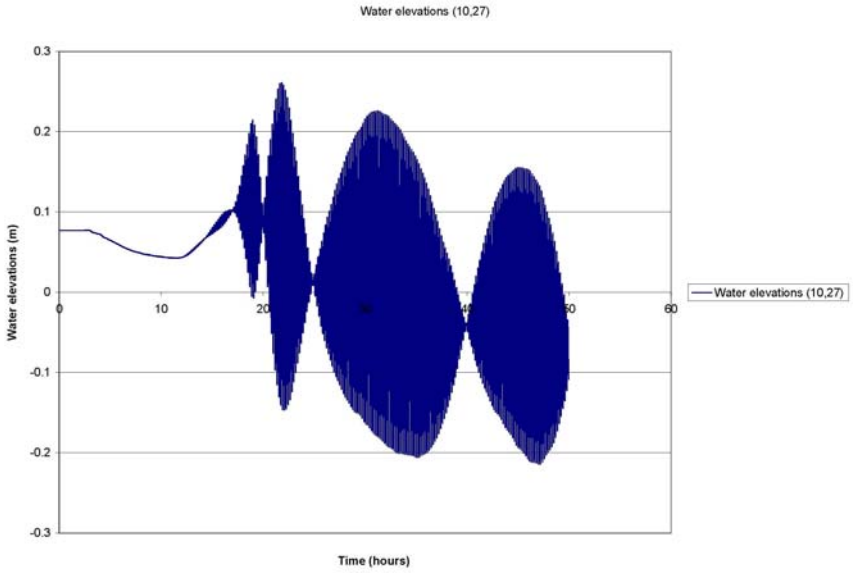

a)

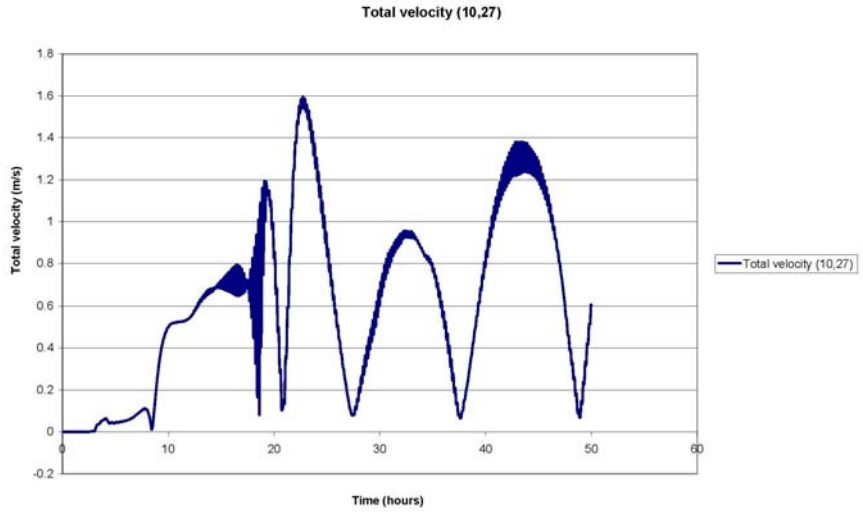

b)

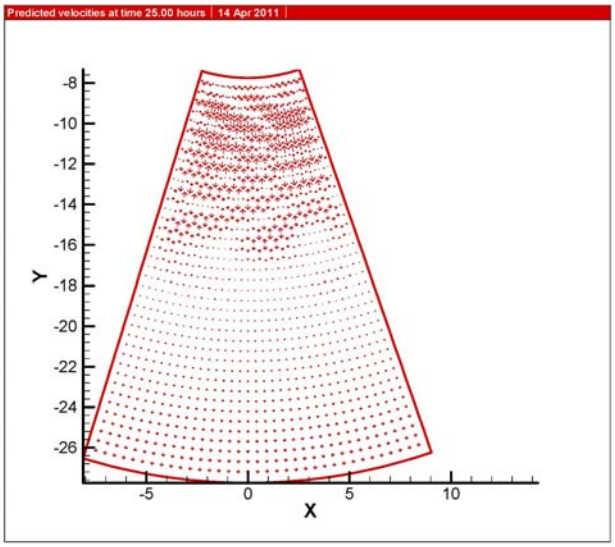

c)

Figure 5.2: Outputs of the model before introducing the Asselin filter: a) water elevations at point (10, 27); b) total velocities at point (10, 27); c) predicted velocities inside domain.

$$F_s^{n+1} = F_c^{n+1} - \frac{\alpha_1(\alpha_2 - 1)}{2}\left(F_c^{n+1} - 2F_s^n + F_{s2}^{n-1}\right) \tag{5.10}$$

where subscripts s, c and $s2$ are used to represent smoothed, computed and doubly smoothed values, respectively. In equations (5.9) and (5.10) the parameter α_1 has the same meaning as in Asselin filter, whereas parameter α_2 controls the amplitude height of the time series. It was empirically found that values of α_2 equal to 0.98, 0.99, 1.00 can be used in the numerical model.

5.3. Case Studies

In all test cases a constant roughness coefficient of 0.2m and no wind is specified in the model. The bottom stress is represented using the quadratic form. A sinusoidal tidal forcing is represented at the outer radius of the domain (OB1) with amplitude A_0=2.077m and tidal period T=12.5 hours.

Three test cases are considered for verification of the numerical model results:

1. horizontal bed with constant scale factors in the radial direction;
2. horizontal bed with one variation of the scale factors in the radial direction;
3. horizontal bed with two variations of the scale factors in the radial direction.

The cylindrical co-ordinates numerical model results are compared with results obtained from similar test cases using robust industry-standard models such as DIVAST (Depth Integrated Velocities and Solute Transport) and EFDC (Environmental Fluid Dynamics Code). A short description of hydrodynamic module of DIVAST model is given in Appendix 12 and it is presented in Appendix 13 for EFDC.

DIVAST is used for results comparison only in the first test case. In DIVAST domain is represented using 61x53 mesh points with constant spatial step ($\Delta x = \Delta y = 353m$) and it is shown in Figure 5.3. Due to the inability of

representing the tidal forcing on a curved boundary within DIVAST, the forcing boundary is represented as a straight line.

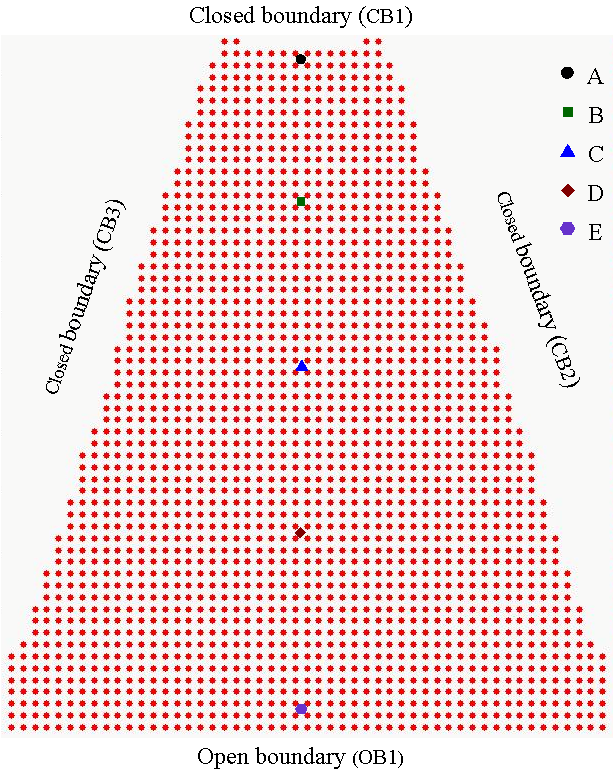

Figure 5.3: Domain representation in DIVAST.

EFDC Explorer version 061009 is used in herein. Model set up for the considered geometry is straightforward and it consists of setting the scale factors and point co-ordinates of the domain in the input files. Domain representation in EFDC is showed in corresponding sections. It is observed that the model does not preserve grid orthogonality at land boundaries, nor at open boundary. The average deviation from grid orthogonality is 0.318º for the first test case [Figure 5.4a)], 0.321º for the second test case [Figure 5.4b)], and 0.3698º for the third test case [Figure 5.4c)].

Comparisons between the results of the three models are done at points corresponding to the following positions in the cylindrical co-ordinates model: A, B, C, D, and E [see Figures 5.3, 5.5 – 5.6, 5.23 – 5.24, 5.37 – 5.38]. For the simulations presented in Section 5.3, the cylindrical co-ordinates numerical model uses a cold start at high water and all plots are shown after two tidal cycles.

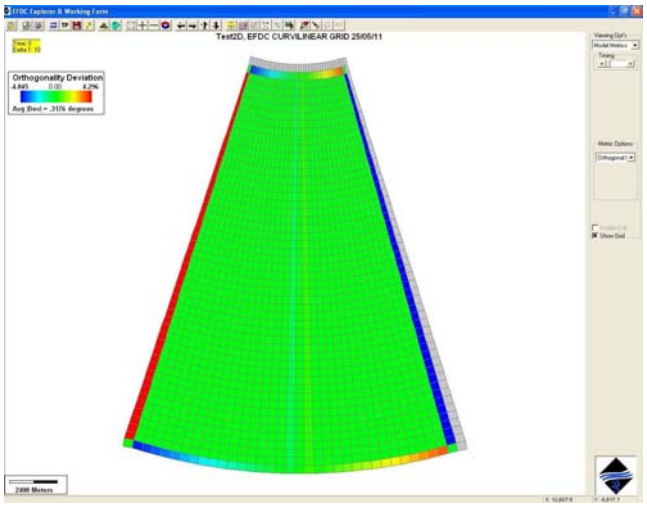

a)

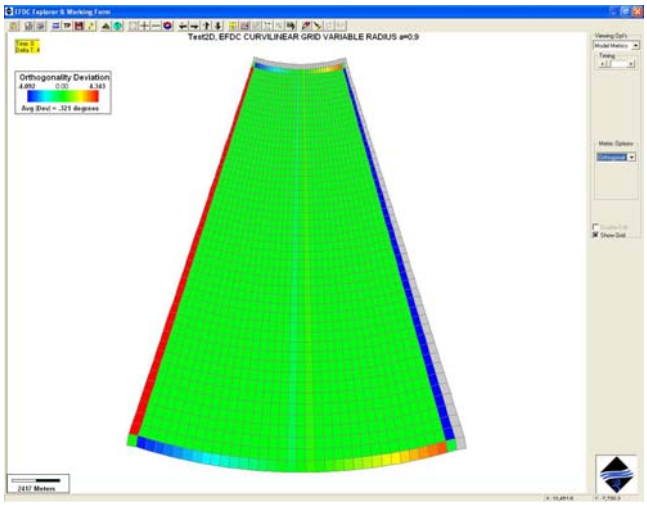

b)

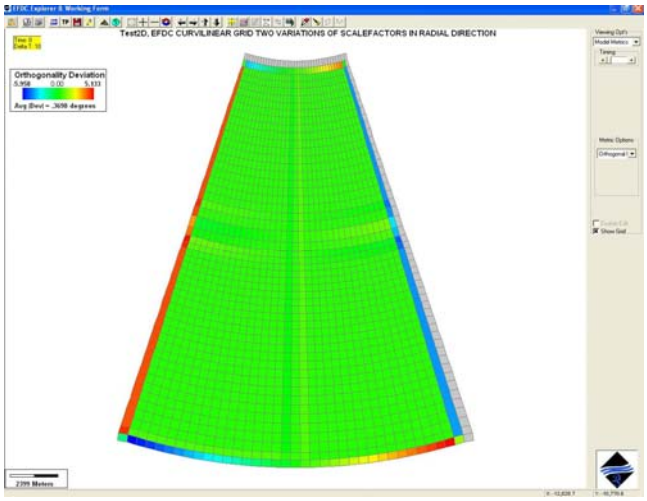

c)

Figure 5.4: Grid orthogonality deviation in EFDC: a) for the horizontal bed with constant step in the radial direction test case; b) for the horizontal bed with one variation of the step in the radial direction test case; c) for the horizontal bed with two variations of the step in the radial direction test case.

In all test cases transformation of the cylindrical co-ordinates numerical model computed water elevations is done according to mathematical relationships given in Annex 11. New model computed water elevations for the three test cases are shown in Figures 5.8 – 5.12, 5.25-5.29 and 5.39-5.43, respectively.

Parameter	**NM**	**DIVAST**
Time step (s)	10.000	10.000
Space step (m)	1.000	1.000
Bed roughness (m)	0.200	0.200
Viscosity(mm)	1.310	1.310
Coefficient of eddy viscosity	1.000	1.000

Table 5.1: Parameters common to the three test cases for the new numerical model, and in the first test case for DIVAST.

Parameter	**EFDC**
Time step (s)	10.000
Space step (m)	1.000
Bed roughness (m)	0.200
Constant horizontal momentum(mm/s)	0.100
Eddy (kinematic) viscosity (mm/s)	10^{-6}
Side wall log law roughness height	0.002
Von Karman constant	0.400
Turbulent constant (B_1)	16.600
Turbulent constant	10.100
Turbulent constant (E_1)	1.800
Turbulent constant (E_2)	1.330
Turbulent constant (E_3)	0.530
Minimum turbulent intensity squared	10^{-8}
Minimum turbulent intensity squared multiplied by length scale	10^{-12}
Minimum dimensionless length scale	0.001

Table 5.2: Parameters common to the three test cases for EFDC.

The no slip closed boundary conditions were represented in terms of Cartesian velocities in DIVAST, volume flux representation [Hirsch (1990)] in the radial direction and based on curvature representation in the angular direction, respectively in the cylindrical co-ordinates numerical model. No slip boundary conditions were used in EFDC, as well.

The parameters in Table 5.1 were common to the three test cases, unless otherwise specified. Hamrick (1992) provides details with regard to the turbulence parameterization used in EFDC and the corresponding parameters are presented in Table 5.2.

5.3.1. Case 1 – Horizontal Bed with Constant Scale Factors in the Radial Direction

For the test described herein a harbour is defined between two concentric circles ($r_1 = 7500m$ and $r_2 = 27900m$) and two radii ($\theta_1 = 252°, \theta_2 = 288°$). According to the chosen geometry, the scale factors of the transformation from the cylindrical onto the computational domain are constant in the radial direction $\left(h_{\xi^r} = 400.0\right)$ and vary from $h_{\xi^\theta} = 130.9$ at the closed boundary to $h_{\xi^\theta} = 486.947$ at the open boundary of the domain along each radius ($\delta r = const.$) [see Table 5.3].

The space step in the computational domain is $\Delta\xi^r = \Delta\xi^\theta = 1$. Domain representation, as well as position of open and closed boundaries, for the cylindrical co-ordinates model is given in Figure 5.5, whereas EFDC domain and boundaries representation is presented in Figure 5.6.

Results of the simulations for a uniform 10m water depth in the three models for the horizontal bed case are shown in Figures 5.10-5.14. The flow is simulated within domain for 144 hours with a time step $\delta t = 10s$. The time step results

Radius	Scale factor in the ξ^r direction	Scale factor in the ξ^θ direction	Point
7500.000	400.000	130.900	
7900.000	400.000	137.881	A
8300.000	400.000	144.862	
8700.000	400.000	151.844	
9100.000	400.000	158.825	
9500.000	400.000	165.806	
9900.000	400.000	172.788	
10300.000	400.000	179.769	
10700.000	400.000	186.750	
11100.000	400.000	193.732	
11500.000	400.000	200.713	
11900.000	400.000	207.694	B
12300.000	400.000	214.676	
12700.000	400.000	221.657	
13100.000	400.000	228.638	
13500.000	400.000	235.619	
13900.000	400.000	242.601	
14300.000	400.000	249.582	
14700.000	400.000	256.563	
15100.000	400.000	263.545	
15500.000	400.000	270.526	
15900.000	400.000	277.507	
16300.000	400.000	284.489	
16700.000	400.000	291.470	
17100.000	400.000	298.451	C
17500.000	400.000	305.433	
17900.000	400.000	312.414	
18300.000	400.000	319.395	
18700.000	400.000	326.377	
19100.000	400.000	333.358	
19500.000	400.000	340.339	
19900.000	400.000	347.321	
20300.000	400.000	354.302	
20700.000	400.000	361.283	
21100.000	400.000	368.265	
21500.000	400.000	375.246	
21900.000	400.000	382.227	D
22300.000	400.000	389.208	
22700.000	400.000	396.190	
23100.000	400.000	403.171	
23500.000	400.000	410.152	
23900.000	400.000	417.134	
24300.000	400.000	424.115	
24700.000	400.000	431.096	
25100.000	400.000	438.078	
25500.000	400.000	445.059	
25900.000	400.000	452.040	
26300.000	400.000	459.022	
26700.000	400.000	466.003	
27100.000	400.000	472.984	E
27500.000	400.000	476.475	
27900.000	400.000	476.475	

Table 5.3: Scale factors for domain representation in the cylindrical co-ordinates numerical model for the first test case.

from the stability criterion given in equation (4.34). The value of Coriolis parameter is 1.165×10^{-4} s^{-1} corresponding to a value of the latitude angle of 53.2ºN. Values of the parameters in the RAW filter are $\alpha_1 = 0.08$, $\alpha_2 = 1.0$.

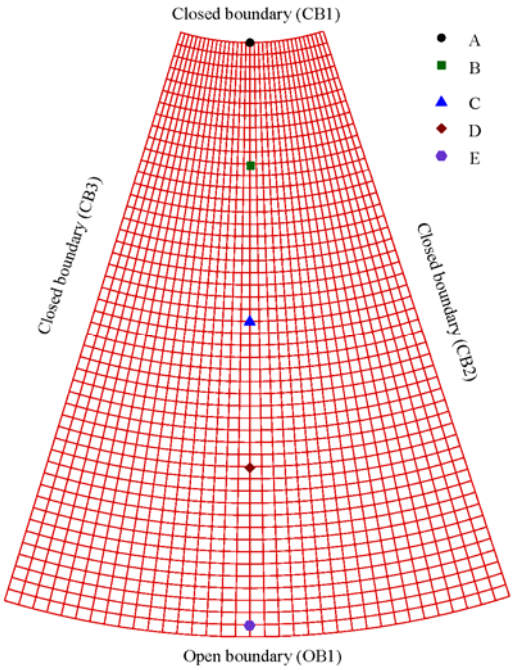

Figure 5.5: Domain representation in the cylindrical co-ordinates numerical model for first test case.

Computed water levels [Figure 5.7] were transformed, based on the Author's own transformation relationship based on the water energy conservation law, given by equation (A11.39), shown below, with theoretical exponent $n = 1.0$ and an exponent computed by the numerical model. The transformation relationships are based on the zeroth order Bessel functions $J_0(kr)$, a detailed description of which can be found in Abramowitz and Stegun (1970). Water elevations resulting from simulations with the three considered models are in phase [Figures 5.8 - 5.12]. The water elevation amplitude errors vary from 0.68 % (at point A), increase to 0.71% (at point B) and decrease to -0.48 % (at point E) with respect to DIVAST values, and 0.52 % (at point A), 0.53% (at point B) and -0.54 % (at point E) with respect to EFDC values, respectively. Table 5.4 gives computed water elevation amplitudes at points A-E inside domain.

$$H_i = H_i^{comp}\left(\frac{B_2}{B_1}\right)^{1/2}\left[\frac{J_0(kr_1)}{J_0(kr_2)}\right]^n\left[\frac{J_0(kr_2)}{J_0(kx_i)}\right]^{2n} \qquad \text{(A11.39)}$$

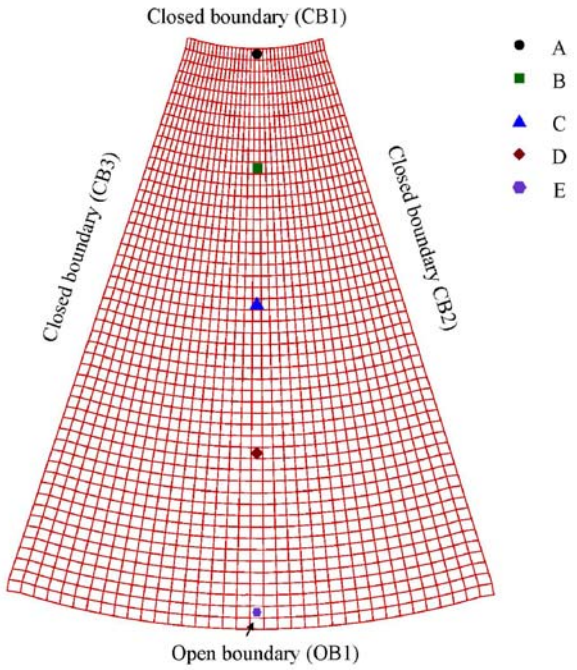

Figure 5.6: Domain representation in EFDC for first test case.

An analysis of the dimensionless water elevation amplitudes shows good agreement between the three models. Dimensionless values are obtained from equation (5.11).

$$A_i' = \frac{A_i}{A_0} \qquad d_i' = \frac{x_i}{l_0} \qquad \text{(5.11)}$$

where A_i' is the dimensionless amplitude at section x_i inside domain, A_i is the model predicted amplitude at section x_i inside domain, and A_0 is the amplitude of the tidal forcing applied at the outer boundary of the domain, d_i' is dimensionless distance, x_i is radius at point i inside domain, l_0 is the total length of the estuary.

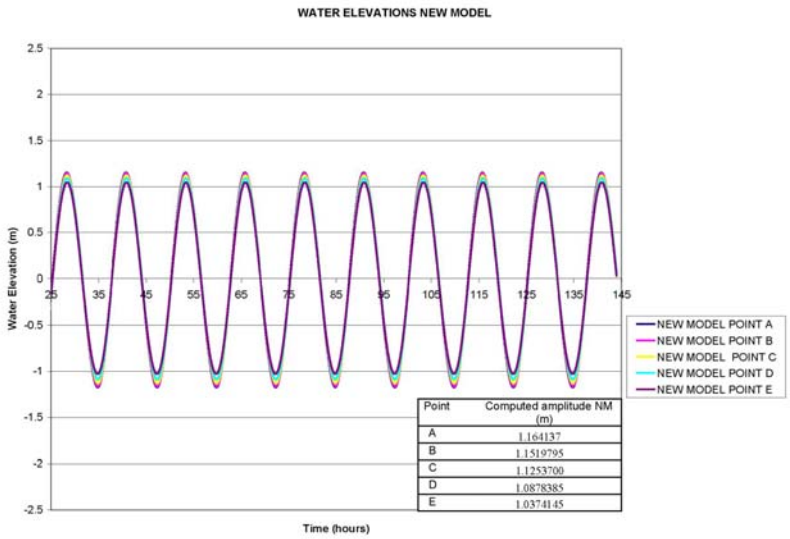

Figure 5.7: Computed water levels from the cylindrical co-ordinates model.

Dimensionless water elevation amplitudes are given in Table 5.5. Figure 5.8a) illustrates dimensionless water elevation amplitude versus distance and it is observed that the maximum dimensionless amplitude error with respect to DIVAST values is obtained at point *B* and has values of 0.758%, whereas the error with respect to EFDC values is 0.642% at point A for $n = 1.0$ [detail in Figure 5.8a)]. The computed exponent term for transformation of water elevation time series is $n = 1.160138$ and Table 5.6 presents the dimensionless water elevation amplitudes at points A-E inside domain in this case.

Point	**Amplitude NM (m)**		**Amplitude DIVAST (m)**	**Amplitude EFDC (m)**
	$n = 1.0$	$n = 1.160138$		
A	2.168	2.155	2.152	2.154
B	2.162	2.152	2.146	2.149
C	2.144	2.140	2.131	2.134
D	2.112	2.114	2.110	2.110
E	2.068	2.079	2.077	2.079

Table 5.4: Water elevation amplitudes at points A-E inside domain for the first test case with $n = 1.0$ and $n = 1.160138$.

With $n = 1.160138$ the maximum error with respect to DIVAST and EFDC values is obtained at point C: 0.392% and 0.260%, respectively. The detail in Figure 5.8b) shows that when using the computed exponent term, the form of the dimensionless water elevation amplitudes along centreline graph becomes similar to both DIVAST and EFDC shapes.

a)

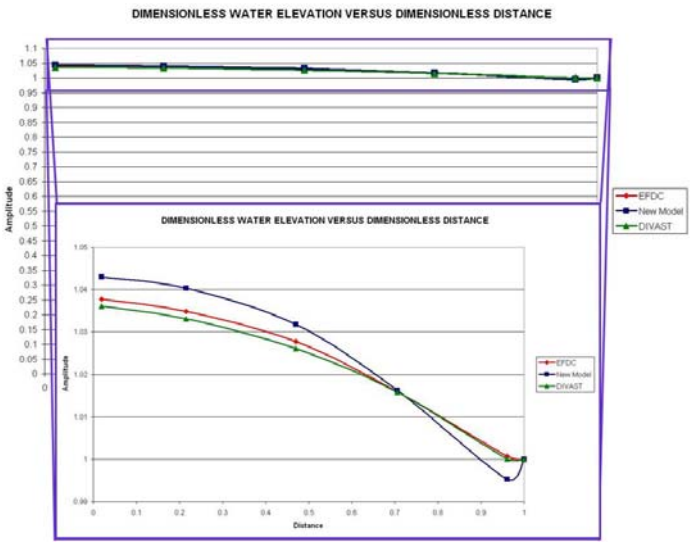

b)

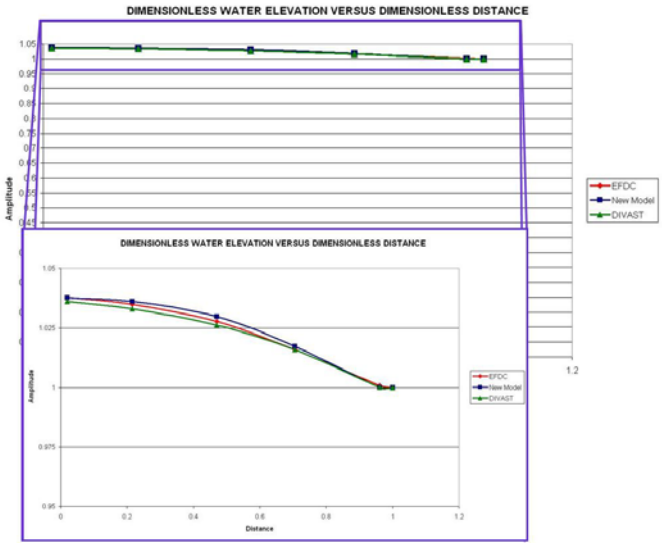

Figure 5.8: Dimensionless water elevation amplitude variation with dimensionless distance for: a) $n = 1.0$; b) $n = 1.160138$ for the first test case.

In general, velocities are in phase [Figures 5.9 - 5.13] and it is observed that in terms of total velocity magnitudes, DIVAST predicted maximum values and EFDC predicted minimum values, except at points B and C, where the

cylindrical co-ordinates numerical model had the smallest and largest values, respectively with errors less than 1.75%. It can be observed that new model predicted total velocities magnitudes lie between values obtained from DIVAST and EFDC. The pattern in terms of variation along centreline of total velocity magnitude resulted from numerical simulations using the three models for the first test case is studied in the time interval 46.8 – 59.3 hours and is described below:

- At point A, where velocities are small, of the order of centimetres/second, total velocities computed by the three models vary considerably in terms of magnitude and period, yet the maximum velocity during ebb tide resulted from the cylindrical co-ordinates numerical model is equal to the value resulted from DIVAST model, whereas the magnitude of the maximum total velocity during flood tide falls between DIVAST and EFDC values [Figure 5.10];

- At point B, the maximum total velocity magnitude at ebb and flood tide resulted from the cylindrical co-ordinates numerical model falls between DIVAST and EFDC values;

- At point C, the cylindrical co-ordinates numerical model over predicts the maximum total velocity magnitude from DIVAST with an error of 0.870% at ebb tide, and 1.377% at flood tide, respectively;

Point	**Dimensionless Amplitude NM**	**Dimensionless Amplitude DIVAST**	**Dimensionless Amplitude EFDC**
A	1.043	1.036	1.037
B	1.041	1.033	1.034
C	1.032	1.026	1.028
D	1.017	1.016	1.016
E	0.996	1.000	1.001

Table 5.5: Dimensionless water elevation amplitudes at points A-E inside domain for horizontal bed test case with $n = 1.0$.

Point	Dimensionless Amplitude NM	Dimensionless Amplitude DIVAST	Dimensionless Amplitude EFDC
A	1.038	1.036	1.037
B	1.036	1.033	1.034
C	1.030	1.026	1.028
D	1.018	1.016	1.016
E	1.001	1.000	1.001

Table 5.6: Dimensionless water elevation amplitudes at points A-E inside domain for horizontal bed test case with $n = 1.160138$.

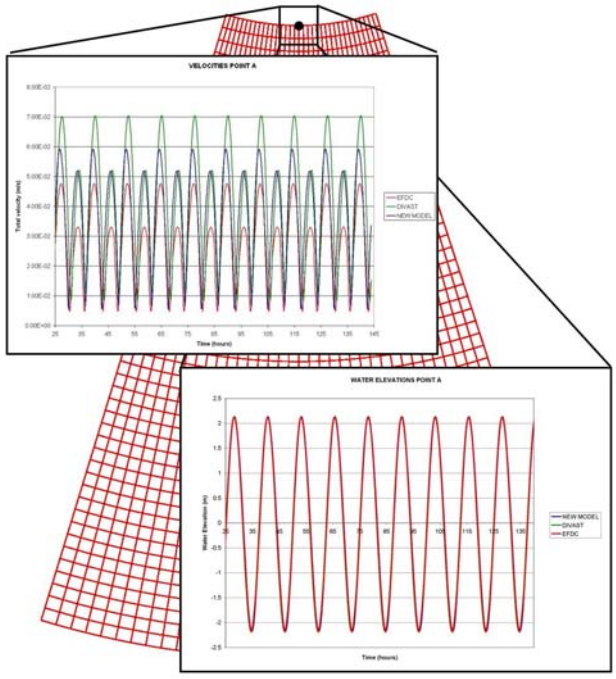

Figure 5.9: Total velocities and water elevation time series comparison between the three models at point A inside domain.

- At point D, the maximum total velocity magnitude obtained from the cylindrical co-ordinates numerical model falls between DIVAST and EFDC values both for ebb and flood tide;

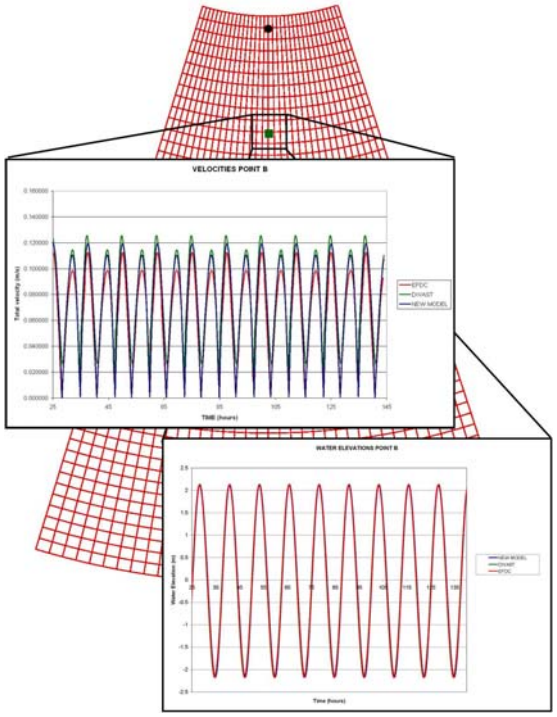

Figure 5.10: Total velocities and water elevation time series comparison between the three models at point B inside domain.

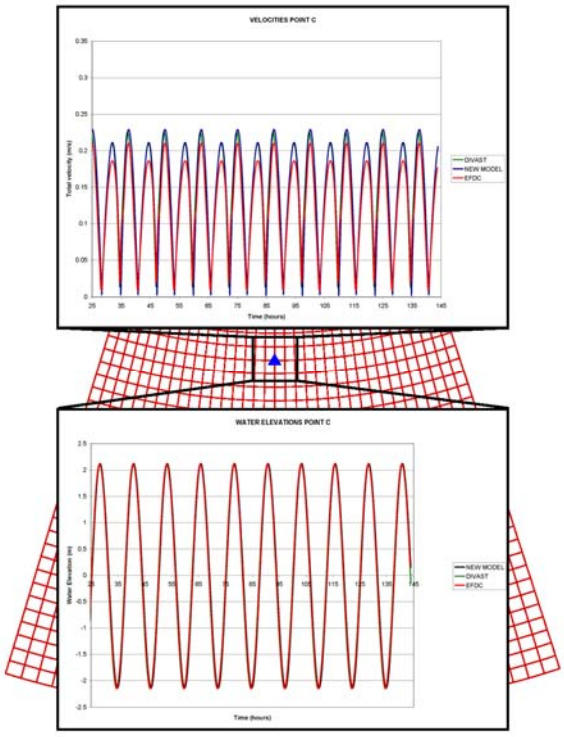

Figure 5.11: Total velocities and water elevation time series comparison between the three models at point C inside domain.

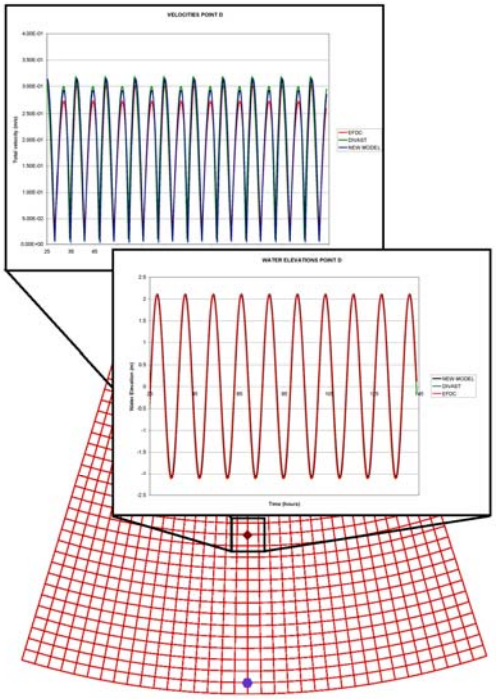

Figure 5.12: Total velocities and water elevation time series comparison between the three models at point D inside domain.

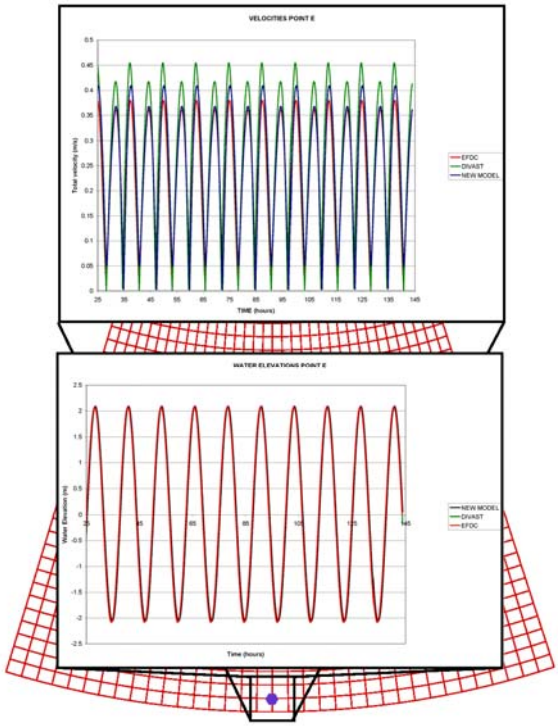

Figure 5.13: Total velocities and water elevation time series comparison between the three models at point E inside domain.

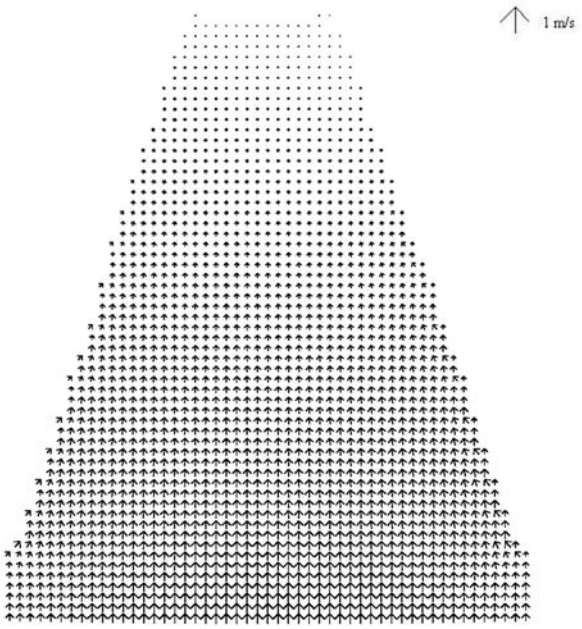

Figure 5.14: Flow inside domain for horizontal bed test case at time 36.00 hours (DIVAST).

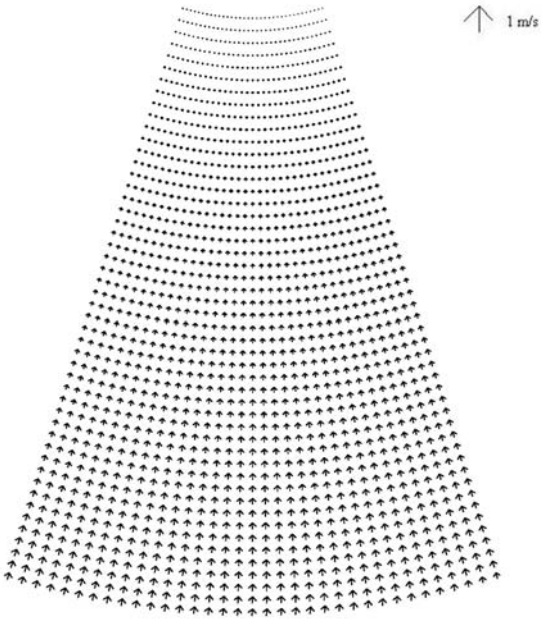

Figure 5.15: Flow inside domain for horizontal bed test case at time 36.00 hours (cylindrical co-ordinates model).

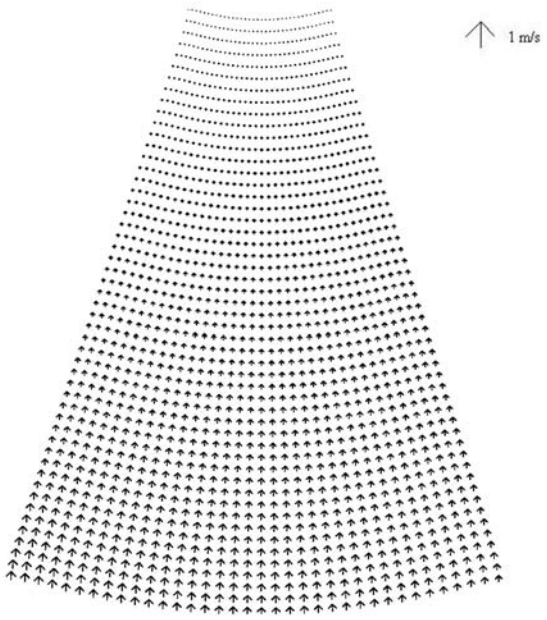

Figure 5.16: Flow inside domain for horizontal bed test case at time 36.00 hours (EFDC).

- At point E, the maximum total velocity magnitude obtained from the cylindrical co-ordinates numerical model is equal to EFDC value at ebb tide and falls between DIVAST and EFDC values at flood tide.

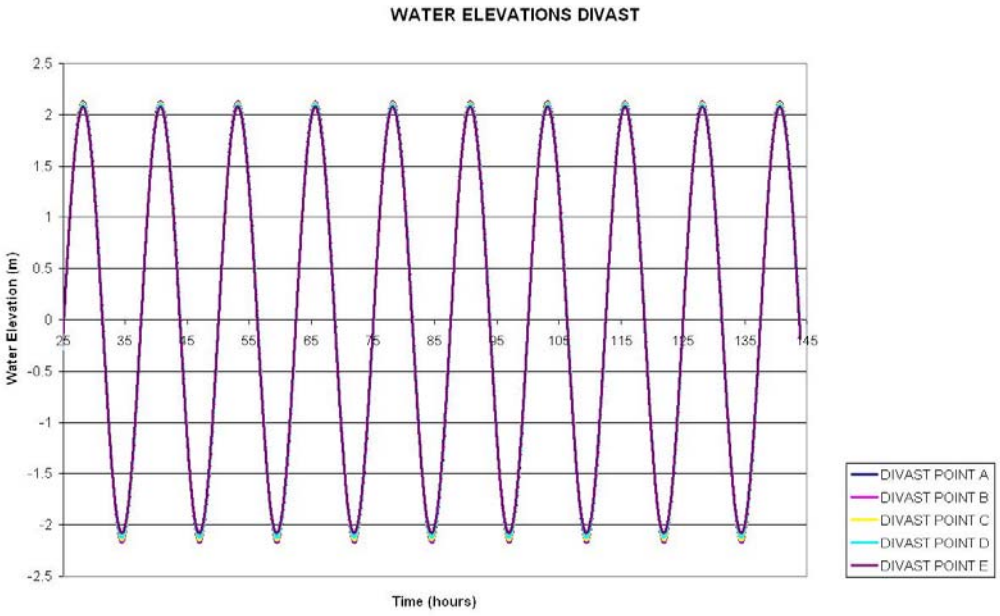

Figure 5.17: Water elevations variation at points A-E inside domain (DIVAST).

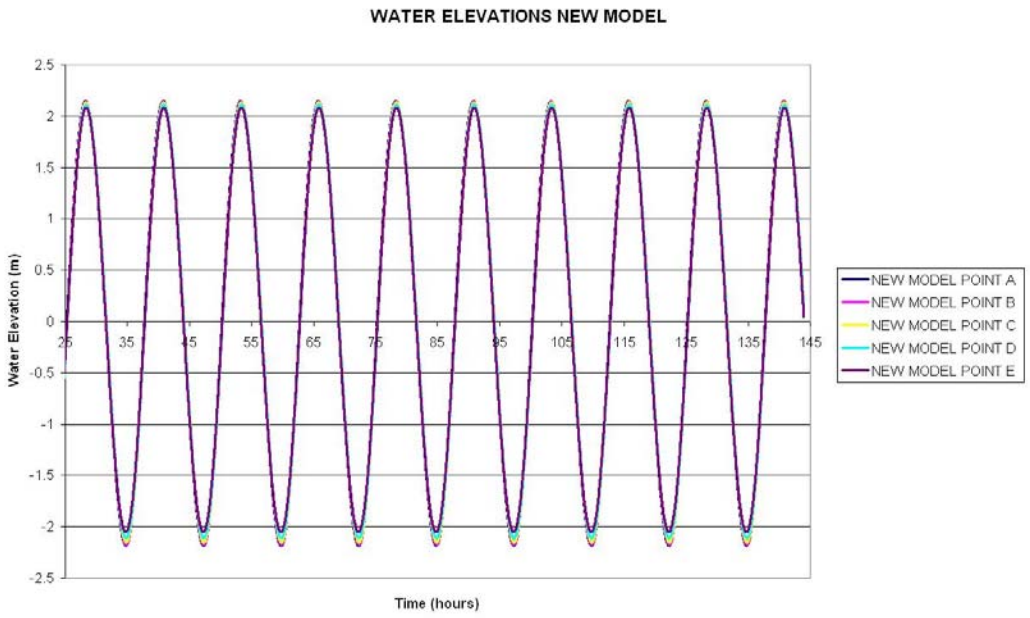

Figure 5.18: Water elevations variation at points A-E inside domain (cylindrical co-ordinates model).

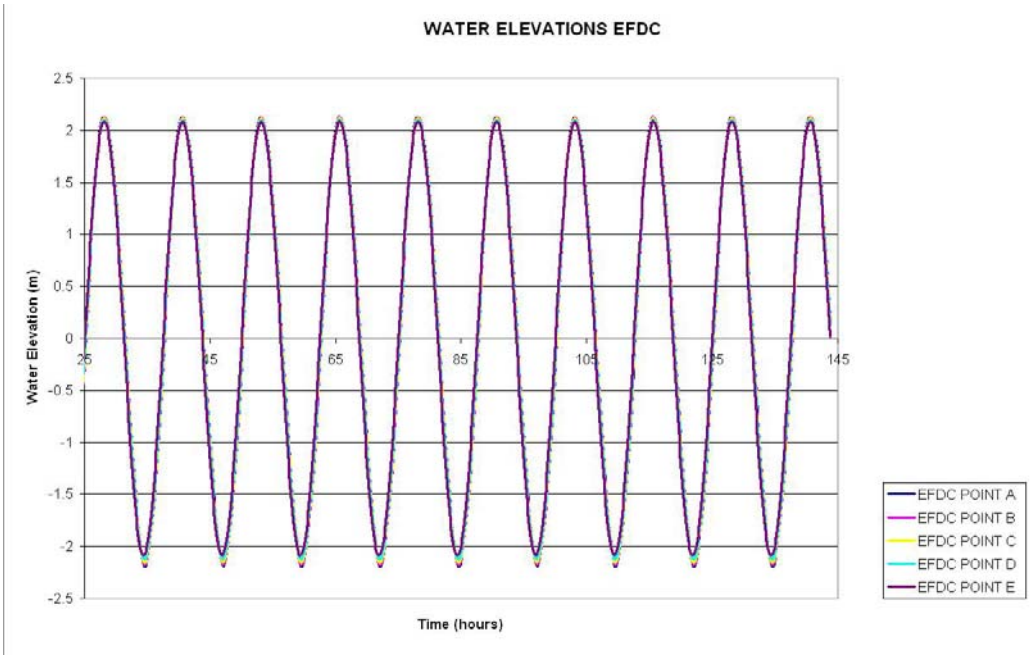

Figure 5.19: Water elevations variation at points A-E inside domain (EFDC).

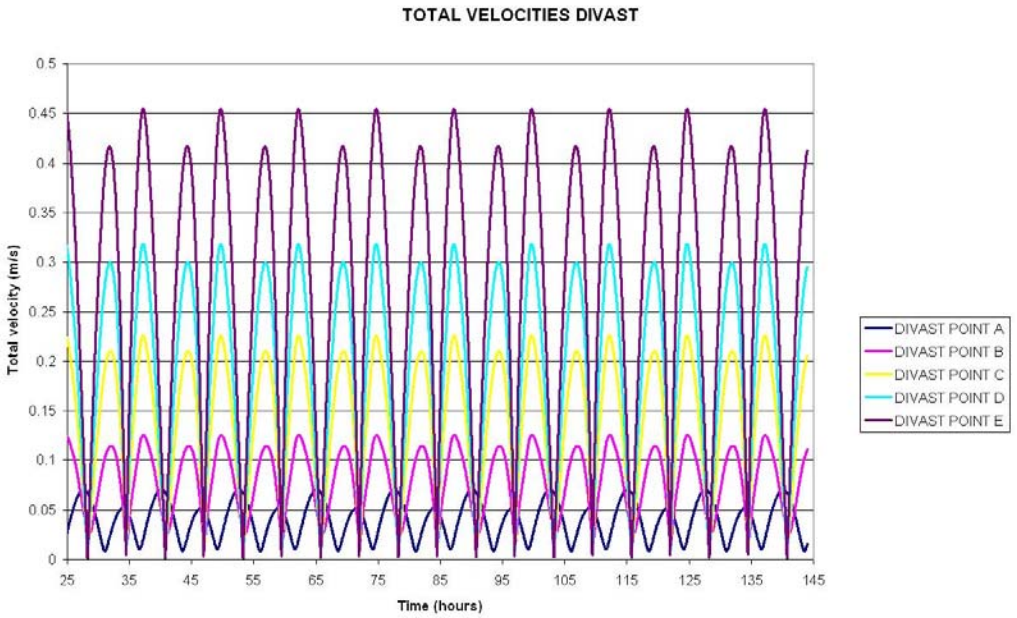

Figure 5.20: Total velocities variation at points A-E inside domain (DIVAST).

Figures 5.14 – 5.16 show current velocity maps at time 36.00 hours for the three models and agreement for directions of velocity vectors is observed. Also, agreement in terms of water elevation time series [Figures 5.17 – 5.19] and total velocity time series [Figures 5.20 – 5.22] variation inside domain is achieved.

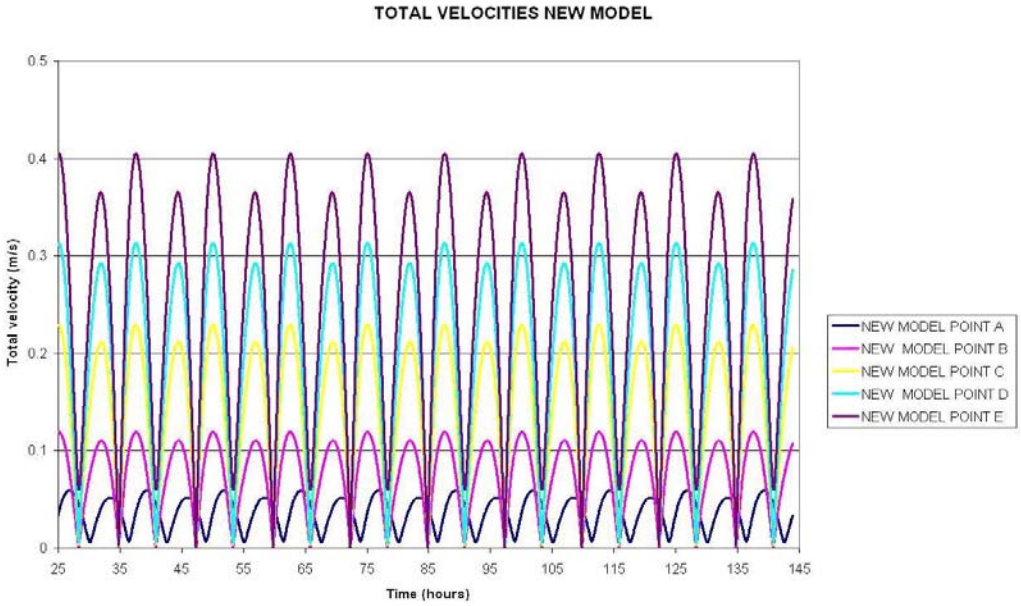

Figure 5.21: Total velocities variation at points A-E inside domain (cylindrical co-ordinates model).

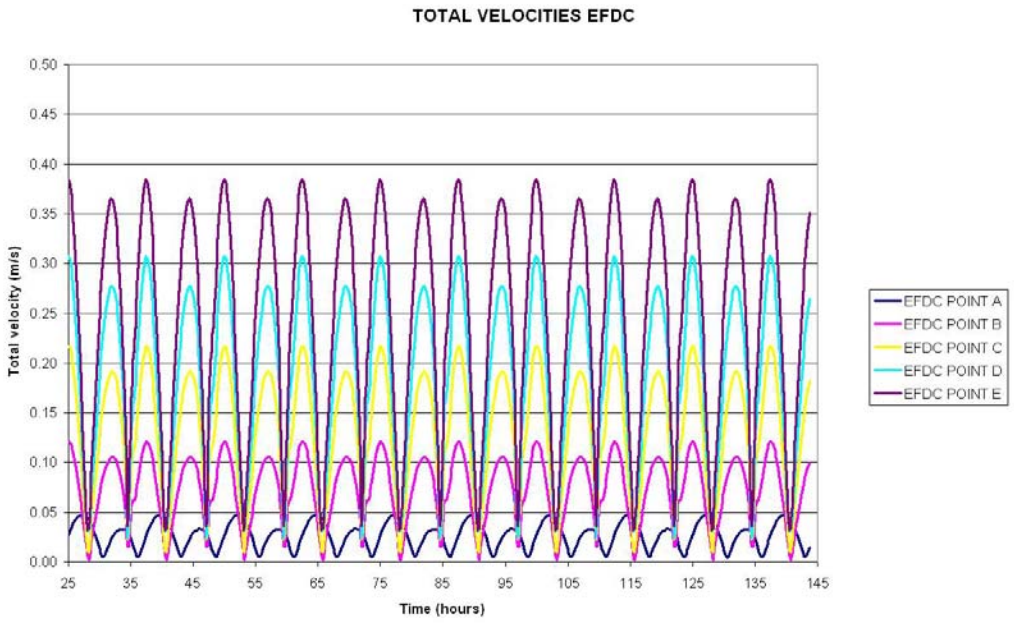

Figure 5.22: Total velocities variation at points A-E inside domain (EFDC).

The computed tidal period for the cylindrical co-ordinates model and DIVAST is 12.497 hours, whereas EFDC value is 12.500 hours. A study of the phase shift, in the time interval 46.8 – 59.3 hours, introduced by the cylindrical co-ordinate system with the water elevation transformation exponent term $n = 1.0$ showed that [Table 5.7]:

a) At point A the phase shift of water elevation time series at high water was 0.083 hours with respect to DIVAST values and 0.008 hours with respect to EFDC values, respectively, whereas the phase shift at low water was 0.306 hours with respect to DIVAST values and 0.269 hours with respect to EFDC values, respectively;

b) At point A the phase shift of total velocity time series at ebb tide was -0.672 hours with respect to DIVAST values and -0.139 hours with respect to EFDC values, respectively; whereas at flood tide the phase shift was -0.825 hours with respect to DIVAST values and -0.458 hours with respect to EFDC values, respectively;

Point A								
	Water Elevation				Total Velocity			
	High Water (HW)		Low Water (LW)		Ebb		Flood	
	Time (hours)	Max (m)	Time (hours)	Min (m)	Time (hours)	Max (m/s)	Time (hours)	Max (m/s)
DIVAST	53.167	2.130	46.964	-2.174	59.033	0.052	52.617	0.070
New Model	53.258	2.148	47.269	-2.188	58.361	0.052	51.792	0.059
EFDC	53.250	2.123	47.000	-2.184	58.500	0.033	52.250	0.048
Point B								
	Water Elevation				Total Velocity			
	High Water (HW)		Low Water (LW)		Ebb		Flood	
	Time (hours)	Max (m)	Time (hours)	Min (m)	Time (hours)	Max (m/s)	Time (hours)	Max (m/s)
DIVAST	53.167	2.125	46.964	-2.167	57.047	0.114	49.745	0.126
New Model	53.289	2.145	47.300	-2.179	56.986	0.111	50.050	0.119
EFDC	53.250	2.120	47.000	-2.178	57.000	0.099	50.000	0.113
Point C								
	Water Elevation				Total Velocity			
	High Water (HW)		Low Water (LW)		Ebb		Flood	
	Time (hours)	Max (m)	Time (hours)	Min (m)	Time (hours)	Max (m/s)	Time (hours)	Max (m/s)
DIVAST	53.167	2.114	46.964	-2.149	56.925	0.210	49.683	0.226
New Model	53.319	2.135	47.300	-2.153	56.956	0.212	50.050	0.229
EFDC	53.250	2.111	47.000	-2.158	57.000	0. 186	50.000	0.210
Point D								
	Water Elevation				Total Velocity			
	High Water (HW)		Low Water (LW)		Ebb		Flood	
	Time (hours)	Max (m)	Time (hours)	Min (m)	Time (hours)	Max (m/s)	Time (hours)	Max (m/s)
DIVAST	53.167	2.099	46.964	-2.121	56.864	0.300	49.653	0.318
New Model	53.350	2.113	47.269	-2.110	56.925	0.293	50.081	0.313
EFDC	53.250	2.096	47.000	-2.124	57.000	0.277	50.000	0.307
Point E								
	Water Elevation				Total Velocity			
	High Water (HW)		Low Water (LW)		Ebb		Flood	
	Time (hours)	Max (m)	Time (hours)	Min (m)	Time (hours)	Max (m/s)	Time (hours)	Max (m/s)
DIVAST	53.167	2.076	46.933	-2.079	56.803	0.417	49.683	0.455
New Model	53.35	2.085	47.239	-2.051	56.864	0.365	50.081	0.405
EFDC	53.25	2.077	47.0	-2.080	57.000	0.365	50.000	0.385

Table 5.7: High and low water levels and maximum total velocity at ebb and flood tide for the first test case for $n = 1.0$.

c) At point E the phase shift of water elevation time series at high water was 0.183 hours with respect to DIVAST values and 0.100 hours with respect to EFDC values, respectively, whereas the phase shift at low water was 0.306 hours with respect to DIVAST values and 0.239 hours with respect to EFDC values, respectively;

d) At point E the phase shift of total velocity time series at ebb tide was 0.061 hours with respect to DIVAST values and -0.136 hours with respect to EFDC values, respectively; whereas at flood tide the phase shift was 0.397 hours with respect to DIVAST values and 0.081 hours with respect to EFDC values, respectively.

Point	**NM** **HW-LW** (hours)	**DIVAST** **HW-LW** (hours)	**EFDC** **HW-LW** (hours)
A	5.989	6.203	6.250
B	5.989	6.203	6.250
C	6.019	6.203	6.250
D	6.081	6.203	6.250
E	6.111	6.233	6.250

Table 5.8: Time period between high water and low water in the three models along centreline.

Point	**NM** **Ebb-Flood** (hours)	**DIVAST** **Ebb-Flood** (hours)	**EFDC** **Ebb-Flood** (hours)
A	6.569	6.416	6.250
B	6.936	7.303	7.000
C	6.906	7.242	7.000
D	6.844	7.211	7.000
E	6.783	7.119	7.000

Table 5.9: Time period between maximum velocity at ebb tide and maximum velocity at flood tide in the three models along centreline.

It was also found that the tidal excursion, representing the time it takes a particle in the water to travel from high water to low water level, varies along centreline from a maximum at point E to a minimum at point B and keeps this value at point A in the cylindrical co-ordinates numerical model, it is constant in EFDC, and changes only at point E in DIVAST [see Table 5.8]. Moreover, the time it

takes a particle to travel from maximum velocity at ebb tide to maximum velocity at flood tide increases from point E to point B and decreases at point A in the cylindrical co-ordinates numerical model, with a similar pattern shown by DIVAST, while EFDC times are constant from E to B and only becomes smaller at point A [see Table 5.9].

5.3.2. Case 2 – Horizontal Bed with Variable Step in the Radial Direction

For the second test case the scale factors vary in the given domain according to the values given in Table 5.10. Figure 5.25 shows domain representation in the cylindrical co-ordinates model, whereas EFDC representation of the same domain is shown in Figure 5.26. The law of variation of the step in the radial direction is given by a "stretching" function [Thompson et al. (1997)]:

$$r_i = f_i r_2 - (1 - f_i) r_1 \tag{5.12}$$

The terms in equation (5.12) are:

$f_i = \dfrac{e^{a \cdot i / i_{\max}} - 1}{e^a - 1}$ is an exponential law of variation of radius inside domain, for $i = 1, ..., i_{\max}$;

a is a parameter which controls the step in the radial direction; $a = 0.9$ in the present study;

r_2 is the maximum (outer) radius, i.e. for $i = i_{\max}$;

r_1 is the minimum (inner) radius, i.e. for $i = 1$.

Results of the simulations for a uniform 10m water depth in the two models for this test case are shown in Figures 5.27 – 5.31. The flow is simulated within domain for 144 hours with a time step δt =4 seconds. The value of Coriolis parameter is the same as in previous test case. The bed roughness was 0.2 m in

Radius	Scale factor in the ξ^r direction	Scale factor in the ξ^θ direction	Point
7348.789	253.171	128.298	
7601.922	257.590	132.717	A
7859.474	262.088	137.213	
8121.522	266.663	141.787	
8388.145	271.319	146.441	
8659.423	276.055	151.177	
8935.437	280.875	155.995	
9216.270	285.779	160.897	
9502.006	290.768	165.885	
9792.730	295.844	170.960	
10088.530	301.009	176.123	
10389.494	306.264	181.377	B
10695.712	311.611	186.722	
11007.276	317.051	192.161	
11324.280	322.586	197.694	
11646.818	328.218	203.324	
11974.987	333.948	209.053	
12308.886	339.778	214.881	
12648.613	345.711	220.812	
12994.272	351.746	226.845	
13345.965	357.887	232.985	
13703.799	364.135	239.231	
14067.879	370.492	245.586	
14438.316	376.960	252.053	
14815.220	383.542	258.632	C
15198.704	390.238	265.326	
15588.883	397.050	272.137	
15985.874	403.982	279.067	
16389.796	411.035	286.117	
16800.769	418.211	293.291	
17218.918	425.512	300.591	
17644.367	432.941	308.017	
18077.243	440.499	315.573	
18517.676	448.190	323.262	
18965.799	456.015	331.084	
19421.745	463.976	339.043	
19885.652	472.076	347.141	D
20357.657	480.318	355.380	
20837.903	488.703	363.763	
21326.533	497.235	372.293	
21823.694	505.916	380.971	
22329.534	514.749	389.801	
22844.206	523.735	398.785	
23367.863	532.879	407.926	
23900.662	542.182	417.226	
24442.763	551.648	426.689	
24994.327	561.278	436.317	
25555.522	571.077	446.113	
26126.514	581.047	456.081	
26707.474	591.192	466.222	E
27298.577	596.263	471.292	
27900.000	601.378	476.417	

Table 5.10: Variation of scale factors inside domain for horizontal bed with variable scale factors in the radial direction test case.

the three models. The values of the parameters in the RAW filter are: $\alpha_1 = 0.05$, $\alpha_2 = 1.00$.

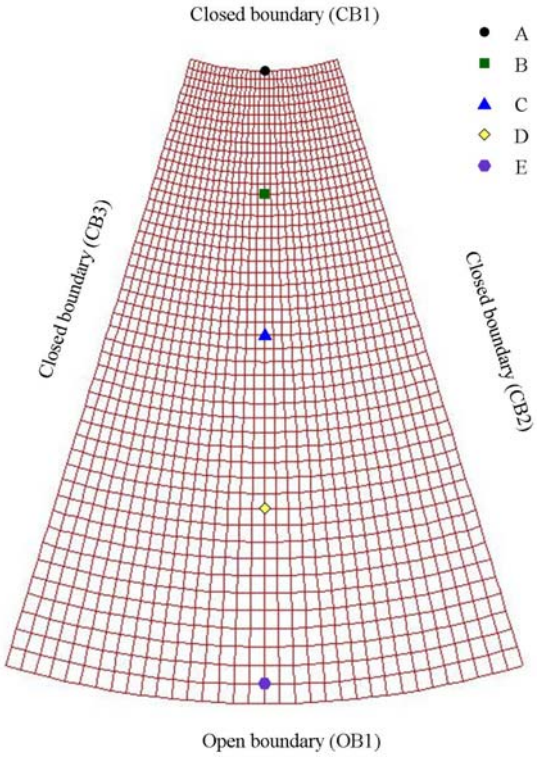

Figure 5.23: Domain representation for second test case in new numerical model.

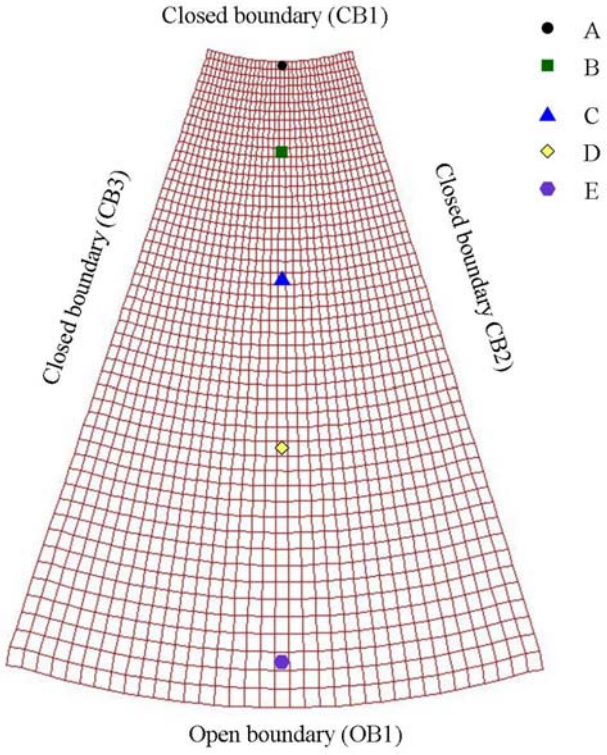

Figure 5.24: Domain representation for second test case in EFDC.

Water elevations resulting from simulations with the two models are in phase [Figures 5.27 – 5.31]. With water elevation transformation exponent term taken as $n = 1.0$, the water elevation amplitude errors vary between 1.096 % (at point A) to 0.591% (at point D) and -0.560 % (at point E).

Point	**Amplitude NM (m)**		**Amplitude EFDC (m)**
	$n = 1.0$	$n = 1.331587$	
A	2.181	2.155	2.157
B	2.178	2.155	2.155
C	2.166	2.151	2.145
D	2.135	2.133	2.122
E	2.070	2.090	2.081

Table 5.11: Water elevation amplitudes at the considered points inside domain for the second test case with $n = 1.0$ and $n = 1.331587$.

The computed value of the water elevation exponent term is $n = 1.331587$, and the errors decrease to -0.117% at point A, 0% at point B and go to 0.515% at point E, respectively. Table 5.11 gives computed water elevation amplitudes at points A-E inside domain for both values of the water elevation transformation exponent term.

In general, total velocities magnitude predicted by the cylindrical co-ordinates numerical model are larger than values predicted by EFDC, except at point A. The reason for this behaviour can be the fact that grid refinement in the cylindrical co-ordinates numerical model introduces errors which propagate to the point nearest the closed boundary. A study of the maximum total velocity magnitude in the time interval 46.8 – 59.3 hours is presented below:

- At point A, the predictions of the cylindrical co-ordinates numerical model under estimate the EFDC values by 23.238% at ebb tide and 38.441% at flood tide;

- At point B, the total velocities magnitude obtained from the cylindrical co-ordinates numerical model over estimate the EFDC values with an error of 11.814% at ebb tide and 6.126% at flood tide;

- At point C, the same as before, with error of 13.187% at ebb tide and 8.418% at flood tide;
- At point D, similar to above with error 6.425% at ebb tide and 3.701% at flood tide;
- At point E, similar to above with error 4.579% at ebb tide and 6.886% at flood tide.

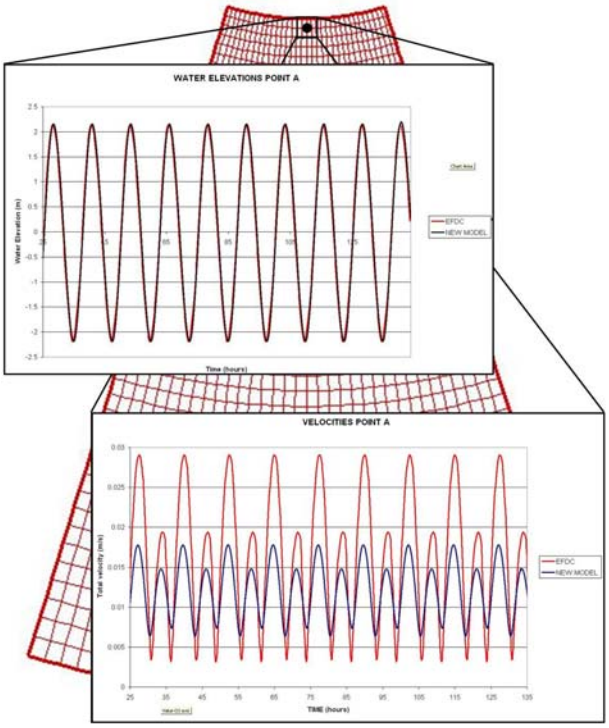

Figure 5.25: Total velocities and water elevation time series comparison between the two models at point A inside domain.

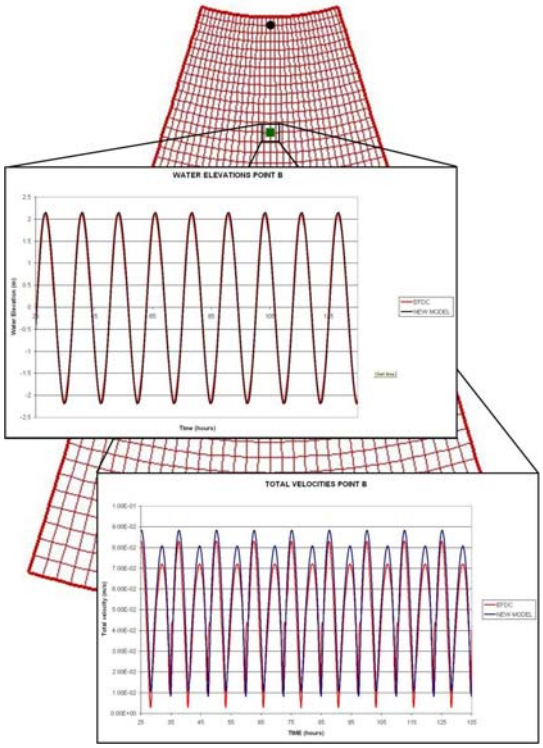

Figure 5.26: Total velocities and water elevation time series comparison between the two models at point B inside domain.

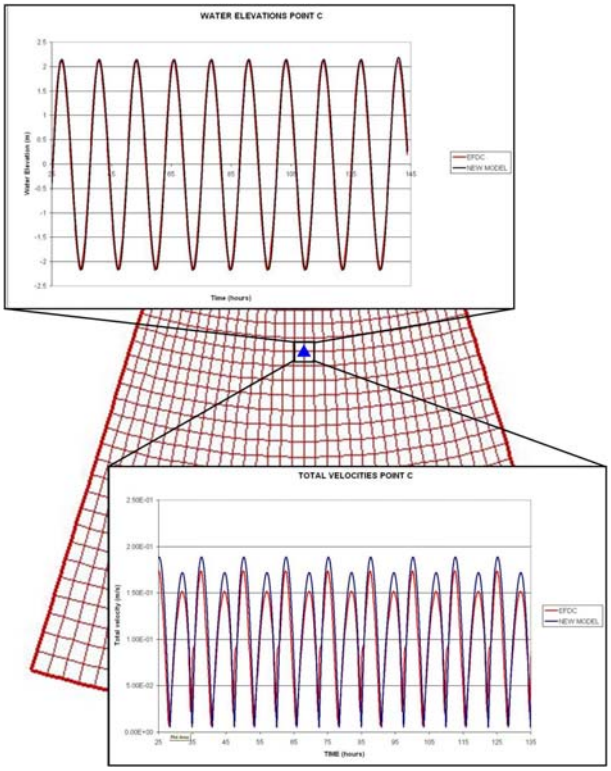

Figure 5.27: Total velocities and water elevation time series comparison between the two models at point C inside domain.

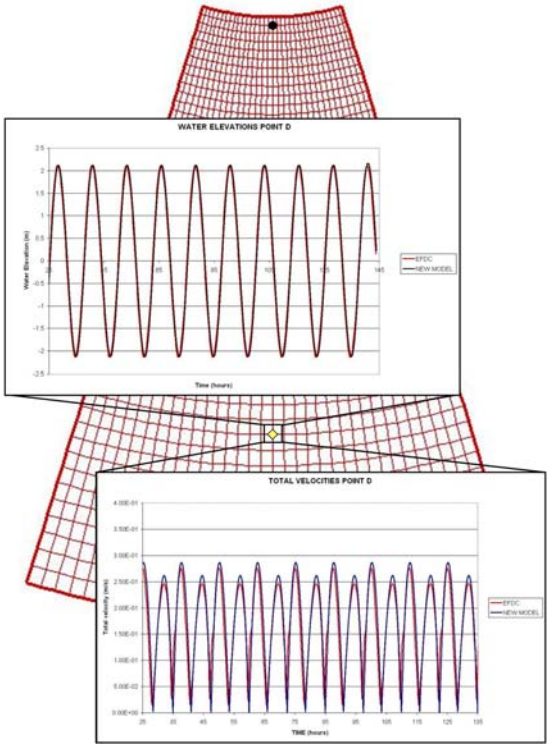

Figure 5.28: Total velocities and water elevation time series comparison between the two models at point D inside domain.

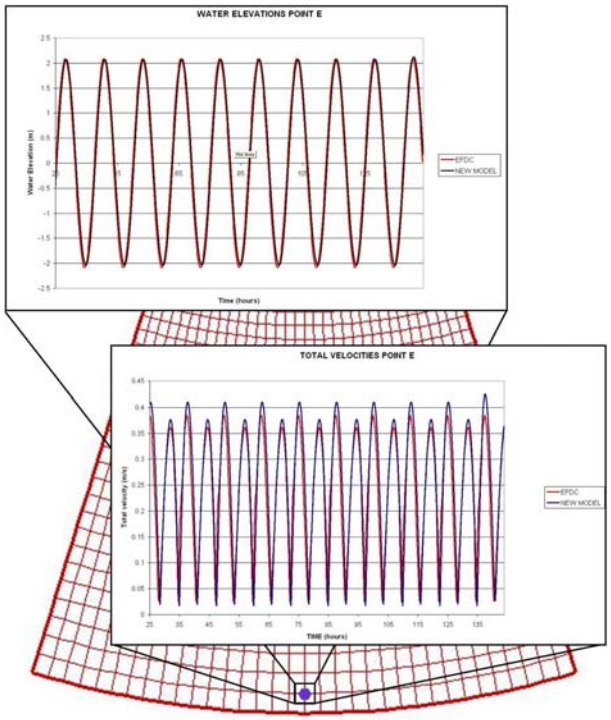

Figure 5.29: Total velocities and water elevation time series comparison between the two models at point E inside domain.

Dimensionless water elevation amplitudes resulted from simulations using the two numerical models are given in Table 5.12, with the exponent term for the transformation of water elevations in the cylindrical co-ordinates model taken as: $n = 1.0$ and $n = 1.331587$, respectively. Figure 5.30a) shows dimensionless water elevation amplitude versus distance for $n = 1.0$ and it is observed that the

a)

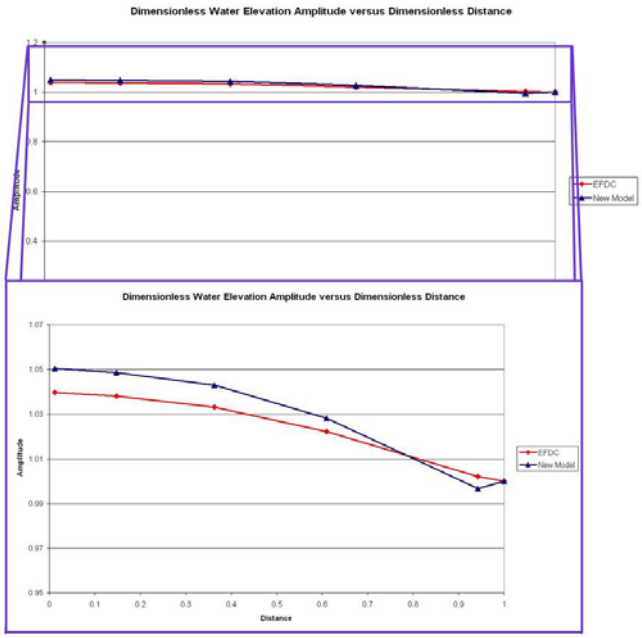

b)

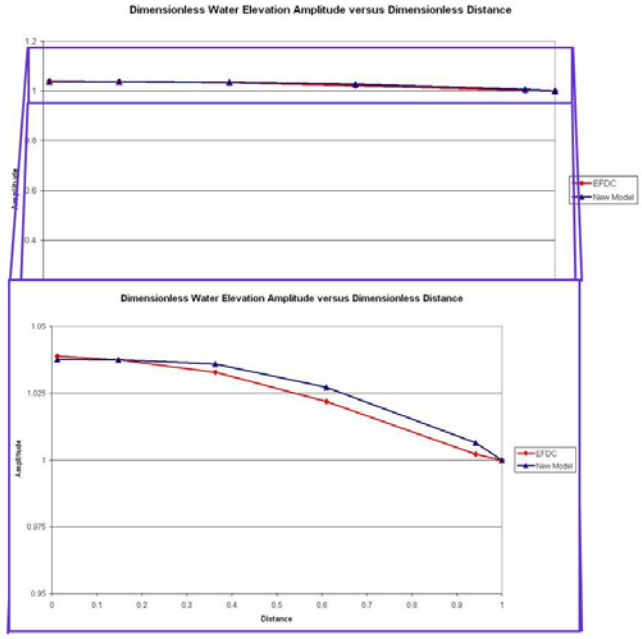

Figure 5.30: Analysis of dimensionless water elevation amplitude versus dimensionless distance for the second test case. Water elevation transformation exponent term in the cylindrical co-ordinates model: a) $n = 1.0$; b) $n = 1.331587$.

maximum dimensionless amplitude error with respect to EFDC values is obtained at point A and has a value of 1.094 % [Figure 5.30a) detail].

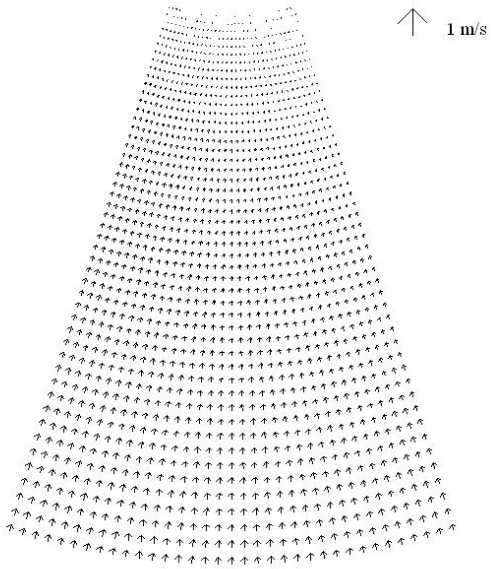

Figure 5.31: Flow inside domain for horizontal bed test case at time 36.00 hours (cylindrical co-ordinates model).

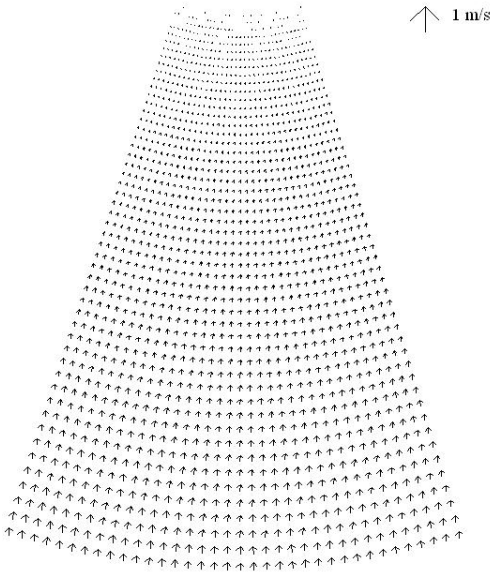

Figure 5.32: Flow inside domain for the second test case at time 36.00 hours (EFDC).

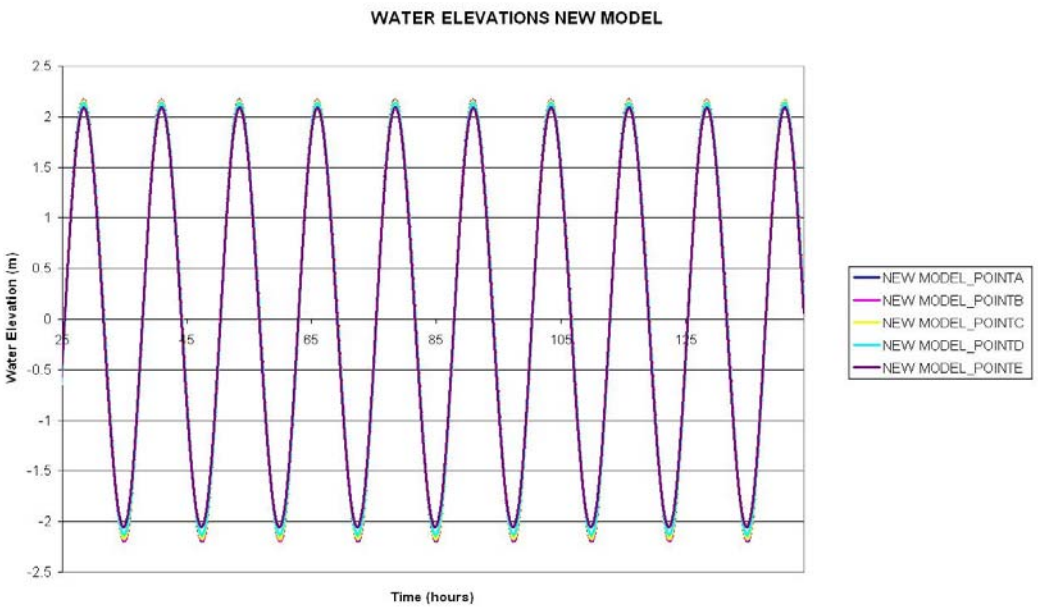

Figure 5.33: Water elevations variation at points A-E inside domain (cylindrical co-ordinates model).

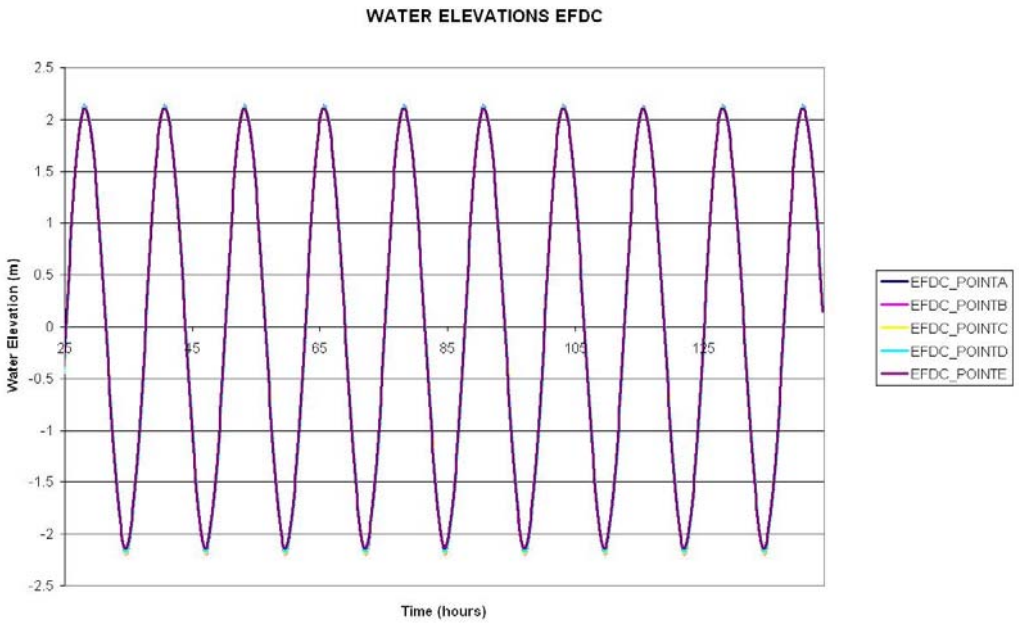

Figure 5.34: Water elevations variation at points A-E inside domain (EFDC).

Figure 5.30b) shows dimensionless water elevation amplitude versus distance for $n = 1.331587$ and it is observed that the maximum dimensionless amplitude error with respect to EFDC values is obtained at point E but it is reduced to 0.515 % [Figure 5.30b) detail].

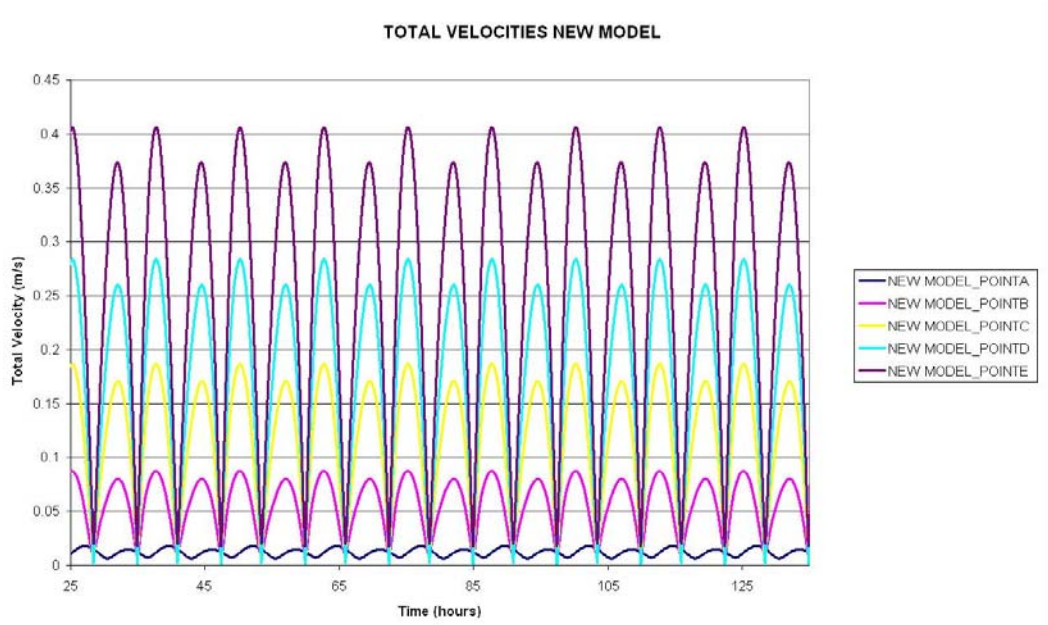

Figure 5.35: Total velocities variation at points A-E inside domain (cylindrical co-ordinates model).

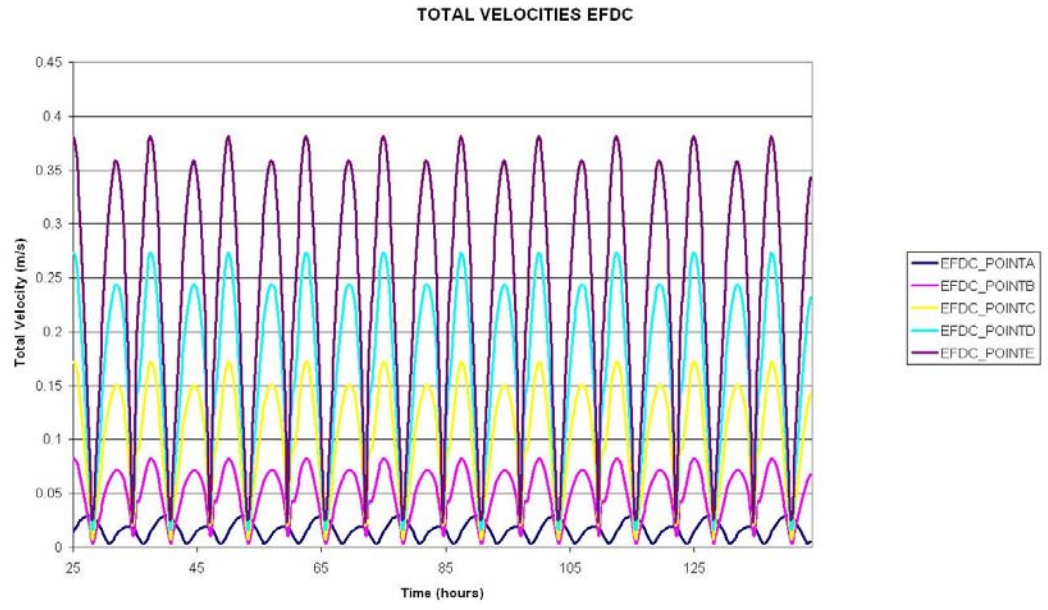

Figure 5.36: Total velocities variation at points A-E inside domain (EFDC).

Velocity vectors are also in phase [Figures 5.27 – 5.31]. Figures 5.33 and 5.34 show current velocities map at time 36.00 hours for the two models and agreement for directions of velocity vectors is observed. In terms of variation of water elevations and velocities inside domain at points A-E, Figures 5.35 and

5.36, and 5.37 and 5.38, respectively, show that agreement is achieved for the two models.

Point	**Dimensionless Amplitude NM**		**Dimensionless Amplitude EFDC**
	$n = 1.0$	$n = 1.331587$	
A	1.050	1.038	1.039
B	1.048	1.037	1.037
C	1.043	1.036	1.033
D	1.028	1.027	1.022
E	0.997	1.007	1.002

Table 5.12: Dimensionless water elevation amplitudes at the considered points inside domain for the second test case with $n = 1.0$ and $n = 1.331587$ in the cylindrical co-ordinates model.

The computed tidal period varies between 12.491 hours and 12.503 hours, with an average value of 12.497 hours in the cylindrical co-ordinates model, and it is constant and equal to 12.500 hours in EFDC. The study of phase shift introduced by the cylindrical co-ordinate system in the time interval 46.8 - 59.3 hours showed that [Table 5.13]:

a) At point A the phase shift of water elevation time series was 0.137 hours at high water and 0.184 hours at low water, respectively, with respect to EFDC values;

b) At point A the phase shift of total velocity time series was -0.456 hours at ebb tide and -0.372 hours at flood tide with respect to EFDC values;

c) At point E the phase shift of water elevation time series was 0.173 hours at high water and 0.312 hours at low water, respectively, with respect to EFDC values;

d) At point E the phase shift of total velocity time series was -0.057 hours at ebb tide and 0.221 hours at flood tide, respectively, with respect to EFDC values.

	Water Elevation				Total Velocity			
	High Water (HW)		Low Water (LW)		Ebb		Flood	
	Time (hours)	Max (m)	Time (hours)	Min (m)	Time (hours)	Max (m/s)	Time (hours)	Max (m/s)
Point A								
New Model	53.387	2.167	47.434	-2.195	58.544	0.015	52.128	0.018
EFDC	53.250	2.127	47.250	-2.188	59.000	0.019	52.500	0.029
Point B								
New Model	53.387	2.164	47.434	-2.191	57.029	0.080	50.172	0.087
EFDC	53.250	2.125	47.000	-2.184	57.000	0.072	50.000	0.082
Point C								
New Model	53.399	2.158	47.410	-2.174	57.041	0.171	50.197	0.187
EFDC	53.250	2.119	47.000	-2.171	57.000	0.151	50.000	0.172
Point D								
New Model	53.411	2.136	47.373	-2.134	57.017	0.260	50.221	0.284
EFDC	53.250	2.105	47.000	-2.140	57.000	0.244	50.000	0.274
Point E								
New Model	53.423	2.088	47.312	-2.052	56.943	0.376	50.221	0.409
EFDC	53.250	2.078	47.000	-2.084	57.000	0.359	50.000	0.382

Table 5.13: High and low water levels and maximum total velocity at ebb and flood tide for the second test case for $n = 1.0$.

In the second test case, it is found that the tidal excursion varies along centreline with the same pattern as in the first test case in the cylindrical co-ordinates numerical model, and it changes only at point A in EFDC [see Table 5.14]. Similarly, the time it takes a particle to travel from maximum velocity at ebb tide

to maximum velocity at flood tide exhibits the same pattern in the cylindrical co-ordinates numerical model and EFDC as in the first test case [see Table 5.15].

Point	**NM** **HW-LW** (hours)	**EFDC** **HW-LW** (hours)
A	5.952	6.000
B	5.952	6.250
C	5.989	6.250
D	6.026	6.250
E	6.123	6.250

Table 5.14: Time period between high water and low water in the three models along centreline.

Point	**NM** **Ebb-Flood** (hours)	**EFDC** **Ebb-Flood** (hours)
A	6.417	6.500
B	6.857	7.000
C	6.844	7.000
D	6.796	7.000
E	6.722	7.000

Table 5.15: Time period between maximum velocity at ebb tide and maximum velocity at flood tide in the three models along centreline.

5.3.3. Case 3 – Horizontal Bed with Two Variations of the Scale Factors in the Radial Direction

For the second test case the scale factors vary in the given domain according to the values given in Table 5.16. Equation (5.26) was used for generation of the grid. The parameter controlling the step size in the radial direction was $a = 0.3$

and up to radius 24 in equation (5.11) and generated the first set of scale factors, followed by the same equation with $a = 0.5$ for the rest of the domain.

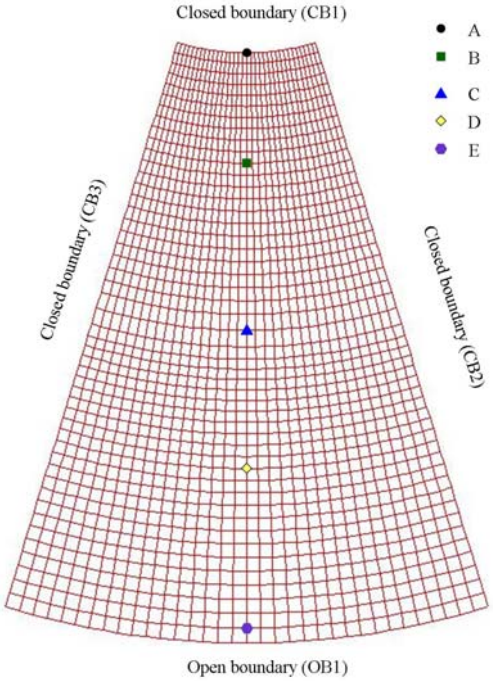

Figure 5.37: Domain representation for third test case in cylindrical co-ordinates numerical model.

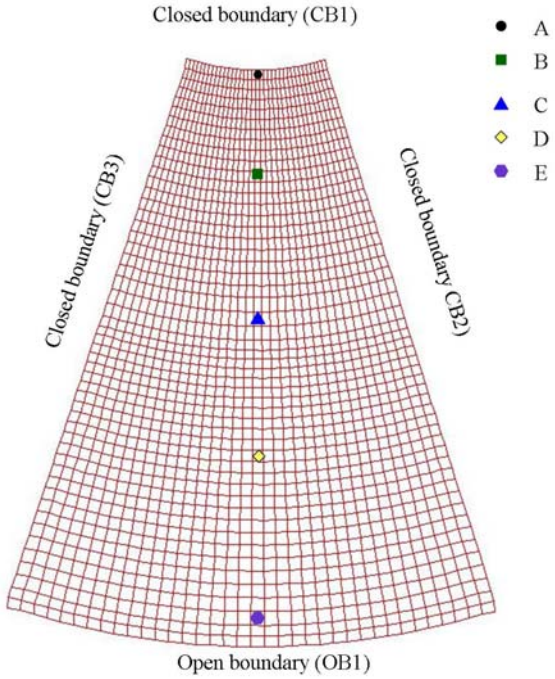

Figure 5.38: Domain representation for third test case in EFDC.

Radius	Scale factor in the ξ^r direction	Scale factor in the ξ^θ direction	Point
7431.259	335.282	129.700	
7766.518	339.330	135.587	A
8105.823	343.427	141.509	
8449.225	347.572	147.503	
8796.773	351.769	153.569	
9148.516	356.015	159.709	
9504.505	360.313	165.922	
9864.792	364.663	172.211	
10229.429	369.065	178.576	
10598.468	373.521	185.017	
10971.962	378.030	191.536	
11349.964	382.594	198.134	B
11732.530	387.212	204.812	
12119.715	391.887	211.570	
12511.574	396.618	218.409	
12908.163	401.406	225.332	
13309.540	406.252	232.338	
13715.763	411.156	239.428	
14126.889	416.120	246.604	
14542.979	421.143	253.867	
14964.092	426.228	261.217	
15390.289	431.373	268.656	
15821.631	514.348	276.185	
16258.181	454.378	285.162	
16855.534	459.866	293.092	C
17327.741	400.197	301.119	
17650.119	328.239	308.103	
17978.306	334.153	313.832	
18312.405	340.174	319.664	
18652.525	346.303	325.601	
18998.773	352.542	331.646	
19351.259	358.894	337.799	
19710.096	365.361	344.062	
20075.398	371.944	350.439	
20447.283	378.645	356.931	
20825.867	385.467	363.539	
21211.273	392.412	370.267	D
21603.623	399.483	377.116	
22003.042	406.681	384.088	
22409.658	414.008	391.186	
22823.600	421.467	398.412	
23245.000	429.061	405.768	
23673.993	436.792	413.257	
24110.715	444.662	420.880	
24555.306	452.673	428.641	
25007.907	460.829	436.541	
25468.663	469.132	444.584	
25937.720	477.585	452.772	
26415.229	486.190	461.108	
26901.342	494.950	469.593	E
27396.213	499.329	473.836	
27900.000	503.747	478.116	

Table 5.16: Variation of scale factors inside domain for horizontal bed with two variations of the space step in the radial direction test case.

The value obtained at radius 25 represented an average value between the value of the scale factor at radius 24 and the computed value from second evaluation of the scale factors based on equation (5.11) at radius 25. Domain representations for the third test case are given in Figures 5.37 and 5.38 for the cylindrical co-ordinates model and EFDC, respectively.

Simulations were performed with the same parameters as in Section 5.5.2. Time step was chosen $\delta t = 8$ seconds. The values of the parameters in the RAW filter are $\alpha_1 = 0.05$, $\alpha_2 = 1.0$. Water elevations amplitude error analysis for $n = 1.0$ shows that maximum water elevation amplitude error occurs at point E and its value is 0.806% with respect to EFDC values, while minimum water elevation amplitude error is 0.168% at point D. With $n = 1.216087$, the maximum water elevation amplitude error is 0.499% at point D and minimum error is 0.019% at point A.

Table 5.17 gives the computed water elevation amplitudes resulted from the simulations using the two models at points A-E inside domain. Dimensionless water elevation amplitudes computed by the cylindrical co-ordinates model, with both $n = 1.0$ and $n = 1.216087$, and EFDC are shown in Table 5.18.

Point	**Amplitude NM (m)**		**Amplitude EFDC (m)**
	$n = 1.0$	$n = 1.216087$	
A	2.172	2.155	2.156
B	2.170	2.156	2.152
C	2.150	2.145	2.138
D	2.122	2.124	2.115
E	2.072	2.085	2.080

Table 5.17: Water elevation amplitudes at the considered points inside domain for third test case for $n = 1.0$ and $n = 1.216087$.

In general, total velocities magnitude predicted by the cylindrical co-ordinates numerical model are larger than values predicted by EFDC, except at point E. A

study of the maximum total velocity magnitude in the time interval 46.8 – 59.3 hours is presented below:

- At point A, the predictions of the cylindrical co-ordinates numerical model over estimate the EFDC values by 175.985% at ebb tide and 112.441% at flood tide. This large difference in values can be explained by the fact that grid is refined twice in this test case and errors are introduced in computations;

- At point B, the total velocities magnitude obtained from the cylindrical co-ordinates numerical model over estimate the EFDC values with an error of 12.059% at ebb tide and 5.942% at flood tide;

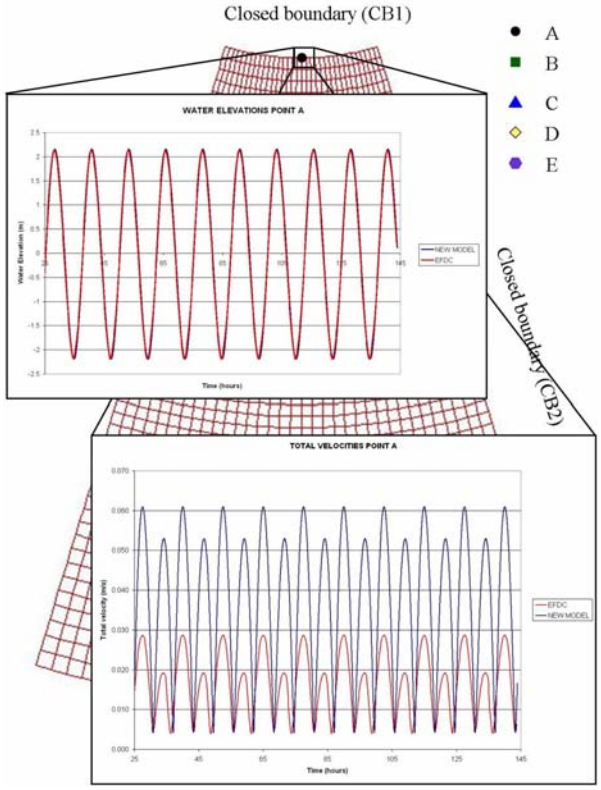

Figure 5.39: Total velocities and water elevation time series comparison between the two models at point A inside domain.

- At point C, the same as before, with error of 14.626% at ebb tide and 10.414% at flood tide;

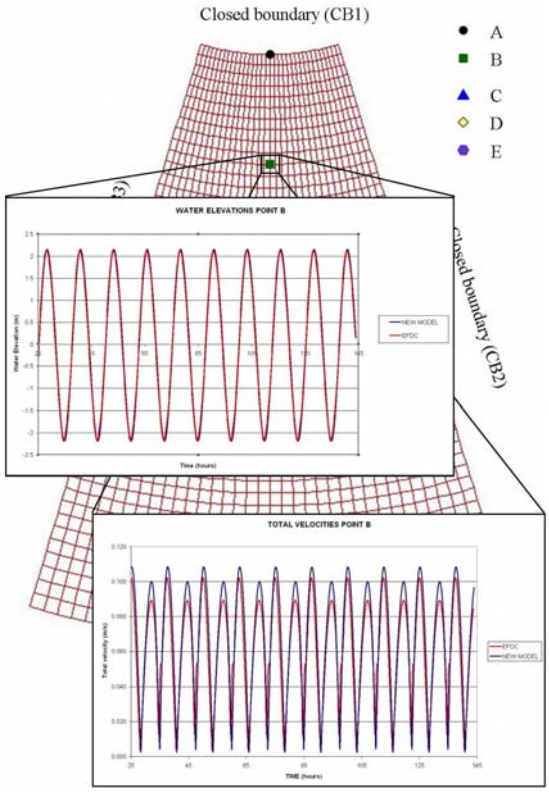

Figure 5.40: Total velocities and water elevation time series comparison between the two models at point B inside domain.

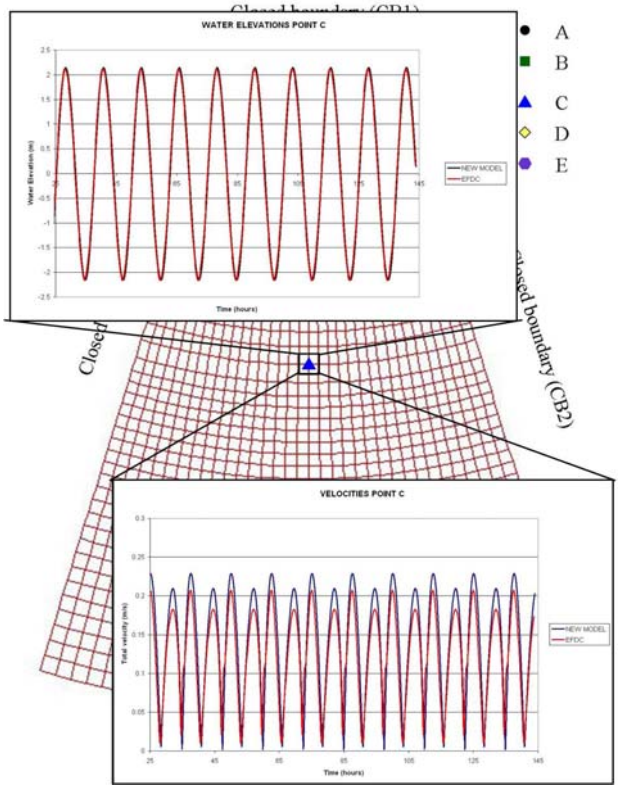

Figure 5.41: Total velocities and water elevation time series comparison between the two models at point C inside domain.

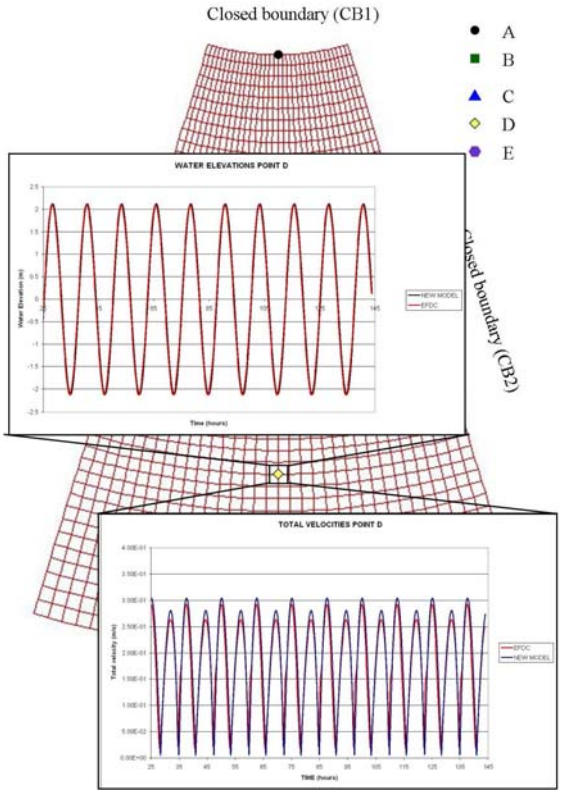

Figure 5.42: Total velocities and water elevation time series comparison between the two models at point D inside domain.

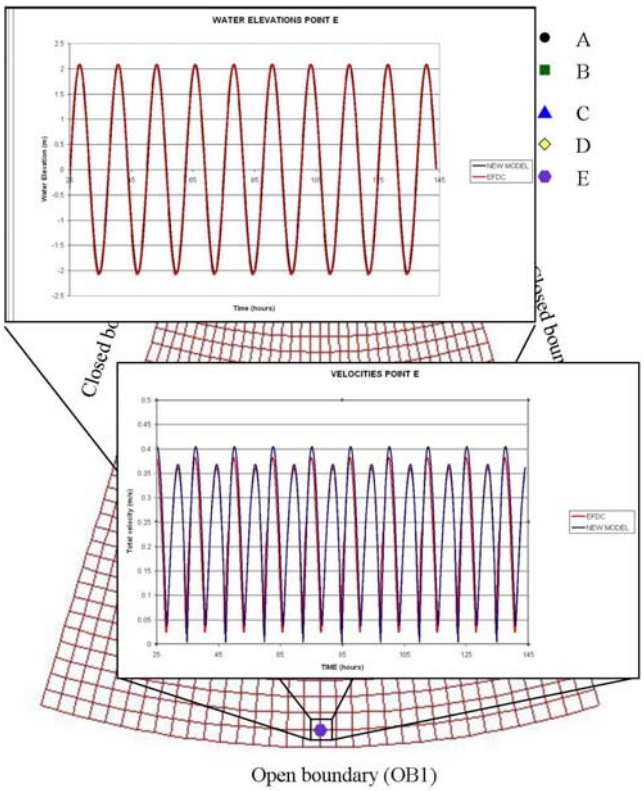

Figure 5.43: Total velocities and water elevation time series comparison between the two models at point E inside domain.

a)

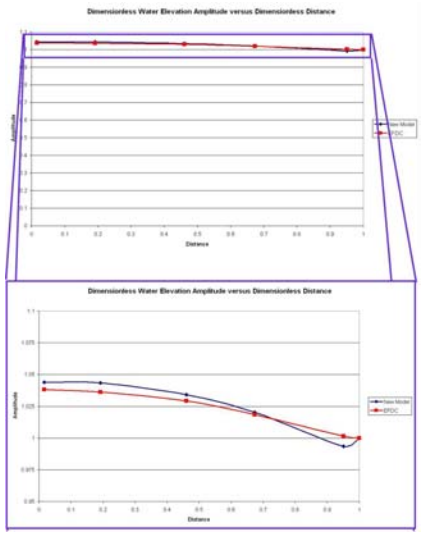

b)

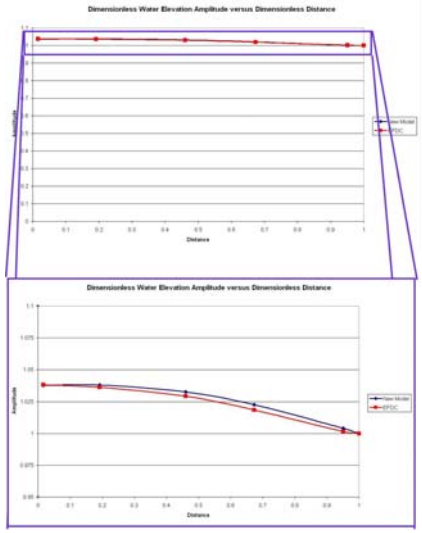

Figure 5.44: Analysis of dimensionless water elevation amplitude versus dimensionless distance for the third test case: a) $n = 1.0$; b) $n = 1.216087$.

Point	**Dimensionless Amplitude NM**		**Dimensionless Amplitude EFDC**
	$n = 1.0$	$n = 1.216087$	
A	1.046	1.038	1.038
B	1.045	1.038	1.036
C	1.036	1.033	1.029
D	1.022	1.022	1.018
E	0.997	1.004	1.001

Table 5.18: Dimensionless water elevation amplitudes at the considered points inside domain for second test case for $n = 1.0$ and $n = 1.216087$.

- At point D, similar to above with error 6.583% at ebb tide and 3.931% at flood tide;

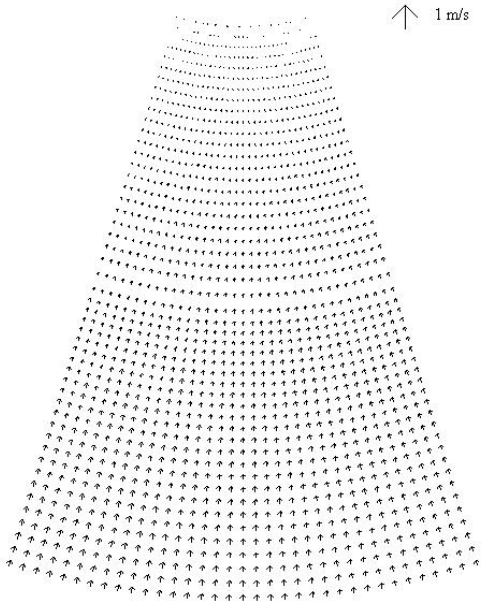

Figure 5.45: Flow inside domain for horizontal bed test case at time 36.00 hours (cylindrical co-ordinates model).

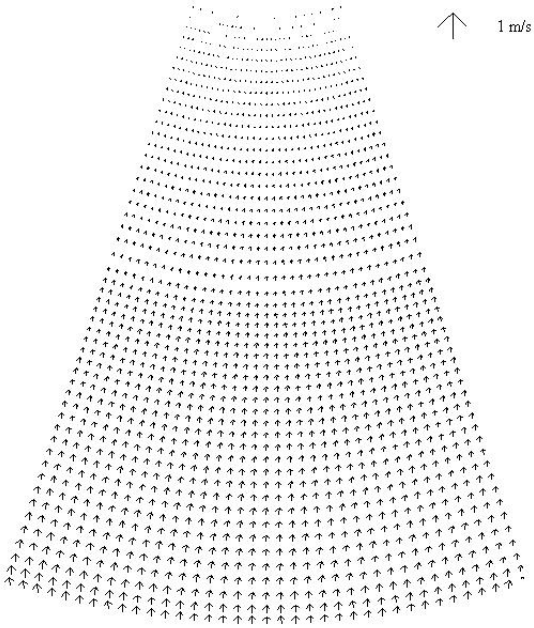

Figure 5.46: Flow inside domain for horizontal bed test case at time 36.00 hours (EFDC).

- At point E, similar to above with error 0.859% at ebb tide and 3.220% at flood tide.

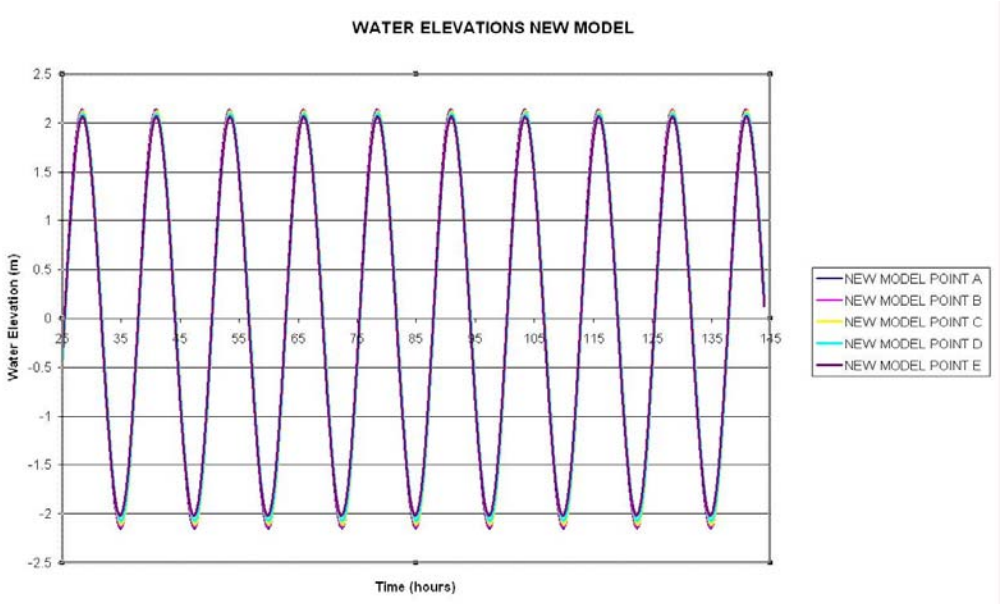

Figure 5.47: Water elevations variation at considered points inside domain (cylindrical co-ordinates model).

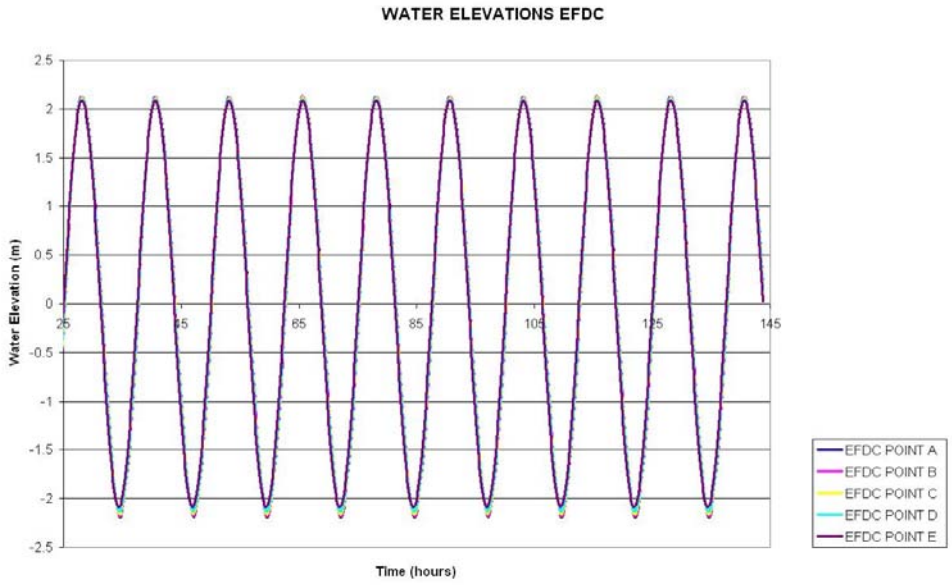

Figure 5.48: Water elevations variation at points A-E inside domain (EFDC).

Figure 5.44a) shows dimensionless water elevation amplitude versus dimensionless distance for $n = 1.0$ and it is observed that the maximum

dimensionless amplitude error with respect to EFDC values is obtained at point E and has a value of and 0.806%. From the detail in Figure 5.44b) it is observed that the shape of the water elevation amplitudes over distance graph is similar for the two models, whereas the detail in Figure 5.44a) shows two different shapes for the same graph. For $n = 1.216087$ the maximum water elevation amplitude error is 0.237% at point D.

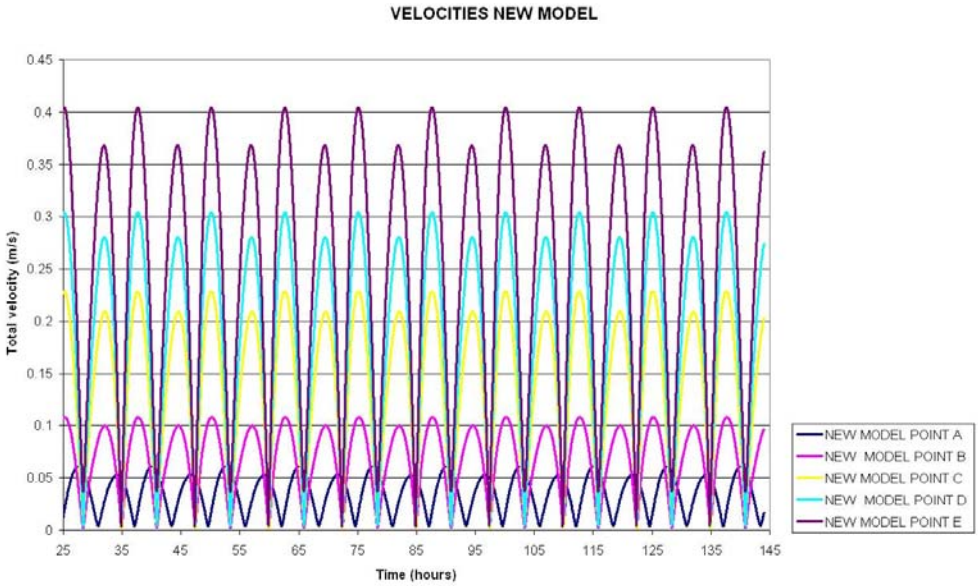

Figure 5.49: Total velocities variation at points A-E inside domain (cylindrical co-ordinates model).

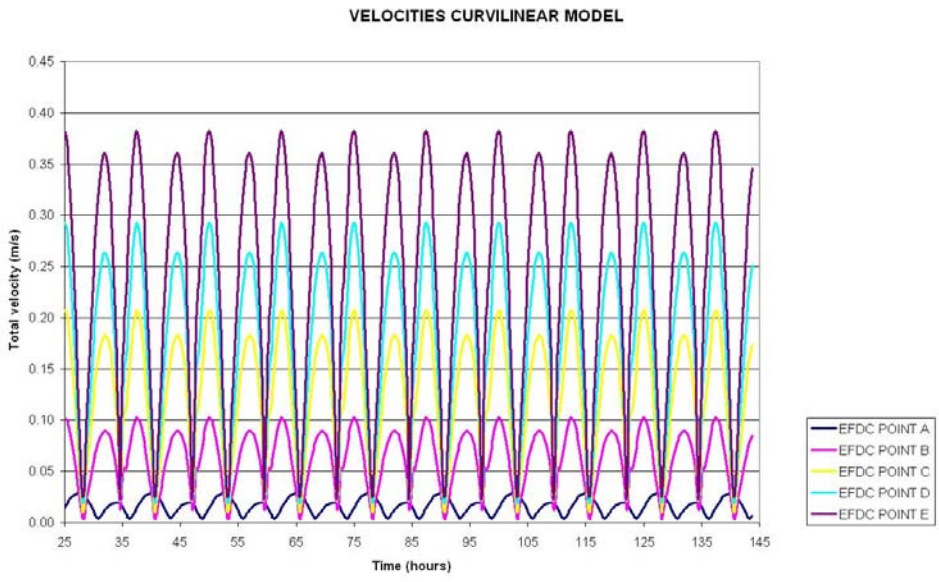

Figure 5.50: Total velocities variation at points A-E inside domain (EFDC).

From Figures 5.39 – 5.43 it can be seen that velocity vectors are in phase. Figures 5.45 and 5.46 show current velocities map at time 36.00 hours for the two models and agreement for directions of velocity vectors is observed.

In terms of variation of water elevations and velocities inside domain at points A-E, Figures 5.47 and 5.48, and Figures 5.49 and 5.50, respectively, show that agreement is achieved for the two models.

Point A								
	Water Elevation				Total Velocity			
	High Water (HW)		Low Water (LW)		Ebb		Flood	
	Time (hours)	Max (m)	Time (hours)	Min (m)	Time (hours)	Max (m/s)	Time (hours)	Max (m/s)
New Model	53.313	2.155	47.324	-2.189	59.156	0.053	52.556	0.061
EFDC	53.250	2.126	47.250	-2.186	59.000	0.019	52.500	0.029
Point B								
	Water Elevation				Total Velocity			
	High Water (HW)		Low Water (LW)		Ebb		Flood	
	Time (hours)	Max (m)	Time (hours)	Min (m)	Time (hours)	Max (m/s)	Time (hours)	Max (m/s)
New Model	53.338	2.155	47.349	-2.184	57.053	0.100	50.184	0.108
EFDC	53.251	2.123	47.000	-2.181	57.000	0.089	50.000	0.102
Point C								
	Water Elevation				Total Velocity			
	High Water (HW)		Low Water (LW)		Ebb		Flood	
	Time (hours)	Max (m)	Time (hours)	Min (m)	Time (hours)	Max (m/s)	Time (hours)	Max (m/s)
New Model	53.362	2.145	47.349	-2.157	57.053	0.209	50.111	0.229
EFDC	53.251	2.114	47.000	-2.161	57.000	0.183	50.000	0.207
Point D								
	Water Elevation				Total Velocity			
	High Water (HW)		Low Water (LW)		Ebb		Flood	
	Time (hours)	Max (m)	Time (hours)	Min (m)	Time (hours)	Max (m/s)	Time (hours)	Max (m/s)
New Model	53.387	2.125	47.324	-2.120	56.980	0.280	50.135	0.304
EFDC	53.251	2.100	47.000	-2.131	57.000	0.263	50.000	0.292
Point E								
	Water Elevation				Total Velocity			
	High Water (HW)		Low Water (LW)		Ebb		Flood	
	Time (hours)	Max (m)	Time (hours)	Min (m)	Time (hours)	Max (m/s)	Time (hours)	Max (m/s)
New Model	53.362	2.088	47.227	-2.055	56.864	0.372	50.050	0.404
EFDC	53.251	2.078	47.000	-2.082	57.000	0.369	50.000	0.391

Table 5.19: High and low water levels and maximum total velocity at ebb and flood tide for the third test case for $n = 1.0$.

The computed tidal period is 12.497 hours for cylindrical co-ordinates model and 12.500 hours for EFDC. The study of phase shift in the time interval 46.8 – 59.3 hours introduced by the cylindrical co-ordinate system showed that [Table 5.19]:

a) At point A the phase shift of water elevation time series was 0.062 hours at high water and 0.324 hours at low water, respectively, with respect to EFDC values;

b) At point A the phase shift of total velocity time series was 0.156 hours at ebb tide and 0.056 hours at flood tide with respect to EFDC values;

c) At point E the phase shift of water elevation time series was 0.111 hours at high water and 0.227 hours at low water, respectively, with respect to EFDC values;

d) At point E the phase shift of total velocity time series was -0.136 hours at ebb tide and 0.050 hours at flood tide, respectively, with respect to EFDC values.

Point	**NM** **HW-LW** (hours)	**EFDC** **HW-LW** (hours)
A	5.989	6.251
B	5.989	6.251
C	6.013	6.251
D	6.062	6.251
E	6.135	6.251

Table 5.20: Time period between high water and low water in the two models along centreline for $n = 1.0$.

In the third test case, it is found that the tidal excursion varies along centreline with the same pattern as in the first test case in the cylindrical co-ordinates numerical model, and it changes only at point A in EFDC [see Table 5.20]. The time it takes a particle to travel from the maximum velocity at ebb tide to the

maximum velocity at flood tide exhibits the same pattern in the cylindrical co-ordinates numerical model as in the first test case and varies in EFDC only at point A [see Table 5.21].

Point	NM Ebb-Flood (hours)	EFDC Ebb-Flood (hours)
A	6.600	6.500
B	6.869	7.000
C	6.942	7.000
D	6.844	7.000
E	6.814	7.000

Table 5.21: Time period between maximum velocity at ebb tide and maximum velocity at flood tide in the three models along centreline.

5.4. Physical Modelling

5.4.1. General Considerations

Coastal engineers avail of three techniques, namely: field observations and measurements, laboratory observations and measurements (physical modelling), and numerical modelling, for study of complex flows which occur in coastal zones [Hughes (1993), Dean and Dalrymple (2002)], as shown in Figure 5.53. The three techniques are complementary in that:

a) field measurements can be used to specify hydrodynamic forcing for both physical and numerical models, as well as validation tools for numerical model results;

b) physical models can be used for validation, in validation test cases, or calibration of numerical models;

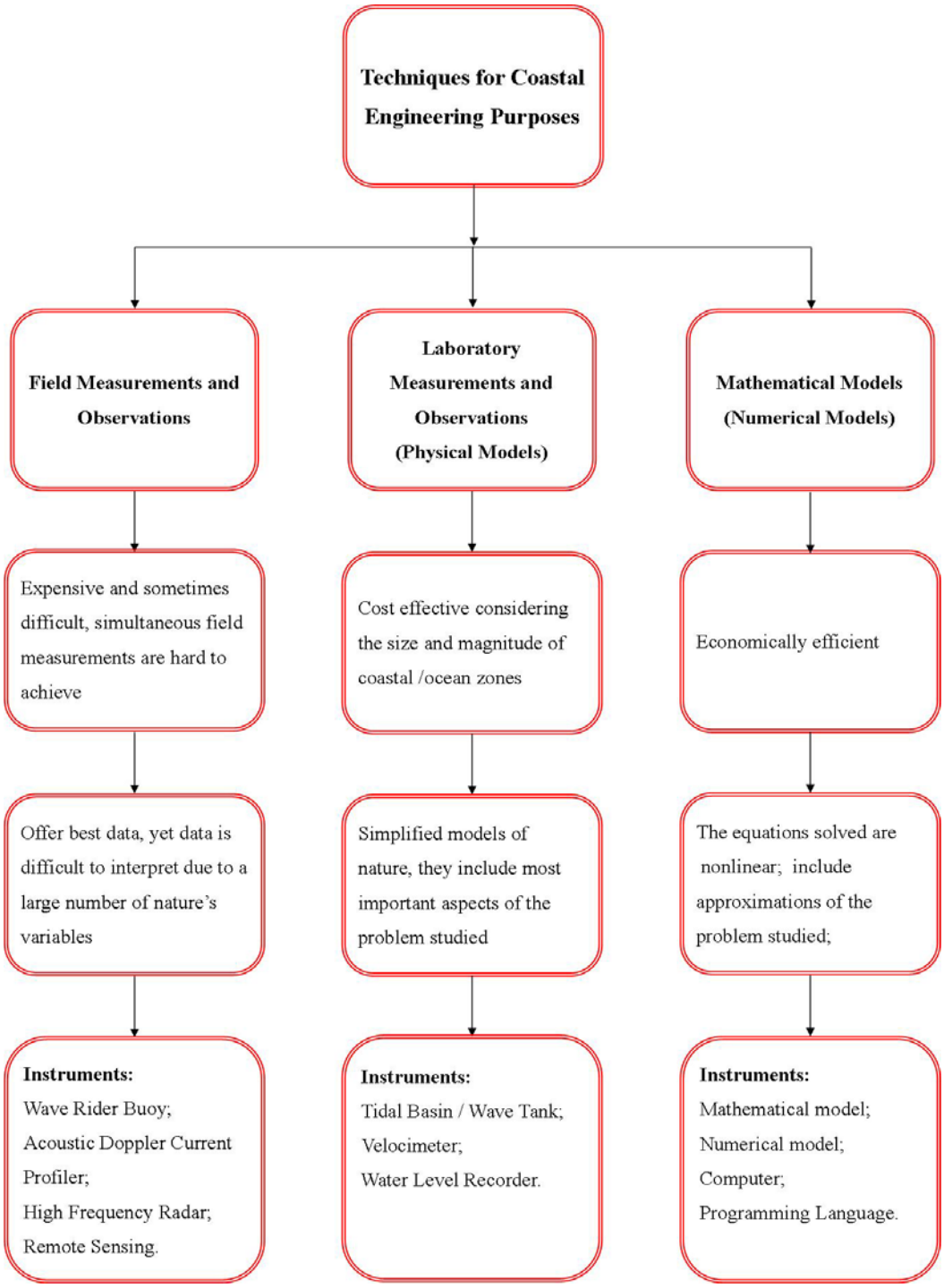

Figure 5.51: Techniques for study of coastal flows.

c) physical model results for complex regions can be used as input or boundary conditions for comprehensive numerical models and this approach is called hybrid modelling;

d) numerical models are useful tools in simulation of near-shore circulation, flows in estuarine tidal systems, or for situations where hydrodynamics is mainly characterized by wave refraction, diffraction or shoaling. Therefore, numerical models can successfully replace the large scale physical models of estuarine zones.

Advantages of using physical modelling are summarized next. Unlike the numerical or analytical models, physical models are based on the non-linear equations governing water flow and accurately represent turbulence and bed friction. Physical models provide easier visualisation of various processes and data collection throughout the flow regime, compared to field measurements and observations, with less expensive equipment required by the first approach. Lastly, the researcher has the ability of varying the environmental conditions inside the physical model.

Disadvantages of using physical modelling are neither small in number, nor insignificant so that they can be overlooked, and they discussed hereafter. Physical models present the scale effect problem, since viscous forces are smaller in the prototype, compared to the scaled model. Furthermore, not all natural forcing and boundary conditions, existing at the moment when field measurements and observations are taken, can be included in the scaled model for the simple reason that they may not be known to the researcher. Also, in some cases, the forcing conditions can be artificially represented by a unidirectional generation of the wave in the physical model, although it may not be the case in the prototype. A significant impact on the quality of the measured data have the physical model boundaries and the less reflective they are, the better the results are. Finally, simulations performed in laboratory are more expensive than those performed using numerical models, since the operational costs of numerical models are smaller than those of physical models.

Based on the arguments presented in the first paragraph of this Chapter, the benefits of physical modelling, with a judicious utilization of the criteria of similitude, can overcome the disadvantages. Since in most cases, due to economical reasons, geometrical scaling is required between the prototype and

physical model, similarity of the phenomena (velocities, accelerations, mass spatial and temporal transport of fluid, resultant forces) must be considered.

A constant value of the linear horizontal and vertical length scale ratios of the prototype and physical model defines geometric similarity. A distorted physical model has two different values of the ratios of the linear dimensions, one for the horizontal and another one for the vertical plane. Therefore, a distorted model is not geometrically similar and cancels the kinematical and dynamical similarity with the prototype. Constant values of the components of velocity ratios at all points specify kinematic similarity. Dynamic similarity assumes that ratios of all forces in the prototype to all forces in the physical model are equal [equation (5.12)]. In most cases, the physical model is smaller than the prototype and equation (5.12) is written for an ideal fluid in this case. Ideally, geometrical, kinematical and dynamical similarity between physical model and prototype define a complete similitude. In reality, dynamic similarity cannot be achieved since scaling of the gravitational acceleration gives a ratio equal to one anywhere on Earth, the same as fluid density and viscosity scale ratios when using the same fluid (water) in the two systems. Hence, the modeller can assess the criteria of similitude and decide the number of criteria that makes it possible to produce results of the physical model that are similar to the prototype. Additionally, the evaluation of governing forces provides supplementary conditions (Froude number and Reynolds number) which ensure similarity of the results.

$$\frac{(F_i)_P}{(F_i)_{PM}} = \frac{(F_p)_P}{(F_p)_{PM}} + \frac{(F_g)_P}{(F_g)_{PM}} + \frac{(F_\nu)_P}{(F_\nu)_{PM}} + \frac{(F_\gamma)_P}{(F_\gamma)_{PM}} + \frac{(F_e)_P}{(F_e)_{PM}} \tag{5.12}$$

where:

subscripts P and PM stand for prototype and physical model, respectively;

$F_i = ma$ is the inertial force, which for geometrical similarity can be written $F_i = \rho L^2 L_V^2$, with L_V the velocity scale, L the geometric scale, mass represented as $m = \rho L^3$, and advective acceleration given by $a = u_i \frac{\partial u_i}{\partial x_i}$ or $a = \frac{L_V^2}{L}$;

$F_p = pL^2$ is pressure force, with p representing unit pressure;

$F_g = mg$ is the gravity force, with its equivalent form $F_g = \rho L^3 g$;

$F_\nu = \tau A$ is the viscous force, written as $F_\nu = \mu L_V L$;

$F_\gamma = \gamma L$, with γ the surface tension, and L the length from a particle on the surface;

$F_e = EA$ is the elasticity force with E the elasticity modulus, $F_e = EL^2$.

Three conditions of similitude [a)-c)] with applicability to both geometrically similar and distorted models, and a fourth condition [d)] which requires a geometrically undistorted model, result from the non-dimensional forms of the depth averaged continuity and momentum equations [Olbert (2006)]:

a) scale ratio of a Froude number:

$$\frac{(L_V)_P}{(L_V)_{PM}} = \sqrt{\frac{(g)_P}{(g)_{PM}} \frac{(L_Z)_P}{(L_Z)_{PM}}} \tag{5.13}$$

b) scale ratio of a Strouhal number:

$$\frac{(L_X)_P}{(L_X)_{PM}} = \frac{(L_V)_P}{(L_V)_{PM}} \frac{(L_T)_P}{(L_T)_{PM}} \tag{5.14}$$

c) scale ratio of a Reynolds number:

$$\frac{(L_V)_P}{(L_V)_{PM}} \frac{(L_X)_P}{(L_X)_{PM}} = \left[\frac{(\nu)_P}{(\nu)_{PM}} \right]^{-1} \tag{5.15}$$

d) scale ratio of vertical viscous shear:

$$\frac{(L_x)_P}{(L_x)_{PM}} = \left[\frac{(L_Z)_P}{(L_Z)_{PM}} \right]^{-1} \tag{5.16}$$

Equation (5.13) can be introduced into equation (5.15) producing the criterion for distorted models which ensures that viscous processes are reproduced correctly in a hydraulic model:

d) scale ratio of vertical viscous shear:

$$\frac{(\nu)_P}{(\nu)_{PM}} = \sqrt{\frac{(L_Z)_P}{(L_Z)_{PM}}} \frac{(L_x)_P}{(L_x)_{PM}} \tag{5.17}$$

where:

L_X is the linear horizontal scale (for distorted models);

L_Z is the linear vertical scale (for distorted models);

L_T is the time scale.

The condition for two models to be geometrically similar can be written mathematically: $L = L_X = L_z$.

5.4.2. Tidal Model Set-Up

A complete description of tidal basin set up [Figures 5.52 and 5.53] at College of Engineering and Informatics, National University of Ireland Galway can be found in Olbert (2006). Tidal basin is made up of three sections in the longitudinal direction: reservoir, manifold chamber and working area, shown in Figure 5.53, which also gives the vertical plane dimensions of the tidal basin.

A 2.0mx5.0mx1.0m water reservoir is separated from the manifold chamber by a vertical weir which controls the variation of water level in the working area. The perforated manifold has the role of uniformly discharging a constant water rate in the working area. The turbulence in the working area is limited by a porous baffle which is positioned between the manifold and working area. Tidal basin can be filled from an external source with 30 m^3 of water in order to perform the simulation, based on a maximum capacity of 40 m^3 of water. The maximum amplitude of water level is 0.15 m. During simulation, water circulation is realized in a closed system, as described below [Figure 5.53b)]:

- water is stored in the reservoir;

- it is next pumped at constant rate into the perforated manifold and then water fills the working area with tidal volume during flood tide or returned immediately to the reservoir at ebb tide;
- the weir overflow system directs excess water from working area to the reservoir.

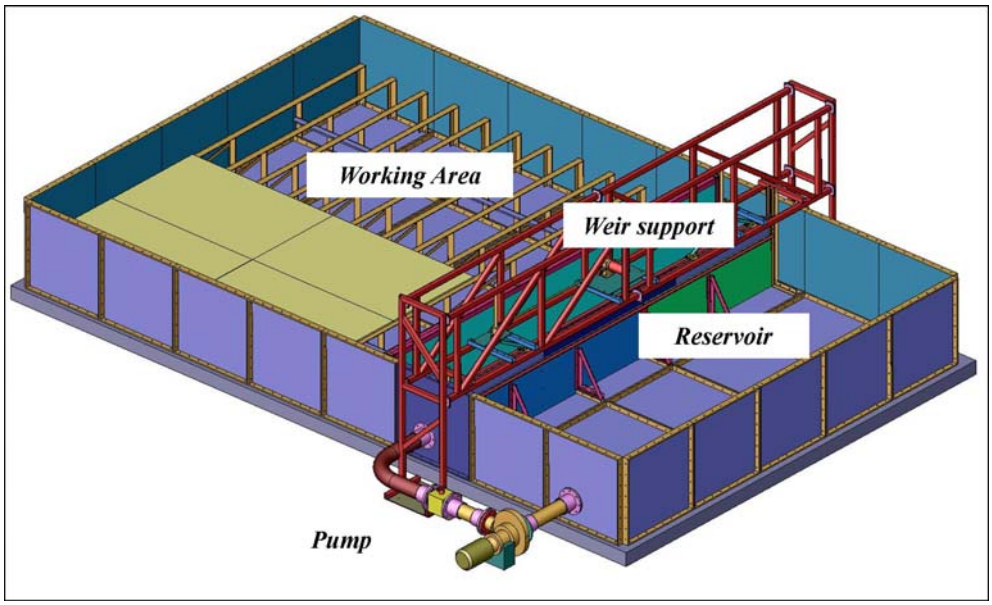

a)

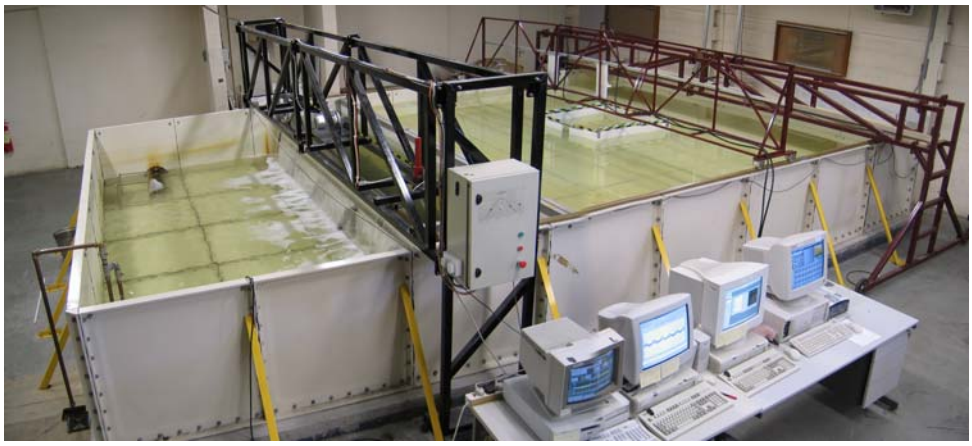

b)

Figure 5.52: Tidal Model set-up [Olbert (2006)]: a) schematic view; b) lab arrangement.

Water elevations are measured with an accuracy of 0.5% by a water level gauge which is best positioned along the wall in order to reduce the effect of the interaction between the device and the mean flow. The water level recorder measures the distance from the head of the displacement transducer to the magnetic field produced by a magnet mounted inside a float moving up and

down the transducer. A data logger takes signal from the gauge every second and transmits it to a computer which further transforms the voltage output into displacement units. At this stage, real time water elevation time series can be both visualized and stored on a computer.

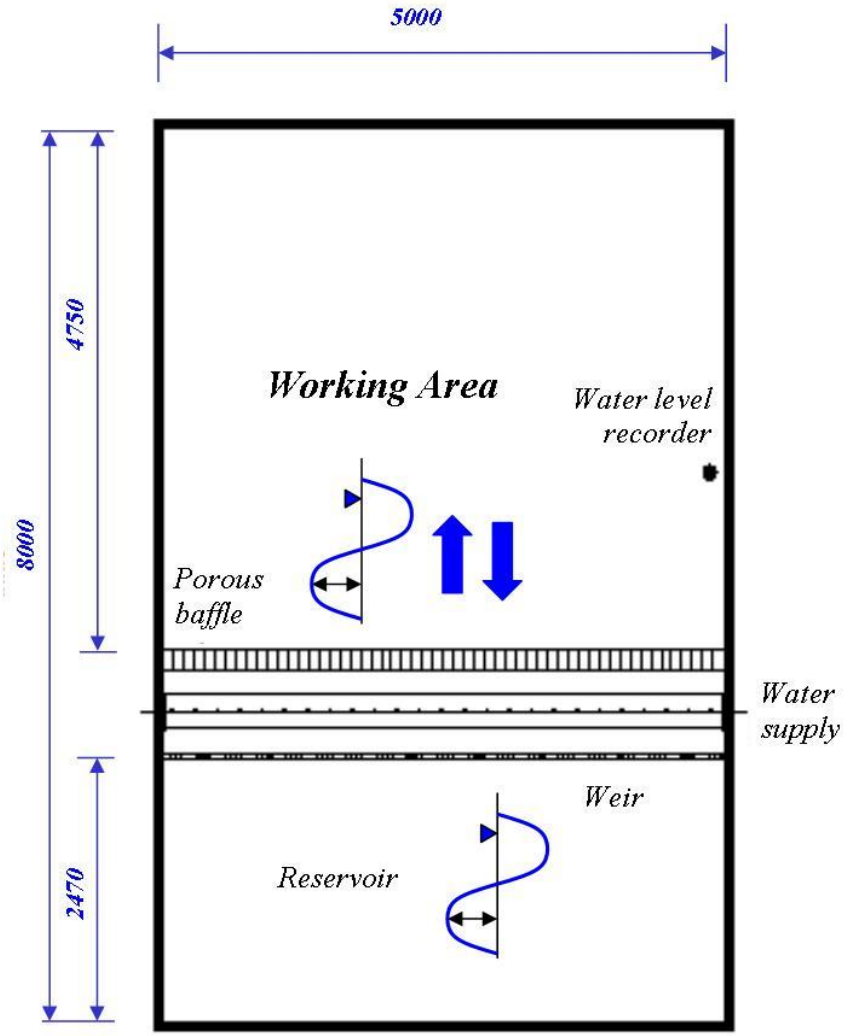

a)

Figure 5.53: Schematic layout of tidal basin [Olbert (2006)]: a) plan view; b) cross-section.

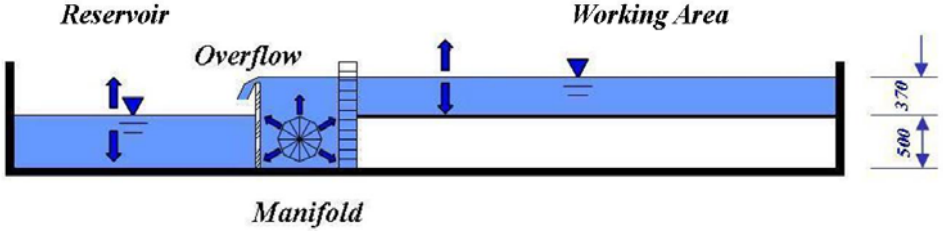

b)

Figure 5.53: Schematic layout of tidal basin [Olbert (2006)]: a) plan view; b) cross-section (*continued*).

Velocity in the working area is recorded by two Nortek Doppler Velocimeters, containing each a probe with a sensor (one transmit and three receive transducers). The velocimeter takes measurements in a small sampling volume (3-9 mm long and circa 6 mm in diameter) positioned 5 cm away from the sensor. A PC card connects the probe to a computer and the Collect V software ensures the online collection of the three components of the velocity vector which are stored on a computer. The noise in velocity measurements, due to the weak flow present in the tidal basin and consequently to low acoustic scattering, can be removed using post-processing techniques, such as the linear filter or a first-order recursive filter. Olbert [2006] observed that second approach produced better results.

5.4.3. Numerical Model Results versus Tidal Basin Measurements – Rectangular Domain from Cylindrical Co-ordinates

Physical model is composed of a rectangular harbour with dimensions: LxBxD=5.0mx4.75mx0.37m [Figures 5.53a) and 5.53b)]. Mean water depth inside the domain is 0.27m. A sinusoidal forcing is applied at the outer radius of domain with amplitude A_0=0.05m and tidal period 0.219 hours (789 seconds).

Characteristic Scale	**Theoretical Froude Scale**	**Computed Froude Scale**
Horizontal length	L_x	400
Vertical length	L_z	50
Time	$L_x/(L_z)^{1/2}$	57
Velocity	$(L_z)^{1/2}$	7.071
Acceleration	L_z/L_x	0.125
Area	L_x^2	160000
Volume	$L_x^2 L_z$	8000000

Table 5.22: Conditions of similitude from Froude ratio Olbert (2006).

For the distorted model presented herein, the Froude similitude was used and the corresponding values are shown in Table 5.22 for all characteristic scales involved.

Physical model corresponds to a prototype with dimensions: LxBxD=2000.0mx1900.0mx18.5m, and a mean water level inside domain of 13.5m. The amplitude of tidal forcing in the prototype is 2.5m and tidal period is 12.5 hours. The variables are summarized in Table 5.23. A distorted model with a horizontal scale L_x=400, a vertical scale L_z=50, and a time scale L_t=57 were used. A bottom roughness coefficient of 0.8 mm, as given by Olbert (2006) was used as input in the physical model. Time step was chosen 0.002 seconds. The simulation parameters used in the new numerical model are presented in Table 5.24 and they are common to all tidal basin test cases, unless otherwise specified.

Variable	**Physical model**	**Prototype**	**Scale**
L (m)	4.75	1900.0	400
B (m)	5.0	2000.0	400
D (m)	0.37	18.5	50
H (m)	0.27	13.5	50
A_0 (m)	0.05	2.5	50
T (hours)	0.219	12.5	57

Table 5.23: Variables used in the physical model and prototype.

Parameter	**NM**
Time step (s)	0.002
Space step (m)	1.000
Bed roughness (m)	0.100
Viscosity(mm)	0.800
Coefficient of eddy viscosity	1.500

Table 5.24: Parameters for tidal basin simulations in the new numerical model.

Tidal basin domain is recovered in a cylindrical co-ordinate system grid when the pole is positioned far enough from the considered domain, i.e. inner radius at

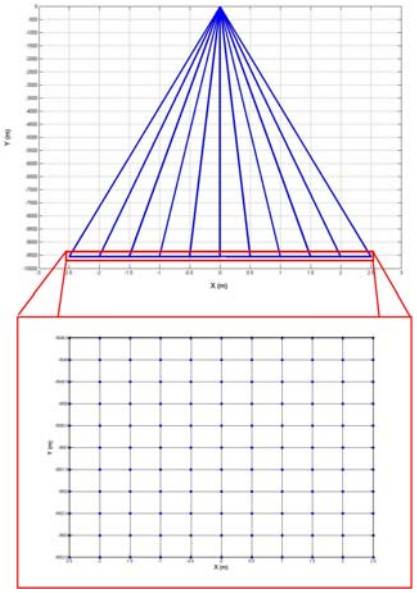

Figure 5.54: Rectangular geometry generation using cylindrical co-ordinates for the scale factors given in Table 5.25.

Point	**Geometric scale factors in the I – direction (m)**	**Geometric scale factors in the J – direction (m)**
J	0.5	0.499958
I	0.5	0.499984
H	0.5	0.500011
G	0.5	0.500037
F	0.5	0.500063
E	0.5	0.500089
D	0.5	0.500115
C	0.5	0.500142
B	0.5	0.500168
A	0.5	0.500194
Forcing	0.5	0.500220

Table 5.25: Scale factors for generation of tidal basin rectangular geometry grid using cylindrical co-ordinates ($\delta r = 0.5m$).

9548.5m and outer radius at 9553.5m, and a very shallow angle ($\theta_1 = 269.985°, \theta_2 = 270.0156°$, $\delta\theta = 0.0006°$) is considered [Figure 5.54].

Table 5.25 gives the values of the scale factors along the south-north direction for grid generation required by the cylindrical co-ordinates numerical model to simulate the conditions for tidal basin. The error in representation of the basin dimension in the $J-$ direction varies from -0.0084% at the closed boundary (point J in Figure 5.57) to 0.044% at the open boundary. Tidal forcing is represented at the outer radius of the domain [Figure 5.55].

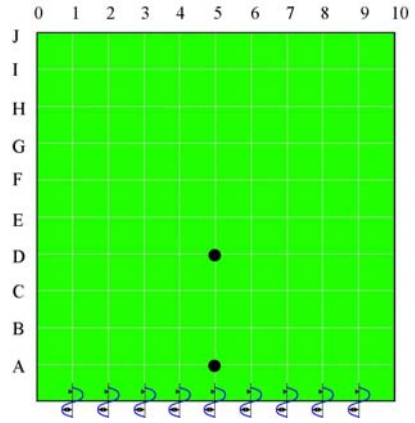

Figure 5.55: Grid representation (11x11 points) of the tidal basin for numerical model simulation ($\delta x = 0.5m$) [Olbert (2006)].

Results from calibration of the tidal basin could be subsequently used for validation of the cylindrical co-ordinates numerical model. However, the numerical model simulation using the coarse grid [Figure 5.55 and Table 5.25], with $\delta r = 0.5m$, did not predict values similar to the ones measured and the grid was successively refined to $\delta r = 0.25m$ and $\delta r = 0.1m$. With the finest grid ($\delta r = 0.1m$), the grid consists of 49x51 points [Figure 5.66] and the errors in representation of the dimension along the $J-$ direction are -0.008% at the closed boundary and 0.043% at the open boundary. Two points are equivalent to A5 and D5 in Olbert (2006): (46, 26) and (31, 26), respectively. The amplitude of radial direction velocity at point A5 is 0.595 cm, while the value predicted by the numerical model is 0.605 cm, resulting in an error of 1.68%. A comparison of

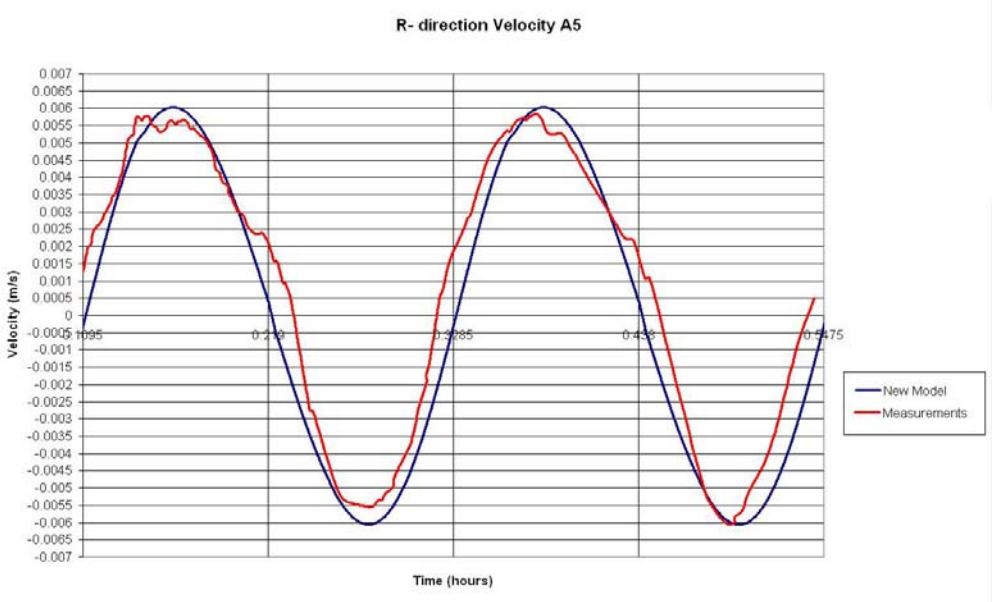

Figure 5.56: Comparison of the measurements and numerical model results for the r – direction velocity component at point A5.

the measurements with numerical model velocity results at point A5 is shown in Figure 5.56.

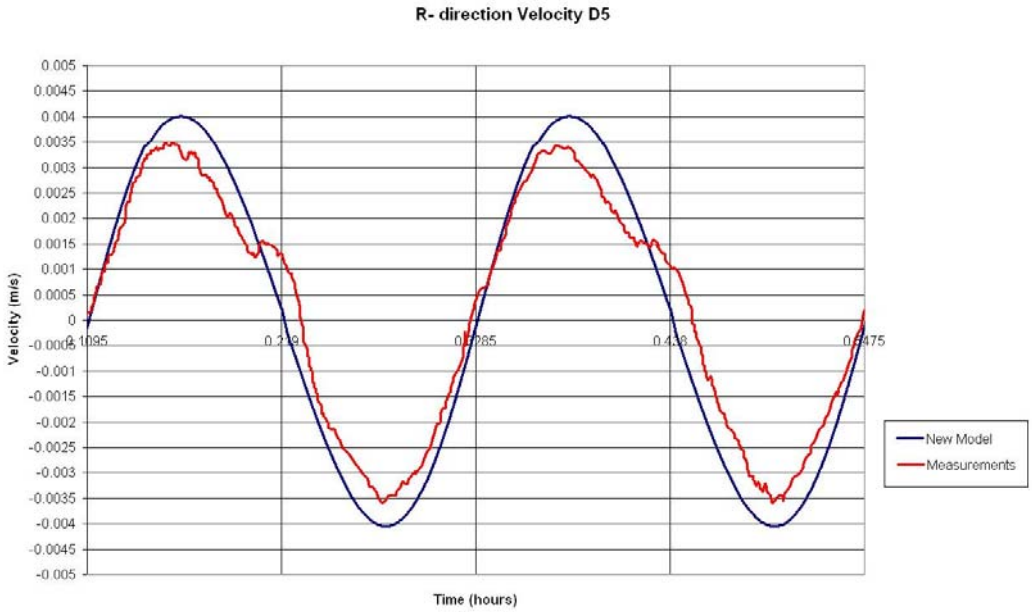

Figure 5.57: Comparison of the r – direction velocity results at point D5.

From Figure 5.57, the measured amplitude of velocity at point D5 is 0.352 cm, while the value predicted by the numerical model is 0.403 cm, resulting in an error of 14.49%.

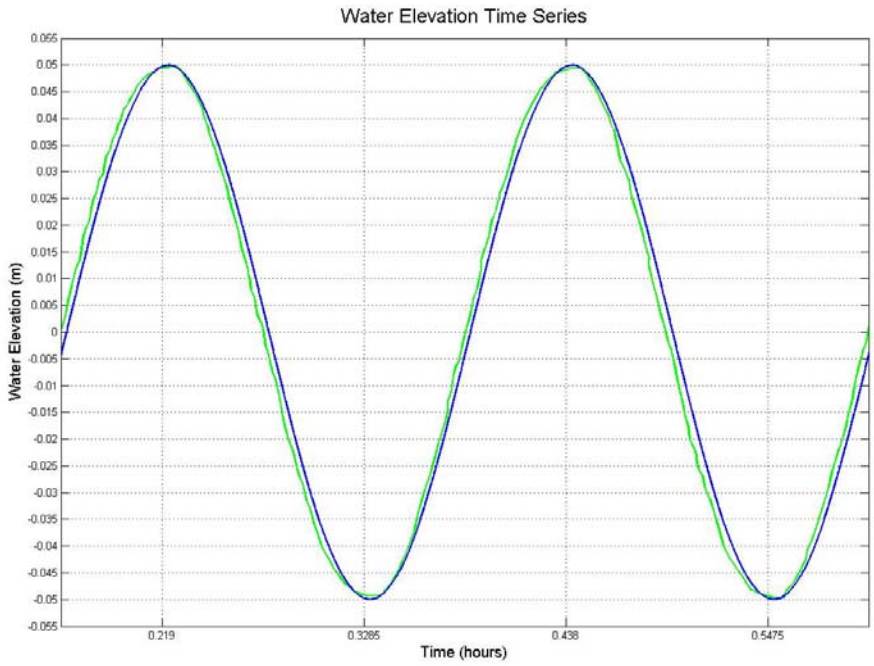

Figure 5.58: Comparison of the water elevation time series resulted from numerical model (blue line) and measurements (green line) at point A5 for two tidal cycles.

A comparison of the measurements with numerical model results for the $r-$ direction velocity component at point D5 is illustrated in Figure 5.57. Water elevation time series comparison between tidal basin measurements and cylindrical co-ordinates numerical model is presented in Figure 5.58. Velocity currents, simulated by the cylindrical co-ordinates numerical model inside tidal basin, present the pattern shown in Figure 5.59. For better visualisation, the magnitude of velocity vectors was magnified by a factor of 125 in Figures 5.59a) and 5.59b), whereas the magnification factor was 12 in Figures 5.59c) and 5.59d). The reference vector was shrunk 0.01 times.

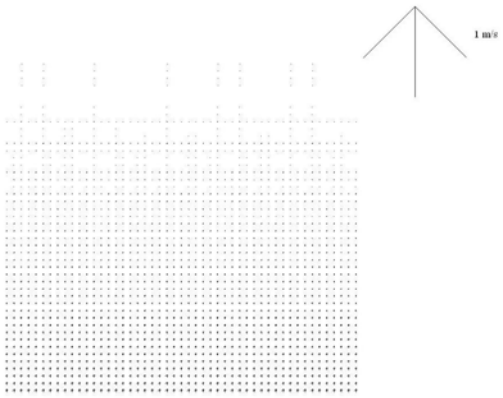

a) High water (HW) at time 0.44 hours

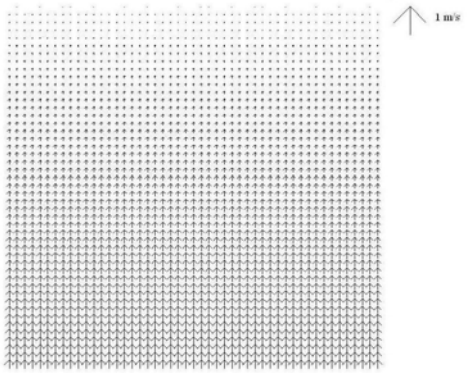

b) Low water (LW) at time 0.55 hours

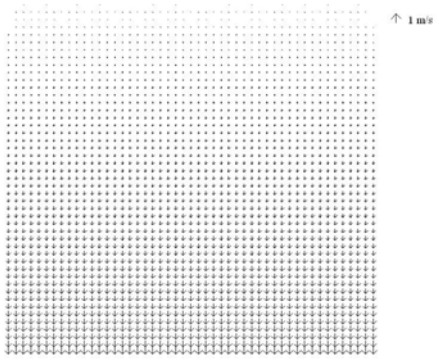

c) Mid-water during ebb tide (MW-ET) at time 0.5 hours

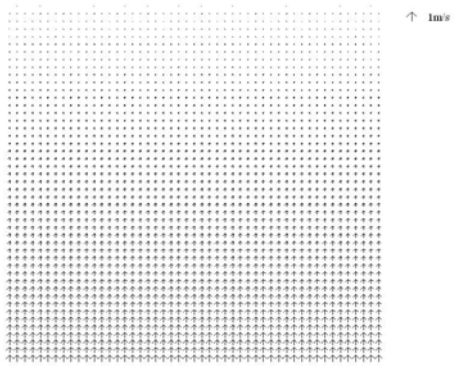

d) Mid-water during flood tide (MW-FT) at time 0.6 hours

Figure 5.59: Velocity currents at various water elevation stages: a) high water; b) low water; c) mid water during ebb tide; d) mid water during flood tide.

5.4.4. Numerical Model Results versus Tidal Basin Measurements – Cylindrical Co-ordinates Numerical Model Transformed into Uniform Cartesian Co-ordinates Numerical Model

The approach for generation of the rectangular geometry from cylindrical co-ordinates, presented in section 5.6.3., is novel in hydrodynamic modelling, at least from the knowledge of the Author. A classical approach for generation of the grid points inside a rectangular domain is to use Cartesian co-ordinates. The

cylindrical co-ordinates numerical model can be transformed into a Cartesian co-ordinates numerical model when the scale factors of the transformation are set equal to one, and the spatial step is specified. Also, closed boundary conditions have to be modified accordingly and the additional terms due to the curvature of the cylindrical grid must be set equal to zero. Moreover, the RAW filter can be turned off ($\alpha_1 = 0, \alpha_2 = 0$).

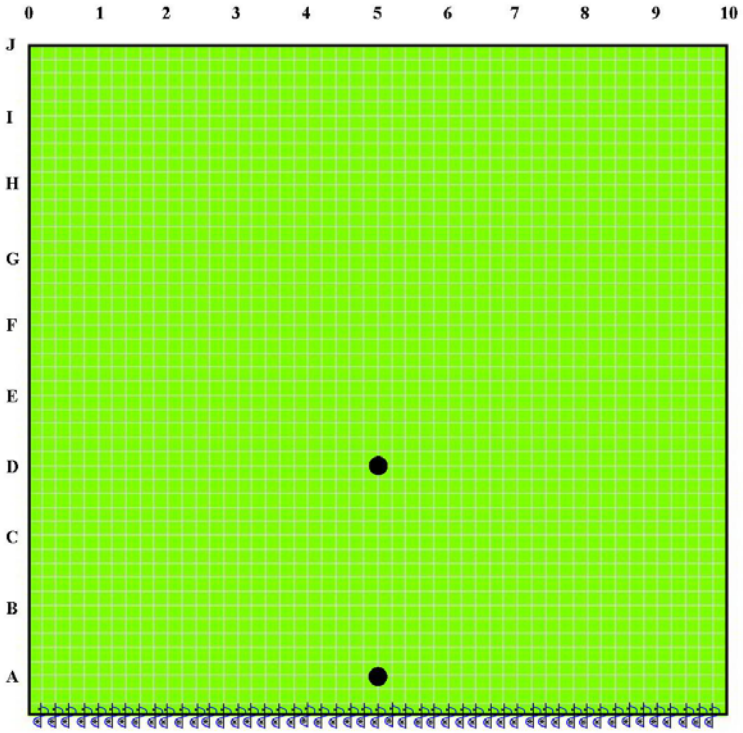

Figure 5.60: Cartesian co-ordinates mesh for representation of tidal basin in numerical model ($\delta x = 0.1m$).

For the numerical simulation in the tidal basin to be performed, a mesh consisting of 49x51 points [Figure 5.61], corresponding to a space step of 0.1m, is chosen, and comparison of both velocities and water elevations with measured data is shown herein. Grid configuration is the same as the one chosen for the rectangular geometry generated from cylindrical co-ordinates described in the previous section.

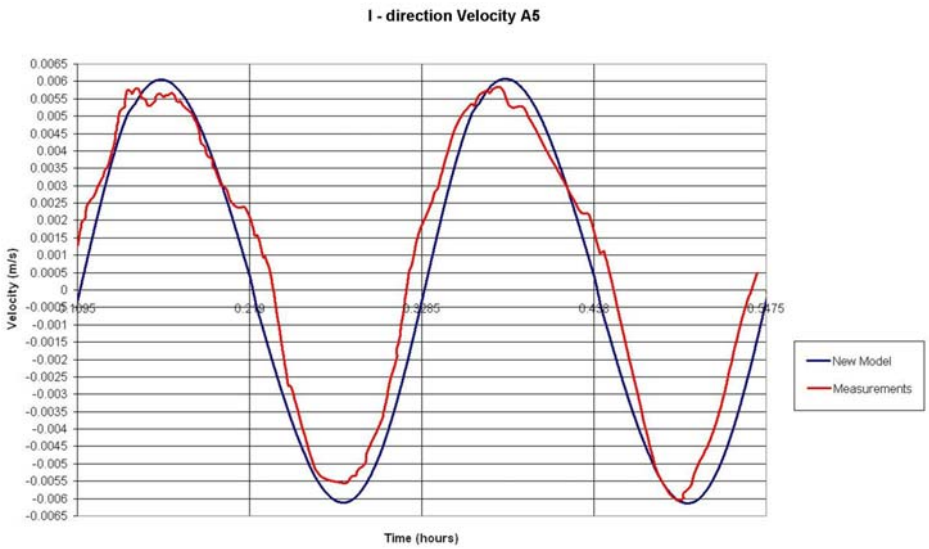

Figure 5.61: Measured data and numerical model predicted I – direction velocity component at point A5 for uniform Cartesian grid.

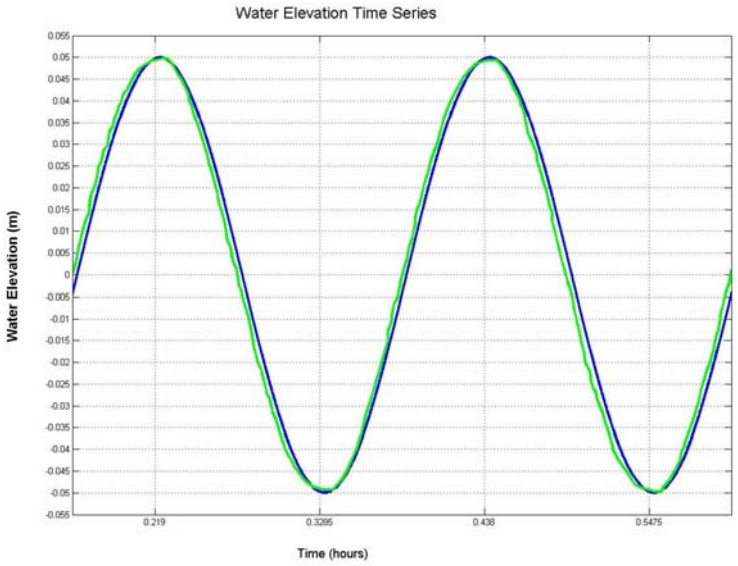

Figure 5.62: Measured data (green line) and numerical model predicted water elevation (blue line) at point A5 for uniform Cartesian grid.

The comparison between measured data and numerical model results at point A5 for the $I-$ direction velocity component is illustrated in Figure 5.61. The velocity error at point A5 is 2.520%, with calculated amplitude of velocity in the $I-$ direction of 0.610 cm. Figure 5.62 presents comparison between measured and numerical model predicted water elevation at point A5.

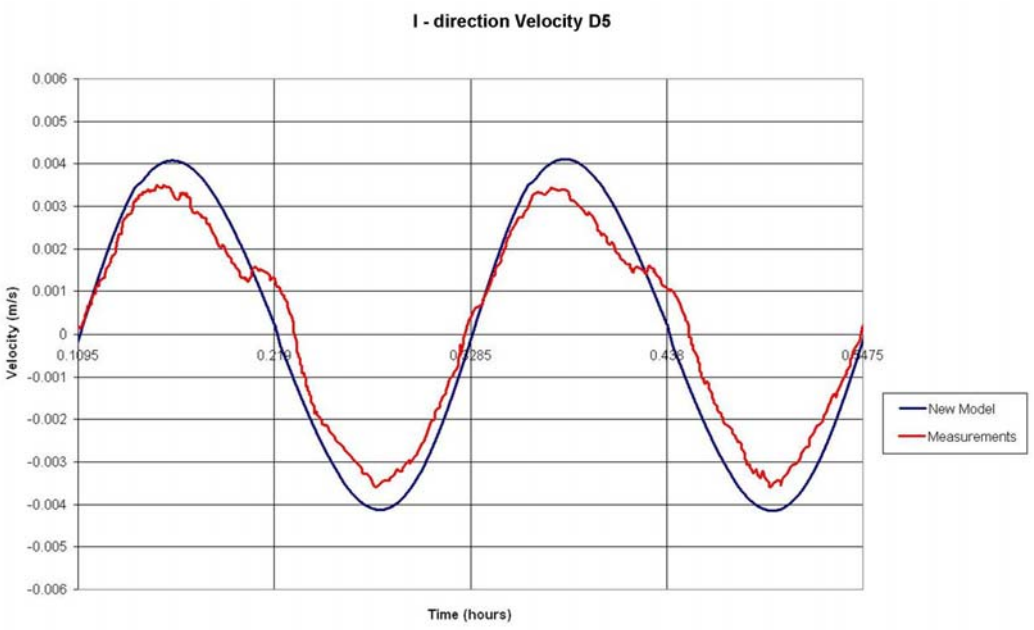

Figure 5.63: Measured data and numerical model predicted I – direction velocity component at point D5 for uniform Cartesian grid.

The $I-$ direction velocity component at point D5 resulted from numerical model is compared against measured data at the same point in Figure 5.63. The $I-$ direction velocity amplitude calculated by the numerical model at point D5 is 0.413 and an error of 17.30% is obtained.

Velocity currents, simulated by the cylindrical co-ordinates numerical model with a uniform Cartesian grid representing tidal basin, present the pattern shown in Figure 5.64. The same magnification factors were used for better visualisation of the velocity currents as in Section 5.4.3. It can be observed that the pattern is similar to the one showed in previous section, though velocities nearest the closed boundaries are not as well represented as in Section 5.4.3.

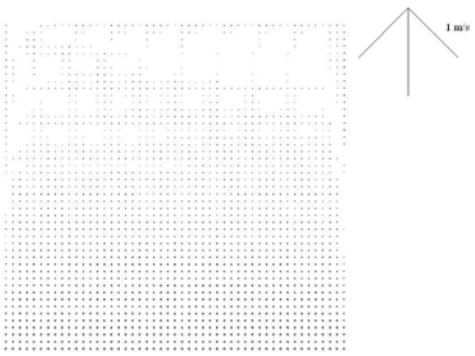

a) High water (HW) at time 0.44 hours

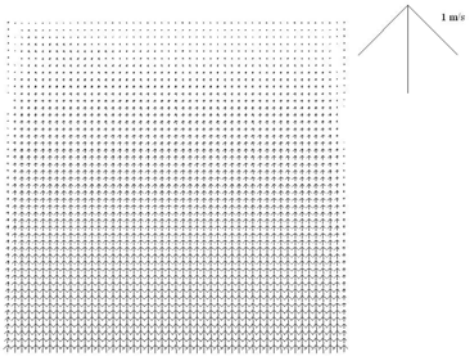

b) Low water (LW) at time 0.55 hours

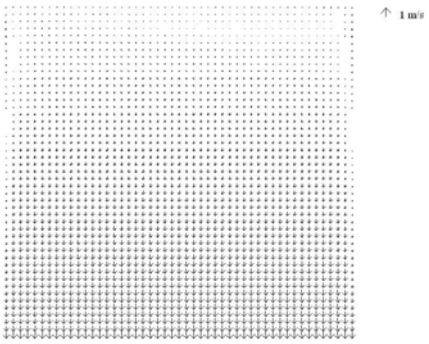

c) Mid-water during ebb tide (MW-ET) at time 0.5 hours

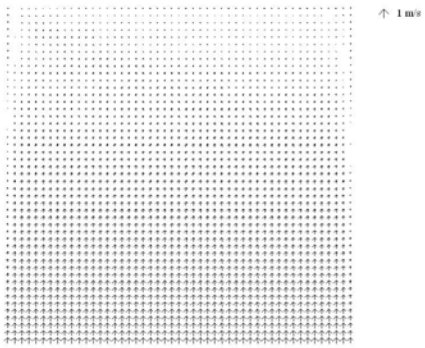

d) Mid-water during flood tide (MW-FT) at time 0.6 hours

Table 5.64: Velocity currents at various water elevation stages: a) high water; b) low water; c) mid water during ebb tide; d) mid water during flood tide.

5.4.5. Numerical Model Results versus Tidal Basin Measurements – Cylindrical Co-ordinates Numerical Model Transformed into Non-Uniform Cartesian Co-ordinates Numerical Model

Tidal basin geometry can be represented using a non-uniform mesh in Cartesian co-ordinates. An example is shown herein. Variation of the space step is assumed in the $I-$ direction, while the space step in the $J-$ direction is kept constant according to the values presented in Table 5.26. For numerical simulation, the parameters used in Section 5.4.4 were used and the results are presented below.

I-direction Point (m)	Space step in the I direction (m)	Space step in the J-direction (m)	Point
100.000	0.062	0.100	
100.061	0.062	0.100	J
100.123	0.063	0.100	
100.186	0.064	0.100	
100.251	0.066	0.100	
100.316	0.067	0.100	
100.383	0.068	0.100	
100.451	0.069	0.100	
100.521	0.071	0.100	I
100.591	0.072	0.100	
100.663	0.073	0.100	
100.736	0.075	0.100	
100.811	0.076	0.100	
100.887	0.077	0.100	
100.964	0.079	0.100	
101.043	0.080	0.100	H
101.123	0.082	0.100	
101.205	0.083	0.100	
101.289	0.085	0.100	
101.373	0.086	0.100	
101.460	0.088	0.100	
101.548	0.090	0.100	G
101.638	0.091	0.100	
101.729	0.093	0.100	
101.822	0.095	0.100	
101.917	0.096	0.100	
102.013	0.098	0.100	F
102.111	0.100	0.100	
102.211	0.102	0.100	
102.313	0.104	0.100	
102.417	0.106	0.100	
102.523	0.108	0.100	E
102.631	0.110	0.100	
102.740	0.112	0.100	
102.852	0.114	0.100	
102.966	0.116	0.100	
103.082	0.118	0.100	D
103.200	0.120	0.100	
103.320	0.123	0.100	
103.443	0.125	0.100	
103.568	0.127	0.100	C
103.695	0.130	0.100	
103.824	0.132	0.100	
103.956	0.134	0.100	
104.090	0.137	0.100	B
104.227	0.139	0.100	
104.366	0.142	0.100	
104.508	0.145	0.100	A
104.653	0.146	0.100	
104.800	0.147	0.100	

Table 5.26: Variation of space step in the I – direction for simulation in the tidal basin.

Comparisons of the I – direction velocity at points (47,26) and (36,26) inside domain, corresponding to A5 and D5 in Olbert (2006), respectively, are illustrated in Figures 5.65 and 5.66, whereas water elevation time series at point A5 are shown in Figure 5.67 for both measured data and numerical model results.

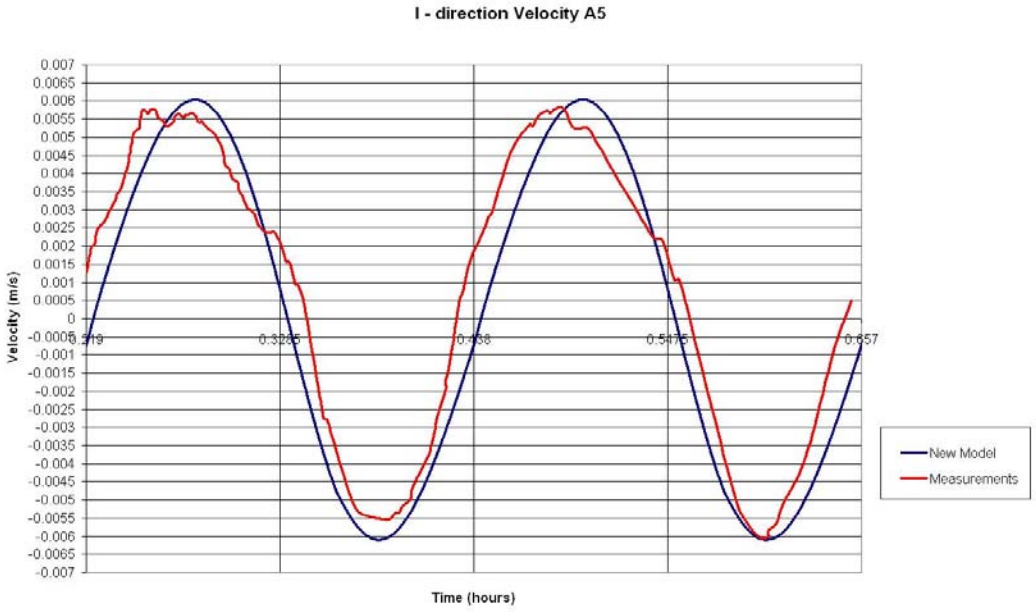

Figure 5.65: Measured data and numerical model predicted I – direction velocity component at point A5 for irregular Cartesian mesh.

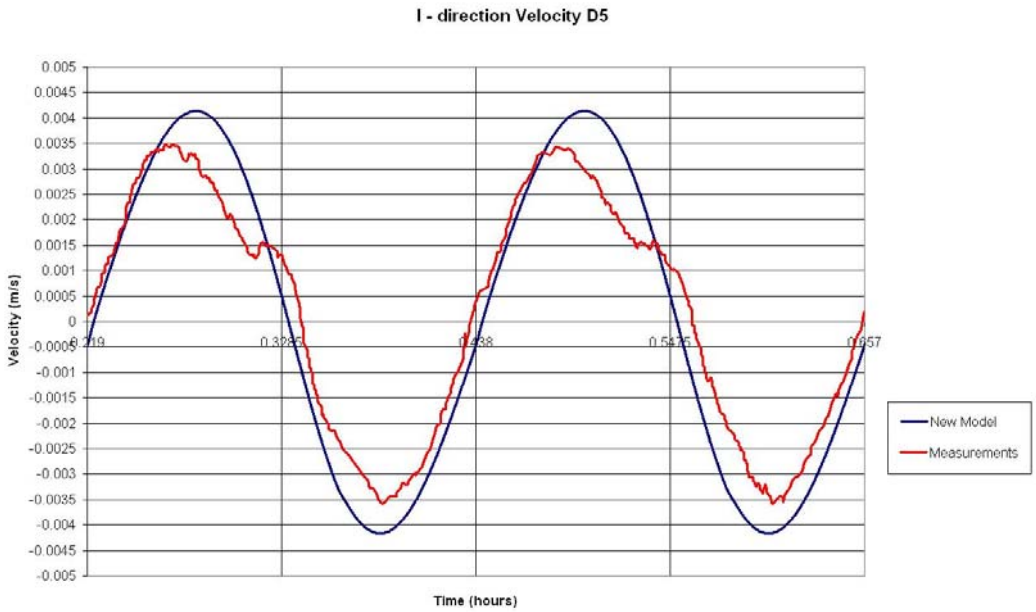

Figure 5.66: Measured data and numerical model predicted I – direction velocity component at point D5 for irregular Cartesian mesh.

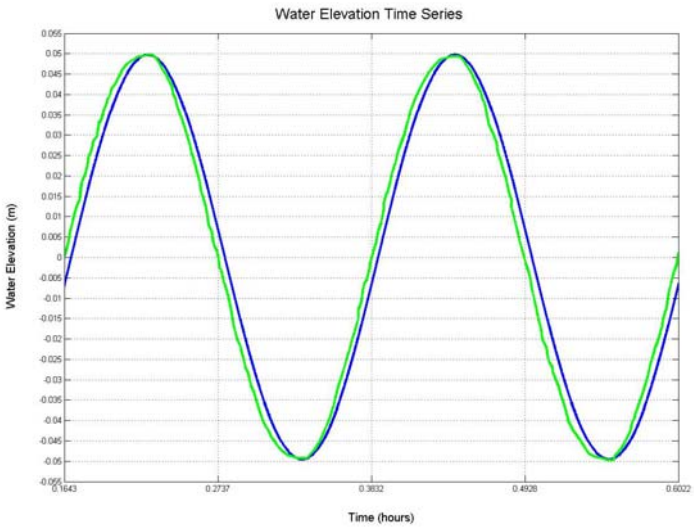

Figure 5.67: Measured data (green line) and numerical model predicted water elevation (blue line) at point A5 for irregular Cartesian mesh.

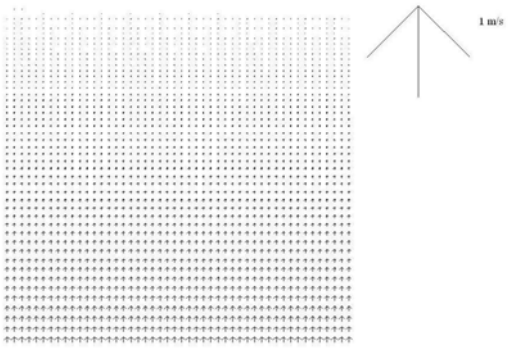

a) High water (HW) at time 0.44 hours

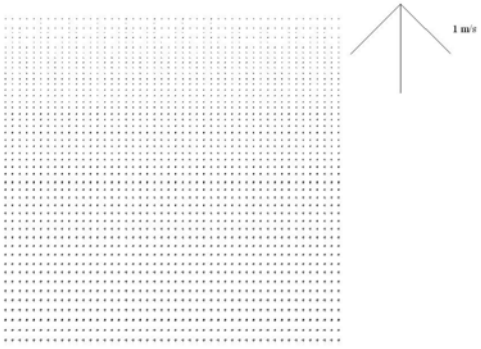

b) Low water (LW) at time 0.55 hours

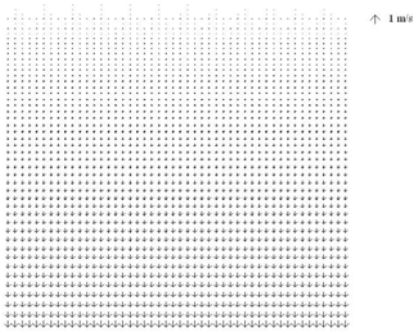

c) Mid-water during ebb tide (MW-ET) at time 0.5 hours

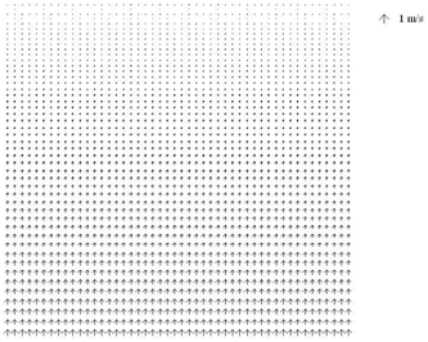

d) Mid-water during flood tide (MW-FT) at time 0.6 hours

Figure 5.68: Velocity currents at various water elevation stages: a) high water; b) low water; c) mid water during ebb tide; d) mid water during flood tide.

Velocity error at point A5 is 0.840%, with calculated amplitude of velocity in the $I-$ direction of 0.600 cm, whereas at point D5 the error is 16.761% and the velocity amplitude has a value of 0.411 cm. Agreement in terms of water elevation amplitude predicted by the numerical model with measured data for two tidal cycles was obtained [Figure 5.67].

Velocity currents, simulated by the cylindrical co-ordinates numerical model with a non-uniform Cartesian grid in the $I-$ direction representing tidal basin, present the pattern shown in Figure 5.68. The same magnification factors were used for better visualisation of the velocity currents as in Section 5.4.3. It can be observed that the pattern is similar to the one showed in Section 5.4.3.

5.5. Application of the Analytical Solution of the Shallow Water Equations in Cylindrical Co-ordinates

5.5.1. General Considerations

Analytical solutions of the simplified shallow water equations in cylindrical co-ordinates [equations (5.17) and (5.18)] for estuarine simulations in terms of Bessel functions were obtained by Lynch and Gray (1978) for four geometries of the bed shape and they are given in Table 5.27. The simplified equations did not include advection, Coriolis and turbulence terms, incorporating a linearized representation of the bed friction term.

$$\frac{\partial \zeta}{\partial t} + \nabla \cdot (HV) = 0 \tag{5.17}$$

$$\frac{\partial v}{\partial t} + g\nabla\zeta + \tau v - \frac{W}{H} = 0 \tag{5.18}$$

where:

ζ is water elevation;

τ is the linearized bottom friction coefficient;

$H = H_0 r^n$ is water depth as function of the constant water depth H_0 and radius r;

n can assume any real value;

$V = (v_r, v_\theta)$ is the depth integrated velocity;

$W = (W_r, W_\theta)$ is the wind stress, assumed to be spatially invariant.

For the considered geometry, boundary conditions were expressed as:

$\frac{\partial \zeta}{\partial r} = 0$ at $r = r_1$ (CB3 in Figure 2.11);

$\zeta = \zeta_0 \cos(\omega t)$ at $r = r_2$ (OB in Figure 2.11), where ω is the frequency of harmonic motion;

$\frac{\partial \zeta}{\partial \theta} = 0$ at $\theta = 0$ (CB1 in Figure 2.11) and $\theta = \varphi$ (CB2 in Figure 2.11).

n	Bathymetry	Solution	Constants
0	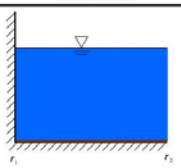	$\zeta(r,t) = \mathrm{Re}\left\{\left[AJ_0(\beta r) + BY_0(\beta r)\right]e^{i\omega t}\right\}$ $V_r(r,t) = \mathrm{Re}\left\{\left[-AJ_1(\beta r) - BY_1(\beta r)\right]\frac{i\omega}{\beta H_0}e^{i\omega t}\right\}$	$A = \frac{\zeta_0 Y_1(\beta r_1)}{J_0(\beta r_2)Y_1(\beta r_1) - J_1(\beta r_1)Y_0(\beta r_2)}$ $B = \frac{-\zeta_0 J_1(\beta r_1)}{J_0(\beta r_2)Y_1(\beta r_1) - J_1(\beta r_1)Y_0(\beta r_2)}$
1	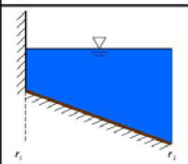	$\zeta(r,t) = \mathrm{Re}\left\{\frac{1}{\sqrt{r}}\left[AJ_1(2\beta\sqrt{r}) + BY_1(2\beta\sqrt{r})\right]e^{i\omega t}\right\}$ $V_r(r,t) = \mathrm{Re}\left\{\frac{1}{\sqrt{r}}\left[-AJ_2(2\beta\sqrt{r}) - BY_2(2\beta\sqrt{r})\right]\frac{i\omega}{\beta H_0}e^{i\omega t}\right\}$	$A = \frac{\zeta_0\sqrt{r_2}Y_2(2\beta\sqrt{r_1})}{J_1(2\beta\sqrt{r_2})Y_2(2\beta\sqrt{r_1}) - J_2(2\beta\sqrt{r_1})Y_1(2\beta\sqrt{r_2})}$ $B = \frac{-\zeta_0\sqrt{r_2}J_2(2\beta\sqrt{r_1})}{J_1(2\beta\sqrt{r_2})Y_2(2\beta\sqrt{r_1}) - J_2(2\beta\sqrt{r_1})Y_1(2\beta\sqrt{r_2})}$
2	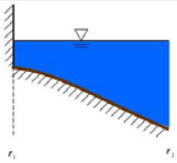	$\zeta(r,t) = \mathrm{Re}\left\{Ar^{s_1} + Br^{s_2}\right\}e^{i\omega t}$ $V_r(r,t) = \mathrm{Re}\left\{\left[s_1 Ar^{s_1-1} - s_2 Br^{s_2-1}\right]\frac{i\omega}{\beta^2 H_0}e^{i\omega t}\right\}$	$A = \frac{\zeta_0 s_2 r_1^{s_2}}{\left(s_2 r_2^{s_1} r_1^{s_2} - s_1 r_1^{s_1} r_2^{s_2}\right)}$ $B = \frac{\zeta_0 s_1 r_1^{s_1}}{\left(s_2 r_2^{s_1} r_1^{s_2} - s_1 r_1^{s_1} r_2^{s_2}\right)}$ $s_1, s_2 = -1 \pm \sqrt{1-\beta^2}$
-2	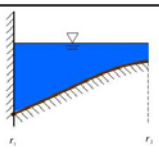	$\zeta = \mathrm{Re}\left\{\zeta_0 \frac{\cosh\left[\frac{\beta}{2}\left(r^2 - r_1^2\right)\right]}{\cosh\left[\frac{\beta}{2}\left(r_2^2 - r_1^2\right)\right]}e^{i\omega t}\right\}$ $\zeta = \mathrm{Re}\left\{\zeta_0 r \frac{\sinh\left[\frac{\beta}{2}\left(r^2 - r_1^2\right)\right]}{\cosh\left[\frac{\beta}{2}\left(r_2^2 - r_1^2\right)\right]}\frac{i\omega}{\beta H_0}e^{i\omega t}\right\}$	
$h(r) = H_0 r^n$; $\beta^2 = (\omega^2 - i\omega\tau)/gH_0$			

Table 5.27: Analytical solutions of the shallow water equations written in cylindrical co-ordinates [Lynch and Gray (1978)].

The equation solved in the absence of wind stress was represented as:

$$\frac{\partial^2 \zeta}{\partial t^2} + \tau \frac{\partial \zeta}{\partial t} - gH_0 r^{n-2}\left[r^2 \frac{\partial^2 \zeta}{\partial r^2} + r(n+1)\frac{\partial \zeta}{\partial r} + \frac{\partial^2 \zeta}{\partial \theta^2} \right] = 0 \qquad (5.19)$$

5.5.2. Numerical Model Results versus Analytical Solution

The numerical model was run with the same simplified form of the governing equations as in the previous section. Model domain and parameters inside domain correspond to the first test case in section 5.5.1.

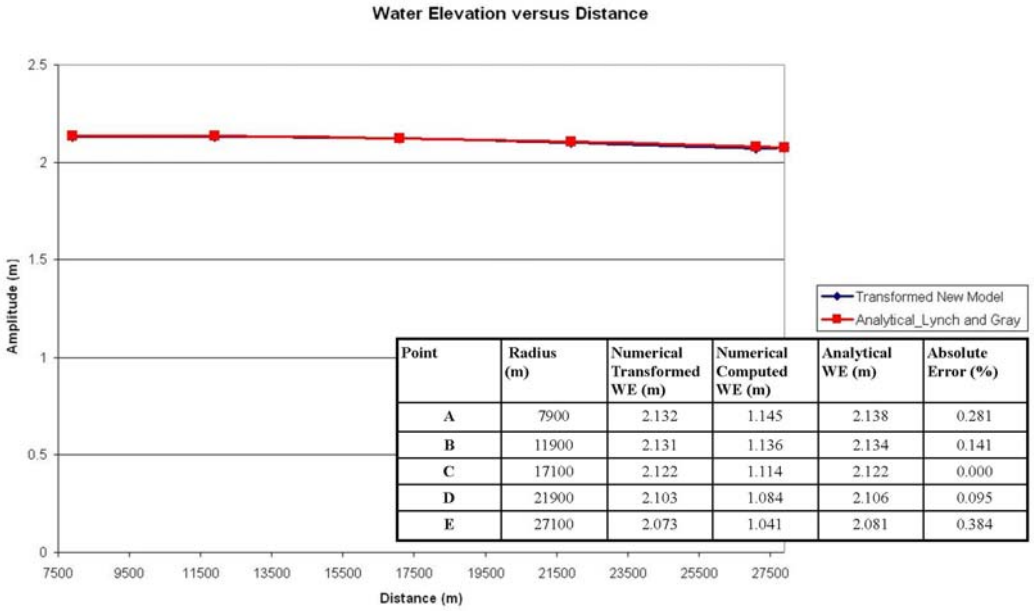

Point	Radius (m)	Numerical Transformed WE (m)	Numerical Computed WE (m)	Analytical WE (m)	Absolute Error (%)
A	7900	2.132	1.145	2.138	0.281
B	11900	2.131	1.136	2.134	0.141
C	17100	2.122	1.114	2.122	0.000
D	21900	2.103	1.084	2.106	0.095
E	27100	2.073	1.041	2.081	0.384

Figure 5.69: Water elevation amplitude at points A-E from cylindrical co-ordinates model and analytical solution of Lynch and Gray (1978) for horizontal bed with constant step in the radial direction.

The parameters used in the RAW filter are: $\alpha_1 = 0.05$; $\alpha_2 = 0.98$; time step is chosen $\delta t = 10$ seconds based on the Courant criterion and the linearized bed friction coefficient is τ=0.0025. A Matlab code was written to generate the analytical solution of Lynch and Gray (1978), corresponding to $n = 0$ in Table

5.25. From Figure 5.69 it is observed that agreement is obtained in terms of water elevation amplitudes at the considered points inside domain, with maximum error approximately 0.384% at point E.

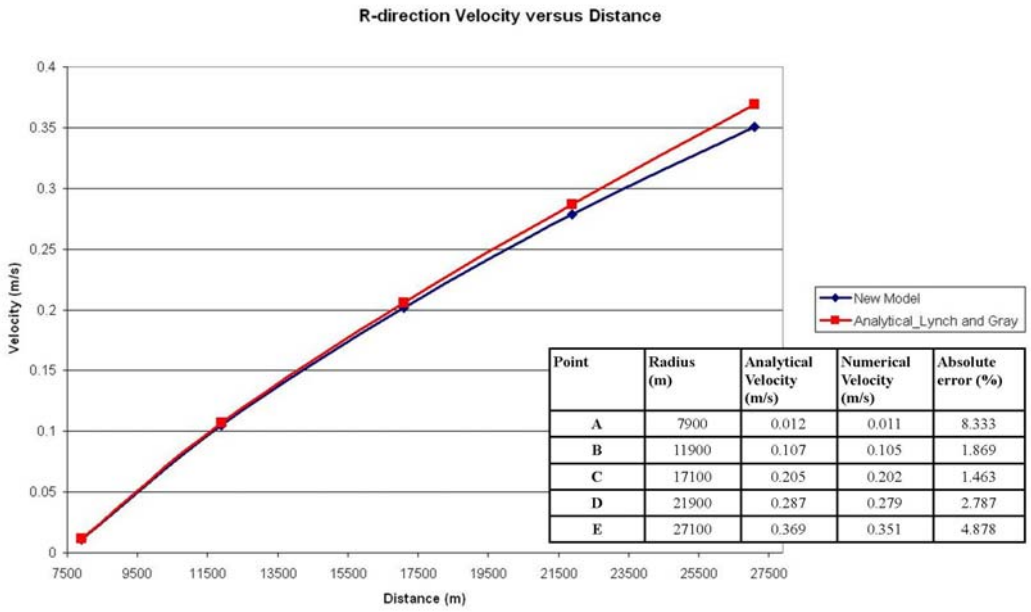

Point	Radius (m)	Analytical Velocity (m/s)	Numerical Velocity (m/s)	Absolute error (%)
A	7900	0.012	0.011	8.333
B	11900	0.107	0.105	1.869
C	17100	0.205	0.202	1.463
D	21900	0.287	0.279	2.787
E	27100	0.369	0.351	4.878

Figure 5.70: $r-$ direction velocity at points A-E from cylindrical co-ordinates model and analytical solution of Lynch and Gray (1978) for horizontal bed with constant step in the radial direction.

Figure 5.70 presents variation of velocities along the centreline and it can be seen that numerical model under predicts the $r-$ direction velocity compared to the values obtained from analytical solution, with a maximum error of 8.333% at point A, where velocities are very small.

5.6. Summary and Conclusions

The present chapter shows the manner in which validation of numerical model results is performed. Firstly, results of two robust numerical models, DIVAST and EFDC, are used to validate results of the numerical model described herein. For simulations, a wedge shaped domain was chosen, defined between $r_1 = 7500m$, $r_2 = 27900m$, $\theta_1 = 252°$, $\theta_2 = 288°$ and a horizontal bed was

considered. Preliminary results indicated the presence of the computational mode in the numerical solution. Therefore, a modified weak filter, namely the Robert – Asselin – Williams filter, was implemented. The values of the RAW filter parameters could be chosen as: $\alpha_1 = 0.05$ or $\alpha_1 = 0.08$, and $\alpha_2 = 0.98$, $\alpha_2 = 0.99$ or $\alpha_2 = 1.00$ and they were established empirically.

Three test cases were considered for research: horizontal bed with constant step in the radial direction, horizontal bed with one variation of the step in the radial direction, and horizontal bed with two variations of the step in the radial direction. For the three test cases presented, cylindrical co-ordinates model showed agreement with results of both DIVAST and EFDC for the first test case, or EFDC for the remaining two test cases. Based on the convergent geometry chosen an increase of water elevation amplitude from open boundary (OB1) towards closed boundary (CB1) was expected from Green's law. Computed water elevations obtained from the cylindrical co-ordinates numerical model required transformation from the computational onto physical plane based on the wave energy conservation law. The transformation relationships were developed by the Author and they were shown in Appendix 11 of the thesis. The water elevations could be transformed based on the theoretical exponent term $n = 1.0$ or a computed exponent term. The computed exponent term generated water elevation amplitudes along the centreline that better approximated the EFDC and DIVAST predictions. In general, from comparison with EFDC and DIVAST it was observed that the cylindrical co-ordinates numerical model with $n = 1.0$ over estimates water elevations at high water, gave a good approximation of water elevations at points in the middle of domain and under predicted them at points near the open boundary (OB1) at low water. For total velocities, it was observed that DIVAST values over estimated EFDC values for total velocities at all points, while numerical model values fell between DIVAST and EFDC values at points B and D. Also, it was observed from the first test case that total velocities predicted by the numerical model were closer in value to DIVAST values at points A and C, whereas better agreement with EFDC values was obtained at point E. The computed tidal period of the cylindrical co-ordinates numerical model was 12.497 hours, the same value was obtained for DIVAST, whereas

EFDC presented a value of 12.500 hours. The remaining two test cases showed good agreement in terms of water elevations and total velocities between the cylindrical co-ordinates numerical model and EFDC values. The general tendency for the cylindrical co-ordinates numerical model was to over estimate the total velocity values obtained from EFDC, but it was shown that this feature was present in DIVAST model, as well. This behaviour can be explained by the errors introduced by the grid refinement technique used in the new cylindrical co-ordinates numerical model.

Secondly, tidal basin measurements were used in three test cases: first one, with the rectangular mesh generated from cylindrical co-ordinates, second one with rectangular grid obtained setting up the scale factors equal to one in both directions, and specifying the cell size (uniform Cartesian co-ordinates), and third one with a non-uniform Cartesian grid in the direction of the flow. Tidal basin dimension were: LxBxD=5.0mx4.75mx0.37m, with a water depth of 0.27m. The applied sinusoidal tidal forcing had amplitude of 0.05cm and period of 789 seconds. Best comparison with measurements was obtained for the mesh containing 49x51 grid points and time step 0.002 seconds. The numerical model was run for four tidal cycles. For validation of the cylindrical co-ordinates numerical model results, the tidal basin measurements of Olbert (2006) were used. For the transformation of the numerical model results an empirical transformation coefficient was used with value equal to two. The error between simulated and measured values of velocity in the direction of flow at the point nearest to the open boundary (A5) was less than 1.700% in the first test case, 2.600% in the second test case and 2.020% in the third test case. For research purposes the results are good, but from the point of view of computational time the approach is far from being advantageous. Furthermore, from the analysis of the results, it was observed that the present numerical model is well suited for cylindrical co-ordinates numerical modelling, but also for modelling on irregular Cartesian meshes.

Finally, comparison with the analytical solution of the shallow water equations in cylindrical co-ordinates showed that the cylindrical co-ordinates numerical model approximates well the analytical solution of Lynch ad Gray (1978). The

same domain as the one employed for validation of the cylindrical co-ordinates numerical model results versus industry standard models was defined, and same parameters, except for the RAW filter, where the values used were: $\alpha_1 = 0.05$ and $\alpha_2 = 0.98$. The numerical model was modified to exclude the Coriolis, advection, and turbulence term, and incorporated a linearized bed friction term with value $\tau = 0.0025$. The maximum error obtained for water elevation amplitudes was 0.384%, and for the $r-$ direction velocity component maximum error was 8.333% at the point nearest to the closed boundary CB1 (point A), where velocity is of the order of centimetres.

From the test cases presented in this Chapter, it can be concluded that the cylindrical co-ordinates numerical model has good potential for estuarine hydrodynamic modelling provided that the model is further enhanced.

Chapter 6

Summary and Final Conclusions

6.1. Summary

The purpose of the present thesis was to develop and test a new two-dimensional estuarine hydrodynamic numerical model written in cylindrical co-ordinates which improves resolution in certain areas without increasing computational costs. The reasons for using the cylindrical co-ordinate system in the research are presented next. Estuarine and coastal zones are very important regions for humanity, since they host over 50% of the world population and offer invaluable resources for life sustainment. A rational usage of these regions is desired, and yet, they are affected by both anthropogenic and natural hazards. In order to elaborate efficient plans for sustainable development of the coastal and estuarine regions, and to better understand the complex mechanisms at the basis of coastal processes, tools for monitoring these areas were developed. Among these, numerical models have an important role in forecasting and simulation and are cost effective. At the moment, structured grid models represent the best alternative in terms of computational costs compared to both unstructured grid and mesh free models. For development of a coastal numerical model the following elements should be specified: mathematical equations, space and time discretization method and solution technique. The choice of the co-ordinate system to represent the grid of points on which spatial discretization can be performed is influenced firstly by the geometry of the domain and secondly by the resolution inside the domain, since computational costs increase with grid refinement and smaller time steps. The literature review presented in Chapter 2 of the thesis revealed that estuarine and coastal zone hydrodynamics could be modelled on structured grids using the cylindrical co-ordinate system based on the following reasons: orthogonality of the grid, built in variable resolution, the smallest number of additional terms added to the mathematical formulation of

the numerical model, compared to spherical, orthogonal and non-orthogonal curvilinear co-ordinate systems, and better representation of the curvature of land boundaries in the angular direction. Furthermore, it was shown that analytical solutions were found only for linearized forms of the Navier-Stokes equations written in cylindrical co-ordinates for estuarine hydrodynamics, or for analyzing scattering of tidal waves around cylindrical islands. Numerical models in cylindrical co-ordinates were traditionally used for three-dimensional pipe flow simulations, and two-dimensional storm surge models were developed as well, the latter approach using simplified formulations of the hydrodynamic equations.

Coastal hydrodynamics numerical models can be developed in either two- or three-dimensions, with two-dimensional models mainly used for well-mixed regions. The cylindrical co-ordinates numerical model presented herein is depth-averaged, and the corresponding assumption that velocities vary after a parabolic law on the vertical, was made. The theoretical considerations involved in development of the equations governing water flow, the continuity and Navier-Stokes equations, which conserve properties such as mass and momentum, were shown in Chapter 3. A time dependent mixing length turbulence model was chosen for the closure of the hydrodynamic equations. Afterwards, the Author's own development of the depth-integrated equations written in cylindrical co-ordinates was presented, followed by the algebraic mapping transformation relationships from the physical onto computational plane. Mapping transformations, as powerful tools in solving the hydrodynamic equations, were chosen because the methods already developed for Cartesian co-ordinates could be extended to other co-ordinate systems. The resulting equations were at the basis of the cylindrical co-ordinates numerical model development.

The solution technique was based on the finite discretization method as shown in Chapter 4. A short review of the finite discretization methods used for discretization of the first and second derivative terms in the governing equations written in both Cartesian co-ordinates and on mapped domains was presented, followed by the discretization scheme used in present research. Spatial discretization was performed on an Arakawa C grid, whereas time discretization scheme was a two-step finite difference Alternating Directions Implicit method.

A general presentation of ADI was also included in Chapter 4. For the proposed discretization technique, the solution was obtained by means of Thomas algorithm. Details regarding implementation of the Thomas algorithm in general and the numerical model were given, as well.

Boundary conditions, both closed and open, played a significant role in improving the quality of the results. The numerical model developed herein specified closed boundary conditions using the no-slip assumption for curved boundaries in the angular direction and the control volume approach in the radial direction. Open boundary conditions were specified as clamped water elevations. A quasi-geostrophic relationship was used to propagate tidal forcing along the angular direction.

For simulations, a wedge shaped domain was chosen, defined between $r_1 = 7500m$, $r_2 = 27900m$, $\theta_1 = 252°$, $\theta_2 = 288°$ and a horizontal bed was considered. A sinusoidal tidal forcing was represented at the outer radius of the domain (OB1) with amplitude A_0=2.077m and tidal period T=12.5 hours. Preliminary results of the cylindrical co-ordinates numerical model presented an odd-even decoupling of the solution, also known as computational mode. The traditional solution for this problem is inclusion of a weak filter, namely the Asselin filter, in the numerical model. An improvement of the Asselin filter is the RAW filter, which not only smoothes the solution but also controls the amplitude height. The latter filter was incorporated in the cylindrical co-ordinates numerical model.

In order to validate the cylindrical co-ordinates numerical model results against industry standard models, three test cases were used: a uniform horizontal bed with constant step in the radial direction; a uniform horizontal bed with one variation of the step in the radial direction, and a uniform horizontal bed with two variations of the step in the radial direction. Variation of the step in the radial direction was obtained with a “stretching” function. The results for each test case were compared against results of two robust numerical models such as DIVAST

and EFDC for the first test case, or EFDC for the two remaining test cases, and agreement was achieved.

Tidal basin measurements were also used for validation and calibration of the cylindrical co-ordinates numerical model. Three approaches were used for validation of the numerical model results versus the tidal basin measurements given by Olbert (2006): first one was to recover the rectangular geometry in cylindrical co-ordinates pushing the pole as far away as possible and using a very shallow angle, second one implied transformation of the numerical model from cylindrical co-ordinates into Cartesian co-ordinates by setting the scale factors equal to one, and specifying a constant spatial step, while the third one defined scale factors as unity and variable step in the direction of flow was used. Tidal basin dimension were: LxBxD=5.0mx4.75mx0.37m, with a water depth of 0.27m. The applied sinusoidal tidal forcing had amplitude of 0.05cm and period of 789 seconds. Best comparison with measurements was obtained for the mesh containing 49x51 grid points and time step 0.002 seconds. The numerical model was run for four tidal cycles. For the transformation of the numerical model results an empirical transformation coefficient was used with value equal to two. The error between simulated and measured values of velocity in the direction of flow at the point nearest to the open boundary (A5) was less than 1.700% in the first test case, 2.600% in the second test case and 2.020% in the third test case. For research purposes the results are good, but from the point of view of computational time the approach is far from being advantageous. Furthermore, from the analysis of the results, it was observed that the present numerical model is well suited for cylindrical co-ordinates numerical modelling, but also for modelling on irregular Cartesian meshes.

The analytical solution of Lynch and Gray (1978) for simplified equations was used to verify numerical model results and very good agreement was observed. The cylindrical co-ordinates numerical model was set up with the same simplified equations as the ones given in Lynch and Gary (1978). Maximum error obtained for water elevation amplitudes was 0.384%, and for the r – direction velocity component maximum error was 8.333% at the point nearest to the closed boundary CB1 (point A), where velocity is of the order of centimetres.

6.2. Discussion and Conclusions

Development and testing of an efficient coastal hydrodynamic model written in cylindrical co-ordinates was shown herein. The model is novel in that, to the Author's best knowledge, this is the first cylindrical co-ordinates model developed for applications to estuarine processes and hydrodynamics. The new model represents an improvement of the existing cylindrical co-ordinate models, in that the model uses the Navier-Stokes equations written in cylindrical co-ordinates in their fully non-linear form to simulate hydrodynamics in the estuarine region, unlike the storm surge models or analytical solutions which use a simplified form of the equations and do not include advection and turbulence effects. Also, compared to the fully non-linear models used in pipe flow simulations, the domain of simulation differs in that an annular section can be used for simulation instead of the full circle, irrotational flow can be assumed and open boundary conditions can be applied on the curved boundary. Moreover, due to the singularity problem, the domain of simulation does not include the pole.

The advantages of the cylindrical o-ordinates numerical model are summarized as follows: unconditional orthogonality of the grid; variable resolution which ensures refined resolution in the area of interest, based on appropriate position of the pole; better representation of the land boundaries due to the curvature of the grid in the angular direction; easy to generate grid. The new model is particularly well suited for V-shaped estuaries with a single river discharging into the sea, since the shape of the grid can naturally fit the shape of the estuary and a fine grid an be automatically generated in the zone of discharge. Additionally, the grid can be further refined in the radial direction using stretching functions and this approach leads to finer resolution in areas of interest such as islands.

The new model was tested and validated against two extensively used industry standard models and the results were encouraging. At the moment, the model is suitable for idealised case simulations with a uniform horizontal sea bed

representation. Also, variable representation of the lateral land boundaries did not give satisfactory results.

The cylindrical co-ordinates model uses a new time filter which helps overcome the initial error, unlike the general orthogonal curvilinear co-ordinates numerical model used for comparison of the results in the research which employs a trapezoidal correction scheme. The quality of the new numerical model results is influenced by the value of the parameters in the Robert-Asselin-Williams filter.

In the cylindrical co-ordinates numerical model, transformation of the water elevations from the computational domain to the physical domain is performed using the Author's own transformation relationships [Appendix 11] based on the water energy conservation law, also known as Green's law. A computed exponent term (n), given in Appendix 11, can be used in the transformation of water elevation and this approach reduces the amplitude error.

Tests with inclusion of a flooding and drying algorithm showed that, at this stage of development, the new model over predicts water elevations at the points nearest to the closed boundary in the direction of flow using the water elevation transformation relationship developed in Appendix 11. Consequently, the flooding and drying algorithm should be modified to better accommodate the cylindrical co-ordinates.

An analysis of computational costs showed that the cylindrical co-ordinates model was four times faster than the Cartesian co-ordinates numerical model ran at the finest resolution in the new model. When compared to the general orthogonal curvilinear co-ordinates numerical model, the cylindrical co-ordinates model was three times slower and this can be explained by the fact that the later model is in the preliminary stage of development, without additional convergence and speed up algorithms. Further development of the cylindrical co-ordinates numerical model is recommended and it should include algorithms to reduce the cost associated with computational time.

6.3. Future Work

From the experiments performed using the cylindrical co-ordinates numerical model developed in this thesis, the following future work is recommended:

i) Representation of boundary conditions can be improved to include radiation conditions, which allow for the computed errors to be radiated outside domain, unlike the reflective conditions used herein;

ii) improvement of the turbulence closure model, since the time dependent mixing length model is not well suited for simulations in tidal basin, as observed by Olbert (2006), and consequently for estuarine and coastal modelling;

iii) Variation of the step in the radial direction should be done using the hyperbolic function, based on the recommendations of Thompson et al. (1977);

iv) Real coastal areas and estuaries present the flooding and drying phenomenon, which is not included in the cylindrical co-ordinates numerical model at the moment;

v) Further tests of the cylindrical co-ordinates numerical model are recommended, such as tests for linearly sloping bed, quadratically varying bed and a more realistic variation of the bed;

vi) Simulations in real harbours, bays, estuaries or coastal areas are desired to evaluate the numerical model;

vii) Inclusion of a water quality and sediment transport module in the existing code to make it applicable to a wider range of problems;

viii) Further development of the numerical model into a three-dimensional version to allow applications not only to well-mixed estuaries and coastal areas, but also to stratified flows.

References and Bibliography

Abramowitz, M. and Stegun, I.A., Ed. (1965). Handbook of Mathematical Functions with Formulas, Graphs and Mathematical Tables. Dover Books on Mathematics. New York, Dover Publications, Inc.

Amezcua, J., Kalnay, E. and Williams, P.D. (2011). The effects of the RAW filter on the climatology and forecast skill of the SPEEDY model. Monthly Weather Review 139(2): 608-619.

Andronosov, A. A., Vol'tzinger, N.E. and Liberman, Y.L. (1997). A two-dimensional model of the Barents Sea. Oceanology 37(1): 16-22.

Andronosov, A. A., Kagan, B.A., Romanenkov, D.A. and Vol'tzinger, N.E. (2002). Numerical modelling of barotropic tidal dynamics in the Strait of Messina. Advances in Water Resources 25: 401-415.

Askelvoll, K. and Moin, P. (1996). An efficient method for temporal integration of the Navier-Stokes equations in confined axisymmetric geometries. Journal of Computational Physics 125(2): 454-463.

Asselin, R. (1972). Frequency filter for time integrations. Monthly Weather Review 100(6): 487-490.

Bao, X. W., Yan, J. and Sun, W.X. (2000). A three-dimensional tidal model in boundary-fitted curvilinear grids. Estuarine, Coastal and Shelf Science 50: 775-788.

Barber, R. W. and Scott, L.J. (2000). Numerical modelling of tidal propagation in the Severn Estuary using a depth-adapted non-orthogonal grid. Environmental Coastal Regions III, WIT Press.

Barbosa, E. and Daube, O. (2005). A finite difference method for 3D incompressible flows in cylindrical coordinates. Computers and Fluids 34: 950-971.

Barth, A., Alvera-Azcarate, A., Rixen, M. and Beckers, J.-M. (2005). Two-way nested model of mesoscale circulation features in the Ligurian Sea. Progress in Oceanography 66: 171-189.

Blayo, E. and Debreu, L. (2005). Revisiting open boundary conditions from the point of view of characteristic variables. Ocean Modelling 9: 231-252.

Blayo, E. and Debreu, L., Ed. (2006). Nesting Ocean Models. Ocean Weather Forecasting. An Integrated View of Oceanography. Chassignet, E.P., Verron, J. Springer Netherlands: 127-146.

Blumberg, A. F., Kantha, L.H. and Mellor, G.L. (1985). Open boundary condition for circulation models. Journal of Hydraulic Engineering (ASCE) 111(2): 237-255.

Blumberg, A. F., and Herring, J.H. (1986). Circulation modelling using orthogonal curvilinear coordinates. Proceedings of the 18th International Liege Colloqium on Ocean Hydrodynamics.

Blumberg, A. F. and Mellor, G., Ed. (1987). A description of a three-dimensional coastal ocean circulation model. Three-Dimensional Coastal Ocean Model. Heaps, N.S. American Geophysical Union, Washington, D.C.: 1-16.

Bonet, J. and Lock, T.-S.L. (1999). Variational and momentum preservation aspects of Smooth Particle Hydrodynamic formulations. Computational Methods in Applied Mechanical Engineering 180: 97-115.

Borthwick, A. G. L. and Barber, R.W. (1992). River and reservoir modelling using the transformed shallow water equations. International Journal for Numerical Methods in Fluids 14(10): 1193-1217.

Borthwick, A. G. L. and Kaar, E.T. (1993). A non-orthogonal curvilinear systems model of species transport in shallow flow domains. Advances in Water Resources 16: 331-350.

Borthwick, A. G. L., Cruz Leon, S. and Jozsa, J. (2001). Adaptive quadtree model of shallow-flow hydrodynamics. Journal of Hydraulic Research 39: 413-424.

Boukas, L. A., Mimikou, N.Th., Missirlis, N.M., Mellor, G.L., Lascaratos, A. and Korres, G. (1999). The parallelization of the Princeton Ocean Model. Proceedings of the 5th International Euro-Par Conference on Parallel Processing, Springer-Verlag London.

Boussinesq, J. (1877). Essai sur la theorie des eaux courantes. Paris, L'Academie des Sciences de L'Institut de France. XXIII: 777.

Carter, G. S. and Merrifield, M.A. (2007). Open boundary conditions for regional tidal simulations. Ocean Modelling 18(3-4): 194-209.

Chapman, D. C. (1985). Numerical treatment of cross-shelf open boundaries in a barotropic coastal ocean model. Journal of Physical Oceanography 15(8): 1060-1075.

Chen, C., Liu, H. and Beardsley, R.C. (2003). An unstructured grid, finite-volume, three-dimensional, primitive equations ocean model: Application to coastal ocean and estuaries. Journal of Atmospheric and Oceanic Technology 20(1): 159-186.

Chen, X. (2003). A fully hydrodynamic model for three-dimensional, free surface flows. International Journal for Numerical Methods in Fluids 42: 929-952.

Chung, T. J. (2002). Computational Fluid Dynamics. Cambridge, Cambridge University Press.

Comer, J., Ed.(2011). Modelling Extreme Flood Events due to Tides, Rivers and Storm Surges. Book of Abstracts NUI Galway - UL Alliance First Annual Engineering and Informatics Research Day. Madden, G. M., Corcoran, P.,Keane & M.,McGrath, S.: 143.

Constantinescu, G. S. and Lele, S.K. (2002). A highly accurate technique for the treatment of flow equations at the polar axis in cylindrical coordinates using series expansions. Journal of Computational Physics 183: 165-186.

Craig, I. J. D. and Sneyd, A.D. (1988). An Alternating Direction Implicit scheme for parabolic equations with mixed derivatives. Computers and Mathematics with Applications 16(4): 341-350.

Dalrymple, R. A. and Rogers, B.D., (2006). Numerical modelling of water waves with the SPH method. Coastal Engineering 53: 141-147.

Davies, A. M., Jones, J.E. and Xing, J. (1997). Review of recent developments in tidal hydrodynamic modelling. I: Spectral methods. Journal of Hydraulic Engineering, ASCE 123(4): 278-292.

De Leffe, M., Le Touze, D. and Alessandrini, B. (2010). SPH modelling of shallow-water coastal flows. Journal of Hydraulic Research 48(extra issue): 118-125.

Dean, R. G. and Dalrymple, R.A. (1991). Water wave mechanics for engineers and scientists. Singapore, World Scientific

Dean, R. G. and Dalrymple, R.A. (2002). Coastal Processes with Engineering Applications, Cambridge University Press.

Dong, S. and Karniadakis, G. Em. (2003). P-refinement and P-threads. Computer Methods Applied in Mechanics and Engineering 192: 2191-2201.

Douglas, J. and Gunn, J.E. (1964). A general formulation of alternating direction methods: parabolic and hyperbolic problems. Numerische Mathematik 6: 428-453. Cited by Hirsch (1988).

Dyke, P. (2007). Modelling coastal and offshore processes, Imperial College Press.

Ebrahimi, K., Falconer, R.A. and Lin, B. (2007). Flow and solute fluxes in integrated wetland and coastal systems. Environmental Modelling and Software 22: 1337-1348.

Eymard, R., Gallouet, T., Herbin, R. (1997). Finite volume methods. Handbook of Numerical Analysis. Ciarlet, P.G., Lions, J.-L. North Holland/Elsevier, Amsterdam: 713-1020. Preprint.

EuroGOOS. Retrieved accessed 28th June 2012.

Fairweather, G. and Navon, I.M. (1980). A linear ADI method for shallow water equations. Journal of Computational Physics 37(1): 1-18.

Falconer, R. A. (1976). Mathematical modelling of jet - forced circulation in reservoirs and harbours. Department of Civil Engineering. London, University of London. PhD: 269.

Falconer, R. A., Wolanski, E. and Mardapitta-Hadjipandeli, L. (1986). Modelling tidal circulation in an island's wake. Journal of Waterway, Port, Coastal, Ocean Engineering (ASCE) 112(2): 234-254.

Falconer, R. A. (1986). A two-dimensional mathematical model of the nitrate levels in an inland natural basin. Water Quality Modelling in the Inland Natural Environment BHRA Fluid Engineering, Bournemouth.

Falconer, R. A. and Chen, Y., Ed. (1996). Modelling transport and water quality processes on tidal floodplains. Floodplain Processes. Anderson, M. G., Walling, D.E., Bates, P.D., Wiley and Sons: 361-398.

Falconer, R. A., Struve, J. and Wu, Y. (1998). DIVAST Manual.

Ferrari, A. (2010). SPH simulation of free surface flow over a sharp-crested weir. Advances in Water Resources 33: 270-276.

Flather, R. A. (1988). A numerical model investigation of tides and diurnal-period continental shelf waves along Vancouver Island. Journal of Physical Oceanography 18: 115-139.

French, J. R. and Clifford, N.J. (2000). Hydrodynamic modelling as a basis for explaining estuarine environmental dynamics: some computational and methodological issues. Hydrological Processes 14: 2089-2108.

Fukagata, K. and Kasagi, N. (2002). Highly energy conservative finite difference method for the cylindrical coordinate system. Journal of Computational Physics 181: 478-498.

Fusco, F. (2012). Real-time forecasting and control for oscillating wave energy devices. Electronic Engineering Department, National University of Ireland Maynooth. PhD: 261.

Galperin, B. L., Kantha, L.H., Hassid, S. and Rosati, A. (1988). A quasi-equilibrium turbulent energy model for geophysical flows. Journal of the Atmospheric Sciences 45(1): 55-62.

George, K. (2007). A depth-averaged tidal numerical model using non-orthogonal curvilinear co-ordinates. Ocean Dynamics 57: 363–374.

Grenier, N., Antuono, M., Colagrossi, A., Le Touze, D. and Alessandrini, B. (2009). A Hamiltonian interface SPH formulation for multi-fluid and free surface flows. Journal of Computational Physics 228: 8380-8393.

Hagen, S. C., Westerink, J. J., Kolar, R. L. and Horstmann, O. (2001). Two dimensional, unstructured mesh generation for tidal models. International Journal for Numerical Methods in Fluids 35: 669-686

Hamrick, J. M. (1992). A three-dimensional Environmental Fluid Dynamics Computer Code: Theoretical and Computational Aspects. The College of William and Mary, Virginia Institute of Marine Science: 63.

Hartnett, M. and Berry, A. (2010). Transport of lead in the Mersey Estuary: The development of a novel approach to deriving partition coefficients. Advances in Engineering Software 41: 84-91.

He, P. and Salcudean, M. (1994). A numerical method for 3D viscous incompressible flows using non-orthogonal grids. International Journal for Numerical Methods in Fluids 18: 449-469.

Hedley, M. and Yau, M.K. (1988). Radiation boundary conditions in numerical modelling. Monthly Weather Review 116(9): 1721-1736.

Henry, R. F. and Walters, R.A. (1993). Geometrically based, automatic generator for irregular triangular networks. Communications in Numerical Methods in Engineering 9: 555-566.

Herzfeld, M. (2009). The role of numerical implementation on open boundary behaviour in limited area ocean models. Ocean Modelling 27(1): 18-32.

Hirsch, C. (1988). Numerical computation of internal and external flows. Vol. 1. Fundamentals of numerical discretization., John Wiley and Sons Ltd.

Hirsch, C., (1990). Numerical computation of internal and external flows. Vol. 2. Computational methods for inviscid and viscous flows. Wiley Series in Numerical Methods in Engineering., John Wiley and Sons Ltd.

Huang, J., Borthwick, A.G.L. and Soulsby, R.L. (1993). Adaptive quadtree simulation of sediment transport. Engineering and Computational Mechanics 163(2): 101-110.

Hughes, S. A. (1993). Physical Models and Laboratory Techniques in Coastal Engineering. Advanced Series on Ocean Engineering. Singapore, World Scientific Publishing Co. Pte. Ltd.

in t'Hout, K. J. and Welfert, B.D. (2007). Stability of ADI schemes applied to convection-diffusion equations with mixed derivative terms. Applied Numerical Mathematics 57(1): 19-35.

Jeffreys, H. (1965). Cartesian Tensors. London, Cambridge University Press.

Jones, J. E. (2002). Coastal and shelf-sea modelling in the European context. Oceanography and Marine Biology: An Annual Review. R. J. Atkinson, Barbes, M. Aberdeen, CRC Press. 40: 37-142.

Jones, J. E., Davies, A.M. (2005). An intercomparison between finite difference and finite element (TELEMAC) approaches to modelling west coast of Britain tides. Ocean Dynamics 55: 178-198.

Kantha, L. H. and Clayson, C.A., Ed. (2000). Numerical Models of Oceans and Oceanic Processes. International Geophysics Series. A series of monographs and textbooks. San Diego, California, Academic Press.

Ketefian, G. S. and Jacobson, M.z., (2011). A mass, energy, vorticity, and potential enstrophy conserving lateral boundary scheme for the shallow water equations using piecewise linear boundary approximations.

Klevanny, K. A., Matveyev, G.V. and Voltzinger, N.E. (1994). An integrated modelling system for coastal area dynamics. International Journal for Numerical Methods in Fluids 19: 181-206.

Kocyigit, M. B., Falconer, R.A. and Lin, B. (2002). Three-dimensional modelling of free surface flows with non-hydrostatic pressure. International Journal for Numerical Methods in Fluids 40(9): 1145-1162.

Korres, G. and Lascaratos, A. (2003). A one-way nested eddy resolving model of the Aegean and Levantine basins: implementation and climatological runs. Annalaes Geophysicae 21: 205-220.

Kowalik, Z. and Marchenko, A.V. (2002). Tidal motion enhancement around islands. Journal of Marine Research 60(4): 551-581.

Lamb, H. (1932). Hydrodynamics. Cambridge, Cambridge University Press.

Larsen, J. C. (1977). Cotidal charts for the Pacific Ocean near Hawaii using f-plane solutions. Journal of Physical Oceanography 7: 100-109.

Lee, D. and Tsuei, Y.M. (1992). A formula for estimation of truncation errors of convection terms in curvilinear coordinate systems. Journal of Computational Physics 98: 90-100.

Lee, S. and Kim, K (1999). Scattering of tidal frequency around a cylindrical island. Journal of Physical Oceanography 29: 436-448.

Lee, S. H. and Kim, K. (1993). Scattering of a Kelvin wave by a cylindrical island. Journal of the Oceanographical Society of Korea 28(3): 177-185.

Legrand, S., Legat, V. and Deleersnijder, E. (2000). Delaunay mesh generation for an unstructured-grid ocean general circulation model. Ocean Modelling 2: 17-28.

LeVeque, R. J. (2003). Finite volume methods for hyperbolic problems, Cambridge University Press, USA.

Lin, B. and Falconer, R.A. (1995). Modelling sediment fluxes in estuarine waters using a curvilinear coordinate grid system. Estuarine, Coastal and Shelf Science 41: 413-428.

Lin, B. and Chandler-Wilde, S.N. (1996). A depth integrated 2D coastal and estuarine model with conformal boundary fitted mesh generation. International Journal for Numerical Methods in Fluids 23: 819-846.

Lindeboom, H. (2002). The Coastal Zone: An Ecosystem under Pressure. . Washington, Island Press.

LOICZ. Retrieved 26th June 2012.

Luettich, R. A., Birkhahn, R.H. and Westerink, J.J. (1991). Application of ADCIRC-2DDI to Masonboro Inlet, North Carolina: A brief numerical modelling study, U.S. army Engineer Waterways Experiment Station.

Lynch, D. R. and Gray, W.G. (1978). Analytic solutions for computer flow. Journal of Hydraulics Division , ASCE 104: 1409-1428.

Lynch, D. R. and Officer, C.B. (1985). Analytic test cases for three-dimensional hydrodynamic models. International Journal for Numerical Methods in Fluids 5: 529-543.

Madala, R. V. and Piacseki, S.A. (1977). A semi-implicit numerical model for baroclinic oceans. Journal of Computational Physics 23: 167-178.

Marchessielo, P., McWilliams, J.C. and Shchepetkin, A. (2001). Open boundary conditions for long-term integration of regional ocean models. Ocean Modelling 3(1): 1-20.

Marsaleix, P., Auclair, F. and Estournel, C. (2006). Considerations on Open Boundary Conditions for Regional and Coastal Ocean Models. Journal of Atmospheric and Oceanic Technology 23: 1604-1613.

Martin, J. L. and McCutcheon, S.C. (1999). Hyrodynamics and transport for water quality modelling. Boca Raton, Lewis Publishers.

Mavriplis, D. J. (1997). Unstructured grid techniques. Annual Review of Fluid Mechanics 29: 473-514.

McCave, I. N., Ed. (2002). Sedimental Settings on Coastal Margins - an Overview. Ocean Margin Systems. Berlin, Springer Verlag .

McKee, S., Wall, D.P. and Wilson, S.K. (1996). An Alternating Direction Implicit scheme for parabolic equations with mixed derivatives and convective terms. Journal of Computational Physics 126(1): 64-76.

Mellor, G., Häkkinen, S., Ezer, T. and Patchen, R., Ed. (2002). A generalization of a sigma coordinate ocean model and an Intercomparison of model vertical grids. . Ocean Forecasting: Conceptual Basis and Analysis. Berlin, Springer.

Mellor, G. L. and Yamada, T. (1982). Development of a turbulence closure model for geophysical fluid problems. Reviews of Geophysics and Space Physics 20(4): 851-875.

Mellor, G. L. and Blumberg, A.F. (1985). Modelling vertical and horizontal diffusivities with the sigma co-ordinate system. Monthly Weather Review 113(8): 1379-1383.

Mellor, G. L. (1996). Introduction to physical oceanography. New York, Springer-Verlag New York, Inc.

Mellor, G. L. (2004). Users guide for a three-dimensional, primitive equation, numerical ocean model.

Mohseni, K. and Colonius, T. (2000). Numerical treatment of polar coordinate singularities. Journal of Computational Physics 157: 787-795.

Mojfeld, H. D. (1980). Effect of vertical viscosity on Kelvin waves. Journal of Physical Oceanography 10: 1039-1050.

Molls, T. and Chaundray, M.H. (1995). Depth-averaged open channel flow model. Journal of Hydraulic Engineering, ASCE 121: 453-465.

Monaghan, J. J. (2005). Smoothed Particle Hydrodynamics. Reports on Progress in Physics 68: 1703-1759.

Moore, S. A. (2004). Lateral boundary conditions in numerical ocean models. Department of Meteorology. Reading, The University of Reading. PhD: 195.

Morinishi, Y., Vasilyev, O.V. and Ogi, T. (2004). Fully conservative finite diference schemein cylindrical coordinates for incompressible flow simulations. Journal of Computational Physics 197: 686-710.

Morton, K. W. and Mayers, D.F. (2005). Numerical solution of partial differential equations: An Introduction, Cambridge University Press.

Muin, M. and Spaulding, M. (1996). Two-dimensional boundary-fitted circulation model in spherical co-ordinates. Journal of Hydraulic Engineering, ASCE 122(9): 512-521.

Muin, M. and Spaulding, M. (1997). Three-dimensional boundary-fitted circulation model. Journal of Hydraulic Engineering, ASCE 123(1): 2-12.

Namin, M., Liu, B. and Falconer, R.A. (2004). Modelling estuarine and coastal flows using an unstructured triangular finite volume algorithm. Advances in Water Resources 27: 1179-1197.

Nash, S., Berry, A. and Hartnett, M. , Ed. (2005). Nutrient dynamics in Cork Harbour. River Basin Management WIT Press.

Nash, S. (2010). Development of an efficient dynamically-nested model for tidal hydraulics and solute transport. Civil Engineering. Galway, NUI Galway. PhD: 382.

Nicholls, R. J. and Small, C. (2002). Improved Estimates of Coastal Population and Exposure to Hazard Released. EOS Transactions of American Geophysical Union 83(28): 301-305.

Nikitin, N. (2006). Finite-difference method for incompressible Navier-Stokes equations in arbitrary orthogonal curvilinear co-ordinates. Journal of Computational Physics 217(2): 759 - 781.

NOAA. Retrieved 13th August 2012.

Nycander, J. and Doos, K. (2003). Open boundary conditions for barotropic flows. Journal of Geophysical Research 108(C5): 3168–3187.

Olbert, A. (2006). Investigations into turbulence processes in tide-induced flows - scale and numerical modelling. Civil Engineering. Galway, National University of Ireland Galway. PhD: 440.

Olbert, A. I. and Hartnett, M. (2010). Storms and surges in Irish Coastal Waters. Ocean Modelling 34: 50-62.

Palma, E. D. and Matano, R.P. (2000). On the implementation of open boundary conditions for a general circulation model: The three dimensional case. Journal of Geophysical Research 105(C4): 8605-8627.

Peaceman, D. W. and Rachford, H.H. (1955). The numerical solution of parabolic and elliptic differential equations. SIAM Journal 3: 28-41. Cited by Hirsch (1988).

Pietrzak, J., Jakobson, J.B., Burchard, H., Vested, H.J. and Petersen, O. (2002). A three-dimensional hydrostatic model for coastal and ocean modelling using a generalised topography following co-ordinate system. Ocean Modelling 4: 173-205.

Post, E. D. and Votta, L.G. (2005). (2005). Computational Science Demands a New Paradigm. Physics Today 58(1): 35-41.

Priymak, V. G. and Miyazaki, T. (1998). Accurate Navier-Stokes investigation of transitional and turbulent flows in a circular pipe. Journal of Computational Physics 142: 370-411.

Rahman, M. M., Paul, G.C. and Hoque, A. (2012). Nested numerical scheme in a polar co-ordinate shallow water model for the coast of Bangladesh. Journal of Coastal Conservation: 1-11.

Riley, K. F. (1974). Mathematical Methods for the Physical Sciences. An informal treatment for students of physics and engineering. London, Cambridge University Press.

Roache, P. J. (1976). Computational Fluid Dynamics. Albuquerque, New Mexico, Hermosa Publishers.

Rodi, W., Majumdar, S. and Schonung, B. (2004). Finite volume methods for two-dimensional incompressible flows with complex boundaries. Computer Methods in Applied Mechanics and Engineering 75: 369-392.

Rodriguez-Paz, M. and Bonet, J. (2005). A corrected smooth particle hydrodynamics formulation of the shallow-water equations. Computers and Structures 83: 1396-1410.

Ross, D. A. (1995). Introduction to Oceanography. New York, Harper Collins College Publishers.

Roy, G. D., Humayun Kabir, A.B.M., Mandal, M.M. and Haque, M.Z. (1999). Polar coordinates shallow water storm surge model for the coast of Bangladesh. Dynamics of Atmospheres and Oceans 29: 397-413.

Sankaranarayanan, S. and Spaulding, M.L. (2003). A study of the effects of grid non-orthogonality in the boundary-fitted coordinate system. Journal of Computational Physics 184: 299–320.

Sankaranarayanan, S. and Ward, M.C. (2006). Development and application of a three-dimensional orthogonal coordinate semi-implicit hydrodynamic model. Continental Shelf Research 26: 1571–1594.

SEAI. Retrieved 17th July 2012.

SETIS. Retrieved 18th July 2012.

Shao, S. and Lo, E.Y.M. (2003). Incompressible SPH method for simulating Newtonian and non-Newtonian flows with a free surface. Advances in Water Resources 26: 787-800.

Sheng, Y.P. (1989). Evolution of a three-dimensional curvilinear-grid hydrodynamic model for estuaries, lakes and coastal waters: CH3D. Estuarine and Coastal Modelling, ASCE: 40-49.

Shi, F., Sun, W. and Wei, G. (1997). A WDM method on a generalized curvilinear grid for calculation of storm surge flooding. Applied Ocean Research 19(4): 275-282.

Shulman, I. and Lewis, J.K. (1994). Modelling open boundary conditions by using the optimization approach., NTIS Technical Report: 19.

Smagorinsky, J. (1963). General circulation experiments with primitive equations. I. The basic experiment. Monthly Weather Review 91(3): 99-164.

Smith, K. M., Cope, W.K. and Vanka, S.P. (1993). A multigrid procedure for three-dimensional flows on non-orthogonal collocated grids. International Journal for Numerical Methods in Fluids 17: 887-904.

Spaulding, M. L. (1984). A vertically averaged circulation model using boundary- fitted coordinates. Journal of Physical Oceanography 14(5): 973–982

Staneva, J., Stanev, E.V., Wolff, J.-O., Badewien, T.H., Reuter, R., Flemming, B., Bartholoma, A. and Bolding, K. (2009). Hydrodynamics and sediment dynamics in German Bight. A focus on observations and modelling in the East Frisian Wadden Sea. Continental Shelf Ressearch 29: 302-319.

Stevens, D. P. (1990). On open boundary conditions for three dimensional primitive equation ocean circulation models. Geophysical and Astrophysical Fluid Dynamics 51: 103-133.

Stewart, R. H. (2008). Introduction to Physical Oceanography.

Swanson, J. G., Spaulding, M., Mathisen, J.P., Jenssen, and Øystein, O.J. (1989). A three dimensional boundary-fitted coordinate hydrodynamic model. Part I: Development and testing. Ocean Dynamics 42: 169-186.

Thompson, J. F., Thames, F.C. and Mastin, C.W. (1977). Boundary-fitted curvilinear coordinate systems for solution of partial differential equations on field containing any number of arbitrary two-dimensional bodies., NASA.

Thompson, J. F., Thames, F.C. and Mastin, C.W. (1977). TOMCAT - A code for numerical generation of boundary fitted coordinate systems on fields containing any number of arbitrary two dimensional bodies. Journal of Computational Physics 24.

Thompson, J. F., Warsi, Z.U.A. and Mastin, C.W. (1982). Boundary-fitted coordinate systems for numerical solution of partial differential equations-a review. Journal of Computational Physiscs 47: 1-108.

UNESCO (2006). IGOS. A Coastal Theme for the IGOS Partnership - For the Monitoring of our Environment from Space and from Earth. Paris. Paris, UNESCO: 60.

Vacondio, R., Rogers, B.D., Stansby, P.K., Mignosa, P. and Feldman, J. (2011). A dynamic particle coalescing and splitting scheme for SPH. 6th International SPHERIC workshop, Hamburg, Germany.

Vacondio, R., Rogers, B.D., Stansby, P.K. and Mignosa, P. (2012). SPH modelling of shallow flow with open boundaries for practical flow simulation. Journal of Hydraulic Engineering (ASCE) 138: 530-541.

Verzzico, R. and Orlandi, P. (1996). A finite difference scheme for three-dimensional incompressible flows in cylindrical coordinates. Journal of Computational Physics 123: 402-414.

Vinokur, M. (1976). The relation of finite element and finite difference methods., NASA.

Walters, R. A. (2005). Coastal ocean models: two useful finite element models. Continental Shelf Research 25.

Wang, P., Song, T.Y., Chao, Y. and Zhang, C. (2005). Parallel computation of the Regional Ocean Modelling System. The International Journal of High Performance Computing Applications 19(4): 375-385.

Warsi, Z. U. A. (2006). Fluid Dynamics. Theoretical and Computational Approaches, Taylor&Francis Group.

Wesseling, P. (2001). Principles of Computational Fluid Dynamics. Springer Series in Computational Mathematics 29.

Westerink, J. J., Luettich, R.A. and Muccino, J.C. (1994). Modelling tides in the western North Atlantic using unstructured graded grids. Tellus A 46(2): 178-199.

White, L. and Deleersnijder, E. (2007). Diagnoses of vertical transport in a three-dimensional finite element model of the tidal circulation around an island. Estuarine, Coastal and Shelf Science 74: 655-669.

Williams, P. D. (2009). A proposed modification to the Roberts - Asselin time filter. Monthly Weather Review 137(8): 2538-2546.

Williams, P. D. (2011). The RAW filter: An improvement to the Robert - Asselin filter in semi - implicit time integrations. Monthly Weather Review 139(6): 1996-2007.

Wu, X. G., Shen, Y.M., Zheng, Y.H. and Yang, Z.F. (2004). Numerical model of flow and pollutant transportation in non-orthogonal curvilinear coordinates. Journal of Environmental Sciences 16: 293-296.

Ye, J., McCorquodale, J.A. and Barron, R.M. (1998). A three-dimensional hydrodynamic model in curvilinear coordinates with collocated grid. International Journal for Numerical Methods in Fluids 28: 1109-1134.

Zhang, W. Z., Hong, H.S., Shang, S.P., Chen, D.W. and Chai, F. (2007). A two-way nested coupled tide-surge model for the Taiwan Strait. Continental Shelf Research 27: 1548–1567.

Orthogonal Co-ordinate Systems

The most widely used orthogonal co-ordinate system is the Cartesian co-ordinate system, developed by the French mathematician René Descartes. A Cartesian co-ordinate system is composed from three intersecting perpendicular axes [Figure A1.1]. Each axis represents the intersection of two perpendicular planes: x axis is the intersection of planes $y = 0$ (xz plane) and $z = 0$ (xy plane); y axis is the intersection of planes $x = 0$ (yz plane) and $z = 0$ (xy plane); z axis is the intersection of planes $x = 0$ (yz plane) and $y = 0$ (xz plane). The intersection of the three axes is called origin.

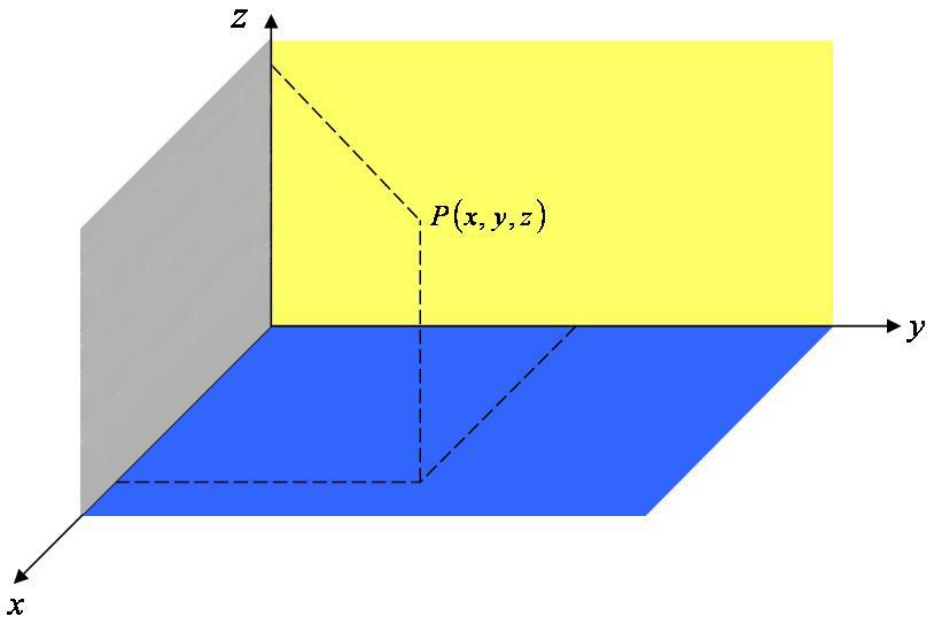

Figure A1.1. Representation of the Cartesian co-ordinate system.

The standard basis in three dimensions comprises the unit vectors (also called versors): $\vec{i}, \vec{j}, \vec{k}$, which have the same direction as the axes x, y, z. The names of the three co-ordinate axes are: $x-$ abscissa, $y-$ ordinate, $z-$ applicate. A three dimensional Cartesian co-ordinate system provides the three physical dimensions of space: length, width, height.

The need of using other than Cartesian types of co-ordinate systems arises in the context of symmetry problems in some physical situations [Riley (1974)]. The

most common non-Cartesian co-ordinate systems are spherical co-ordinates [Figure A1.2], and cylindrical co-ordinates [Figure A1.3] as orthogonal curvilinear co-ordinate systems. An example of a general orthogonal curvilinear co-ordinate system is shown in Figure A1.4. Spherical co-ordinates are given by:

$$\begin{aligned} x &= r\sin\theta\cos\phi \\ y &= r\sin\theta\sin\phi \\ z &= r\cos\theta \end{aligned} \qquad \text{(A1.1)}$$

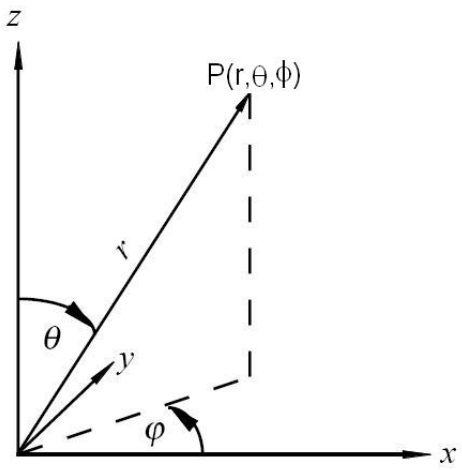

Figure A1.2. Spherical polar co-ordinate system.

Cylindrical co-ordinates are defined as follows:

$$\begin{aligned} x &= r\cos\phi \\ y &= r\sin\phi \\ z &= z \end{aligned} \qquad \text{(A1.2)}$$

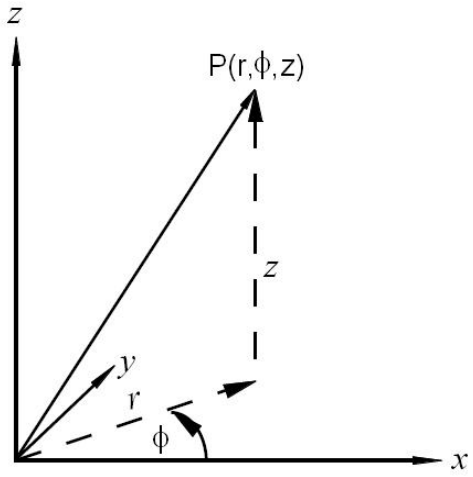

Figure A1.3. Cylindrical polar co-ordinate system.

The elements describing the three co-ordinate systems are presented in Table A1.1.

	Cartesian	Spherical polar	Cylindrical polar
$u_1u_2u_3$	$x\ \ y\ \ z$	$r\ \ \theta\ \ \phi$	$r\ \ \phi\ \ z$
$h_1h_2h_3$	1 1 1	$1\ \ r\ \ r\sin\theta$	$1\ \ r\ 1$
$(dr)^2$	$dx^2+dy^2+dz^2$	$dr^2+r^2d\theta^2+r^2\sin^2\theta d\phi$	$dr^2+r^2d\phi^2+dz^2$
dS_1	$dydz$	$r^2\sin\theta d\theta d\phi$	$rd\phi dz$
dS_2	$dxdz$	$r\sin\theta drd\phi$	$drdz$
dS_3	$dxdy$	$rdrd\theta$	$rdrd\phi$
dV	$dxdydz$	$r^2\sin\theta drd\theta d\phi$	$rdrd\phi dz$

Table A1.1: Elements describing Cartesian, spherical and cylindrical co-ordinate systems

where:

u_i are the three co-ordinates describing the position of a point in space, $i=1,2,3$;

h_i are the scale or metric factors and are defined using the subsequent equation:

$$\left|d\vec{r}\right|^2 = \sum_{i=1}^{3} h_i^2 \left(du_i\right)^2 \tag{A1.3}$$

$d\vec{r}$ is the position vector (in Cartesian co-ordinates) or the line element (in curvilinear co-ordinates);

dS_1 is the surface of face delimited by dy, dz or $u_1 = const.$;

dS_2 is the surface of face delimited by dx, dz or $u_2 = const.$;

dS_3 is the surface of face delimited by dx, dy or $u_3 = const.$ (given by the subsequent equation);

$$dS_3 = \left(\frac{\partial \vec{r}}{\partial u_1} \times \frac{\partial \vec{r}}{\partial u_2} \right) du_1 du_2 \tag{A1.4}$$

dV is the elemental volume, given by the Jacobian:

$$dV = \begin{vmatrix} \dfrac{\partial x}{\partial u_1} & \dfrac{\partial x}{\partial u_2} & \dfrac{\partial x}{\partial u_3} \\ \dfrac{\partial y}{\partial u_1} & \dfrac{\partial y}{\partial u_2} & \dfrac{\partial y}{\partial u_3} \\ \dfrac{\partial z}{\partial u_1} & \dfrac{\partial z}{\partial u_2} & \dfrac{\partial z}{\partial u_3} \end{vmatrix} du_1 du_2 du_3 \tag{A1.5}$$

or the equivalent relationship:

$$dV = \left(\frac{\partial \vec{r}}{\partial u_1} \times \frac{\partial \vec{r}}{\partial u_2} \right) \cdot \frac{\partial \vec{r}}{\partial u_3} du_1 du_2 du_3 \tag{A1.6}$$

It has positive values if u_1, u_2, u_3 are included into a right-handed frame and negative otherwise.

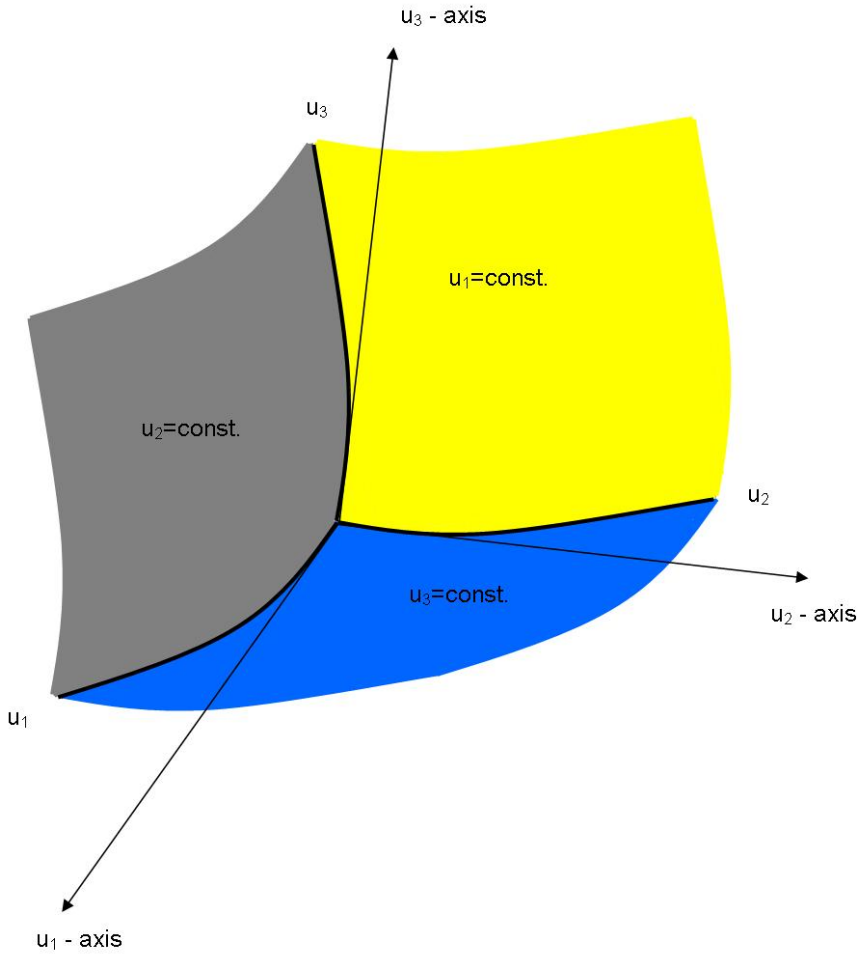

Figure A1.4. General orthogonal curvilinear co-ordinate system. The angle between any two axes is $90°$.

APPENDIX 2

Vector Operators in Orthogonal Co-ordinate Systems

Vector operators are useful tools for derivation of the equations governing hydrodynamics and mass conservation, written in tensors form, in various Eulerian co-ordinate systems. The cylindrical co-ordinate system will be considered in detail in Appendix 6. For the co-ordinate systems defined in Appendix 1, the following vector operators can be expressed in these co-ordinate systems:

1. Gradient

The gradient is, by definition, the rate of change with distance. In the co-ordinate systems considered, the gradient is a vector as follows:

- General orthogonal curvilinear co-ordinate system:

$$grad\Phi = \nabla\Phi = \frac{1}{h_1}\frac{\partial\Phi}{\partial u_1}\vec{e}_1 + \frac{1}{h_2}\frac{\partial\Phi}{\partial u_2}\vec{e}_2 + \frac{1}{h_3}\frac{\partial\Phi}{\partial u_3}\vec{e}_3 \qquad \text{(A2.1)}$$

where:

$\Phi(x, y, z)$ is a scalar field;

$\vec{e}_1, \vec{e}_2, \vec{e}_3$ are the versors of the three axes considered ($\vec{i}, \vec{j}, \vec{k}$ for the Cartesian co-ordinate system).

- Cartesian co-ordinate system:

$$grad\Phi \equiv \frac{\partial\Phi}{\partial x}\vec{i} + \frac{\partial\Phi}{\partial y}\vec{j} + \frac{\partial\Phi}{\partial z}\vec{k} \qquad \text{(A2.2)}$$

- Spherical co-ordinate system:

$$grad\Phi = \nabla\Phi = \frac{\partial\Phi}{\partial r}\vec{e}_1 + \frac{1}{r}\frac{\partial\Phi}{\partial\theta}\vec{e}_2 + \frac{1}{r\sin\theta}\frac{\partial\Phi}{\partial\phi}\vec{e}_3 \qquad \text{(A2.3)}$$

- Cylindrical co-ordinate system:

$$grad\Phi = \nabla\Phi = \frac{\partial\Phi}{\partial r}\vec{e}_1 + \frac{1}{r}\frac{\partial\Phi}{\partial\phi}\vec{e}_2 + \frac{\partial\Phi}{\partial z}\vec{e}_3 \qquad \text{(A2.4)}$$

2. Divergence

The divergence is, by definition, the way that vector fields vary with position. In the co-ordinate systems considered, the divergence is a scalar described by the subsequent equations:

- General orthogonal curvilinear co-ordinate system:

$$\nabla\cdot\vec{a} = \frac{1}{h_1h_2h_3}\left[\frac{\partial}{\partial u_1}\left(h_2h_3a_1\right) + \frac{\partial}{\partial u_2}\left(h_3h_1a_2\right) + \frac{\partial}{\partial u_3}\left(h_1h_2a_3\right)\right] \qquad \text{(A2.5)}$$

- Cartesian co-ordinate system:

$$div\vec{a} = \frac{\partial a_x}{\partial x} + \frac{\partial a_y}{\partial y} + \frac{\partial a_z}{\partial z} \equiv \nabla\cdot\vec{a} \qquad \text{(A2.6)}$$

where:

$\vec{a} = \left(a_x, a_y, a_z\right)$ is the considered vector field.

- Spherical co-ordinate system:

$$\nabla\cdot\vec{a} = \frac{1}{r^2}\frac{\partial}{\partial r}\left(r^2a_r\right) + \frac{1}{r\sin\theta}\frac{\partial}{\partial\theta}\left(\sin\theta a_\theta\right) + \frac{1}{r\sin\theta}\frac{\partial a_\phi}{\partial\phi} \qquad \text{(A2.7)}$$

- Cylindrical co-ordinate system:

$$\nabla \cdot \vec{a} = \frac{1}{r}\frac{\partial}{\partial r}\left(r a_r\right) + \frac{1}{r}\frac{\partial a_\phi}{\partial \phi} + \frac{\partial a_z}{\partial z} \tag{A2.8}$$

3. Curl

The curl is, by definition, a vector operator that describes the infinitesimal rotation of a three-dimensional vector field. In the co-ordinate systems considered, the curl is a vector with components given by the following equations:

- General orthogonal curvilinear co-ordinate system:

$$\begin{aligned}
\left(curl\vec{a}\right)_3 &= \frac{1}{h_1 h_2}\left[\frac{\partial}{\partial u_1}\left(h_2 a_2\right) - \frac{\partial}{\partial u_2}\left(h_1 a_1\right)\right] \\
\left(curl\vec{a}\right)_1 &= \frac{1}{h_2 h_3}\left[\frac{\partial}{\partial u_2}\left(h_3 a_3\right) - \frac{\partial}{\partial u_3}\left(h_2 a_2\right)\right] \\
\left(curl\vec{a}\right)_2 &= \frac{1}{h_3 h_1}\left[\frac{\partial}{\partial u_3}\left(h_1 a_1\right) - \frac{\partial}{\partial u_1}\left(h_3 a_3\right)\right]
\end{aligned} \tag{A2.9}$$

- Cartesian co-ordinate system:

$$curl\vec{a} = \left(\frac{\partial a_z}{\partial y} - \frac{\partial a_y}{\partial z}\right)\vec{i} + \left(\frac{\partial a_x}{\partial z} - \frac{\partial a_z}{\partial x}\right)\vec{j} + \left(\frac{\partial a_y}{\partial x} - \frac{\partial a_x}{\partial y}\right)\vec{k} \tag{A2.10}$$

- Spherical co-ordinate system:

$$\left(curl\vec{a}\right)_r = \left(\frac{1}{r}\frac{\partial a_\phi}{\partial \theta} + \frac{\cot\theta}{r}a_\phi - \frac{1}{r\sin\theta}\frac{\partial a_\theta}{\partial \phi}\right) \tag{A2.11}$$

$$\left(curl\vec{a}\right)_\theta = \left(\frac{1}{r\sin\theta}\frac{\partial a_r}{\partial \phi} - \frac{a_\phi}{r} - \frac{\partial a_\phi}{\partial r}\right) \tag{A2.11}$$

continued

$$\left(curl\vec{a}\right)_{\phi} = \left(\frac{a_{\theta}}{r} + \frac{\partial a_{\theta}}{\partial r} - \frac{1}{r}\frac{\partial a_{r}}{\partial \theta}\right)$$

- Cylindrical co-ordinate system:

$$\left(curl\vec{a}\right)_{r} = \left(\frac{1}{r}\frac{\partial a_{z}}{\partial \phi} - \frac{\partial a_{\phi}}{\partial z}\right)$$

$$\left(curl\vec{a}\right)_{\phi} = \left(\frac{\partial a_{r}}{\partial z} - \frac{\partial a_{z}}{\partial r}\right) \qquad \text{(A2.12)}$$

$$\left(curl\vec{a}\right)_{z} = \left(\frac{a_{\phi}}{r} + \frac{\partial a_{\phi}}{\partial r} - \frac{1}{r}\frac{\partial a_{r}}{\partial \phi}\right)$$

4. The Laplacian operator ∇^2

The Laplacian (∇^2) is, by definition, a linear differential operator acting upon a vector with the vector itself consisting of a sum of unit vectors multiplied by components. In the co-ordinate systems considered, the Laplacian operator is a scalar as follows (for the particular case: $\vec{a} = \nabla\Phi$):

- General orthogonal curvilinear co-ordinate system:

$$\nabla^2\Phi = \frac{1}{h_1 h_2 h_3}\left[\frac{\partial}{\partial u_1}\left(\frac{h_2 h_3}{h_1}\frac{\partial\Phi}{\partial u_1}\right) + \frac{\partial}{\partial u_2}\left(\frac{h_3 h_1}{h_2}\frac{\partial\Phi}{\partial u_2}\right) + \frac{\partial}{\partial u_3}\left(\frac{h_1 h_2}{h_3}\frac{\partial\Phi}{\partial u_3}\right)\right] \qquad \text{(A2.13)}$$

- Cartesian co-ordinate system:

$$\left[\nabla^2\vec{a}\right]_x = \frac{\partial^2 a_x}{\partial x^2} + \frac{\partial^2 a_x}{\partial y^2} + \frac{\partial^2 a_x}{\partial z^2} \qquad \text{(A2.14)}$$

- Spherical co-ordinate system:

$$\nabla^2\Phi = \frac{1}{r^2}\frac{\partial}{\partial r}\left(r^2\frac{\partial\Phi}{\partial r}\right) + \frac{1}{r^2\sin\theta}\frac{\partial}{\partial\theta}\left(\sin\theta\frac{\partial\Phi}{\partial\theta}\right) + \frac{1}{r^2\sin\theta}\frac{\partial^2\Phi}{\partial\phi^2} \qquad \text{(A2.15)}$$

- Cylindrical co-ordinate system:

$$\nabla^2\Phi = \frac{1}{r}\frac{\partial}{\partial r}\left(r\frac{\partial\Phi}{\partial r}\right) + \frac{1}{r^2}\frac{\partial^2\Phi}{\partial\theta^2} + \frac{\partial^2\Phi}{\partial z^2} \qquad \text{(A2.16)}$$

Non-orthogonal Curvilinear Co-ordinate Systems

Non-orthogonal curvilinear systems are characterized by that the co-ordinates are not orthogonal and the length of the natural basis vectors (h_i) does not fully determine the geometry. Figure A3.1 illustrates a general curvilinear co-ordinate system.

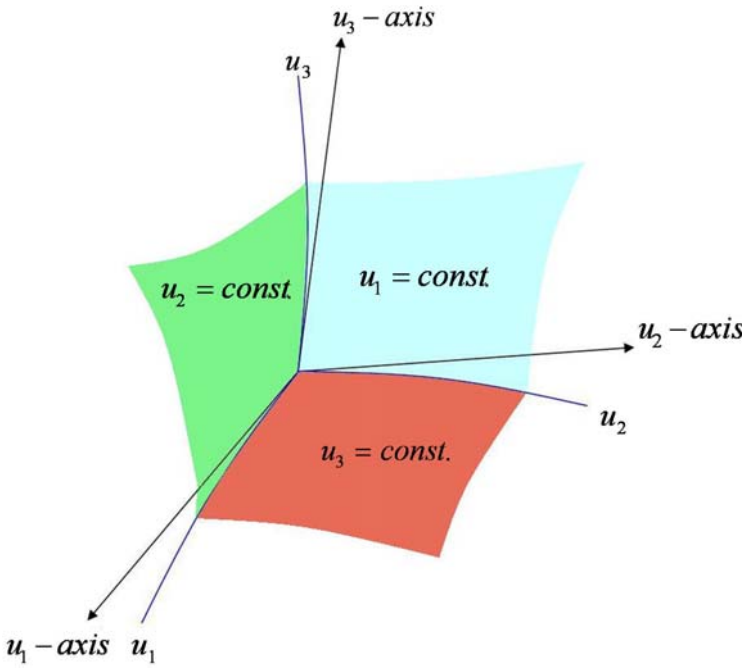

Figure A3.1. Representation of the generalised curvilinear co-ordinate system.

The expression of the metric coefficients is given by the dot product:

$$g_{ij} = \frac{\partial \vec{r}}{\partial u^i} \cdot \frac{\partial \vec{r}}{\partial u^j} = \sum_{l=1}^{3} \frac{\partial x_l}{\partial u^i} \frac{\partial x_l}{\partial u^j} \tag{A3.1}$$

The reciprocal basis vectors in the non-orthogonal co-ordinates ($\nabla u_i, i = 1,2,3$) are perpendicular to the $u_i = const.$ surface, but they are not parallel to $\frac{\partial \vec{r}}{\partial u_i}$ (displacement or natural basis). Their length is not equal to unity and the dot

product of the natural basis and reciprocal basis is 1 or 0, as well as in the case of orthogonal co-ordinates:

$$\frac{\partial \vec{r}}{\partial u_i} \cdot \nabla u_j = \sum_{l=1}^{3} \frac{\partial x_l}{\partial u_i} \frac{\partial u_j}{\partial x_l} = \frac{\partial u_j}{\partial u_i} = \delta_{ij} \tag{A3.2}$$

where:

δ_{ij} is the Kronecker delta.

In tensor representation, a vector $\vec{v}$ can be expressed as the sum of the products of each of its components times the basis vector belonging to that component in two ways:

$$\vec{v} = v^i \vec{e}_i = v_i \vec{e}^{\,i} \tag{A3.3}$$

where:

v^i are the contravariant components of $\vec{v}$;

v_i are the covariant components of $\vec{v}$;

$\vec{e}_i$ are covariant basis vectors;

$\vec{e}^{\,i}$ are the contravariant basis vectors.

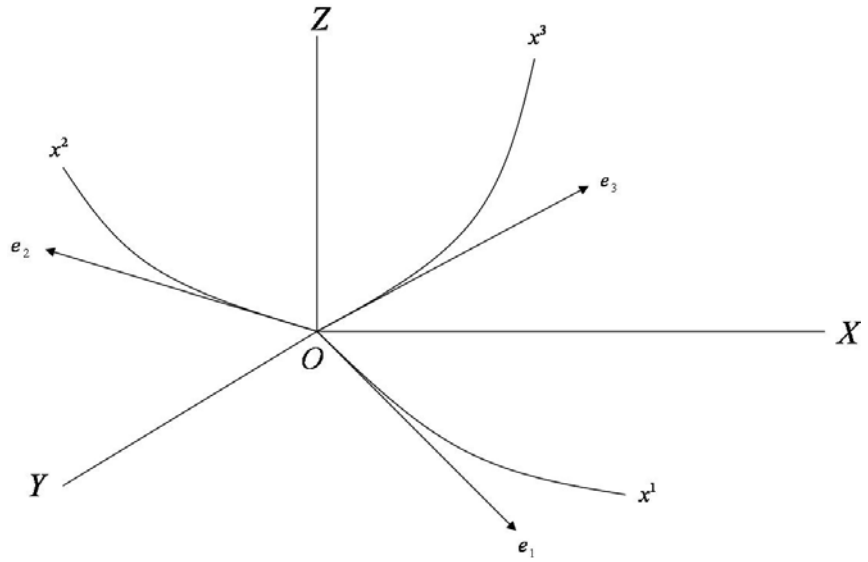

Figure A3.2. Covariant basis vectors for curvilinear co-ordinates [Warsi (2006)].

In equation (A3.1) repeated indices are assumed to sum according to the Einstein summation convention:

$$\bar{v}_j \frac{\partial x_l}{\partial u^i}\frac{\partial x_l}{\partial u^j} \equiv \sum_j \sum_l \bar{v}_j \frac{\partial x_l}{\partial u^i}\frac{\partial x_l}{\partial u^j} \tag{A3.4}$$

Equation (A3.3) is satisfied if and only if the elements in the equation transform from $\bar{x}^i$ co-ordinates to x^i co-ordinates (where x^i are differentiable functions of $\bar{x}^i$, and vice versa) according to the rules:

$$\begin{aligned} v^i &= \bar{v}^j \frac{\partial x^i}{\partial \bar{x}^j},\ v_i = \bar{v}_j \frac{\partial \bar{x}^j}{\partial x^i} \\ e^i &= \bar{e}^j \frac{\partial x^i}{\partial \bar{x}^j},\ e_i = \bar{e}_j \frac{\partial \bar{x}^j}{\partial x^i} \end{aligned} \tag{A3.5}$$

where the overbared components and basis vectors represent $\vec{v}$ in the co-ordinates $\bar{x}^i$:

$$\vec{v} = \bar{v}^i \vec{\bar{e}}_i = \bar{v}_i \vec{\bar{e}}^i \tag{A3.6}$$

The inverse relations can be written as:

$$\begin{aligned} \bar{v}^i &= v^j \frac{\partial \bar{x}^i}{\partial x^j},\ \bar{v}_i = v_j \frac{\partial x^j}{\partial \bar{x}^i} \\ \bar{e}^i &= e^j \frac{\partial \bar{x}^i}{\partial x^j},\ \bar{e}_i = e_j \frac{\partial x^j}{\partial \bar{x}^i} \end{aligned} \tag{A3.7}$$

The inverse functions defined by equations (A3.7) exist only if the Jacobian $J \equiv \det\left(\frac{\partial x_i}{\partial \bar{x}_i}\right)$ is not singular. By using equation (A3.5) equation (A3.3) defining $\vec{v}$ can be written in the form:

$$\vec{v} = v^i \vec{e}_i = v_i \vec{e}^{\,i} \Rightarrow v^i \vec{e}_i = \bar{v}^j \frac{\partial x^i}{\partial \bar{x}^j} \bar{e}_j \frac{\partial \bar{x}^j}{\partial x^i} = \bar{v}_j \frac{\partial \bar{x}^j}{\partial x^i} \bar{e}_j \frac{\partial x^i}{\partial \bar{x}^j} = \bar{v}_j \vec{\bar{e}}^{\,j} \tag{A3.8}$$

The above relationship preserves the invariance of the tensor representation, by that vector components that transform in a covariant manner are paired with basis vectors which transform in a contravariant manner.

The metric coefficients relating the covariant and contravariant vectors are as follows:

$$\begin{aligned} g_{ij} &\equiv \frac{\partial \vec{r}}{\partial u^i} \cdot \frac{\partial \vec{r}}{\partial u^j} = \sum_l \frac{\partial x_l}{\partial u^i} \frac{\partial x_l}{\partial u^j} \\ g^{ij} &\equiv \nabla u_i \cdot \nabla u_j = \sum_l \frac{\partial u_i}{\partial x_l} \frac{\partial u_j}{\partial x_l} \end{aligned} \tag{A3.9}$$

where the metric coefficients g_{ij} (covariant metric tensor) and g^{ij} (contravariant metric tensor) specify all the lengths and angles of the bases $\frac{\partial \vec{r}}{\partial u_i}$ and ∇u_i, $i = 1,2,3$, respectively.

Vector Operators in Non-orthogonal Curvilinear Co-ordinate Systems

Gradient of a vector $\vec{v}$ in curvilinear co-ordinates is:

$$grad\vec{v} = \frac{\partial \vec{v}}{\partial x^i} \vec{e}^{\,i} \tag{A3.10}$$

The covariant derivative of the contravariant components can be written as:

$$v^k_{,i} = \frac{\partial v^k}{\partial x^i} + v^r \Gamma^k_{ir} \tag{A3.11}$$

where:

Γ_{ij}^{m} are Christoffel symbols of the second kind described by:

$$\Gamma_{ij}^{m} = g^{mk}[ij,k] \tag{A3.12}$$

and $[ij,k]$ are Christoffel symbols of the first kind:

$$[ij,k] = \frac{1}{2}\left(\frac{\partial g_{ik}}{\partial x^{j}} + \frac{\partial g_{jk}}{\partial x^{i}} + \frac{\partial g_{ij}}{\partial x^{k}}\right) \tag{A3.13}$$

It results that the gradient of a vector has the expression:

$$grad\vec{v} = v_{,i}^{k}\vec{e}_{k}\vec{e}^{\,i} \tag{A3.14}$$

Divergence of a vector $\vec{v}$ is:

$$div\vec{v} = \frac{\partial \vec{v}^{\,i}}{\partial x^{i}} \cdot \vec{e}^{\,i} \tag{A3.15}$$

or

$$div\vec{v} = v_{,i}^{i} \tag{A3.16}$$

which leads to:

$$div\vec{v} = \frac{1}{\sqrt{g}}\frac{\partial}{\partial x^{i}}\left(\sqrt{g}v^{i}\right) = \frac{1}{\sqrt{g}}\frac{\partial}{\partial x^{i}}\left(\sqrt{g}\vec{v}\cdot\vec{e}^{\,i}\right) \tag{A3.17}$$

where: $g = \det(g_{ij})$.

In covariant components, divergence of a vector is:

$$div\vec{v} = g^{ik} v_{i,k} \tag{A3.18}$$

where: $v_{k,i}$ is the covariant derivative of covariant components, defined by:

$$v_{k,i} = \frac{\partial v_k}{\partial x^i} - v^r \Gamma_{ik}^r \tag{A3.19}$$

In curvilinear co-ordinates, the curl of a vector is:

$$curl\vec{v} = \vec{e}_i \times \frac{\partial \vec{v}}{\partial x^i} \tag{A3.20}$$

Considering the following identities:

$$\begin{aligned} \vec{e}_j \times \vec{e}_k &= \sqrt{g} a_{ijk} \vec{e}^{\,i} \\ \vec{e}^{\,j} \times \vec{e}^{\,k} &= \sqrt{g} a^{ijk} \vec{e}_i \end{aligned} \tag{A3.21}$$

the curl can be written:

$$curl\vec{v} = \frac{1}{\sqrt{g}} a^{ijk} v_{k,j} \vec{e}_i \tag{A3.22}$$

where: a^{ijk} and a_{ijk} are permutation symbols and superscripted symbols used only to have a consistent notation for summation on repeated upper and lower indices.

The contravariant components of curl are as follows:

$$\left(curl\vec{v}\right)^i = \frac{1}{\sqrt{g}} \left(\frac{\partial v_k}{\partial x^j} - \frac{\partial v_j}{\partial x^k} \right) \tag{A3.23}$$

where: i, j, k are to be taken cyclically in the order 1,2,3.

APPENDIX 4

Continuity Equation Written in Various Co-ordinate Systems

In tensors form, continuity equation was obtained for incompressible flows in equation (3.6). The equation can be written in various co-ordinate systems as follows:

- **Cartesian co-ordinate system** (x, y, z) in Figure A1.1, with physical velocity components on the axes (v_x, v_y, v_z):

$$\frac{\partial v_x}{\partial x} + \frac{\partial v_y}{\partial y} + \frac{\partial v_z}{\partial z} = 0 \tag{A4.1}$$

- **Spherical co-ordinate system** (r, θ, φ) in Figure A1.2, with radius r, longitude θ, and colatitude φ, with physical velocity components on the axes $(v_r, v_\theta, v_\varphi)$:

$$\frac{1}{r\sin\theta}\frac{\partial v_\varphi}{\partial \varphi} + \frac{1}{r\sin\theta}\frac{\partial}{\partial \theta}\left(v_\theta \sin\theta\right) + \frac{1}{r^2}\frac{\partial\left(r^2 v_r\right)}{\partial r} = 0 \tag{A4.2}$$

Scale factors: $h_r = 1$; $h_\theta = r\sin\varphi$; $h_\varphi = r$. Jacobian: $J = r^2 \sin\varphi$.

- **General orthogonal curvilinear co-ordinate system** (u^1, u^2, u^3) in Figure A1.4, with physical velocity components on the axes (v_1, v_2, v_3):

$$\frac{1}{h_1 h_2 h_3}\left\{\frac{\partial}{\partial u^1}\left[h_2 h_3 v_1\right] + \frac{\partial}{\partial u^2}\left[h_1 h_3 v_2\right] + \frac{\partial}{\partial u^3}\left[h_1 h_2 v_3\right]\right\} = 0 \tag{A4.3}$$

Scale factors: h_1 ; h_2 ; h_3. Jacobian: $J = h_1 h_2 h_3$.

- **General non-orthogonal curvilinear co-ordinate system** (u^1, u^2, u^3) in Figure A3.1, with physical velocity components on the axes $v(1), v(2), v(3)$:

$$\frac{1}{g^{1/2}} \frac{\partial}{\partial u^i} \left[\left(\frac{g}{g^{ii}} \right)^{1/2} v(i) \right] = 0 , \; i = 1,2,3 \tag{A4.4}$$

Jacobian: $g^{1/2}$; g_{ii} are the first diagonal components of matrix g , which consists of typical elements g_{ij} .

APPENDIX 5

Momentum Equations Written in Various Co-ordinate Systems

In tensors form, the Navier-Stokes equation was obtained for incompressible flows in equation (3.22). Derivation of the Navier-Stokes equations in terms of physical components of the vectors, in cylindrical co-ordinate system, will be treated in Appendix 6. Equation (3.22) can be written in various Eulerian co-ordinate systems, other than cylindrical co-ordinate system, as follows:

- **Cartesian co-ordinate system** (x, y, z) in Figure A1.1, with physical velocity components v_x, v_y, v_z on the axes:

x – direction momentum equation:

$$\frac{\partial v_x}{\partial t} + v_x \frac{\partial v_x}{\partial x} + v_y \frac{\partial v_x}{\partial y} + v_z \frac{\partial v_x}{\partial z} = X - \frac{1}{\rho}\frac{\partial P}{\partial x} + \frac{\partial}{\partial x}\left(\frac{E_x}{\rho}\frac{\partial v_x}{\partial x}\right) + \frac{\partial}{\partial y}\left(\frac{E_y}{\rho}\frac{\partial v_x}{\partial y}\right) + \frac{\partial}{\partial z}\left(\frac{E_z}{\rho}\frac{\partial v_x}{\partial z}\right) \tag{A5.1}$$

y – direction momentum equation:

$$\frac{\partial v_y}{\partial t} + v_x \frac{\partial v_y}{\partial x} + v \frac{\partial v_y}{\partial y} + v_z \frac{\partial v_y}{\partial z} = Y - \frac{1}{\rho}\frac{\partial P}{\partial y} + \frac{\partial}{\partial x}\left(\frac{E_x}{\rho}\frac{\partial v_y}{\partial x}\right) + \frac{\partial}{\partial y}\left(\frac{E_y}{\rho}\frac{\partial v_y}{\partial y}\right) + \frac{\partial}{\partial z}\left(\frac{E_z}{\rho}\frac{\partial v_y}{\partial z}\right) \tag{A5.2}$$

z – direction momentum equation:

$$\frac{\partial v_z}{\partial t} + v_x \frac{\partial v_z}{\partial x} + v_y \frac{\partial v_z}{\partial y} + w \frac{\partial v_z}{\partial z} = Z - \frac{1}{\rho}\frac{\partial P}{\partial z} + \frac{\partial}{\partial x}\left(\frac{E_x}{\rho}\frac{\partial v_z}{\partial x}\right) + \frac{\partial}{\partial y}\left(\frac{E_y}{\rho}\frac{\partial v_z}{\partial y}\right) + \frac{\partial}{\partial z}\left(\frac{E_z}{\rho}\frac{\partial v_z}{\partial z}\right) \tag{A5.3}$$

where:

Symbol	Definition	Components on the three axes of a Cartesian system	Unit
V	instantaneous velocity	v_x, v_y, v_z	LT^{-1}
t	time	-	T
ρ	fluid density	-	ML^{-3}
F	body forces, acting per volume unit	X, Y, Z	MLT^{-2}
P	pressure	-	$ML^{-1}T^{-2}$
g	gravitational acceleration	-	LT^{-2}
E	eddy viscosity	E_x, E_y, E_z	$ML^{-1}T^{-1}$

- **Spherical co-ordinate system** (r, θ, φ) in Figure A1.2, with radius r, longitude θ, and colatitude φ, and physical velocity components v_r, v_θ, v_φ on the axes:

$\varphi-$ direction momentum equation:

$$\begin{aligned}&\frac{\partial v_\varphi}{\partial t}+v_r\frac{\partial v_\varphi}{\partial r}+\frac{v_\varphi}{r}\frac{\partial v_\varphi}{\partial \theta}+\frac{v_\varphi}{r\sin\theta}\frac{\partial v_\varphi}{\partial \varphi}+\frac{v_\varphi v_r\cot\theta}{r}+\frac{v_r v_\varphi}{r}\\&=f_\varphi-\frac{1}{\rho}\frac{1}{r\sin\theta}\frac{\partial p}{\partial \varphi}\\&+E_\varphi\left(\nabla^2 v_\varphi-\frac{v_\varphi}{r^2\sin^2\theta}+\frac{2}{r^2\sin\theta}\frac{\partial v_r}{\partial \varphi}+\frac{2\cos\theta}{r^2\sin^2\theta}\frac{\partial v_\theta}{\partial \varphi}\right)\end{aligned} \tag{A5.4}$$

$\theta-$ direction momentum equation:

$$\begin{aligned}&\frac{\partial v_\theta}{\partial t}+v_r\frac{\partial v_\theta}{\partial r}+\frac{v_\theta}{r}\frac{\partial v_\theta}{\partial \theta}+\frac{v_\varphi}{r\sin\theta}\frac{\partial v_\theta}{\partial \varphi}-\frac{v_\theta^2\cot\theta}{r}+\frac{v_r v_\theta}{r}\\&=f_\theta-\frac{1}{\rho}\frac{\partial p}{r\partial \theta}\\&+E_\theta\left(\nabla^2 v_\theta-\frac{v_\theta}{r^2\sin^2\theta}+\frac{2}{r^2}\frac{\partial v_r}{\partial \theta}-\frac{2\cos\theta}{r^2\sin^2\theta}\frac{\partial v_\varphi}{\partial \varphi}\right)\end{aligned} \tag{A5.5}$$

$r-$ direction momentum equation:

$$\frac{\partial v_r}{\partial t}+v_r\frac{\partial v_r}{\partial r}+\frac{v_\theta}{r}\frac{\partial v_r}{\partial \theta}+\frac{v_\varphi}{r\sin\theta}\frac{\partial v_r}{\partial \varphi}-\frac{v_\theta^2+v_\varphi^2}{r}=$$
$$=f_r-\frac{1}{\rho}\frac{\partial p}{\partial r}+ \qquad \text{(A5.6)}$$
$$+E_r\left(\nabla^2 v_r-\frac{2}{r^2}\frac{\partial v_\theta}{\partial \theta}-\frac{2v_r}{r^2}-\frac{2v_\theta\cot\theta}{r^2}-\frac{2}{r^2\sin^2\theta}\frac{\partial v_\varphi}{\partial \varphi}\right)$$

Scale factors: $h_r=1$; $h_\theta=r\sin\varphi$; $h_\varphi=r$. Jacobian: $J=r^2\sin\varphi$. Laplacian:

$$\nabla^2=\frac{1}{r^2}\frac{\partial}{\partial r}\left(r^2\frac{\partial}{\partial r}\right)+\frac{1}{r^2\sin\theta}\frac{\partial}{\partial \theta}\left(\sin\theta\frac{\partial}{\partial \theta}\right)+\frac{1}{r^2\sin^2\theta}\frac{\partial^2}{\partial \varphi^2} \qquad \text{(A5.7)}$$

where:

Symbol	**Definition**	**Components in r, θ and φ directions**	**Unit**
V	instantaneous velocity	v_r, v_θ, v_φ	LT^{-1}
F	body forces, acting per volume unit	f_r, f_θ, f_φ	MLT^{-2}
E	eddy viscosity/diffusivity	E_r, E_θ, E_φ	$ML^{-1}T^{-1}$

- **General orthogonal co-ordinate system** (u^1,u^2,u^3) in Figure A1.4 with physical velocity components $v(1),v(2),v(3)$ on the axes:

u^1- direction momentum equation:

$$\frac{\partial v(1)}{\partial t}+\frac{v(1)}{h_1}\left[\frac{\partial v(1)}{\partial u^1}\right]+\frac{v(2)}{h_2}\left[\frac{\partial v(1)}{\partial u^2}+\frac{v(1)}{h_1}\frac{\partial h_1}{\partial u^2}-\frac{v(2)}{h_1}\frac{\partial h_2}{\partial u^1}\right]$$
$$+\frac{v(3)}{h_3}\left[\frac{\partial v(1)}{\partial u^3}+\frac{v(1)}{h_1}\frac{\partial h_1}{\partial u^3}-\frac{v(3)}{h_1}\frac{\partial h_3}{\partial u^1}\right] \qquad \text{(A5.8)}$$
$$=f(1)-\frac{1}{\rho}\frac{1}{h_1}\frac{\partial p}{\partial u^1}+E_1h_1\nabla^2\left[h_1v(1)\right]$$

u^2 – direction momentum equation:

$$\frac{\partial v(2)}{\partial t}+\frac{v(1)}{h_1}\left[\frac{\partial v(2)}{\partial u^1}+\frac{v(2)}{h_2}\frac{\partial h_2}{\partial u^1}-\frac{v(1)}{h_2}\frac{\partial h_1}{\partial u^2}\right]+\frac{v(2)}{h_2}\left[\frac{\partial v(2)}{\partial u^2}\right]$$
$$+\frac{v(3)}{h_3}\left[\frac{\partial v(2)}{\partial u^3}+\frac{v(2)}{h_2}\frac{\partial h_2}{\partial u^3}-\frac{v(3)}{h_2}\frac{\partial h_3}{\partial u^2}\right] \qquad \text{(A5.9)}$$
$$= f(2)-\frac{1}{\rho}\frac{1}{h_2}\frac{\partial p}{\partial u^2}+E_2 h_2\nabla^2\left[h_2 v(2)\right]$$

u^3 – direction momentum equation:

$$\frac{\partial v(3)}{\partial t}+\frac{v(1)}{h_1}\left[\frac{\partial v(3)}{\partial u^1}+\frac{v(3)}{h_3}\frac{\partial h_3}{\partial u^1}-\frac{v(1)}{h_3}\frac{\partial h_1}{\partial u^3}\right]$$
$$+\frac{v(2)}{h_2}\left[\frac{\partial v(3)}{\partial u^2}+\frac{v(3)}{h_3}\frac{\partial h_3}{\partial u^2}-\frac{v(2)}{h_3}\frac{\partial h_2}{\partial u^3}\right]+\frac{v(3)}{h_3}\left[\frac{\partial v(2)}{\partial u^2}\right] \qquad \text{(A5.10)}$$
$$= f(3)-\frac{1}{\rho}\frac{1}{h_3}\frac{\partial p}{\partial u^3}+E_3 h_3\nabla^2\left[h_3 v(3)\right]$$

Scale factors: h_1; h_2; h_3. Jacobian: $J = h_1 h_2 h_3$.

Vector Laplacian in general orthogonal curvilinear co-ordinates has the expression:

$$\nabla^2\vec{V}$$
$$=\left\{\frac{1}{h_1}\frac{\partial}{\partial u^1}\left\{\frac{1}{J}\frac{\partial}{\partial u^1}\left[v(1)\frac{J}{h_1}\right]+\frac{1}{J}\frac{\partial}{\partial u^2}\left[v(2)\frac{J}{h_2}\right]\right.\right.$$
$$\left.\left.+\frac{1}{J}\frac{\partial}{\partial u^3}\left[\frac{J}{h_3}v(3)\right]\right\}-\frac{1}{h_2}\frac{\partial}{\partial u^2}\left\{\frac{1}{h_1}\frac{\partial v(2)}{\partial u^1}-\frac{1}{h_2}\frac{\partial v(1)}{\partial u^2}\right.\right.$$
$$\left.\left.+\frac{h_3}{J}\left[v(2)\frac{\partial h_2}{\partial u^1}-v(1)\frac{\partial h_1}{\partial u^2}\right]\right\}+\left\{\frac{1}{h_3}\frac{\partial v(1)}{\partial u^3}-\frac{1}{h_1}\frac{\partial v(3)}{\partial u^1}\right. \qquad \text{(A5.12)}$$
$$\left.+\frac{h_2}{J}\left[v(1)\frac{\partial h_1}{\partial u^3}-v(3)\frac{\partial h_3}{\partial u^1}\right]\right\}\frac{h_1}{J}\frac{\partial h_2}{\partial u^3}$$
$$+\frac{1}{h_3}\frac{\partial}{\partial u^3}\left\{\frac{1}{h_3}\frac{\partial v(1)}{\partial u^3}-\frac{1}{h_1}\frac{\partial v(3)}{\partial u^1}\right.$$
$$\left.+\frac{h_2}{J}\left[v(1)\frac{\partial h_1}{\partial u^3}-v(3)\frac{\partial h_3}{\partial u^1}\right]\right\}-\left\{\frac{1}{h_1}\frac{\partial v(2)}{\partial u^1}-\frac{1}{h_2}\frac{\partial v(1)}{\partial u^2}\right.$$

$$
\begin{aligned}
&+\frac{h_3}{J}\left[v(2)\frac{\partial h_2}{\partial u^1}-v(1)\frac{\partial h_1}{\partial u^2}\right]\Bigg\}\frac{h_1}{J}\frac{\partial h_3}{\partial u^2}\Bigg\}\vec{e}_{\xi^1}\\
&+\left\{\frac{1}{h_2}\frac{\partial}{\partial u^2}\left\{\frac{1}{J}\frac{\partial}{\partial u^1}\left[v(1)\frac{J}{h_1}\right]+\frac{1}{J}\frac{\partial}{\partial u^2}\left[v(2)\frac{J}{h_2}\right]\right.\right.\\
&\left.\left.+\frac{1}{J}\frac{\partial}{\partial u^3}\left[\frac{J}{h_3}v(3)\right]\right\}-\frac{1}{h_3}\frac{\partial}{\partial u^3}\left\{\frac{1}{h_2}\frac{\partial v(3)}{\partial u^2}-\frac{1}{h_3}\frac{\partial v(2)}{\partial u^3}\right.\right.\\
&\left.\left.+\frac{1}{h_2h_3}\left[v(3)\frac{\partial h_3}{\partial u^2}-v(2)\frac{\partial h_2}{\partial u^3}\right]\right\}+\left\{\frac{1}{h_1}\frac{\partial v(2)}{\partial u^1}-\frac{1}{h_2}\frac{\partial v(1)}{\partial u^2}\right.\right.\\
&\left.\left.+\frac{1}{h_1h_2}\left[v(2)\frac{\partial h_2}{\partial u^1}-v(1)\frac{\partial h_1}{\partial u^2}\right]\right\}\frac{1}{h_1h_3}\frac{\partial h_3}{\partial u^1}\right.\\
&+\frac{1}{h_1}\frac{\partial}{\partial u^1}\left\{\frac{1}{h_1}\frac{\partial v(2)}{\partial u^1}-\frac{1}{h_2}\frac{\partial v(1)}{\partial u^2}\right.\\
&\left.+\frac{1}{h_1h_2}\left[v(2)\frac{\partial h_2}{\partial u^1}-v(1)\frac{\partial h_1}{\partial u^2}\right]\right\}-\left\{\frac{1}{h_2}\frac{\partial v(3)}{\partial u^2}-\frac{1}{h_3}\frac{\partial v(2)}{\partial u^3}\right.\\
&\left.+\frac{1}{h_2h_3}\left[v(3)\frac{\partial h_3}{\partial u^2}-v(2)\frac{\partial h_2}{\partial u^3}\right]\right\}\frac{1}{h_1h_3}\frac{\partial h_1}{\partial u^3}\Bigg\}\vec{e}_{\xi^2}\\
&+\left\{\frac{1}{h_3}\frac{\partial}{\partial u^3}\left\{\frac{1}{J}\frac{\partial}{\partial u^1}\left[v(1)\frac{J}{h_1}\right]+\frac{1}{J}\frac{\partial}{\partial u^2}\left[v(2)\frac{J}{h_2}\right]\right.\right.\\
&\left.\left.+\frac{1}{J}\frac{\partial}{\partial u^3}\left[\frac{J}{h_3}v(3)\right]\right\}-\frac{1}{h_1}\frac{\partial}{\partial u^1}\left\{\frac{1}{h_3}\frac{\partial v(1)}{\partial u^3}-\frac{1}{h_1}\frac{\partial v(3)}{\partial u^1}\right.\right.\\
&\left.\left.+\frac{h_2}{J}\left[v(1)\frac{\partial h_1}{\partial u^3}-v(3)\frac{\partial h_3}{\partial u^1}\right]\right\}+\left\{\frac{1}{h_2}\frac{\partial v(3)}{\partial u^2}-\frac{1}{h_3}\frac{\partial v(2)}{\partial u^3}\right.\right.\\
&\left.\left.+\frac{h_1}{J}\left[v(3)\frac{\partial h_3}{\partial u^2}-v(2)\frac{\partial h_2}{\partial u^3}\right]\right\}\frac{h_3}{J}\frac{\partial h_1}{\partial u^2}\right.\\
&+\frac{1}{h_2}\frac{\partial}{\partial u^2}\left\{\frac{1}{h_2}\frac{\partial v(3)}{\partial u^2}-\frac{1}{h_3}\frac{\partial v(2)}{\partial u^3}\right.\\
&\left.+\frac{h_1}{J}\left[v(3)\frac{\partial h_3}{\partial u^2}-v(2)\frac{\partial h_2}{\partial u^3}\right]\right\}-\left\{\frac{1}{h_3}\frac{\partial v(1)}{\partial u^3}-\frac{1}{h_1}\frac{\partial v(3)}{\partial u^1}\right.\\
&\left.+\frac{h_2}{J}\left[v(1)\frac{\partial h_1}{\partial u^3}-v(3)\frac{\partial h_3}{\partial u^1}\right]\right\}\frac{h_3}{J}\frac{\partial h_2}{\partial u^1}\Bigg\}\vec{e}_{\xi^3}
\end{aligned}
\qquad \text{(A5.12)}
$$

continued

where:

Symbol	Definition	Components in u^1, u^2 and u^3 directions	Unit
V	instantaneous velocity	v^1, v^2, v^3	LT^{-1}
F	body forces, acting per volume unit	f^1, f^2, f^3	MLT^{-2}
E	eddy viscosity/diffusivity	E_1, E_2, E_3	$ML^{-1}T^{-1}$

- **General non-orthogonal co-ordinate system** (u^1, u^2, u^3) in Figure A3.1, with physical velocity components on the axes $v(1), v(2), v(3)$:

u^i – direction momentum equation:

$$g_{ii}^{1/2}\left\{\frac{\partial\left[v(i)/\,g_{ii}^{1/2}\right]}{\partial t}+\frac{\partial\left[v(i)/\,g_{ii}^{1/2}\right]}{\partial u^j}\frac{v(j)}{g_{jj}^{1/2}}\right.$$
$$\left.+\frac{1}{g_{jj}^{1/2}g_{kk}^{1/2}}\left\{\begin{matrix} i \\ j \quad k \end{matrix}\right\}v(j)v(k)\right\} \qquad \text{(A5.13)}$$
$$= f(i)-\frac{1}{\rho}g_{ii}^{1/2}g^{ij}p_{,j}+E_i g_{ii}^{1/2}\nabla^2\left[g_{ii}^{1/2}v(i)\right]$$

for $i=1,2,3$, $j=1,2,3$.

Jacobian: $g^{1/2}$; in two dimensions it can be written: $g^{1/2}=g_{11}g_{22}-g_{12}g_{21}$.

g_{ii} are the main diagonal components of matrix g, with typical elements

$$g_{ij}=\sum_{k=1}^{3}\frac{\partial y^k}{\partial x^i}\frac{\partial y^k}{\partial x^j};$$

$\left\{\begin{matrix} i \\ j \quad k \end{matrix}\right\}$ are Christoffel symbols of the second kind.

Vector Laplacian in general non-orthogonal curvilinear co-ordinates can be derived in terms of physical components of the vectors from:

$$\nabla^2\vec{v}=grad(div\vec{v})-curl\left(curl\vec{v}\right) \qquad \text{(A5.14)}$$

APPENDIX 6

Derivation of Fundamental Equations of Hydrodynamics in Cylindrical Polar Co-ordinates

In the following derivation the summation convention is used. According to this convention, any index repeated once in the upper position and once in the lower position in a product of terms is called a dummy index and held to be summed over the range of its values [equation (A3.4)]. Any index not repeated is called free and may take any value in its range.

Present derivation follows the work of Aris (1989) in terms of general orthogonal curvilinear co-ordinates with application to cylindrical co-ordinates. Cartesian co-ordinates for derivation of the hydrodynamic equations in cylindrical co-ordinates are:

$$\begin{aligned} x &= r\cos\theta \\ y &= r\sin\theta \\ z_{Cartesian} &= z_{cylindrical} \end{aligned} \qquad \text{(A6.1)}$$

Cylindrical co-ordinates r, θ, z can be written as:

$$\begin{aligned} r &= \sqrt{x^2 + y^2} \\ \theta &= \tan^{-1}\frac{y}{x} \\ z_{cylindrical} &= z_{Cartesian} \end{aligned} \qquad \text{(A6.2)}$$

Throughout the text the cylindrical co-ordinates are also written as: $\bar{x}^i$, $i = 1,2,3$, with $\bar{x}^1 = r$; $\bar{x}^2 = \theta$; $\bar{x}^3 = z$. Similarly, Cartesian co-ordinates are written in tensor notation: x^j, $j = 1,2,3$, with: $x^1 = x$; $x^2 = y$; $x^3 = z$.

Partial derivatives of the Cartesian co-ordinates with respect to cylindrical co-ordinates are:

$$\frac{\partial x}{\partial r}=\cos\theta \qquad \frac{\partial x}{\partial \theta}=-r\sin\theta \qquad \frac{\partial x}{\partial z_{cylindrical}}=0$$
$$\frac{\partial y}{\partial r}=\sin\theta \qquad \frac{\partial y}{\partial \theta}=r\cos\theta \qquad \frac{\partial y}{\partial z_{cylindrical}}=0 \tag{A6.3}$$
$$\frac{\partial z_{Cartesian}}{\partial r}=0 \qquad \frac{\partial z_{Cartesian}}{\partial \theta}=0 \qquad \frac{\partial z_{Cartesian}}{\partial z_{cylindrical}}=1$$

Partial derivatives of cylindrical co-ordinates with respect to Cartesian co-ordinates are:

$$\frac{\partial r}{\partial x}=\frac{x}{\sqrt{(x)^2+(y)^2}} \qquad \frac{\partial r}{\partial y}=\frac{y}{\sqrt{(x)^2+(y)^2}} \qquad \frac{\partial r}{\partial z_{Cartesian}}=0$$
$$\frac{\partial \theta}{\partial x}=-\frac{y}{(x)^2+(y)^2} \qquad \frac{\partial \theta}{\partial y}=\frac{x}{(x)^2+(y)^2} \qquad \frac{\partial \theta}{\partial z_{Cartesian}}=0 \tag{A6.4}$$
$$\frac{\partial z_{cylindrical}}{\partial x}=0 \qquad \frac{\partial z_{cylindrical}}{\partial y}=0 \qquad \frac{\partial z_{cylindrical}}{\partial z_{Cartesian}}=1$$

or:

$$\frac{\partial r}{\partial x}=\frac{r\cos\theta}{r}=\cos\theta \qquad \frac{\partial r}{\partial y}=\frac{r\sin\theta}{r}=\sin\theta \qquad \frac{\partial r}{\partial z_{Cartesian}}=0$$
$$\frac{\partial \theta}{\partial x}=-\frac{\sin\theta}{r} \qquad \frac{\partial \theta}{\partial y}=\frac{\cos\theta}{r} \qquad \frac{\partial \theta}{\partial z_{Cartesian}}=0 \tag{A6.5}$$
$$\frac{\partial z_{cylindrical}}{\partial x}=0 \qquad \frac{\partial z_{cylindrical}}{\partial y}=0 \qquad \frac{\partial z_{cylindrical}}{\partial z_{Cartesian}}=1$$

In the Cartesian co-ordinate system, the distance between two points can be represented as:

$$ds^2=dx^2+dy^2+dz^2 \tag{A6.6}$$

The same distance in the general curvilinear orthogonal co-ordinate system can be defined:

$$ds^2 = g_{ij} d\bar{x}^i d\bar{x}^j \tag{A6.7}$$

The co-ordinate metric tensor, which defines the relationship between distance and the infinitesimal co-ordinate increments, can be written:

$$g_{ij} = \sum_{k=1}^{3} \frac{\partial x^k}{\partial \bar{x}^i} \frac{\partial x^k}{\partial \bar{x}^j} \tag{A6.8}$$

The orthogonal co-ordinates have a special property:

$$g_{ii} = h_i^2 \tag{A6.9}$$

where h_i are called scale factors. The scale factors represent the ratio of distance to co-ordinate difference.

The values g_{ij} of the metric tensor of the transformation from Cartesian co-ordinates to cylindrical co-ordinates are:

$$\begin{aligned}
g_{11} &= \frac{\partial x^1}{\partial \bar{x}^1} \frac{\partial x^1}{\partial \bar{x}^1} + \frac{\partial x^2}{\partial \bar{x}^1} \frac{\partial x^2}{\partial \bar{x}^1} + \frac{\partial x^3}{\partial \bar{x}^1} \frac{\partial x^3}{\partial \bar{x}^1} \\
g_{11} &= \cos^2 \bar{x}^2 + \sin^2 \bar{x}^2 \\
g_{11} &= 1 \\
g_{22} &= \frac{\partial x^1}{\partial \bar{x}^2} \frac{\partial x^1}{\partial \bar{x}^2} + \frac{\partial x^2}{\partial \bar{x}^2} \frac{\partial x^2}{\partial \bar{x}^2} + \frac{\partial x^3}{\partial \bar{x}^2} \frac{\partial x^3}{\partial \bar{x}^2} \\
g_{22} &= \left(\bar{x}^1\right)^2 \cos^2 \bar{x}^2 + \left(\bar{x}^1\right)^2 \sin^2 \bar{x}^2 \\
g_{22} &= \left(\bar{x}^1\right)^2 \leftrightarrow \bar{g}_{22} = r^2 \\
g_{33} &= \frac{\partial x^1}{\partial \bar{x}^3} \frac{\partial x^1}{\partial \bar{x}^3} + \frac{\partial x^2}{\partial \bar{x}^3} \frac{\partial x^2}{\partial \bar{x}^3} + \frac{\partial x^3}{\partial \bar{x}^3} \frac{\partial x^3}{\partial \bar{x}^3} \\
g_{33} &= 1
\end{aligned} \tag{A6.10}$$

$$
\begin{aligned}
g_{12} = g_{21} &= \frac{\partial x^1}{\partial \bar{x}^1}\frac{\partial x^1}{\partial \bar{x}^2} + \frac{\partial x^2}{\partial \bar{x}^1}\frac{\partial x^2}{\partial \bar{x}^2} + \frac{\partial x^3}{\partial \bar{x}^1}\frac{\partial x^3}{\partial \bar{x}^2} \\
g_{12} = g_{21} &= \left(-\bar{x}^1 \sin \bar{x}^2\right)\cos \bar{x}^2 + \sin \bar{x}^2 \left(\bar{x}^1 \cos \bar{x}^2\right) \\
g_{12} = g_{21} &= 0 \\
g_{13} = g_{31} &= \frac{\partial x^1}{\partial \bar{x}^1}\frac{\partial x^1}{\partial \bar{x}^3} + \frac{\partial x^2}{\partial \bar{x}^1}\frac{\partial x^2}{\partial \bar{x}^3} + \frac{\partial x^3}{\partial \bar{x}^1}\frac{\partial x^3}{\partial \bar{x}^3} \\
g_{13} = g_{31} &= \left(\cos \bar{x}^2\right)\cdot 0 + \left(\sin \bar{x}^2\right)\cdot 0 + 0 \cdot 1 \\
g_{13} = g_{31} &= 0 \\
g_{23} = g_{32} &= \frac{\partial x^1}{\partial \bar{x}^2}\frac{\partial x^1}{\partial \bar{x}^3} + \frac{\partial x^2}{\partial \bar{x}^2}\frac{\partial x^2}{\partial \bar{x}^3} + \frac{\partial x^3}{\partial \bar{x}^2}\frac{\partial x^3}{\partial \bar{x}^3} \\
g_{23} = g_{32} &= \left(-\bar{x}^1 \sin \bar{x}^2\right)\cdot 0 + \left(\bar{x}^1 \cos \bar{x}^2\right)\cdot 0 + 0 \cdot 1 \\
g_{23} = g_{32} &= 0
\end{aligned}
\qquad \text{(A6.10)}
$$

continued

The scale factors are defined as follows:

$$
\begin{aligned}
h_r &= \sqrt{g_{11}} = 1 \\
h_\theta &= \sqrt{g_{22}} = r \\
h_z &= \sqrt{g_{33}} = 1
\end{aligned}
\qquad \text{(A6.11)}
$$

Since θ is an angle, variation of distance in the angular direction can be written as $ds = h_\theta d\theta = r d\theta$.

The Jacobian is the ratio of an elementary material volume to its initial volume, also known as dilatation or expansion:

$$
\bar{J} = \begin{vmatrix}
\dfrac{\partial \bar{x}^1}{\partial x^1} & \dfrac{\partial \bar{x}^2}{\partial x^1} & \dfrac{\partial \bar{x}^3}{\partial x^1} \\
\dfrac{\partial \bar{x}^1}{\partial x^2} & \dfrac{\partial \bar{x}^2}{\partial x^2} & \dfrac{\partial \bar{x}^3}{\partial x^2} \\
\dfrac{\partial \bar{x}^1}{\partial x^3} & \dfrac{\partial \bar{x}^2}{\partial x^3} & \dfrac{\partial \bar{x}^3}{\partial x^3}
\end{vmatrix}
\qquad \text{(A6.12)}
$$

The Jacobian of the transformation to **Cartesian co-ordinates** is:

$$J = \begin{vmatrix} \dfrac{\partial x}{\partial r} & \dfrac{\partial y}{\partial r} & \dfrac{\partial z_{Cartesian}}{\partial r} \\ \dfrac{\partial x}{\partial \theta} & \dfrac{\partial y}{\partial \theta} & \dfrac{\partial z_{Cartesian}}{\partial \theta} \\ \dfrac{\partial x}{\partial z_{cylindrical}} & \dfrac{\partial y}{\partial z_{cylindrical}} & \dfrac{\partial z_{Cartesian}}{\partial z_{cylindrical}} \end{vmatrix} \tag{A6.13}$$

$$J = \frac{\partial x}{\partial r}\left(\frac{\partial y}{\partial \theta}\frac{\partial z_{Cartesian}}{\partial z_{cylindrical}} - \frac{\partial z_{Cartesian}}{\partial \theta}\frac{\partial y}{\partial z_{cylindrical}}\right)$$
$$- \frac{\partial y}{\partial r}\left(\frac{\partial x}{\partial \theta}\frac{\partial z_{Cartesian}}{\partial z_{cylindrical}} - \frac{\partial z_{Cartesian}}{\partial \theta}\frac{\partial x}{\partial z_{cylindrical}}\right)$$
$$+ \frac{\partial z_{Cartesian}}{\partial r}\left(\frac{\partial x}{\partial \theta}\frac{\partial y}{\partial z_{cylindrical}} - \frac{\partial y}{\partial \theta}\frac{\partial x}{\partial z_{cylindrical}}\right) \tag{A6.13}$$
continued

$$J = \frac{\partial x}{\partial r}\frac{\partial y}{\partial \theta} - \frac{\partial x}{\partial \theta}\frac{\partial y}{\partial r}$$
$$J = (\cos\theta) r\cos\theta - (-r\sin\theta)\sin\theta$$
$$J = r\left(\cos^2\theta + \sin^2\theta\right)$$
$$J = r$$

Let:

$$g = \det\left(g_{ij}\right) \tag{A6.14}$$

$$g = \begin{vmatrix} g_{11} & g_{12} & g_{13} \\ g_{21} & g_{22} & g_{23} \\ g_{31} & g_{32} & g_{33} \end{vmatrix} \leftrightarrow \bar{g} = \begin{vmatrix} 1 & 0 & 0 \\ 0 & r^2 & 0 \\ 0 & 0 & 1 \end{vmatrix}$$
$$g = g_{11}\left(g_{22}g_{33} - g_{23}g_{32}\right) - g_{12}\left(g_{21}g_{33} - g_{23}g_{31}\right) +$$
$$+ g_{13}\left(g_{21}g_{32} - g_{22}g_{31}\right) \tag{A6.15}$$
$$g = r^2$$

This means that the scalar g is the square of the Jacobian $\left|\dfrac{\partial x}{\partial \bar{x}}\right|$ of the transformation from **cylindrical co-ordinates** to **Cartesian co-ordinates**. By definition, $\sqrt{g}$ is the length of the normal to the plane containing two covariant tangents.

Contravariant vectors

The velocity vector transforms from Cartesian co-ordinates (x^j , $j = x, y, z$) to cylindrical co-ordinates ($\bar{x}^i$, $i = r, \theta, z$) according to:

$$\bar{v}^i = \frac{\partial \bar{x}^i}{\partial x^j} v^j \qquad \text{with single summation on } j \tag{A6.16}$$

resulting in:

$$\begin{aligned}
&v^r = \frac{\partial r}{\partial x} v^x + \frac{\partial r}{\partial y} v^y + \frac{\partial r}{\partial z_{Cartesian}} v^z \rightarrow v^r = v^x \cos\theta + v^y \sin\theta \\
&v^\theta = r\frac{\partial \theta}{\partial x} v^x + r\frac{\partial \theta}{\partial y} v^y + r\frac{\partial \theta}{\partial z} v^z \rightarrow v^\theta = -v^x \sin\theta + v^y \cos\theta \\
&\left(v^z\right)_{cylindrical} = \frac{\partial z_{cylindrical}}{\partial x} v^x + \frac{\partial z_{cylindrical}}{\partial y} v^y + \frac{\partial z_{cylindrical}}{\partial z_{Cartesian}} v^z \\
&\rightarrow \left(v^z\right)_{cylindrical} = \left(v^z\right)_{Cartesian}
\end{aligned} \tag{A6.17}$$

Going from cylindrical co-ordinates to Cartesian co-ordinates, contravariant vector transformation relationships can be written as:

$$v^j = \frac{\partial x^j}{\partial \bar{x}^i} \bar{v}^i \tag{A6.18}$$

or:

$$\begin{aligned}
&v^x = \frac{\partial x}{\partial r} v^r + \frac{\partial x}{\partial \theta} v^\theta + \frac{\partial x}{\partial z} v^z \rightarrow v^x = v^r \cos\theta - v^\theta r \sin\theta \\
&v^y = \frac{\partial y}{\partial r} v^r + \frac{\partial y}{\partial \theta} v^\theta + \frac{\partial y}{\partial z} v^z \rightarrow v^y = v^r \sin\theta + v^\theta r \cos\theta \\
&\left(v^z\right)_{Cartesian} = \frac{\partial z}{\partial r} v^r + \frac{1}{r}\frac{\partial z}{\partial \theta} v^\theta + \frac{\partial z}{\partial z} v^z \rightarrow \left(v^z\right)_{Cartesian} = \left(v^z\right)_{cylindrical}
\end{aligned} \tag{A6.19}$$

Figure A6.1 illustrates transformation of vector components from Cartesian to cylindrical co-ordinate system and vice versa:

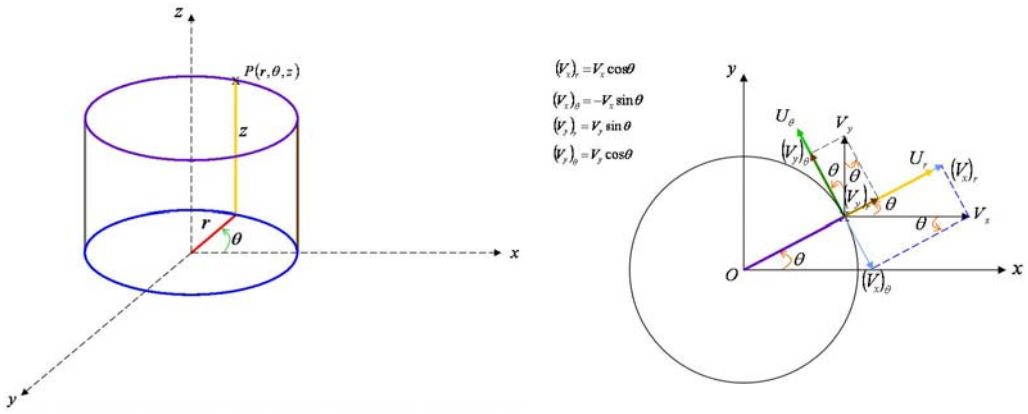

Figure A6.1. Graphical transformation of vector components from cylindrical co-ordinates to Cartesian co-ordinates.

Physical components of a vector in orthogonal co-ordinate systems:

For a general orthogonal system the magnitude of a vector can be written as:

$$|A|^2 = \left(h_1 A^1\right)^2 + \left(h_2 A^2\right)^2 + \left(h_3 A^3\right)^2 \tag{A6.20}$$

where:

A^i, $i = 1,2,3$ are contravariant components of the vector;

h_i, $i = 1,2,3$ are the scale factors.

This approach ensures that $h_i A^i$ have the same physical dimensions as the magnitude of the vector A.

The unit contravariant vectors, tangent to the three co-ordinate lines, are:

$$e^i_{(1)} = \frac{\delta^i_1}{h_1}, \quad e^i_{(2)} = \frac{\delta^i_2}{h_2}, \quad e^i_{(3)} = \frac{\delta^i_3}{h_3} \tag{A6.21}$$

If the contravariant vector A^i is represented as a linear combination of these base vectors:

$$A^i = A(1)e^i_{(1)} + A(2)e^i_{(2)} + A(3)e^i_{(3)} \tag{A6.22}$$

which gives:

$$A(1) = h_1 A^1, \quad A(2) = h_2 A^2, \quad A(3) = h_3 A^3 \tag{A6.23}$$

where:

$A(i)$ are called the physical components of the contravariant vector A^i, with the same physical dimensions as the magnitude of A.

The physical components of a covariant vector A_i can be constructed in the same way by the representation:

$$A_i = A(1)e_{(1)i} + A(2)e_{(2)i} + A(3)e_{(3)i} \tag{A6.24}$$

Since $e_{(j)i} = \delta_i^j h_j$, we have:

$$A(1) = \frac{A_1}{h_1}, \quad A(2) = \frac{A_2}{h_2}, \quad A(3) = \frac{A_3}{h_3} \tag{A6.25}$$

However, $A_1 = h_1^2 A^1$, etc, so that both of these sets of formulae define the same physical components. Physical components do not transform as tensors. Their transformation law in a new co-ordinate system $\overline{A}(i) = \overline{h}_i \overline{A}^i$ is:

$$\overline{A}(i) = \overline{h}_i \overline{A}^i = \overline{h}_i \frac{\partial \overline{x}^i}{\partial x^j} A^j = \frac{\overline{h}_i}{h^j} \frac{\partial \overline{x}^i}{\partial x^j} A(j) \tag{A6.26}$$

Where there is no sum on i but a single summation on j. Consider the angle θ_{ij} between $\overline{e}^p_{(i)}$ in the new co-ordinate system and $e^q_{(j)}$ in the old. This angle can be calculated by bringing both unit vectors into the same co-ordinate system. In the new co-ordinate system $e^q_{(j)}$ becomes:

$$\bar{e}^{r}_{(j)} = \frac{\partial \bar{x}^{r}}{\partial x^{q}} e^{q}_{(j)} = \frac{1}{h_j} \frac{\partial \bar{x}^{r}}{\partial x^{j}} \tag{A6.27}$$

However this is a unit vector since:

$$\bar{g}_{rs} \bar{e}^{r}_{(j)} \bar{e}^{s}_{(j)} = \frac{1}{h_j} \bar{g}_{rs} \frac{\partial \bar{x}^{r}}{\partial x^{j}} \frac{\partial \bar{x}^{s}}{\partial x^{j}} = \frac{1}{h_j^2} \bar{g}_{jj} = 1 \tag{A6.28}$$

And so θ_{ij} is given by:

$$\begin{aligned} \cos\theta_{ij} &= \bar{g}_{pr} \bar{e}^{p}_{(i)} \bar{e}^{r}_{(j)} = \bar{h}_i^{2} \left(\frac{1}{\bar{h}_i} \right) \left(\frac{1}{h_j} \frac{\partial \bar{x}^{i}}{\partial x^{j}} \right) \\ \cos\theta_{ij} &= \frac{\bar{h}_i}{h^{j}} \frac{\partial \bar{x}^{i}}{\partial x^{j}} \end{aligned} \tag{A6.29}$$

Hence the transformation law for physical components can be written:

$$\bar{A}(i) = \cos\theta_{ij} A(j) \tag{A6.30}$$

Equation (A6.30) gives the transformation law for physical components as the sum of projections of the three components on the new direction. In Cartesian systems the physical, covariant and contravariant components are identical. It can be shown that the physical components are the lengths of projections of a vector on the tangents to the co-ordinate lines in orthogonal systems, which can be written:

$$|A||B|\cos\theta = \sum_{i=1}^{3} A(i) B(i) \tag{A6.31}$$

Physical components of tensors:

Higher order tensors usually occur in such formulae as that for stress, defined by $t^i = p^i_j n^j$. The purpose of this section is to show that stress can be written in terms of physical components as $t(i) = p(ij)n(j)$. In an orthogonal co-ordinate system, physical components of a tensor are:

$$t(i) = h_i t^i = h_i p^i_{.j} n^j = \frac{h_i}{h_j} p^i_{.j} n(j) \tag{A6.32}$$

So that the following relationship can be written:

$$p(ij) = \frac{h_i}{h_j} p^i_{.j} \tag{A6.33}$$

In equation (A6.33) each index can be treated as the corresponding covariant or contravariant index of the vector:

$$A(ijk) = \frac{h_i h_j A^{ij}_k}{h_k} \tag{A6.34}$$

where none of the indices is summed. In orthogonal co-ordinate systems, the physical components of tensors $p^i_{.j}$ and $p^j_{i.}$ use the same representation since:

$$p(ij) = \frac{h_i}{h_j} p^i_{.j} = \frac{h_i}{h_j} g^{im} g_{jn} p^n_{m.} = \frac{h_j}{h_i} p^j_{i.} \tag{A6.35}$$

it can be observed that the diagonal elements of a mixed second order tensor are the same as their physical components:

$$p(ii) = p^i_{.i} = p^i_{i.} \tag{A6.36}$$

where the equations for $p^{i}_{.j}$ and $p^{j}_{i.}$ can be derived from the following formulae:

$$T^{ij}_{.k} = \frac{\partial T^{ij}}{\partial x^k} + \Gamma^{i}_{mk} T^{mj} + \Gamma^{j}_{mk} T^{im} \tag{A6.37}$$

$$T_{ij.k} = \frac{\partial T^{ij}}{\partial x^k} - \Gamma^{m}_{ik} T_{mj} - \Gamma^{m}_{jk} T_{im} \tag{A6.38}$$

$$T^{i}_{j.k} = \frac{\partial T^{i}_{j}}{\partial x^k} + \Gamma^{i}_{mk} T^{m}_{j} - \Gamma^{m}_{jk} T^{i}_{m} \tag{A6.39}$$

$$p^{i}_{,j} = \frac{\partial p^{i}}{\partial x^j} + \left\{ \begin{matrix} i \\ j \quad k \end{matrix} \right\} p^{k} \tag{A6.40}$$

$$T^{j}_{i.} = g_{ik} T^{kj} \tag{A6.41}$$

Christoffel symbols:

By definition, the metric coefficients are given by equations (A6.6). Derivatives of g_{ij} can be written:

$$\begin{aligned}
\frac{\partial g_{ij}}{\partial x^k} &= \sum_{p=1}^{3} \left[\frac{\partial^2 y^p}{\partial x^i \partial x^k} \frac{\partial y^p}{\partial x^j} + \frac{\partial y^p}{\partial x^i} \frac{\partial^2 y^p}{\partial x^j \partial x^k} \right] \\
\frac{\partial g_{ik}}{\partial x^j} &= \sum_{p=1}^{3} \left[\frac{\partial^2 y^p}{\partial x^i \partial x^j} \frac{\partial y^p}{\partial x^k} + \frac{\partial y^p}{\partial x^i} \frac{\partial^2 y^p}{\partial x^j \partial x^k} \right] \\
\frac{\partial g_{jk}}{\partial x^i} &= \sum_{p=1}^{3} \left[\frac{\partial^2 y^p}{\partial x^i \partial x^j} \frac{\partial y^p}{\partial x^k} + \frac{\partial y^p}{\partial x^j} \frac{\partial^2 y^p}{\partial x^i \partial x^k} \right]
\end{aligned} \tag{A6.42}$$

From which the expression of the Christoffel symbol of the first kind is obtained:

$$[jk,i]=\sum_{p=1}^{3}\frac{\partial^2 y^p}{\partial x^i \partial x^j}\frac{\partial y^p}{\partial x^k}=\frac{1}{2}\left(\frac{\partial g_{ij}}{\partial x^k}+\frac{\partial g_{ik}}{\partial x^j}-\frac{\partial g_{jk}}{\partial x^i}\right) \tag{A6.43}$$

The product:

$$g^{ir}[jk,i]=\frac{1}{2}g^{ir}\left(\frac{\partial g_{ri}}{\partial x^k}+\frac{\partial g_{rk}}{\partial x^j}-\frac{\partial g_{jk}}{\partial x^r}\right) \tag{A6.44}$$

is the Christoffel symbol of the second kind. The following notations are possible: $\left\{ \begin{matrix} r \\ j \quad k \end{matrix} \right\}$ or Γ_{jk}^{r}. Christoffel symbols of first and second kind are also known as connection coefficients, dependent on the co-ordinate system.

Christoffel symbols of the first and second kind transform according to the law:

$$\overline{[lm,n]}=\frac{\partial x^p}{\partial \overline{x}^l}\frac{\partial x^q}{\partial \overline{x}^m}\frac{\partial x^r}{\partial \overline{x}^n}[pq,r]+\frac{\partial^2 x^p}{\partial \overline{x}^l \partial \overline{x}^m}\frac{\partial x^q}{\partial \overline{x}^n}g_{pq} \tag{A6.45}$$

and, respectively:

$$\overline{\left\{ \begin{matrix} n \\ l \quad m \end{matrix} \right\}}=\frac{\partial x^p}{\partial \overline{x}^l}\frac{\partial x^q}{\partial \overline{x}^m}\frac{\partial x^r}{\partial \overline{x}^n}\left\{ \begin{matrix} r \\ p \quad q \end{matrix} \right\}+\frac{\partial^2 x^p}{\partial \overline{x}^l \partial \overline{x}^m}\frac{\partial x^n}{\partial \overline{x}^p} \tag{A6.46}$$

In an orthogonal system of co-ordinates $g_{pq}=0$ if $p\neq q$ and $g_{ii}=h_i^2$, the Christoffel symbols are relatively simple and involve only one term. Christoffel symbol of the first kind $[12,3]$ is zero since it is composed of derivatives of g_{12},g_{23},g_{31} which all vanish. Using equation (6.46), the two remaining non-zero Christoffel symbols are:

$$[12,1]=\frac{1}{2}\left(\frac{\partial g_{11}}{\partial x^2}+\frac{\partial g_{12}}{\partial x^1}-\frac{\partial g_{12}}{\partial x^1}\right)\Rightarrow[12,1]=\frac{1}{2}\frac{\partial\left(h_1^2\right)}{\partial x^2}\Rightarrow[12,1]=h_1\frac{\partial h_1}{\partial x^2} \tag{A6.47}$$

and:

$$\begin{aligned}[22,1] &= \frac{1}{2}\left(\frac{\partial g_{12}}{\partial x^2} + \frac{\partial g_{12}}{\partial x^2} - \frac{\partial g_{22}}{\partial x^1}\right) \\ [22,1] &= -\frac{1}{2}\frac{\partial\left(h_2^2\right)}{\partial x^1} \Rightarrow [22,1] = -h_2\,\frac{\partial h_2}{\partial x^1}\end{aligned} \tag{A6.48}$$

In general, Christoffel symbols of the first kind can be written:

$$[pq,r] = \pm h_i\,\frac{\partial h_i}{\partial x^j} \tag{A6.49}$$

when: $p = q = r = i = j$ with the positive sign;

$q = r = i$, $p = j$ with the positive sign;

$r = p = i$, $q = j$ with the positive sign;

$p = q = i$, $r = j$ with the negative sign;

and is zero if p, q, r are all different.

Since $\left\{ \begin{matrix} i \\ j \quad k \end{matrix} \right\} = \frac{1}{h_i^2}[jk,i]$ with no sum on j, we have:

$$\left\{ \begin{matrix} i \\ j \quad k \end{matrix} \right\} = \begin{cases} 0 & \text{when p, q, r are all different;} \\ \dfrac{1}{h_i}\dfrac{\partial h_i}{\partial x^j} & \begin{matrix}\text{when p = q = r = i = j;} \\ \text{or q = r = i, p = j;} \\ \text{or r = p = i, q = j;}\end{matrix} \\ -\dfrac{h_i}{h_j^2}\dfrac{\partial h_i}{\partial x^j} & \text{when p = q = i, r = j.} \end{cases} \tag{A6.50}$$

In a Cartesian co-ordinate system the value of Christoffel symbols is zero. In cylindrical co-ordinates the only non-zero Christoffel symbols are:

$$
\begin{aligned}
\left[12,2\right] &= \frac{1}{2}\left(\frac{\partial g_{21}}{\partial x^2} + \frac{\partial g_{22}}{\partial x^1} - \frac{\partial g_{12}}{\partial x^2} \right) \\
\left[12,2\right] &= \frac{1}{2}\frac{\partial\left(h_2^2\right)}{\partial x^1} \\
\left[12,2\right] &= h_2 \frac{\partial h_2}{\partial x^1} \\
\left[12,2\right] &= r
\end{aligned}
\tag{A6.51}
$$

$$
\begin{aligned}
\left[22,1\right] &= \frac{1}{2}\left(\frac{\partial g_{12}}{\partial x^2} + \frac{\partial g_{12}}{\partial x^2} - \frac{\partial g_{22}}{\partial x^1} \right) \\
\left[22,1\right] &= -\frac{1}{2}\frac{\partial\left(h_2^2\right)}{\partial x^1} \\
\left[22,1\right] &= -h_2 \frac{\partial h_2}{\partial x^1} \\
\left[22,1\right] &= -r
\end{aligned}
\tag{A6.52}
$$

$$
\begin{aligned}
&\left\{ \begin{matrix} 1 \\ 2 \end{matrix} \quad \begin{matrix} \\ 2 \end{matrix} \right\} = -r \\
&\left\{ \begin{matrix} 2 \\ 1 \end{matrix} \quad \begin{matrix} \\ 2 \end{matrix} \right\} = \left\{ \begin{matrix} 2 \\ 2 \end{matrix} \quad \begin{matrix} \\ 1 \end{matrix} \right\} = \frac{1}{h_2^2}\left[12,2\right] \Leftrightarrow \left\{ \begin{matrix} 2 \\ 1 \end{matrix} \quad \begin{matrix} \\ 2 \end{matrix} \right\} = \left\{ \begin{matrix} 2 \\ 2 \end{matrix} \quad \begin{matrix} \\ 1 \end{matrix} \right\} = \frac{1}{r}
\end{aligned}
\tag{A6.53}
$$

where the scale factors are: $h_1 = 1$, $h_2 = r$, $h_3 = 1$, and co-ordinates are: $x^1 = r$, $x^2 = \theta$, $x^3 = z$.

Covariant derivative

The covariant derivative of a contravariant vector can be computed using:

$$
A^j_{,k} = \frac{\partial A^j}{\partial x^k} + \left\{ \begin{matrix} j \\ i \end{matrix} \quad \begin{matrix} \\ k \end{matrix} \right\} A^i \tag{A6.54}
$$

whereas the covariant derivative of a covariant vector is given by:

$$A_{j,k} = \frac{\partial A^j}{\partial x^k} - \left\{ \begin{matrix} i \\ j \quad k \end{matrix} \right\} A_i \qquad \text{(A6. 55)}$$

The Laplacian, divergence and curl

This section shows the manner in which the vector operators in Appendix 2 were derived, based on derivation of each operator in general orthogonal curvilinear co-ordinates.

The Laplacian of φ is:

$$\nabla^2 \varphi = g^{ij} \varphi_{,ij} \qquad \text{(A6.56)}$$

or

$$\nabla^2 \varphi = \frac{1}{g^{1/2}} \frac{\partial}{\partial x^j} \left(g^{1/2} g^{ij} \frac{\partial \varphi}{\partial x^i} \right) \qquad \text{(A6.57)}$$

In orthogonal co-ordinates it can be written:

$$\nabla^2 \Phi = \frac{1}{h_1 h_2 h_3} \left[\frac{\partial}{\partial x^1} \left(\frac{h_2 h_3}{h_1} \frac{\partial \varphi}{\partial x^1} \right) + \frac{\partial}{\partial x^2} \left(\frac{h_3 h_1}{h_2} \frac{\partial \varphi}{\partial x^2} \right) + \frac{\partial}{\partial x^3} \left(\frac{h_1 h_2}{h_3} \frac{\partial \varphi}{\partial x^3} \right) \right] \qquad \text{(A6.58)}$$

Divergence of a vector $\vec{A}$ is:

$$div\vec{A} = g^{ij} A_{i,j} \qquad \text{(A6.59)}$$

or

$$div\vec{A} = \frac{1}{g^{1/2}} \frac{\partial}{\partial x^i} \left(g^{1/2} A^i \right)$$
$$div\vec{A} = \frac{1}{g^{1/2}} \frac{\partial}{\partial x^j} \left(g^{1/2} g^{ij} A_i \right) \tag{A6.60}$$

In terms of physical components the relationship defining divergence of a vector is:

$$div\vec{A} = \frac{1}{g^{1/2}} \frac{\partial}{\partial x^i} \left[\left(\frac{g}{g^{ii}} \right)^{1/2} A(i) \right] \tag{A6.61}$$

which in orthogonal co-ordinates is:

$$div\vec{A} = \frac{1}{h_1 h_2 h_3} \left[\frac{\partial}{\partial x^1} \left(A(1) h_2 h_3 \right) + \frac{\partial}{\partial x^2} \left(h_1 A(2) h_3 \right) + \frac{\partial}{\partial x^3} \left(h_1 h_2 A(3) \right) \right] \tag{A6.62}$$

Curl is:

$$curl\vec{A} = \varepsilon^{ijk} A_{k,j} \tag{A6.63}$$

$$curl\vec{A} = \varepsilon^{ijk} g_{kp} A^p_{,j} \tag{A6.64}$$

In an orthogonal system the physical components of $A_{k,j}$ are:

$$A(k,j) = \frac{1}{h_j h_k} A_{k,j} \tag{A6.65a}$$

$$A(k,j) = \frac{1}{h_j h_k} \left\{ \frac{\partial}{\partial x^j} \left[h_k A(k) \right] - h_p A(p) \left\{ \begin{matrix} p \\ j \quad k \end{matrix} \right\} \right\} \tag{A6.65b}$$

The two Christoffel symbols that appear are with $p = j$ or $p = k$:

$$\left\{ \begin{matrix} j \\ j \quad k \end{matrix} \right\} = \frac{1}{h_j} \frac{\partial h_j}{\partial x^k}, \left\{ \begin{matrix} k \\ j \quad k \end{matrix} \right\} = \frac{1}{h_k} \frac{\partial h_k}{\partial x^j} \tag{A6.66}$$

and equation (A6.65b) can be written:

$$\begin{aligned} A(k, j) &= \frac{1}{h_j} \frac{\partial A(k)}{\partial x^j} + A(k) \frac{1}{h_j h_k} \frac{\partial h_k}{\partial x^j} \\ &- A(j) \frac{1}{h_j h_k} \frac{\partial h_j}{\partial x^k} - A(k) \frac{1}{h_j h_k} \frac{\partial h_k}{\partial x^j} \end{aligned} \tag{A6.67a}$$

$$A(k, j) = \frac{1}{h_j} \frac{\partial A(k)}{\partial x^j} - A(j) \frac{1}{h_j h_k} \frac{\partial h_j}{\partial x^k} \tag{A6.67b}$$

The following convention is used:

$$\varepsilon^{ijk} = \begin{cases} \dfrac{1}{h_1 h_2 h_3} & \text{if i, j, k is an even permutation of 123;} \\ -\dfrac{1}{h_1 h_2 h_3} & \text{if i, j, k is an odd permutation of 123.} \end{cases} \tag{A6.68}$$

Let ijk be fixed as an even permutation of 123 then the ith component of $curl\vec{A}$ is:

$$\begin{aligned} h_i \varepsilon^{ijk} A_{k,j} &= \frac{h_i}{h_1 h_2 h_3} h_j h_k \left[A(k, j) - A(j, k) \right] \\ h_i \varepsilon^{ijk} A_{k,j} &= A(k, j) - A(j, k) \\ h_i \varepsilon^{ijk} A_{k,j} &= \left\{ \frac{1}{h_j} \frac{\partial A(k)}{\partial x^j} - \frac{1}{h_k} \frac{\partial A(j)}{\partial x^k} + \frac{1}{h_j h_k} \left[A(k) \frac{\partial h_k}{\partial x^j} - A(j) \frac{\partial h_j}{\partial x^k} \right] \right\} \end{aligned} \tag{A6.69}$$

Intrinsic derivatives

The relationship for derivation of acceleration can be written as:

$$a^i = \frac{\partial v^i}{\partial t} + v^j v^i_{,j}$$

$$a^i = \frac{\partial v^i}{\partial t} + \frac{\partial v^i}{\partial x^j} v^j + \left\{ \begin{matrix} i \\ j \quad k \end{matrix} \right\} v^j v^k \qquad \text{(A6.70)}$$

In an orthogonal co-ordinate system the physical components of velocity and acceleration are:

$$v(i) = h_i v^i \ , \ a(i) = h_i a^i \qquad \text{(A6.71)}$$

Using equation (A6.71), equation (A6.70) becomes:

$$a(i) = \frac{\partial v(i)}{\partial t} + \frac{h_i}{h_j} v(j) \frac{\partial}{\partial x^j} \frac{v(i)}{h_i} + \frac{h_i}{h_j h_k} \left\{ \begin{matrix} i \\ j \quad k \end{matrix} \right\} v(j) v(k) \qquad \text{(A6.72)}$$

no sum on i

which subsequently becomes:

$$a(i) = \frac{\partial v(i)}{\partial t} + \sum_{j=1}^{3} \frac{v(j)}{h_j} \left[\frac{\partial v(i)}{\partial x^j} + \frac{v(i)}{h_i} \frac{\partial h_i}{\partial x^j} - \frac{v(j)}{h_i} \frac{\partial h_j}{\partial x^i} \right] \qquad \text{(A6.73)}$$

The three components of acceleration vector in cylindrical co-ordinates are:

$$a(1) = \frac{\partial v(1)}{\partial t} + \frac{v(1)}{h_1} \left[\frac{\partial v(1)}{\partial x^1} + \frac{v(1)}{h_1} \frac{\partial h_1}{\partial x^1} - \frac{v(1)}{h_1} \frac{\partial h_1}{\partial x^1} \right] +$$
$$+ \frac{v(2)}{h_2} \left[\frac{\partial v(1)}{\partial x^2} + \frac{v(1)}{h_1} \frac{\partial h_1}{\partial x^2} - \frac{v(2)}{h_1} \frac{\partial h_2}{\partial x^1} \right]$$
$$+ \frac{v(3)}{h_3} \left[\frac{\partial v(1)}{\partial x^3} + \frac{v(1)}{h_1} \frac{\partial h_1}{\partial x^3} - \frac{v(3)}{h_1} \frac{\partial h_3}{\partial x^1} \right]$$

$$a(1)=\frac{\partial v(1)}{\partial t}+v(1)\left[\frac{\partial v(1)}{\partial x^1}+v(1)\frac{\partial h_1}{\partial x^2}-v(2)\frac{\partial h_2}{\partial x^1}\right]+$$
$$+\frac{v(2)}{h_2}\left[\frac{\partial v(1)}{\partial x^2}+v(1)\frac{\partial h_1}{\partial x^2}-v(2)\frac{\partial h_2}{\partial x^1}\right]+$$
$$+v(3)\left[\frac{\partial v(1)}{\partial x^3}+v(1)\frac{\partial h_1}{\partial x^3}-v(3)\frac{\partial h_3}{\partial x^1}\right]$$
$$a(1)=\frac{\partial v(1)}{\partial t}+v(1)\left[\frac{\partial v(1)}{\partial x^1}\right]+\frac{v(2)}{h_2}\left[\frac{\partial v(1)}{\partial x^2}-v(2)\frac{\partial h_2}{\partial x^1}\right]+v(3)\left[\frac{\partial v(1)}{\partial x^3}\right] \qquad \text{(A6.74)}$$

$$a(2)=\frac{\partial v(2)}{\partial t}+\frac{v(1)}{h_1}\left[\frac{\partial v(2)}{\partial x^1}+\frac{v(2)}{h_2}\frac{\partial h_2}{\partial x^1}-\frac{v(1)}{h_2}\frac{\partial h_1}{\partial x^2}\right]+$$
$$+\frac{v(2)}{h_2}\left[\frac{\partial v(2)}{\partial x^2}+\frac{v(2)}{h_2}\frac{\partial h_2}{\partial x^2}-\frac{v(2)}{h_2}\frac{\partial h_2}{\partial x^2}\right]+$$
$$+\frac{v(3)}{h_3}\left[\frac{\partial v(2)}{\partial x^3}+\frac{v(2)}{h_2}\frac{\partial h_2}{\partial x^3}-\frac{v(3)}{h_2}\frac{\partial h_3}{\partial x^2}\right]$$
$$a(2)=\frac{\partial v(2)}{\partial t}+v(1)\left[\frac{\partial v(2)}{\partial x^1}+\frac{v(2)}{r}\right]+\frac{v(2)}{r}\left[\frac{\partial v(2)}{\partial x^2}\right]+v(3)\left[\frac{\partial v(2)}{\partial x^3}\right] \qquad \text{(A6.75)}$$

$$a(3)=\frac{\partial v(3)}{\partial t}+\frac{v(1)}{h_1}\left[\frac{\partial v(3)}{\partial x^1}+\frac{v(3)}{h_3}\frac{\partial h_3}{\partial x^1}-\frac{v(1)}{h_3}\frac{\partial h_1}{\partial x^3}\right]+$$
$$+\frac{v(2)}{h_2}\left[\frac{\partial v(3)}{\partial x^2}+\frac{v(3)}{h_3}\frac{\partial h_3}{\partial x^2}-\frac{v(2)}{h_3}\frac{\partial h_2}{\partial x^3}\right]+$$
$$+\frac{v(3)}{h_3}\left[\frac{\partial v(3)}{\partial x^3}+\frac{v(3)}{h_3}\frac{\partial h_3}{\partial x^3}-\frac{v(3)}{h_3}\frac{\partial h_3}{\partial x^2}\right]$$
$$a(3)=\frac{\partial v(3)}{\partial t}+v(1)\left[\frac{\partial v(3)}{\partial x^1}\right]+\frac{v(2)}{r}\left[\frac{\partial v(3)}{\partial x^2}\right]+v(3)\left[\frac{\partial v(3)}{\partial x^3}\right] \qquad \text{(A6.76)}$$

where:

$h_1=1,\ h_2=r,\ h_3=1$ are the scale factors in cylindrical co-ordinates;

$$\frac{\partial h_1}{\partial x^1}=0,\ \frac{\partial h_1}{\partial x^2}=0,\ \frac{\partial h_1}{\partial x^3}=0$$

$$\frac{\partial h_2}{\partial x^1}=1,\ \frac{\partial h_2}{\partial x^2}=0,\ \frac{\partial h_2}{\partial x^3}=0$$

$$\frac{\partial h_3}{\partial x^1} = 0\,,\ \frac{\partial h_3}{\partial x^2} = 0\,,\ \frac{\partial h_3}{\partial x^3} = 0$$

$$x^1 = r\,,\ x^2 = \theta\,,\ x^3 = z$$

The components of acceleration can also be written:

$$a(r) = \frac{\partial v(r)}{\partial t} + v(r)\left[\frac{\partial v(r)}{\partial r}\right] + \frac{v(\theta)}{r}\frac{\partial v(r)}{\partial \theta} - \frac{v^2(\theta)}{r} + v(z)\frac{\partial v(r)}{\partial z} \qquad \text{(A6.77)}$$

$$a(\theta) = \frac{\partial v(\theta)}{\partial t} + v(r)\frac{\partial v(\theta)}{\partial r} + \frac{v(\theta)}{r}\frac{\partial v(\theta)}{\partial \theta} + v(z)\frac{\partial v(\theta)}{\partial z} + v(r)\frac{v(\theta)}{r} \qquad \text{(A6.78)}$$

$$a(z) = \frac{\partial v(z)}{\partial t} + v(r)\left[\frac{\partial v(z)}{\partial r}\right] + \frac{v(\theta)}{r}\left[\frac{\partial v(z)}{\partial \theta}\right] + v(z)\left[\frac{\partial v(z)}{\partial z}\right] \qquad \text{(A6.79)}$$

In equations (A6.77), (A6.78) and (A6.79) the following notations were used: $a(1) = a(r)$; $a(2) = a(\theta)$; $a(3) = a(z)$; $v(1) = v(r)$; $v(2) = v(\theta)$; $v(3) = v(z)$.

The continuity equation

The equation of continuity for compressible fluids has the expression given in equation (3.5):

$$\frac{d\rho}{dt} + \rho v^i_{,i} = \frac{\partial \rho}{\partial t} + \left(\rho v^i\right)_{,i} = 0 \qquad \text{(A6.80)}$$

In cylindrical co-ordinates the $\left(\rho v^i\right)_{,i}$ term can be written based on equation (A6.60):

$$\left(\rho v^i\right)_{,i} = \frac{1}{g^{1/2}}\frac{\partial}{\partial x^i}\left[g^{1/2}\left(\rho v^i\right)\right] \qquad \text{(A6.81)}$$

In physical components the $\left(\rho v^i\right)_{,i}$ term becomes, based on equation (A6.63):

$$\frac{1}{r}\left\{\frac{\partial}{\partial r}[r\rho v(1)]+\frac{\partial}{\partial \theta}[\rho v(2)]+\frac{\partial}{\partial z}[r\rho v(3)]\right\}$$
$$=\frac{1}{r}\frac{\partial[r\rho v(r)]}{\partial r}+\frac{1}{r}\frac{\partial[\rho v(\theta)]}{\partial \theta}+\frac{1}{r}\frac{\partial[r\rho v(z)]}{\partial z}$$

And the continuity equation (A6.80) can be written as:

$$\frac{1}{r}\frac{\partial[r\rho v(r)]}{\partial r}+\frac{1}{r}\frac{\partial[\rho v(\theta)]}{\partial \theta}+\frac{\partial[\rho v(z)]}{\partial z}=0 \qquad \text{(A6.82)}$$

For incompressible fluids equation (A6.82) becomes:

$$\frac{1}{r}\frac{\partial[rv(r)]}{\partial r}+\frac{1}{r}\frac{\partial v(\theta)}{\partial \theta}+\frac{\partial v(z)}{\partial z}=0 \qquad \text{(A6.83)}$$

The equation of motion

The Cauchy equation of fluid motion (3.12) can be written as:

$$a^i = f^i + \frac{T^{ij}_{,j}}{\rho} \qquad \text{(A6.84)}$$

Using equation (A6.70), equation (A6.84) gives:

$$\frac{\partial v^i}{\partial t} + v^j v^i_{,j} = f^i + \frac{T^{ij}_{,j}}{\rho} \qquad \text{(A6.85)}$$

where:

$$T^{ij}_{,j} = \frac{1}{g^{1/2}} \frac{\partial}{\partial x^j} \left(g^{1/2} T^{ij} \right) + T^{jk} \left\{ \begin{matrix} i \\ j \quad k \end{matrix} \right\} \tag{A6.86}$$

In orthogonal co-ordinates the physical components of equation (A6.86) may be written:

$$\rho\left[a(i) - f(i)\right] = T(ij, j)$$

$$= \frac{h_i}{h_1 h_2 h_3} \frac{\partial}{\partial x^j} \left[\frac{h_1 h_2 h_3}{h_i h_j} T(ij) \right] + \frac{h_i}{h_j h_k} \left\{ \begin{matrix} i \\ j \quad k \end{matrix} \right\} T(jk) \tag{A6.87}$$

no sum on i

Developing equations (A6.87) for the three dimensions r, θ, z results:

$$\rho\left[a(1) - f(1)\right] = T(1j, j)$$

$$= \frac{h_1}{h_1 h_2 h_3} \frac{\partial}{\partial x^1} \left[\frac{h_1 h_2 h_3}{h_1 h_1} T(11) \right] + \frac{\partial}{\partial x^2} \left[\frac{h_1 h_2 h_3}{h_1 h_2} T(12) \right]$$
$$+ \frac{\partial}{\partial x^3} \left[\frac{h_1 h_2 h_3}{h_1 h_3} T(13) \right] + \frac{h_1}{h_1 h_1} \left\{ \begin{matrix} 1 \\ 1 \quad 1 \end{matrix} \right\} T(11) + \frac{h_1}{h_1 h_2} \left\{ \begin{matrix} 1 \\ 1 \quad 2 \end{matrix} \right\} T(12)$$
$$+ \frac{h_1}{h_1 h_3} \left\{ \begin{matrix} 1 \\ 1 \quad 3 \end{matrix} \right\} T(13) + \frac{h_1}{h_2 h_1} \left\{ \begin{matrix} 1 \\ 2 \quad 1 \end{matrix} \right\} T(21) + \frac{h_1}{h_2 h_2} \left\{ \begin{matrix} 1 \\ 2 \quad 2 \end{matrix} \right\} T(22)$$
$$+ \frac{h_1}{h_2 h_3} \left\{ \begin{matrix} 1 \\ 2 \quad 3 \end{matrix} \right\} T(23) + \frac{h_1}{h_3 h_1} \left\{ \begin{matrix} 1 \\ 3 \quad 1 \end{matrix} \right\} T(31) + \frac{h_1}{h_3 h_2} \left\{ \begin{matrix} 1 \\ 3 \quad 2 \end{matrix} \right\} T(32)$$
$$+ \frac{h_1}{h_3 h_3} \left\{ \begin{matrix} 1 \\ 3 \quad 3 \end{matrix} \right\} T(33)$$

$$\rho\left[a(1) - f(1)\right] = T(1j, j)$$

$$= \frac{1}{h_2} \left\{ \frac{\partial}{\partial x^1} \left[h_2 T(11) \right] + \frac{\partial T(12)}{\partial x^2} + \frac{\partial}{\partial x^3} \left[h_2 T(13) \right] \right\}$$

$$\rho\left[a(1) - f(1)\right] = \frac{1}{r} \left\{ \frac{\partial}{\partial r} \left[r T(rr) \right] + \frac{\partial T(r\theta)}{\partial \theta} + \frac{\partial}{\partial z} \left[r T(rz) \right] \right\}$$

$$= \frac{\partial T(rr)}{\partial r} + \frac{1}{r} \frac{\partial T(r\theta)}{\partial \theta} + \frac{\partial T(rz)}{\partial z} + \frac{T(rr)}{r} - \frac{T(\theta\theta)}{r}$$

$$\rho\left[a(1) - f(1)\right] = \frac{\partial T(rr)}{\partial r} + \frac{1}{r} \frac{\partial T(r\theta)}{\partial \theta} + \frac{\partial T(rz)}{\partial z} + \frac{T(rr)}{r} - \frac{T(\theta\theta)}{r} \tag{A6.88}$$

$$\rho[a(2)-f(2)]=T(2j,j)$$

$$=\frac{h_2}{h_1h_2h_3}\frac{\partial}{\partial x^1}\left[\frac{h_1h_2h_3}{h_2h_1}T(21)\right]+\frac{\partial}{\partial x^2}\left[\frac{h_1h_2h_3}{h_2h_2}T(22)\right]$$

$$+\frac{\partial}{\partial x^3}\left[\frac{h_1h_2h_3}{h_2h_3}T(23)\right]+\frac{h_2}{h_1h_1}\begin{Bmatrix}2\\1&1\end{Bmatrix}T(11)+\frac{h_2}{h_1h_2}\begin{Bmatrix}2\\1&2\end{Bmatrix}T(12)$$

$$+\frac{h_2}{h_1h_3}\begin{Bmatrix}2\\1&3\end{Bmatrix}T(13)+\frac{h_2}{h_2h_1}\begin{Bmatrix}2\\2&1\end{Bmatrix}T(21)+\frac{h_2}{h_2h_2}\begin{Bmatrix}2\\2&2\end{Bmatrix}T(22)$$

$$+\frac{h_2}{h_2h_3}\begin{Bmatrix}2\\2&3\end{Bmatrix}T(23)+\frac{h_2}{h_3h_1}\begin{Bmatrix}2\\3&1\end{Bmatrix}T(31)+\frac{h_2}{h_3h_2}\begin{Bmatrix}2\\3&2\end{Bmatrix}T(32)$$

$$+\frac{h_2}{h_3h_3}\begin{Bmatrix}2\\3&3\end{Bmatrix}T(33)$$

$$\rho[a(2)-f(2)]=T(2j,j)$$

$$=\frac{\partial T(21)}{\partial x^1}+\frac{\partial}{\partial x^2}\left[\frac{1}{h_2}T(22)\right]+\frac{\partial T(23)}{\partial x^3}+\frac{T(12)}{h_2}+\frac{T(21)}{h_2}$$

$$=\frac{\partial T(r\theta)}{\partial r}+\frac{\partial}{\partial\theta}\left[\frac{1}{r}T(\theta\theta)\right]+\frac{\partial T(\theta z)}{\partial z}+\frac{T(r\theta)}{r}+\frac{T(\theta r)}{r}$$

$$=\frac{\partial T(r\theta)}{\partial r}+\frac{1}{r}\frac{\partial T(\theta\theta)}{\partial\theta}+\frac{\partial T(\theta z)}{\partial z}+2\frac{T(r\theta)}{r}$$

$$\rho[a(\theta)-f(\theta)]=\frac{\partial T(r\theta)}{\partial r}+\frac{1}{r}\frac{\partial T(\theta\theta)}{\partial\theta}+\frac{\partial T(\theta z)}{\partial z}+2\frac{T(r\theta)}{r} \qquad \text{(A6.89)}$$

$$\rho[a(3)-f(3)]=T(3j,j)$$

$$=\frac{h_3}{h_1h_2h_3}\frac{\partial}{\partial x^1}\left[\frac{h_1h_2h_3}{h_3h_1}T(31)\right]+\frac{\partial}{\partial x^2}\left[\frac{h_1h_2h_3}{h_3h_2}T(32)\right]$$

$$+\frac{\partial}{\partial x^3}\left[\frac{h_1h_2h_3}{h_3h_3}T(33)\right]+\frac{h_3}{h_1h_1}\begin{Bmatrix}3\\1&1\end{Bmatrix}T(11)+\frac{h_3}{h_1h_2}\begin{Bmatrix}3\\1&2\end{Bmatrix}T(12)$$

$$+\frac{h_3}{h_1h_3}\begin{Bmatrix}3\\1&3\end{Bmatrix}T(13)+\frac{h_3}{h_2h_1}\begin{Bmatrix}3\\2&1\end{Bmatrix}T(21)+\frac{h_3}{h_2h_2}\begin{Bmatrix}3\\2&2\end{Bmatrix}T(22)$$

$$+\frac{h_3}{h_2h_3}\begin{Bmatrix}3\\2&3\end{Bmatrix}T(23)+\frac{h_3}{h_3h_1}\begin{Bmatrix}3\\3&1\end{Bmatrix}T(31)+\frac{h_3}{h_3h_2}\begin{Bmatrix}3\\3&2\end{Bmatrix}T(32)$$

$$+\frac{h_3}{h_3h_3}\begin{Bmatrix}3\\3&3\end{Bmatrix}T(33)$$

$$\rho[a(3)-f(3)]=T(3j,j)$$

$$=\frac{1}{h_2}\left\{\frac{\partial}{\partial x^1}[h_2T(31)]+\frac{\partial T(32)}{\partial x^2}+\frac{\partial}{\partial x^3}[h_2T(33)]\right\}$$

$$=\frac{1}{r}\frac{\partial[rT(zr)]}{\partial r}+\frac{1}{r}\frac{\partial T(z\theta)}{\partial\theta}+\frac{1}{r}\frac{\partial[rT(zz)]}{\partial z}$$

$$=\frac{\partial T(zr)}{\partial r}+\frac{1}{r}\frac{\partial T(z\theta)}{\partial\theta}+\frac{\partial T(zz)}{\partial z}+\frac{T(zr)}{r}$$

$$\rho[a(z)-f(z)]=\frac{\partial T(zr)}{\partial r}+\frac{1}{r}\frac{\partial T(z\theta)}{\partial\theta}+\frac{\partial T(zz)}{\partial z}+\frac{T(zr)}{r} \qquad \text{(A6.90)}$$

In general curvilinear co-ordinates the stress tensor for a Newtonian fluid can be written:

$$T^{ij}=\left(-p+\lambda e^m_m\right)g^{ij}+2\mu e^{ij} \qquad \text{(A6.91)}$$

where:

$e^{ij}=\frac{1}{2}\left(v_{j,i}+v_{i,j}\right)$ is the symmetric part of v_i

$$v_i=g_{ij}v^j\Rightarrow\begin{cases}v_{i,j}=\left(g_{ik}v^k\right)_{,j}=g_{ik}v^k_{,j}\\ v_{j,i}=\left(g_{jk}v^k\right)_{,i}=g_{jk}v^k_{,i}\end{cases}$$

$$v(i,j)=\frac{1}{h_ih_j}\left[\frac{\partial}{\partial x^j}\frac{v(i)}{h_i}+\begin{Bmatrix}i\\ m\quad j\end{Bmatrix}\frac{v(m)}{h_m}\right]g_{ii}$$

$$v(j,i)=\frac{1}{h_ih_j}\left[\frac{\partial}{\partial x^i}\frac{v(j)}{h_j}+\begin{Bmatrix}j\\ m\quad i\end{Bmatrix}\frac{v(m)}{h_m}\right]g_{jj}$$

$$h_ih_je^{ij}=\frac{1}{2}\frac{1}{h_ih_j}\left\{\left[\frac{\partial}{\partial x^j}\frac{v(i)}{h_i}+\begin{Bmatrix}i\\ m\quad j\end{Bmatrix}\frac{v(m)}{h_m}\right]g_{ii}+\left[\frac{\partial}{\partial x^i}\frac{v(j)}{h_j}+\begin{Bmatrix}j\\ m\quad i\end{Bmatrix}\frac{v(m)}{h_m}\right]g_{jj}\right\}$$

Since $e^m_m=v^i_{,i}$ is the dilatation so that for an incompressible fluid:

$$T^{ij}=-pg^{ij}+2\mu e^{ij} \qquad \text{(A6.92)}$$

with:

$$g^{ij} = \begin{cases} 0 & \text{for i} \neq \text{j} \\ & \text{in the orthogonal case} \\ \dfrac{1}{g_{ii}} & \text{for i} = \text{j} \end{cases}$$

$$e(11) = \frac{\partial[v(1)/h_1]}{\partial x^1} \Rightarrow e(rr) = \frac{\partial v(r)}{\partial r},\ h_1 = 1$$

$$e(22) = \left[\frac{1}{h_2}\frac{\partial v(2)}{\partial x^2} + \frac{v(1)}{h_2}\right] \Rightarrow e(\theta\theta) = \left[\frac{1}{r}\frac{\partial v(\theta)}{\partial \theta} + \frac{v(r)}{r}\right],\ h_2 = r$$

$$e(33) = \frac{\partial[v(3)/h_3]}{\partial x^3} \Rightarrow e(zz) = \frac{\partial v(z)}{\partial z},\ h_3 = 1$$

$$e(23) = \frac{1}{2}\frac{h_2}{h_3}\left[\frac{\partial v(2)/h_2}{\partial x^3}\right] + \frac{1}{2}\frac{h_3}{h_2}\left[\frac{\partial v(3)/h_3}{\partial x^2}\right] \qquad \text{(A6.93)}$$

$$\Rightarrow e(\theta z) = \frac{1}{2}\left[\frac{1}{r}\frac{\partial v(z)}{\partial \theta} + \frac{\partial v(\theta)}{\partial z}\right]$$

$$e(31) = \frac{1}{2}\frac{h_3}{h_1}\frac{\partial[v(3)/h_3]}{\partial x^1} + \frac{1}{2}\frac{h_1}{h_3}\frac{\partial[v(1)/h_1]}{\partial x^3}$$

$$\Rightarrow e(rz) = \frac{1}{2}\left[\frac{\partial v(r)}{\partial z} + \frac{\partial v(z)}{\partial r}\right]$$

$$e(12) = \frac{1}{2}\frac{h_1}{h_2}\left\{\frac{\partial[v(1)/h_1]}{\partial x^2} - \frac{v(2)}{h_2}r\right\} + \frac{1}{2}\frac{h_2}{h_1}\left\{\frac{\partial[v(2)/h_2]}{\partial x^1}\right\} \Rightarrow$$

$$\Rightarrow e(r\theta) = \frac{1}{2}\left[\frac{1}{r}\frac{\partial v(r)}{\partial \theta} + \frac{\partial v(\theta)}{\partial r} - \frac{v(\theta)}{r}\right]$$

$$T_{ij} = g_{ii}g_{jj}T^{ij}$$

In cylindrical polar co-ordinates the physical components of stress for an incompressible fluid are:

$$T(rr) = -p + 2\mu\frac{\partial v(r)}{\partial r} \qquad \text{(A6.94a)}$$

$$T(\theta\theta) = -p + 2\mu\left[\frac{1}{r}\frac{\partial v(\theta)}{\partial \theta} + \frac{v(r)}{r}\right] \qquad \text{(A6.94b)}$$

$$T(zz) = -p + 2\mu \frac{\partial v(z)}{\partial z} \tag{A6.94c}$$

$$T(\theta z) = \mu\left[\frac{\partial v(\theta)}{\partial z} + \frac{1}{r}\frac{\partial v(z)}{\partial \theta}\right] \tag{A6.94d}$$

$$T(zr) = \mu\left[\frac{\partial v(z)}{\partial r} + \frac{\partial v(r)}{\partial z}\right] \tag{A6.94e}$$

$$T(r\theta) = \mu\left[\frac{1}{r}\frac{\partial v(r)}{\partial \theta} + \frac{\partial v(\theta)}{\partial r} - \frac{v(\theta)}{r}\right] \tag{A6.94f}$$

The Navier-Stokes equations

For an incompressible fluid equation (3.22) can be written in terms of physical components as:

$$a(i) = f(i) - g_{ii}^{1/2} g^{ij} \frac{1}{\rho} p_{,j} + \frac{\mu}{\rho} g_{ii}^{1/2} \nabla^2 \left[g_{ii}^{1/2} v(i)\right] \tag{A6.95}$$

or:

$$\begin{aligned} a(r) &= f(r) - \frac{1}{\rho}\frac{\partial p}{\partial r} \\ &+ \nu\left\{\frac{\partial^2 v(r)}{\partial r^2} + \frac{1}{r^2}\frac{\partial^2 v(r)}{\partial \theta^2} + \frac{\partial^2 v(r)}{\partial z^2} + \frac{1}{r}\frac{\partial v(r)}{\partial r} - \frac{v(r)}{r^2} - \frac{2}{r^2}\frac{\partial v(\theta)}{\partial \theta}\right\} \end{aligned} \tag{A6.96}$$

$$\begin{aligned} a(\theta) &= f(\theta) - \frac{1}{\rho r}\frac{\partial p}{\partial \theta} \\ &+ \nu\left\{\frac{\partial^2 v(\theta)}{\partial r^2} + \frac{1}{r^2}\frac{\partial^2 v(\theta)}{\partial \theta^2} + \frac{\partial^2 v(\theta)}{\partial z^2} + \frac{1}{r}\frac{\partial v(\theta)}{\partial r} - \frac{v(\theta)}{r} + \frac{2}{r}\frac{\partial v(r)}{\partial \theta}\right\} \end{aligned} \tag{A6.97}$$

$$\begin{aligned} a(z) &= f(z) - \frac{1}{\rho}\frac{\partial p}{\partial z} \\ &+ \nu\left\{\frac{\partial^2 v(z)}{\partial r^2} + \frac{1}{r^2}\frac{\partial^2 v(z)}{\partial \theta^2} + \frac{\partial^2 v(z)}{\partial z^2} + \frac{1}{r}\frac{\partial v(z)}{\partial r}\right\} \end{aligned} \tag{A6.98}$$

Using equations (A6.77)-(A6.79) physical components of the Navier-Stokes equations in cylindrical co-ordinates become:

$$\begin{aligned}&\frac{\partial v(r)}{\partial t}+v(r)\frac{\partial v(r)}{\partial r}+\frac{v(\theta)}{r}\frac{\partial v(r)}{\partial \theta}+v(z)\frac{\partial v(r)}{\partial z}-\frac{v^2(\theta)}{r}\\&=f(r)-\frac{1}{\rho}\frac{\partial p}{\partial r}\\&+\nu\left[\frac{\partial^2 v(r)}{\partial r^2}+\frac{1}{r^2}\frac{\partial^2 v(r)}{\partial \theta^2}+\frac{\partial^2 v(r)}{\partial z^2}+\frac{1}{r}\frac{\partial v(r)}{\partial r}\right.\\&\left.-\frac{2}{r^2}\frac{\partial v(\theta)}{\partial \theta}-\frac{v(r)}{r^2}\right]\end{aligned} \tag{A6.99}$$

$$\begin{aligned}&\frac{\partial v(\theta)}{\partial t}+v(r)\frac{\partial v(\theta)}{\partial r}+\frac{v(\theta)}{r}\frac{\partial v(\theta)}{\partial \theta}+v(z)\frac{\partial v(\theta)}{\partial z}+v(r)\frac{v(\theta)}{r}\\&=f(\theta)-\frac{1}{\rho r}\frac{\partial p}{\partial \theta}+\nu\left[\frac{\partial^2 v(\theta)}{\partial r^2}+\frac{1}{r^2}\frac{\partial^2 v(\theta)}{\partial \theta^2}+\frac{\partial^2 v(\theta)}{\partial z^2}\right.\\&\left.+\frac{1}{r}\frac{\partial v(\theta)}{\partial r}+\frac{2}{r^2}\frac{\partial v(r)}{\partial \theta}-\frac{v(\theta)}{r^2}\right]\end{aligned} \tag{A6.100}$$

$$\begin{aligned}&\frac{\partial v(z)}{\partial t}+v(r)\left[\frac{\partial v(z)}{\partial r}\right]+\frac{v(\theta)}{r}\left[\frac{\partial v(z)}{\partial \theta}\right]+v(z)\left[\frac{\partial v(z)}{\partial z}\right]\\&=f(z)-\frac{1}{\rho}\frac{\partial p}{\partial z}+\nu\left[\frac{\partial^2 v(z)}{\partial r^2}+\frac{1}{r^2}\frac{\partial^2 v(z)}{\partial \theta^2}+\frac{\partial^2 v(z)}{\partial z^2}+\frac{1}{r}\frac{\partial v(z)}{\partial r}\right]\end{aligned} \tag{A6.101}$$

In obtaining the final form of the Navier-Stokes equations, the derivative of continuity equation with respect to the r – direction was used:

$$\frac{\partial}{\partial r}\left\{\frac{1}{r}\frac{\partial[rv(r)]}{\partial r}+\frac{1}{r}\frac{\partial v(\theta)}{\partial \theta}+\frac{\partial v(z)}{\partial z}\right\}=0 \tag{A6.102}$$

$$\begin{aligned}&-\frac{v(r)}{r^2}+\frac{1}{r}\frac{\partial v(r)}{\partial r}+\frac{\partial^2 v(r)}{\partial r^2}-\frac{1}{r^2}\frac{\partial v(\theta)}{\partial \theta}+\frac{1}{r}\frac{\partial^2 v(\theta)}{\partial r\partial \theta}\\&+\frac{\partial^2 v(z)}{\partial r\partial z}=0\end{aligned} \tag{A6.103}$$

Other useful relationships are:

$$\frac{\partial}{\partial r}\left\{\frac{1}{r}\frac{\partial[rv(r)]}{\partial r}\right\}=-\frac{v(r)}{r^2}+\frac{1}{r}\frac{\partial v(r)}{\partial r}+\frac{\partial^2 v(r)}{\partial r^2} \tag{A6.104}$$

$$\frac{\partial}{\partial r}\left\{\frac{1}{r}\frac{\partial}{\partial \theta}[v(\theta)]\right\}=-\frac{1}{r^2}\frac{\partial v(\theta)}{\partial \theta}+\frac{1}{r}\frac{\partial^2 v(\theta)}{\partial r\partial \theta} \tag{A6.105}$$

$$\frac{\partial}{\partial r}\left\{\frac{1}{r}\frac{\partial}{\partial z}[rv(z)]\right\}=\frac{\partial^2 v(z)}{\partial r\partial z} \tag{A6.106}$$

$$\begin{aligned}&\frac{1}{r}\frac{\partial}{\partial r}\left\{r\frac{\partial[v(r)]}{\partial r}\right\}=\frac{1}{r}\frac{\partial v(r)}{\partial r}+\frac{\partial^2 v(r)}{\partial r^2}\\&\frac{1}{r}\frac{\partial}{\partial \theta}\left\{\frac{1}{r}\frac{\partial[v(r)]}{\partial \theta}\right\}=\frac{1}{r^2}\frac{\partial^2 v(r)}{\partial \theta^2}\\&\frac{1}{r}\frac{\partial}{\partial z}\left\{r\frac{\partial[v(r)]}{\partial z}\right\}=\frac{\partial^2 v(r)}{\partial z^2}\end{aligned} \tag{A6.107}$$

$\nu=\dfrac{\mu}{\rho}$ is the kinematic viscosity;

μ is the dynamic coefficient of viscosity;

λ is the second coefficient of viscosity;

$\left(\lambda+\dfrac{2}{3}\mu\right)$ is the coefficient of bulk viscosity.

In derivation of the NSE written in cylindrical co-ordinates, the expression of the Laplacian of a vector was written:

$$\begin{aligned}&\nabla^2\vec{v}\\&=\left[\frac{\partial^2 v(r)}{\partial r^2}+\frac{1}{r^2}\frac{\partial^2 v(r)}{\partial \theta^2}+\frac{\partial^2 v(r)}{\partial z^2}+\frac{1}{r}\frac{\partial v(r)}{\partial r}-\frac{2}{r^2}\frac{\partial v(\theta)}{\partial \theta}-\frac{v(r)}{r^2}\right]\vec{e}_r\\&+\left[\frac{\partial^2 v(\theta)}{\partial r^2}+\frac{1}{r^2}\frac{\partial^2 v(\theta)}{\partial \theta^2}+\frac{\partial^2 v(\theta)}{\partial z^2}+\frac{1}{r}\frac{\partial v(\theta)}{\partial r}+\frac{2}{r^2}\frac{\partial v(r)}{\partial \theta}-\frac{v(\theta)}{r^2}\right]\vec{e}_\theta\\&+\left[\frac{\partial^2 v(z)}{\partial r^2}+\frac{1}{r^2}\frac{\partial^2 v(z)}{\partial \theta^2}+\frac{\partial^2 v(z)}{\partial z^2}+\frac{1}{r}\frac{\partial v(z)}{\partial r}\right]\vec{e}_z\end{aligned} \tag{A6.108}$$

Calculus for Depth Integration of the $r-$direction Momentum Equation Written in Cylindrical Polar Coordinates

Depth integration of the $r-$ direction momentum equation between free surface (ζ) and bed $(-h)$, over the water column ($H=\zeta+h$), is performed using Leibnitz's rule (3.64) so that equation (3.74) can be written for identification of terms:

$$\underbrace{\int_{-h}^{\zeta}\frac{\partial v_r}{\partial t}dz}_{1}+\underbrace{\int_{-h}^{\zeta}\frac{\partial v_r^2}{\partial r}dz}_{2}+\underbrace{\int_{-h}^{\zeta}\frac{1}{r}\frac{\partial v_r v_\theta}{\partial \theta}dz}_{3}+\underbrace{\int_{-h}^{\zeta}\frac{\partial v_r v_z}{\partial z}dz}_{4}$$
$$+\underbrace{\int_{-h}^{\zeta}\left(\frac{v_r^2}{r}-\frac{\overline{v_r' v_r'}}{r}\right)dz}_{5}-\underbrace{\int_{-h}^{\zeta}\left(\frac{v_\theta^2}{r}-\frac{\overline{v'_\theta v'_\theta}}{r}\right)dz}_{6}=$$
$$\underbrace{\int_{-h}^{\zeta}f_C v_\theta dz}_{7}-\underbrace{\int_{-h}^{\zeta}\frac{1}{\rho}\frac{\partial p}{\partial r}dz}_{8}+\underbrace{\int_{-h}^{\zeta}\frac{\partial}{\partial r}\left(E\frac{\partial v_r}{\partial r}-\overline{v'_r v'_r}\right)dz}_{9}+ \tag{3.74}$$
$$+\underbrace{\int_{-h}^{\zeta}\frac{1}{r}\frac{\partial}{\partial \theta}\left(\frac{1}{r}E\frac{\partial v_r}{\partial \theta}-\overline{v'_r v'_\theta}\right)dz}_{10}+\underbrace{\int_{-h}^{\zeta}\frac{\partial}{\partial z}\left(E\frac{\partial v_r}{\partial z}-\overline{v'_r v'_z}\right)dz}_{11}+$$
$$+\underbrace{\int_{-h}^{\zeta}\left(\frac{1}{r}E\frac{\partial v_r}{\partial r}\right)dz}_{12}-\underbrace{\int_{-h}^{\zeta}\left(\frac{2}{r^2}E\frac{\partial v_\theta}{\partial \theta}\right)dz}_{13}-\underbrace{\int_{-h}^{\zeta}E\frac{v_r}{r^2}dz}_{14}$$

Equation (3.74) contains 14 integral terms, which are treated as follows:

- term 1:

$$\int_{-h}^{\zeta}\frac{\partial v_r}{\partial t}dz=\frac{\partial}{\partial t}\int_{-h}^{\zeta}v_r dz-(\bar{v}_r)_\zeta\frac{\partial \zeta}{\partial t}+(v_r)_{-h}\frac{\partial(-h)}{\partial t}$$
$$=\frac{\partial V_r H}{\partial t}-(v_r)_\zeta\frac{\partial \zeta}{\partial t}+(v_r)_{-h}\frac{\partial(-h)}{\partial t} \tag{A7.1}$$

- term 2:

$$\int_{-h}^{\zeta} \frac{\partial (v_r)^2}{\partial r}\, dz = \frac{\partial}{\partial r} \int_{-h}^{\zeta} (v_r)^2\, dz - (v_r)_{\zeta}^2 \frac{\partial \zeta}{\partial t} + (v_r)_{-h}^2 \frac{\partial (-h)}{\partial t} \qquad \text{(A7.2)}$$

The term $\frac{\partial}{\partial r} \int_{-h}^{\zeta} (v_r)^2\, dz$ may be integrated assuming a one seventh power law for velocity distribution:

$$v_r = V_{r\max} \frac{(h+z)^{1/7}}{(h+\zeta)^{1/7}} = \left(1 + \frac{1}{7}\right) V_r \frac{(h+z)^{1/7}}{(h+\zeta)^{1/7}}$$

$$\int_{-h}^{\zeta} (v_r)^2\, dz = \left(\frac{8}{7} V_r\right)^2 \int_{-h}^{\zeta} \left[\frac{(h+z)^{1/7}}{(h+\zeta)^{1/7}}\right]^2 dz$$

$$= \left(\frac{8}{7} V_r\right)^2 \frac{1}{(h+\zeta)^{2/7}} \frac{7}{9} (h+z)^{9/7} \Big|_{-h}^{\zeta}$$

$$= \left(\frac{8}{7} V_r\right)^2 \frac{1}{(h+\zeta)^{2/7}} \frac{7}{9} (h+\zeta)^{9/7}$$

$$= \left(\frac{8}{7}\right)^2 \frac{7}{9} (h+\zeta) V_r^2$$

$$\int_{-h}^{\zeta} (v_r)^2\, dz = 1.016 (h+\zeta) V_r^2$$

$$\frac{\partial}{\partial r} \int_{-h}^{\zeta} \bar{v}_r \bar{v}_r\, dz = \frac{\partial}{\partial r} \left[1.016 (h+\zeta) V_r^2\right] = 1.016 \frac{\partial V_r^2 (h+\zeta)}{\partial r} = \beta \frac{\partial V_r^2 H}{\partial r}$$

The final expression of term 2 becomes:

$$\int_{-h}^{\zeta} \frac{\partial (v_r)^2}{\partial r}\, dz = \beta \frac{\partial V_r^2 H}{\partial r} - (v_r)_{\zeta}^2 \frac{\partial \zeta}{\partial r} + (v_r)_{-h}^2 \frac{\partial (-h)}{\partial r} \qquad \text{(A7.3)}$$

- term3:

$$\int_{-h}^{\zeta} \frac{1}{r} \frac{\partial (v_r v_\theta)}{\partial \theta} dz = \frac{1}{r} \frac{\partial}{\partial \theta} \int_{-h}^{\zeta} v_r v_\theta\, dz - \frac{1}{r} (v_r v_\theta)_{\zeta} \frac{\partial \zeta}{\partial \theta} + \frac{1}{r} (v_r v_\theta)_{-h} \frac{\partial (-h)}{\partial \theta} \qquad \text{(A7.4)}$$

Following the approach for development of term 2 and assuming that velocity components in both directions can be postulated by a logarithmic law, equation (A7.4) becomes:

$$\int_{-h}^{\zeta} \frac{1}{r} \frac{\partial (v_r v_\theta)}{\partial \theta} dz = \beta \frac{1}{r} \frac{\partial V_r V_\theta H}{\partial \theta} - (v_r v_\theta)_\zeta \frac{1}{r} \frac{\partial \zeta}{\partial \theta} + (v_r v_\theta)_{-h} \frac{1}{r} \frac{\partial (-h)}{\partial \theta} \tag{A7.5}$$

- term 4:

$$\int_{-h}^{\zeta} \frac{\partial (v_r v_z)}{\partial z} dz = (v_r v_z)_\zeta - (v_r v_z)_{-h} \tag{A7.6}$$

- term 5 uses the same derivation as term 3:

$$\begin{aligned} &\frac{1}{r} \int_{-h}^{\zeta} \left[(v_r)^2 - \overline{v_r' v_r'} \right] dz \\ &= 1.016 \frac{V_r^2 H}{r} + \frac{1}{r} \int_{-h}^{\zeta} \left[E_t \left(2 \frac{\partial v_r}{\partial r} \right) - \frac{2}{3} k \right] dz \\ &= \beta \frac{V_r^2 H}{r} + \frac{2}{r} \left(\bar{E}_t H \frac{\partial V_r}{\partial r} \right) - \frac{2}{3} \bar{k} H \end{aligned} \tag{A7.7}$$

- term 6 uses the same derivation as term 3:

$$\begin{aligned} &\frac{1}{r} \int_{-h}^{\zeta} \left[(v_\theta)^2 - \overline{v'_\theta v'_\theta} \right] dz \\ &= 1.016 \frac{V_\theta^2 H}{r} + \frac{1}{r} \int_{-h}^{\zeta} \left[2 \bar{E}_t \left(\frac{1}{r} \frac{\partial v_\theta}{\partial \theta} + \frac{v_r}{r} \right) - \frac{2}{3} k \right] \\ &= \beta \frac{V_\theta^2 H}{r} + \frac{2}{r^2} \left(\bar{E}_t H \frac{\partial V_\theta}{\partial \theta} \right) + \frac{2}{r} \left(\bar{E}_t H \frac{V_r}{r} \right) - \frac{2}{3} \bar{k} H \end{aligned} \tag{A7.8}$$

- term7:

$$f_C \int_{-h}^{\zeta} v_\theta dz = f_C V_\theta H \tag{A7.9}$$

- term 8:

$$\int_{\zeta}^{-h}\frac{1}{\rho}\frac{\partial p}{\partial r}dz=\left[\int_{\zeta}^{-h}pdz-(p)_{-h}\frac{\partial(-h)}{\partial r}+(p)_{\zeta}\frac{\partial\zeta}{\partial r}\right] \tag{A7.10}$$

With the hydrostatic assumption term 8 can be written:

$$g\frac{\partial}{\partial r}\int_{-h}^{\zeta}\zeta dz=g\frac{\partial\zeta}{\partial r}\int_{-h}^{\zeta}dz=g\frac{\partial\zeta}{\partial r}z\Big|_{-h}^{\zeta}=g\frac{\partial\zeta}{\partial r}(\zeta+h)=gH\frac{\partial\zeta}{\partial r} \tag{A7.11}$$

- term 9:

$$\begin{aligned}&\int_{-h}^{\zeta}\frac{\partial}{\partial r}\left(E\frac{\partial v_r}{\partial r}-\overline{v'_r\,v'_r}\right)dz=\int_{-h}^{\zeta}\frac{\partial}{\partial r}\left[E\frac{\partial v_r}{\partial r}+E_t\left(2\frac{\partial v_r}{\partial r}\right)-\frac{2}{3}k\right]dz\\&=\frac{\partial}{\partial r}\left(EH\frac{\partial V_r}{\partial r}\right)+2\frac{\partial}{\partial r}\left(\overline{E}_tH\frac{\partial V_r}{\partial r}\right)-\frac{2}{3}\frac{\partial}{\partial r}\left(\bar{k}H\right)\end{aligned} \tag{A7.12}$$

- term 10:

$$\begin{aligned}&\frac{1}{r}\int_{-h}^{\zeta}\frac{\partial}{\partial\theta}\left(\frac{1}{r}E\frac{\partial v_r}{\partial\theta}-\overline{v'_r\,v'_\theta}\right)dz\\&=\frac{1}{r}\int_{-h}^{\zeta}\frac{\partial}{\partial\theta}\left[\frac{1}{r}E\frac{\partial v_r}{\partial\theta}+E_t\left(\frac{\partial v_\theta}{\partial r}-\frac{v_\theta}{r}+\frac{1}{r}\frac{\partial v_r}{\partial\theta}\right)\right]dz\\&=\frac{1}{r^2}\frac{\partial}{\partial\theta}\left(EH\frac{\partial V_r}{\partial\theta}\right)+\frac{1}{r}\frac{\partial}{\partial\theta}\left(\overline{E}_tH\frac{\partial V_\theta}{\partial r}\right)-\frac{1}{r}\frac{\partial}{\partial\theta}\left(\overline{E}_tH\frac{V_\theta}{r}\right)\\&+\frac{1}{r^2}\frac{\partial}{\partial\theta}\left(\overline{E}_tH\frac{\partial V_r}{\partial\theta}\right)\end{aligned} \tag{A7.13}$$

- term 11:

$$\begin{aligned}&\int_{-h}^{\zeta}\frac{\partial}{\partial z}\left(E\frac{\partial v_r}{\partial z}-\overline{v'_r\,v'_z}\right)dz\\&=\int_{-h}^{\zeta}\frac{\partial}{\partial z}\left[E\frac{\partial v_r}{\partial z}+E_t\left(\frac{\partial v_z}{\partial r}+\frac{\partial v_r}{\partial z}\right)\right]dz\\&=\frac{1}{\rho}\left(\tau_{rz\zeta}-\tau_{rz-h}\right)\end{aligned} \tag{A7.14}$$

- term 12:

$$\int_{-h}^{\zeta}\frac{1}{r}E\frac{\partial v_r}{\partial r}dz=\frac{1}{r}E\frac{\partial V_r\left(h+\zeta\right)}{\partial r}=\frac{1}{r}E\frac{\partial V_r H}{\partial r} \tag{A7.15}$$

- term 13:

$$\int_{-h}^{\zeta}\left(\frac{2}{r^2}E\frac{\partial v_\theta}{\partial\theta}\right)dz=\frac{2}{r^2}E\frac{\partial V_\theta\left(h+\zeta\right)}{\partial\theta}=\frac{2}{r^2}EH\frac{\partial V_\theta}{\partial\theta} \tag{A7.16}$$

- term 14:

$$\int_{-h}^{\zeta}E\frac{v_r}{r^2}dz=\frac{1}{r^2}E\int_{-h}^{\zeta}v_r dz=\frac{1}{r^2}EV_r\left(h+\zeta\right)=\frac{1}{r^2}EHV_r \tag{A7.17}$$

Subsequently, momentum equation in the $r-$direction becomes:

$$\begin{aligned}
&\underbrace{\frac{\partial V_r H}{\partial t}-\left(v_r\right)_\zeta\frac{\partial\zeta}{\partial t}+\left(v_r\right)_{-h}\frac{\partial\left(-h\right)}{\partial t}}_{1}\\
&+\underbrace{\beta\frac{\partial V_r^2 H}{\partial r}-\left(v_r\right)_\zeta^2\frac{\partial\zeta}{\partial r}+\left(v_r\right)_{-h}^2\frac{\partial\left(-h\right)}{\partial r}}_{2}\\
&+\underbrace{\beta\frac{1}{r}\frac{\partial V_r V_\theta H}{\partial\theta}-\frac{1}{r}\left(v_r v_\theta\right)_\zeta\frac{\partial\zeta}{\partial\theta}+\frac{1}{r}\left(v_r v_\theta\right)_{-h}\frac{\partial\left(-h\right)}{\partial\theta}}_{3}\\
&+\underbrace{\left(v_r v_z\right)_\zeta-\left(v_r v_z\right)_{-h}}_{4}+\underbrace{\beta\frac{V_r^2 H}{r}}_{5a}+\underbrace{\frac{2}{r}\left(\overline{E}_t H\frac{\partial V_r}{\partial r}\right)}_{5b}-\underbrace{\frac{2}{3}\overline{k}H}_{5'}\\
&-\underbrace{\beta\frac{V_\theta^2 H}{r}}_{6a}+\left[\underbrace{-\frac{2}{r^2}\left(\overline{E}_t H\frac{\partial V_\theta}{\partial\theta}\right)-\frac{2}{r}\left(\overline{E}_t H\frac{V_r}{r}\right)}_{6b}+\underbrace{\frac{2}{3}\overline{k}H}_{6'}\right]\\
&=\underbrace{f_C V_\theta H}_{7}-\underbrace{gH\frac{\partial\zeta}{\partial r}}_{8}+\underbrace{\frac{\partial}{\partial r}\left(EH\frac{\partial V_r}{\partial r}\right)+2\frac{\partial}{\partial r}\left(\overline{E}_t H\frac{\partial V_r}{\partial r}\right)}_{9}\\
&\underbrace{-\frac{2}{3}\frac{\partial}{\partial r}\left(\overline{k}H\right)}_{9'}+\underbrace{\frac{1}{r^2}\frac{\partial}{\partial\theta}\left(EH\frac{\partial V_r}{\partial\theta}\right)+\frac{1}{r}\frac{\partial}{\partial\theta}\left(\overline{E}_t H\frac{\partial V_\theta}{\partial r}\right)}_{10}
\end{aligned} \tag{A7.18}$$

$$\underbrace{-\frac{1}{r}\frac{\partial}{\partial\theta}\left(\overline{E}_t H\frac{V_\theta}{r}\right)+\frac{1}{r^2}\frac{\partial}{\partial\theta}\left(\overline{E}_t H\frac{\partial V_r}{\partial\theta}\right)}_{10}+\underbrace{\frac{1}{\rho}\left(\tau_{rz\zeta}-\tau_{rz-h}\right)}_{11} \qquad \text{(A7.18)}$$

continued

$$+\underbrace{\frac{1}{r}E\frac{\partial V_r H}{\partial r}}_{12}-\underbrace{\frac{2}{r^2}EH\frac{\partial V_\theta}{\partial\theta}}_{13}-\underbrace{\frac{1}{r^2}EHV_r}_{14}$$

At the free surface the kinematic boundary condition is written as condition (3.71) multiplied by $v_{r\zeta}$:

$$v_{r\zeta}\left(\frac{\partial\zeta}{\partial t}+v_{r\zeta}\frac{\partial\zeta}{\partial r}+\frac{1}{r}v_{\theta\zeta}\frac{\partial\zeta}{\partial\theta}-v_{z\zeta}\right)=0 \qquad \text{(A7.19)}$$

which reduces to zero the summed contribution of the terms containing $v_{r\zeta}, v_{\theta\zeta}, v_{z\zeta}$. At the impermeable bed the no slip condition (3.68) is used, resulting in that the terms including $(v_r)_{-h}$, $(v_\theta)_{-h}$ and $(v_z)_{-h}$ become zero. The primed terms including the depth averaged turbulent kinetic energy are neglected.

Equation (A7.21) becomes:

$$\begin{aligned}
&\underbrace{\frac{\partial V_r H}{\partial t}}_{1}+\underbrace{\beta\frac{\partial V_r^2 H}{\partial r}}_{2}+\underbrace{\beta\frac{1}{r}\frac{\partial V_r V_\theta H}{\partial\theta}}_{3}+\underbrace{\beta\frac{V_r^2 H}{r}}_{5a}+\underbrace{\frac{2}{r}\left(\overline{E}_t H\frac{\partial V_r}{\partial r}\right)}_{5b}\\
&\underbrace{-\beta\frac{V_\theta^2 H}{r}}_{6a}\underbrace{-\frac{2}{r^2}\left(\overline{E}_t H\frac{\partial V_\theta}{\partial\theta}\right)-\frac{2}{r}\left(\overline{E}_t H\frac{V_r}{r}\right)}_{6b}\\
&=\underbrace{f_C V_\theta H}_{7}-\underbrace{gH\frac{\partial\zeta}{\partial r}}_{8}+\underbrace{\frac{\partial}{\partial r}\left(EH\frac{\partial V_r}{\partial r}\right)+2\frac{\partial}{\partial r}\left(\overline{E}_t H\frac{\partial V_r}{\partial r}\right)}_{9}\\
&\underbrace{+\frac{1}{r^2}\frac{\partial}{\partial\theta}\left(EH\frac{\partial V_r}{\partial\theta}\right)+\frac{1}{r}\frac{\partial}{\partial\theta}\left(\overline{E}_t H\frac{\partial V_\theta}{\partial r}\right)}_{10}\\
&\underbrace{-\frac{1}{r}\frac{\partial}{\partial\theta}\left(\overline{E}_t H\frac{V_\theta}{r}\right)+\frac{1}{r^2}\frac{\partial}{\partial\theta}\left(\overline{E}_t H\frac{\partial V_r}{\partial\theta}\right)}_{10}+\underbrace{\frac{1}{\rho}\left(\tau_{rz\zeta}-\tau_{rz-h}\right)}_{11}
\end{aligned} \qquad \text{(A7.20)}$$

$$+\underbrace{\frac{1}{r}EH\frac{\partial V_r}{\partial r}}_{12}-\underbrace{\frac{2}{r^2}EH\frac{\partial V_\theta}{\partial \theta}}_{13}-\underbrace{\frac{1}{r^2}EHV_r}_{14} \qquad \text{(A7.20)}$$

continued

Terms 2, 3, 5 and 6 have a common factor which is β, so that equation (A7.20) can be written:

$$\begin{aligned}
&\underbrace{\frac{\partial V_r H}{\partial t}}_{1}+\beta\left(\underbrace{\frac{\partial V_r^2 H}{\partial r}}_{2}+\underbrace{\frac{1}{r}\frac{\partial V_r V_\theta H}{\partial \theta}}_{3}+\underbrace{\frac{V_r^2 H}{r}}_{5a}-\underbrace{\frac{V_\theta^2 H}{r}}_{6a}\right)\\
&=\underbrace{f_C V_\theta H}_{7}-\underbrace{gH\frac{\partial \zeta}{\partial r}}_{8}+\underbrace{\frac{\partial}{\partial r}\left(EH\frac{\partial V_r}{\partial r}\right)+2\frac{\partial}{\partial r}\left(\overline{E}_t H\frac{\partial V_r}{\partial r}\right)}_{9}\\
&\underbrace{+\frac{1}{r^2}\frac{\partial}{\partial \theta}\left(EH\frac{\partial V_r}{\partial \theta}\right)+\frac{1}{r}\frac{\partial}{\partial \theta}\left(\overline{E}_t H\frac{\partial V_\theta}{\partial r}\right)}_{10}\\
&\underbrace{-\frac{1}{r}\frac{\partial}{\partial \theta}\left(\overline{E}_t H\frac{V_\theta}{r}\right)+\frac{1}{r^2}\frac{\partial}{\partial \theta}\left(\overline{E}_t H\frac{\partial V_r}{\partial \theta}\right)}_{10}+\underbrace{\frac{1}{\rho}\tau_{rz\zeta}-\frac{1}{\rho}\tau_{rz-h}}_{11}\\
&+\underbrace{\frac{1}{r}EH\frac{\partial V_r}{\partial r}}_{12}-\underbrace{\frac{2}{r^2}EH\frac{\partial V_\theta}{\partial \theta}}_{13}-\underbrace{\frac{1}{r^2}EHV_r}_{14}+\underbrace{\frac{2}{r}\left(\overline{E}_t H\frac{\partial V_r}{\partial r}\right)}_{5b}\\
&\underbrace{-\frac{2}{r^2}\left(\overline{E}_t H\frac{\partial V_\theta}{\partial \theta}\right)-\frac{2}{r}\left(\overline{E}_t H\frac{V_r}{r}\right)}_{6b}
\end{aligned} \qquad \text{(A7.21)}$$

The two dimensional depth-integrated form of the $r-$direction momentum equation becomes:

$$\begin{aligned}
&\frac{\partial V_r H}{\partial t}+\beta\left[\frac{\partial\left(V_r^2 H\right)}{\partial r}+\frac{1}{r}\frac{\partial\left(V_r V_\theta H\right)}{\partial \theta}+\frac{V_r^2 H-V_\theta^2 H}{r}\right]=\\
&f_C V_\theta H-gH\frac{\partial \zeta}{\partial r}+\frac{1}{\rho}\tau_{rw}-\frac{1}{\rho}\tau_{rb}\\
&+\frac{\partial}{\partial r}\left[\left(E+2\overline{E}_t\right)H\frac{\partial V_r}{\partial r}\right]+\frac{1}{r}\frac{\partial}{\partial \theta}\left[\left(E+\overline{E}_t\right)H\frac{1}{r}\frac{\partial V_r}{\partial \theta}\right]\\
&+\frac{1}{r}\frac{\partial}{\partial \theta}\left(\overline{E}_t H\frac{\partial V_\theta}{\partial r}\right)-\frac{1}{r^2}\left(3\overline{E}_t+2E\right)H\frac{\partial V_\theta}{\partial \theta}
\end{aligned} \qquad \text{(A7.22)}$$

$$+\frac{1}{r}\left(E+2\overline{E}_t\right)H\frac{\partial V_r}{\partial r}-\left(E+2\overline{E}_t\right)H\frac{V_r}{r^2} \qquad \text{(A7.22) } \textit{continued}$$

where:

$$\frac{1}{r^2}\frac{\partial}{\partial\theta}\left(\overline{E}_t V_\theta H\right)=\frac{1}{r^2}\overline{E}_t H\frac{\partial V_\theta}{\partial\theta}+\frac{1}{r^2}V_\theta\frac{\partial\left(\overline{E}_t H\right)}{\partial\theta}$$

Variation of the averaged turbulent viscosity is assumed to be very small: $\frac{1}{r^2}V_\theta H\frac{\partial\overline{E}_t}{\partial\theta}\approx 0$. At the free surface: $\tau_{rz\zeta}=\tau_{rw}$ is the wind shear stress component in the $r-$direction. At the bed: $\tau_{rz-h}=\tau_{rb}$ is the bed shear stress component in the $r-$direction.

Equation (A7.22) can be written:

$$\begin{aligned}&\frac{\partial V_r H}{\partial t}+\beta\left[\frac{\partial\left(V_r^2 H\right)}{\partial r}+\frac{1}{r}\frac{\partial\left(V_r V_\theta H\right)}{\partial\theta}+\frac{V_r^2 H-V_\theta^2 H}{r}\right]=\\&f_C V_\theta H-gH\frac{\partial\zeta}{\partial r}+\frac{1}{\rho}\tau_{rw}-\frac{1}{\rho}\tau_{rb}+\frac{\partial}{\partial r}\left[2\overline{E}_t H\frac{\partial V_r}{\partial r}\right]\\&+\frac{1}{r}\frac{\partial}{\partial\theta}\left[\overline{E}_t H\frac{1}{r}\frac{\partial V_r}{\partial\theta}\right]+\frac{1}{r}\frac{\partial}{\partial\theta}\left(\overline{E}_t H\frac{\partial V_\theta}{\partial r}\right)-\frac{3}{r^2}\overline{E}_t H\frac{\partial V_\theta}{\partial\theta}\\&+\frac{1}{r}\frac{\partial}{\partial\theta}\left(\overline{E}_t H\frac{\partial V_\theta}{\partial r}\right)+\frac{2}{r}\overline{E}_t H\frac{\partial V_r}{\partial r}-2\overline{E}_t H\frac{V_r}{r^2}\end{aligned} \qquad \text{(A7.23)}$$

Knowing that:

$$\frac{\partial}{\partial r}\left[\frac{1}{r}\frac{\partial}{\partial r}\left(rV_r\right)\right]=\frac{\partial^2 V_r}{\partial r^2}+\frac{1}{r}\frac{\partial V_r}{\partial r}-\frac{1}{r^2}V_r$$

equation (A7.23) further transforms into:

$$\begin{aligned}&\frac{\partial V_r H}{\partial t}+\beta\left[\frac{\partial\left(V_r^2 H\right)}{\partial r}+\frac{1}{r}\frac{\partial\left(V_r V_\theta H\right)}{\partial\theta}+\frac{V_r^2 H-V_\theta^2 H}{r}\right]=\\&f_C V_\theta H-gH\frac{\partial\zeta}{\partial r}+\frac{1}{\rho}\tau_{rw}-\frac{1}{\rho}\tau_{rb}\end{aligned} \qquad \text{(A7.24)}$$

$$+2\frac{\partial}{\partial r}\left[\overline{E}_t H\frac{1}{r}\frac{\partial\left(rV_r\right)}{\partial r}\right]+\frac{1}{r}\frac{\partial}{\partial\theta}\left[\overline{E}_t H\frac{1}{r}\frac{\partial V_r}{\partial\theta}\right] \tag{A7.24}$$

$$+\frac{1}{r}\frac{\partial}{\partial\theta}\left(\overline{E}_t H\frac{\partial V_\theta}{\partial r}\right)-\frac{3}{r^2}\overline{E}_t H\frac{\partial V_\theta}{\partial\theta}$$ *continued*

APPENDIX 8

Calculus for Depth Integration of the $\theta-$ direction Momentum Equation Written in Cylindrical Polar Coordinates

Depth integration of the $\theta-$ direction momentum equation between free surface (ζ) and bed $(-h)$, over the water column ($H=\zeta+h$), is performed using Leibnitz's rule (3.64) so that equation (3.79) can be written for identification of terms:

θ – direction momentum equation

$$\underbrace{\int_{-h}^{\zeta}\frac{\partial\overline{v}_\theta}{\partial t}dz}_{1}+\underbrace{\int_{-h}^{\zeta}\frac{\partial\overline{v}_r\overline{v}_\theta}{\partial r}dz}_{2}+\underbrace{\int_{-h}^{\zeta}\frac{1}{r}\frac{\partial\overline{v}_\theta^2}{\partial\theta}dz}_{3}+\underbrace{\int_{-h}^{\zeta}\frac{\partial\overline{v}_z\overline{v}_\theta}{\partial z}dz}_{4}+\underbrace{\int_{-h}^{\zeta}2\frac{\overline{v}_r\overline{v}_\theta}{r}dz}_{5}=$$
$$\underbrace{-\int_{-h}^{\zeta}f_C\overline{v}_r dz}_{6}\underbrace{-\int_{-h}^{\zeta}\frac{1}{\rho r}\frac{\partial\overline{p}}{\partial\theta}dz}_{7}+\underbrace{\int_{-h}^{\zeta}\frac{\partial}{\partial r}\left(E\frac{\partial\overline{v}_\theta}{\partial r}-\overline{v'_r\,v'_\theta}\right)dz}_{8}+$$
$$\underbrace{+\int_{-h}^{\zeta}\frac{1}{r}\frac{\partial}{\partial\theta}\left(\frac{1}{r}E\frac{\partial\overline{v}_\theta}{\partial\theta}-\overline{v'_\theta\,v'_\theta}\right)dz}_{9}+\underbrace{\int_{-h}^{\zeta}\frac{\partial}{\partial z}\left(E\frac{\partial\overline{v}_\theta}{\partial z}-\overline{v'_\theta\,v'_z}\right)dz}_{10}+ \qquad (3.79)$$
$$\underbrace{+\int_{-h}^{\zeta}\frac{1}{r}E\frac{\partial\overline{v}_\theta}{\partial r}dz}_{11}+\underbrace{\int_{-h}^{\zeta}\frac{2}{r^2}E\frac{\partial\overline{v}_r}{\partial\theta}dz}_{12}\underbrace{-\int_{-h}^{\zeta}E\frac{\overline{v}_\theta}{r^2}dz}_{13}-$$
$$\underbrace{-2\int_{-h}^{\zeta}\frac{\overline{v'_r\,v'_\theta}}{r}dz}_{14}$$

where Leibnitz's rule is written for each term as follows:

- term 1:

$$\int_{-h}^{\zeta}\frac{\partial\overline{v}_\theta}{\partial t}dz=\frac{\partial}{\partial t}\int_{-h}^{\zeta}\overline{v}_\theta dz-\left(\overline{v}_\theta\right)_\zeta\frac{\partial\zeta}{\partial t}+\left(\overline{v}_\theta\right)_{-h}\frac{\partial(-h)}{\partial t}$$

- term 2:

$$\int_{-h}^{\zeta}\frac{\partial\left(\overline{v}_r\overline{v}_\theta\right)}{\partial r}dz=\frac{\partial}{\partial r}\int_{-h}^{\zeta}\overline{v}_r\overline{v}_\theta dz-\left(\overline{v}_r\overline{v}_\theta\right)_\zeta\frac{\partial\zeta}{\partial r}+\left(\overline{v}_r\overline{v}_\theta\right)_{-h}\frac{\partial(-h)}{\partial r}$$

- term 3:

$$\int_{-h}^{\zeta}\frac{1}{r}\frac{\partial\left(\overline{v}_\theta\overline{v}_\theta\right)}{\partial\theta}dz=\frac{1}{r}\frac{\partial}{\partial\theta}\int_{-h}^{\zeta}\overline{v}_\theta\overline{v}_\theta dz-\frac{1}{r}\left(\overline{v}_\theta\overline{v}_\theta\right)_\zeta\frac{\partial\zeta}{\partial\theta}+\frac{1}{r}\left(\overline{v}_\theta\overline{v}_\theta\right)_{-h}\frac{\partial(-h)}{\partial\theta}$$

$$\frac{1}{r}\frac{\partial}{\partial\theta}\int_{-h}^{\zeta}\overline{v}_\theta\overline{v}_\theta dz=\beta\frac{1}{r}\frac{\partial V_\theta^2(h+\zeta)}{\partial\theta}$$

$$\int_{-h}^{\zeta}\frac{1}{r}\frac{\partial\left(\overline{v}_\theta\overline{v}_\theta\right)}{\partial\theta}dz=\beta\frac{1}{r}\frac{\partial V_\theta^2(h+\zeta)}{\partial\theta}-\frac{1}{r}\left(\overline{v}_\theta\overline{v}_\theta\right)_\zeta\frac{\partial\zeta}{\partial\theta}+\frac{1}{r}\left(\overline{v}_\theta\overline{v}_\theta\right)_{-h}\frac{\partial(-h)}{\partial\theta}$$

- term 4:

$$\int_{-h}^{\zeta}\frac{\partial\left(\overline{v}_\theta\overline{v}_z\right)}{\partial z}dz=\left(\overline{v}_\theta\overline{v}_z\right)_\zeta-\left(\overline{v}_\theta\overline{v}_z\right)_{-h}$$

- term 5:

$$\int_{-h}^{\zeta}2\frac{\overline{v}_r\overline{v}_\theta}{r}dz=2\beta\frac{V_rV_\theta H}{r}$$

Terms 6 and 7 are derived analogously to the corresponding terms in the r – direction.

- term 8:

$$\int_{-h}^{\zeta}\frac{\partial}{\partial r}\left(E\frac{\partial\overline{v}_\theta}{\partial r}-\overline{v'_r\,v'_\theta}\right)dz=\int_{-h}^{\zeta}\frac{\partial}{\partial r}\left[E\frac{\partial\overline{v}_\theta}{\partial r}+E_t\left(\frac{\partial\overline{v}_\theta}{\partial r}-\frac{\overline{v}_\theta}{r}+\frac{1}{r}\frac{\partial\overline{v}_r}{\partial\theta}\right)\right]dz=$$

$$\frac{\partial}{\partial r}\left[EH\frac{\partial V_\theta}{\partial r}\right]+\frac{\partial}{\partial r}\left[\overline{E}_tH\frac{\partial V_\theta}{\partial r}\right]-\frac{\partial}{\partial r}\left[\overline{E}_tH\frac{V_\theta}{r}\right]+\frac{\partial}{\partial r}\left[\overline{E}_tH\frac{1}{r}\frac{\partial V_r}{\partial\theta}\right]$$

$$\overline{k}=\frac{1}{2}\left(\overline{v'}_r^2+\overline{v'}_\theta^2+\overline{v'}_z^2\right)$$

- term 9:

$$\frac{1}{r}\int_{-h}^{\zeta}\frac{\partial}{\partial\theta}\left(\frac{1}{r}E\frac{\partial\overline{v}_\theta}{\partial\theta}-\overline{v'_\theta\,v'_\theta}\right)dz=\frac{1}{r}\int_{-h}^{\zeta}\frac{\partial}{\partial\theta}\left[\frac{1}{r}E\frac{\partial\overline{v}_\theta}{\partial\theta}+2E_t\left(\frac{1}{r}\frac{\partial\overline{v}_\theta}{\partial\theta}+\frac{\overline{v}_r}{r}\right)-\frac{2}{3}k\right]dz=$$

$$\frac{1}{r^2}\frac{\partial}{\partial\theta}\left[EH\frac{\partial V_\theta}{\partial\theta}\right]+\frac{2}{r^2}\frac{\partial}{\partial\theta}\left[\overline{E}_tH\frac{\partial V_\theta}{\partial\theta}+\overline{E}_tHV_r\right]-\frac{2}{3}\overline{k}H$$

- term 10:

$$\int_{-h}^{\zeta}\frac{\partial}{\partial z}\left(E\frac{\partial \bar{v}_\theta}{\partial z}-\overline{v'_\theta\, v'_z}\right)dz=\frac{1}{\rho}\left(\tau_{\theta z\zeta}-\tau_{\theta z-h}\right)$$

At free surface: $\tau_{\theta z\zeta}=\tau_{\theta w}$ is the wind shear stress component in θ – direction.

At bed: $\tau_{\theta z-h}=\tau_{\theta b}$ is the bed shear stress component in θ – direction.

- term 11:

$$\int_{-h}^{\zeta}\frac{1}{r}E\frac{\partial \bar{v}_\theta}{\partial r}dz=\frac{1}{r}EH\frac{\partial V_\theta}{\partial r}$$

-term 12:

$$\frac{2}{r^2}\int_{-h}^{\zeta}E\frac{\partial \bar{v}_r}{\partial \theta}dz=\frac{2}{r^2}EH\frac{\partial V_r}{\partial \theta}$$

- term 13:

$$\int_{-h}^{\zeta}E\frac{\bar{v}_\theta}{r^2}dz=\frac{1}{r^2}E\int_{-h}^{\zeta}\bar{v}_\theta dz=\frac{1}{r^2}EHV_\theta$$

- term 14:

$$-\frac{2}{r}\int_{-h}^{\zeta}\overline{v'_r\, v'_\theta}dz=\frac{2}{r}\int_{-h}^{\zeta}\left[E_t\left(\frac{\partial \bar{v}_\theta}{\partial r}-\frac{\bar{v}_\theta}{r}+\frac{1}{r}\frac{\partial \bar{v}_r}{\partial \theta}\right)\right]dz=\frac{2}{r}\left[\bar{E}_t H\frac{\partial V_\theta}{\partial r}\right]-\frac{2}{r}\bar{E}_t H\frac{V_\theta}{r}+$$
$$+\frac{2}{r^2}\bar{E}_t H\frac{\partial V_r}{\partial \theta}$$

Using the above relationships, equation (3.79) can be written:

θ – direction momentum equation

$$\underbrace{\frac{\partial V_\theta H}{\partial t}-\left(\bar{v}_\theta\right)_\zeta\frac{\partial \zeta}{\partial t}+\left(\bar{v}_\theta\right)_{-h}\frac{\partial(-h)}{\partial t}}_{1} \qquad \text{(A8.1)}$$

$$+\underbrace{\beta\frac{1}{r}\frac{\partial V_r V_\theta(h+\zeta)}{\partial\theta}-(\overline{v}_r\overline{v}_\theta)_\zeta\frac{\partial\zeta}{\partial r}+(\overline{v}_r\overline{v}_\theta)_{-h}\frac{\partial(-h)}{\partial r}}_{2}$$

$$+\underbrace{\beta\frac{1}{r}\frac{\partial V_\theta^2(h+\zeta)}{\partial\theta}-\frac{1}{r}(\overline{v}_\theta\overline{v}_\theta)_\zeta\frac{\partial\zeta}{\partial\theta}+\frac{1}{r}(\overline{v}_\theta\overline{v}_\theta)_{-h}\frac{\partial(-h)}{\partial\theta}}_{3}$$

$$+\underbrace{(\overline{v}_\theta\overline{v}_z)_\zeta-(\overline{v}_\theta\overline{v}_z)}_{4}+\underbrace{2\beta\frac{V_r V_\theta H}{r}}_{5}$$

$$=-\underbrace{f_C V_r}_{6}-\underbrace{\frac{1}{r}gH\frac{\partial\zeta}{\partial\theta}}_{7}$$

$$+\underbrace{\frac{\partial}{\partial r}\left[EH\frac{\partial V_\theta}{\partial r}\right]+\frac{\partial}{\partial r}\left[\overline{E}_t H\frac{\partial V_\theta}{\partial r}\right]-\frac{\partial}{\partial r}\left[\overline{E}_t H\frac{V_\theta}{r}\right]}_{8}$$

$$+\underbrace{\frac{\partial}{\partial r}\left[\frac{1}{r}\overline{E}_t H\frac{\partial V_r}{\partial\theta}\right]}_{8}$$

$$+\underbrace{\frac{1}{r^2}\frac{\partial}{\partial\theta}\left[EH\frac{\partial V_\theta}{\partial\theta}\right]+\frac{2}{r^2}\frac{\partial}{\partial\theta}\left[\overline{E}_t H\frac{\partial V_\theta}{\partial\theta}+\overline{E}_t H V_r\right]-\frac{2}{3}\overline{k}H}_{9}$$

$$+\underbrace{\frac{1}{\rho}(\tau_{\theta z\zeta}-\tau_{\theta z-h})}_{10}$$

$$+\underbrace{\frac{1}{r}EH\frac{\partial V_\theta}{\partial r}}_{11}+\underbrace{\frac{2}{r^2}EH\frac{\partial V_r}{\partial\theta}}_{12}-\underbrace{\frac{1}{r^2}EHV_\theta}_{13}$$

$$+\underbrace{\frac{2}{r}\left[\overline{E}_t H\frac{\partial V_\theta}{\partial r}\right]-\frac{2}{r}\overline{E}_t H\frac{V_\theta}{r}+\frac{2}{r^2}\overline{E}_t H\frac{\partial V_r}{\partial\theta}}_{14} \qquad \text{(A8.1)}$$

continued

Grouping terms resulted from turbulence modelling in the terms with same number one gets:

θ – direction momentum equation

$$\underbrace{\frac{\partial V_\theta H}{\partial t}-(\overline{v}_\theta)_\zeta\frac{\partial\zeta}{\partial t}+(\overline{v}_\theta)_{-h}\frac{\partial(-h)}{\partial t}}_{1} \qquad \text{(A8.2)}$$

$$
\begin{aligned}
&+\underbrace{\beta\frac{1}{r}\frac{\partial V_r V_\theta (h+\zeta)}{\partial\theta}-(\overline{v}_r\overline{v}_\theta)_\zeta\frac{\partial\zeta}{\partial r}+(\overline{v}_r\overline{v}_\theta)_{-h}\frac{\partial(-h)}{\partial r}}_{2}\\
&+\underbrace{\beta\frac{1}{r}\frac{\partial V_\theta^2 (h+\zeta)}{\partial\theta}-\frac{1}{r}(\overline{v}_\theta\overline{v}_\theta)_\zeta\frac{\partial\zeta}{\partial\theta}+\frac{1}{r}(\overline{v}_\theta\overline{v}_\theta)_{-h}\frac{\partial(-h)}{\partial\theta}}_{3}\\
&+\underbrace{(\overline{v}_\theta\overline{v}_z)_\zeta-(\overline{v}_\theta\overline{v}_z)}_{4}+\underbrace{2\beta\frac{V_r V_\theta H}{r}}_{5}\\
&=-\underbrace{f_C V_r}_{6}-\underbrace{\frac{1}{r}gH\frac{\partial\zeta}{\partial\theta}}_{7}\\
&+\underbrace{\frac{\partial}{\partial r}\left[(EH+\overline{E}_t H)\frac{\partial V_\theta}{\partial r}\right]-\frac{\partial}{\partial r}\left[\overline{E}_t H\frac{V_\theta}{r}\right]+\frac{\partial}{\partial r}\left[\frac{1}{r}\overline{E}_t H\frac{\partial V_r}{\partial\theta}\right]}_{8}\\
&+\underbrace{\frac{1}{r^2}\frac{\partial}{\partial\theta}\left[(EH+2\overline{E}_t H)\frac{\partial V_\theta}{\partial\theta}\right]+\frac{2}{r^2}\frac{\partial}{\partial\theta}\left[\overline{E}_t H V_r\right]}_{9}\\
&+\underbrace{\frac{1}{\rho}(\tau_{\theta z\zeta}-\tau_{\theta z-h})}_{10}+\underbrace{\frac{1}{r}EH\frac{\partial V_\theta}{\partial r}}_{11}+\underbrace{\frac{2}{r^2}EH\frac{\partial V_r}{\partial\theta}}_{12}-\underbrace{\frac{1}{r^2}EHV_\theta}_{13}\\
&+\underbrace{\frac{2}{r}\left[\overline{E}_t H\frac{\partial V_\theta}{\partial r}\right]-\frac{2}{r}\overline{E}_t H\frac{V_\theta}{r}+\overline{E}_t H\frac{2}{r^2}\frac{\partial V_r}{\partial\theta}}_{14}
\end{aligned}
\qquad \text{(A8.2)}
$$

continued

Further grouping of the turbulence terms gives:

θ – direction momentum equation

$$
\begin{aligned}
&\underbrace{\frac{\partial V_\theta H}{\partial t}-(\overline{v}_\theta)_\zeta\frac{\partial\zeta}{\partial t}+(\overline{v}_\theta)_{-h}\frac{\partial(-h)}{\partial t}}_{1}\\
&+\underbrace{\beta\frac{1}{r}\frac{\partial V_r V_\theta (h+\zeta)}{\partial\theta}-(\overline{v}_r\overline{v}_\theta)_\zeta\frac{\partial\zeta}{\partial r}+(\overline{v}_r\overline{v}_\theta)_{-h}\frac{\partial(-h)}{\partial r}}_{2}\\
&+\underbrace{\beta\frac{1}{r}\frac{\partial V_\theta^2 (h+\zeta)}{\partial\theta}-\frac{1}{r}(\overline{v}_\theta\overline{v}_\theta)_\zeta\frac{\partial\zeta}{\partial\theta}+\frac{1}{r}(\overline{v}_\theta\overline{v}_\theta)_{-h}\frac{\partial(-h)}{\partial\theta}}_{3}\\
&+\underbrace{(\overline{v}_\theta\overline{v}_z)_\zeta-(\overline{v}_\theta\overline{v}_z)}_{4}+\underbrace{2\beta\frac{V_r V_\theta H}{r}}_{5}
\end{aligned}
\qquad \text{(A8.3)}
$$

$$= -\underbrace{f_C V_r}_{6} - \underbrace{\frac{1}{r} gH \frac{\partial \zeta}{\partial \theta}}_{7} + \frac{1}{\rho}\left(\tau_{\theta z\zeta} - \tau_{\theta z-h}\right)$$

$$+ \frac{\partial}{\partial r}\left[\left(EH + \overline{E}_t H\right)\frac{\partial V_\theta}{\partial r}\right] + \frac{1}{r^2}\frac{\partial}{\partial \theta}\left[\left(EH + 2\overline{E}_t H\right)\frac{\partial V_\theta}{\partial \theta}\right] \qquad \text{(A8.3)}$$

$$+ \frac{1}{r}\left[\left(2\overline{E}_t H + EH\right)\frac{\partial V_\theta}{\partial r}\right] - \frac{\partial}{\partial r}\left[\overline{E}_t H \frac{V_\theta}{r}\right] - \frac{1}{r^2}\left(EH + 2\overline{E}_t H\right)V_\theta \qquad \textit{continued}$$

$$+ \left(\overline{E}_t H + EH\right)\frac{2}{r^2}\frac{\partial V_r}{\partial \theta} + \frac{2}{r^2}\frac{\partial}{\partial \theta}\left[\overline{E}_t H V_r\right] + \frac{\partial}{\partial r}\left[\overline{E}_t H \frac{1}{r}\frac{\partial V_r}{\partial \theta}\right]$$

Kinematic and no-slip boundary conditions can be applied at the free surface and bed, respectively so that equation (A8.3) becomes:

θ – direction momentum equation

$$\frac{\partial V_\theta H}{\partial t} + \beta \frac{1}{r}\frac{\partial V_r V_\theta H}{\partial \theta} + \beta \frac{1}{r}\frac{\partial V_\theta^2 (h+\zeta)}{\partial \theta} + 2\beta \frac{V_r V_\theta H}{r} \qquad \text{(A8.4)}$$

$$= -f_C V_r - \frac{1}{r} gH \frac{\partial \zeta}{\partial \theta} + \frac{1}{\rho}\left(\tau_{\theta z\zeta} - \tau_{\theta z-h}\right)$$

$$+ \frac{\partial}{\partial r}\left[\overline{E}_t H \frac{\partial V_\theta}{\partial r}\right] + \frac{2}{r^2}\frac{\partial}{\partial \theta}\left[\overline{E}_t H \frac{\partial V_\theta}{\partial \theta}\right]$$

$$+ \frac{2}{r}\left[\overline{E}_t H \frac{\partial V_\theta}{\partial r}\right] - \frac{1}{r}\frac{\partial}{\partial r}\left[\overline{E}_t H V_\theta\right] + \frac{1}{r^2}\overline{E}_t H V_\theta - \frac{2}{r^2}\overline{E}_t H V_\theta$$

$$+ \overline{E}_t H \frac{2}{r^2}\frac{\partial V_r}{\partial \theta} + \frac{2}{r^2}\frac{\partial}{\partial \theta}\left[\overline{E}_t H V_r\right] + \frac{1}{r}\frac{\partial}{\partial r}\left[\overline{E}_t H \frac{\partial V_r}{\partial \theta}\right] - \overline{E}_t H \frac{1}{r^2}\frac{\partial V_r}{\partial \theta}$$

APPENDIX 9

Calculus for Transformation of the Depth Integrated Governing Equations Written in Cylindrical Coordinates from the Physical onto Computational Domain

Continuity Equation

Continuity equation (3.73) transforms according to transformation relationships (3.103) in:

$$\frac{\partial \zeta}{\partial t}+\frac{1}{r}\frac{1}{h_{\xi^r}}\frac{\partial}{\partial \xi^r}\left(rq_{\xi^r}\right)+\frac{1}{h_{\xi^\theta}}\frac{\partial q_{\xi^\theta}}{\partial \xi^\theta}=0 \Rightarrow \tag{A9.1}$$

$$\frac{\partial \zeta}{\partial t}+\frac{1}{r}\frac{1}{h_{\xi^r}}\frac{r}{h_r}\frac{\partial q_{\xi^r}}{\partial \xi^r}+\frac{1}{r}\frac{1}{h_{\xi^r}}q_{\xi^r}\frac{\partial r}{\partial \xi^r}+\frac{1}{h_{\xi^\theta}}\frac{\partial q_{\xi^\theta}}{\partial \xi^\theta}=0 \tag{A9.2}$$

because:

$$\frac{J}{h_r}=r$$

and $\frac{\partial r}{\partial \xi^r}=\Delta r$

the third term in the above equation becomes:

$$\frac{1}{r}\frac{1}{h_{\xi^r}}q_{\xi^r}\frac{\partial}{\partial \xi^r}\left(\frac{r}{h_r}\right)=\frac{q_{\xi^r}}{r}$$

$J=h_r h_\theta;\ h_r=1;\ h_\theta=r$

$h_{\xi^r}, h_{\xi^\theta}$ are the scale factors of the transformation from cylindrical co-ordinates to computational plane.

$q_{\xi^r}, q_{\xi^\theta}$ are the components of discharge per unit width in the two directions ξ^r, ξ^θ of the computational plane.

Equation (A9.2) can be written as:

$$\frac{\partial \zeta}{\partial t}+\frac{1}{h_{\xi^r}}\frac{\partial q_{\xi^r}}{\partial \xi^r}+\frac{1}{r}q_{\xi^r}+\frac{1}{h_{\xi^\theta}}\frac{\partial q_{\xi^\theta}}{\partial \xi^\theta}=0 \tag{A9.3}$$

The following work can be done on equation (A9.3):

$$\frac{h_{\xi^r}h_{\xi^\theta}}{J_\xi}\frac{\partial \zeta}{\partial t}+\frac{1}{r}\frac{h_{\xi^\theta}}{J_\xi}\frac{\partial\left(rq_{\xi^r}\right)}{\partial \xi^r}+\frac{h_{\xi^r}}{J_\xi}\frac{\partial q_{\xi^\theta}}{\partial \xi^\theta}=0$$

$$\frac{h_{\xi^r}h_{\xi^\theta}}{J_\xi}\frac{\partial \zeta}{\partial t}+\frac{h_{\xi^\theta}}{J_\xi}\frac{\partial q_{\xi^r}}{\partial \xi^r}+\frac{1}{r}\frac{h_{\xi^\theta}}{J_\xi}q_{\xi^r}\frac{\partial r}{\partial \xi^r}+\frac{h_{\xi^r}}{J_\xi}\frac{\partial q_{\xi^\theta}}{\partial \xi^\theta}=0$$

$$\frac{h_{\xi^r}h_{\xi^\theta}}{J_\xi}\frac{\partial \zeta}{\partial t}+\frac{h_{\xi^\theta}}{J_\xi}\frac{\partial q_{\xi^r}}{\partial \xi^r}+\frac{1}{r}q_{\xi^r}+\frac{1}{J_\xi}\frac{\partial\left(h_{\xi^r}q_{\xi^\theta}\right)}{\partial \xi^\theta}=0$$

$$\frac{h_{\xi^r}h_{\xi^\theta}}{J_\xi}\frac{\partial \zeta}{\partial t}+\frac{1}{J_\xi}\frac{\partial\left(h_{\xi^\theta}q_{\xi^r}\right)}{\partial \xi^r}-\frac{1}{J_\xi}q_{\xi^r}\frac{\partial h_{\xi^\theta}}{\partial \xi^r}+\frac{1}{r}q_{\xi^r}+\frac{1}{J_\xi}\frac{\partial\left(h_{\xi^r}q_{\xi^\theta}\right)}{\partial \xi^\theta}=0$$

$$\frac{h_{\xi^r}h_{\xi^\theta}}{J_\xi}\frac{\partial \zeta}{\partial t}+\frac{1}{J_\xi}\frac{\partial\left(h_{\xi^\theta}q_{\xi^r}\right)}{\partial \xi^r}-\frac{1}{r}q_{\xi^r}+\frac{1}{r}q_{\xi^r}+\frac{1}{J_\xi}\frac{\partial\left(h_{\xi^r}q_{\xi^\theta}\right)}{\partial \xi^\theta}=0$$

$$\frac{\partial \zeta}{\partial t}+\frac{1}{J_\xi}\frac{\partial\left(h_{\xi^\theta}q_{\xi^r}\right)}{\partial \xi^r}+\frac{1}{J_\xi}\frac{\partial\left(h_{\xi^r}q_{\xi^\theta}\right)}{\partial \xi^\theta}=0 \tag{A9.4}$$

where:

$$\frac{\partial h_{\xi^\theta}}{\partial \xi^r}=\frac{\partial\left(r\Delta\theta\right)}{\partial \xi^r}=\Delta\theta\frac{\partial r}{\partial \xi^r}=\Delta r\Delta\theta$$

$$\frac{1}{J_\xi}\frac{\partial h_{\xi^\theta}}{\partial \xi^r}=\frac{1}{r}$$

and $h_{\xi^r}=\Delta r\neq f\left(\xi^\theta\right)$.

Equation (A8.4) gives the continuity equation after mapping transformations are performed from the physical domain onto the computational domain.

Acceleration terms

The acceleration term in the $r-$direction momentum equation (3.92) is:

$r-$direction

$$a(r)=\frac{\partial q_r}{\partial t}+\left(\frac{\partial V_r V_r H}{\partial r}+\frac{1}{r}\frac{\partial V_r V_\theta H}{\partial \theta}+\frac{V_r^2 H-V_\theta^2 H}{r}\right)\Leftrightarrow \tag{A9.5}$$

$$a(r)=\left(\frac{\partial V_r q_r}{\partial r}+\frac{1}{r}\frac{\partial V_\theta q_r}{\partial \theta}+\frac{V_r q_r-V_\theta q_\theta}{r}\right)$$

Using transformation relationships (3.105a), equation (A9.5) becomes:

$$a\left(\xi^r\right)=\frac{h_{\xi^r}}{h_r}\frac{\partial \xi^r}{\partial r}a(r)+\frac{h_{\xi^r}}{h_\theta}\frac{\partial \xi^r}{\partial \theta}a(\theta)\Rightarrow$$

$$a\left(\xi^r\right)=\frac{h_{\xi^r}}{h_r}\frac{\partial \xi^r}{\partial r}\left(\frac{\partial q_r}{\partial t}+\frac{1}{h_r}\frac{\partial V_r q_r}{\partial r}+\frac{1}{h_\theta}\frac{\partial V_\theta q_r}{\partial \theta}+\frac{V_r q_r-V_\theta q_\theta}{h_\theta}\right) \tag{A9.6}$$

$$+\frac{h_{\xi^r}}{h_\theta}\frac{\partial \xi^r}{\partial \theta}\left(\frac{\partial q_\theta}{\partial t}+\frac{1}{h_r}\frac{\partial V_r q_\theta}{\partial r}+\frac{1}{h_\theta}\frac{\partial V_\theta q_\theta}{\partial \theta}+2\frac{V_r q_\theta}{h_\theta}\right)$$

$$a\left(\xi^r\right)=\frac{h_{\xi^r}}{h_r}\frac{\partial \xi^r}{\partial r}\left(\frac{\partial V_r q_r}{\partial r}+\frac{1}{r}\frac{\partial V_\theta q_r}{\partial \theta}+\frac{V_r q_r-V_\theta q_\theta}{r}\right) \tag{A9.7}$$

Since $\frac{\partial \xi^r}{\partial \theta}=0$ and knowing that $\frac{\partial \xi^r}{\partial r}=\frac{1}{\Delta r}$, $h_{\xi^r}=\Delta r$, $h_r=1$, equation (A9.7) results in:

$$a\left(\xi^r\right)=\frac{\partial q_{\xi^r}}{\partial t}+\frac{1}{h_{\xi^r}}\frac{\partial V_{\xi^r} q_{\xi^r}}{\partial \xi^r}+\frac{1}{h_{\xi^\theta}}\frac{\partial V_{\xi^\theta} q_{\xi^r}}{\partial \xi^\theta}+\frac{V_{\xi^r} q_{\xi^r}-V_{\xi^\theta} q_{\xi^\theta}}{r} \tag{A9.8}$$

$$a\left(\xi^r\right)=\frac{\partial q_{\xi^r}}{\partial t}+\frac{1}{h_{\xi^r}}\frac{\partial V_{\xi^r} q_{\xi^r}}{\partial \xi^r}+\frac{1}{h_{\xi^\theta}}\frac{\partial V_{\xi^\theta} q_{\xi^r}}{\partial \xi^\theta}+\frac{1}{J_\xi}\frac{\partial h_{\xi^\theta}}{\partial \xi^r}\left(V_{\xi^r} q_{\xi^r}-V_{\xi^\theta} q_{\xi^\theta}\right)$$

Similarly, the left hand side term in the $\theta-$direction momentum equation (3.93):

θ – direction

$$a(\theta)=\left(\frac{\partial q_\theta}{\partial t}+\frac{\partial V_r q_\theta}{\partial r}+\frac{1}{r}\frac{\partial V_\theta q_\theta}{\partial \theta}+2\frac{V_r q_\theta}{r}\right)\Leftrightarrow$$

$$a(\theta)=\left(\frac{\partial q_\theta}{\partial t}+\frac{\partial V_r q_\theta}{\partial r}+\frac{1}{r}\frac{\partial V_\theta q_\theta}{\partial \theta}+2\frac{V_r q_\theta}{r}\right) \tag{A9.9}$$

is transformed into:

ξ^θ – direction

$$a(\xi^\theta)=\frac{h_{\xi^\theta}}{h_r}\frac{\partial \xi^\theta}{\partial r}a(r)+\frac{h_{\xi^\theta}}{h_\theta}\frac{\partial \xi^\theta}{\partial \theta}a(\theta)\Leftrightarrow$$

$$a(\xi^\theta)=\frac{h_{\xi^\theta}}{h_r}\frac{\partial \xi^\theta}{\partial r}\left(\frac{\partial q_r}{\partial t}+\frac{1}{h_r}\frac{\partial V_r q_r}{\partial r}+\frac{1}{h_\theta}\frac{\partial V_\theta q_r}{\partial \theta}+\frac{V_r q_r - V_\theta q_\theta}{h_\theta}\right) \tag{A9.10}$$

$$+\frac{h_{\xi^\theta}}{h_\theta}\frac{\partial \xi^\theta}{\partial \theta}\left(\frac{\partial q_\theta}{\partial t}+\frac{1}{h_r}\frac{\partial V_r q_\theta}{\partial r}+\frac{1}{h_\theta}\frac{\partial V_\theta q_\theta}{\partial \theta}+2\frac{V_r q_\theta}{h_\theta}\right)$$

A similar analysis to the one performed for equation (A9.8) leads to:

ξ^θ – direction

$$a(\xi^\theta)=\frac{\partial q_{\xi^\theta}}{\partial t}+\frac{1}{h_{\xi^r}}\frac{\partial V_{\xi^r} q_{\xi^\theta}}{\partial \xi^r}+\frac{1}{h_{\xi^\theta}}\frac{\partial V_{\xi^\theta} q_{\xi^\theta}}{\partial \xi^\theta}+2\frac{V_{\xi^r} q_{\xi^\theta}}{r} \tag{A9.11}$$

$$a(\xi^\theta)=\frac{\partial q_{\xi^\theta}}{\partial t}+\frac{1}{h_{\xi^r}}\frac{\partial V_{\xi^r} q_{\xi^\theta}}{\partial \xi^r}+\frac{1}{h_{\xi^\theta}}\frac{\partial V_{\xi^\theta} q_{\xi^\theta}}{\partial \xi^\theta}+2\frac{1}{J_\xi}\frac{\partial h_{\xi^\theta}}{\partial \xi^r}V_{\xi^r} q_{\xi^\theta}$$

Turbulence terms

The Laplacian of a vector in two-dimensional general orthogonal coordinates (ξ^1,ξ^2) is:

$$\nabla^2\vec{A}=\left\{\frac{1}{h_{\xi^1}}\frac{\partial}{\partial\xi^1}\left[\frac{1}{J}\frac{\partial}{\partial\xi^1}\left(h_{\xi^2}A_{\xi^1}\right)\right]+\frac{1}{h_{\xi^2}}\frac{\partial}{\partial\xi^2}\left(\frac{1}{h_{\xi^2}}\frac{\partial A_{\xi^1}}{\partial\xi^2}\right)\right.$$
$$+\frac{1}{h_{\xi^1}}\frac{\partial}{\partial\xi^1}\left[\frac{1}{J}\frac{\partial}{\partial\xi^2}\left(h_{\xi^1}A_{\xi^2}\right)\right]-\frac{1}{h_{\xi^2}}\frac{\partial}{\partial\xi^2}\left(\frac{1}{h_{\xi^1}}\frac{\partial A_{\xi^2}}{\partial\xi^1}\right) \qquad \text{(A9.12)}$$
$$\left.-\frac{1}{h_{\xi^2}}\frac{\partial}{\partial\xi^2}\left[\frac{1}{J}\left(A_{\xi^2}\frac{\partial h_{\xi^2}}{\partial\xi^1}-A_{\xi^1}\frac{\partial h_{\xi^1}}{\partial\xi^2}\right)\right]\right\}\vec{e}_{\xi^1}$$

$$+\left\{\frac{1}{h_{\xi^1}}\frac{\partial}{\partial\xi^1}\left(\frac{1}{h_{\xi^1}}\frac{\partial A_{\xi^2}}{\partial\xi^1}\right)+\frac{1}{h_{\xi^2}}\frac{\partial}{\partial\xi^2}\left[\frac{1}{J}\frac{\partial}{\partial\xi^2}\left(h_{\xi^1}A_{\xi^2}\right)\right]\right.$$
$$-\frac{1}{h_{\xi^1}}\frac{\partial}{\partial\xi^1}\left(\frac{1}{h_{\xi^2}}\frac{\partial A_{\xi^1}}{\partial\xi^2}\right)+\frac{1}{h_{\xi^2}}\frac{\partial}{\partial\xi^2}\left[\frac{1}{J}\frac{\partial}{\partial\xi^1}\left(h_{\xi^2}A_{\xi^1}\right)\right] \qquad \text{(A9.12)}$$
$$\left.+\frac{1}{h_{\xi^1}}\frac{\partial}{\partial\xi^1}\left[\frac{1}{J}\left(A_{\xi^2}\frac{\partial h_{\xi^2}}{\partial\xi^1}-A_{\xi^1}\frac{\partial h_{\xi^1}}{\partial\xi^2}\right)\right]\right\}\vec{e}_{\xi^2} \qquad \textit{continued}$$

or:

$$\nabla^2\vec{A}=\left\{\frac{1}{h_{\xi^1}}\frac{\partial}{\partial\xi^1}\left[\frac{1}{J}\frac{\partial}{\partial\xi^1}\left(h_{\xi^2}A_{\xi^1}\right)\right]+\frac{1}{h_{\xi^2}}\frac{\partial}{\partial\xi^2}\left(\frac{1}{J}\frac{\partial h_{\xi^1}A_{\xi^1}}{\partial\xi^2}\right)\right.$$
$$\left.+\frac{1}{h_{\xi^1}}\frac{\partial}{\partial\xi^1}\left[\frac{1}{J}\frac{\partial}{\partial\xi^2}\left(h_{\xi^1}A_{\xi^2}\right)\right]-\frac{1}{h_{\xi^2}}\frac{\partial}{\partial\xi^2}\left(\frac{1}{J}\frac{\partial h_{\xi^2}A_{\xi^2}}{\partial\xi^1}\right)\right\}\vec{e}_{\xi^1} \qquad \text{(A9.13)}$$
$$+\left\{\frac{1}{h_{\xi^1}}\frac{\partial}{\partial\xi^1}\left(\frac{1}{J}\frac{\partial h_{\xi^2}A_{\xi^2}}{\partial\xi^1}\right)+\frac{1}{h_{\xi^2}}\frac{\partial}{\partial\xi^2}\left[\frac{1}{J}\frac{\partial}{\partial\xi^2}\left(h_{\xi^1}A_{\xi^2}\right)\right]\right.$$
$$\left.-\frac{1}{h_{\xi^1}}\frac{\partial}{\partial\xi^1}\left(\frac{1}{J}\frac{\partial h_{\xi^1}A_{\xi^1}}{\partial\xi^2}\right)+\frac{1}{h_{\xi^2}}\frac{\partial}{\partial\xi^2}\left[\frac{1}{J}\frac{\partial}{\partial\xi^1}\left(h_{\xi^2}A_{\xi^1}\right)\right]\right\}\vec{e}_{\xi^2}$$

where: h_{ξ^1}, h_{ξ^2} are the scale factors in the two considered directions, A_{ξ^1}, A_{ξ^2} are components of vector $\vec{A}$ in the two orthogonal directions ξ^1 and ξ^2, respectively, and $J = h_{\xi^1}h_{\xi^2}$ is the Jacobian of the transformation from general orthogonal to Cartesian co-ordinates.

The component of the Laplacian of a vector in the r – direction transforms according to equations (3.105a):

$$\nabla^2 V\left(\xi^r\right)=\frac{h_{\xi^r}}{h_r}\frac{\partial \xi^r}{\partial r}\nabla^2 V(r)+\frac{h_{\xi^r}}{h_\theta}\frac{\partial \xi^r}{\partial \theta}\nabla^2 V(\theta)\Rightarrow$$

$$\nabla^2 V\left(\xi^r\right)$$
$$=\frac{h_{\xi^r}}{h_r}\frac{\partial \xi^r}{\partial r}\left(\frac{\partial^2 V_r}{\partial r^2}+\frac{1}{r^2}\frac{\partial^2 V_r}{\partial \theta^2}+\frac{1}{r}\frac{\partial V_r}{\partial r}-\frac{2}{r^2}\frac{\partial V_\theta}{\partial \theta}-\frac{V_r}{r^2}\right)$$
$$+\frac{h_{\xi^r}}{h_\theta}\frac{\partial \xi^r}{\partial \theta}\left(\frac{\partial^2 V_\theta}{\partial r^2}+\frac{1}{r^2}\frac{\partial^2 V_\theta}{\partial \theta^2}+\frac{1}{r}\frac{\partial V_\theta}{\partial r}+\frac{2}{r^2}\frac{\partial V_r}{\partial \theta}-\frac{V_\theta}{r^2}\right)$$

$$\nabla^2 V\left(\xi^r\right)$$
$$=\frac{h_{\xi^r}}{h_r}\frac{\partial \xi^r}{\partial r}\left[\frac{\partial}{\partial r}\left(\frac{\partial V_r}{\partial r}\right)+\frac{1}{r^2}\frac{\partial}{\partial \theta}\left(\frac{\partial V_r}{\partial \theta}\right)+\frac{1}{r}\frac{\partial V_r}{\partial r}-\frac{2}{r^2}\frac{\partial V_\theta}{\partial \theta}-\frac{V_r}{r^2}\right]$$

$$\nabla^2 V\left(\xi^r\right)=\frac{1}{h_{\xi^r}}\frac{\partial}{\partial \xi^r}\left(\frac{1}{h_{\xi^r}}\frac{\partial V_{\xi^r}}{\partial \xi^r}\right)+\frac{1}{h_{\xi^\theta}}\frac{\partial}{\partial \xi^\theta}\left(\frac{1}{h_{\xi^\theta}}\frac{\partial V_{\xi^r}}{\partial \xi^\theta}\right)$$
$$+\frac{1}{r}\frac{1}{h_{\xi^r}}\frac{\partial V_{\xi^r}}{\partial \xi^r}-\frac{1}{r}\frac{2}{h_{\xi^\theta}}\frac{\partial V_{\xi^\theta}}{\partial \xi^\theta}-\frac{V_{\xi^r}}{r^2}$$

$$\nabla^2 V\left(\xi^r\right)$$
$$=\frac{1}{h_{\xi^r}}\frac{\partial}{\partial \xi^r}\left(\frac{1}{h_{\xi^r}}\frac{\partial V_{\xi^r}}{\partial \xi^r}\right)+\frac{1}{h_{\xi^\theta}}\frac{\partial}{\partial \xi^\theta}\left(\frac{1}{h_{\xi^\theta}}\frac{\partial V_{\xi^r}}{\partial \xi^\theta}\right)$$
$$+\frac{1}{h_{\xi^r}}\frac{\partial}{\partial \xi^r}\left(\frac{V_{\xi^r}}{r}\right)-\frac{1}{r}\frac{2}{h_{\xi^\theta}}\frac{\partial V_{\xi^\theta}}{\partial \xi^\theta}-V_{\xi^r}\left(\frac{1}{J_\xi}\frac{\partial h_{\xi^\theta}}{\partial \xi^r}\right)^2$$

$$\nabla^2 V\left(\xi^r\right)$$
$$=\underbrace{\frac{1}{h_{\xi^r}}\frac{\partial}{\partial \xi^r}\left(\frac{1}{h_{\xi^r}}\frac{\partial V_{\xi^r}}{\partial \xi^r}\right)}_{1}+\underbrace{\frac{1}{h_{\xi^\theta}}\frac{\partial}{\partial \xi^\theta}\left(\frac{1}{h_{\xi^\theta}}\frac{\partial V_{\xi^r}}{\partial \xi^\theta}\right)}_{2}$$
$$+\underbrace{\frac{1}{J_\xi}\frac{\partial h_{\xi^\theta}}{\partial \xi^r}\frac{1}{h_{\xi^r}}\frac{\partial V_{\xi^r}}{\partial \xi^r}}_{3}-\underbrace{\frac{1}{r}\frac{2}{h_{\xi^\theta}}\frac{\partial V_{\xi^\theta}}{\partial \xi^\theta}}_{4}-\underbrace{V_{\xi^r}\left(\frac{1}{J_\xi}\frac{\partial h_{\xi^\theta}}{\partial \xi^r}\right)^2}_{5} \qquad \text{(A9.14)}$$

The following treatment is applied to the first, third and fifth terms of equation (A9.14):

$$\frac{1}{h_{\xi^r}}\frac{\partial}{\partial\xi^r}\left(\frac{1}{h_{\xi^r}}\frac{\partial V_{\xi^r}}{\partial\xi^r}\right)+\left(\frac{1}{J_\xi}\frac{\partial h_{\xi^\theta}}{\partial\xi^r}\right)\frac{1}{h_{\xi^r}}\frac{\partial V_{\xi^r}}{\partial\xi^r}-V_{\xi^r}\left(\frac{1}{J_\xi}\frac{\partial h_{\xi^\theta}}{\partial\xi^r}\right)^2$$
$$=\frac{1}{h_{\xi^r}}\frac{\partial}{\partial\xi^r}\left(\frac{h_{\xi^\theta}}{J_\xi}\frac{\partial V_{\xi^r}}{\partial\xi^r}+V_{\xi^r}\frac{1}{J_\xi}\frac{\partial h_{\xi^\theta}}{\partial\xi^r}\right) \qquad \text{(A9.15)}$$
$$=\frac{1}{h_{\xi^r}}\frac{\partial}{\partial\xi^r}\left[\frac{1}{J_\xi}\frac{\partial\left(h_{\xi^\theta}V_{\xi^r}\right)}{\partial\xi^r}\right]$$

The second term in equation (A8.14) can be written as:

$$\frac{1}{h_{\xi^\theta}}\frac{\partial}{\partial\xi^\theta}\left(\frac{1}{h_{\xi^\theta}}\frac{\partial V_{\xi^r}}{\partial\xi^\theta}\right)$$
$$=\frac{1}{h_{\xi^\theta}}\frac{\partial}{\partial\xi^\theta}\left(\frac{h_{\xi^r}}{J_\xi}\frac{\partial V_{\xi^r}}{\partial\xi^\theta}\right)$$
$$=\frac{1}{h_{\xi^\theta}}\frac{\partial}{\partial\xi^\theta}\left[\frac{1}{J_\xi}\frac{\partial\left(h_{\xi^r}V_{\xi^r}\right)}{\partial\xi^\theta}-\frac{1}{J_\xi}V_{\xi^r}\frac{\partial h_{\xi^r}}{\partial\xi^\theta}\right] \qquad \text{(A9.16)}$$
$$=\frac{1}{h_{\xi^\theta}}\frac{\partial}{\partial\xi^\theta}\left[\frac{1}{J_\xi}\frac{\partial\left(h_{\xi^r}V_{\xi^r}\right)}{\partial\xi^\theta}\right]-\frac{1}{h_{\xi^\theta}}\frac{\partial}{\partial\xi^\theta}\left(V_{\xi^r}\frac{1}{J_\xi}\frac{\partial h_{\xi^r}}{\partial\xi^\theta}\right)$$

Since $h_{\xi^r}\neq f\left(\xi^\theta\right)$, then $\frac{1}{h_{\xi^\theta}}\frac{\partial}{\partial\xi^\theta}\left(V_{\xi^r}\frac{1}{J_\xi}\frac{\partial h_{\xi^r}}{\partial\xi^\theta}\right)=0$, and this term can be added to equation (A9.16) to give:

$$\frac{1}{h_{\xi^\theta}}\frac{\partial}{\partial\xi^\theta}\left(\frac{1}{h_{\xi^\theta}}\frac{\partial V_{\xi^r}}{\partial\xi^\theta}\right)=\frac{1}{h_{\xi^\theta}}\frac{\partial}{\partial\xi^\theta}\left[\frac{1}{J_\xi}\frac{\partial\left(h_{\xi^r}V_{\xi^r}\right)}{\partial\xi^\theta}\right] \qquad \text{(A9.17)}$$

The fourth term in equation (9.14) is treated as follows:

$$\frac{1}{r}\frac{2}{h_{\xi^\theta}}\frac{\partial V_{\xi^\theta}}{\partial\xi^\theta}$$

$$= 2\frac{1}{J_\xi}\frac{\partial h_{\xi^\theta}}{\partial \xi^r}\frac{1}{h_{\xi^\theta}}\frac{\partial V_{\xi^\theta}}{\partial \xi^\theta}$$

$$= \left(\frac{1}{J_\xi}\frac{\partial h_{\xi^\theta}}{\partial \xi^r}\frac{1}{h_{\xi^\theta}}\frac{\partial V_{\xi^\theta}}{\partial \xi^\theta}\right) + \left(\frac{1}{h_{\xi^\theta}}\frac{\partial V_{\xi^\theta}}{\partial \xi^\theta}\frac{1}{J_\xi}\frac{\partial h_{\xi^\theta}}{\partial \xi^r}\right)$$

$$= \left[\frac{1}{J_\xi}\frac{\partial}{\partial \xi^r}\left(\frac{h_{\xi^\theta}}{h_{\xi^\theta}}\frac{\partial V_{\xi^\theta}}{\partial \xi^\theta}\right) - h_{\xi^\theta}\frac{1}{J_\xi}\frac{\partial}{\partial \xi^r}\left(\frac{1}{h_{\xi^\theta}}\frac{\partial V_{\xi^\theta}}{\partial \xi^\theta}\right)\right]$$
$$+ \left[\frac{1}{h_{\xi^\theta}}\frac{\partial}{\partial \xi^\theta}\left(V_{\xi^\theta}\frac{1}{J_\xi}\frac{\partial h_{\xi^\theta}}{\partial \xi^r}\right) - \frac{V_{\xi^\theta}}{h_{\xi^\theta}}\frac{\partial}{\partial \xi^\theta}\left(\frac{1}{J_\xi}\frac{\partial h_{\xi^\theta}}{\partial \xi^r}\right)\right]$$

$$= \left[\frac{1}{J_\xi}\frac{\partial}{\partial \xi^r}\left(\frac{\partial V_{\xi^\theta}}{\partial \xi^\theta}\right) - \frac{1}{h_{\xi^r}}\frac{\partial}{\partial \xi^r}\left(\frac{1}{h_{\xi^\theta}}\frac{\partial V_{\xi^\theta}}{\partial \xi^\theta}\right)\right]$$
$$+ \left[\frac{1}{h_{\xi^\theta}}\frac{\partial}{\partial \xi^\theta}\left(\frac{1}{J_\xi}\frac{\partial\left(V_{\xi^\theta}h_{\xi^\theta}\right)}{\partial \xi^r}\right) - \frac{1}{h_{\xi^\theta}}\frac{\partial}{\partial \xi^\theta}\left(\frac{h_{\xi^\theta}}{J_\xi}\frac{\partial V_{\xi^\theta}}{\partial \xi^r}\right)\right. \qquad \text{(A9.18)}$$
$$\left. - \frac{V_{\xi^\theta}}{h_{\xi^\theta}}\frac{\partial}{\partial \xi^\theta}\left(\frac{1}{J_\xi}\frac{\partial h_{\xi^\theta}}{\partial \xi^r}\right)\right]$$

$$= \left[\frac{1}{J_\xi}\frac{\partial}{\partial \xi^r}\left(\frac{\partial V_{\xi^\theta}}{\partial \xi^\theta}\right) - \frac{1}{h_{\xi^r}}\frac{\partial}{\partial \xi^r}\left(\frac{1}{J_\xi}\frac{\partial\left(h_{\xi^r}V_{\xi^\theta}\right)}{\partial \xi^\theta}\right)\right.$$
$$\left. + \frac{1}{h_{\xi^r}}\frac{\partial}{\partial \xi^r}\left(\frac{V_{\xi^\theta}}{J_\xi}\frac{\partial h_{\xi^r}}{\partial \xi^\theta}\right)\right]$$
$$+ \left[\frac{1}{h_{\xi^\theta}}\frac{\partial}{\partial \xi^\theta}\left(\frac{1}{J_\xi}\frac{\partial\left(V_{\xi^\theta}h_{\xi^\theta}\right)}{\partial \xi^r}\right) - \frac{1}{h_{\xi^\theta}}\frac{\partial}{\partial \xi^\theta}\left(\frac{1}{h_{\xi^r}}\frac{\partial V_{\xi^\theta}}{\partial \xi^r}\right)\right.$$
$$\left. - \frac{V_{\xi^\theta}}{h_{\xi^\theta}}\frac{\partial}{\partial \xi^\theta}\left(\frac{1}{J_\xi}\frac{\partial h_{\xi^\theta}}{\partial \xi^r}\right)\right]$$

$$= -\left[\frac{1}{h_{\xi^r}}\frac{\partial}{\partial \xi^r}\left(\frac{1}{J_\xi}\frac{\partial\left(h_{\xi^r}V_{\xi^\theta}\right)}{\partial \xi^\theta}\right)\right]$$
$$+ \left[\frac{1}{J_\xi}\frac{\partial}{\partial \xi^r}\left(\frac{\partial V_{\xi^\theta}}{\partial \xi^\theta}\right) + \frac{1}{h_{\xi^r}}\frac{\partial}{\partial \xi^r}\left(\frac{V_{\xi^\theta}}{J_\xi}\frac{\partial h_{\xi^r}}{\partial \xi^\theta}\right)\right]$$
$$- \left[\frac{1}{h_{\xi^\theta}}\frac{\partial}{\partial \xi^\theta}\left(\frac{1}{h_{\xi^r}}\frac{\partial V_{\xi^\theta}}{\partial \xi^r}\right) + \frac{V_{\xi^\theta}}{h_{\xi^\theta}}\frac{\partial}{\partial \xi^\theta}\left(\frac{1}{J_\xi}\frac{\partial h_{\xi^\theta}}{\partial \xi^r}\right)\right]$$

$$
\begin{aligned}
&+\left[\frac{1}{h_{\xi^\theta}}\frac{\partial}{\partial\xi^\theta}\left(\frac{1}{J_\xi}\frac{\partial\left(V_{\xi^\theta}h_{\xi^\theta}\right)}{\partial\xi^r}\right)\right]\\
&=-\left[\frac{1}{h_{\xi^r}}\frac{\partial}{\partial\xi^r}\left(\frac{1}{J_\xi}\frac{\partial\left(h_{\xi^r}V_{\xi^\theta}\right)}{\partial\xi^\theta}\right)\right]+\left[\frac{1}{h_{\xi^\theta}}\frac{\partial}{\partial\xi^\theta}\left(\frac{1}{J_\xi}\frac{\partial\left(V_{\xi^\theta}h_{\xi^\theta}\right)}{\partial\xi^r}\right)\right]\\
&+\left[\frac{1}{J_\xi}\frac{\partial}{\partial\xi^r}\left(\frac{\partial V_{\xi^\theta}}{\partial\xi^\theta}\right)+\frac{1}{h_{\xi^r}}\frac{\partial}{\partial\xi^r}\left(\frac{V_{\xi^\theta}}{J_\xi}\frac{\partial h_{\xi^r}}{\partial\xi^\theta}\right)\right]\\
&-\left[\frac{1}{h_{\xi^\theta}}\frac{\partial}{\partial\xi^\theta}\left(\frac{1}{h_{\xi^r}}\frac{\partial V_{\xi^\theta}}{\partial\xi^r}\right)+\frac{V_{\xi^\theta}}{h_{\xi^\theta}}\frac{\partial}{\partial\xi^\theta}\left(\frac{1}{J_\xi}\frac{\partial h_{\xi^\theta}}{\partial\xi^r}\right)\right]
\end{aligned}
\qquad \text{(A9.18)}
$$

continued

In equation (A9.18) the third and the fifth term cancel each other, since:

$$
\frac{1}{J_\xi}\frac{\partial}{\partial\xi^r}\left(\frac{\partial V_{\xi^\theta}}{\partial\xi^\theta}\right)=\frac{1}{h_{\xi^\theta}}\frac{\partial}{\partial\xi^\theta}\left(\frac{1}{h_{\xi^r}}\frac{\partial V_{\xi^\theta}}{\partial\xi^r}\right)=\frac{1}{J_\xi}\frac{\partial}{\partial\xi^\theta}\left(\frac{\partial V_{\xi^\theta}}{\partial\xi^r}\right) \qquad \text{(A9.19)}
$$

The fourth term in equation (A9.18) is zero, because the scale factor in the ξ^r direction is not a function of ξ^θ. The sixth term is also zero, since $\frac{\partial}{\partial\xi^\theta}\left(\frac{1}{J_\xi}\frac{\partial h_{\xi^\theta}}{\partial\xi^r}\right)=0$, i.e. radius is not a function of ξ^θ.

Using the above rationalisation and equations (A9.17) and (A9.18), the laplacian of a vector in the ξ^r direction can be written as:

$$
\begin{aligned}
&\nabla^2 V\left(\xi^r\right)\\
&=\frac{1}{h_{\xi^r}}\frac{\partial}{\partial\xi^r}\left[\frac{1}{J_\xi}\frac{\partial\left(h_{\xi^\theta}V_{\xi^r}\right)}{\partial\xi^r}\right]+\frac{1}{h_{\xi^\theta}}\frac{\partial}{\partial\xi^\theta}\left[\frac{1}{J_\xi}\frac{\partial\left(h_{\xi^r}V_{\xi^r}\right)}{\partial\xi^\theta}\right]\\
&+\left[\frac{1}{h_{\xi^r}}\frac{\partial}{\partial\xi^r}\left(\frac{1}{J_\xi}\frac{\partial\left(h_{\xi^r}V_{\xi^\theta}\right)}{\partial\xi^\theta}\right)\right]-\left[\frac{1}{h_{\xi^\theta}}\frac{\partial}{\partial\xi^\theta}\left(\frac{1}{J_\xi}\frac{\partial\left(V_{\xi^\theta}h_{\xi^\theta}\right)}{\partial\xi^r}\right)\right]
\end{aligned}
\qquad \text{(A9.20)}
$$

The component of Laplacian of a vector in θ – direction transforms according to equation (3.105b):

$$\nabla^2 V\left(\xi^\theta\right)=\frac{h_{\xi^\theta}}{h_r}\frac{\partial\xi^\theta}{\partial r}\nabla^2 V(r)+\frac{h_{\xi^\theta}}{h_\theta}\frac{\partial\xi^\theta}{\partial\theta}\nabla^2 V(\theta)\Rightarrow$$

$$\nabla^2 V\left(\xi^\theta\right)=\frac{h_{\xi^\theta}}{h_r}\frac{\partial\xi^\theta}{\partial r}\left(\frac{\partial^2 V_r}{\partial r^2}+\frac{1}{r^2}\frac{\partial^2 V_r}{\partial\theta^2}+\frac{1}{r}\frac{\partial V_r}{\partial r}-\frac{2}{r^2}\frac{\partial V_\theta}{\partial\theta}-\frac{V_r}{r^2}\right) \tag{A9.21}$$

$$+\frac{h_{\xi^\theta}}{h_\theta}\frac{\partial\xi^\theta}{\partial\theta}\left(\frac{\partial^2 V_\theta}{\partial r^2}+\frac{1}{r^2}\frac{\partial^2 V_\theta}{\partial\theta^2}+\frac{1}{r}\frac{\partial V_\theta}{\partial r}+\frac{2}{r^2}\frac{\partial V_r}{\partial\theta}-\frac{V_\theta}{r^2}\right)$$

$$\nabla^2 V\left(\xi^\theta\right)$$

$$=\frac{h_{\xi^\theta}}{h_\theta}\frac{\partial\xi^\theta}{\partial\theta}\left(\frac{\partial^2 V_\theta}{\partial r^2}+\frac{1}{r^2}\frac{\partial^2 V_\theta}{\partial\theta^2}+\frac{1}{r}\frac{\partial V_\theta}{\partial r}+\frac{2}{r^2}\frac{\partial V_r}{\partial\theta}-\frac{V_\theta}{r^2}\right) \tag{A9.22}$$

Following the development used for the expression of the laplacian in the ξ^r – direction, the laplacian in the ξ^θ – direction becomes:

$$\nabla^2 V\left(\xi^\theta\right)$$

$$=\frac{1}{h_{\xi^r}}\frac{\partial}{\partial\xi^r}\left[\frac{1}{J_\xi}\frac{\partial\left(h_{\xi^\theta}V_{\xi^\theta}\right)}{\partial\xi^r}\right]+\frac{1}{h_{\xi^\theta}}\frac{\partial}{\partial\xi^\theta}\left[\frac{1}{J_\xi}\frac{\partial\left(h_{\xi^r}V_{\xi^\theta}\right)}{\partial\xi^\theta}\right] \tag{A9.23}$$

$$-\left[\frac{1}{h_{\xi^r}}\frac{\partial}{\partial\xi^r}\left(\frac{1}{J_\xi}\frac{\partial\left(h_{\xi^r}V_{\xi^r}\right)}{\partial\xi^\theta}\right)\right]+\left[\frac{1}{h_{\xi^\theta}}\frac{\partial}{\partial\xi^\theta}\left(\frac{1}{J_\xi}\frac{\partial\left(V_{\xi^r}h_{\xi^\theta}\right)}{\partial\xi^r}\right)\right]$$

APPENDIX 10

Finite Difference Discretizations of the Terms in the Navier-Stokes Equations

In the $\xi^r -$ direction the terms in equation (3.115) are discretized as follows:

- term 1 – local acceleration:

$$\frac{\partial q_{\xi^r}}{\partial t} \approx \frac{q_{\xi^r}\Big|_{i+1/2,j}^{n+1/2} - q_{\xi^r}\Big|_{i+1/2,j}^{n-1/2}}{\Delta t}$$

- term 2 – advective acceleration:

$$\beta\left\{\frac{1}{J_\xi}\left[\frac{\partial}{\partial\xi^r}\left(\frac{J_\xi}{h_{\xi^r}}V_{\xi^r}q_{\xi^r}\right)+\frac{\partial}{\partial\xi^\theta}\left(\frac{J_\xi}{h_{\xi^\theta}}V_{\xi^r}q_{\xi^\theta}\right)\right]+\frac{V_\theta}{J_\xi}\left(q_{\xi^r}\frac{\partial h_{\xi^r}}{\partial\xi^\theta}-q_{\xi^\theta}\frac{\partial h_{\xi^\theta}}{\partial\xi^r}\right)\right\}\approx$$

$$\beta\frac{1}{J_\xi\Big|_{i+1/2,j}}\left\{\frac{1}{\Delta\xi^r}\left[\left(h_{\xi^\theta}V'_{\xi^r}q'_{\xi^r}\Big|_{i+1,j}^{n}\right)-\left(h_{\xi^\theta}V'_{\xi^r}q'_{\xi^r}\Big|_{i,j}^{n}\right)\right]\right.$$

$$+\frac{1}{\Delta\xi^\theta}\left[\left(h_{\xi^r}q_{\xi^\theta}\right)_{i+1/2,j+1/2}^{n}V'_{\xi^r}\Big|_{i+1/2,j+a}^{n}-\left(h_{\xi^r}q_{\xi^\theta}\right)_{i+1/2,j-1/2}^{n}V'_{\xi^r}\Big|_{i+1/2,j-1+b}^{n}\right.$$

$$+V_{\xi^\theta}\Big|_{i+1/2,j}^{n}\left[q'_{\xi^r}\Big|_{i+1/2,j}^{n}\frac{1}{\Delta\xi^\theta}\left(h_{\xi^r}\Big|_{i+1/2,j+1/2}^{n}-h_{\xi^r}\Big|_{i+1/2,j-1/2}^{n}\right)\right.$$

$$\left.\left.\left.-q_{\xi^\theta}\Big|_{i+1/2,j}^{n}\frac{1}{\Delta\xi^r}\left(h_{\xi^\theta}\Big|_{i+1,j}-h_{\xi^\theta}\Big|_{i,j}\right)\right]\right\}$$

- term 3 – Coriolis acceleration:

$$fq_{\xi^\theta} \approx f\,q_{\xi^\theta}\Big|_{i+1/2,j}^{n}$$

- term 4 – pressure gradient:

$$\frac{1}{h_{\xi^r}}gH\frac{\partial\zeta}{\partial\xi^r}\approx\frac{g}{2}\frac{1}{\Delta\xi^r}\left(\frac{H}{h_{\xi^r}}\right)\Bigg|_{i+1/2,j}^{n}\left(\zeta\Big|_{i+1,j}^{n+1/2}-\zeta\Big|_{i,j}^{n+1/2}+\zeta\Big|_{i+1,j}^{n-1/2}-\zeta\Big|_{i,j}^{n-1/2}\right)$$

- term 5 – wind shear force:

$$\frac{\rho_a}{\rho}\gamma W_{\xi^r}W\approx\frac{\rho_a}{\rho}\gamma W_{\xi^r}W\Big|_{i+1/2,j}^{n-1/2}$$

- term 6 - bed shear resistance:

$$g\frac{V_{\xi^r}V}{C^2}\approx g\left(\frac{V}{HC^2}\right)\Bigg|_{i+1/2,j}^{n}\left(\frac{q_{\xi^r}\Big|_{i+1/2,j}^{n+1/2}+q_{\xi^r}\Big|_{i+1/2,j}^{n-1/2}}{2}\right)$$

- term 7 (7a+7b) – turbulence induced shear force:

$$\overline{E}H\left\{\frac{1}{h_{\xi^r}}\frac{\partial}{\partial\xi^r}\left[\frac{1}{J_\xi}\frac{\partial}{\partial\xi^r}\left(h_{\xi^\theta}V_{\xi^r}\right)\right]+\frac{1}{h_{\xi^\theta}}\frac{\partial}{\partial\xi^\theta}\left(\frac{1}{J_\xi}\frac{\partial h_{\xi^r}V_{\xi^r}}{\partial\xi^\theta}\right)\right.$$

$$\left.+\frac{1}{h_{\xi^r}}\frac{\partial}{\partial\xi^r}\left[\frac{1}{J_\xi}\frac{\partial}{\partial\xi^\theta}\left(h_{\xi^r}V_{\xi^\theta}\right)\right]-\frac{1}{h_{\xi^\theta}}\frac{\partial}{\partial\xi^\theta}\left(\frac{1}{J_\xi}\frac{\partial h_{\xi^\theta}V_{\xi^\theta}}{\partial\xi^r}\right)\right\}\approx$$

$$\left(\overline{E}H\right)\Big|_{i+1/2,j}^{n}\left\{\frac{1}{h_{\xi^r}\Big|_{i+1/2,j}}\frac{1}{\Delta\left(\xi^r\right)^2}\left[\frac{1}{J_\xi\Big|_{i+1,j}}\left(h_{\xi^\theta}V_{\xi^r}^{'}\right)_{i+3/2,j}^{n}-\frac{1}{J_\xi\Big|_{i+1,j}}\left(h_{\xi^\theta}V_{\xi^r}^{'}\right)_{i+1/2,j}^{n}\right]\right.$$

$$-\frac{1}{h_{\xi^r}\Big|_{i+1/2,j}}\frac{1}{\Delta\left(\xi^r\right)^2}\frac{1}{J_\xi\Big|_{i,j}}\left[\left(h_{\xi^\theta}V_{\xi^r}^{'}\right)_{i+1/2,j}^{n}-\left(h_{\xi^\theta}V_{\xi^r}^{'}\right)_{i-1/2,j}^{n}\right]$$

$$+\frac{1}{h_{\xi^\theta}\Big|_{i+1/2,j}}\frac{1}{\Delta\left(\xi^\theta\right)^2}\left[\frac{1}{J_\xi\Big|_{i+1/2,j+1/2}}\left(h_{\xi^r}V_{\xi^r}^{'}\right)_{i+1/2,j+1}^{n}-\frac{1}{J_\xi\Big|_{i+1/2,j+1/2}}\left(h_{\xi^r}V_{\xi^r}^{'}\right)_{i+1/2,j}^{n}\right]$$

$$-\frac{1}{h_{\xi^\theta}\Big|_{i+1/2,j}}\frac{1}{\Delta\left(\xi^\theta\right)^2}\left[\frac{1}{J_\xi\Big|_{i+1/2,j-1/2}}\left(h_{\xi^r}V_{\xi^r}^{'}\right)_{i+1/2,j}^{n}-\frac{1}{J_\xi\Big|_{i+1/2,j-1/2}}\left(h_{\xi^r}V_{\xi^r}^{'}\right)_{i+1/2,j-1}^{n}\right]$$

$$+\frac{1}{h_{\xi^r}\Big|_{i+1/2,j}}\frac{1}{\Delta\xi^r\Delta\xi^\theta}\left[\frac{1}{J_\xi\Big|_{i+1,j}}\left(h_{\xi^r}V_{\xi^\theta}\right)_{i+1,j+1/2}^{n}-\frac{1}{J_\xi\Big|_{i+1,j}}\left(h_{\xi^r}V_{\theta}\right)_{i+1,j-1/2}^{n}\right.$$

$$\left.-\frac{1}{J_\xi\Big|_{i,j}}\left(h_{\xi^r}V_{\xi^\theta}\right)_{i,j+1/2}^{n}+\frac{1}{J_\xi\Big|_{i,j}}\left(h_{\xi^r}V_{\xi^\theta}\right)_{i,j-1/2}^{n}\right]$$

$$-\frac{1}{\left(h_{\xi^\theta}\right)_{i+1/2,j}}\left[\frac{1}{J_\xi\Big|_{i+1/2,j+1/2}}\left(h_{\xi^\theta}V_{\theta}\right)_{i+1,j+1/2}^{n}-\frac{1}{J_\xi\Big|_{i+1/2,j+1/2}}\left(h_{\xi^\theta}V_{\xi^\theta}\right)_{i,j+1/2}^{n}\right.$$

$$\left.\left.-\frac{1}{J_\xi\Big|_{i+1/2,j-1/2}}\left(h_{\xi^\theta}V_{\xi^\theta}\right)_{i+1,j-1/2}^{n}+\frac{1}{J_\xi\Big|_{i+1/2,j-1/2}}\left(h_{\xi^\theta}V_{\xi^\theta}\right)_{i,j-1/2}^{n}\right]\right\}$$

In the $\xi^\theta-$ direction the terms in equation (3.116) are discretized as follows:

- term 1 – local acceleration:

$$\frac{\partial q_{\xi^\theta}}{\partial t}\approx\frac{q_{\xi^\theta}\Big|_{i,j+1/2}^{n+1}-q_{\xi^\theta}\Big|_{i,j+1/2}^{n}}{\Delta t}$$

- term 2 (2a and 2b): advective acceleration:

$$\beta\left\{\frac{1}{J_\xi}\left[\frac{\partial}{\partial\xi^r}\left(\frac{J_\xi}{h_{\xi^r}}V_{\xi^r}q_{\xi^\theta}\right)+\frac{\partial}{\partial\xi^\theta}\left(\frac{J_\xi}{h_{\xi^\theta}}V_{\xi^\theta}q_{\xi^\theta}\right)\right]\right.$$
$$\left.+\frac{V_{\xi^r}}{J_\xi}\left(q_{\xi^\theta}\frac{\partial h_{\xi^\theta}}{\partial\xi^r}-q_{\xi^r}\frac{\partial h_{\xi^r}}{\partial\xi^\theta}\right)\right\}$$

$$\approx\frac{\beta}{J_\xi\big|_{i,j+1/2}}\left\{\frac{1}{\Delta\xi^r}\left[\left(h_{\xi^\theta}q_{\xi^r}\right)^{n+1/2}_{i+1/2,j+1/2}V'_{\xi^\theta}\Big|^{n+1/2}_{i+a^*,j+1/2}-\left(h_{\xi^\theta}q_{\xi^r}\right)^{n+1/2}_{i+1/2,j-1/2}V'_{\xi^\theta}\Big|^{n+1/2}_{i-1+b^*,j+1/2}\right]\right.$$
$$+\frac{1}{\Delta\xi^\theta}\left[\left(h_{\xi^r}V'_{\xi^\theta}q'_{\xi^\theta}\right)^{n+1/2}_{i,j+1}-\left(h_{\xi^r}V'_{\xi^\theta}q'_{\xi^\theta}\right)^{n+1/2}_{i,j+1}\right]$$
$$+V_{\xi^r}\Big|^{n+1/2}_{i,j+1/2}\left[q'_{\xi^\theta}\Big|^{n+1/2}_{i,j+1/2}\frac{1}{\Delta\xi^r}\left(h_{\xi^\theta}\Big|^{n+1/2}_{i+1,j}-h_{\xi^\theta}\Big|^{n+1/2}_{i,j}\right)\right.$$
$$\left.\left.-q_{\xi^r}\Big|^{n+1/2}_{i,j+1/2}\frac{1}{\Delta\xi^\theta}\left(h_{\xi^r}\Big|^{n+1/2}_{i+1/2,j+1/2}-h_{\xi^r}\Big|^{n+1/2}_{i+1/2,j-1/2}\right)\right]\right\}$$

- term 3 – Coriolis acceleration:

$$fq_{\xi^r}\approx f\,q_{\xi^r}\Big|^{n+1/2}_{i,j+1/2}$$

- term 4 – pressure gradient:

$$\frac{1}{h_{\xi^\theta}}gH\frac{\partial\zeta}{\partial\xi^\theta}\approx\frac{g}{2}\frac{1}{\Delta\xi^\theta}\left(\frac{H}{h_{\xi^\theta}}\right)\Bigg|^{n+1/2}_{i,j+1/2}\left(\zeta|^n_{i,j+1}-\zeta|^n_{i,j}+\zeta|^{n+1}_{i,j+1}-\zeta|^{n+1}_{i,j}\right)$$

- term 5 - wind shear force:

$$\frac{\rho_a}{\rho}\gamma W_{\xi^\theta}W\approx\frac{\rho_a}{\rho}\gamma W_{\xi^\theta}W|^n_{i,j+1/2}$$

- term 6 - bed shear resistance:

$$g\frac{V_{\xi^\theta}V}{C^2}\approx g\left(\frac{V}{HC^2}\right)\Bigg|^{n+1/2}_{i,j+1/2}\left(\frac{q_{\xi^\theta}\Big|^{n+1}_{i,j+1/2}+q_{\xi^\theta}\Big|^{n}_{i,j+1/2}}{2}\right)$$

- term 7 (7a+7b) – turbulence induced shear force:

$$\overline{E}H\left\{\frac{1}{h_{\xi^r}}\frac{\partial}{\partial\xi^r}\left(\frac{1}{J_\xi}\frac{\partial h_{\xi^\theta}V_{\xi^\theta}}{\partial\xi^r}\right)+\frac{1}{h_{\xi^\theta}}\frac{\partial}{\partial\xi^\theta}\left[\frac{1}{J_\xi}\frac{\partial}{\partial\xi^\theta}\left(h_{\xi^r}V_{\xi^\theta}\right)\right]\right.$$
$$\left.-\frac{1}{h_{\xi^r}}\frac{\partial}{\partial\xi^r}\left(\frac{1}{J_\xi}\frac{\partial h_{\xi^r}V_{\xi^r}}{\partial\xi^\theta}\right)+\frac{1}{h_{\xi^\theta}}\frac{\partial}{\partial\xi^\theta}\left[\frac{1}{J_\xi}\frac{\partial}{\partial\xi^r}\left(h_{\xi^\theta}V_{\xi^r}\right)\right]\right\}$$

$$\approx \left(\overline{E}H\right)\Big|_{i,j+1/2}^{n+1/2}\left\{\frac{1}{h_{\xi^r}\Big|_{i,j+1/2}}\frac{1}{\left(\Delta\xi^r\right)^2}\frac{1}{J_\xi\Big|_{i+1/2,j+1/2}}\left[\left(h_{\xi^\theta}V'_{\xi^\theta}\right)\Big|_{i+1,j+1/2}^{n+1/2}-\left(h_{\xi^\theta}V'_{\xi^\theta}\right)_{i,j+1/2}^{n+1/2}\right]\right.$$

$$-\frac{1}{h_{\xi^r}\Big|_{i,j+1/2}}\frac{1}{\left(\Delta\xi^r\right)^2}\frac{1}{J_\xi\Big|_{i-1/2,j+1/2}}\left[\left(h_{\xi^\theta}V'_{\xi^\theta}\right)\Big|_{i,j+1/2}^{n+1/2}-\left(h_{\xi^\theta}V'_{\xi^\theta}\right)_{i-1,j+1/2}^{n+1/2}\right]$$

$$+\frac{1}{h_{\xi^\theta}\Big|_{i,j+1/2}}\frac{1}{\left(\Delta\xi^\theta\right)^2}\left[\frac{1}{J_\xi\Big|_{i,j+1}}\left(h_{\xi^r}V'_{\xi^\theta}\right)_{i,j+3/2}^{n+1/2}-\frac{1}{J_\xi\Big|_{i,j+1}}\left(h_{\xi^r}V'_{\xi^\theta}\right)_{i,j+1/2}^{n+1/2}\right]$$

$$-\frac{1}{h_{\xi^\theta}\Big|_{i,j+1/2}}\frac{1}{\left(\Delta\xi^\theta\right)^2}\left[\frac{1}{J_\xi\Big|_{i,j}}\left(h_{\xi^r}V'_{\xi^\theta}\right)_{i,j+1/2}^{n+1/2}-\frac{1}{J_\xi\Big|_{i,j}}\left(h_{\xi^r}V'_{\xi^\theta}\right)_{i,j-1/2}^{n+1/2}\right]$$

$$+\frac{1}{h_{\xi^r}\Big|_{i,j+1/2}}\frac{1}{\Delta\xi^r\Delta\xi^\theta}\left[\frac{1}{J_\xi\Big|_{i+1/2,j+1/2}}\left(h_{\xi^r}V_{\xi^r}\right)_{i+1/2,j+1}^{n+1/2}\right.$$

$$-\frac{1}{J_\xi\Big|_{i+1/2,j+1/2}}\left(h_{\xi^r}V_{\xi^r}\right)_{i+1/2,j}^{n+1/2}$$

$$\left.-\frac{1}{J_\xi\Big|_{i-1/2,j+1/2}}\left(h_{\xi^r}V_{\xi^r}\right)_{i-1/2,j+1}^{n+1/2}+\frac{1}{J_\xi\Big|_{i-1/2,j+1/2}}\left(h_{\xi^r}V_{\xi^r}\right)_{i-1/2,j}^{n+1/2}\right]$$

$$-\frac{1}{h_{\xi^\theta}\Big|_{i,j+1/2}}\frac{1}{\Delta\xi^r\Delta\xi^\theta}\left[\frac{1}{J_\xi\Big|_{i,j+1}}\left(h_{\xi^\theta}V_{\xi^r}\right)_{i+1/2,j+1}^{n+1/2}-\frac{1}{J_\xi\Big|_{i,j+1}}\left(h_{\xi^\theta}V_{\xi^r}\right)_{i-1/2,j+1}^{n+1/2}\right.$$

$$\left.\left.-\frac{1}{J_\xi\Big|_{i,j}}\left(h_{\xi^\theta}V_{\xi^r}\right)_{i+1/2,j}^{n+1/2}+\frac{1}{J_\xi\Big|_{i,j}}\left(h_{\xi^\theta}V_{\xi^r}\right)_{i-1/2,j}^{n+1/2}\right]\right\}$$

APPENDIX 11

Wave Energy Conservation

A11.1. Analytical Solution of the Wave Equation for Convergent Geometry and Uniform Water Depth in the Frictionless Case

According to Dean and Dalrymple (1991) solution of the wave equation for a variable cross section channel (figure A11.1) is obtained writing the linearized one-dimensional equations along the channel centreline:

$$\frac{\partial(UhB)}{\partial x} = -B\frac{\partial \zeta}{\partial t} \tag{A11.1}$$

$$B\frac{\partial U}{\partial t} = -gB\frac{\partial \zeta}{\partial x} \tag{A11.2}$$

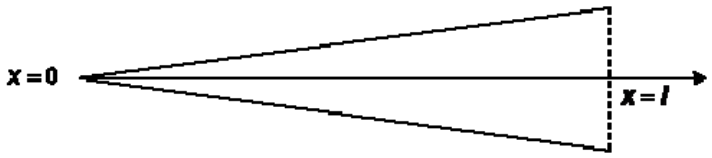

Figure A11.1. Domain for the study of analytical solution in convergent geometry.

Differentiation of the first equation with respect to time gives:

$$\frac{\partial}{\partial x}\left(hB\frac{\partial U}{\partial t}\right) = -B\frac{\partial^2 \zeta}{\partial t^2} \tag{A11.3}$$

Introducing equation (A11.2) into equation (A11.3) gives:

$$\frac{\partial}{\partial x}\left[h\left(-gB\frac{\partial \zeta}{\partial x}\right)\right] = -B\frac{\partial^2 \zeta}{\partial t^2} \tag{A11.4}$$

which results into:

$$\frac{g}{B}\frac{\partial}{\partial x}\left(hB\frac{\partial\zeta}{\partial x}\right)=\frac{\partial^2\zeta}{\partial t^2} \tag{A11.5}$$

or:

$$\frac{g}{B}\frac{\partial}{\partial x}\left[hB\frac{\partial\zeta(x)}{\partial x}\right]+\omega^2\zeta=0 \tag{A11.6}$$

where $\zeta(x,t)=\zeta(x)\cos\omega t$. From this one gets: $\frac{\partial\zeta}{\partial t}=-\omega\zeta(x)\sin\omega t$ and $\frac{\partial^2\zeta}{\partial t^2}=-\omega^2\zeta(x)\cos\omega t \Leftrightarrow \frac{\partial^2\zeta}{\partial t^2}=-\omega^2\zeta$. Equation (A11.5) is the wave equation for constant channel width B and water depth below mean water level h .

For an estuary with an uniform depth ($h=const.$) whose width is linearly increasing with distance from zero toward the mouth at $x=l$, the tidal surface elevations due to co-oscillating tide are obtained from the equation:

$$\frac{\partial^2\zeta(x)}{\partial x^2}+\frac{1}{x}\frac{\partial\zeta(x)}{\partial x}+k^2\zeta(x)=0 \tag{A11.7}$$

where: $k=\frac{\omega}{c}\Rightarrow k=\frac{\omega}{\sqrt{gh}}$.

Equation (A11.7) is a Bessel equation of order zero which is solved in terms of Bessel functions and has the general solution of the form:

$$\zeta(x,t)=\left[\tilde{A}J_0(kx)+\tilde{B}Y_0(kx)\right]\cos\omega t \tag{A11.8}$$

with: $\tilde{A},\tilde{B}$ constants to be determined. At $x=0$, the end of the channel, $Y_0(0)\to-\infty$ which would be unrealistic for $\zeta(0,t)$; therefore $\tilde{B}=0$. To

evaluate constant $\tilde{A}$, the tide at $x = l$, is taken to be $\zeta(l,t) = \frac{H}{2}\cos\omega t$, where H is the local tidal range.

$$\zeta(l,t) = \tilde{A}J_0(kl)\cos\omega t = \frac{H}{2}\cos\omega t \tag{A11.9}$$

Equation (A11.9) gives the expression for constant $\tilde{A}$ as:

$$\tilde{A} = \frac{H}{2J_0(kl)} \tag{A11.10}$$

Subsequently, solution of equation (A11.7) has the expression:

$$\zeta(x,t) = \frac{H}{2}\frac{J_0(kx)}{J_0(kl)}\cos\omega t \tag{A11.11}$$

"The zero-th order Bessel function calls for a large increase in tidal height into the estuary or bay, with a corresponding wave length decrease in the near field (about 25% over the first half wave length). If the estuary length l corresponds to a zero of the Bessel function, then again the possibility for resonance occurs." [Dean and Dalrymple (1991)]

A11.2. Analytical Solution of the Wave Equation for Convergent Geometry and Variable Water Depth in the Frictionless Case

According to Rahman (1994) for an estuary with variable depth $h = h_0(x/l)$ and breadth $B = B_0(x/l)$, solution of the one dimensional wave equation is obtained using equation (A11.5) and expressing water depth as variable:

$$\frac{\partial^2\zeta}{\partial t^2} = \frac{gh_0}{l}\left(x\frac{\partial^2\zeta}{\partial x^2} + 2\frac{\partial\zeta}{\partial x}\right) \tag{A11.12}$$

A simple harmonic tide can be written as in the previous section as $\zeta(x,t)=\zeta(x)\cos\omega t$ and equation (A11.12) becomes:

$$-\omega^2\zeta(x)=\frac{gh_0}{l}\left(x\frac{\partial^2\zeta(x)}{\partial x^2}+2\frac{\partial\zeta(x)}{\partial x}\right) \tag{A11.13}$$

or:

$$-\frac{\omega^2}{\frac{gh_0}{l}}\zeta(x)=\left(x\frac{\partial^2\zeta(x)}{\partial x^2}+2\frac{\partial\zeta(x)}{\partial x}\right) \tag{A11.14}$$

Writing: $k^2=\frac{\omega^2 l}{gh_0}$ and dividing by x equation (A11.14) is written as:

$$\frac{\partial^2\zeta(x)}{\partial x^2}+\frac{2}{x}\frac{\partial\zeta(x)}{\partial x}+\frac{k^2}{x}\zeta(x)=0 \tag{A11.15}$$

The generalized Bessel differential equation has the form:

$$\frac{\partial^2 y}{\partial x^2}+\frac{(2\alpha-2\beta\nu+1)}{x}\frac{\partial y}{\partial x}+\left[\beta^2\gamma^2x^{2\beta-2}+\frac{\alpha(\alpha-2\beta\nu)}{x^2}\right]y=0 \tag{A.3.16}$$

and its complete general solution is:

$$y=x^{\beta\nu-\alpha}\left[A_1J_\nu(\gamma x^\beta)+B_1Y_\nu(\gamma x^\beta)\right] \tag{A11.17}$$

Identifying coefficients in equation (A11.16) gives:

$$(2\alpha-2\beta\nu+1)=2 \tag{A11.18a}$$

$$x^{2\beta-2}=\frac{1}{x} \tag{A11.18b}$$

$$\beta^2\gamma^2 = k^2 \tag{A11.18c}$$

$$\alpha(\alpha - 2\beta\nu) = 0 \tag{A11.18d}$$

Solution of the system of equations (A11.18a,b,c,d) is: $\alpha_1 = 0$, $\alpha_2 = 1$ $\beta = \frac{1}{2}$, $\gamma = 2k$, $\nu_1 = -1$, $\nu_2 = 1$. According to this, solution of equation (A11.14) is:

$$\zeta(x) = x^{-1/2}\left[\tilde{A}_1 J_1\left(2kx^{1/2}\right) + \tilde{B}_1 Y_1\left(2kx^{1/2}\right)\right] \tag{A11.19}$$

In order for the solution to be bounded at $x = 0$ the constant $\tilde{B}_1$ is equal to zero. Boundary condition at the outer boundary $x = l$ requires that: $\tilde{A}_1 = \frac{H}{2} l^{1/2} \frac{1}{J_1\left(2kl^{1/2}\right)}$. Subsequently, equation (A.3.19) becomes:

$$\zeta(x) = \frac{H}{2}\frac{l^{1/2}}{x^{1/2}}\frac{J_1\left(2kx^{1/2}\right)}{J_1\left(2kl^{1/2}\right)} \tag{A11.20}$$

and water elevation varies according to:

$$\zeta(x,t) = \frac{H}{2}\frac{l^{1/2}}{x^{1/2}}\frac{J_1\left(2kx^{1/2}\right)}{J_1\left(2kl^{1/2}\right)}\cos\omega t \tag{A11.21}$$

A11.3. Transformation of Water Elevation Solution obtained from the Numerical Model

For the problem described herein, the domain is defined between two concentric circles with minimum and maximum values of the radius $\left(r_1 = 7500m\right.$, $\left.r_2 = 27900m\right)$ and two radii positioned with respect to the positive value of the $x-$ axis of a Cartesian co-ordinate system at $\left(\theta_1 = 252^\circ, \theta_2 = 288^\circ\right)$. Tidal forcing is specified at the outer boundary of the domain $\left(r_2 = 27900m\right)$ by means of water elevation amplitude: $\zeta = H_2 \sin\left(\omega t + \Phi\right)$. A closed boundary is

considered at $r_1 = 7500m$ [Figure A11.2]. A constant water level of 10m and a horizontal bed are assumed in the domain.

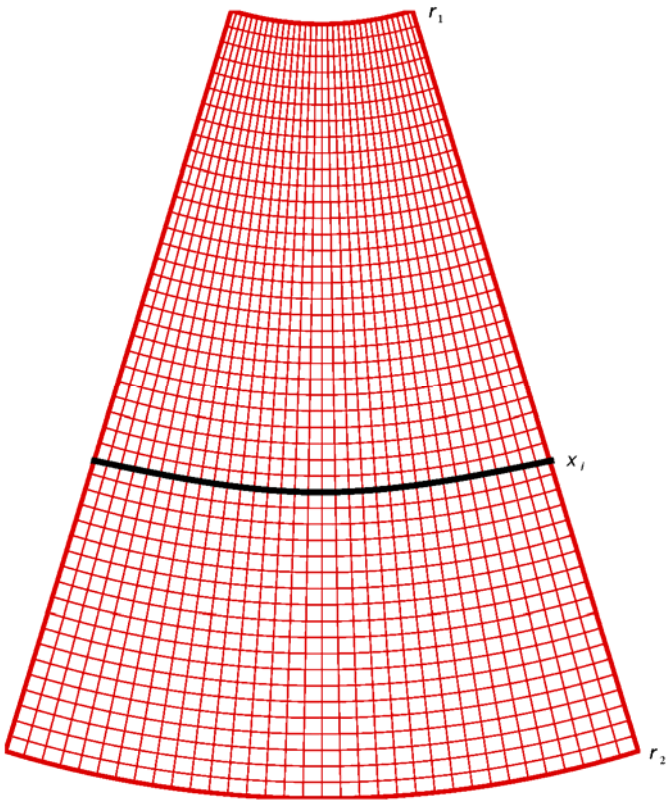

Figure A11.2. Domain representation for water elevation transformation.

Analytical solution of the simplified problem is given as in equation (A11.11), with H expressing not the tidal range, but the amplitude of the tidal forcing:

$$H_1 = H_2 \frac{J_0(kr_1)}{J_0(kr_2)} \tag{A11.22}$$

Water energy conservation relationship equivalent to Green's law in rectangular domain:

$$H_1 = H_2 \left(\frac{B_2}{B_1} \right)^{1/2} \tag{A11.23}$$

The solutions given by equations (A11.22) and (A11.23) have the same value provided that:

$$\left(\frac{B_2}{B_1}\right)^{1/2} = \frac{J_0(kr_1)}{J_0(kr_2)} \tag{A11.24}$$

Since it is not the case, the following approach is used:

- the water energy conservation relationship (Green's law) is written as:

$$H_1 = H_2^{comp}\left(\frac{B_2}{B_1}\right)^{1/2} \tag{A11.25}$$

or, in flux representation form:

$$H_2 = H_1^{comp}\left(\frac{B_2}{B_1}\right)^{1/2} \tag{A11.26}$$

- the analytical solution of the problem is written for the computed solution as:

$$H_1^{comp} = H_2^{comp}\left[\frac{J_0(kr_1)}{J_0(kr_2)}\right]^n \tag{A11.27}$$

- the real solutions are obtained as functions of the computed solutions using the subsequent relationships:

$$H_1 = H_1^{comp}\left(\frac{B_2}{B_1}\right)^{1/2}\left[\frac{J_0(kr_2)}{J_0(kr_1)}\right]^n \tag{A11.28}$$

$$H_2 = H_2^{comp}\left(\frac{B_2}{B_1}\right)^{1/2}\left[\frac{J_0(kr_1)}{J_0(kr_2)}\right]^n \tag{A11.29}$$

For any point x_i inside the considered domain the analytical solution and the relationship equivalent to Green's law with respect to the open boundary r_2 of the domain can be written as:

$$H_i^{comp} = H_2^{comp}\left[\frac{J_0(kx_i)}{J_0(kr_2)}\right]^n \tag{A11.30}$$

$$H_i = H_2^{comp}\left(\frac{B_2}{B_i}\right)^{1/2} \tag{A11.31}$$

$$H_2 = H_i^{comp}\left(\frac{B_2}{B_i}\right)^{1/2} \tag{A11.32}$$

So that the computed solution of the problem can be transformed into the real solution using:

$$H_i = H_i^{comp}\left(\frac{B_2}{B_i}\right)^{1/2}\left[\frac{J_0(kr_2)}{J_0(kx_i)}\right]^n \tag{A11.33}$$

and water elevation applied at the outer boundary can be expressed as a function of the computed solution based on the values at point x_i as:

$$H_2 = H_2^{comp}\left(\frac{B_2}{B_i}\right)^{1/2}\left[\frac{J_0(kx_i)}{J_0(kr_2)}\right]^n \tag{A11.34}$$

From equations (A11.12) and (A11.13) the ratio H_i / H_2 has the form:

$$\frac{H_i}{H_2} = \frac{H_i^{comp}\left(\frac{B_2}{B_i}\right)^{1/2}\left[\frac{J_0(kr_2)}{J_0(kx_i)}\right]^n}{H_2^{comp}\left(\frac{B_2}{B_i}\right)^{1/2}\left[\frac{J_0(kx_i)}{J_0(kr_2)}\right]^n}$$

$$\frac{H_i}{H_2} = \frac{H_i^{comp}}{H_2^{comp}}\left[\frac{J_0(kr_2)}{J_0(kx_i)}\right]^{2n} \tag{A11.35}$$

But the real solution variation is given by equation (A11.22), which introduced in equation (A11.35) gives:

$$\frac{H_i^{comp}}{H_2^{comp}}\left[\frac{J_0(kr_2)}{J_0(kx_i)}\right]^{2n} = \frac{J_0(kx_i)}{J_0(kr_2)} \tag{A11.36}$$

or:

$$\frac{H_i^{comp}}{H_2^{comp}} = \left[\frac{J_0(kx_i)}{J_0(kr_2)}\right]^{2n+1} \tag{A11.37}$$

Equation (A11.37) gives the variation of the computed amplitudes with respect to the computed value of the amplitude at the open boundary in the model. Equation (A11.29) and equation (A11.30) produce:

$$H_i = H_2^{comp}\left(\frac{B_2}{B_1}\right)^{1/2}\left[\frac{J_0(kr_1)}{J_0(kr_2)}\right]^n \frac{J_0(kx_i)}{J_0(kr_2)} \tag{A11.38}$$

Expressing H_2^{comp} as a function of H_i^{comp} from equation (A11.37) and introducing the result into equation (A11.38) gives:

$$H_i = H_i^{comp}\left(\frac{B_2}{B_1}\right)^{1/2}\left[\frac{J_0(kr_1)}{J_0(kr_2)}\right]^n\left[\frac{J_0(kr_2)}{J_0(kx_i)}\right]^{2n} \tag{A11.39}$$

The exponent in equation (A11.39) is obtained writing the equation between r_1 and r_2:

$$\frac{H_1^{comp}}{H_2^{comp}} = \left[\frac{J_0(kr_1)}{J_0(kr_2)}\right]^{2n+1} \tag{A11.40}$$

Since $H_2 = H_2^{comp}\left(\frac{B_2}{B_1}\right)^{1/2}\left[\frac{J_0(kr_1)}{J_0(kr_2)}\right]^n$ one gets the computed value of the tidal range at the open boundary as:

$$H_2^{comp} = H_2\left(\frac{B_1}{B_2}\right)^{1/2}\left[\frac{J_0(kr_2)}{J_0(kr_1)}\right]^n \tag{A11.41}$$

which is next introduced in equation (A11.40) resulting in:

$$\frac{H_1^{comp}}{H_2}\left(\frac{B_2}{B_1}\right)^{1/2}\left[\frac{J_0(kr_1)}{J_0(kr_2)}\right]^n = \left[\frac{J_0(kr_1)}{J_0(kr_2)}\right]^{2n+1} \tag{A11.42}$$

or:

$$\frac{H_1^{comp}}{H_2}\left(\frac{B_2}{B_1}\right)^{1/2} = \left[\frac{J_0(kr_1)}{J_0(kr_2)}\right]^{n+1} \tag{A11.43}$$

Applying the natural logarithm to equation (A11.43) gives:

$$\ln\left[\frac{H_1^{comp}}{H_2}\left(\frac{B_2}{B_1}\right)^{1/2}\right] = (n+1)\ln\left[\frac{J_0(kr_1)}{J_0(kr_2)}\right] \tag{A11.44}$$

and subsequently n is obtained as:

$$n = \frac{\ln\left[\frac{H_1^{comp}}{H_2}\left(\frac{B_2}{B_1}\right)^{1/2}\right]}{\ln\left[\frac{J_0(kr_1)}{J_0(kr_2)}\right]} - 1 \qquad \text{(A11.45)}$$

In equation (A11.45) all values are known except for the computed tidal range H_1^{comp} at the next point near the closed boundary of the domain (r_1). This is obtained from the model within one tidal cycle , i.e. T=75-87.5 hours.

Nomenclature:

r_1	Value of radius at the closed boundary of the domain
r_2	Value of radius at the open boundary of the domain
H_1	Real amplitude at the closed boundary (r_1) of the domain
H_2	Specified amplitude at the open boundary (r_2) of the domain
H_i	Real amplitude at point x_i inside domain
H_i^{comp}	Computed amplitude at point x_i inside domain
B_1	Width of the domain at the closed boundary of the domain
B_2	Width of the domain at the open boundary of the domain
B_i	Width of the domain at point x_i inside domain
h_1	Water depth at the nearest point to the closed boundary (r_1)
h_2	Water depth at the nearest point to the open boundary (r_2)
h_i	Water depth at section x_i inside domain
k	Wavenumber (specified as in DIVAST)
$J_0(kx_i)$, i=1,2,…,	Zero-th order Bessel function of the first kind
$J_1(2kx_i^{1/2})$, i=1,2,…,	First order Bessel function of the first kind
ω	Angular frequency of the tidal wave
t	Time
Φ	Phase

APPENDIX 12

DIVAST Model Description

The Depth Integrated Velocities and Solute Transport (DIVAST) model is a two-dimensional Cartesian co-ordinates model developed by Prof. Roger A. Falconer at Cardiff University, Wales. The model consists of four modules: bathymetric, hydrodynamic, solute transport and water quality module. A versatile model, DIVAST is under continuous development with a large number of industrial applications in tidal [Falconer et al. (1986)], sediment transport [Falconer and Chen (1996)], water quality [Falconer (1986)], heavy metals [Hartnett and Berry (2010)], and physical modelling [Ebrahimi et al. (2007)]. A large number of water quality parameters can be simulated in DIVAST: salinity, biochemical oxygen demand, dissolved oxygen, total and faecal coliforms, nitrogen (organic, ammoniac, nitrate), phosphorus (organic and inorganic), and phytoplankton. The relationship between the hydrodynamic and the three remaining modules is as follows: the bathymetric module is used as input for hydrodynamics, and the outputs of the hydrodynamic module are used as inputs for any of the sediment transport or water quality modules.

Detailed descriptions of DIVAST can be found in Olbert (2006) who further developed the model to include a more advanced turbulence parameterization, namely the $k-\varepsilon$ scheme, and Nash (2010) who modified the original structure to incorporate both basic and adaptive nested schemes. Below, a short presentation of the mathematical equations and numerical scheme included in DIVAST for hydrodynamic modelling are presented.

A12.1. DIVAST Equations for Hydrodynamic Modelling

For a well-mixed estuary, the equations governing hydrodynamics in DIVAST can be written in a Cartesian co-ordinate system presented in Figure A1.1 [Falconer and Chen (1996)]:

continuity equation

$$\frac{\partial \zeta}{\partial t} + \frac{\partial UH}{\partial x} + \frac{\partial VH}{\partial y} = 0 \tag{A12.1}$$

$x-$ direction momentum equation

$$\underbrace{\frac{\partial UH}{\partial t}}_{1} + \underbrace{\beta\left(\frac{\partial U^2 H}{\partial x} + \frac{\partial UVH}{\partial y}\right)}_{2} = \tag{A12.2}$$

$$\underbrace{fVH}_{3} + \underbrace{gH\frac{\partial \zeta}{\partial x}}_{4} + \underbrace{\gamma\frac{\rho_a}{\rho}W_x W}_{5} - \underbrace{g\frac{UV_t}{C^2}}_{6} + \underbrace{\bar{\varepsilon}H\left(\frac{\partial^2 U}{\partial x^2} + \frac{\partial^2 U}{\partial y^2}\right)}_{7}$$

$y-$ direction momentum equation

$$\frac{\partial VH}{\partial t} + \beta\left(\frac{\partial UVH}{\partial x} + \frac{\partial V^2 H}{\partial y}\right) = \tag{A12.3}$$

$$-fUH + gH\frac{\partial \zeta}{\partial y} + \gamma\frac{\rho_a}{\rho}W_y W - g\frac{VV_t}{C^2} + \bar{\varepsilon}H\left(\frac{\partial^2 V}{\partial x^2} + \frac{\partial^2 V}{\partial y^2}\right)$$

where:

$(U,V) = \frac{1}{H}\int_{-h}^{\zeta}(\bar{u},\bar{v})dz$ are depth-averaged velocities of the time averaged quantities $(\bar{u},\bar{v})$ in the $x-$ and $y-$ directions, respectively;

$V_t = \sqrt{U^2 + V^2}$ is the depth-averaged fluid speed;

(W_x, W_y) are wind velocity components in the $x-$ and $y-$ directions, respectively;

$W = \sqrt{W_x^2 + W_y^2}$ is wind speed;

$\bar{\varepsilon}$ is depth-averaged eddy viscosity.

Equations (5.1)-(5.3) assume that fluid is Newtonian, incompressible, velocity gradients on the vertical direction are not significant and fluctuations in fluid density are small. Turbulence closure is represented with a dynamic mixing

length model. The seven terms in equation (5.2) correspond to the terms presented in Chapter 2, Section 2.2.7.

A12.2. DIVAST Boundary Conditions

No-slip boundary conditions for straight walls [equation (3.119)] are used in DIVAST for closed boundaries. The model uses reflective open boundary conditions which can be expressed in terms of prescribed velocities or water elevations. For water elevations, the quasi-geostrophic equation can be used to describe evolution of the water level along an $x = const.$ open boundary:

$$\frac{\partial \zeta}{\partial y} = -\frac{fU}{g} \tag{A12.4}$$

A12.3. DIVAST Finite Difference Scheme

The non-linear system of equations (5.1) - (5.3) has three unknowns: water elevation (ζ), and velocity components (U and V) along the two axes of the Cartesian co-ordinate system. DIVAST uses a uniform staggered grid system for representation of variables inside domain. According to Figure 5.1, water elevations are represented at point (i, j), velocity component in the $x-$ direction is represented at point $(i+1/2, j)$, while velocity component in the $y-$ direction is represented at point $(i, j+1/2)$.

Time discretization in DIVAST is performed with an economical two-level Alternating Directions Implicit method [equations (4.30) – (4.31)]. ADI method reduces the non-linear problem to two linearized one-dimensional systems of equations to be solved in each direction. The variables solved implicitly at first half time step are water elevation and the $x-$ direction velocity components, while the $y-$ direction velocity components are evaluated explicitly. Similarly,

at second half time step, implicit representations of water elevation and the $y-$ direction velocity components are used, complemented by explicit discretization of the $x-$ direction velocity component. The resulting tridiagonal systems of equations, in terms of the unknowns $\zeta_{i,j}^{n+1/2}$ and $q_x\big|_{i+1/2,j}^{n+1/2}$ in the $x-$direction, and $\zeta_{i,j}^{n+1}$ and $q_y\big|_{i,j+1/2}^{n+1}$ in the $y-$direction respectively, are solved at each half time step using Thomas algorithm.

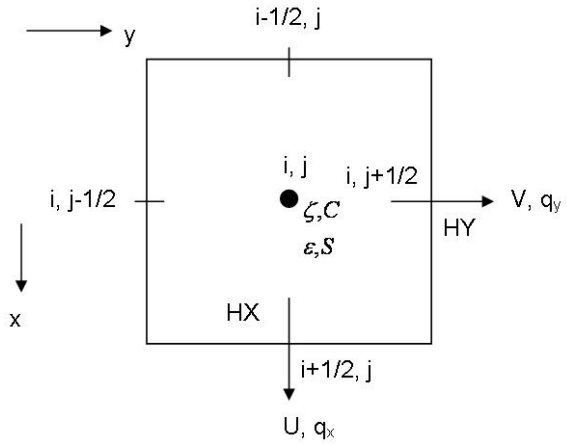

Figure A12.1: Representation of variables in DIVAST.

Discretization of the continuity equation is done at point (i, j) with a second order accurate scheme which is fully centred in both time and space over one time step [Falconer et al. (1998)]. Equations (A12.5) and (A12.6) represent the finite difference approximations to equations (A12.1) and (A12.2), respectively, during first time step, from $t_1 = n\delta t$ to $t_{1+1/2} = (n+1/2)\delta t$, where n is an integer representing the number of time step. Finite difference approximations for equation (5.2) are centred at point $(i+1/2, j)$.

continuity equation

$$\frac{\zeta\big|_{i,j}^{n+1/2} - \zeta\big|_{i,j}^{n}}{\delta t/2} = -\frac{1}{\delta x}\left[(q_x)\big|_{i+1/2,j}^{n+1/2} - (q_x)\big|_{i-1/2,j}^{n+1/2}\right] - \frac{1}{\delta y}\left[(q_y)\big|_{i,j+1/2}^{n} - (q_y)\big|_{i,j-1/2}^{n}\right] \tag{A12.5}$$

$x-$ direction momentum equation

$$
\begin{aligned}
&q_x\big|_{i+1/2,j}^{n+1/2} - q_x\big|_{i+1/2,j}^{n-1/2} = \\
&-\beta\frac{\delta t}{2\delta x}\left[\left(U'q'_x\right)\big|_{i+3/2.j}^{n} - \left(U'q'_x\right)\big|_{i-1/2.j}^{n}\right] \\
&-\beta\frac{\delta t}{\delta y}\left[\left(U'q_y\right)_{i+1/2.j+1/2}^{n} - \left(U'q_y\right)_{i+1/2.j-1/2}^{n}\right] \\
&+\delta t f\, q_y\big|_{i+1/2,j}^{n} - gH\big|_{i+1/2,j}\frac{\delta t}{2\delta x}\left(\zeta\big|_{i+1,j}^{n+1/2} + \zeta\big|_{i+1,j}^{n-1/2} - \zeta\big|_{i,j}^{n+1/2} - \zeta\big|_{i,j}^{n-1/2}\right) \\
&+\delta t\frac{\gamma\rho_a}{\rho}W_x W - \frac{\delta t g}{2C^2}\left(U\big|_{i+1/2,j}^{n+1/2} + U\big|_{i+1/2,j}^{n-1/2}\right)\sqrt{U^2+V^2}\Big|_{i+1/2,j}^{n} \\
&\bar{\varepsilon}\frac{\delta t}{(\delta x)^2}H\big|_{i+1/2,j}\left(U'\big|_{i+3/2,j}^{n} - 2U'\big|_{i+1/2,j}^{n} + U'\big|_{i-1/2,j}^{n}\right)
\end{aligned}
\qquad \text{(A12.6)}
$$

The finite difference approximations to equations (A12.1) and (A12.3) can be written for the second half time step, from $t_{1+1/2} = (n+1/2)\delta t$ to $t_2 = (n+1)\delta t$, with discretized $y-$ direction momentum equation centred at point $(i, j+1/2)$:

continuity equation

$$
\begin{aligned}
&\frac{\zeta\big|_{i,j}^{n+1} - \zeta\big|_{i,j}^{n+1/2}}{\delta t/2} = \\
&-\frac{1}{\delta x}\left[\left(q_x\right)_{i+1/2,j}^{n+1/2} - \left(q_x\right)_{i-1/2,j}^{n+1/2}\right] - \frac{1}{\delta y}\left[\left(q_y\right)_{i,j+1/2}^{n+1} - \left(q_y\right)_{i,j-1/2}^{n+1}\right]
\end{aligned}
\qquad \text{(A12.7)}
$$

$y-$ direction momentum equation

$$
\begin{aligned}
&q_y\big|_{i,j+1/2}^{n+1} - q_y\big|_{i,j+1/2}^{n} = \\
&-\beta\frac{\delta t}{\delta x}\left[\left(V'q'_x\right)\big|_{i+1/2,j+1/2}^{n} - \left(V'q'_x\right)\big|_{i-1/2,j+1/2}^{n}\right] \\
&-\beta\frac{\delta t}{2\delta y}\left[\left(V'q_y\right)_{i,j+3/2}^{n} - \left(V'q_y\right)_{i,j-1/2}^{n}\right] \\
&-\delta t f\, q_x\big|_{i,j+1/2}^{n} - gH\big|_{i,j+1/2}\frac{\delta t}{2\delta x}\left(\zeta\big|_{i,j+1}^{n+1} + \zeta\big|_{i,j+1}^{n} - \zeta\big|_{i,j}^{n+1} - \zeta\big|_{i,j}^{n}\right) \\
&+\delta t\frac{\gamma\rho_a}{\rho}W_y W - \frac{\delta t g}{2C^2}\left(V_{i,j+1/2}^{n+1} + V\big|_{i,j+1/2}^{n}\right)\sqrt{U^2+V^2}\Big|_{i,j+1/2}^{n+1/2}
\end{aligned}
\qquad \text{(A12.8)}
$$

$$\bar{\varepsilon}\frac{\delta t}{(\delta y)^2}H\Big|_{i,j+1/2}^{n+1/2}\left(V'\Big|_{i,j+3/2}^{n+1/2}-2V'\Big|_{i,j+1/2}^{n+1/2}+V'\Big|_{i,j-1/2}^{n+1/2}\right)$$

In the finite difference approximations of the continuity, $x-$ and $y-$ direction momentum equations (A12.5), (A12.7), (A12.6) and (A12.8) a convenient change in variables notation was performed: $q_x = UH$ and $q_y = VH$. The primed terms in the momentum equations represent values corrected by time iterations.

In DIVAST, advection terms in momentum equations (A12.6) and (A12.8) are approximated using the second order central difference for direct products $\left(U'q_x'\right)$ or $\left(V'q_y'\right)$, while cross-products $\left(U'q_y'\right)$ or $\left(V'q_x'\right)$ are represented with the first order upwind algorithm. In the $x-$ direction momentum equation the first order upwind algorithm gives the values of U':

$$U'\Big|_{i+1/2,j+1/2}^{n}=\begin{cases}U\Big|_{i+1/2,j+1}^{n} & if \quad q_y\Big|_{i+1/2,j+1/2}^{n}<0\\ U\Big|_{i+1/2,j-1}^{n} & if \quad q_y\Big|_{i+1/2,j-1/2}^{n}>0\end{cases} \tag{A12.9}$$

where:

$$q_y\Big|_{i+1/2,j+1/2}^{n}=\frac{1}{2}\left(q_y\Big|_{i,j+1/2}^{n}+q_y\Big|_{i+1,j+1/2}^{n}\right)$$

$$q_y\Big|_{i+1/2,j-1/2}^{n}=\frac{1}{2}\left(q_y\Big|_{i,j-1/2}^{n}+q_y\Big|_{i+1,j-1/2}^{n}\right)$$

Computational accuracy of DIVAST scheme presented herein requires that time step is restricted by the Courant number given in equation (4.33).

EFDC Model Description

Environmental Fluid Dynamics Code (EFDC) was developed by John Hamrick at Virginia Institute of Marine Science in 1992. EFDC is a both two-dimensional and three-dimensional general orthogonal curvilinear co-ordinates model, which offers the choice of Cartesian grids to be generated as well. This versatile model has four modules, namely hydrodynamics, solute transport, water quality, and toxics. The model is currently used by the US Environmental Protection Agency. A description of EFDC is given next, based on the work of Hamrick (1992).

A13.1. EFDC Two-Dimensional Equations for Hydrodynamic Modelling

The depth-averaged forms of the three-dimensional continuity and horizontal momentum equations given in Hamrick (1992) are obtained by integration with respect to z over the interval $(0,1)$, with addition of vertical boundary conditions, vertical velocity in the dimensionless vertical co-ordinate is $w = 0$ at $z = (0,1)$, considering $k = 1, K$ vertical layers and introducing some convenient notations: $\overline{V}_x = h_y H\overline{u}$, $\overline{V}_y = h_x H\overline{v}$, $V_x\big|_k = h_y H u_k$, $V_y\big|_k = h_y H v_k$.

continuity equation

$$\frac{\partial \zeta}{\partial t} + \frac{1}{J}\frac{\partial V_x}{\partial x} + \frac{1}{J}\frac{\partial V_y}{\partial y} = 0 \tag{A13.1}$$

$x-$ direction momentum equation

$$\underbrace{\frac{\partial \overline{V}_x}{\partial t}}_{1} = \underbrace{-\frac{h_y}{h_x} Hg \frac{\partial \zeta}{\partial x}}_{2} \underbrace{-\frac{h_y}{h_x} H \frac{\partial p_s}{\partial x}}_{3} + \underbrace{\frac{h_y}{h_x} Hg\left(\overline{b}\frac{\partial h}{\partial x} - \overline{B}\frac{\partial H}{\partial x} - \frac{1}{2}H\frac{\partial \overline{\beta}}{\partial x}\right)}_{4} \tag{A13.2}$$

$$\underbrace{-\frac{1}{h_x}\sum_{k=1}^{K}\delta_k\left[\frac{\partial\left(V_x\big|_k u_k\right)}{\partial x}+\frac{\partial\left(V_y\big|_k u_k\right)}{\partial y}\right]}_{5}$$

$$+\underbrace{\frac{1}{h_x}\sum_{k=1}^{K}\delta_k\left[Jf+v_k\frac{\partial h_y}{\partial x}-u_k\frac{\partial h_x}{\partial y}\right]Hv_k}_{6} \qquad \text{(A13.2)}$$

continued

$$+\underbrace{h_y\left(\tau_{xz}\right)_K}_{7}-\underbrace{h_y\left(\tau_{xz}\right)_0}_{8}+\underbrace{\frac{\overline{Q}_u}{h_x}}_{9}$$

$y-$ direction momentum equation

$$\frac{\partial\overline{V}_y}{\partial t}=$$

$$-\frac{h_x}{h_y}Hg\frac{\partial\zeta}{\partial y}-\frac{h_x}{h_y}H\frac{\partial p_s}{\partial y}+\frac{h_x}{h_y}Hg\left(\overline{b}\frac{\partial h}{\partial y}-\overline{B}\frac{\partial H}{\partial y}-\frac{1}{2}H\frac{\partial\overline{\beta}}{\partial y}\right)$$

$$-\frac{1}{h_y}\sum_{k=1}^{K}\delta_k\left[\frac{\partial\left(V_x\big|_k v_k\right)}{\partial x}+\frac{\partial\left(V_y\big|_k v_k\right)}{\partial y}\right] \qquad \text{(A13.3)}$$

$$-\frac{1}{h_y}\sum_{k=1}^{K}\delta_k\left[Jf+v_k\frac{\partial h_y}{\partial x}-u_k\frac{\partial h_x}{\partial y}\right]Hu_k$$

$$+h_x\left(\tau_{yz}\right)_K-h_x\left(\tau_{yz}\right)_0+\frac{\overline{Q}_v}{h_y}$$

where:

$J=h_xh_y$ is the Jacobian of the orthogonal transformation from physical plane onto computational domain;

$$\sum_{k=1}^{K}\delta_k u_k=\overline{u}$$

$$\sum_{k=1}^{K}\delta_k v_k=\overline{v}$$

$\overline{Q}_u,\overline{Q}_v$ are depth averaged values of the momentum source-sink terms;

p_s is the physical pressure at the free surface by the reference density;

$$\overline{\beta}=\sum_{k=1}^{K}\delta_k\beta_k$$

$$\beta_k = \sum_{j=k}^{K} \delta_j b_j - \frac{1}{2}\delta_k b_k$$

$$\overline{B} = \sum_{k=1}^{K}\left[\delta_k \beta_k + \frac{1}{2}\delta_k (z_k + z_{k-1}) b_k \right]$$

$(\tau_{xz})_k = \frac{1}{H}(A_v)_k \frac{u_{k+1} - u_k}{(\delta_{k+1} + \delta_k)/2}$ is the turbulent shear stress at the cell layer interface in the $x-$ direction;

$(\tau_{yz})_k = \frac{1}{H}(A_v)_k \frac{v_{k+1} - v_k}{(\delta_{k+1} + \delta_k)/2}$ is the turbulent shear stress at the cell layer interface in the $y-$ direction.

In equation (A13.2) nine terms are identified and they represent the following:

1. time rate of change of depth integrated volumetric transports;
2. pressure gradient associated with free surface slope;
3. pressure gradient associated with atmospheric pressure;
4. pressure gradient associated with buoyancy;
5. advective accelerations;
6. Coriolis and curvature accelerations;
7. free surface tangential stress;
8. bottom tangential stress;
9. general source/sink term.

In EFDC turbulence closure is provided by a second moment turbulence model of Mellor and Yamada (1982) modified by Galperin et al. (1982). The vertical turbulent viscosity A_v and the vertical turbulent diffusivity A_b are given in equations (A13.4) and (A13.5), respectively, as functions of the turbulent intensity q, turbulent length scale l and a Richardson number Ri_q [equation (A13.6)]. Solutions of a pair of transport equations (A13.7) and (A13.8) provide the values of the turbulence intensity and turbulence length scale.

$$A_v = \frac{0.4\left(1+8Ri_q\right)ql}{\left(1+36Ri_q\right)\left(1+6Ri_q\right)} \tag{A13.4}$$

$$A_b = \frac{0.5ql}{\left(1+36Ri_q\right)} \tag{A13.5}$$

$$Ri_q = \frac{gH\,\partial b/\partial z}{q^2}\left(\frac{l}{H}\right)^2 \tag{A13.6}$$

turbulence intensity equation

$$\begin{aligned}&\frac{\partial\left(JHq^2\right)}{\partial t}+\frac{\partial\left(h_yHuq^2\right)}{\partial x}+\frac{\partial\left(h_xHvq^2\right)}{\partial y}+\frac{\partial\left(Jwq^2\right)}{\partial z}=\\&\frac{\partial}{\partial z}\left(\frac{J}{H}A_q\frac{\partial q^2}{\partial z}\right)+Q_q+2\frac{J}{H}A_v\left[\left(\frac{\partial u}{\partial z}\right)^2+\left(\frac{\partial v}{\partial z}\right)^2\right]+2JA_b\frac{\partial b}{\partial z}-2\frac{JH}{B_1l}q^3\end{aligned} \tag{A13.7}$$

turbulence length scale equation

$$\begin{aligned}&\frac{\partial\left(JHq^2l\right)}{\partial t}+\frac{\partial\left(h_yHuq^2l\right)}{\partial x}+\frac{\partial\left(h_xHvq^2l\right)}{\partial y}+\frac{\partial\left(Jwq^2l\right)}{\partial z}=\\&\frac{\partial}{\partial z}\left(\frac{J}{H}A_q\frac{\partial q^2l}{\partial z}\right)+Q_l+\frac{J}{H}E_1lA_v\left[\left(\frac{\partial u}{\partial z}\right)^2+\left(\frac{\partial v}{\partial z}\right)^2\right]+JE_1E_3A_b\frac{\partial b}{\partial z}\\&-\frac{JH}{B_1}\left[1+\frac{E_2l^2}{\left(kL\right)^2}\right]q^3\end{aligned} \tag{A13.8}$$

where:

$$\frac{1}{L}=\frac{1}{H}\left[\frac{1}{z}+\frac{1}{\left(1-z\right)}\right]$$

Q_b, Q_l are additional source-sink terms (subgrid scale horizontal diffusion);

$B_1 = 16.6$ as given by Mellor and Yamada (1982);

$\left(E_1, E_2, E_3\right) = \left(1.8, 1.33, 0.25\right)$ are empirical constants.

A13.2. EFDC Boundary Conditions

EFDC incorporates both free surface and rigid lid boundary conditions for specification of water surface. Helmholtz equation for water surface, equation (A13.9), or surface pressure is written on the boundaries where V_x and V_y are specified.

$$\frac{\partial \zeta}{\partial t} - g\frac{1}{J}\left[\frac{\partial}{\partial x}\left(\frac{h_y}{h_x}H\frac{\partial \zeta}{\partial x}\right)+\frac{\partial}{\partial y}\left(\frac{h_x}{h_y}H\frac{\partial \zeta}{\partial y}\right)\right]-\phi = 0 \qquad \text{(A13.9)}$$

where ϕ incorporates all previously evaluated terms and transport boundary conditions.

A13.3. EFDC Finite Difference Scheme

Finite difference approximations to equations (A13.1)-(A13.3) are given by equations (A13.10)-(A13.12). Variables are represented on the staggered grid shown in Figure A13.1. Grid cell is centred at *u* velocity and h_y scale factor location, with water elevation, Jacobian and buoyancy represented at eastern and western boundaries of the cell, and *v* velocity and h_x scale factor positioned at the corners of the cell. Finite difference approximations of the horizontal spatial derivatives with second order accurate central differences on the grid in Figure A13.1 ensure conservation of mass, momentum and energy. In terms of time differentiation, a three time level scheme, introduced by Madala and Piacsek (1977) for the study of baroclinic oceans, is used.

continuity equation

$$\zeta\Big|^{n+1} - \zeta\Big|^{n-1} + \frac{\delta t}{\Delta_\zeta^{1/2} J}\left[\overline{\Delta}_x^{\zeta}\left(\overline{V}_x^{\,n+1} + \overline{V}_x^{\,n-1}\right) + \overline{\Delta}_y^{\zeta}\left(\overline{V}_y^{\,n+1} + \overline{V}_y^{\,n-1}\right)\right] \qquad \text{(A13.10)}$$

$$= 0$$

$x-$ direction momentum equation

$$
\begin{aligned}
&\overline{V}_x\Big|^{n+1} = \overline{V}_x\Big|^{n-1} \\
&-\delta t\left[\left(\frac{h_y}{h_x}H\right)^u\right] g\left[\overline{\Delta}_x^u\left(\zeta\Big|^{n+1}+\zeta\Big|^{n-1}\right)\right]-2\delta t t\left[\left(\frac{h_y}{h_x}H\right)^u\right]\overline{\Delta}_x^u p_s \\
&+2\delta t\left[\left(\frac{h_y}{h_x}H\right)^u\right] g\left(\overline{b}^u\overline{\Delta}_x^u h-\overline{B}^u\overline{\Delta}_x^u H-\frac{1}{2}H^u\overline{\Delta}_x^u\overline{\beta}\right) \\
&-2\delta t\left(\frac{1}{h_x}\right)^u\sum_{k=1}^{K}\delta_k\left[\overline{\Delta}_x^u\left(V_x\big|_k u_k\right)+\overline{\Delta}_x^u\left(V_y\big|_k u_k\right)\right] \\
&+2\delta t\left(\frac{1}{h_x}\right)^u\sum_{k=1}^{K}\delta_k\left[\left(mf+v_k\frac{\partial h_y}{\partial x}-u_k\frac{\partial h_x}{\partial y}\right)Hv_k\right]^u \\
&+2\delta t\left(h_y\right)^u\left[\left(\tau_{xz}^{n-1}\right)_K-\left(\tau_{xz}^{n-1}\right)_0\right]^u \\
&+2\delta t\left(\frac{1}{h_x}\right)^u\sum_{k=1}^{K}\delta_k\left[\overline{\Delta}_x\left(h_y H\tau_{xx}^{n-1}\right)+\overline{\Delta}_y\left(h_x H\tau_{xy}^{n-1}\right)+\overline{\Delta}_y\left(h_x\right)H\tau_{xy}^{n-1}\right. \\
&\left.-\overline{\Delta}_x\left(h_y\right)H\tau_{yy}^{n-1}\right]_k^u
\end{aligned}
\tag{A13.11}
$$

$y-$ direction momentum equation

$$
\begin{aligned}
&\overline{V}_y\Big|^{n+1} = \overline{V}_y\Big|^{n-1} \\
&-\delta t\left[\left(\frac{h_x}{h_y}H\right)^v\right] g\left[\overline{\Delta}_y^v\left(\zeta\Big|^{n+1}+\zeta\Big|^{n-1}\right)\right]-2\delta t t\left[\left(\frac{h_x}{h_y}H\right)^v\right]\overline{\Delta}_y^v p_s \\
&+2\delta t\left[\left(\frac{h_x}{h_y}H\right)^v\right] g\left(\overline{b}^v\overline{\Delta}_y^v h-\overline{B}^v\overline{\Delta}_y^v H-\frac{1}{2}H^v\overline{\Delta}_y^v\overline{\beta}\right) \\
&-2\delta t\left(\frac{1}{h_y}\right)^v\sum_{k=1}^{K}\delta_k\left[\overline{\Delta}_y^v\left(V_x\big|_k v_k\right)+\overline{\Delta}_y^v\left(V_y\big|_k v_k\right)\right] \\
&+2\delta t\left(\frac{1}{h_y}\right)^v\sum_{k=1}^{K}\delta_k\left[\left(mf+v_k\frac{\partial h_y}{\partial x}-u_k\frac{\partial h_x}{\partial y}\right)Hu_k\right]^v \\
&+2\delta t\left(h_x\right)^v\left[\left(\tau_{yz}^{n-1}\right)_K-\left(\tau_{yz}^{n-1}\right)_0\right]^u
\end{aligned}
\tag{A13.12}
$$

$$+2\delta t\left(\frac{1}{h_y}\right)^u \sum_{k=1}^{K}\delta_k\left[\overline{\Delta}_x\left(h_y H\tau_{yx}^{n-1}\right)+\overline{\Delta}_y\left(h_x H\tau_{yy}^{n-1}\right)-\overline{\Delta}_y\left(h_x\right)H\tau_{xx}^{n-1}\right.$$

$$\left.+\overline{\Delta}_x\left(h_y\right)H\tau_{yx}^{n-1}\right]_k^v \qquad \text{(A13.12)}$$

continued

where the horizontal stress tensor is represented as [Mellor and Blumberg (1985)]:

$$\left(\tau_{xx}\right)_k=\frac{2}{h_x}A_H\frac{\partial u_k}{\partial x} \qquad \text{(A13.13a)}$$

$$\left(\tau_{xy}\right)_k=\left(\tau_{yx}\right)_k=2A_H\left(\frac{1}{h_x}\frac{\partial v_k}{\partial x}+\frac{1}{h_y}\frac{\partial u_k}{\partial y}\right) \qquad \text{(A13.13b)}$$

$$\left(\tau_{yy}\right)_k=\frac{2}{h_y}A_H\frac{\partial v_k}{\partial y} \qquad \text{(A13.13c)}$$

where A_H is the horizontal diffusion coefficient, specified as a minimum constant value when central difference form of advection acceleration is used, or established as in Smagorinski (1963) when the horizontal turbulent diffusion represents sub-grid scale mixing.

In equations (A13.10)-(A13.12) variables are specified at central time step n, unless otherwise defined. The superscripts (ζ, u, v) indicate the spatial point where a variable is either centred or evaluated. The subscripts of the spatial central difference operators indicate direction of differentiation.

The elliptic system of equations (A13.9) for water elevation is discretized with spatial central difference operators. Reduced systems conjugate gradient methods with multicolour or red-black ordering of the cells can be used to solve the system of finite difference approximations to equation (A13.9) and an approximate solution of the free surface displacement is obtained at time $n+1$. Next, water elevations at forward time step are substituted into equations (A13.11) and (A13.12) to give $\overline{V}_x\Big|^{n+1}$ and $\overline{V}_y\Big|^{n+1}$, respectively. Mass

conservation requires a revised value of the water elevation at time $n+1$, representing solution of continuity equation (A13.10) after introduction of computed values $\overline{V}_x\Big|^{n+1}$ and $\overline{V}_y\Big|^{n+1}$. In order to overcome the computational mode of the numerical solution, a trapezoidal scheme is used as a correction step.

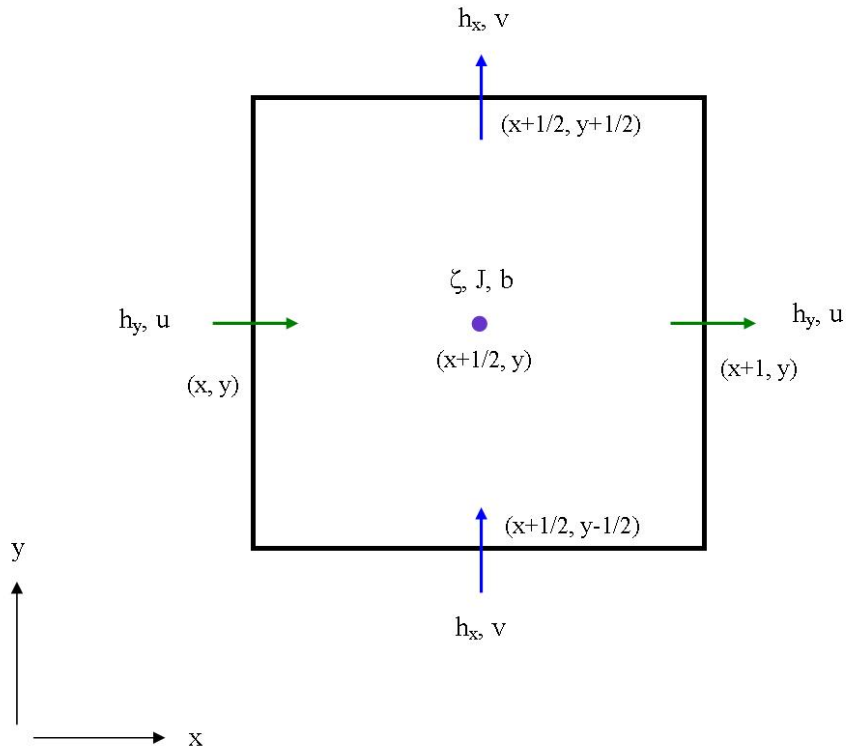

Figure A13.1: Staggered grid representation of variables in EFDC.